Identification of Novel Cow's Milk Derived Protein Hydrolysates to Support Immune and Skeletal Muscle Function

A thesis submitted for the degree of PhD

By

Conor Patrick Akintola, B.Sc.

January 2022



Based on research conducted at:

The School of Biotechnology

Dublin City University

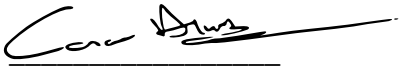
Glasnevin

Dublin 9

Under the Supervision of Prof. Christine Loscher

Declaration

I hereby certify that this material, which I now submit for assessment on the programme of study leading to the award of Doctor of Philosophy is entirely my own work, and that I have exercised reasonable care to ensure that the work is original, and does not to the best of my knowledge breach any law of copyright, and has not been taken from the work of others save and to the extent that such work has been cited and acknowledged within the text of my work.

Signed: 

ID No.: 11321601

Date: 10/01/2022

Table of Contents

Dedication i
Acknowledgements ii
Abbreviations iv
List of Figures v
List of Supplementary Figures xiii
List of Tables xiv
Presentations xvi
Publications xvi
Education and Outreach xvii
Abstract xviii

Chapter 1 1
General Introduction 1
1.1 Introduction 2
1.2 Food for Health Ireland (FHI) 6
1.2.1 Cow's Milk Derived Bioactive Hydrolysates Peptides: 7
1.3 The Immune System: 10
1.3.1 Overview of the Innate Immune System 10
1.3.2 Macrophage 11
1.3.3 Cytokines 14
1.4 Skeletal Muscle: 19
1.4.1 Glucoregulatory Functions of Skeletal Muscle 20
1.4.2 Muscle Maintenance – Anabolic Efficiency: 22
1.4.4 The immune system co-ordinates skeletal muscle repair 27
1.4.5 A dysfunctional immune response impairs skeletal muscle recovery 29
1.5 Therapeutic application of immunomodulators to drive healing skeletal muscle healing 30
1.6 Thesis Aims 31

Chapter 2 32
Materials and Methods 32
2.1 Materials 33
2.2 Methods 40
2.2.1 Sample Preparation: 40
2.2.2 Cell Culture: 40
2.2.3 Cell Numeration 45
2.2.4 Flow Cytometry 46
2.2.4.2 Cell Surface Marker Staining Protocol 47
2.2.5 Enzyme Linked Immuno-Sorbent Assay (ELISA) 48
2.2.6 Measurement of Nitric Oxide (NO) Secretion 50
2.2.7 Measurement of Arginase 1 Activity in J74A.1 Murine Macrophage and Murine BMDMs 51
2.2.8 MTS Cell Viability Assay 53
2.2.9 Optical Detection of Cell Surface GLUT4 in L6-GLUT4myc Myoblasts and Myotubes 54
2.2.10 Detection of p4E-BP1$^{(Th37.46)}$ by Western Blot Analysis in L6 Myotubes: 56
2.2.11 Measurement of *in vitro* wound closure using a scratch assay method. 58
2.2.12 Generation of J774A.1 Macrophage Conditioned Growth Medium 59
2.2.13 Generation of Activated J774A.1 Macrophage for C-Culture Experimentation 59
2.2.14 Statistical Analysis 60

Chapter 3: 61
Establishment of an *in vitro* Model of M1 and M2 Macrophage Polarisation for Assessing the Immunomodulatory Activity of Cow's Milk Protein Hydrolysates 61
3.1 Introduction: 62
3.2 Results 65

3.2.1 Polarisation of J774A.1 Macrophage *in vitro* : 65
3.2.3 Isolation and Polarisation of Primary Bone Marrow Derived Macrophage: 75
3.2.4 Casein Derived Protein Hydrolysates Modulate the Activity of M1 and M2 Polarised J774A.1 Macrophage 79
3.2.5 Optimisation of Hydrolysate Incubation in J774A.1 Macrophage 84
3.2.6 Analysis of Casein Derived and Whey Protein Derived Hydrolysates on M1 and M2 Polarised J774A.1 Macrophage. 89
3.3 Figures 94
3.4 Discussion 126

Chapter 4 135
Establishment of *in vitro* Screening Platforms to Study the Effect of Cows Milk Protein Hydrolysates on Glucose Metabolism, Protein Anabolism and Wound Healing in Skeletal Muscle 135
4.1 Introduction 136
4.2 Results 140
4.2.1 Growth and Culture of L6 GLUT4myc Rat Derived Skeletal Muscle Cells 140
4.2.2 100nM Insulin Induces GLUT4myc Translocation to the cell surface of both myoblasts and myotubes 140
4.2.3 Treatment of L6 GLUT4myc Myoblasts with 100ng/mL of Th1 and Th2 cytokines, impacts basal and insulin stimulated GLUT4myc. 141
4.2.4 Assessment of a 96 well GLUT4myc Assay Format 142
4.2.5 Optimisation of an in vitro screening platform for the detection of cell surface GLUT4 in L6 GLUT4myc myoblasts and myotubes. 144
4.2.5.2 Time course analysis of GLUT4myc translocation in response to 1μM Insulin in L6 GLUT4myc myoblasts 145
4.2.6 Representative doses of recombinant Th1 and Th2 cytokines secreted from J774A.1 macrophage modulate GLUT4 translocation in L6 GLUT4myc myotubes 146
4.2.7 Preliminary Analysis of the Effect of Casein Derived Protein Hydrolysates on GLUT4myc Translocation in L6 GLUT4myc Myoblasts 147
4.2.8 Casein and Whey derived protein hydrolysates differentially modulate GLUT4 translocation to the cell surface of L6 GLUT4myc Myotubes. 148
4.2.9 Detection and Quantification of phospho-4EBP1 in L6 Myotubes 153
4.2.10 Development of an in vitro model of wound healing in L6 Myoblasts 159
4.3 Figures 164
4.4 Discussion 204

Chapter 5 216
Establishment of *in vitro* Conditioned Medium and Co-Culture Models to Assess the Impact of Candidate Cow's Milk Protein Hydrolysate Modulated Immune Profiles on Outputs of Skeletal Muscle Function 216
5.1 Introduction 217
5.2 Results: 220
5.2.1 Generation of Differentially Activated Macrophage Conditioned Medium 220
5.2.2 The Effect of M1 and M2 Macrophage Conditioned medium on GLUT4 Translocation in L6 GLUT4myc Myotubes. 224
5.2.3 The Effect of M1 and M2 Macrophage Conditioned medium on p4E-BP1$^{Thr37/46}$ activation in L6 Myotubes. 227
5.2.4 The Effect of M1 and M2 Macrophage Conditioned medium on Wound Healing In vitro 228
The final parameter we assessed was the potential impact of hydrolysate-modulated M1 and M2 macrophages on muscle repair using the scratch assay. We first examined the effects of M1 and M2 media alone in this assay. 228
5.2.4.1 Naïve, M1 and M2 Conditioned growth medium promotes wound healing in vitro 229
5.2.5 The Effect of Co-Culture with modulated and non-modulated J774A.1 Macrophage on Critical Outputs of Skeletal Muscle Function. 233
5.3 Figures: 242
5.4 Discussion: 287

Chapter 6: 298
General Discussion 298
Chapter 7: 312
Supplementary Figures 312
Chapter 8: 330
Bibliography 330

Dedication

This Thesis is Dedicated to

Selwyn James Akintola

Home is behind, the world ahead

And there are many paths to tread

Through shadow, to the edge of night

Until the stars are all alight

Mist and shadow

Cloud and shade

All shall fade

All shall fade

J.R.R Tolkien

Acknowledgements

A PhD can often be viewed as this mammoth task that you undertake alone. This cannot be further from the truth, there is an long list of people who have helped me along the way.

Central to a PhD is a charismatic and supportive Supervisor. Thank you, Christine, for taking me on, giving me the chance and believing in me from day one. You embody all the attributes that make a fantastic supervisor and mentor. I have benefited hugely from your experience, knowledge, and guidance throughout this journey. You are the scientist that I aspire to, thank you for everything.

A special thank you, to the incredible technical staff of the School of Biotechnology. Your efforts enabling my peers and I, to get back into the lab to finish off this PhD during the pandemic cannot be praised enough. Always there to help! Thank you, Graham, Monica, Deirdre, Allison, David, Carmen, Trish, Kasia, and Janice.

To the immunomodulation research group members, past and present. From the very start, you all made me feel very welcome and helped me settle into the lab. Thank you to Laura, Iza, Kathy, Alisha, and Catherine. Particularly I would like to particularly thank Niamh and Kim, who were never short of providing a lot of laughs and advice along the way. Always still a WhatsApp or phone call away if I ever needed anything! To Dearbhla, when you arrived as a 4th year undergrad, I knew you would be the perfect fit for the group, just promise me that you will continue to uphold a high standard of tube labelling in the lab! To my friends in research groups across the school. Thank you for always being there to lend a buffer, an ear, and the craic. Shout out to Eoin, Denise, Susan, Yousif and Arabelle!

There was a time when I was the only person active in the lab and our research group office, and this was a lonely time to say the least. However, one day in 2019, that all changed when Niamh, Molly and Paola managed to swing their way into the free spaces in the office and hijack our Roche light cycler. I could not have asked for three better people to share in an office and a friendship with. The laughs, the tears, the procrastination, the rants, and the emotional support you have given me over the last two years cannot be justly summarized

in a single paragraph. You are incredible people, and I will be forever grateful for your friendship everything you have done for me! Looking forward to many, many more years of friendship!

Phil, Ciarán, Kevin, Liam, Emmet and Ruaidhri...what can I say? I've lost count of how many years we have been friends. Through thick and thin, you have always been a constant. A source of comedic relief, serious talk and emotional support. You all have helped more than you will ever know. I count myself lucky to know such kind and supportive men and more so to be able to call you all my friends! Much love lads!

To Jennie, you were there at the very start of this journey and now here we are at the end. I don't think I'll ever be able to put into words how much you have supported me along the way. Always there to pick me up, keep me grounded, make me laugh, make me smile and make me feel whole. You are a very special human being, and I cannot wait to start the next chapter of our lives together. Love you loads Jenzo!

To my Mam and Lizzi, we have been through the worst of it. Despite that, the three of us have held each other up to keep our heads above the water. Your love is all that I needed to get through. From watching Emmerdale and Corry to whipping the Tequila out for no reason other than the fun of it. The two of you have carried me through life and this PhD. Always telling me that I am able and that I am good enough, even when I felt I wasn't, you made me believe in myself more than I ever thought I could. I love you two all the way to the moon and back! Special mention also, to the Jess, the best little fat kitty cat!

Finally, to my Dad, it is hard for me to fathom that it has been twelve years since we lost you. Some will say I am biased; you were the best Dad. You never discouraged me from trying new things, from archery to golf to learning to play the guitar. You always said that I could do and be anything that I wanted, and that no matter what, that you would always be proud of me. This PhD thesis is for you, and I hope that I have made you proud

Abbreviations

AR	Anabolic Resistance
BMDC	Bone Marrow Derived Dendritic Cells
BMDM	Bone Marrow Derived Macrophage
BCAAs	Branched chain amino acids
BAPs	Bioactive peptides
BSA	Bovine Serum Albumin
DHA	Docosahexaenoic Acid
DAMPs	Damage associated molecular patterns
EPA	Eicosapentaenoic Acid
EDTA	Ethylenediaminetetraacetic acid
ELISA	Enzyme Linked Immunosorbent Assay
4EBP1	4E Binding protein 1
eIF4e	Eukaryotic Translation Initiation Factor 4E
ECL	Electro chemi luminescent substrate
FBS	Foetal Bovine Serum
FACS	Fluorescent activated cell sorting
FHI	Food for Health Ireland
GM-CSF	Granulocyte-macrophage colony stimulating factor
HRP	Horseradish Peroxidase
IR	Insulin Resistance
IFN	Interferon
IL	Interleukin
IR	Insulin resistance
kDa	Kilo-Dalton
LPS	Lipopolysaccharide
mTOR	Mammalian Target of Rapamycin
MPS	Muscle Protein Synthesis
M-CSF	Macrophage colony stimulating factor
NaCN	Sodium Caseinate
NSAID	Non-steroidal anti-inflammatory
MHC	Major Histocompatibility complex
PAGE	Polyacrylamide Gel Electrophoresis
PAMPs	Pathogen associated molecular patters
PBS	Phosphate Buffered Saline
SM	Skeletal Muscle
RT	Room Temperature
RD	Reagent Diluent
T2DM	Type 2 Diabetes Mellitus
TLR	Toll Like receptor
Th	T-helper
TNF	Tumour necrosis factor
TGF	Transforming growth factor
TBS	Tris Buffered Saline
UTC	Untreated Control

List of Figures

Figure 1.1 Workflow for the generation and isolation of bioactive peptides from whole, intact whey and casein and their known functions (Marcone, Simone et al., 2017), Page 9

Figure 1.2 Overview of Toll-like signalling pathways in innate immunity (R&D Systems). Page 17

Figure 1.3 Overview of principal macrophage phenotypes, their modes of activation and their key function *in vivo* (Martinez and Gordon, 2014). Page 18

Figure 1.4 Schematic representation of the signalling cascade that induces GLUT4 translocation in skeletal muscle (Huang and Czech, 2007). Page 21

Figure 1.5 Overview of the mammalian Target of Rapamycin (mTOR) signalling pathway (R&D Systems). Page 25

Figure 1.6 Schematic representation of the cellular and humoral interactions between muscle and the immune system during regenerations (James G. Tidball, 2017) Page 28

Figure 3.1 Stimulation of J774A.1 Macrophage with M1 Polarising factors affects cytokine secretion in a dose dependant manner. Page 94

Figure 3.2 Stimulation of J774A.1 Macrophage with M2 Polarising factors affects cytokine secretion in a dose dependant manner. Page 95

Figure 3.3 Polarised J774A.1 exhibit a differential cytokine profile. Page 96

Figure 3.4 Indicative phenotypic markers of M1 and M2 polarised J774A.1 macrophage. Page 97

Figure 3.5 IL-4 and IL-13 Stimulation leads to variability in M2 marker IL-10 secretion. Page 98

Figure 3.6 Stimulation of J774A.1 Macrophage with IL-4 and TGFβ affects cytokine secretion in a Dose Dependant Manner. Page 99

Figure 3.7 J774A.1 Macrophage polarised with 20ng/mL IL-4/IL-13 or 20ng/mL IL-4/TGFβ display differing M2 cytokine secretome profiles. Page 100

Figure 3.8 Co-Stimulation with 100mM PGE2 and 100ng/mL LPS Suppresses the Secretion of M1 Associated Cytokines and Drives Expression of M2 Associated IL-10. Page 101

3.9 Co-Stimulation with 100mM PGE2 and 100ng/mL LPS Gives Rise to an M2-Like cytokine Secretion Profile. Page 102

Figure 3.10 Co-Stimulation with 100mM PGE2 and 100ng/mL Drives a Significant Increase in Nitric Oxide Secretion Compared to M2 Polarised Macrophage. Page 103

Figure 3.11 Co-Stimulation with 100mM PGE2 and 100ng/mL LPS Fails to Drive the Activity of M2 Specific Marker Arginase 1. Page 104

Figure 3.12 Cell surface marker analysis of M1 and M2 polarised J774A.1 macrophage. Page 105

Figure 3.13 J774A.1 macrophage do not secrete key inflammatory cytokines, IL-12p40 and IL-23. Page 106

Figure 3.14 IFNγ, IL-4 and TGFβ affect cytokine secretion in BMDMs. Page 107

Figure 3.15 BMDMs exhibit differential cytokine profiles consistent with M1 and M2 macrophage phenotypes. Page 108

Figure 3.16 - Casein derived hydrolysates show the ability to modulate the cytokine secretion in naïve J774A.1 macrophage. Page 109

Figure 3.17 - Casein derived hydrolysates show the ability to modulate the cytokine secretion in M1 polarised J774A.1 macrophage. Page 110

Figure 3.18 - Casein derived hydrolysates show the ability to modulate the M2 driven phenotype in J774A.1 macrophage. Page 111

Figure 3.19 - Casein derived hydrolysates show the ability to modulate the M2 driven phenotype in J774A.1 macrophage. Page 112

Figure 3.20 - Casein derived hydrolysates show the ability to modulate Nitrite production polarised in J774A.1 macrophage. Page 113

Figure 3.21 - Candidate casein derived hydrolysates show the ability to modulate the activity of key M2 macrophage marker Arginase 1. Page 114

Figure 3.22 - Casein Derived Protein Hydrolysates Modulate Expression of Cytokines in Naïve J774A.1 Macrophage in a Time Dependant Manner. Page 115

Figure 3.23 - Casein Derived Hydrolysates Demonstrate loss of TNFα and IL-6 Suppressive Bioactivity as Length of Pre-Incubation Increases. Page 116

Figure 3.24 - Re-Stimulation of J774A.1 Macrophage with Casein Derived Hydrolysates Recovers Anti-Inflammatory Bioactivity in M1 Polarised J774A.1 Macrophage. Page 117

Figure 3.25 - Casein Derived Protein Hydrolysates Modulate Expression of Cytokines in Naïve J774A.1 Macrophage in a Time Dependant Manner at a Dose of 2mg/mL. Page 118

Figure 3.26 - Casein Derived Protein Hydrolysates Modulate Expression of Cytokines in M1 Stimulated J774A.1 Macrophage in a Time Dependant Manner at a Dose of 2mg/mL. Page 119

Figure 3.27 – Casein (NaCN) and Whey Protein (WPC) derived hydrolysates show the ability to modulate the cytokine secretion in naïve J774A.1 macrophage. Page 120

Figure 3.28– Casein and Whey protein derived hydrolysates show the ability to modulate the cytokine secretion in M1 polarised J774A.1 macrophage. Page 121

Figure 3.29 - Casein and Whey protein derived hydrolysates show the ability to modulate the M2 driven phenotype in J774A.1 macrophage. Page 122

Figure 3.30 - Whey Protein (WPC) derived hydrolysates 2-47 and its regenerates show the ability to modulate the cytokine secretion in naïve J774A.1 macrophage. Page 123

Figure 3.31 - Whey Protein (WPC) derived hydrolysates 2-47 and its regenerates show the ability to modulate the cytokine secretion in M1 Polarised J774A.1 macrophage. Page 124

Figure 3.32 - Whey Protein (WPC) derived hydrolysates 2-47 and its regenerates show the ability to modulate the cytokine secretion in M2 Polarised J774A.1 macrophage. Page 125

Figure 4.1 Myogenic differentiation of L6 and L6 GLUT4myc myoblasts. Page 164

Figure 4.2 Insulin from bovine pancreas at super physiological concentrations induce GLUT4 translocation to the cell membrane in L6 GLUT4myc Myoblasts and Myotubes. Page 165

Figure 4.3 Recombinant Murine Th1 and Th2 cytokines modulate GLUT4 translocation in L6 GLUT4myc Myoblasts in the presence and absence of 100nM Insulin. Page 166

Figure 4.4 Variability and inconsistencies in detectable fold changes between the unstimulated control and insulin-stimulated control lead to an inability to interpret the effects of casein and casein derived hydrolysates on basal GLUT4myc translocation. Page 167

Figure 4.5 Variability and inconsistencies in detectable fold changes between the unstimulated control and insulin-stimulated control lead to an inability to interpret the effects of casein derived hydrolysates on insulin stimulated GLUT4myc translocation. Page 168

Figure 4.6 Insulin drives GLUT4 Translocation in L6 GLUT4myc Myoblasts in a dose dependant manner. Page 169

Figure 4.7 Time course Insulin drives GLUT4 Translocation in L6 GLUT4myc Myoblasts. Page 170

Figure 4.8 Dose response of GLUT4myc translocation to the cell membrane of L6 GLUT4myc myoblasts in response to stimulation with 1μM Bovine Insulin. Page 171

Figure 4.9 Time course Insulin drives GLUT4 Translocation in L6 GLUT4myc Myoblasts. Page 172

Figure 4.10 Recombinant Murine Th1 and Th2 Macrophage specific cytokines modulate GLUT4 translocation in L6 GLUT4myc Myotubes in a dose dependant manner in the presence and absence of 1μM Insulin. Page 173

Figure 4.11 Analysis of the effects of casein derived hydrolysates on the basal expression of cell surface GLUT4myc in L6 GLUT4myc Myoblasts. Page 174

Figure 4.12 Analysis of the effects of casein derived hydrolysates on the basal expression of cell surface GLUT4myc in L6 GLUT4myc Myoblasts. Page 175

Figure 4.13 Whey protein derived protein hydrolysates modulate the translocation of GLUT4 to the cell surface of L6 GLUT4myc Myotubes. Page 176

Figure 4.14 Whey protein derived protein hydrolysates modulate the translocation of GLUT4 to the cell surface of L6 GLUT4myc Myotubes. Page 177

Figure 4.15 Whey protein derived protein hydrolysates modulate the translocation of GLUT4 to the cell surface of L6 GLUT4myc Myotubes. Page 178

Figure 4.16 Whey protein derived protein hydrolysates modulate the translocation of GLUT4 to the cell surface of L6 GLUT4myc Myotubes. Page 179

Figure 4.17 Whey protein derived protein hydrolysates modulate the translocation of GLUT4 to the cell surface of L6 GLUT4myc Myotubes. Page 180

Figure 4.18 Whey protein derived protein hydrolysates modulate the translocation of GLUT4 to the cell surface of L6 GLUT4myc Myotubes. Page 181

Figure 4.19 Whey and Casein Derived Hydrolysates affect basal and insulin stimulated GLUT4 translocation in L6 GLUT4myc Myotubes. Page 182

Figure 4.20 Representative western blot image of phospho-4EBP1$^{(Thr37/46)}$ activation and associated densitometric data derived using Image J image analysis software. Page 183

Figure 4.21: The effect of insulin on the levels of p4-EPB1$^{Thr(37/46)}$ in L6 myotubes. Page 184

Figure 4.22: The effect of insulin incubation time on the levels of p4-EPB1$^{Thr(37/46)}$ in L6 myotubes. Page 185

Figure 4.23: The effect of whey (WPC) and casein (NaCN) derived hydrolysates on the on the levels of basal p4-EPB1$^{Thr(37/46)}$ in L6 myotubes. Page 186

Figure 4.24: The effect of whey (WPC) and casein (NaCN) derived hydrolysates on the on the levels of insulin stimulated p4-EPB1$^{Thr(37/46)}$ in L6 myotubes. Page 187

Figure 4.25: Recombinant Th1 and Th2 cytokines modulate wound healing in an in vitro assay of wound healing. Page 188

Figure 4.26: Recombinant Th1 and Th2 cytokines modulate wound healing in an in vitro assay of wound healing. Page 189

Figure 4.27: Recombinant Th1 and Th2 cytokines induce CCL2/MCP-1 chemokine secretion in L6 myoblasts associated with increased rates of in vitro wound closure. Page 190

Figure 4.28: Whey and Casein derived hydrolysates drive CCL2/MCP-1 secretion in TNFα activated L6 myoblasts/ Page 191

Figure 4.29: Whey (WPC) derived hydrolysates modulate the recovery of an in vitro wound in L6 myoblasts. Page 192

Figure 4.30: Whey (WPC) derived hydrolysates modulate the recovery of an in vitro wound in L6 myoblasts. Page 193

Figure 4.31: Whey (WPC) derived hydrolysates modulate the recovery of an in vitro wound in L6 myoblasts. Page 194

Figure 4.32: Whey (WPC) derived hydrolysates modulate the recovery of an in vitro wound in TNFα activated L6 myoblasts. Page 195

Figure 4.33: Whey (WPC) derived hydrolysates modulate the recovery of an in vitro wound in TNFα activated L6 myoblasts. Page 196

Figure 4.34: Whey (WPC) derived hydrolysates modulate the recovery of an in vitro wound in TNFα activated L6 myoblasts. Page 197

Figure 4.35: Casein (NaCN) derived hydrolysates modulate the recovery of an in vitro wound in L6 myoblasts. Page 198

Figure 4.36: Casein (NaCN) derived hydrolysates modulate the recovery of an in vitro wound in L6 myoblasts. Page 199

Figure 4.37: Casein (NaCN) derived hydrolysates modulate the recovery of an in vitro wound in L6 myoblasts. Page 200

Figure 4.38: Casein (NaCN) derived hydrolysates modulate the recovery of an in vitro wound in TNFα activated L6 myoblasts. Page 201

Figure 4.39: Casein (NaCN) derived hydrolysates modulate the recovery of an in vitro wound in TNFα activated L6 myoblasts. Page 202

Figure 4.40: Casein (NaCN) derived hydrolysates modulate the recovery of an in vitro wound in TNFα activated L6 myoblasts. Page 203

Figure 5.1 Increasing ratios of αMEM to DMEM growth medium negatively impacts on J774A.1 macrophage cell viability. Page 242

Figure 5.2 Increasing ratios of αMEM to DMEM growth medium modulates cytokine secretion in LPS activated J774A.1 macrophage. Page 243

Figure 5.3 The effect of different medium supplementation on M1 and M2 polarised J774A.1 macrophage. Page 244

Figure 5.4 The effect of different medium supplementation on M1 and M2 polarised J774A.1 macrophage cytokine secretion profiles. Page 245

Figure 5.5 Varying seeding density of cells concentrates detectable levels of secreted cytokines in M1 Polarised J774A.1 Macrophage. Page 246

Figure 5.6 Varying seeding density of cells concentrates detectable levels of secreted cytokines in M2 Polarised J774A.1 Macrophage. Page 247

Figure 5.7 Candidate Casein and Whey Derived Hydrolysates Exhibit Anti-Inflammatory Bioactivity in M1 Polarised J774A.1 Macrophage. Page 248

Figure 5.8 Candidate Casein and Whey Derived Hydrolysates Exhibit Anti-Inflammatory Bioactivity in M2 Polarised J774A.1 Macrophage. Page 249

Figure 5.9 Concentrating the levels of secreted M1 and M2 specific cytokines modulates translocation of GLUT4 in L6 GLUT4myc myotubes. Page 250

Figure 5.10 NacN, 2-18 and 2-132 Hydrolysate Modulated M1 J774A.1 Macrophage Conditioned medium promotes GLUT4 translocation in L6 GLUT4myc Myotyubes. Page 251

Figure 5.11 NacN, 2-18 and 2-132 Hydrolysate Modulated M2 J774A.1 Macrophage Conditioned medium promotes GLUT4 translocation in L6 GLUT4myc Myotyubes. Page 252

Figure 5.12 WPC, 2-47 and 2-152 Hydrolysate Modulated M1 J774A.1 Macrophage Conditioned medium promotes GLUT4 translocation in L6 GLUT4myc Myotyubes. Page 253

Figure 5.13 WPC, 2-47 and 2-152 Hydrolysate Modulated M2 J774A.1 Macrophage Conditioned medium promotes GLUT4 translocation in L6 GLUT4myc Myotyubes. Page 254

Figure 5.14 Concentrated M1 and M2 J774A.1 macrophage conditioned medium differentially modulates basal p4E-BP1$^{(Thr37/46)}$ in L6 Myotubes. Page 255

Figure 5.15 Concentrated M1 and M2 J774A.1 macrophage conditioned medium differentially modulate insulin stimulated p4E-BP1$^{(Thr37/46)}$ in L6 Myotubes. Page 256

Figure 5.16 NacN, 2-18 and 2-132 Hydrolysate Modulated M1 J774A.1 Macrophage Conditioned medium beneficially modulates basal p4E-BP1$^{(Thr37/46)}$ in L6 Myotubes. Page 257

Figure 5.17 NacN, 2-18 and 2-132 Hydrolysate Modulated M2 J774A.1 Macrophage Conditioned medium beneficially modulates basal p4E-BP1$^{(Thr37/46)}$ in L6 Myotubes. Page 258

Figure 5.18 NacN, 2-18 and 2-132 Hydrolysate Modulated M1 J774A.1 Macrophage Conditioned medium beneficially modulates insulin stimulated p4E-BP1$^{(Thr37/46)}$ in L6 Myotubes. Page 259

Figure 5.19 NacN, 2-18 and 2-132 Hydrolysate Modulated M2 J774A.1 Macrophage Conditioned medium beneficially modulates insulin stimulated p4E-BP1$^{(Thr37/46)}$ in L6 Myotubes. Page 260

Figure 5.20 WPC, 2-47, 2-152 Hydrolysate Modulated M1 J774A.1 Macrophage Conditioned medium beneficially modulates basal p4E-BP1$^{(Thr37/46)}$ in L6 Myotubes. Page 261

Figure 5.21 WPC, 2-47, 2-152 Hydrolysate Modulated M2 J774A.1 Macrophage Conditioned medium beneficially modulates basal p4E-BP1$^{(Thr37/46)}$ in L6 Myotubes. Page 262

Figure 5.22 WPC, 2-47, 2-152 Hydrolysate Modulated M1 J774A.1 Macrophage Conditioned medium beneficially modulates insulin stimulated p4E-BP1$^{(Thr37/46)}$ in L6 Myotubes. Page 263

Figure 5.23 WPC, 2-47, 2-152 Hydrolysate Modulated M2 J774A.1 Macrophage Conditioned medium beneficially modulates insulin stimulated p4E-BP1$^{(Thr37/46)}$ in L6 Myotubes. Page 264

Figure 5.24 Naïve, M1 and M2 Modulated Macrophage Conditioned Medium Beneficially modulated wound healing in vitro . Page 265

Figure 5.25 NacN, 2-18 and 2-132 Hydrolysate Modulated Conditioned Medium Beneficially modulates wound healing in vitro . Page 266

Figure 5.26 NacN, 2-18 and 2-132 Hydrolysate Modulated Conditioned Medium Beneficially modulates wound healing in vitro . Page 267

Figure 5.27 WPC, 2-47 and 2-152 Hydrolysate Modulated Conditioned Medium Beneficially modulates wound healing in vitro . Page 268

Figure 5.28 WPC, 2-47 and 2-152 Hydrolysate Modulated Conditioned Medium Beneficially modulates wound healing in vitro . Page 269

Figure 5.29 Co-Culture of M1 and M2 Activated J774A.1 Macrophage drives GLUT4 translocation in L6 GLUT4myc Myotubes. Page 270

Figure 5.30 Co-Culture with NaCN, 2-18 and 2-132 modulated M1 J77A.1 macrophage promotes GLUT4 translocation in L6 GLUT4myc Myotubes. Page 271

Figure 5.31 Co-Culture with NaCN, 2-18 and 2-132 modulated M2 J77A.1 macrophage promotes GLUT4 translocation in L6 GLUT4myc Myotubes. Page 272

Figure 5.32 Co-Culture with WPC, 2-47 and 2-152 modulated M1 J77A.1 macrophage promotes GLUT4 translocation in L6 GLUT4myc Myotubes. Page 273

Figure 5.33 Co-Culture with WPC, 2-47 and 2-152 modulated M2 J77A.1 macrophage promotes GLUT4 translocation in L6 GLUT4myc Myotubes. Page 274

Figure 5.34 Co-Culture with NacN, 2-18 and 2-132 Hydrolysate Modulated M1 J774A.1 Macrophage beneficially modulates basal p4E-BP1$^{(Thr37/46)}$ in L6 Myotubes. Page 275

Figure 5.35 Co-Culture with NacN, 2-18 and 2-132 Hydrolysate Modulated M2 J774A.1 Macrophage beneficially modulates basal p4E-BP1$^{(Thr37/46)}$ in L6 Myotubes. Page 276

Figure 5.36 Co-Culture with NacN, 2-18 and 2-132 Hydrolysate Modulated M1 J774A.1 Macrophage beneficially modulates insulin stimulated p4E-BP1$^{(Thr37/46)}$ in L6 Myotubes. Page 277

Figure 5.37 Co-Culture with NacN, 2-18 and 2-132 Hydrolysate Modulated M2 J774A.1 Macrophage beneficially modulates insulin stimulated p4E-BP1$^{(Thr37/46)}$ in L6 Myotubes. Page 278

Figure 5.38 Co-Culture with WPC, 2-47 and 2-152 Hydrolysate Modulated M1 J774A.1 Macrophage beneficially modulates basal p4E-BP1$^{(Thr37/46)}$ in L6 Myotubes. Page 279

Figure 5.39 Co-Culture with WPC, 2-47 and 2-152 Hydrolysate Modulated M2 J774A.1 Macrophage modulates basal p4E-BP1$^{(Thr37/46)}$ in L6 Myotubes. Page 280

Figure 5.40 Co-Culture with WPC, 2-47 and 2-152 Hydrolysate Modulated M1 J774A.1 Macrophage modulates insulin stimulated p4E-BP1$^{(Thr37/46)}$ in L6 Myotubes. Page 281

Figure 5.41 Co-Culture with WPC, 2-47 and 2-152 Hydrolysate Modulated M2 J774A.1 Macrophage modulates insulin stimulated p4E-BP1$^{(Thr37/46)}$ in L6 Myotubes. Page 282

Figure 5.42 Co-Culture with NaCN, 2-18 and 2-132 Hydrolysate Modulated M1 J774A.1 Macrophage beneficially modulate wound healing in vitro . Page 283

Figure 5.43 Co-Culture with NaCN, 2-18 and 2-132 Hydrolysate Modulated M2 J774A.1 Macrophage beneficially modulate wound healing in vitro . Page 284

Figure 5.44 Co-Culture with WPC, 2-47 and 2-152 Hydrolysate Modulated M1 J774A.1 Macrophage beneficially modulate wound healing in vitro . Page 285

Figure 5.45 Co-Culture with WPC, 2-47 and 2-152 Hydrolysate Modulated M2 J774A.1 Macrophage beneficially modulate wound healing in vitro . Page 286

List of Supplementary Figures

SF1.1 - M1 and M2 polarising factors do not impact J774A.1 Cell Viability Page 313

SF1.2 - IL-4 and TGFβ does not negetitvely impact on J774A.1 Macrophage cell viability Page 314

SF1.3 - Co-Stimulation with 100mM PGE2 and 100ng/mL LPS does not Negatively Impact J774A.1 Cell Viability Page 315

SF1.4- Increasing doses of LPS do not negetively on J774A.1 Macrophage Viability, Page 316

SF1.5 - Isolated Bone Marrow Derived Macrophage Express Key Surface Markers of the Macrophage Lineage F4/80 and CD11, Page 317

SF1.6 - Isolated Bone Marrow Derived Macrophage Express differential levels of key Dendritic cell marker CD11c, Page 318

SF1.7 - Varying doses of IFNγ, IL-4 and TGFβ do not negatively impact of BMDM viability, Page 319

SF1.8 J774A.1 Murine Macrophage viability is not negatively impacted by hydrolysate stimulation in the presence and absence of M1 and M2 polarising factors, Page 320

SF1.9 - J774A.1 Murine Macrophage viability is not negatively impacted my hydrolysate stimulation in the presence and absence M2 polarising factors, Page 321

SF1.10 - J774A.1 Murine Macrophage viability is not negatively impacted by casein and whey protein hydrolysate stimulation in the presence and absence of M1 and M2 polarising factors, Page 322

SF1.11 - Whey Protein (WPC) derived hydrolysates 2-47 and its regenerates do not negatively affect polarised J774A.1 Viability, Page 323

SF1.12 - 100nM Insulin stimulation leads to varied response in cell surface GLUT4myc in a 96 well plate format of the GLUT4 translocation assay, Page 324

SF1.13 Insulin fails to induce a significant change in cell surface GLUT4 in L6 GLUT4myc Myoblasts in a dose dependant manner, Page 325

SF1.14 100nM Insulin Stimulates 4EBP1 phosphorylation in L6 Myotubes, Page 326

SF1.14 - Detection of phospho-4EBP1 in L6 Myotubes using a chemi-luminescent substrate, Page 327

SF1.16 Exposure times dictate relative intensity of signal observable in Western Blot, 1-minute exposure time, Page 328

SF1.17 Exposure times dictate relative intensity of signal observable in Western Blot - 5 minute exposure time, Page 329

List of Tables

Table 2.1 List of Cell Lines. Page 33

Table 2.2 General Equipment. Page 33

Table 2.3 Cell Culture Materials and Reagents. Page 34

Table 2.4 Recombinant Cytokines and Stimulation Factors. Page 35

Table 2.5 Stock Buffers. Page 35

Table 2.6 ELISA Kits and Materials. Page 36

Table 2.7 GLUT4 Optical Detection Assay Materials and Reagents. Page 36

Table 2.8 Flow Cytometry Materials and Reagents. Page 37

Table 2.9 Western Blotting Materials and Reagents. Page 38

Table 2.10 Assay Kits. Page 39

Table 2.11 Software and Analysis Tools. Page 39

Table 4.1: Summary of the effect of NaCN and WPC derived protein hydrolysates at 1mg/mL, on the translocation of GLUT4 in L6 GLUT4myc myotubes. Page 151

Table 4.2: Summary of the dose response effect of NaCN and WPC derived protein hydrolysates at on the translocation of GLUT4 in L6 GLUT4myc myotubes. Page 153

Table 5.1 Tabular representation of statistical analysis of M1 NaCN Hydrolysate Modulated wound healing in vitro . Page 230

Table 5.2 Tabular representation of statistical analysis of M2 NaCN Hydrolysate Modulated wound healing in vitro . Page 231

Table 5.3 Tabular representation of statistical analysis of M1 WPC Hydrolysate Modulated wound healing in vitro . Page 232

Table 5.4 Tabular representation of statistical analysis of M2 WPC Hydrolysate Modulated wound healing in vitro . Page 233

Table 5.5 Tabular representation of statistical analysis of NaCN Hydrolysate M1 Modulated Cells on wound healing in vitro . Page 238

Table 5.6 Tabular representation of statistical analysis of NaCN Hydrolysate M2 Modulated Cells wound healing in vitro . Page 239

Table 5.7 Tabular representation of statistical analysis of WPC Hydrolysate M1 Modulated Cells wound healing in vitro . Page 240

Table 5.8 Tabular representation of statistical analysis of WPC Hydrolysate M2 Modulated Cells wound healing in vitro . Page 241

Presentations

School of Biotechnology Annual Research Day, January 2021

Modulating the Immune Response to Improve Muscle Function – Oral Presentation

Conor Akintola, Christine E. Loscher

Faculty of Sports and Exercise Medicine Annual Research Conference, RCSI September 2019

Modulating the Immune Response to Improve Muscle Function – Poster Presentation

Conor Akintola, Brendan Egan, Christine E. Loscher

Irish Society of Immunology Annual Meeting, TBSI. September 2019

Modulating the Immune Response to Improve Muscle Function – Poster Presentation

Conor Akintola, Christine E. Loscher

School of Biotechnology Research Day, January 2019

Modulating Immune Response to Improve Muscle Function – Oral Presentation

Conor Akintola, Christine E. Loscher

School of Biotechnology Research Day, January 2018

Modulating Immune Response to Improve Muscle Function – Oral Presentation

Conor Akintola, Christine E. Loscher

Publications

Chapter 6 of Advances in Nutraceuticals and Functional Foods: Concepts and Applications, ***in press***, 2021
Apple Academic Press (APA)

Nutrition Nutraceuticals: A Proactive Approach for Healthcare
Conor P. Akintola, Dearbhla Finnegan, Niamh Hunt, Richard Lalor, Sandra O'Neill, and Christine Loscher

Education and Outreach

EUSO 2019, Almada, Portugal, May 4th to May 11th 2019

European Union Science Olympiad is an annual event which aims to enthuse students for science and to challenge them to get the best out of themselves and to meet like-minded students from across the EU. The European Union Science Olympiad (EUSO) is a team-based practical science competition consisting of integrated tasks across biology, chemistry and physics. This design ensures that not only do students use their scientific knowledge and practical skills, they must also collaborate and share tasks effectively. The Ireland teams were selected in Ireland through a lengthy process which started in September 2018, when we invited the top students (identified by the State Examination Commission) who achieved the highest grades in Maths & Science in the Junior Certificate Examination, to participate in IrEUSO in DCU in November 2018. Age eligible students from the previous year were also invited to participate. Therefore this group consists of 5 th year students as well as TY students. Over 350 students participated in the theoretical Round 1 exam. The practical Round 2 test took place in DCU in January 2019, following two days of Laboratory training in DCU. The final teams were selected after Round 2. The EUSO 2019 edition seen Team Ireland win Gold and Silver medals. Teams were mentored and accompanied to the competition by Conor Akintola, School of Biotechnology (biology mentor), Ass. Prof. Paul van Kamden, School of Physical Sciences (physics mentor) and Ass. Prof. Odilia Finlayson, School of Chemical Sciences (country co-ordinator and chemistry mentor).

Biological Research Society Committee Member

Media officer, 2017/2018

Volunteering Co-ordinator 2018/2019

The Biological Research Society (BRS) is a social and representative body for academic staff and students within the School of Biotechnology and related institutes in Dublin City University. The BRS is comprised of an elected committee of postgraduate students that entrusted to represent its members year-round.

Abstract

Identification of Novel Cow's Milk Derived Protein Hydrolysates to Support Immune and Skeletal Muscle Function

Conor Akintola B.Sc.

In recent years, the impact of immune function on muscle health has become apparent. The immune system has been identified as a key arbiter of muscle recovery and regeneration following injury or modified muscle use. The regulatory interactions between the immune system and muscle during regeneration are intricate and orchestrated by a plethora of innate and adaptive immune cell phenotypes. Principal among these are Macrophage. Briefly, damage to muscle drives a pro-inflammatory immune response. This response is characterised by the presence and activity of M1 polarised macrophage. M1 macrophage clears the site of injury and drive the proliferation of quiescent muscle progenitor cells. As healing progresses the immune microenvironment shifts, characterised by the increased prevalence of anti-inflammatory M2 macrophage, which promotes myoblast to myotube differentiation and quenches residual inflammation at the site of injury. Through ageing and lifestyle factors, inflammation can persist to become chronic, which detrimentally impacts the regenerative and metabolic functions of muscle tissue. Chronic inflammation in skeletal muscle is thought to increase lipid accumulation in muscle which further exacerbates the inflammatory response, which damages muscle tissue further resulting in a deleterious, degenerative loss of muscle mass and function overtime. Due to the role that macrophage have in regeneration, and the extent at which their dysfunction can impair muscle function, modulating macrophage activity may offer a potential therapeutic avenue to treat chronic muscle disease. Functional foods contain bioactive ingredients, that beneficially impact consumer health. This research highlights the potential application of immunomodulatory cow's milk derived hydrolysates to promote muscle health through modulation of M1 and M2 macrophage phenotypes in vitro . We further identify that cow's milk derived hydrolysates possess myomodulatory activity, able to promote glucoregulatory and anabolic pathways and promote wound healing *in vitro* . Additionally, this research also highlights the impact that modulated immune function has on key aspects of muscle function including glucose metabolism, protein anabolism and wound healing. Novel, food derived immunomodulators may provide an alternative, natural route for the treatment of inflammation induced muscle damage and metabolic implications.

Chapter 1

General Introduction

1.1 Introduction

Our diets play a significant role in modulating the function and efficiency of our bodies. The colloquialisms "you are, what you eat" and "Let food be thy medicine, and medicine be thy food" a phrase allegedly spoken by Hippocrates in 400 BC, have never been more applicable than in the modern age (Witkamp and van Norren, 2018a). Maintaining physical activity and eating healthy are essential for longevity and prosperity as we age. However, worrying trends are emerging in Ireland and on the global stage. As of 2020, the WHO estimates that in a population of 7.8 billion people, an astonishing 1.9 billion of these are overweight, with 650 million people classes as obese (WHO). Alarmingly, according to the Irish Heart Foundation, 1 in 5 primary school children are overweight or obese. This, in combination with decrease in childhood activity rates in Ireland, does not bode well for the long term health of future generations (Woods et al., 2018). With higher rates of obesity, there is an unprecedented prevalence of diet and lifestyle related non-communicable disease such as cardiovascular disease, inflammatory disorders and metabolic syndromes, that put tremendous pressure on national health care systems (Pi-Sunyer, 2010). The WHO estimates that 71% of deaths globally are as a result of chronic disease. Moreover, with the advent of medical and scientific advances, the global average life expectancy has increased from 66.8 to 73.4 years between the year 2000 and 2019 (WHO). In spite of this, although people may be living longer, they may not be living healthier.

Chronic disease, as a result of obesity and ageing is directly linked with an increase in basal inflammation within the body (Lee and Olefsky, 2021). Treatments around targeting chronic inflammation are a current strategy being pursued to combat chronic inflammatory disease. This increase in basal inflammation can detrimentally impair metabolic homeostasis in the body increasing the likelihood of developing metabolic and inflammatory disorders (Ferrucci and Fabbri, 2018). Pharmaceutical strategies to tackle this issue are limited and could in fact exacerbate the issue around modulating immunity in chronic disease. For example, Rheumatoid arthritis (RA) is a condition where joints of an individual become inflamed and as a result the function of the joint becomes diminished overtime (Guo et al., 2018). A key immunological characteristic of RA is the over expression of a pro-inflammatory cytokine Tumour necrosis factor-α (TNFα) (Farrugia and Baron, 2016). Observed as a biomarker and therapeutic target of RA, an anti-TNFα biologic therapy

is often used in combating RA and other inflammatory diseases. However, patients being treated with anti-TNF biologics such as Infliximab, can in the first instance become immunosuppressed as a result of systemic TNFα down regulation, but resistance to Infliximab treatment does occur overtime due to the generation of inhibitory antibodies, leaving limited options to alleviate disease symptoms (Sidiropoulos and Boumpas, 2006).

The term "functional foods" was coined in recent years and describes a set of foods identified to possess the ability to beneficially enhance the health and wellbeing of the consumer (PROESTOS, 2018). Broadly speaking, all foods can be considered functional in some respects. Once digested the macro and micro nutrients absorbed into the body can influence the body's systems, such as modulating immune function, driving cellular proliferation, influencing muscle mass and cardiac function (PROESTOS, 2018). However, Functional foods are foods that contain added specific bioactive ingredients, that when consumed can beneficially impact the consumer in several ways, beyond the effects of basic "wild type" nutrition (Hasler, 2002). Functional foods a have been linked with direct improvements in consumer health in areas such as cardiovascular health, metabolic and chronic inflammatory disease (El Sohaimy, 2012).

Bioactive ingredients, that define functional foods are mined from both plant and animal sources. Plant sources of functional ingredients include specific plant components such as phytochemicals, namely flavonoids, carotenoids, and vitamin complexes (Gylling et al., 2014; Witkamp and van Norren, 2018b) One plant food component that is considered the golden bullet of nutrition is Curcumin, the bioactive component of the commonly available spice Turmeric. Curcumin has been shown to have an arsenal of health boosting properties. In a rat model of RA, Dai et. al demonstrated that Curcumin was able to reduce disease severity through the down regulation of over-active mTOR activity in the synovial microenvironment. Reduction in disease severity was positively associated with a reduction of inflammatory cells and inflammatory cytokines IL-1 and TNFα (Dai et al., 2018).

Whole plant foods are also considered bioactive. For examples these include commonly available food stuffs such oregano and garlic. Coriander has been shown to have functional ability as a food additive by displaying antioxidant, antimicrobial and even anticancer potential (Hasler, 2002). Garlic has also been examined in depth for its potential functional

ability as a food additive. Garlic displays many functional attributes including anti-hypertensive properties and anticancer functionality, particularly in relation to cancer of the GI tract (Koca and Tasci, 2016). A meta-analysis of several clinical trials concerning garlic, found that ingestion of powdered garlic or garlic oil reduced cholesterol by as much as 4%-6% compared to placebo controls (Stevinson, 2000).

Of particular interest, however, are functional foods and functional ingredients derived from animal origins. Marine animals offer a wealth of potential functional foods, most notably omega n-3 fatty acids. Oily fish like mackerel are prime sources of n-3 fatty acids such as EPA and DHA. Many studies have indicated that consumption of marine fish fatty acids may reduce the risk of coronary heart disease, benefit pregnancy and improve cognitive function in subjects with Alzheimer's disease (Hasler, 2002; Swanson et al., 2012).

Functional proteins and functional bioactive peptides (BAPs) are garnering much attention for their potential therapeutic benefits. Isolated from both animal and plant sources alike, bioactive proteins and peptide sequences have exhibited the potential to modulate several aspects of human health including; immune function, cardiovascular function neuronal function and overall cellular function (Hartmann and Meisel, 2007; Hasler, 2002; Li-chan, 2015). Functional ingredients derived from protein can take two forms. They can take the guise of a heterogenous mix of macro- and micro-peptide sequences called a "hydrolysate" or exist as an individual functional peptide sequence called bioactive peptides (BP). Whether a hydrolysate or a BP, the specific peptide sequences encrypted within each are within a parent protein. These sequences have the potential to be released from the parent protein following digestion and are then free to exert health promoting effects (Udenigwe and Aluko, 2012). The natural bioavailability of bioactive peptide sequences from whole foods is dependent on the digestibility of the initial protein source, and other physiochemical conditions that dictate digestion. Consequently, a consistently efficacious bioavailability of a specific peptide or mix of peptides may not be achievable from the native whole food or protein source.

There are two avenues by which bioactive peptides and hydrolysates can be identified. The first stream of identification is referred to as the empirical approach, this method involves the native protein source undergoing proteolytic hydrolysis, using enzymes such as pepsin, trypsin, and chemo-trypsin to model the digestive process *in vitro* or through a bacterial digestion process called fermentation, which fragments the proteins. This produces an array of hydrolysates which are fractionated to recover potentially BPs, which are then screened for bioactive potential *in vitro* and *in vivo*. This is the approach we took in this study. Recently however, a bioinformatic approach has been taken in some instances to identify bioactive hydrolysates. This method sees the *in silico* analysis of protein sequences to predict potentially bioactivity peptide sequences. These sequences are then artificially synthesised, and their activity is assessed (Li-chan, 2015). The Irish start-up Nuritias, has developed and patented an Artificial Intelligence (A.I) algorithm which uses this bioinformatic approach, and have identified several bioactive peptides with commercial and therapeutic potential.

As functional hydrolysates and functional foods are considered natural, and to date their effects appear to beneficially impact a number of body systems there is much interest in employing functional foods to support healthy by alleviating symptoms and inducers of chronic disease such as metabolic syndromes, auto-immune conditions and cardiac disease (Calder and Kew, 2018; Hartmann and Meisel, 2007; Hasler, 2002; Marcone, Simone et al., 2017; PROESTOS, 2018). Unlike common pharmaceutical compounds currently employed to negate the symptoms of NCD, no evidence exists to date that functional foods accumulate in the body's tissues during prolonged usage thus, it is unlikely that there will the negative side effects as can be associated with pharmaceuticals (Hartmann and Meisel, 2007; Kiewiet, Mensiena; Faas, Maria; de Vos, 2018; Udenigwe and Aluko, 2012). This environment and knowledge has led to the growth of a functional foods industry, estimated to be worth $309 billion US dollars by 2027 according to a recent report by Precedence Research. Thus mining protein sources for novel functional bioactives presents a promising commercial opportunity.

1.2 Food for Health Ireland (FHI)

The Immunomodulation Research group at Dublin City University focuses on Identifying novel bio-active compounds that can beneficially modulate the immune system for therapeutic benefit. The research group operate under the Food for Health Ireland (FHI) Technology centre. The FHI centre is a partnership between multinational industry leaders in human nutrition and public research organisations with the singular goal of researching, developing, manufacturing, and marketing novel, bioactive food ingredients isolated from bovine milk that have a proven health benefit. The FHI Technology Centre focuses on researching bioactive milk compounds for applications in areas such as: Technology and Healthy Cheeses, Infant Nutrition, Appetite Modulation, Glycaemic Management, Performance Nutrition and Healthy Ageing.

Specifically, the novel ingredients in question take the form of hydrolysed bioactive peptides isolated from cow's milk protein. FHI partners, isolate the protein fractions of whey and casein from whole cow's milk. These fractions are then subjected to enzymatic hydrolysis, using both *in vivo* and *in vitro* digestive technologies to fragment whole parent, whey and casein proteins. Digestive, proteolytic enzymes such as trypsin and chymotrypsin are often used in the digestive processes (figure 1.1). These enzymes cleave at specific protein sequence sites. However, due to the complexity of parent protein sources, it is likely that there are multiple cleavage sites for specific enzymes. The subsequent fractions generated by this hydrolysis contain a heterogenous mixture of several peptide of varying length, each potentially with its own unique bioactivity (Marcone, Simone et al., 2017). Parallel studies under the FHI initiative are currently working to identify the specific sequences of the bioactive peptides using a combination of bioinformatic and mass spectrometry analysis to identify the valuable bioactive sequences.

1.2.1 Cow's Milk Derived Bioactive Hydrolysates Peptides:

Cow's milk protein is dominated by two major families of protein, whey, and casein. Whey accounts for approximately 20% of total protein and casein, approximately 80% of total protein in cow's milk. Over the past decades, there has been a considerable number of bioactive peptide sequences isolated from both whey and casein proteins alike (Marcone, Simone et al., 2017). The therapeutic and modulatory effects of whey and casein hydrolysates range from antihypertensive to anti-oxidant, insulinotrophic effects to immunomodulatory properties (Marcone, Simone et al., 2017; Reyes-Diaz et al., 2018).

1.2.1.1 Whey Protein Derived Bioactive Hydrolysates and Peptides

Whey protein as mentioned comprises 20% of the protein content of cow's milk. Whole whey protein is comprised of a heterogenous mix of growth factors, functional enzymes and protein complexes. Whey protein is often considered for use in supporting athletic performance. This is due in part to the solubility of whey in acid and the need to have rapid nutrient absorption following exercise to support recovery (Phillips, 2011).

Whole whey protein alone has health boosting properties such as promoting insulin sensitivity and metabolic function (Adams and Broughton, 2016). When hydrolysed however, whey produces a plethora of bioactive hydrolysates and bioactive peptides. Several whey hydrolysates have been shown to promote glucose metabolism through promotion of the glucose metabolic pathway in skeletal muscle and adipose tissue (D'Souza et al., 2020; Morato et al., 2013). Furthermore, several whey derived peptides and hydrolysates have been shown to have ACE inhibitory bioactivity, improving measures of cardiovascular health (Silva et al., 2014). A commercially available hydrolysed whey ingredient BioZate, produced by Agropur, has proven to positively regulate hypertension (Dullius et al., 2018).

1.2.1.2 Casein

Casein makes up the remaining 80% of cow's milk protein content made up by four subunits α_{s1}-, α_{s2}-, β-, and κ-casein (Marcone, Simone et al., 2017). Casein, in direct contrast to whey protein, is not acid soluble and coagulates once ingested. As a result, this reduces the digestibility of casein, resulting in a slower release of protein and amino acids (Wang et al., 2018). Due to the low digestibility of native caseins in cow's milk, casein protein presents a unique opportunity to mine novel health boosting bioactive hydrolysates and peptides for commercialisation.

Casein hydrolysates have shown considerable immunomodulatory potential. Mukhopadhya et al. demonstrated that a casein hydrolysate can reduce inflammation in colonic tissue, through down regulation of IL-1α/β, IL-8, TNFα and IFN$\boldsymbol{\gamma}$ (Mukhopadhya et al., 2014). Lalor et. al showed that a k-casein fragment can promote an anti-inflammatory M2 phenotype in macrophage, whilst also inhibiting T cell proliferation (Lalor and O'Neill, 2019a). The activities of casein derived hydrolysates and peptides extend to tissue healing and maintenance. Casein hydrolysates were also shown to promote intestinal wound healing in a CACO2 *in vitro* injury model (Nielsen et al., 2019). Moreover, ingestion of casein hydrolysates promoted anabolic signalling in a human exercise trial (Cogan et al., 2018). The previously mentioned bioactivities do provide evidence that cow's milk protein is a well of bioactive hydrolysates and peptides. Further investigation into the potential bioactivities of milk derived protein functional foods is required to identify applications for health promoting and commercial opportunity.

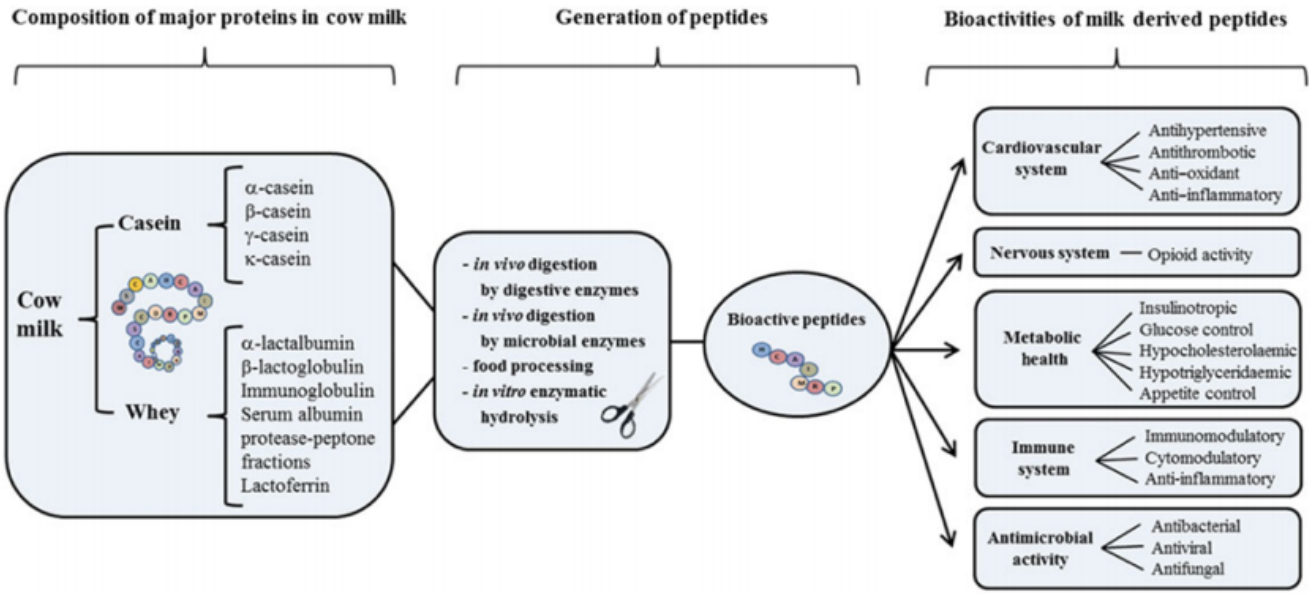


Figure 1.1 *Workflow for the generation and isolation of bioactive peptides from whole, intact whey and casein and their known functions* (Marcone, Simone et al., 2017). Whole whey and caseins may be enzymatically digested *in vitro* or *in vivo*. Subsequent peptides produced from this hydrolysis may be fractioned and screened for bioactivity in modulating aspects of human and animal health.

1.3 The Immune System:

The immune system is a complex system of cellular and biochemical interactions that enables multicellular life to defend itself from pathological infection. The immune system can be broadly separated into two categories: innate immunity and adaptive immunity. Innate immunity consists of several barriers: including physical and cellular, to infection. The adaptive immunity consists of both cellular and antibody-based responses, and unlike innate immunity, can specifically target a single pathogen and develop a "memory" for specific target to mount a rapid response should the antigen be encountered again. There are two classically known immune responses, the Type-1 and a Type-2 response. The Type-1 response is a pro-inflammatory response, characterised by the presence of inflammatory cytokines such as IFNγ and TNFα. This response is activated in response to pathogen invasion and damage. It is essential for the immune system to clear an infection (Chaplin, 2010). The Type-2 response in contrast, is anti-inflammatory. The Type-2 phenotype is characterised by high levels of anti-inflammatory cytokines such as IL-10, IL-4 and IL-13 and has a key role in immunoregulation (Kaiko et al., 2008).

1.3.1 Overview of the Innate Immune System

Innate immunity is the first line of defence protecting the host from infection and regulating the immune response to tissue damage. The innate immune system consists, initially of physical barriers to infection such as the skin, mucosal and epithelial layers. If these physical barriers are breached through damage, or through internal tissue damage, the cellular immune response is the first responder to tissue damage and pathogen infection. The innate immune cell response is characterised by the presence of myeloid derived cell populations such as neutrophil, macrophage and dendritic cells that have essential functions in promoting an effective inflammatory response, phagocytosis, and antigen presentation to the adaptive immune system. Each of these cell types possess unique set intercellular and cell surface receptors that mediate activation and deactivation of inflammation. Integral to the activation of the innate immune response is a group of pattern recognition receptors (PRRs) called toll-like receptors (TLRs) (Lester and Li, 2014). There are nine recognised TLRs that mediate distinct activation profiles of neutrophils,

macrophage, and dendritic cells alike (figure 1.2). TLR3/7/9 for example are found in the intercellular compartment and recognise DNA and RNA ligands related to viral infection. In contrast, TLR2/4 recognise bacterial pathogens. Each TLR receptor activates a cascade of inflammatory signalling that leads to distinct secretome profiles and cell surface marker expression (Collins, 2014). TLRs have also been identified as receptors for damage associated molecular patterns (DAMPs) which are released during both sterile and non-sterile tissue injury (Gong et al., 2020). TLR2 and TLR4 have been identified as key receptors for a plethora of DAMPs and have been even identified as playing pivotal roles in the progression of auto-immune disease and chronic inflammatory disease (Roh and Sohn, 2018)

1.3.2 Macrophage

Macrophage are a key cell type involved in the cellular innate immune response. They are responsible for phagocytic clearance of necrotic cells, cellular debris, bacteria and virally infected and function as antigen presenting cells. Macrophage are derived from hematopoietic stem cells in the bone where they are released and, in the body, exist in broadly two states; circulating monocyte-derived macrophage and mature tissue resident macrophage that exist in a quiescent state ready to mount a response to any given stimuli be that infection or tissue damage. Circulating monocytes replenish resident macrophage populations, where upon maturation adopt location specific characteristics and becoming distinct subpopulations of macrophage; such as osteoclasts in the bone marrow and Kupffer cells in the liver (Gordon and Taylor, 2005). Macrophage are a highly plastic and diverse lineage of cells (Martinez and Gordon, 2014). In 1986, pioneering work identified that *in vivo*, the immune system operates under the Th1 and Th2 specific phenotypes previously mentioned (Mosmann et al., 1986). In 2000, Mills et. al provided the first evidence that like T cells, macrophage can be polarised to effect either Th1 or Th2 functions (Mills et al., 2000). Macrophages operate under two distinct phenotypes. The first, is referred to as the “classically activated” inflammatory M1 macrophage. The second phenotype is the “alternatively activated” anti-inflammatory M1, M2 macrophage. Figure 1.3 illustrates modes of macrophage function.

1.3.2.1 M1 macrophage

The M1 phenotype is characterised by markers and behaviours consistent with a type 1 or Th1 immune response. Termed M1 to reflect this, M1 macrophage are highly inflammatory cell types. They have pivotal roles in the bodies first response to infection and tissue damage. M1 macrophage are activated *in vivo* and in vitro by toll like receptor (TLR) ligands such as lipopolysaccharide (LPS), which binds via *TLR4*. IFNs, a T cell derived cytokine family, which in the context of macrophage activation is responsible for driving M1 specific gene expression via JAK1/2 STAT1/2 signalling pathway. In combination with a TLR4 ligand such as LPS, that drives MyD88 mediated NF-κB activation an M1 phenotype is generated (Murray et al., 2014). The importance of IFN in a polarising cocktail is important as LPS vs. LPS/IFN activated macrophage exhibit differential inflammatory gene activation profiles. DAMPs, which are released in response to injury are also responsible for driving the M1 phenotype via TLR4 binding, and in combination with IFN secreted from CD8+ T cells in response to infection or tissue damage, drives the polarisation of the local and infiltrating macrophage population to an M1 inflammatory phenotype. *In vitro* , an M1 like macrophage phenotype can be driven using a combination of LPS and the pro-inflammatory cytokine IFNγ (Krzyszczyk et al., 2018; Martinez and Gordon, 2014). Reports also suggest that TNF can mediated M1 activation via TNFR1 and TNFR2 signalling pathways (Wajant and Siegmund, 2019). M1 macrophage secrete pro-inflammatory mediators such as IL-1, IL-6, IL-10, IL-12p40 and TNF with concomitant activation of iNOS producing reactive oxygen species. Moreover, co-stimulatory cell surface receptors including CD86 and MHCII are considerably upregulated and phagocytic activity is also enhanced (Orecchioni et al., 2019).

1.3.2.2 M2 Macrophage

M2 macrophage or "alternatively activated" macrophage, in contrast to the M1 phenotype, are an anti-inflammatory subset of macrophage that have key functions in allergy, parasite killing and importantly immunoregulation. Broadly speaking, M2 macrophage are typically activated by Th2 derived cytokines such as IL-4, IL-13 and TGFβ (Wang et al., 2014). However, in recent years the term M2 has become an overarching designation for a family of distinct macrophage subsets. There are currently three broadly recognised subsets of M2 macrophage. M2a macrophage, are considered the typical example of the M2 macrophage. M2a macrophage are activated in response to Th2 cytokines IL-4 and IL-13, which signal through the Jak1/3/STAT6 signalling pathways. M2a macrophage have a key role in promoting a Th2 immune response. M2a macrophage secrete low levels of the M1 associated cytokines and high levels of IL-10. M2a macrophage also have high levels of Arginase 1 enzyme activity (Orecchioni et al., 2019).

M2b macrophage express a different but slightly overlapping gene expression profile than M2a macrophage. For examples M2b macrophage secrete higher levels of IL-10 buts also secrete the M1 associated TNFα, IL-1, IL-6 and exhibit some phagocytic activity. M2b macrophage are activated in response to immune complexes, TLR ligands an IL-1R agonists (Murray et al., 2014). M2b macrophage have been implicated in the promotion of tumour growth and parasitic infection through downregulation of inflammatory pathways but have also been shown to be functional in reducing tissue damage in areas such as the spinal cord (Wang et al., 2019).

The third M2 subtype is the M2c macrophage, dubbed the immunoregulatory macrophage. M2c macrophage differentiation achieved through IL-10 signalling via the JAK1/3/STAT3 signalling pathway. Once activated M2c macrophage secrete high levels of the Th2 immunoregulatory cytokines IL-10 and TGFβ. M2c activity down regulates inflammatory activity to reduce local tissue damage because of inflammatory immune cells phenotypes (Martinez and Gordon, 2014). Moreover, M2c macrophage are pro-fibrotic and have critical roles in promoting wound healing and tissue remodelling. M2c macrophage also exhibit a degree of phagocytic activity, key in resolving wound injury (Wang et al., 2019).

1.3.3 Cytokines

Cytokines are key signalling molecules that propagate and regulate immune system activity. Cytokines are secreted by numerous typically non-immune cell types such as muscle and adipose tissue, that function similarly in the recruitment and orchestration of the immune response in each micro- or systemic environment (Altan-Bonnet and Mukherjee, 2019; Arango Duque and Descoteaux, 2014). Cytokines can be grouped broadly into two categories: pro- and anti-inflammatory. Pro-inflammatory cytokines are responsible for propagating the immune response to infection and tissue damage. Anti-inflammatory cytokines in contrast, regulate and deactivate inflammation, which is a critical step in maintaining tissue and whole-body homeostasis and long-term health (Dinarello, 2007). Due to the critical role of these cytokines in the immune response, and the detriment to which dysregulation of inflammatory pathways can have in states of chronic inflammatory disease, cytokines and their receptors have been identified as potential therapeutic targets and for use as therapies themselves in inflammatory disease (Lai and Dong, 2016). In the context of macrophage phenotypes there are four cytokines that have been extensively characterised: IL-1β, IL-6, IL-10 and TNFα.

1.3.3.1 IL-1β

IL-1β is a Th1 pro-inflammatory cytokine produced by myeloid derived immune cells such as macrophage and dendritic cells. IL-1β, secreted in response to TLR ligation, has an array of effects inducing inflammatory cytokine secretion in immune cells, and in other tissues. IL-1 is found in two forms, inactive and active. Cleavage of pro-IL-1β by caspase-1 releases the active IL-1β, where it is free to drive lymphocyte proliferation (Vijayaraj et al., 2021). Overabundance of IL-1β has been implicated in the progression of many chronic inflammatory diseases. For example, IL-1β in the gut drives secretion of IL-8 from gut endothelial cells which is associated with gut inflammation and inflammatory bowel disease (Daig, 2000). It has also been implicated in the onset of T2DM by impacting β-cell function (Zhao et al., 2014).

1.3.3.2 IL-6

IL-6 is a pleotropic cytokine that modulates inflammation. IL-6 is produced by a range of cell types, from macrophage, T cells, to endothelial cells. Secreted through TLR ligation and even skeletal muscle contraction, IL-6 possess a wide range of functions (Rogeri et al., 2020). In the context of inflammation, it has key roles driving the immune response to an array of infections. Recently, IL-6 was identified as a mediator of severe disease occurrence in patients diagnosed with COVID19 (Sabaka et al., 2021). Similarly to IL-1β, IL-6 has been implicated in the occurrence of chronic inflammatory disease such as rheumatoid arthritis (RA) (Hirano, 2021). IL-6 also possess some anti-inflammatory properties, that are time dependant. IL-6 has been shown to drive the development of the anti-inflammatory Th2 T cell subset through induction of IL-4 secretion and blocking IFNγ secretion (Scheller et al., 2011). Moreover, IL-6 secreted from muscle tissue is known to facilitate nutrient uptake and utilisation (Marko et al., 2020)

1.3.3.3 IL-10

IL-10 is a potent immunoregulatory cytokine. Produced by dendritic cells, macrophage and an array of T cell subsets, notably Tregs, IL-10 is critical for regulating inflammation progression in the body. IL-10 down regulates Th1 response by reducing inflammatory cytokine secretion. Moreover IL-10 has also been shown to block proliferation of Th1 cells and interfere with chemotactic pathways critical for the progression of inflammation (Iyer and Cheng, 2012). The importance of IL-10 in regulating inflammation was demonstrated by Zhang et. al. Researchers demonstrated that IL-$10^{(-/-)}$ knockout mice suffered spontaneous gut inflammation in the absence of pathogenic agents (Zhang et al., 2014). IL-10 is a key stimulator of M2c immunoregulatory and Treg subsets that regulate and dampen inflammation to maintain homeostasis (Martinez and Gordon, 2014; Zhang et al., 2014).

1.3.3.4 TNFα

TNFα is perhaps one of the most well-known inflammatory cytokines. TNFα secretion is promoted via TLR ligation and subsequent NF-κB activity in an array of immune cell types including macrophage, dendritic cells and various T cell subsets. Secreted TNFα signals immune and non-immune cell types through the cell surface receptors TNFR1 and TNFR2. Binding of TNFα to these receptors drives NF-κB mediated pro-inflammatory cytokine secretion including more TNFα, which drives autocrine propagation of inflammation. Chronic, elevated TNFα levels have been implicated in the progression of chronic inflammatory diseases including diabetes, inflammatory bowel disease and RA (Blandizzi et al., 2014). In fact, the role of TNFα in inflammatory disease has been so well characterised that it has become a prime therapeutic target for next generation biologic therapies (Papamichael et al., 2019).

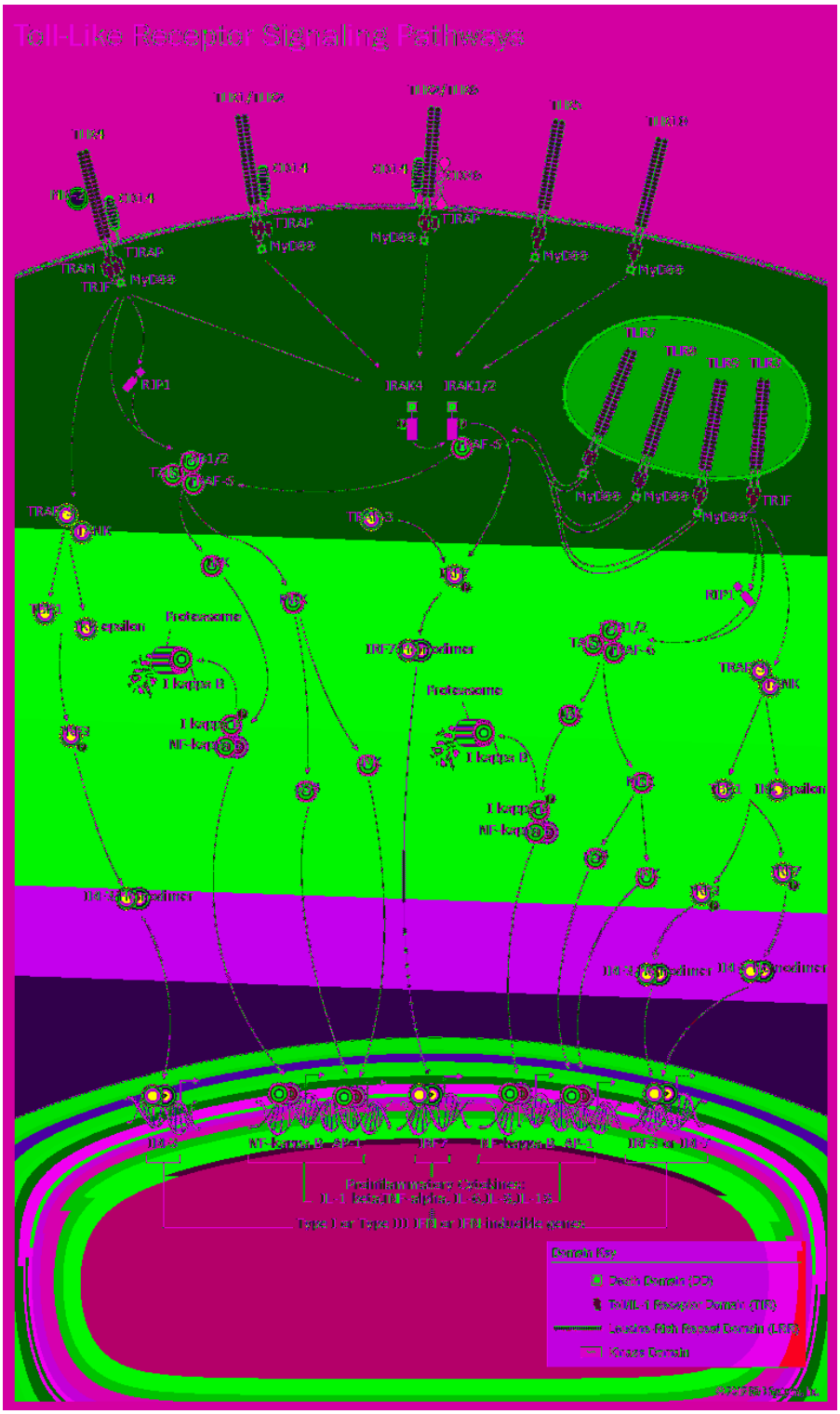


Figure 1.2 Overview of Toll-like signalling pathways in innate immunity (R&D Systems). Toll-like receptors (TLRs) are innate immune sensors, that recognise an array of extra- and inter-cellular antigenic signals. TLR activation drives inflammatory immune signalling and inflammasome activation culminating in the production of pro-inflammatory cytokines and the expression of co-stimulatory molecules on innate immune cell surfaces.

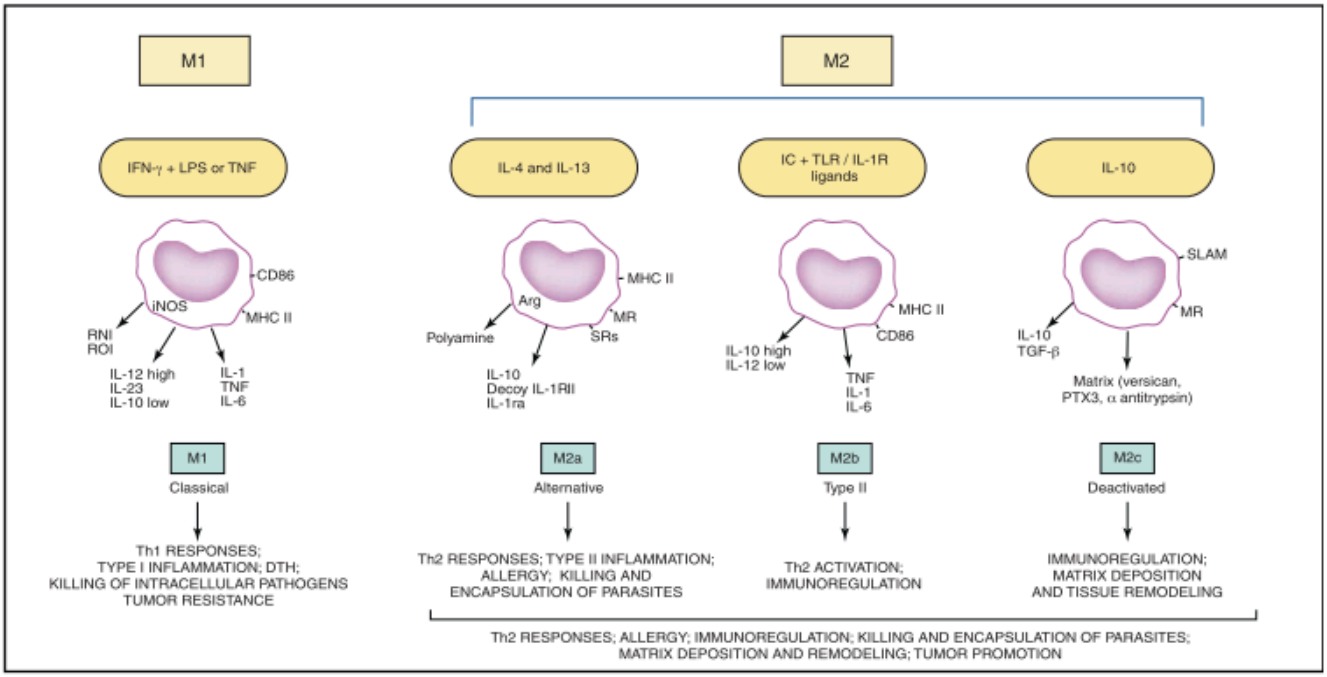


Figure 1.3 Overview of principal macrophage phenotypes, their modes of activation and their key function *in vivo* (Martinez and Gordon, 2014). Macrophage exhibit a wide degree of plasticity with regard to their phenotype. M1 macrophage are pro-inflammatory and are often activated through LPS and IFNγ/TNFα activation. The M2 phenotype consists of a wide range of anti-inflammatory sub-M2 phenotypes. *In vitro* , the M2a macrophage is often used to represent the M2 phenotype, activated through IL-4 and/or IL-13 stimulation.

1.4 Skeletal Muscle:

Skeletal muscle (SM) accounts for approximately 40% of total body mass in mammals (Egan and Zierath, 2013a). SM allows mammals to socially interact and survive by enabling locomotion, postural behaviour, communication and breathing. It is a fibrous, dense tissue comprised of several different fibre types (Egan and Zierath, 2013a; Frontera and Ochala, 2015). The whole muscle is contained in a connective tissue layer called the epimysium, where bundles of contractile fibres called myofibrils are contained within layers known as the perimysium. Both arteries and veins weave through the musculature to provide oxygen and nutrients and to remove waste. Nerve endings are also located in the fibre bundles to allow for appropriate communication between the neuronal system and the muscle (Frontera and Ochala, 2015).

Muscle fibre types can be generally classified into two categories as slow-twitch (type 1) and fast-twitch (type 2) muscle fibres. The two fibre classifications are defined by their contractile properties. However, there are physiological differences to support their contrasting properties. For example, type 1 fibres in humans are known to have a smaller cross-sectional area and a higher density of mitochondria. They also express differing myosin heavy-chain (MHC) isoforms. Type 1 muscle fibres express MHC1 and Type 2 express MHC2A. Type 1 muscle fibres are also less prone to fatigue compared to type 2 fibres (Egan and Zierath, 2013a).

In addition to its key function in locomotion and social interaction, skeletal muscle has been identified as a primary metabolic site in the human body. The primary metabolic functions including are energy production, glycaemic control and maintaining muscle mass and as a result, stabilising whole body metabolic homeostasis (Egan and Zierath, 2013a; Frontera and Ochala, 2015; Richter and Hargreaves, 2013).

1.4.1 Glucoregulatory Functions of Skeletal Muscle

It is estimated that when at rest, SM accounts for approximately 30% of overall energy expenditure. This increases significantly when moving or performing exercise. Unsurprisingly, skeletal muscle is equipped with energy stores such as glycogen, amino acids and creatine and is also very sensitive to insulin which induces glucose uptake and utilization in the muscle. Glucose that is unused during exercise is stored as glycogen within the muscle. This glycogen can be readily catalysed in a hypoglycaemic environment to provide energy (Egan and Zierath, 2013a).

Glucose uptake in skeletal muscle is facilitated by a family of transmembrane glucose transporters called GLUT transporters. A key protein in the glucose metabolic pathway of skeletal muscle is the insulin-regulated glucose transporter GLUT4. During exercise and the absorption of nutrients, the transport of glucose across the cell membrane is essential to regulating blood glucose levels, and replenishing glycogen stores. In adipose and muscle tissue, GLUT4 is the primary glucose transporter. In a basal state, GLUT4 is absent from the plasma membrane however, following stimulation with proteinaceous factors like Insulin or extrinsic factors such as exercise, GLUT4 is recruited to the membrane to facilitate glucose transport (Bryant et al., 2002). GLUT4 translocation to the plasma membrane can be initiated through insulin via the PI3K signalling pathway and by muscle contraction, likely mediated via AMPK signalling (figure.1.4) (Huang and Czech, 2007)

Several studies have implicated dysfunction in GLUT4 translocation in Type 2 Diabetes Mellitus. Dysfunction in GLUT4 translocation is a direct consequence of insulin resistance (Samuel and Shulman, 2012). Insulin resistance (IR) is defined as a diminished capacity of tissues to respond to insulin stimulation (Samuel and Shulman, 2012). In skeletal muscle, this leads to a reduction in glucose uptake by muscle cells and culminates in a hyperglycaemia and the consequences of sustained high levels of serum glucose (Defronzo, 2009). There are several factors that can contribute to IR, these include; ectopic fat accumulation in muscle tissue and chronic inflammation (Samuel and Shulman, 2012; Shoelson et al., 2006). High levels of circulating inflammatory cytokines such as TNFα, have

been linked to the incidence of insulin resistance (Navarro and Mora, 2006; Pillon et al., 2012).

It has been documented that diets high in refined sugar and fat are deleterious to whole-body glucose homeostasis. Chronic low grade inflammation is also thought to contribute to insulin resistance in skeletal muscle (Navarro and Mora, 2006). However, there are certain foods which have been shown to enhance the response of muscle cells to insulin. For example, whey protein has been shown to increase the whole body responsiveness to insulin in obese, healthy and insulin resistant subjects (Sousa et al., 2012). Casein protein however has not been studied in terms of its effects on glucose metabolism. Although whey protein is more potent at promoting insulin sensitivity, there is a case to be made for casein. Several studies concerning casein isolated peptides have demonstrated that they are capable of inducing insulin sensitivity (Matsunaga et al., 2017; Song et al., 2017).

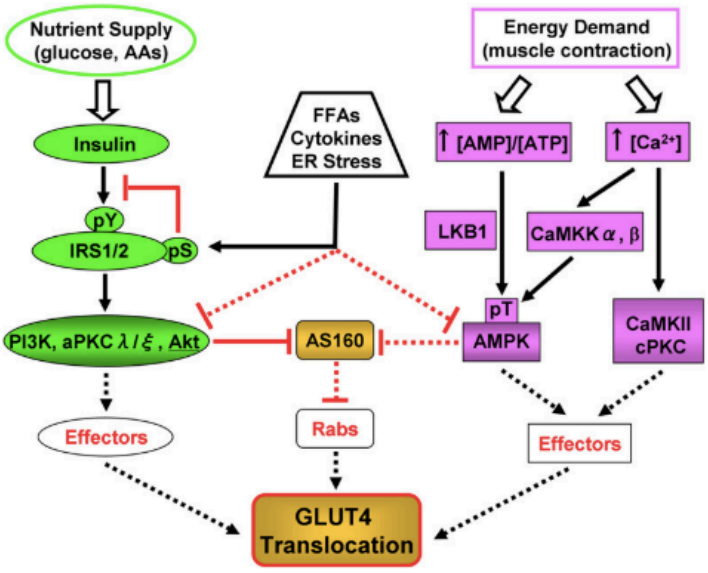


Figure 1.4 Schematic representation of the signalling cascade that induces GLUT4 translocation in skeletal muscle (Huang and Czech, 2007). Ingestion of nutrients drives secretion of insulin which induces GLUT4 translocation via IRS1 signalling in a plethora of cell types. Muscle contraction, and subsequent energy demand also drives GLUT4 translocation which is linked to AMPK and PKC signalling pathways.

1.4.2 Muscle Maintenance – Anabolic Efficiency:

Skeletal muscle is sensitive to many endogenous and exogenous signals that influence its function. Muscle can undergo states of atrophy (loss of muscle mass) and hypertrophy (gain in muscle mass). The trophic state of muscle is critical for overall health. Muscle atrophy is linked to disease, frailty and increased mortality. The mammalian target of rapamycin (mTOR) signalling pathway is the principal regulator of muscle hypertrophy, the pathway is outlined in figure 1.5 (Yoon, 2017).

Following anabolic stimulus, such as nutrient ingestion and exercise, the mTOR pathway and its downstream effectors are activated to regulate various aspects of the MPS process such as ribosome biogenesis and translation initiation (Yoon, 2017). Exercise is known to induce mTOR signalling in healthy muscle tissue, however this response does become stunted in elderly individuals following exercise (Breen and Phillips, 2011; Deldicque et al., 2005). There are two functional mTOR complexes within the cell, mTORC1 and mTORC2 (fig 1.5). mTORC2 is responsible for regulating cell survival and cytoskeletal arrangements, whereas mTORC1, the main complex that regulates skeletal muscle mass and its activation is sensitive to augmentation by amino acids, growth factors and cytokines (Showkat et al., 2014; Yoon, 2017). Downstream of mTORC1, there is what is considered a key marker of mTOR activation, 4-EBP1 (Qin et al., 2016). 4-EBP1 is a member of a group of small proteins that are inhibitors of translation (Qin et al., 2016). 4-EBP1 inhibits translation via interaction with the translation initiator eIF4E (Musa et al., 2016). In an inactive state, 4-EBP1 is unphosphorylated and bound directly to eIF4E, however upon phosphorylation at specific sites, 4-EBP1 dissociates from eIF4E which allows for translation initiation (Musa et al., 2016; Qin et al., 2016). Thus, by directly measuring the levels of phosphorylated 4-EBP1, it can be directly correlated to levels of mTOR signalling and thus MPS (Haran et al., 2012; Qin et al., 2016; Saini et al., 2016).

Anabolic resistance (AR) is defined as the diminished capacity of tissues and cells to upregulate anabolic protein processes in response to anabolic stimuli (Haran et al., 2012). In skeletal muscle, this impaired response to anabolic stimuli skews the balance of muscle protein synthesis to muscle protein degradation, inducing a loss of muscle mass over time. This is defined as muscle atrophy (Haran et al., 2012). Anabolic stimuli include intrinsic factors such as hormones, amino acids and cytokines, that are known to increase the rate of protein synthesis in young, healthy skeletal muscle (Haran et al., 2012). Extrinsic factors such as exercise and nutrition have major effects on protein metabolism (Cartee et al., 2016). Combinations of exercise and protein supplementation, in several human studies, has been shown to increase muscle mass and the rate of MPS in the elderly and young subjects (Atherton et al., 2017; Rasmussen et al., 2018).

AR is a key pathology in a metabolic syndrome known as sarcopenia (Dardevet et al., 2012; Haran et al., 2012). Sarcopenia is characterised by the age related loss of muscle mass over time, with a primary loss of type 2 muscle fibres (Kalyani et al., 2014). As well as displaying resistance to anabolic stimuli, sarcopenic individuals often display a resistance to insulin, T2DM and obesity. However, a causal link between these characteristics and sarcopenia has yet to be established (Kalinkovich and Livshits, 2017). Sarcopenia is a deleterious condition that can result in a significant reduction in quality of life with regards to mobility and overall health (Breen and Phillips, 2011; Dardevet et al., 2012; Haran et al., 2012). With the global population of individuals over 60 projected to be over 2 billion in the next 30 years, the rate of sarcopenia is potentially set to rise (Breen and Phillips, 2011) and has the potential to strain the already under pressure national health services.

There are several potential mechanisms in which AR in relation to sarcopenia may be induced. Initially, protein malnutrition is known to be a key element. Protein malnutrition, reduces the amount of bioavailable amino acids necessary for protein synthesis (Breen and Phillips, 2011; Haran et al., 2012). Ageing muscle can also reduce the sensitivity of muscle to amino acid stimulus, as ageing is known to increase the anabolic threshold of skeletal muscle (Dardevet et al., 2012; Haran et al., 2012). Inactivity has also been demonstrated to induce AR, even in young adults (Breen and Phillips, 2011; Cartee et al., 2016).

It is also believed that inflammation may directly impact the anabolic sensitivity of skeletal muscle. Studies in both rodents and human subjects have indicated that there is a negative correlation between the rate of MPS and the concentration of circulating inflammatory markers (Breen and Phillips, 2011; Toth, 2004). As we age, the human body becomes an increasingly inflammatory environment, with documented increases in circulating inflammatory cytokines in people over 60. This is a phenomenon known as “inflammaging” (Álvarez-Rodríguez et al., 2012; Haran et al., 2012). Chronic inflammation is known to have deleterious effects on muscle mass (Breen and Phillips, 2011; Chazaud, 2016; Tidball and Villalta, 2010). Chronic inflammation in skeletal muscle is thought to increase lipid accumulation in skeletal muscle which further exacerbates the inflammatory response, which damages muscle tissue further resulting in a deleterious, degenerative loss of muscle mass and function over time (Haran et al., 2012; Tidball and Villalta, 2010). It is postulated that reducing inflammation using anti-inflammatory substrates could offer a potential avenue to further treat AR and Sarcopenia in the elderly (Breen and Phillips, 2011).

In the elderly, mTOR signalling has been found to be reduced, thus allowing for AR and muscle atrophy to take hold (Haran et al., 2012). Specifically, 4-EBP1 phosphorylation and 70S6K, a second marker of mTOR activation, was found to be blunted in elderly muscle compared to young muscle (Breen and Phillips, 2011; Kumar et al., 2009). Supplementation with protein combined with exercise has proven effective in overcoming and enhancing mTOR signalling (Breen and Phillips, 2011; Haran et al., 2012), and we postulate that supplementation with a bioactive casein hydrolysate may offer a therapeutic strategy to combat sarcopenia.

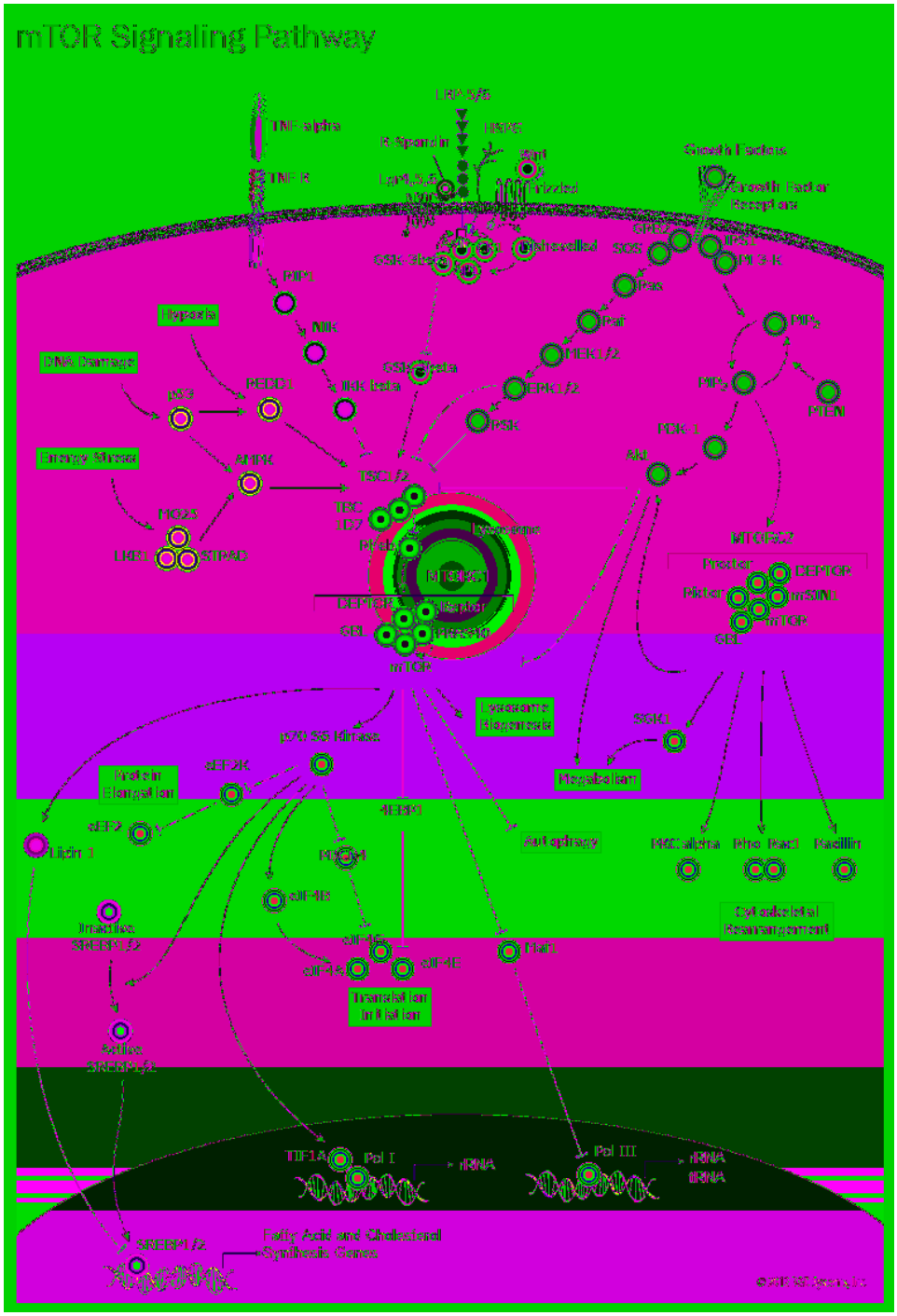


Figure 1.5 Overview of the mammalian Target of Rapamycin (mTOR) signalling pathway (R&D Systems). mTOR is the key regulator of muscle protein synthesis. Principally, the mTORC1 complex is responsible for regulating translation initiation, protein elongation, lysosome biogenesis and autophagy. The mTORC2 complex regulates cytoskeletal rearrangement. Both mTORC1 and mTORC2 activation is mediated by nutrients, growth factor and cytokine signalling.

1.4.3 Muscle Repair and Regeneration – Myogenesis:

Skeletal muscle is considered to be a stable tissue which has a very low turnover rate of nuclei relative to other tissues (Yin et al., 2013). This stability however does become unsettled following intense exercise, injury, and modified muscle usage. SM displays incredible regenerative potential with correct healing resulting in maintenance or increase of muscle mass, restoration of contractile potential and full revascularisation of the muscle (Yin et al., 2013). Myogenesis is the process by which adult muscle forms new muscle fibres and heals itself. Broadly speaking there are three stages in the process of myogenesis. The initial stage of muscle regeneration is known as the "proliferative stage". Here, quiescent adult stem cells resident in the musculature, called satellite cells, are activated and begin to proliferate, expressing myogenic markers such as MyoD. When satellite cell numbers have bolstered, the cells begin the process of differentiating into myoblasts, precursors to mature myotubes. These cells express the markers Myogenin, MEF2 and Myf4. These markers, together with the already active Myf5 and MyoD induce expression of muscle specific genes to initiate the final stage of myogenesis called "terminal differentiation". During terminal differentiation myoblasts fuse together to form a multinucleated myotube which integrates into the existing muscle infrastructure to form a complete myofiber. Myogenesis is an intricate and temporal process in which there is a stepwise activation of and deactivation of specific genes and enzymes. Krook et. al demonstrated in human muscle cells, the differential expression of Myogenin, Myf5, Desmin and MyoD throughout a ten-day differentiation of human myoblasts to myotubes (Krook et al., 2014).. The complexity of myogenesis and regeneration is confounded when the role that the immune system plays in the process of muscle recovery is considered.

1.4.4 The immune system co-ordinates skeletal muscle repair

The regulatory interactions between the immune system and skeletal muscle during repair and regeneration are highly intricate and occur in a step wise temporal manner. The interaction and process is illustrated in figure 1.6. Initially, approximately 1 to 2 hours post injury, there is a rapid invasion of inflammatory neutrophils from circulation into the damaged area of muscle. The neutrophils secrete high levels of IFNγ and TNFα, whose function is two-fold in this scenario. Firstly, they condition the site of injury to support a pro-inflammatory response and drive a M1 phenotype in resident Macrophage in the muscle and drive infiltrating monocytes to differentiate into the M1 macrophage subtype. Secondly, IFNγ and TNFα both act directly upon the satellite cells located in the muscle (James G. Tidball, 2017). TNFα and IFNγ induces the proliferation of these cells in order to bolster numbers sufficiently to support correct recovery of skeletal muscle (Tidball et al., 2015). In the early stages of muscle recovery, the M1 induced macrophage together with $CD8^+$ T-lymphocytes recruit more inflammatory monocytes via CCL2 signalling to the site of injury and secrete high levels of nitric oxide (NO) to lyse damaged and necrotic muscle fibres. The M1 macrophage phagocytose the cellular debris to clear the site of injury and allow space for new muscle fibres to take their place in whole tissue (Rigamonti et al., 2014).

As necrotic muscle tissue is removed, and satellite cells are differentiating there is a phenotypic and environmental shift from a pro-inflammatory to an anti-inflammatory phenotype. Phagocytosis induces the M1 to M2 shift in the macrophage and they begin to secrete Th2 cytokines such as IL-10 and TGFβ. These cytokines are profibrotic and promote the differentiation and maturation of myoblasts to myotubes to myofibers. Eosinophils act on resident fibradipogenic (FAP) cells and drive their differentiation into fibroblasts, which are responsible for the deposition of the connective extracellular matrix. At this point a population of muscle specific T regulatory (Treg) cells expressing FoxP3, CD4, CD25 and IL-33r are drawn to the site of injury via an IL-33 secreted by FAP cells and secrete anti-inflammatory cytokines that promote a Th2 micro-environment. It is also worth noting that, Dendritic Cells (DCs) are also present in injured muscle during the regeneration, perhaps as sentinel guards against infection (Burzyn et al., 2013; Wirsdörfer et al., 2016).

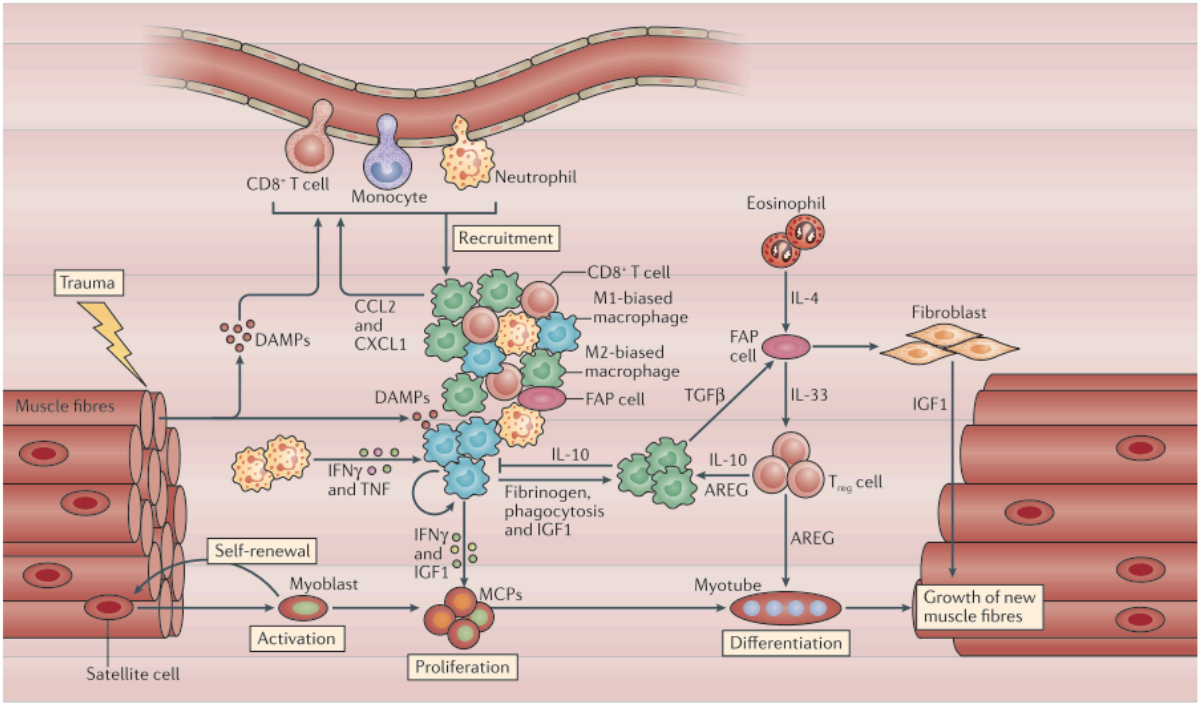


Figure 1.6 *Schematic representation of the cellular and humoral interactions between muscle and the immune system during regenerations* (James G. Tidball, 2017). Damage to skeletal muscle drives a pro-inflammatory immune response. This response is characterised by the presence and activity of M1 polarised macrophage. M1 macrophage clears the site of injury and drive the proliferation of quiescent muscle progenitor cells. As healing progresses the immune microenvironment shifts, characterised by the increased prevalence of anti-inflammatory M2 macrophage, which promotes myoblast to myotube differentiation and quenches residual inflammation at the site of injury.

1.4.5 A dysfunctional immune response impairs skeletal muscle recovery

As presented above, immune system interactions with skeletal muscle are highly intricate and time dependant, and unfortunately do not function correctly as often as desired. In many scenarios, the resolution of muscle related inflammation is impaired (James G. Tidball, 2017). This can be influenced by age, lifestyle, and nutrition. The effects of inflammatory cytokines such as TNFα and IFNγ have been shown to impair muscle regeneration by interfering with the proliferation and differentiation of muscle resident stem cells called satellite cells (Costamagna et al., 2015; James G. Tidball, 2017). Saclier et. al also demonstrated that M1 macrophage both directly and indirectly inhibit myoblast to myotube fusion, which is a critical event in muscle healing (Saclier et al., 2013). Furthermore, incorrect resolution and prolonged inflammation during muscle recovery can drive a pro-fibrotic transitional macrophage phenotype. These transitional macrophage phenotypes, exhibit an intermediate phenotype between both M1 and M2 subtypes. A critical distinction however is the fact that these transitional macrophages are unable to induce apoptosis in FAP cells. FAP cell apoptosis occurs naturally in acute muscle injury, thus excess accumulation of connective tissue deposition is abrogated resulting in minimal scarring. This is not the case in chronic injury where sustained populations of transitional macrophage cannot induce FAP cell apoptosis., This results in persistent deposition of connective tissue and subsequent scarring, which in turn, exacerbates muscle injury and its ability to regenerate (James G. Tidball, 2017). Consequently, inadequate regeneration and associated inflammation can deleteriously impact on muscle mass and function, and indeed overall health.

1.5 Therapeutic application of immunomodulators to drive healing skeletal muscle healing

Due to the prominent role that macrophage play in wound healing as a whole, there is much interest in modulating their function to promote healing (Krzyszczyk et al., 2018; T Koh and L DiPietro, 2013). Many therapeutic strategies exist around the *in situ* activation of host derived macrophage and re-introduction to the site of injury (T Koh and L DiPietro, 2013). There are also experimental strategies involving modulating endogenous host macrophage (Krzyszczyk et al., 2018). For example, Goren et. al documented that administration of anti-TNFα and anti-F4/80 antibodies, to inhibit inflammatory macrophage, one week post injury resulted in enhanced healing (Goren et al., 2007).

Another therapeutic strategy is the use of mesenchymal stromal cells (MSCs). Conditioned growth media from MSCs was found to increase macrophage proliferation *in vitro* and growth factors secreted by MSCs can also induce M2-like characteristics (Chen et al., 2008; Németh et al., 2009). Applying this knowledge, Zhang et. al, demonstrated *in vivo* that application of MSCs to a subcutaneous wound area enhanced M2 like characteristics in the wound-resident macrophage and critically, promoted an increased healing rate of the wound (Zhang et al., 2010).

The above strategies are evidence of the therapeutic potential of immunomodulation to promote wound healing. However, none of the above models use muscle damage as a wound model. To our knowledge, there is no current literature that observes the impact of therapeutically modulated immune function on muscle regeneration. Current strategies to promote muscle healing revolve around established methods such as physiotherapy and biomaterial scaffolds (Schilling et al., 2018).

1.6 Thesis Aims

With people living longer and becoming more physically active, the occurrence of muscle related health issues, both mechanical and metabolic, is potentially set to rise. As presented above, inflammation is the common denominator between poor muscle regeneration, insulin resistance and anabolic resistance. Therapeutic immunomodulatory avenues to promote muscle healing are invasive and have the potential to carry significant side effects in humans. It is propose that, an anti-inflammatory casein and/or whey derived hydrolysates, can benefit muscle health in three ways: 1) suppress inflammation, through macrophage modulation, in skeletal muscle to promote healing 2) reduce systemic inflammation and potentially benefit the insulin and anabolic sensitivity of whole body skeletal muscle and 3) act directly on skeletal muscle to drive insulin and anabolic sensitivity. An added benefit is that the hydrolysates in question are natural and derived from food, thus are unlikely to have added side effects as possible with other methods of immunomodulation. This is also believed to be a novel method and driving muscle injury healing.

The aims of this thesis are as follows;

1. To screen a panel of casein and whey derived hydrolysates for immunomodulatory bioactivity and their ability to modulate M1 and M2 macrophage polarisation.

2. To establish whether casein and whey derived hydrolysates can influence muscle metabolism by assessing their effects on GLUT4 activity. and phosphorylation levels of 4EBP1.

3. To establish whether casein and whey derived hydrolysates could promote healing in a muscle injury model using the scratch assay model.

4. To develop an *in vitro* muscle-macrophage co-culture model to determine whether casein and whey hydrolysates that modulate M1 and M2 macrophages can impact on muscle metabolism due to these immunomodulatory effects.

Chapter 2

Materials and Methods

2.1 Materials

Table 2.1 Cell Lines

Cell Lines	Biosafety Class	Source
J774A.1 Macrophage	I	ECACC
L6 Myoblasts	I	Kerafast, Boston, MA, USA
L6 GLUT4myc Myoblasts	I	Donated by Dr. Brendan Egan, SHHP, DCU

Table 2.2 General Equipment

Class II laminar flow biosafety cabinet	Holtan Air
CO_2 steri-cylce incubator	Thermo-fisher
Universal 32R Refrigerated Centrifuge	Hettich
CKX31 Inverse Microscope	Olympus
LabCam^{TM} iDu Optics iPhone 6 microscope bracket	iDu Optics

Table 2.3 Cell Culture Materials and Reagents

Material/Reagent	Supplier
1X DPBS	Biosciences
Foetal Bovine Serum (FBS)	Biosciences
RPMI culture medium	Biosciences
αMEM culture medium	Biosciences
DMEM culture medium	Sigma Aldrich
100X Penicillin-Streptomycin Antibiotic	Biosciences
100X Antibiotic-Antimycotic	Biosciences
1X Trypsin EDTA	Biosciences
0.4% Trypan Blue	Sigma Aldrich
6, 24,96 well Nunc^{TM} cell culture plates	Fisher Scientific
T75 Nunc^{TM} cell culture flasks	Fisher Scientific
10cm petri dishes	Lennox
5mL, 10mL, 25mL pasteur pipettes	Lennox
15mL, 50mL self-standing falcon tubes	Lennox
Sterile Cell Scrapers	Sarstedt
19G, 21G needles	VWR
1mL and 10mL syringe fillers	VWR
Whatman 2μm cellulose acetate filters	Sigma Aldrich

Table 2.4 Recombinant Cytokines and Stimulation Factors

Material/Reagent	Supplier
Recombinant murine IFNγ	Biosciences
Recombinant murine IL-2	Peprotech
Recombinant murine IL-1β	Peprotech
Recombinant murine IL-4	Peprotech
Recombinant murine IL-13	Peprotech
Recombinant murine IL-6	Peprotech
Recombinant murine IL-10	Peprotech
Recombinant human TGFβ	Peprotech
Recombinant murine TNFα	Biosciences
Recombinant Murine M-CSF	Biosciences
E.coli Lipopolysaccharide	Enzo Life Sciences
Insulin from Bovine Pancreas	Sigma Aldrich

Table 2.5 Stock Buffers

Material/Reagent	Formulation
10X phosphate buffered saline (PBS)	80g/L NaCl, 11.6g/L Na_2HPO_4, 2g/L KH_2PO_4, 2g/L KCL
10X tris buffered saline (TBS)	24.2g/L Tris Base, 87.6g/L NaCl
PBS Tween 20 (PBST)	0.05% Tween 20 v/v in 1X PBS
TBS Tween 20 (TBST)	0.05% Tween 20 v/v in 1X TBS
Reagent Diluent (ELISA)	1% BSA in 1X DPBS
Dilution/Blocking Buffer (GLUT4)	5% goat serum in 1X DPBS
RIPA lysis buffer	8.7g/L NaCL, 6.05g/L Trizma base, 1% v/v triton X-100, 1X Halt Protease/Phosphatase inhibitor
3M HCL	24.9mL 37% HCL and 75.1 mL diH_2O
2N H_2SO_4	28mL 95% H_2SO_4 and 472mL diH_2O

Table 2.6 ELISA Kits and Materials

Material/Reagent	Source
IL-1β	R&D Biotechne
IL-6	R&D Biotechne
IL-10	R&D Biotechne
IL-12p40	R&D Biotechne
IL-12p70	R&D Biotechne
IL-23	R&D Biotechne
TNFα	R&D Biotechne
CCL2/MCP-1	R&D Biotechne
96 well Nunc™ ELISA Plates	Biosciences
3,3',5,5'-tetramethylbenzidine (TMB)	BDOptEIA™
Bovine Serum Albumin (BSA)	Sigma Aldrich

Table 2.7 GLUT4 Optical Detection Assay Materials and Reagents

Material/Reagent	Source
SIGMAFAST™ OPD (*o*-Phenylenediamine dihydrochloride)	Sigma Aldrich
Goat Serum	Biosciences
Paraformaldehyde	Sigma Aldrich
Anti-c-myc primary antibody	Sigma Aldrich
Goat Anti-Rabbit HRP conjugate secondary antibody	Jackson ImmunoResearch

Table 2.8 Flow Cytometry Materials and Reagents

Material/Reagent	Fluorophore	Source/Formulation
Anti-mouse TLR4	PE	BD
Anti-mouse MHCII	FITC	BD
Anti-mouse CD80	PE	BD
Anti-mouse CD86	FITC	BD
Anti-mouse CD11c	APC	BD
Anti-mouse CD11b	PE-Cy7	BD
Anti-mouse F4/80	APC	BD
FACs Buffer	N/A	(10mL FBS, 0.25g NaN_3, 1mL 0.5M EDTA)/ 500mL 1X DPBS
FACs Tubes	N/A	VWR

Table 2.9 Western Blotting Materials and Reagents

Material	Formulation	Source
Novex™ Wedge Well precast protein gels	12% Tris-HCL	Thermofisher
2X Laemmli Loading Buffer	50µl B-ME/950µL Buffer	Bio-Rad
Ammonium Persulfate	10% w/v in diH_2O	Sigma Aldrich
SDS Stock	10% w/v in diH_2O	Sigma Aldrich
TEMED	N/A	Sigma Aldrich
Kaleidoscope^{TM} molecular weight marker	N/A	Bio-Rad
Nitrocellulose iBlot Transfer Membranes	N/A	Thermofisher
iBlot Transfer System	N/A	Thermofisher
Rabbit anti-Phospho-4EBP1$^{(Thr37/46)}$	1:1000	Cell Signaling technologies
Rabbit anti-β-actin	1:1000	Cell Signaling Technologies
Anti-Rabbit HRP	1:1000	Cell Signaling Technologies
Tris-Cl	pH8.8, 1.5M	Sigma Aldrich
Tris-Cl	pH6.8 1.0M	Sigma Aldrich
ECL Western Blot Substrate	N/A	Thermofisher Scientific

Table 2.10 Assay Kits

Kit	Source
Arginase 1 Activity Assay	Sigma Aldrich
BCA Protein Assay Kit	Thermofisher
Greiss Reagent Assay	Promega (MyBio)
MTS Cell Viability Assay	Promega (MyBio)

Table 2.11 Software and Analysis Tools

Software	Source
GraphPad V5.0	GraphPad Software
FlowJo V10	FlowJo
FACSDiva V6.0	BD Biosciences
ImageJ Photo Analysis Software	https://imagej.nih.gov/ij/download.html

2.2 Methods

2.2.1 Sample Preparation:

Following the Food for Health Ireland, cross institutional SOP for hydrolysate resuspension, agreed upon in 2015, samples were prepared as follows. Powders stored at -20°C in a frost free freezer, were removed and allowed to equilibrate to room temperature for 15min. 0.015g of each sample was carefully weighed into 1.5mL sterile Eppendorf tubes. Samples were resuspended in 1.5mL of sterile, molecular grade water (Sigma), resulting in a 10mg/mL stock. Samples were gently agitated for 30min to allow for complete dispersion of the powder. Samples were centrifuged at 5,000 x *g* for 5min at room temperature. Supernatants were removed and filtered through 0.2μm cellulose acetate filters (Whatman). Samples were prepared fresh and before usage at a desired working concentration.

2.2.2 Cell Culture:

All Cell culture was conducted in a Holton Air Laminar Flow Class II Biosafety cabinet under sterile, aseptic conditions. The biosafety cabinet was cleaned with 70% IMS before use and after use, all materials entered into the biosafety cabinet were sterilised with 70% IMS.

2.2.2.1 J774A.1 Murine Macrophage:

J774A.1 macrophage cell line was purchased from the European Collective of Authenticated Cell Cultures (ECACC). Cells were maintained in DMEM supplemented with 10% FBS and 1% Pen-Strep in nunc treated T75 cell culture vessels at 37°C in 5% CO_2. Cells were passaged every three to four days at 80% confluency. Cells were removed from the culture surface using a sterile cell scraper. Cell suspension was collected in 50mL falcon tubes and centrifuged at 1250 x g for 5min at room temperature. Cells were sub-cultured in a ratio of 1:10. Cells were seeded for experimentation at a concentration of 1x10^{6}cells/mL, unless stated otherwise. To drive M1 and M2 polarisation cells were treated with; 100ng/mL LPS and 20ng/mL IFNγ; 20ng/mL IL-4 and 20ng/mLTGFβ or IL-13 for 24hr at 37°C in 5% CO_2.

2.2.2.2 Isolation and Culture of Primary Bone Marrow Derived Macrophage (BMDM):

Balb/C female mice were housed in a specific pathogen free (SPF) environment in the bio-resource unit at Dublin City University. Mice were 6-8 weeks old and purchased from Charles River, UK. Work was carried out under HPRA individual authorisation AE19115/I043. Training in animal handling and cervical dislocation was delivered and signed off on by head veterinarian Damian O' Donohue.

Day 0: Mice were euthanised via cervical dislocation. Mice were sprayed in 70% ethanol and placed in a Class II Biosafety cabinet. All subsequent steps were performed under aseptic conditions within the class II biosafety cabinet. Hind limbs from each mouse were removed and the fur, muscle and fat were stripped away to expose the femur and tibia bones. Femur and tibia bones were separated and placed in a petri dish containing 10mLs of RPMI growth media supplemented with 10% FBS and 2% Pen/Strep. Using sterile forceps and scissors the end of each bone was cut to expose the bone barrow. The bone marrow was flushed out with media using a 27-gauge needle. Bone marrow was collected in a sterile 50mL Falcon tube. Once all of the bone marrow was collected, bone marrow was dispersed by repeated aspiration through a 19-gauge needle. Bone marrow was centrifuged at 250 x g for 5 min at room temperature. Bone marrow pellet was resuspended in complete RPMI containing 50ng/mL rM-CSF and plated onto cell culture petri dishes at a ratio of one bone per plate. Plates were incubated at 37°C in 5% CO_2.

Day 3: Cells were fed with an extra 10mL of complete RPMI containing 50ng/mL rM-CSF, totalling 20mL per plate.

Day 6:, Isolated BMDMs were harvested on day six for experimentation. The dish was carefully tilted to remove old medium. 10mL of fresh complete RPMI containing 50ng/mL rM-CSF was added. Cells were scraped using a sterile cell scraper and collected in sterile 50mL falcon tubes. Cells were centrifuged at 250 x g for 5 min. Cells were resuspended and counted using a haemocytometer. Isolated BMDMs were plated for experimentation at $1x10^6$cells/mL. To drive M1 and M2 polarisation cells were treated with; 100ng/mL LPS and 20ng/mL IFNγ; 20ng/mL IL-4, TGFβ for 24hr at 37°C in 5% CO_2.

2.2.2.3 L6 GLUT4myc Myoblast Cell Line

L6 Rat GLUT4myc myoblast cell line was donated by Dr. Brendan Egan (DCU, SHHP) and Dr. Karl Cogan (UCD, FHI). Cells were maintained in αMEM Growth Medium (GM) supplemented with 10% FBS and 1% Antibiotic-Antimycotic solution and 2μg/mL Blasticidn-HCL in T75 cell culture vessels at 37°C in 5% CO_2. Cells were maintained for 10-15 passages and sub-cultured every 3 to four days at approximately 60% confluency. Briefly, confluent cells were washed twice with sterile 1X PBS. 3mL of 1X Trypsin-EDTA solution was added for 3 min. Cells were observed under the microscope for rounding. At this time 5mL of fresh GM was added and the underside of the flask tapped gently to dislodge the cells. The cell suspension was transferred to a 50mL falcon and centrifuged at 500 x g at room temperature. Cells were resuspended in 5mL of GM and passaged at a ratio of 1:20. Myoblasts were seeded at $8x10^4$cells/mL for experimentation and $4x10^4$cells/mL for differentiation into myotubes for experimentation. L6 GLUT4myc Myoblasts were differentiated into Myotubes by culturing the Myoblast monolayers for four days in GM and four days in Differentiation Media (DM), αMEM supplemented with 2% FBS and 1% Antibiotic-Antimycotic. Prior to experimentation, cells were serum starved in αMEM supplemented with 1% pen/strep.

2.2.2.4 L6 Myoblast Cell Line

L6 myoblast cell line was originally purchased from Kerafast, Boston, MA, USA. Cells were maintained in αMEM Growth Media (GM) supplemented with 10% FBS and 1% Antibiotic-Antimycotic solution in T75 cell culture vessels at 37°C in 5% CO_2. Cells were maintained for 10-15 passages and sub-cultured every 3 days at approximately 70% confluency. Briefly, confluent cells were washed twice with sterile 1X PBS. 3mL of 1X Trypsin-EDTA solution was added for 5 min. Cells were observed under the microscope for rounding. At this time 5mL of fresh GM was added and the underside of the flask tapped gently to dislodge the cells. The cell suspension was transferred to a 50mL falcon and centrifuged at 500 x g at room temperature. Cells were resuspended in 5mL of GM and passaged 1:10. Myoblasts were seeded at $8x10^4$cells/mL for experimentation and $4x10^4$cells/mL for differentiation into myotubes for experimentation. L6 Myoblasts were differentiated into Myotubes by culturing the Myoblast monolayers for four days in GM and four days in Differentiation Media (DM), αMEM supplemented with 2% FBS and 1% Antibiotic-Antimycotic. Prior to experimentation, cells were serum starved in αMEM supplemented with 1% pen/strep.

2.2.3 Cell Numeration

To determine cell numbers and extrapolate cell concentration for experimentation, cell suspensions were counted using a haemocytometer. 100μL of cell suspension was added to a 1.5mL Eppendorf tube containing 150μL sterile 1x PBS and 250μL of 0.1% Trypan Blue staining solution. This cocktail was mixed and incubated at room temperature for 5 min. During this time the haemocytometer was cleaned with 70% IMS and a cover slip was placed on top of the grid. 10μL of the Trypan Blue/Cell cocktail was carefully placed underneath the coverslip, ensuring no air bubbles were formed. Cells were counted in four gridded sections. An average value was taken between the four sections and used in the following equation to calculate cell concentration.

$$N \, x \, 5 \, x \, 10^4 = X \, cells/mL$$

Where "*N*" is the average cells count, "*5*" is the dilution factor and "10^4"corresponds to the surface area of the haemocytometer. Once calculated cells were diluted to the desired concentration in the respective cell culture medium.

2.2.4 Flow Cytometry

2.2.4.1 Basic Principles of Flow Cytometry:

Flow cytometry is an essential technique in cell surface phenotype analysis. Flow cytometry allows the user to analyse specific cellular characteristic from size, complexity to specific markers expressed both intra and extra- cellularly. The flow cytometer instrument is comprised of three primary systems; Fluids, Optics and Electronics. The fluidics channels the cell targets in a single file format to the optical sensors. The optics system is comprised of lasers that excite the target cell of interest and a combination of mirrors and filters collect the light signals given off when the target has been interrogated. The electronics system then deciphers the light signals and converts them into electrical signals that can be read by the computer and displayed as numerical data.

The point at which the laser beam hits the target cell is known as the point of interrogation. When the laser hits the target cell, it sends light scattering is several directions. Light that is scattered axial to the light source is called forward scatter (FSC). FSC is an indicator of cell surface area and size. Light scattered perpendicular to the laser is called side scatter (SSC) and is indicative of the internal complexity of a cell. Using antibodies conjugated to light-excitable fluorochromes such as PE, FITC and APC can be used to tag specific cell surface markers. When excited by the laser, these fluorochromes will emit light that can be collected and interpreted.

2.2.4.2 Cell Surface Marker Staining Protocol:

J77A.1 macrophage and primary BMDMs were seeded in 6 well plates at a concentration of $1x10^6$cells/mL. Cells were stimulated with M1 and M2 polarising molecules as described previously. Following incubation, cells were scrapped and collected in 15mL centrifuge tubes. An equal volume of heat inactivated FBS was added at room temperature for 15min to block non-specific binding. Cells were then centrifuged at 300 x g for 5 mins at 4°C. Cells were resuspending in 1mL of FACs buffer. 200μL of this cell suspension (approx. 400,000 cells) was added to a designated well of a 96 well round bottom plate, in duplicate. The plate was spun down at 300 x g for 5 mins at 4°C. Supernatants were aspirated, and cells resuspended in 100μL of 1:1000 dilutions of respective antibodies and incubated for 30 min at 4°C. Cells were then washed three times in FACs buffer by resuspending in 200μL of FACs buffer and centrifuging 300 x g for 5 mins at 4°C. Once washing was completed, cells were resuspending in 100μL and transferred to FACs loading tubes containing 400μL of FACs buffer. Cells were then analysed using the BD FACSAria 1 system. Raw FCS files were analysed, and data graphed using V10.0 FlowJo software.

2.2.5 Enzyme Linked Immuno-Sorbent Assay (ELISA)

2.2.5.1 Basic Principles of ELISA

The ELISA is a robust, antibody-based method used to identify the concentrations of a specific analyte in a respective sample. In the research presented, a sandwich ELISA format was used to determine the concentration of specific cytokines secreted by J774A.1 murine macrophage and BMDMs. In this format of ELISA, the analyte of interested in detected between two specific antibodies, a capture and a detection. Each antibody binds to a unique epitope on the analyte in question allowing it to be sandwiched between the antibodies. The detection antibody is coupled to a biotin tag which allows for binding of specific detection agent, in this case Streptavidin-HRP. Streptavidin-HRP, as horse radish peroxidase, catalyses the conversion of the substrate solution, tetramethylbenzidine (TMB) to a coloured product. The optical density (OD) of this product is measured using a 96 well microplate reader. This intensity of this colour is directly proportional to the amount of analyte in the sample in question. Quantities in unknown samples are determined using a standard curve generated for each specific analyte.

2.2.5.2 Cytokine ELISA Protocol

The concentrations of the cytokines IL-1β, IL-6, IL-10, IL-12p40, IL-23, TNFα and CCL2/MCP-1 were determined using the sandwich ELISA kits provided my R&D Systems and performed according to the manufacturer's instructions. Briefly, the capture antibody was diluted to an appropriate concentration and 50μL/well was added. Plates were incubated overnight, at room temperature. Next, plates were washed, three times, in wash buffer (1X PBS + 0.05% Tween-20). To overcome non-specific binding, plates were blocked at room temperature, for 1 hour in reagent diluent (1% BSA + 1X PBS). Plates were once again washed three times and 50μL/well of appropriately diluted standard and sample was added to each plate. Plates were incubated at 4°C overnight. The following day, plates were washed three times and 50μL/well of appropriately diluted biotinylated detection antibody was added and incubated at room temperature for 2 hours. Plates were washed three times and 50μL/well of a 1:40 streptavidin-HRP solution was added for 20 min, at room temperature protected from light. Plates were washed once again and 50μL/well of fresh TMB substrate was added and incubated for 20 min at room temperature, protected from light until a blue colour developed. This was followed by the addition of 25μL/well of 2N sulphuric acid, to stop the reaction. The optical density was determined at 450nm using a Versamax^{TM} microplate reader. Each sample and standard were analysed in triplicate.

2.2.6 Measurement of Nitric Oxide (NO) Secretion

2.2.6.1 Basic Principles of the Griess Reagent System

Nitric Oxide (NO) is an indictive marker of macrophage polarisation. Concentrations of NO were measured in fresh cell supernatants derived from J774A.1 murine macrophage using the Griess Reagent System (Promega). This system measures the concentration of Nitrite (NO_2^-), which is non-volatile breakdown product of NO formation. This system uses Sulphanilamide and N-1-napthylethylenediamine (NED), under acidic conditions, to form a coloured azo-compound in the presence of NO_2^-. The intensity of the coloured azo-compound is directly proportional to the levels of NO_2^- in the supernatant from which the concentration of NO can be inferred.

2.2.6.2 Griess Reagent System Protocol

The measurement of NO_2^- was conducted according to the manufacturer's instructions. Briefly, a serial dilution of a 100μM Nitrite standard was prepared using complete DMEM and 50μL was added in triplicate to the wells of a 96 well plate. 50μL of appropriately diluted sample was added in triplicate to the 96 well plate. 50μL of Sulphanilamide solution was added to each standard and sample and incubated for 10 min at room temperature, protected from light. This was followed by 50μL of NED solution to each standard and sample and incubated for 10 min and room temperature protected from light. A purple/magenta colour began to form immediately. OD was measured at 535nm using a Versamax™ microplate reader. NO_2^- in samples were determined by comparing absorbance values to that of the values located within the standard curve.

2.2.7 Measurement of Arginase 1 Activity in J74A.1 Murine Macrophage and Murine BMDMs

2.2.7.1 Basic Principles of the Arginase 1 Assay

Arginase 1 (Arg1) is a manganese-containing enzyme that is responsible for the catalysis of arginine to urea. As with NO, Arg1 activity is considered an indicative marker of macrophage polarisation. Arg1 is located in the cytoplasm of the cell and thus in order to analyse its activity cells must undergo lysis. In the assay reaction, Arg1 converts arginine to urea and ornithine. The urea product reacts with a substrate, inducing a colour change in which, the colour intensity is directly proportional to the activity of Arg1. As a baseline, 1 unit of Arg1 will convert 1.0μmoles of L-Arginine to urea and ornithine per minute at p9.5 at 37°C. The assay kit used here (Sigma) has a detection lower detection limit of 0.3units/L for a 2 hour, 96 well plate reaction.

2.2.7.2 Arginase 1 Assay Protocol

The assay protocol was followed as per the manufacturer's instructions (Sigma). Briefly, approximately 1x10^{6} cells were harvested and washed with sterile PBS. Cells were centrifuged at 1,000 x g for 10 min at 4°C. Cell pellets were resuspended in 100μL of lysis buffer (10mM TRIS-HCL, 1μM Pepstatin A, 1μM Leupeptin-HCL and 0.4% Triton X-100) and kept on ice for 10 min. Samples were centrifuged at 13,000 x g to remove insoluble debris. Supernatants were retained and 40μL of sample was added to two assigned wells of a 96 well plate, one of these will act as a sample blank. 50μL of a1mM urea standards was added to an assigned well of a 96 well plate beside a well filled with 50μL of diH_2O. 10μL of 5X substrate buffer was added to both sample wells. The plate was then incubated at 37°C for 2 hours. 200μL of prepared Urea Reagent was then added to each sample and sample blank wells, the urea standard and the diH_2O. 10μL of 5X substrate buffer was added immediately to each of the sample blank wells also. The plate was incubated at room temperature for 1 hour. The OD was then measured at 430nm using a Versamax^{TM} microplate reader.

2.2.7.3 Calculation of Arginase 1 Activity

Arg1 activity was calculated with the respective absorbance values using the following equation:

$$Activity = \frac{(Abs\ Sample) - (Abs\ Blank)}{(Abs\ Standard) - (Abs\ Water)}\ x\ \frac{(1mM\ x\ 50\ x\ 10^3)}{(V\ x\ T)}$$

Where "Abs" is the OD value, "V" is the total volume of sample used, "1mM" is the concentration of the urea standard, "50" is the reaction volume in μL, "T" is the reaction time and "10^3" is the mM to μM conversion factor.

2.2.8 MTS Cell Viability Assay

2.2.8.1 Basic Principles of the MTS Cell Viability Assay

The MTS is assay is a commonly used method for assaying the viability of cells *in vitro* under certain conditions. In this assay, the starting compound MTS tetrazolium (yellow) is catalysed by dehydrogenase enzymes, in the mitochondria of living and active cells, to a coloured formazan product (purple). The intensity of the resulting colour is directly proportional to the percentage of viable cells in a population.

2.2.8.2 MTS Cell Viability Assay Protocol

The assay system used was the CellTiter 96® AQueous One Solution Cell Proliferation Assay. The assay was conducted as per the manufacturer's instructions. Each assay was performed in triplicate and a positive control (untreated cells) and negative control (10% DMSO) was included. 100μL of a $1x10^6$cells/mL cell suspension was added in triplicate to designated wells of a 96 well plate. Cells were then stimulated accordingly and incubated overnight at 37°C in 5% CO_2. The Following day, 20μL of CellTiter 96® AQueous One Solution was added to each well and incubated at 37°C in 5% CO_2. The OD was determined every hour for a total of three hours using a Versamax™ microplate reader at 490nm. Cell viability was expressed as a percentage of the Positive, untreated control which is considered 100%.

2.2.9 Optical Detection of Cell Surface GLUT4 in L6-GLUT4myc Myoblasts and Myotubes

2.2.9.1 Basic Principles:

GLUT4 is the primary insulin stimulated glucose receptor expressed in mammalian cells. L6 GLUT4myc Cells are stably transfected with a plasmid that express a myc tagged GLUT4. Subsequently, due to the ability of this cell line to over express a myc tagged GLUT4, they have become a key model to study glucose metabolism *in vitro* . This allows for the analysis of glucose uptake levels in myoblast and myotube stage of muscle development. An OPD substrate based, colourmetric assay optical detection assay initially described by Ishikura *et. al* was used to measure insulin stimulated GLUT4 translocation in myoblasts and myotubes (Ishikura et al., 2010a). Described below are protocols for the established 24 well plate format and an optimised 96 well assay format.

2.2.9.2 OPD GLUT4myc Optical Detection Assay: 24 Well Plate Assay

Initially, myoblasts were seeded in 24 well plates at the densities previously described. Following stimulation, cells were starved in serum free αMEM supplemented with 1% antibiotic-antimitotic (Gibco), for three hours at 37°C. Next, designated cells were stimulated with Bovine Insulin (Sigma Aldrich) for 20 min at 37°C. Next, cells were washed twice in ice cold PBS and fixed in 300μL of ice cold 3% paraformaldehyde for 10mins on ice and a further 20mins at room temperature. Supernatant was aspirated, and cells were washed three times in room temperature PBS. Cells were blocked for 15 min in 5% Goat Serum-PBS. All wells, excluding wells designated to assess background, were incubated with 1μg/mL primary GLUT4myc antibody (Sigma-Aldrich) for 60mins at 4°C. Wells were washed five times in PBS. Appropriate wells were then incubated with a 1:500 dilution of a secondary HRP-conjugated goat anti-rabbit antibody (Jackson Immunoresearch) for 45 min at 4°C. Cells were wash five times in PBS. 1mL of freshly prepared OPD Substrate (Sigma Aldrich) was added to each well and incubated in the dark for 30 min. The reaction was stopped with 250μL of 3M HCL. 200μL of each sample was transferred to a designated well of a 96 well plate. Samples were read at 492nm using a Versamax^{TM} microplate reader.

Values for each replicate were normalised to the unstained cells and results expressed as a fold change of the non-insulin stimulated cells.

2.2.9.3 OPD GLUT4myc Optical Detection Assay: 96 Well Plate Assay

Initially, L6 GLUT4myc myoblasts were seeded on 96 well plates at the densities previously described. Following stimulation, cells were starved in serum free DMEM supplemented with 1% antibiotic-antimitotic (Gibco), for three hours at 37°C. Next, designated cells were stimulated with 100nM Bovine Insulin (Sigma Aldrich) for 20 min at 37°C. Cells were then fixed with 100μL of 3% paraformaldehyde for 10mins on ice and a further 20mins at room temperature. Next, cells were washed with 200μL of 0.1mM Glycine for 5 min on a plate shaker. Next, cells were washed three times in PBS and blocked in 5% Goat Serum-PBS. Next, wells were incubated with a 1:1000 dilution of primary GLUT4myc antibody (Sigma-Aldrich) for 60mins at 4°C. Some wells are left unstained to assess background. Next, cells were washed five times in PBS. Appropriate wells were then incubated with a 1:500 dilution of a secondary HRP-conjugated goat anti-rabbit antibody (Jackson Immunoresearch) for 45 min at 4°C. Cells were washed five times in PBS. Cells are then incubated in 100μL of freshly prepared OPD reagent for 30mins in the dark at room temperature. The reaction was stopped with 25μL of 3M HCL per well. The plate was read directly at 492nm using a Versamax^{TM} microplate reader. Values for each replicate was normalised to the unstained cells and results expressed as a fold change of the non-insulin stimulated cells.

2.2.10 Detection of p4E-BP1$^{(Th37.46)}$ by Western Blot Analysis in L6 Myotubes:

2.2.10.1 Preparation of L6 Cell Lysates:

L6 myoblasts were seeded and differentiate into mature myotubes as previously described. Myoblasts were stimulated with 1mg/mL NaCN or Whey protein, at 37°C in 5% CO_2. For 24hr. Following this incubation, cells were washed twice in sterile, ice cold 1X DPBS. Cells were scraped and centrifuged at 500 x g at 4°C. Cells were resuspended in 300μL of ice cold RIPA lysis buffer containing 1X Protease-Phosphatase inhibitor cocktail. Cells were lysed by vigorously passing them through a 21 gauge needle several times and incubating for 30 min on ice. Lysates were centrifuged at 13,000 x g at 4°C for 15 min to remove insoluble cellular debris. Supernatants were retained and kept on ice or stored at -20°C.

2.2.10.2 Determination of Total Protein Concentration via BCA Assay:

Total protein concentration was determined using the BCA protein assay kit provided by Thermo-Fischer Scientific. The 96 well assay protocol was performed as per the manufacturer's instructions. Briefly, a Bovine Serum Albumin (BSA) standard curve was prepared in triplicate with concentrations ranging from 2,000μg/mL to 25μg/mL. 25μL of each sample and standard was added in triplicate per well of a 96 well plate. Following this, 200μL of prepared working reagent (WR) was added to each well. The plate was then covered and incubated at 37°C for 30 min. The plate was then cooled to room temperature for 5 min. The plate was read directly at 562nm using a Versamax™ microplate reader. Sample protein concentration was extrapolated from the standard curve absorbance values.

2.2.10.3 Separation of Proteins via SDS-PAGE:

15μg of protein was prepared in activated 2X Laemmli loading buffer by boiling at 100°C for 5 min. Samples were centrifuged briefly to ensure all protein was collected for loading. 10μg of protein was loaded into each well of a 12% pre-cast SDS-PAGE gel. 5μL of molecular weight marker was loaded along with each sample. Samples were separated down the length of the gel for one hour at 180V until separation was complete. Once separation was complete, the gel assembly was broken down and the complete SDS-PAGE gel placed onto a nitrocellulose transfer membrane using the iBlot™ transfer system. Transfer was confirmed by the presence of the pre-stained molecular weight markers on the nitrocellulose membranes.

2.2.10.4 Immunoblotting:

Membranes were removed and blocked in 5% BSA for 1 hour at room temperature with gentle agitation. Membranes were then washed in TBST three times, for 5 min with gentle agitation at room temperature. Rabbit Phospho-4E-BP1$^{(Thr37/46)}$ and Mouse β-actin primary antibodies at a 1:1000 dilution in antibody dilution buffer. Membranes were incubated overnight at 4°C with gentle agitation. Next, membranes were washed in TBST three times, for 5 min with gentle agitation at room temperature. Anti-Rabbit HRP and Anti-Mouse HRP conjugated antibodies were incubated and 1:1000 dilutions in antibody dilution buffer and incubated for 1 hour at room temperature. Membranes were then washed in TBST three times, for 5 min with gentle agitation at room temperature. Membranes where then incubated in 15mL of western blot specific TMB substrate for 20min, or 5mL of electro chemiluminescent (ECL) reagent for 2 min protected from light. Following this incubation, images were captured with a lighted background for TMB incubated blots and in a G-Box for ECL incubated blots. Western blot images were quantified using ImageJ analysis software.

2.2.11 Measurement of *in vitro* wound closure using a scratch assay method.

2.2.11.1 Basic Principles

The ability of cells to migrate and proliferate is a key pilar of wound healing and resolution of tissue damage. The rate at which cells of a given tissue dictates the how quickly a wound or other forms of tissue damage can heal. Although a plethora of *in vivo* and *in vitro* methods are employed to study the progression wound closure, these are costly and time consuming. The scratch assay method involves scratching a uniform line down the centre of a confluent layer of cells, and subsequently tracking the rate at which cells migrate to cover and heal the wounded area, through live imaging or static timepoint photography. This method has been employed extensively to elucidate the effect that certain treatments have on wound healing in vitro , in many cell types.

2.2.11.2 Scratch Assay

L6 myoblasts were seeded in 24 well cell culture plates at $8x10^4$cells/mL. Cells were grown to confluence but not allowed to differentiate into mature myotubes. Once confluent, a uniform scratch was made down the centre of each well containing cells using a guide ruler and sterile P1000 pipette tip. Once the sterile wound was made, cells were twice in prewarmed sterile 1X DPBS to remove dead/floating cells. Cells were then fed with growth medium and/or treated as required. Images were taken at time points 0hr, 24hr and 48hr using an Apple iPhone 6 mounted to a LabCam™ iDu Optics microscope bracket under 40X magnification. Images were taken at a specific, predetermined pointed within each well following wounding at each of the previously mentioned time points. The rate of wound closure for each treated condition is expressed as a percentage of the initial wound area for each treated condition using the following formula, where "i" represents the initial wound area and "t" represents each respective time point.

$$\%\ Closure = \frac{(Ti - Tt)}{Ti}\ x\ 100$$

2.2.12 Generation of J774A.1 Macrophage Conditioned Growth Medium

J774A.1 macrophage were seeded in 6 well cell culture plates at $1x10^6$cells/mL. Cells were cultured in supplemented DMEM at 37°C for 3hr in 5% CO_2. Following which they were polarised to either M1 or M2 phenotypes as previously described 37°C for 24hr in 5% CO_2. Once this incubation was complete, conditioned supernatant was harvested, and centrifuged at 250 x g for 5mins to remove floating cells and/or insoluble cellular debris. Secreted cytokine concentrations were determined by cytokine specific ELISA as previously described. Conditioned supernatants were stored at -20°C until required. To generate hydrolysate modulated conditioned growth medium, cells were preincubated with 1mg/mL of each hydrolysate or whole protein control prior to M1 and M2 polarisation. Hydrolysate modulated supernatant was harvested and processed in the same manner and unmodulated M1 and M2 supernatant as previously described. Conditioned supernatants were added directly to L6 GLUT4myc/L6 myoblasts and myotubes to study the effects of M1 and M2 modulated secretome profiles on outputs of skeletal muscle function.

2.2.13 Generation of Activated J774A.1 Macrophage for C-Culture Experimentation

J774A.1 macrophage were seeded in 6 well cell culture plates at $1x10^6$cells/mL. Cells were cultured at 37°C for 3hr in 5% CO_2. Following which they were polarised to either M1 or M2 phenotypes as previously described 37°C for 4hr in 5% CO_2. Once this incubation was complete, supernatant was removed, and cell were washed twice in prewarmed sterile 1X DPBS. Activated cells were removed by gentle scraping with a sterile cell scraper. Activated cells were collected by centrifugation and resuspend in L6 GM. Cells were added directly into L6 myoblast cultures at numbers ranging from 5,000 to 100,000 cells per well. To generate hydrolysate modulated M1/M2 J774A.1 activated cells, cells were preincubated with 1mg/mL of each hydrolysate or whole protein control prior to M1 and M2 polarisation. Hydrolysate modulated cells were harvested and processed in the same manner and unmodulated M1 and M2 cells previously described. Modulated and unmodulated cells were added directly to L6 GLUT4myc/L6 myoblasts and myotubes to study the effects of M1 and M2 modulated cell contact on outputs of skeletal muscle function.

2.2.14 Statistical Analysis

Results are presented as mean ± standard error of the mean (±SEM). Data analysis was between groups was performed using a one-way ANOVA followed by a Newman-Keuls/Dunnetts post test or a two-way ANOVA followed by a Holm-Sidak post-test, where stated. All data was analysed using Prism analysis software V8.2 (GraphPad Software, Inc.). Values of less that $p<0.05$ were considered statistically significant.

Chapter 3:

Establishment of an *in vitro* Model of M1 and M2 Macrophage Polarisation for Assessing the Immunomodulatory Activity of Cow's Milk Protein Hydrolysates

3.1 Introduction:

Macrophage are a monocyte derived cell type, that form a critical part of the innate immune response. Macrophage are heterogenous and highly plastic in their phenotypic properties which is modulated by their mode of activation (Shapouri-Moghaddam et al., 2018). Generally there is considered to be two subgroups of macrophage, that differ in their phenotypic and functional properties as illustrated in figure 3.1.1 (Martinez and Gordon, 2014; Shapouri-Moghaddam et al., 2018).

The first of the macrophage phenotype is referred to as the classically activated or M1 macrophage (Martinez and Gordon, 2014). M1 macrophage are highly inflammatory and have key functions in phagocytosis of necrotic cells, virally infected cells and bacteria. They also secrete high levels of pro-inflammatory cytokines and reactive oxygen species (ROS). M1 macrophage are generally activated *in vivo* by TLR ligands such as LPS, which binds via TLR4 (Martinez and Gordon, 2014). Damage associated molecular patterns (DAMPs), which are released in response to injury are also responsible for driving an M1 phenotype (James G Tidball, 2017; Tidball and Villalta, 2010). In contrast, M2 macrophage exhibit an anti-inflammatory phenotype. M2 macrophage function is associated with wound healing, allergy response and immunoregulation (Martinez and Gordon, 2014; Shapouri-Moghaddam et al., 2018). M2 macrophage are considered a more complex phenotype of macrophage as they themselves are sub divided into three distinct M2 phenotypes: M2a, M2b and M2c macrophage. Although, subtle differences in phenotype occur between these subtypes, one parameter is constant; M2 polarised macrophage are anti-inflammatory.

Macrophage are considered the major players in the regenerative process of skeletal muscle (Saini et al., 2016; Tidball and Villalta, 2010; Wynn and Vannella, 2016). As described previously in *1.5.1* there is a series of complex and time sensitive interactions between the immune system and skeletal muscle. Briefly, macrophage are initially polarised towards the inflammatory M1 phenotype following exposure to DAMPs released from damaged muscle tissue and conditioning by inflammatory factors secreted by neutrophils (Chazaud, 2016;

James G Tidball, 2017). M1 macrophage infiltrate the muscle tissue and begin to phagocytose necrotic and damaged muscle cells. (Chazaud, 2016). The inflammatory cytokines TNFα and IFNγ secreted by M1 macrophage act directly upon muscle progenitor cells to drive the proliferation of these cells in order to bolster numbers sufficiently to support correct recovery of skeletal muscle (Tidball et al., 2015). There is a phenotypic shift in the immune environment at the site of injury. M1 macrophage shift polarity to become anti-inflammatory M2 macrophage. M2 macrophage are considered the "healer" immune phenotype in the context of wound and injury recovery, and allow for the final differentiation of myoblasts into mature myofibers and myotubes whilst also quenching any residual inflammation in the injury microenvironment (Arnold et al., 2007; James G Tidball, 2017). However, in many cases this inflammation can persist and have detrimental effects on muscle health.

Chronic inflammation in skeletal muscle can severally impact the ability that muscle tissue has to regenerate (Chazaud, 2016). Saclier *et. al* previously demonstrated that both myoblast differentiation into mature myotubes was hampered when exposed to M1 conditioned growth medium and when co-cultured with M1 polarised human-derived macrophage. Interestingly incubation with conditioned medium and co-culture with M2a- and M2c- polarised human macrophage encouraged differentiation of myoblasts into mature myotubes (Saclier et al., 2013). As discussed previously, it is also believed that inflammation plays a direct role in the development of insulin resistance and anabolic resistance, two key metabolic pathways not only important for muscle health, but for whole body health (Breen and Phillips, 2011; Shoelson et al., 2006).

Due to the primary role that macrophage have in wound healing and muscle recovery, and the extent at which their dysfunction can impair muscle function, modulation of macrophage function as a therapeutic strategy is an avenue that is being explored (Krzyszczyk et al., 2018). For example, wound healing was accelerated in a mouse model of injury by attenuating M1 macrophage function with administration of anti-TNFα and anti-F4/80 antibodies (Goren et al., 2007). Novel, food derived immunomodulators may provide an alternative, natural route for the treatment of inflammation induced muscle damage.

The aims of this chapter are:

1. To develop an *in vitro* M1 and M2 macrophage polarisation model, in both an immortalised J774A.1 cell line and in primary Bone Marrow Derived Macrophage.

2. To use this model of polarisation to provide preliminary data on the effect of that whole casein (NaCN) and whey (WPC) derived hydrolysates have on a macrophages' ability to polarise to the M1 and M2 phenotypes.

3.2 Results

3.2.1 Polarisation of J774A.1 Macrophage *in vitro*

In order to study the immunomodulatory effects of milk derived bioactive hydrolysates, it was necessary to devise an *in vitro* M1 and M2 polarised macrophage cell model. J774A.1 macrophage (ATCC) were chosen as the cell line. It has been well established that induction of an inflammatory M1 phenotype is achieved through stimulation with *E.coli* lipopolysaccharide (LPS) in combination with the inflammatory cytokine IFNγ. In contrast, induction of the anti-inflammatory M2 phenotype is achieved through stimulation with the Th2 cytokines, IL-4 and IL-13. J774A.1 macrophage were stimulated with varying concentrations of M1 and M2 phenotype inducers in order to establish an effective polarisation method. Stimulated cells were cultured for 24hr at 37°C in 5% CO_2.

3.2.1.1 Cell Viability Assessment.

J774A.1 macrophage were seeded at 1x10^6 cells/mL. Cells were subsequently stimulated with M1 and M2 polarising factors (LPS and IFNγ, IL-4 and IL-13 respectively) at concentrations ranging from 10ng/mL to 100ng/mL. Cell viability was assessed using the the CellTiter® Aqueous One Solution cell proliferation assay, as previously described in section 2.2.8. A negative control, of 10% DMSO in DMEM was used to induce cell death ($p<0.001$). As illustrated in supplementary figure SF1.1, both M1 and M2 polarising factors have no significant impact on cell viability, as determined by comparison to the positive and negative controls.

3.2.1.2 Stimulation of J774A.1 Macrophage with M1 Polarising factors affects cytokine secretion in a dose dependant manner

J774A.1 macrophage were seeded at $1x10^6$ cells/mL. Cells were subsequently stimulated with LPS and the M1 polarising factors LPS and IFNγ, at concentrations ranging from 10ng/mL to 100ng/mL. Stimulated cells were cultured for 24hr at 37°C in 5% CO_2. Concentrations of IL-1β, IL-6, TNFα and IL-10 were quantified using specific ELISA duosets (R&D) as previously described in section 2.2.5. LPS, a known inflammatory inducer, signals through toll-like receptor 4 (TLR4), which initiates a signalling cascade that ultimately drives secretion of pro-inflammatory cytokines among other hallmarks of inflammation. Stimulation with 100ng/mL LPS induced IL-1β, IL-6, IL-10 and TNFα secretion by J774A.1 macrophage. In order to induce a true M1 phenotype however, IFNγ is required. As illustrated in figure 3.1, IFNγ in the presence of LPS, affected cytokine secretion in a dose dependant manner. IL-6 and TNFα ($p<0.05$) secretion was enhanced in the presence of IFNγ whereas IL-1β secretion, while maintained, was down regulated compared to LPS alone. Interestingly, inclusion of IFNγ was able to down regulate IL-10 secretion compared to LPS alone, suggesting that polarisation to a true M1 phenotype was being observed.

3.2.1.3 Stimulation of J774A.1 Macrophage with M2 Polarising factors affects cytokine secretion in a dose dependant manner

J774A.1 macrophage were seeded at $1x10^6$ cells/mL. Cells were subsequently stimulated with LPS and the M2 polarising factors, IL-4 and IL-13, at concentrations ranging from 10ng/mL to 100ng/mL. Stimulated cells were cultured for 24hr at 37°C in 5% CO_2. Concentrations of IL-1β, IL-6, TNFα and IL-10 were quantified using specific ELISA duosets (R&D) as previously described in section 2.2.5. Cytokine secretion was modulated by stimulation with IL-4 and IL-13 in a dose dependant manner as illustrated in figure 3.2. As expected, IL-4 and IL-13 stimulation did not induce production of pro-inflammatory factors when compared to LPS induction. Although, low levels of IL-1β, IL-6 and TNFα ($p<0.001$) were observed. Crucially, M2 macrophage are required to drive IL-10 secretion in combination with comparably low levels on key inflammatory cytokines. IL-10 secretion was indeed affected in a dose dependant manner, and secretion peaks at concentrations of 20ng/mL IL-4 and IL-13 ($p<0.05$). Collectively, IL-10 induction and low levels of inflammatory cytokines indicate polarisation towards an M2 phenotype.

3.2.1.4 Polarised J774A.1 macrophage exhibit differential cytokine profiles consistent with M1 and M2 macrophage phenotypes.

We next confrimed our M1 and M2 profiles by polarising macrophage in the same expeiment so we could directly compare them. J774A.1 macrophage were seeded at $1x10^6$ cells/mL. Cells were subsequently stimulated with M1 and M2 polarising factors. Naïve, M1 and M2 polarised J774A.1 macrophage display divergent cytokine profiles consistent with each phenotype as outlined in figure 3.3. In dose response experiments, 100ng/mL LPS and 20ng/mL IFNγ appears to be sufficient to drive an M1 phenotype in J774A.1 macrophage. This is characterised by high levels of secreted IL-1β, IL-6 and TNFα and crucially, low levels of IL-10. Deriving from the M2 polarisation dose response, 20ng/mL IL-4 and 20ng/mL IL-13 are sufficient to polarise J774A.1 macrophage towards and M2 phenotype. This is indicated through high expression of IL-10 and crucially low levels of IL-1β, IL-6 and TNFα secretion. Of note, naïve J774A.1 macrophage seem to have a low basal expression of IL-1β, IL-10 and TNFα. Stimulation with IL-4 and IL-13 alters this profile by driving IL-10 secretion and knocking out IL-1β and TNFα production. Low levels of IL-6 are also detectable in M2 polarised macrophage. The profiles from this experiment provide data to confirm the M1 and M2 phenotype.

3.2.1.5 Polarised J774A.1 macrophage express key phenotypic marker's consistent with M1 and M2 macrophage phenotypes.

To further confirm the M1 and M2 phenotype we examined other markers of the phenotype. J774A.1 macrophage were seeded at $1x10^6$ cells/mL. Cells were subsequently stimulated with M1 polarising factors 20ng/mL IFNγ and 100ng/mL LPS, and M2 polarising factors 20ng/mL IL-4 and 20ng/mL IL-13. There are two indicative phenotypic markers that are distinct for each macrophage subtype. In M1 macrophage, the enzyme iNOS is activated. iNOS produces nitric oxide which is a critical mediator of inflammatory macrophage activity. iNOS is inactive in M2 macrophage. In contrast, Arginase 1 catalyses the conversion of arginine to polyamines which orchestrate several cellular processes, Arginase 1 activity is unique to anti-inflammatory M2 macrophage. M1 stimulation induced iNOS in M1 macrophage and not M2 macrophage ($p<0.001$) (Figure 3.4). M2 stimulation induced Arginase 1 activity in M2 macrophage ($p<0.05$). M1 Arginase activity was unchanged relative to the unstimulated control cells (Figure 3.5). The differential expression of these two key markers further confirms, that polarisation towards M1 and M2 phenotypes is indeed occurring.

3.2.1.6 M2 Polarisation Leads to Inconsistent Secretion of IL-10 in J774A.1 Macrophage

Polarisation of J774A.1 macrophage with the afore mentioned IL-4 and IL-13 cocktail, leads to induction of IL-10 secretion with accompanied low levels or complete absence of pro-inflammatory cytokines and markers. However, we found that IL-10 secretion between the M1 IL-10 secretion and M2 IL-10 secretion to be highly variable. As illustrated in figure 3.5, in several cases, M1 secreted IL-10 is significantly higher than that of the M2 polarised macrophage ($p<0.001$). In contrast, there are several experiments where IL-10 secretion is higher in the M2 polarised macrophage, as is expected ($p<0.05$, $p<0.001$). What is constant however, is that stimulation of J774A.1 macrophage with 20ng/mL IL-4 and IL-13 leads to induction of IL-10 in M2 macrophage compared to the unstimulated J774A.1 macrophage. Due to these in consistencies, alternate polarisation molecules will be explored in an attempt to increase IL-10 secretion in the M2 polarised macrophage.

3.2.2 Alternate M2 Polarisation in M2 Macrophage

3.2.2.1 Cell Viability Assessment

TGFβ is a potent immunoregulatory cytokine that is known to drive a Th2 phenotype in several immune cell types. Due to its immunoregulatory potential, it was decided to attempt combinations of TGFβ and IL-4 to drive a high IL-10 secreting M2 phenotype in J774A.1 Macrophage. J774A.1 macrophage were seeded at $1x10^6$ cells/mL. Cells were subsequently stimulated with alternate M2 polarising, IL-4 and TGFβ, factors at concentrations ranging from 10ng/mL to 100ng/mL. Cell viability was assessed using the the CellTiter® Aqueous One Solution cell proliferation assay. A negative control, of 10% DMSO in DMEM was used to induce cell death. As illustrated in supplementary figure SF1.2, alternate M2 polarising factors do not impact on cell viability, as determined by comparison to the positive and negative controls.

3.2.2.2 Stimulation of J774A.1 Macrophage with Alternate M2 Polarising Factors Affects Cytokine Secretion in a Dose Dependant Manner

J774A.1 macrophage were seeded at $1x10^6$ cells/mL. Cells were subsequently stimulated with alternate M2 polarising factors, IL-4 and TGFβ, at concentrations ranging from 10ng/mL to 100ng/mL. Stimulated cells were cultured for 24hr at 37°C in 5% CO_2. Concentrations of IL-1β, IL-6, TNFα and IL-10 were quantified using specific ELISA duo sets. As outlined in figure 3.6, stimulation with IL-4 and TGFβ, did not induce expression of high levels of pro-inflammatory cytokines, however low levels of IL-1β and IL-6 were induced. Critically, IL-10 secretion was significantly upregulated ($p<0.001$) in all doses of IL-4 and TGFβ. There was no statistically significant difference between the 20ng/mL and 50ng/mL doses.

3.2.2.3 Stimulation of J774A.1 Macrophage with IL-4/IL-13 and IL-4/TGFβ M2 Polarising Factors Leads to an Alternate M2-like Cytokine Profile in J774A.1 Macrophage

20ng/mL IL-4/IL-13 and 20ng/mL IL-4/TGFβ stimulation in J774A.1 macrophage both drive a cytokine profile consistent with an M2 profile (Figure 3.7). IL-4/IL-13 stimulation leads to low IL-6 secretion and high IL-10 secretion. There was no detectable IL-1β and TNFα secretion from J774A.1 macrophage polarised in this manner. Conversely, Low levels of pro-inflammtory cytokines were induced by stimulation with IL-4 and TGFβ, however, this upregulation was determined to be not significant. Most notabley, IL-10 secretion, following stimulation with IL-4 and TGFβ, was doubled significantly compared to the levels observed in macrophage polarised with IL-4 and IL-13 ($p<0.001$).

3.2.2.4 Stimulation of J774A.1 Macrophage with M1 Polarising Factors, 20ng/mL IL-4/TGFβ and 100ng/mL LPS and 100mM PGE2 does not Affect Cell Viability.

Protaglanden E2 (PGE2) is an immunoregulatory molecule produced by the enzymatic conversion of Arachadonic Acid by Cyclooxygenase 2 (COX2). PGE2 and LPS stimulation is known to induce immunoregulatory phenotypes in macrophage characterized by high IL-10 and low TNFα secretion (Montero et al., 2016; Treffkorn et al., 2004). J774A.1 macrophage were seeded at $1x10^6$ cells/mL. Cells were stimulated with M1 polarising molecules 20ng/mL IFNγ and 100ng/mL LPS, M2 polarising factors 20ng/mL IL-4 and 20ng/mL TGFβ and 100ng/mL LPS and 100mM PGE2. As illustrated in supplementary figure SF1.3, cell viability is not significantly affected by stimulation with the afore mention factors.

3.2.2.5 100ng/mL LPS and 100mM PGE2 Suppresses Secretion of M1 Related Cytokines and Drives Secretion of M2 Associated IL-10.

J774A.1 macrophage were seeded at $1x10^6$ cells/mL. Cells were stimulated with M1 polarising molecules 20ng/mL IFNγ and 100ng/mL LPS, M2 polarising factors 20ng/mL IL-4 and 20ng/mL TGFβ and 100ng/mL LPS and 100mM PGE2. Stimulated cells were cultured for 24hr at 37°C in 5% CO_2. Concentrations of IL-1β, IL-6, TNFα and IL-10 were quantified using specific ELISA duosets. As outlined in figure 3.11, 100ng/mL LPS and 20ng/mL IFNγ drives secretion of pro-inflammatory IL-1β, IL-6, and TNFα, with some IL-10 induction. Conversely stimulation with M2 polarising factors 20ng/mL IL-4 and 20ng/mL TGFβ leads to the generation of a typical M2 phenotype characterised by comparaitvely high secretion of IL-10 and low IL-1β, IL-6, and TNFα. Interestingly, co-stimulation with 100ng/mL LPS and 100mM PGE2 negates the known pro-inflammatory effects of LPS. There was no significant change in IL-1β, IL-6, and TNFα secretion compared to the M2 stimulated cells. IL-10 secretion was significantly enhanced by LPS and PGE2 ($p<0.001$). Taken together, it has been determined that LPS and PGE2 co-stimulation induces an M2 like cytokine secretion profile in J774A.1 macrophage, as illustrated figure 3.8.

3.2.2.6 100ng/mL LPS and 100mM PGE2 Suppresses Secretion of M1 maker Nitric Oxide

J774A.1 macrophage were seeded at $1x10^6$ cells/mL. Cells were stimulated with M1 polarising molecules 20ng/mL IFNγ and 100ng/mL LPS, M2 polarising factors 20ng/mL IL-4 and 20ng/mL TGFβ and 100ng/mL LPS and 100mM PGE2. Stimulated cells were cultured for 24hr at 37°C in 5% CO_2. Nitric oxide concentrations were determined using the Greiss Reagent assay system as previously described. As illustrated in Figure 3.9, LPS and PGE2, suppressed the secretion of M1 associated Nitric oxide. However, there was a significant increase in nitric oxide secretion in the LPS and PGE2 stimulated cells and the M2 stimulated cells ($p<0.01$). The secretion of nitric oxide in LPS and PGE2 stimulated cells is higher than the unstimulated cells and the M2 stimulated cells, which is uncharacteristic for an M2 phenotype.

3.2.2.7 100ng/mL LPS and 100mM PGE2 Fails to Drive the Activity of M2 Specific Marker Arginase 1

J774A.1 macrophage were seeded at $1x10^6$ cells/mL. Cells were stimulated with M1 polarising molecules 20ng/mL IFNγ and 100ng/mL LPS, M2 polarising factors 20ng/mL IL-4 and 20ng/mL TGFβ and 100ng/mL LPS and 100mM PGE2. Stimulated cells were cultured for 24hr at 37°C in 5% CO_2. Arginase 1 activity was determined using the Arginase Activity Assay as previously described in section 2.2.7. 20ng/mL IL-4 and 20ng/mL TGFβ, induced the activity of Arginase 1 (Figure 3.10). Conversely M1 polarised cells, did not exhibit the same upregulated activity. No obeservable change was observed between M1 stimulated cells and LPS and 100mM PGE2 stimulated cells. There was a significant difference in Arginase 1 activity between the M2 stimulated cells and LPS and 100mM PGE2 stimulated cells ($p<0.001$).

3.2.2.8 M1 (20ng/mL IFNγ and 100ng/mL LPS) and M2 (20ng/mL IL-4 and 20ng/mL TGFβ) Polarised Cells Exhibit differential Surface Marker Profiles Consistent with Each Phenotype

J774A.1 macrophage were seeded at $1x10^6$ cells/mL. Cells were stimulated with M1 polarising molecules 20ng/mL IFNγ and 100ng/mL LPS, M2 polarising factors 20ng/mL IL-4 and 20ng/mL TGFβ. Stimulated cells were cultured for 24hr at 37°C in 5% CO_2. Naïve and polarised cells were stained with antibodies against TLR4, MHCII, CD80, CD86, CD14, CD40, Ly6C and Dectin-1. Analysis of cell markers showed that TLR4 ($p<0.05$), MHCII ($p<0.01$), [CD80, CD86, CD14, CD40 and Ly6C] ($p<0.001$) were all elevated in the M1 polarised macrophage compared to the M2 macrophage, as represented in Figure 3.15. M2 macrophage expressed lower levels of co-stimulatory molecules compared to the unstimulated control and the M2 polarised macrophage. Dectin-1, an M2 marker, was also upregulated in M2 polarised macrophage compared to M1 macrophage ($p<0.001$). Interestingly, M2 macrophage expressed MHCII higher than the unstimulated, naïve macrophage. It has been documented in previous studies that M2 macrophage can also express MHCII, despite the fact expression of MHCII is more strongly associated with an inflammatory phenotype. Due to the inflammatory nature of M1 macrophage, and the role they play in driving both innate the adaptive immune, and the contrasting function of M2

macrophage, the results illustrated in figure 3.11 are consistent with the known functions and characteristics of both M1 and M2 polarised macrophage.

3.2.2.9 J774A.1 macrophage do not secrete key inflammatory cytokines, IL-12p40 and IL-23

IL-12p40 and IL-23 are key members of the IL-12 family of inflammatory cytokines. Previous data (not presented in this thesis) generated by the Immunomodulation Research Group has indicated 100ng/mL LPS can induce expression of high levels of IL-12p40 and IL-23 in several immune cell types. In order to assess whether J774A.1 macrophage are capable of secreting IL-12p40 and IL-23, a dose response of *E.coli* LPS was performed in J774A.1 macrophage. J774A.1 macrophage were incubated with the following concentrations of LPS; 0ng/mL, 100ng/mL, 250ng/mL, 500ng/mL, 750ng/mL and 1μg/mL. Cells were subsequently incubated for 24hr at 37°C in 5% $CO_{2.}$ Specific cytokine concentrations were determined using specific ELISA kits for IL-12p40, IL-23 and IL-27p28 (R&D). Cell viability was also assessed using CellTiter® Aqueous One Solution cell proliferation assay. Varying doses of LPS did not negatively impact cell viability of J774A.1 macrophage, illustrated in supplementary figure SF1.4. J774A.1 macrophage secrete low levels of IL-27p28, and this was affected in a dose dependant manner as illustrated in figure 3.12. IL-12p40 secretion was only induced at super physiological concentrations of LPS at 750ng/mL and 1μg/mL. Even at these LPS concentrations, cytokine secretion is very low and is expected to be in the range of 10^3-10^4pg/mL. Similarly, IL-23 expression was only induced on the higher end of the LPS dose spectrum, but to only very low levels.

3.2.3 Isolation and Polarisation of Primary Bone Marrow Derived Macrophage:

Due to the potential application of these bioactive hydrolysates in nutritional strategies to support athletes and the ageing population, it is important that the *in vitro* screening process is as physiologically relevant as possible. With this in mind, assessing hydrolysate activity in primary derived cells is essential. Additionally, an integral part of this study, will be to determine whether it is possible to overcome the limitations of the J774A.1 polarisation mode, namely secretion of the IL-12 family cytokines; IL-12p40 and IL-23, and previously discussed issues with IL-10 secretion variability. In this study, murine Bone Marrow Derived Macrophage (BMDM) were isolated from femoral and tibial bone marrow from 6 to 8 week old Balb/c mice. These mice were housed in an SPF environment. Raw bone marrow was isolated as previously described, in a class II laminar flow hood, under aseptic conditions. Isolated bone marrow cells were cultured in RPMI growth medium supplemented with 25ng/mL recombinant M-CSF. BMDMs were polarised to an M1 phenotype 20ng/mL IFNγ and 100ng/mL LPS, and to an M2 phenotype using 20ng/mL IL-4 and 20ng/mL IL-13, due to the known increased sensitivity of primary cells over established cell lines.

3.2.3.1 Isolated Bone Marrow Derived Macrophage Express Key Surface Markers of the Macrophage Lineage F4/80 and CD11b while Isolated Bone Marrow Dendritic Cells do not.

Bone marrow from 6-8 week old Balb/C female mice was isolated as previously described. Bone marrow progenitor cells were cultured for 7 days in the presence of 25ng/mL M-CSF to drive Macrophage and 50ng/mL GM-CSF to drive Dendritic cells. Following cell culture and differentiation, cells were scrapped and collected for flow cytometry analysis. Cells were stained with antibodies against CD11b, CD11c and F4/80. Flow cytometry data was analsyed using FlowJo software. Bone marrow progenitor cells cultured in 25ng/mL M-CSF expressed high levels of CD11b and F4/80, represented in figure 3.18. CD11c expression was also observed (figure 3.19). Bone marrow progenitor cells cultured in 50ng/mL GM-CSF, in contrast, expressed no F4/80, similar levels of CD11b (supplementary figure SF1.5) and increased levels of CD11c (supplementary figure SF1.6). Cells exhibiting the following profile, **$CD11b^{+}CD11c^{+}F4/80^{+}$** are indicative of cells beloning to the macrophage lineage. Bone marrow derived dendritic cells express CD11c and do not express F4/80. Thus the **$CD11b^{+}CD11c^{Hi}F4/80^{-}$** are dendritic cells. These differences in surface marker expression, induced by the different growth factors in the two primary derived lineages, allow for confirmation that isolation and culture of a primary macrophage cell line has occurred successfully.

3.2.3.2 Varying doses of IFNγ, IL-4 and TGFβ do not negatively impact of BMDM viability

BMDMs were seeded at $1x10^{6}$ cells/mL. Cells were subsequently stimulated with M1 and M2 polarising factors at concentrations ranging from 10ng/mL to 100ng/mL. Cell viability was assessed using the the CellTiter® Aqueous One Solution cell proliferation assay. A negative control, of 10% DMSO in DMEM was used to induce cell death. Neither M1 or M2 polarisation factors, at each of the varying doses, had a negative impact on cell viability in BMDMs as presented in supplementary figure SF1.7.

3.2.3.4 Stimulation of BMDMs with M1 Polarising factors affects cytokine secretion in a dose dependant manner

BMDMs were seeded at $1x10^6$ cells/mL. Cells were subsequently stimulated with LPS and IFNγ at concentrations ranging from 10ng/mL to 100ng/mL. Stimulated cells were cultured for 24hr at 37°C in 5% CO_2. Concentrations of IL-1β, IL-6, IL-12p40, IL-23,TNFα, and IL-10 were quantified using specific ELISA duosets. Expression of inflammatory cytokines was induced relative to the control(unstimulated BMDMs) at all doses of IFNγ in the presence of 100ng/mL LPS, as illustrated in figure 3.13. At doses of 50ng/mL IFNγ, the highest induction of inflammatory cytokines is observed. However, in all cases, the margin of error seems to be greater than that observed in the other doses. IL-10 secretion was unaffected at all doses of IFNγ. Thus, 20ng/mL IFNγ in the presence of 100ng/mL LPS will continue to be used for M1 polarisation of BMDMs *in vitro* .

3.2.3.5 Stimulation of BMDMs with M2 Polarising factors affects cytokine secretion in a dose dependant manner

BMDMs were seeded at $1x10^6$ cells/mL. Cells were subsequently stimulated with LPS and IFNγ at concentrations ranging from 10ng/mL to 100ng/mL. Stimulated cells were cultured for 24hr at 37°C in 5% CO_2. Concentrations of IL-1β, IL-6, IL-12p40, IL-23, TNFα, and IL-10 were quantified using specific ELISA duosets (R&D). Data is presented in figure 3.14. IL-4 and TGFβ did not induce expression of IL-6, IL-12p40 and TNFα. IL-4 and TGFβ treatment, decreased expression of IL-1β, and IL-23 in a dose dependant manner. IL-10 secretion was negatively affected at doses of 50ng/mL and 100ng/mL IL-4 and TGFβ. IL-10 concentrations were relatively unaffected at the lower doses of 10ng/mL and 20ng/mL.

3.2.3.6 Polarised BMDMs exhibit differential cytokine profiles consistent with M1 and M2 macrophage phenotypes.

BMDMs were seeded at $1x10^6$ cells/mL. Cells were subsequently stimulated with M1 and M2 polarising factors as previously described. Extrapolated from the dose response experiments previously mentioned, 100ng/mL LPS and 20ng/mL IFNγ will continue to be used for M1 polarisation. BMDMs treated in this way secrete high levels of inflammatory IL-1β, IL-6, IL-12p40, IL-23 and TNFα. IL-10 secretion remained unchanged relative to the control. M2 polarisation dose response experiments revealed that, 20ng/mL IL-4 and 20ng/mL TGFβ may be sufficient to drive an M2-like phenotype in BMDMs This is indicated through maintained expression of IL-10 and crucially low levels of pro-inflammatory markers. Naïve BMDMs share a broadly similar cytokine profile to M2-like polarised BMDMs. Differences occur due to small increases in IL-1β, IL-6, IL-12p40, IL-23 and TNFα secretion in M2-like polarised macrophage. Naïve, M1 and M2-like polarised cytokine profiles are illustrated in figure 3.15.

3.2.4 Casein Derived Protein Hydrolysates Modulate the Activity of M1 and M2 Polarised J774A.1 Macrophage

3.2.4.1 Casein Derived Protein Hydrolysates do not Negatively Impact the Viability of Polarised J774A.1 Macrophage

J774A.1 macrophage were seeded at $1x10^6$ cells/mL and preincubated with 1mg/mL of casein hydrolysate for 1hr at 37°C in 5% CO_2. Cells were subsequently stimulated with M1 polarising factors 20ng/mL IFNγ and 100ng/mL LPS, and M2 polarising factors 20ng/mL IL-4 and 20ng/mL IL-13. As a negative control, cells were incubated in 10% DMSO to induce cell death. Cell viability was determined using the CellTiter® Aqueous One Solution cell proliferation assay. As illustrated in supplementary figure SF1.8, stimulation with candidate samples did not adversely affect the viability of the naïve, M1 and M2 stimulated J774.1 macrophage

3.2.4.2 Casein Derived Protein Hydrolysates Modulate the Expression of Specific Cytokines in Naïve J774A.1 Macrophage.

In order to determine whether caesin hydrolysates could modulate M1 and M2 differentiation, we first examined their effect on naïve unpolarised macrophages. J774A.1 macrophage were seeded at $1x10^6$ cells/mL and preincubated with 1mg/mL of individual casein hydrolysates or the whole parent protein control for 1hr at 37°C in 5% CO_2. Concentrations of IL-1β, IL-6, TNFα and IL-10 were quantified using specific ELISA duosets. As represented in figure 3.16, levels of both inflammatory and anti-inflammatory markers were increased following stimulation with 1mg/mL casein derived protein hydrolysate compared to both the unstimulated control and the whole parent protein controls (NaCN). Significant increases were seen in IL-1β and TNFα following treatment with sample 2-29 ($p<0.05$), which also increased IL-6 secretion. IL-10 was significantly downregulated in response to sample 2-29 ($p<0.05$). In many cases, hydrolysates that drove production of inflammatory cytokines also drove the production of IL-10. This suggests that there is no specific pro or anti-inflammatory bioactivity for several samples such as 2-21 and 2-30.

3.2.4.3 Casein Derived Protein Hydrolysates Exhibit Anti-Inflammatory Bioactivities in M1 Polarised J774A.1 macrophage.

J774A.1 macrophage were seeded at $1x10^6$ cells/mL and preincubated with 1mg/mL of casein hydrolysate for 1hr at 37°C in 5% CO_2. Cells were subsequently polarised to an M1 phenotype using 20ng/mL IFNγ and 100ng/mL LPS. Concentrations of IL-1β, IL-6, TNFα and IL-10 were quantified using specific ELISA duosets. Data is illustrated in Figure 3.17. Regarding IL-1β, in all cases excluding sample 2-28, IL-1β was suppressed in M1 polarised macrophage. IL-6 and TNFα secretion was also suppressed significantly in many cases. Significant increases in IL-10 were also observed, particularly with samples 2-18 ($p<0.01$), 2-21 ($p<0.001$), 2-22 ($p<0.001$), 2-23 ($p<0.05$) and 2-30 ($p<0.05$). This suppression of inflammatory cytokines with corresponding increases in anti-inflammatory IL-10 highlight the anti-inflammatory, immunomodulatory potential of these hydrolysates. However, in the case of sample 2-132, suppression in IL-1β, IL-6 ($p<0.001$) and TNFα secretion was observed. IL-10 secretion was unaffected by 2-132 stimulation. This effect is also indicative of anti-inflammatory bioactivity.

3.2.4.4 Casein Derived Protein Hydrolysates Modulate the Expression of Specific Cytokines in M2 Polarised J774A.1 Macrophage.

J774A.1 macrophage were seeded at $1x10^6$ cells/mL and preincubated with 1mg/mL of casein hydrolysate for 1hr at 37°C in 5% CO_2. Cells were subsequently polarised to an M2 phenotype using 20ng/mL IL-4 and 20ng/mL IL-13. Concentrations of IL-1β, IL-6, TNFα and IL-10 were quantified using specific ELISA duosets (R&D). As illustarted in figure 3.18, similar to the naïve J774A.1 macrophage, casein derived hydrolysates and the whole parent control differentially affected the secretion of pro-inflammatory cytokines compared to the unstimulated and M2 controls. Of note however, is that in most cases, IL-10 secretion was maintained or enhanced, significantly in the case of 2-30 ($p<0.01$). This suggests, that this panel of casein derived hydrolysates may be beneficial in maintaining the activity of M2 anti-inflammatory macrophage.

3.2.4.5 Casein Derived Protein Hydrolysates do not Negatively Impact the Viability of Polarised alternately polarised M2 J774A.1 Macrophage

We also examined the effect of the caesin hydrolysates on M2 macrophages when they were polarised using the alternative factors IL-4 and TGFβ. J774A.1 macrophage were seeded at $1x10^6$ cells/mL and preincubated with 1mg/mL of casein hydrolysate for 1hr at 37°C in 5% CO_2. Cells were subsequently stimulated with M2 polarising factors 20ng/mL IL-4 and TGFβ. As a negative control, cells were incubated in 10% DMSO to induce cell death. Cell viability was determined using the CellTiter® Aqueous One Solution cell proliferation assay. As presented in supplementary figure SF1.9, in all but two cases, stimulation with candidate samples did not adversely affect the viability of M2 stimulated J774.1 macrophage, . Samples 2-28 and 2-30, in combination with 20ng/mL IL-4 and TGFβ, appear to have cytotoxic effects in J774A.1 macrophage.

3.2.4.6 Casein Derived Protein Hydrolysates Modulate the Expression of Key Cytokines in Alternatively M2 polarised J774A.1 Macrophage

We next examined the effect of the caesin hydrolysates on cytokines sdecretion from alternatively activated M2 macrophages. J774A.1 macrophage were seeded at $1x10^6$ cells/mL and preincubated with 1mg/mL of casein hydrolysate for 1hr at 37°C in 5% CO_2. Cells were subsequently polarised to an M2 phenotype using 20ng/mL IL-4 and TGFβ. Concentrations of IL-1β, IL-6, TNFα and IL-10 were quantified using specific ELISA duosets (R&D). Data is illustrated in figure 3.19. In many cases, IL-1β secretion was down regulated compared to the M2 and whole protein control (NaCN). IL-6 secretion was differentially upregulated, as observed previously in the IL-4 and IL-13 treated macrophage. TNFα was upregulated in the cases of samples 2-34, 2-84, 2-132, 2-133 and 2-134, however these levels were still lower than that of the untreated control wells. TNFα secretion was down regulated compared to the untreated control cells in the remaining samples compared to the M2 stimulated control. IL-10 secretion was not significantly affected in many cases compared to the M2 stimulated control. There was significant IL-10 down regulation in samples 2-135, 2-27, 2-28, 2-29 and 2-30 ($p<0.001$). However, hydrolysates displayed an opposing effect on IL-10 secretion compared to whole casein (NaCN). Samples 2-34, 2-84, 2-132, 2-133 ($p<0.001$), 2-134 ($p<0.01$) 2-21 ($P<0.001$), 2-22, 2-23, 2-24 ($p<0.05$) and 2-27 ($p<0.001$) increased IL-10 secretion significantly. Hydrolysates appear to have similar effects on IL-4/IL-13 and IL-4/TGFβ polarised M2 J774A.1 macrophage. Thus, these hydrolysates may be beneficial in maintaining the activity of M2 anti-inflammatory macrophage.

3.2.4.7 Casein Derived Hydrolysates Modulate Nitric Oxide Secretion in polarised J774A.1 Macrophage

J774A.1 macrophage were seeded at $1x10^6$ cells/mL. J774A.1 murine macrophage were stimulated with M1 polarising factors 20ng/mL IFNγ and 100ng/mL LPS and M2 polarising factors 20ng/mL IL-4 and 20ng/mL TGFβ in the presence and absence of 1mg/mL casein derived hydrolysate and whole protein control NaCN. Nitrite production was measured using the Greiss Reagent Assay system as previously described in section 2.2.7. As illustrated in figure 3.20, whole casein and the hydrolysates did not induce nitrite production in naïve and M2 polarised macrophage. However, in M1 polarised macrophage, casein derived hydrolysates all significantly ($p<0.001$) down regulated the secretion of nitrite.. Nitrite production, through the activity of the enzyme iNOS, is a hallmark feature of inflammatory M1 macrophage. Thus, reduction in the production of nitrite may correlate to subtle changes in phenotype polarisation of J774A.1 macrophage.

3.2.4.8 Candidate Hydrolysates 2-132, 2-18, 2-21 and 2-22 show potential in modulating Arginase 1 Activity in Naïve and Polarised J774A.1 Macrophage

J774A.1 murine macrophage were stimulated with M1 polarising factors 20ng/mL IFNγ and 100ng/mL LPS and M2 polarising factors 20ng/mL IL-4 and 20ng/mL TGFβ in the presence and absence of 1mg/mL specific casein derived hydrolysate and whole protein control NaCN. Arginase 1 activity was measured as previously described using the Arg1 activity assay kit. Hydrolysates 2-132, 2-18, 2-21 and 2-22 were selected due to their anti-inflammatory potential in M1 and M2 J774A.1 macrophage. As illustrated is figure 3.21, Arginase 1 activity is enhanced in M1 J774A.1 macrophage, specifically with sample 2-132. Sample 2-132 ($p<0.05$) and samples 2-22 were also able to increase Arginase 1 activity in M2 polarised J774A.1 macrophage with NaCN, 2-18 and 2-21 ($p<0.01$, $p<0.001$) suppressing Arginase 1 activity. Arginase 1 activity was moderately enhanced in naïve J774A.1 macrophage. This information adds weight to our evidence that these hydrolysates are anti-inflammatory and can impact on different markers of inflammation and macrophage function and phenotype.

3.2.5 Optimisation of Hydrolysate Incubation in J774A.1 Macrophage

Food for Health Ireland incorporates the workflow from several research groups, across several research institutions. In order to maintain consistency in mining milk derived hydrolysate activity, a standardised sample preparation and stimulation protocol was established. This procedure has been described previously in the Materials and Methods section. This established protocol allows for stimulation of immune cells with 1mg/mL of milk derived hydrolysate for one hour, before stimulation with polarising cocktails. Data presented to this point has used this method. However, it is important that different time points are assessed to ensure that optimal bioactivity from these samples can be observed.

3.2.5.1 Casein Derived Protein Hydrolysates Modulate the Secretion of Cytokines from Naïve J774A.1 Macrophage Over Time

J774A.1 macrophage were seeded at $1x10^6$ cells/mL and stimulated with 1mg/mL of casein hydrolysate for 1hr, 6hr and 12hr at 37°C in 5% CO_2. Concentrations of IL-1β, IL-6, TNFα and IL-10 were quantified using specific ELISA duosets (R&D) as previously described. The data is represented in figure 3.22. No significant changes in cytokine secretion was observed with IL-1β, IL-6, IL-10 and TNFα. Despite this, there are observable changes in cytokine concentrations, as illustrated in figure 3.31. Initially after 1hr, it can be observed that IL-1β and TNFα secretion is suppressed relative to the unstimulated J774A.1s. Concurrently, IL-10 secretion is enhanced in many cases. IL-6 secretion is maintained but there is some increase seen from sample 2-18 through 2-30. After 6hr and 12hr IL-10 levels begin to normalise to the control, with some exceptions. IL-1β, IL-6 and TNFα follow this trend. This may indicate that the hydrolysate has been metabolised extensively by this point.

3.2.5.2 Casein Derived Protein Hydrolysates Modulate the Secretion of Cytokines from M1 Polarised J774A.1 Macrophage Over Time

J774A.1 macrophage were seeded at $1x10^6$ cells/mL and preincubated with 1mg/mL of casein hydrolysate for 6hr and 12hr at 37°C in 5% CO_2. Cells were subsequently polarised to an M1 phenotype using 20ng/mL IFNγ and 100ng/mL LPS as previously described. Concentrations of IL-1β, IL-6, TNFα and IL-10 were quantified using specific ELISA duosets. The data is represented in figure 3.32. To date the effect of hydrolysates on M1 polarisation after 1hr has been eluded to. However, the effect after 6hr and 12hr is still unknown. Previously, it has been observed that these hydrolysates have significant effects on the secretion of IL-6 and TNFα. Although we see significant suppression of IL-6, at 6hr with samples NaCN ($p<0.01$), 2-135 ($p<0.001$) and 2-28 ($p<0.01$), there is loss of the IL-6 suppressive capacity at 6hr and 12hr. No significant suppression of TNFα is observed at 6hr. At 12hr, the only notable suppression is seen with, NaCN ($p<0.01$), 2-135 ($p<0.001$) and 2-28 ($p<0.001$). IL-1β secretion is broadly maintained at 6hr and 12hr, with non-significant increases observed at 12hr with samples 2-133, 2-135 and 2-28. Interestingly, at 6hr IL-10 secretion is suppressed with the exception of samples 2-34, 2-84 and 2-29. Significant IL-10 downregulation at 6hr is observed with sample 2-28 ($p<0.05$). After 12hr IL-10 secretion appears to trend back to the levels seen in the M1 stimulated J774A.1 macrophage. Significant IL-10 down regulation is still observed at 12hr with sample 2-135 ($p<0.05$) and 2-29 ($p<0.05$). Together, the data presented in Figure 3.23, indicates that over time the effect of the hydrolysate is diminished perhaps due to the sample being metabolised by the cells.

3.2.5.3 Re-Stimulation with Casein Derived Protein Hydrolysates at 6hr and 12hr Restores the Anti-Inflammatory Effects in M1 Polarised J774A.1 Macrophage Over Time

J774A.1 macrophage were seeded at $1x10^6$ cells/mL and preincubated with 1mg/mL of casein hydrolysate for 6hr and 12hr at 37°C in 5% CO_2. Upon polarisation to an M1 phenotype using 20ng/mL IFNγ and 100ng/mL LPS, a further does of 1mg/mL of each candidate hydrolysate was administered. Cells were incubated for 24hr at 37°C in 5% CO_2 Concentrations of IL-1β, IL-6, TNFα and IL-10 were quantified using specific ELISA duosets. Outlined in figure 3.24, at 6hr, reintroduction of the hydrolysates at the point of polarisation to an M1 phenotype resulted in suppression of IL-1β (ns). There was selective suppression of IL-6 and TNFα. For example, sample 2-132 suppresses both IL-6 ($p<0.01$) and TNFα (ns). Sample 2-28, significantly suppresses IL-6 ($p<0.001$) and TNFα ($p<0.001$) at 6hr. IL-10 is blanketly suppressed ($p<0.001$) at 6hr. At 12hr there is blanket suppression of IL-1β (ns), IL-6 ($p<0.001$) and TNFα ($p<0.001$). The blanket suppression of IL-10 at 6hr, is somewhat mitigated at 12hr with less significant suppression. Sample 2-34 and 2-132 show the ability to maintain IL-10 levels, an effect previously seen at 1mg/mL stimulation for 1hr (figure 3.24).

3.2.5.4 Casein Derived Hydrolysates at a Concentration of 2mg/mL Modulates Cytokine Secretion in Naïve J774A.1 Macrophage

It has previously been demonstrated that reintroduction of a hydrolysate at the point of polarisation to an M1 phenotype in J774A.1 macrophage restores the ant-inflammatory bioactivity overtime. However, the question remains, is this effect due to the fact there is more hydrolysate present, or is it due to fresh un-metabolised hydrolysate being present? J774A.1 macrophage were seeded at $1x10^6$ cells/mL and stimulated with 2mg/mL of casein hydrolysate for 1hr, 6hr and 12hr at 37°C in 5% CO_2. Concentrations of IL-1β, IL-6, TNFα and IL-10 were quantified using specific ELISA duosets. The data is represented in figure 3.25. With regard to IL-1β, no significant increase was observed at 1hr by any samples. NaCN enhanced IL-1β secretion at 6hr ($p<0.001$) and 12hr ($p<0.001$). At 12hr sample 2-134 ($p<0.001$) and 2-135 ($p<0.05$) increased IL-1β secretion. Although not significant, IL-6 secretion was suppressed by all samples at 1hr except for NaCN. IL-6 levels remained suppressed after 6hr with the exception of NaCN (ns) and 2-28 ($p<0.05$). After 12hr, IL-6 levels remained suppressed with only NaCN ($p<0.001$) and 2-28(ns) driving noticeable increases. IL-10 levels showed no significant change despite some fluctuations. Consistently, samples 2-18 through 2-30, maintained IL-10 expression overtime. Suppression of IL-10 secretion was observed with samples 2-84 through 2-135. As with IL-10, although non-significant, observable changes in TNFα secretion were observed overtime. For example, sample 2-134 suppressed TNFα secretion at all time points. Conversely, sample 2-18 either maintained or enhanced TNFα secretion.

3.2.5.5 Casein Derived Hydrolysates at a Concentration of 2mg/mL Modulates Cytokine Secretion in M1 Polarised J774A.1 Macrophage

J774A.1 macrophage were seeded at $1x10^6$ cells/mL and stimulated with 2mg/mL of casein hydrolysate for 1hr, 6hr and 12hr at 37°C in 5% CO_2. Cells were subsequently polarised to an M1 phenotype using 20ng/mL IFNγ and 100ng/mL LPS as previously described Concentrations of IL-1β, IL-6, TNFα and IL-10 were quantified using specific ELISA duosets. The data is represented in figure 3.26. At 2mg/mL, NaCN significantly increased the secretion of IL-1β and 1hr, 6hr and 12hr pre incubation time points ($p<0.001$). Sample 2-135 and 2-28 showed consistent upregulation at all time points with significant increases at 12hr ($p<0.001$). Significant increase were also observed at 12hr with sample 2-18 ($p<0.001$) and sample 2-29 ($p<0.01$). Sample 2-132 suppressed IL-1β at 12hr ($p<0.05$). 2-132 also suppressed IL-1β at 1hr and 6hr (ns). Significant impacts on IL-6 secretion were also observed across all timepoints. Notably, 2-132 continued to show the same anti-inflammatory effects at 1hr ($p<0.001$), 6hr and 12hr ($p<0.001$). Selective suppression of TNFα was observed at 2mg/mL across all time points. Consistently however samples NaCN (1hr $p<0.001$; 6hr $p<0.05$; 12hr $p<0.001$), 2-132 (1hr $p<0.01$; 6hr ns; 12hr $p<0.01$), 2-135 (1hr $p<0.01$; 6hr $p<0.01$; $p<0.001$) and sample 2-28 (1hr $p<0.05$; 6hr $p<0.05$, 12hr $p<0.001$) demonstrated suppressive effects on TNFα. IL-10 secretion was sporadically effected at all time points with no significant changes being detected. With the exception of sample 2-135 at 6hr, 2-18 at 12hr and 2-30 at 12hr, samples either maintained or suppressed the secretion of IL-10. This fact in combination with the suppressive effect on other cytokines may indicate that at 2mg/mL, samples become immunosuppressive rather than selectively anti-inflammatory as observed at 1mg/mL.

3.2.6 Analysis of Casein Derived and Whey Protein Derived Hydrolysates on M1 and M2 Polarised J774A.1 Macrophage.

Based on the analysis presented above, it is believed that that hydrolysate simulation at 1mg/mL for 1hr prior to polarisation to M1 and M2 phenotypes is the optimal stimulation procedure to determine the bioactive effects of milk derived protein hydrolysates. With this in mind it was decided to screen additional samples, that have previously displayed pro-Th2 characteristics in our other cell screening models. The data presented below comprises of samples derived from both the Whey and Casein fractions of Cows Milk, including regenerate samples from samples of interest determined by previous FHI investigations.

3.2.6.1 Cell Viability Assessment

J774A.1 macrophage were seeded at $1x10^6$ cells/mL and preincubated with 1mg/mL of casein or whey protein hydrolysate for 1hr at 37°C in 5% CO_2. Cells were subsequently stimulated with M1 polarising factors 20ng/mL IFNγ and 100ng/mL LPS, and M2 polarising factors 20ng/mL IL-4 and 20ng/mL TGFβ. As a negative control, cells were incubated in 10% DMSO to induce cell death. Cell viability was determined using the CellTiter® Aqueous One Solution cell proliferation assay. As illustrated in supplementary figure SF1.10, stimulation with candidate samples did not adversely affect the viability of the naïve, M1 and M2 stimulated J774.1 macrophage. Although significant decreases in M1 polarised cells was observed with sample 2-44 ($p<0.01$) and 2-32 ($p<0.05$), viability remains +80% and is consider non-cytotoxic. Sample 2-12 also had a similar affect in M2 polarised cells ($p<0.05$).

3.2.6.2 Casein Derived and Whey Protein Derived Hydrolysates Modulate Cytokine Secretion in Naïve J774A.1 Macrophage

J774A.1 macrophage were seeded at $1x10^6$ cells/mL and preincubated with 1mg/mL of casein and whey protein hydrolysate for 1hr at 37°C in 5% CO_2. Concentrations of IL-1β, IL-6, TNFα and IL-10 were quantified using specific ELISA duosets. Data is represented in figure 3.27. Although there was enhanced secretion of pro-inflammatory IL-1β, IL-6 and TNFα, none of which is statistically significant, levels of pro-inflammatory factors remained low. In Contrast, IL-10 secretion was noticeably enhanced by all samples presented, when compared to the unstimulated control.

3.2.6.3 Casein Derived and Whey Protein Derived Hydrolysates Modulate Cytokine Secretion in M1 Polarised J774A.1 Macrophage

J774A.1 macrophage were seeded at $1x10^6$ cells/mL and stimulated with 1mg/mL of casein and whey protein hydrolysate for 1hr 37°C in 5% CO_2. Cells were subsequently polarised to an M1 phenotype using 20ng/mL IFNγ and 100ng/mL LPS as previously described Concentrations of IL-1β, IL-6, TNFα and IL-10 were quantified using specific ELISA duosets. Data is represented in figure 3.28. Broadly, IL-1β remains unaffected compared to the M1 stimulated control. NaCN ($p<0.001$), 2-12, 2-41, 2-43 and 2-19 exhibit pro-IL-1β characteristics. Full coverage of IL-6 suppression is observed with the exception of NaCN, which has previously demonstrated pro-IL-1β/IL-6 properties. Observable increases in TNFα levels are seen with hydrolysate 2-01, 2-12, 2-41, 2-42, 2-43 and 2-31. Remaining hydrolysates either maintain or suppress TNFα secretion. In relation to IL-10, both casein and whey protein derived hydrolysates maintain or drive IL-10 secretion with the exception of NaCN, 2-25 and 2-32. Significant increases in IL-10 secretion were observed with 2-01 ($p<0.05$), 2-03 ($p<0.01$) and 2-13 ($p<0.05$).

3.2.6.4 Casein Derived and Whey Protein Derived Hydrolysates Modulate Cytokine Secretion in M2 Polarised J774A.1 Macrophage

J774A.1 macrophage were seeded at $1x10^6$ cells/mL and preincubated with 1mg/mL of casein and whey protein derivied hydrolysates for 1hr at 37°C in 5% CO_2. Cells were subsequently polarised to an M2 phenotype using 20ng/mL IL-4 and TGFβ. Concentrations of IL-1β, IL-6, TNFα and IL-10 were quantified using specific ELISA duosets. Data is represented in Figure 3.29. As observed in naïve stimulated J774A.1 macrophage. Samples do not drive the expression of pro inflammatory cytokines. As expected NaCN enhances IL-1β and IL-6 secretion when compared to the M2 stimulated cells. NaCN also down regulates IL-10 ($p<0.01$) and TNFα ($p<0.001$). IL-10 secretion was maintained in many cases. 2-01, 2-03 and 2-10 enhance IL-10 expression while concurrently suppressing IL-1β, IL-6 and TNFα suggesting pro-M2 like properties.

3.2.6.5 Whey Protein (WPC) derived hydrolysate 2-47 and its regenerates do not negatively affect J774A.1 cell viability

Previous work conducted within FHI, identified that sample 2-47 was bioactive across a range of *in vitro* and *in vivo* biological systems outside of the immune space. As a result, the sample was regenerated, either through upscaling of production at an industrial scale or at a smaller scale in an attempt to improve functional aspects such as bioactivity and solubility. Samples 2-151 through 2-154 are the regernated 2-47 sample, here after refered to as regenerates. J774A.1 macrophage were seeded at $1x10^6$ cells/mL and preincubated with 1mg/mL of casein and whey protein derivied hydrolysates 2-47 and its regenerates for 1hr at 37°C in 5% CO_2. Cells were subsequently stimulated with M1 polarising factors 20ng/mL IFNγ and 100ng/mL LPS, and M2 polarising factors 20ng/mL IL-4 and 20ng/mL TGFβ. As a negative control, cells were incubated in 10% DMSO to induce cell death. Cell viability was determined using the CellTiter® Aqueous One Solution cell proliferation assay. There was no significant effect on polarised J774A.1 cell viability (supplementary figure SF1.11).

3.2.6.5 Whey Protein (WPC) derived hydrolysates 2-47 and its regenerates show the ability to modulate the cytokine secretion in naïve J774A.1 macrophage

J774A.1 macrophage were seeded at $1x10^6$ cells/mL and preincubated with 1mg/mL of whey protein hydrolysate for 1hr at 37°C in 5% CO_2. Concentrations of IL-1β, IL-6, TNFα and IL-10 were quantified using specific ELISA duosets. As illustrated in Figure 3.30, there is no significant increase in pro-inflammatory cytokine secretion. IL-10 secretion is maintained by all samples, except for sample 2-153.

3.2.6.6 Whey Protein (WPC) derived hydrolysates 2-47 and its regenerates show the ability to modulate the cytokine secretion in M1 Polarised J774A.1 macrophage

J774A.1 macrophage were seeded at $1x10^6$ cells/mL and preincubated with 1mg/mL of whey protein hydrolysate for 1hr at 37°C in 5% CO_2Cells were subsequently polarised to an M1 phenotype using 20ng/mL IFNγ and 100ng/mL LPS as previously described Concentrations of IL-1β, IL-6, TNFα and IL-10 were quantified using specific ELISA duosets. Significant anti-inflammatory bioactivity were displayed by the 2-47 regenerate samples in M1 polarised cells (figure 3.31). Namely, sample 2-152. 2-152 suppressed the expression of IL-1β ($p<0.01$), IL-6 ($p<0.001$) and TNFα ($p<0.001$) with an associated increase in IL-10 concentrations (ns).

3.2.6.7 Whey Protein (WPC) derived hydrolysates 2-47 and its regenerates show the ability to modulate the cytokine secretion in M2 Polarised J774A.1 macrophage

J774A.1 macrophage were seeded at $1x10^6$ cells/mL and preincubated with 1mg/mL of whey protein hydrolysate for 1hr at 37°C in 5% CO_2Cells were subsequently polarised to an M2 phenotype using 20ng/mL IL-4 and 20ng/mL TGFβ as previously described. Concentrations of IL-1β, IL-6, TNFα and IL-10 were quantified using specific ELISA duosets. Sample 2-47 and its regenerates maintained their anti-inflammatory capacity in M2 polarised J774A.1 cells (figure 3.32). This indicated by suppression of IL-1β, IL-6 and TNFα with maintenance of IL-10 expression. Sample 2-152 continued to suppress IL-1β and IL-6 and increase the secretion of IL-10. IL-6 secretion was unaffected. Taken in combination with data gathered from M1 polarised J774A.1 cells, it can be determined that sample 2-47 and its regenerate have the capacity to be a pro M2 anti-inflammatory ingredient.

3.3 Figures

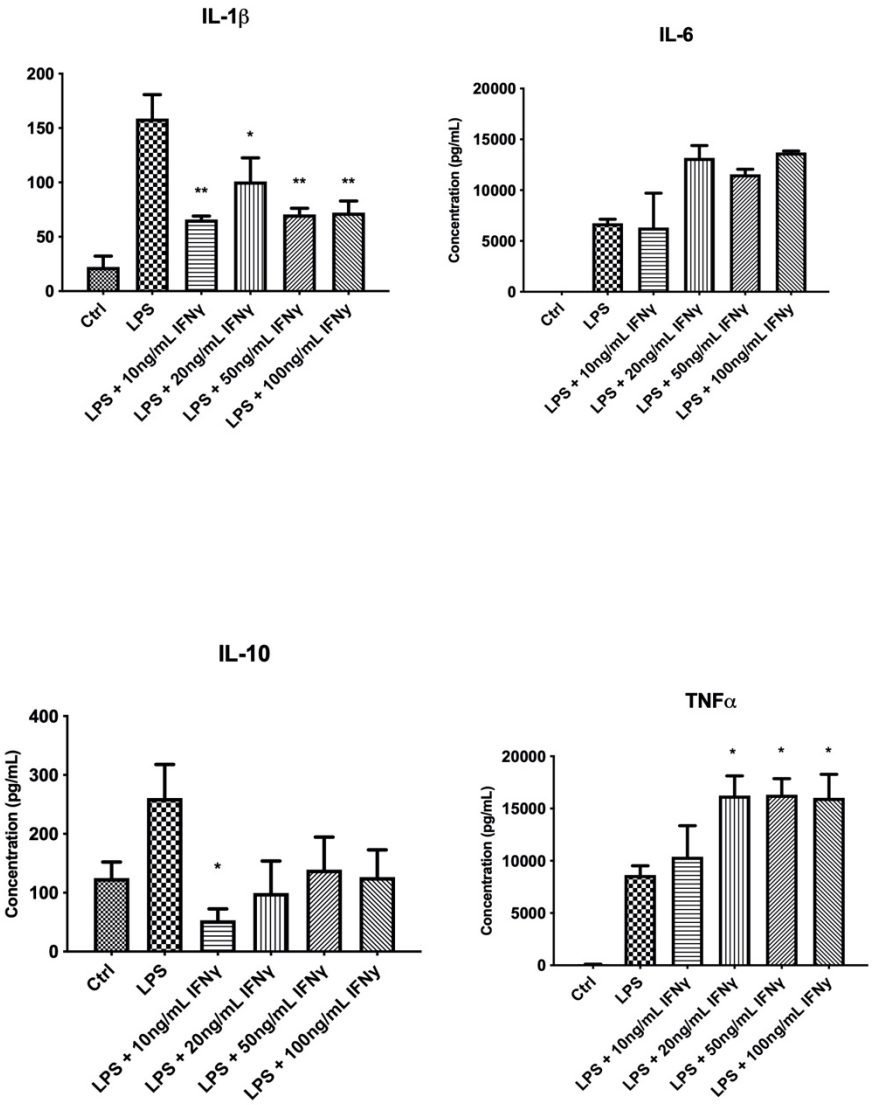


Figure 3.1 - Stimulation of J774A.1 Macrophage with M1 Polarising factors affects cytokine secretion in a dose dependant manner J774A.1 Macrophage were stimulated with 100ng/mL LPS and a dose range of 10ng/mL to 100ng/mL IFNγ. Specific cytokine concentrations were assessed using ELISA kits as previously described in section 2.2.5. Data is presented as mean ± SEM of three replicates. ***p<0.001, **p<0.01, *p<0.05 comparing LPS stimulated cells vs. IFNγ and LPS stimulated cells. Significance was determined using one- way ANOVA with a Newman-Keuls post-test.

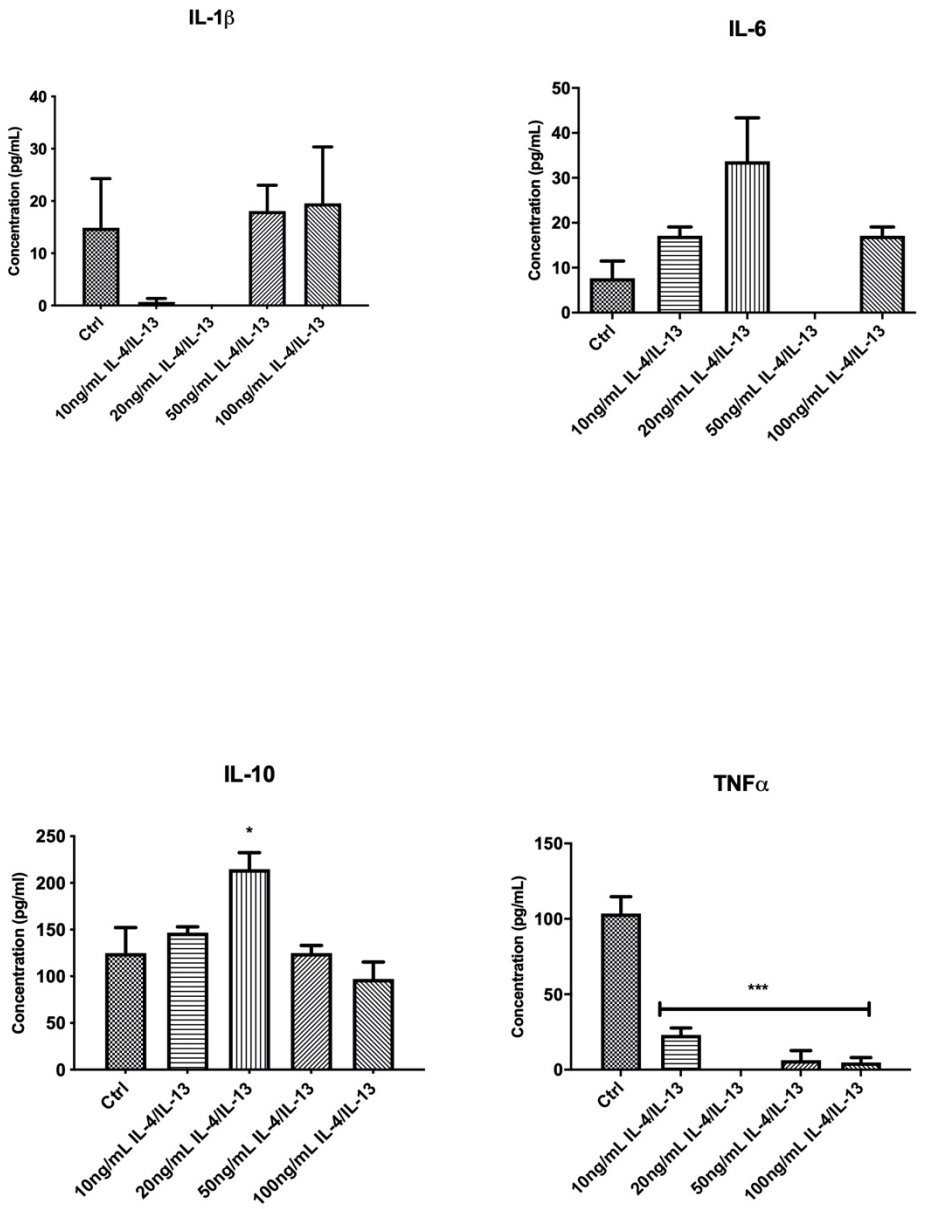


Figure 3.2 - Stimulation of J774A.1 Macrophage with M2 Polarising factors affects cytokine secretion in a dose dependant manner J774A.1 Macrophage were stimulated with and a dose range of 10ng/mL to 100ng/mL IL-4 and IL-13. Specific cytokine concentrations were assessed using ELISA kits as previously described in section 2.2.5. Data is presented as mean ± SEM of three replicates. ***p<0.001, **p<0.01, *p<0.05 comparing the means of each data set. Significance was determined using one- way ANOVA with a Newman-Keuls post-test.

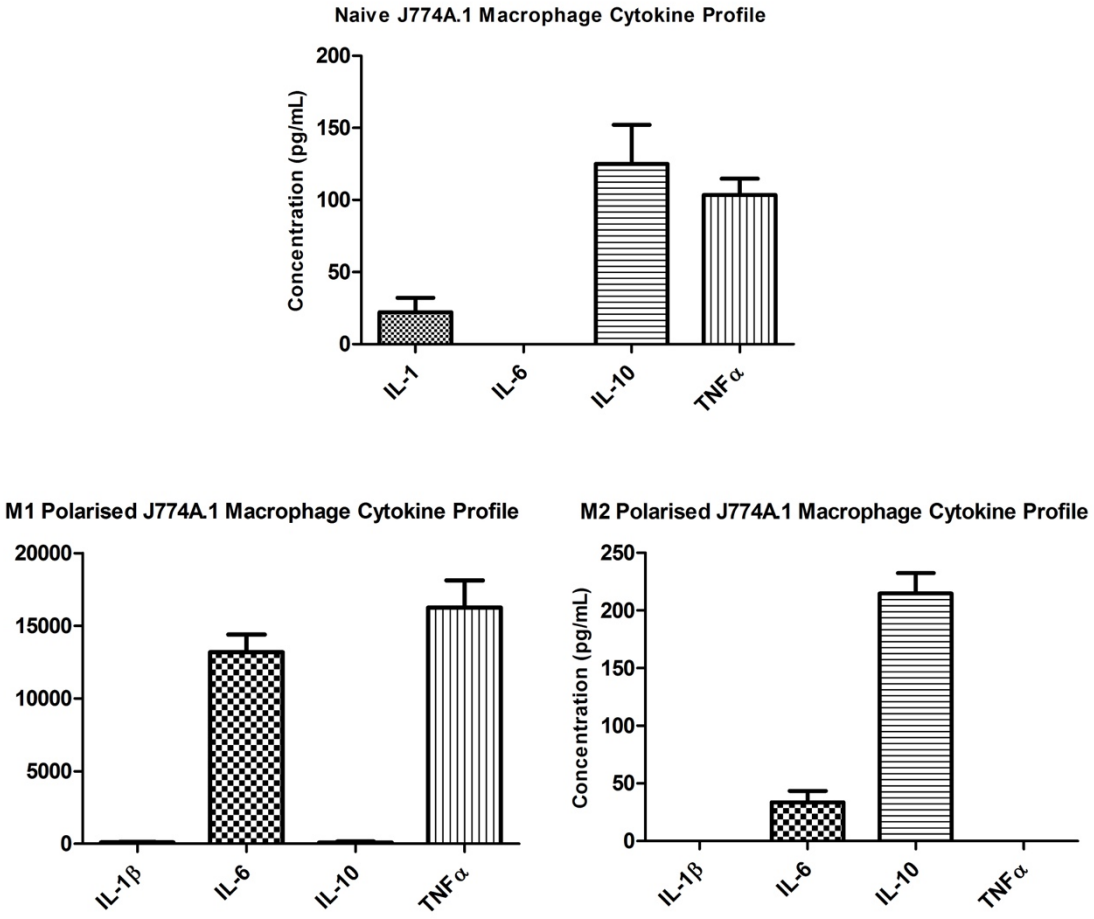


Figure 3.3 - Polarised J774A.1 exhibit a differential cytokine profile. J774A.1 were stimulated with M1 polarising factors 20ng/mL IFNγ and 100ng/mL LPS, and M2 polarising factors 20ng/mL IL-4 and 20ng/mL IL-13 for 24hr at 37°C in 5% CO_2. Polarisation of J774A.1 macrophage to M1 and M2 subtypes elicits differing cytokine profiles, illustrated above, in naïve M1 and M2 polarised macrophage. Data is presented as mean ± SEM of three replicates.

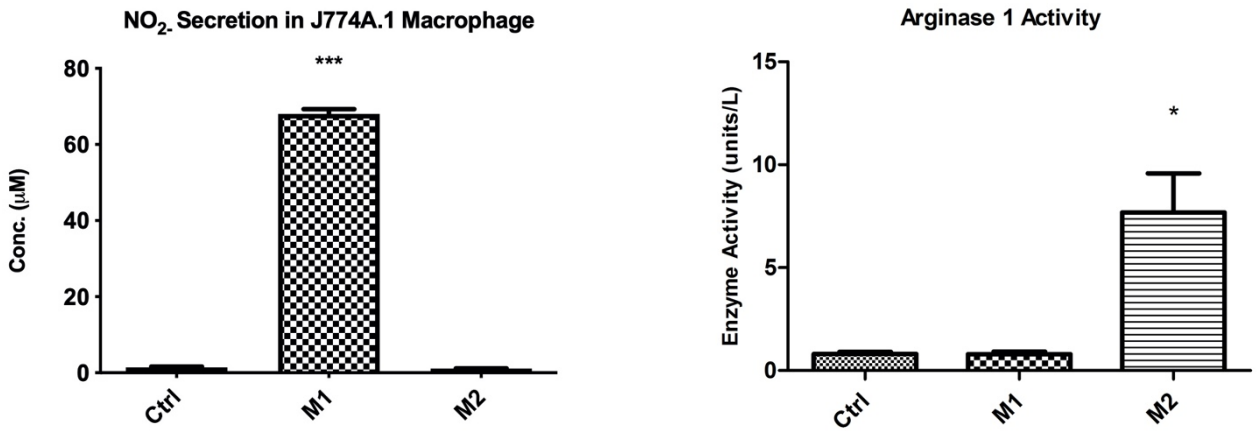


Figure 3.4 - Indicative phenotypic markers of M1 and M2 polarised J774A.1 macrophage. J774A.1 were stimulated with M1 polarising factors 20ng/mL IFNγ and 100ng/mL LPS, and M2 polarising factors 20ng/mL IL-4 and 20ng/mL IL-13 for 24hr at 37°C in 5% CO_2. A) Nitrite production in M1 and M2 polarised cells was determined using the Greiss Reagent system as previously described in section 2.2.6. B) Arginase 1 activity was assessed in M1 and M2 polarised macrophage using the Arginase 1 Activity Kit as previously described in section 2.2.7. Data is presented as mean ± SEM of three replicates. ***p<0.001, **p<0.01, *p<0.05 comparing M1 vs. M2 stimulated cells. Significance was determined using one- way ANOVA with a Newman-Keuls post-test.

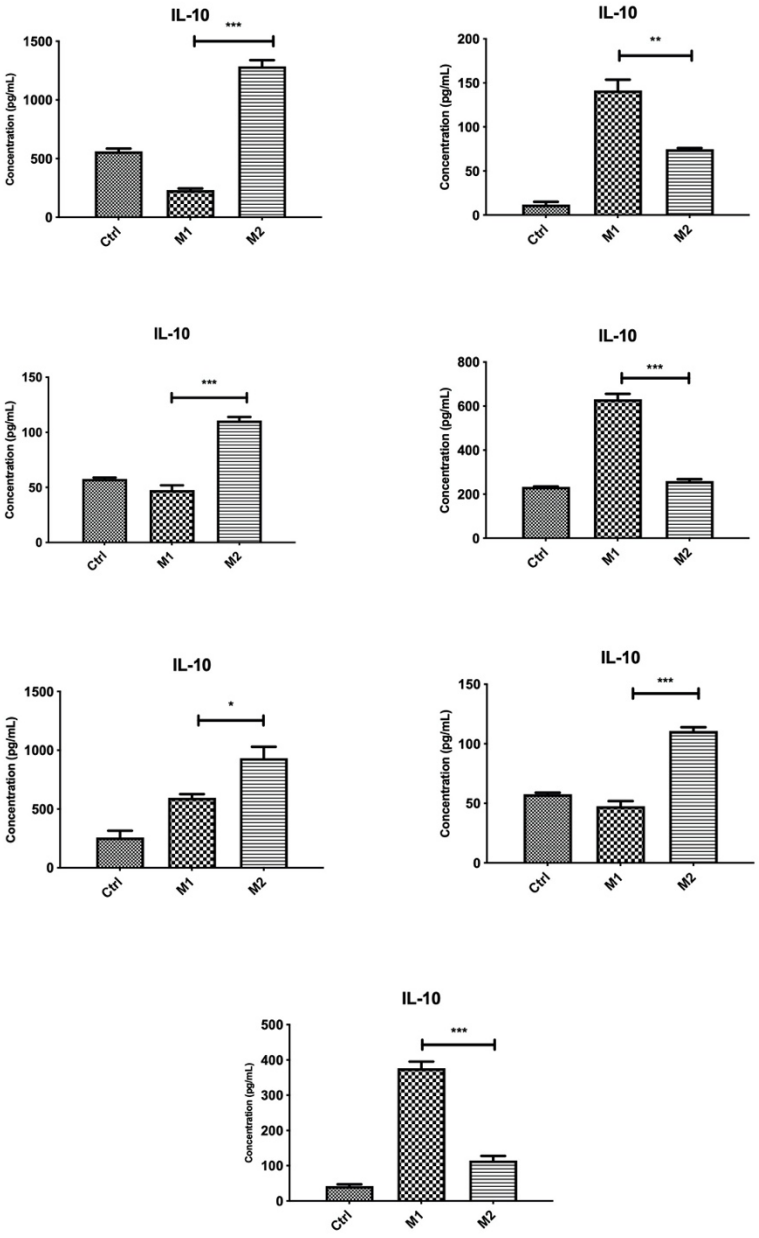


Figure 3.5 – IL-4 and IL-13 Stimulation leads to variability in M2 marker IL-10 secretion J774A.1 macrophage were polarised to a M1 and M2 macrophage phenotype previously described. IL-10 secretion was measured using specific ELISA kits as previously described in section 2.2.5. The above data illustrates the variation in IL-10 expression between M1 and M2 polarised macrophage Data is presented as mean ± SEM of three replicates. . ***p<0.001, **p<0.01, *p<0.05 comparing M1 vs. M2 stimulated cells. Significance was determined using one- way ANOVA with a Newman-Keuls post-test.

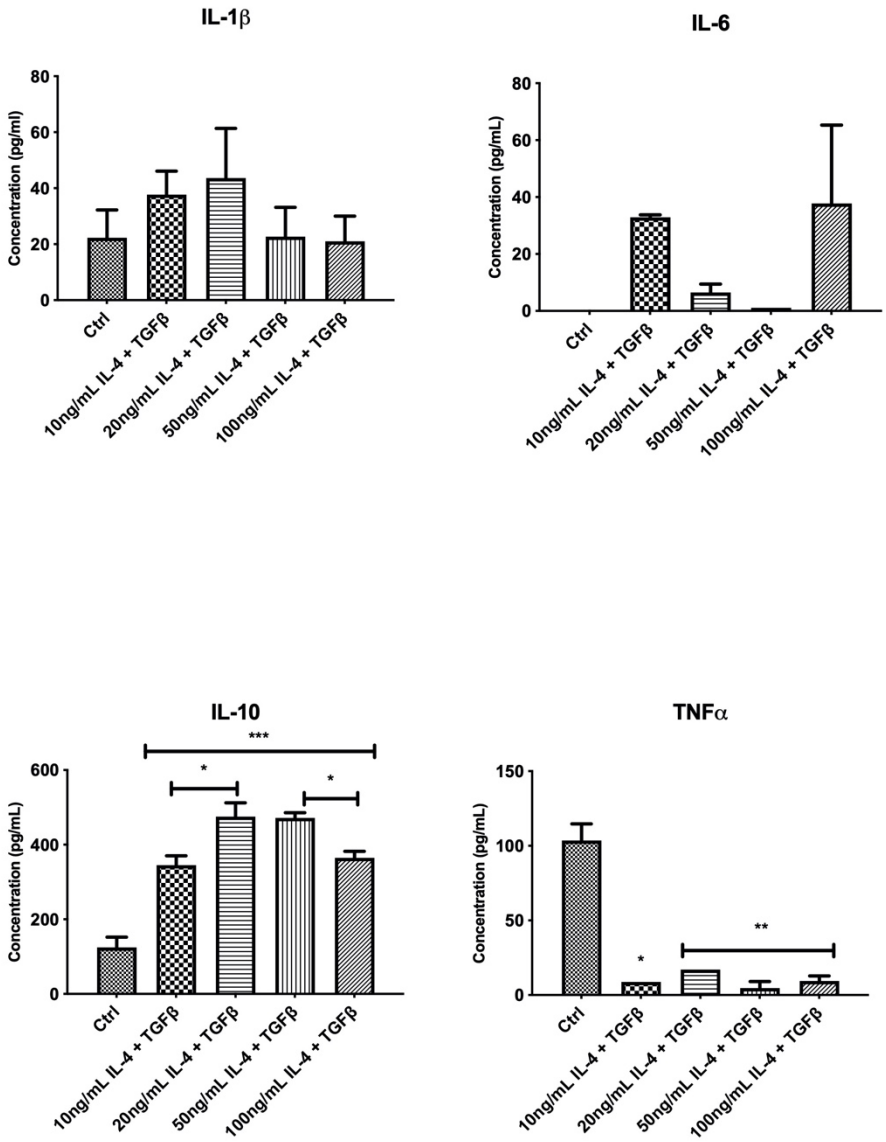


Figure 3.6 - Stimulation of J774A.1 Macrophage with IL-4 and TGFβ affects cytokine secretion in a Dose Dependant Manner J774A.1 Macrophage were stimulated with and a dose range of 10ng/mL to 100ng/mL IL-4 and IL-13. Specific cytokine concentrations were assessed using ELISA kits as previously described in section 2.2.5. Data is presented as mean ± SEM of three replicates. ***p<0.001, **p<0.01, *p<0.05 comparing the means of each data set. Significance was determined using one- way ANOVA with a Newman-Keuls post-test

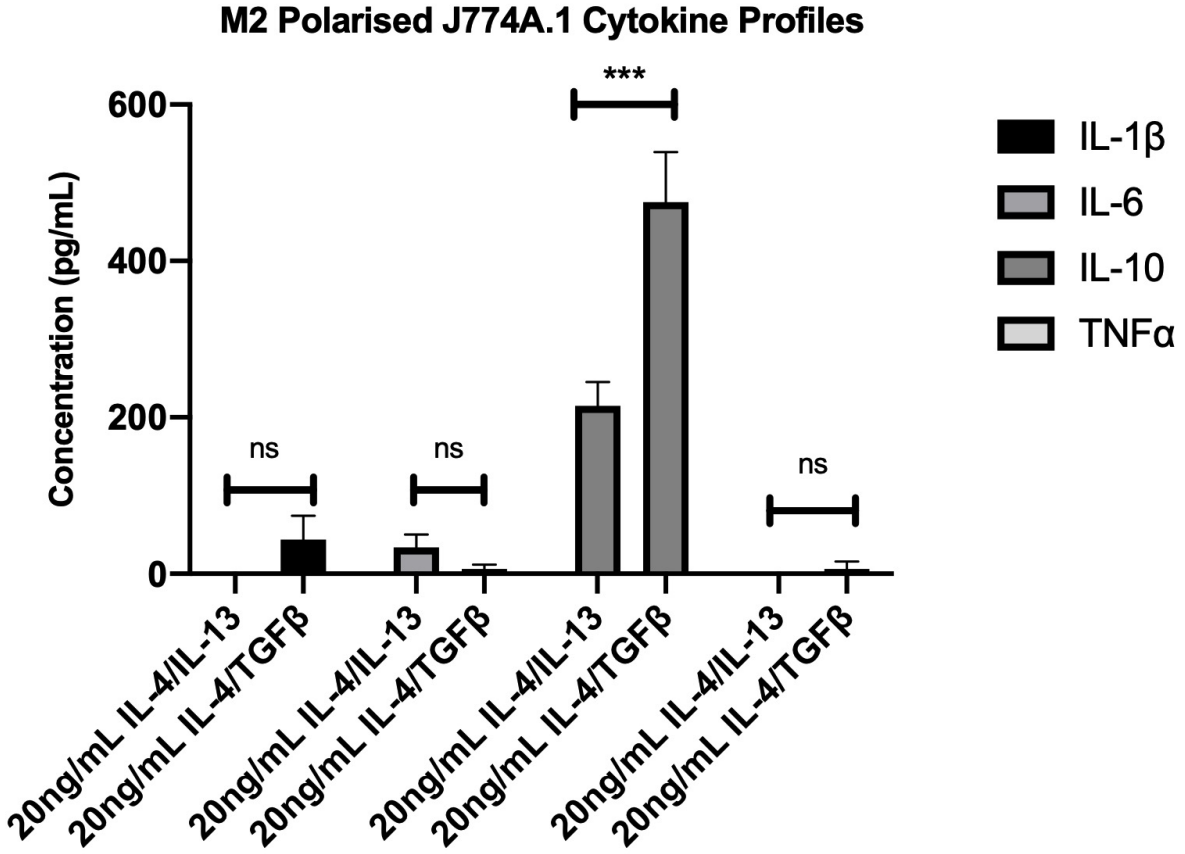


Figure 3.7 - J774A.1 Macrophage polarised with 20ng/mL IL-4/IL-13 or 20ng/mL IL-4/TGFβ display differing M2 cytokine secretome profiles. J774A.1 Macrophage were stimulated with 20ng/mL IL-4/IL-13 and 20ng/mL IL-4/TGFβ Specific cytokine concentrations were assessed using ELISA kits as previously described in section 2.2.5. Data is presented as mean ± SEM of three replicates. ***p<0.001, **p<0.01, *p<0.05 comparing specific cytokine concentrations. Significance was determined using one- way ANOVA with a Newman-Keuls post-test.

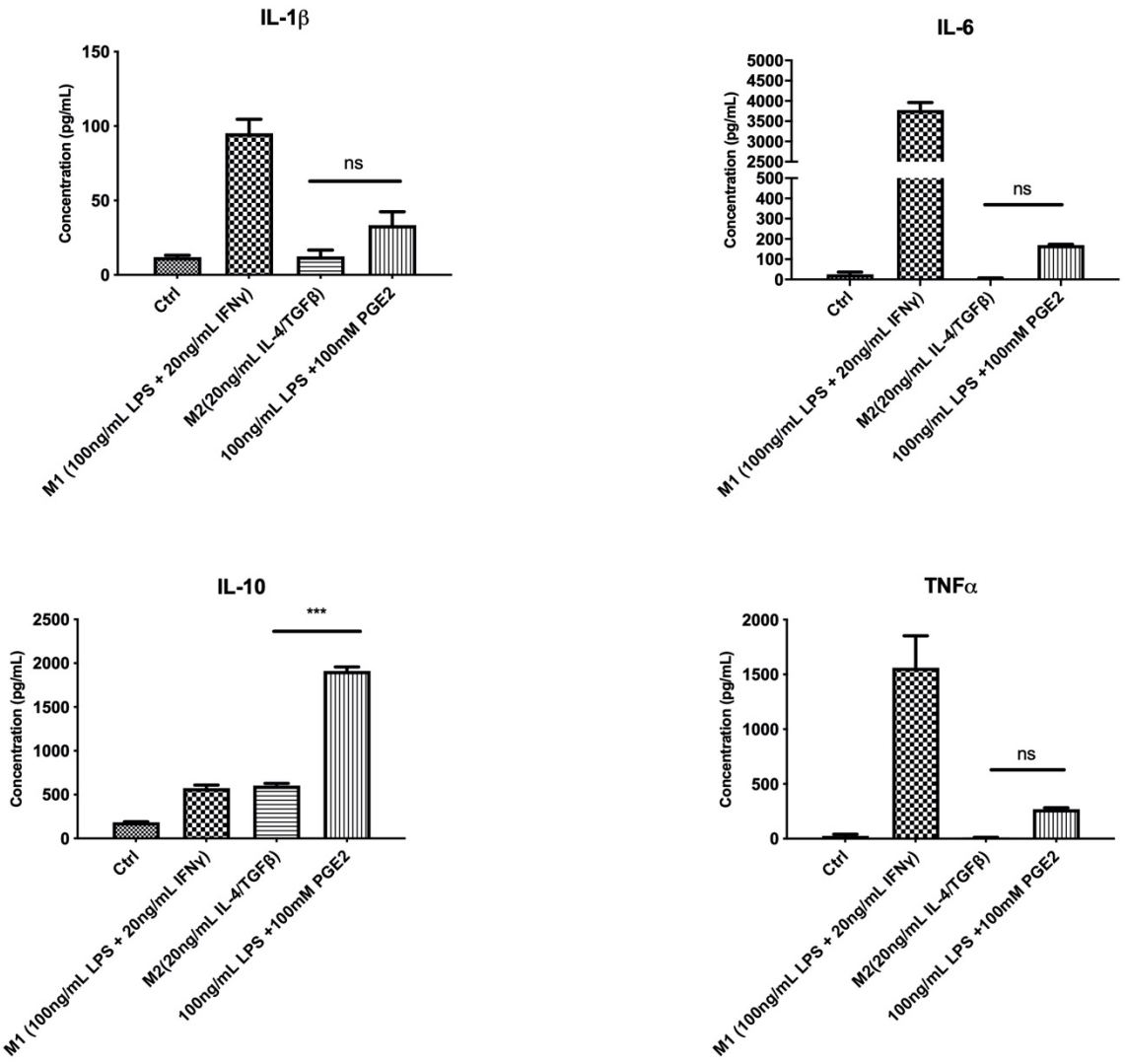
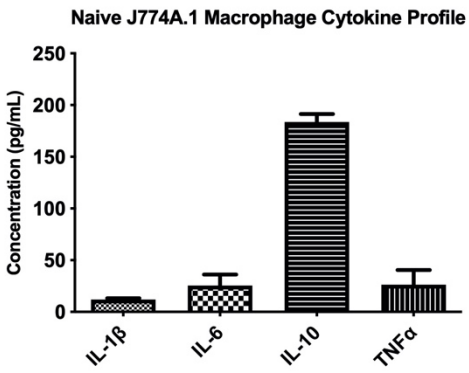
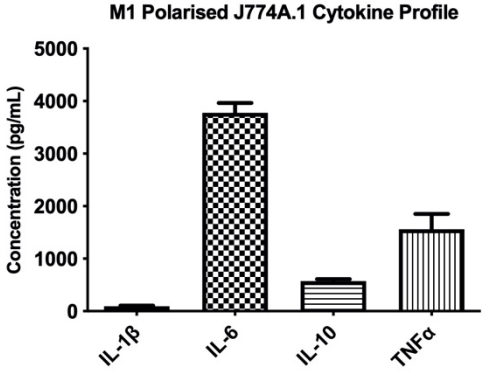
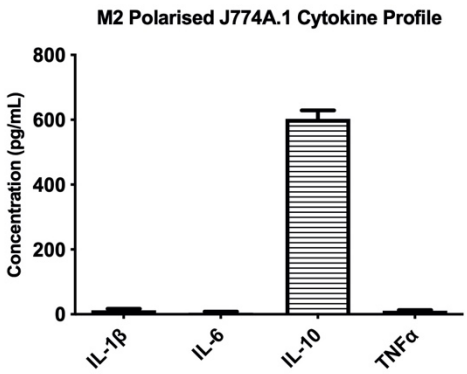
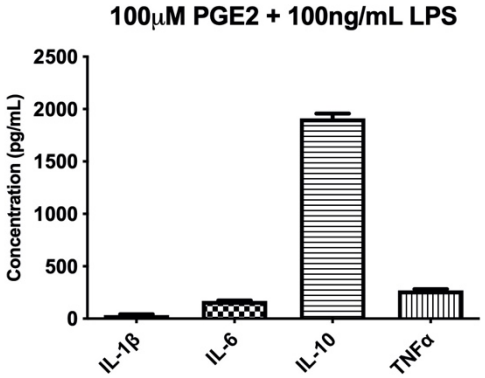


Figure 3.8 - Co-Stimulation with 100mM PGE2 and 100ng/mL LPS Suppresses the Secretion of M1 Associated Cytokines and Drives Expression of M2 Associated IL-10. J774A.1 Macrophage were seeded at $1x10^6$cells/mL and stimulated with M1 polarising factors 20ng/mL IFNγ and 100ng/mL LPS, M2 polarising factors 20ng/mL IL-4 and 20ng/mL TGFβ , and 100mM PGE2 and 100ng/mL LPS for 24hr at 37°C in 5% CO_2. Specific cytokine concentrations were assessed using ELISA kits as previously described in section 2.2.5. Data is presented as mean ± SEM of three replicates. ***p<0.001, **p<0.01, *p<0.05 comparing M2 polarised cells vs. 100mM PGE2 and 100ng/mL LPS stimulated cells. Significance was determined using one-way ANOVA with a Newman-Keuls post-test.









3.9 – Co-Stimulation with 100mM PGE2 and 100ng/mL LPS Gives Rise to an M2-Like cytokine Secretion Profile. J774A.1 Macrophage were seeded at $1x10^6$cells/mL and stimulated with M1 polarising factors 20ng/mL IFNγ and 100ng/mL LPS, M2 polarising factors 20ng/mL IL-4 and 20ng/mL TGFβ , and 100mM PGE2 and 100ng/mL LPS for 24hr at 37°C in 5% CO_2. Specific cytokine concentrations were assessed using ELISA kits as previously described in section 2.2.5. Data is presented as mean ± SEM of three replicates.

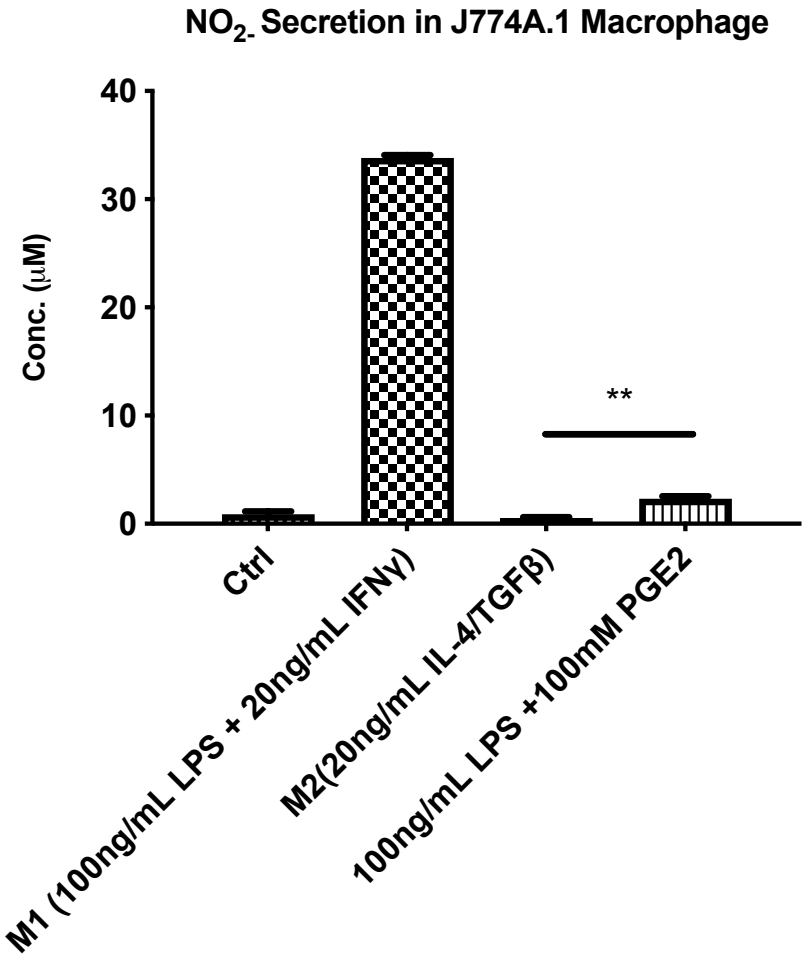


Figure 3.10 - Co-Stimulation with 100mM PGE2 and 100ng/mL Drives a Significant Increase in Nitric Oxide Secretion Compared to M2 Polarised Macrophage. J774A.1 Macrophage were seeded at $1x10^6$cells/mL and stimulated with M1 polarising factors 20ng/mL IFNγ and 100ng/mL LPS, M2 polarising factors 20ng/mL IL-4 and 20ng/mL TGFβ , and 100mM PGE2 and 100ng/mL LPS for 24hr at 37°C in 5% CO_2. Nitric Oxide production in polarised cells was determined using the Greiss Reagent system as previously described in section 2.2.6. Data is presented as mean $\pm$ SEM of three replicates. ***p<0.001, **p<0.01, *p<0.05 comparing M2 polarised cells vs. 100mM PGE2 and 100ng/mL LPS stimulated cells. Significance was determined using one-way ANOVA with a Newman-Keuls post-test.

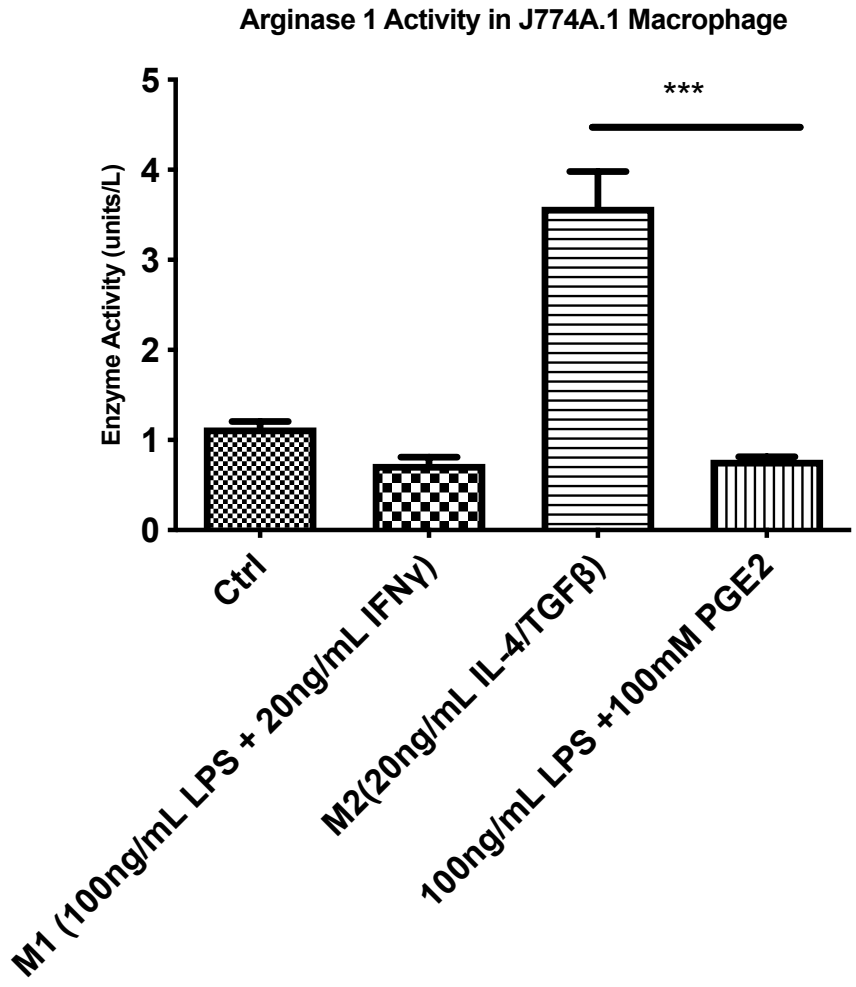


Figure 3.11 - Co-Stimulation with 100mM PGE2 and 100ng/mL LPS Fails to Drive the Activity of M2 Specific Marker Arginase 1. J774A.1 Macrophage were seeded at $1x10^6$cells/mL and stimulated with M1 polarising factors 20ng/mL IFNγ and 100ng/mL LPS, M2 polarising factors 20ng/mL IL-4 and 20ng/mL TGFβ , and 100mM PGE2 and 100ng/mL LPS for 24hr at 37°C in 5% CO_2. Arginase 1 activity was assessed using the Arginase 1 Activity Kit as previously described in section 2.2.7. Data is presented as mean ± SEM of three replicates. ***p<0.001, **p<0.01, *p<0.05 comparing M2 polarised cells vs. 100mM PGE2 and 100ng/mL LPS stimulated cells. Significance was determined using one-way ANOVA with a Newman-Keuls post-test.

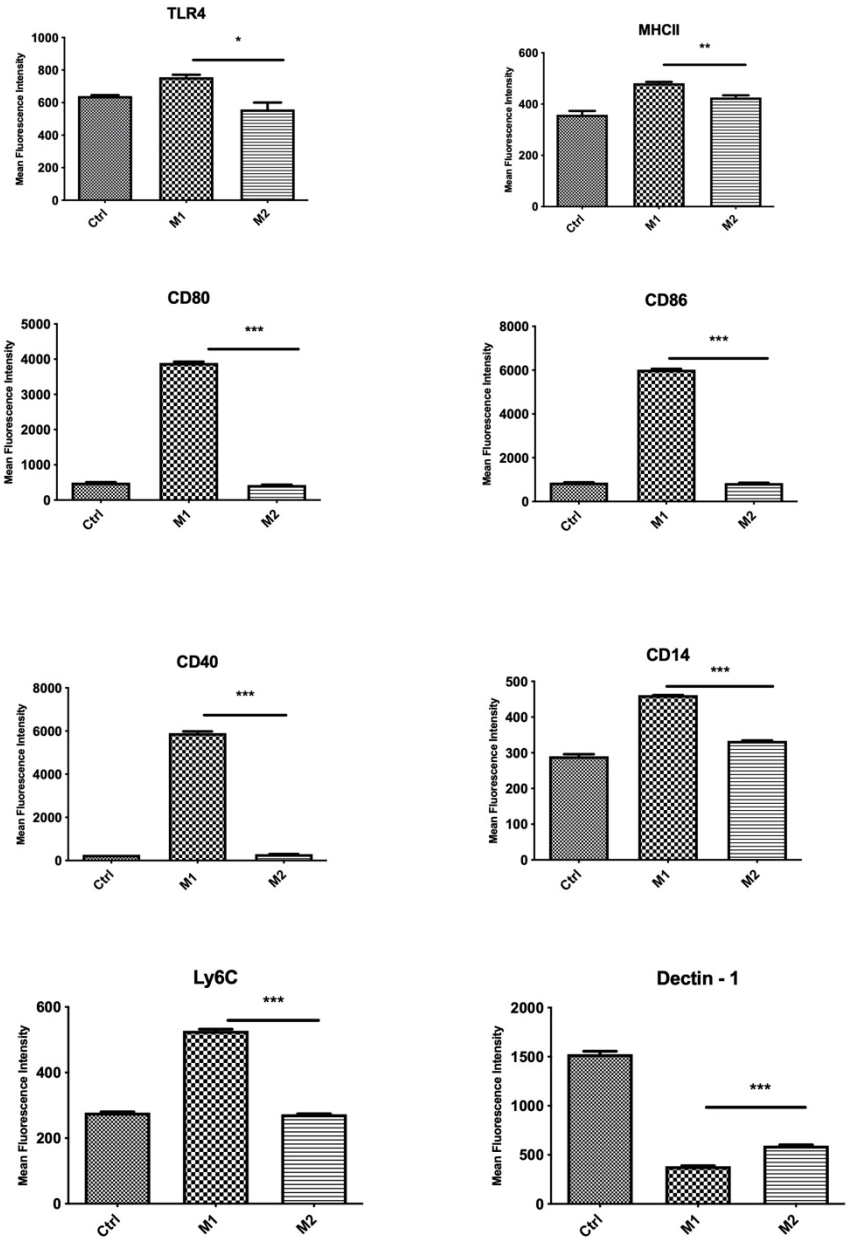


Figure 3.12 - Cell surface marker analysis of M1 and M2 polarised J774A.1 macrophage: J774A.1 macrophage were stimulated with M1 polarising factors 20ng/mL IFNγ and 100ng/mL LPS, and M2 polarising factors 20ng/mL IL-4 and 20ng/mL TGFβfor 24hr at 37°C in 5% CO_2. Naïve and polarised cells were stained with antibodies against TLR4, MHCII, CD80, CD86, CD14, CD40, Ly6C and Dectin-1. Data is presented as mean ± SEM of three replicates normalised to a population of unstained J774A.1 Macrophage. ***p<0.001, **p<0.01, *p<0.05 comparing M1 vs. M2 stimulated cells. Significance was determined using one- way ANOVA with a Newman-Keuls post-test.

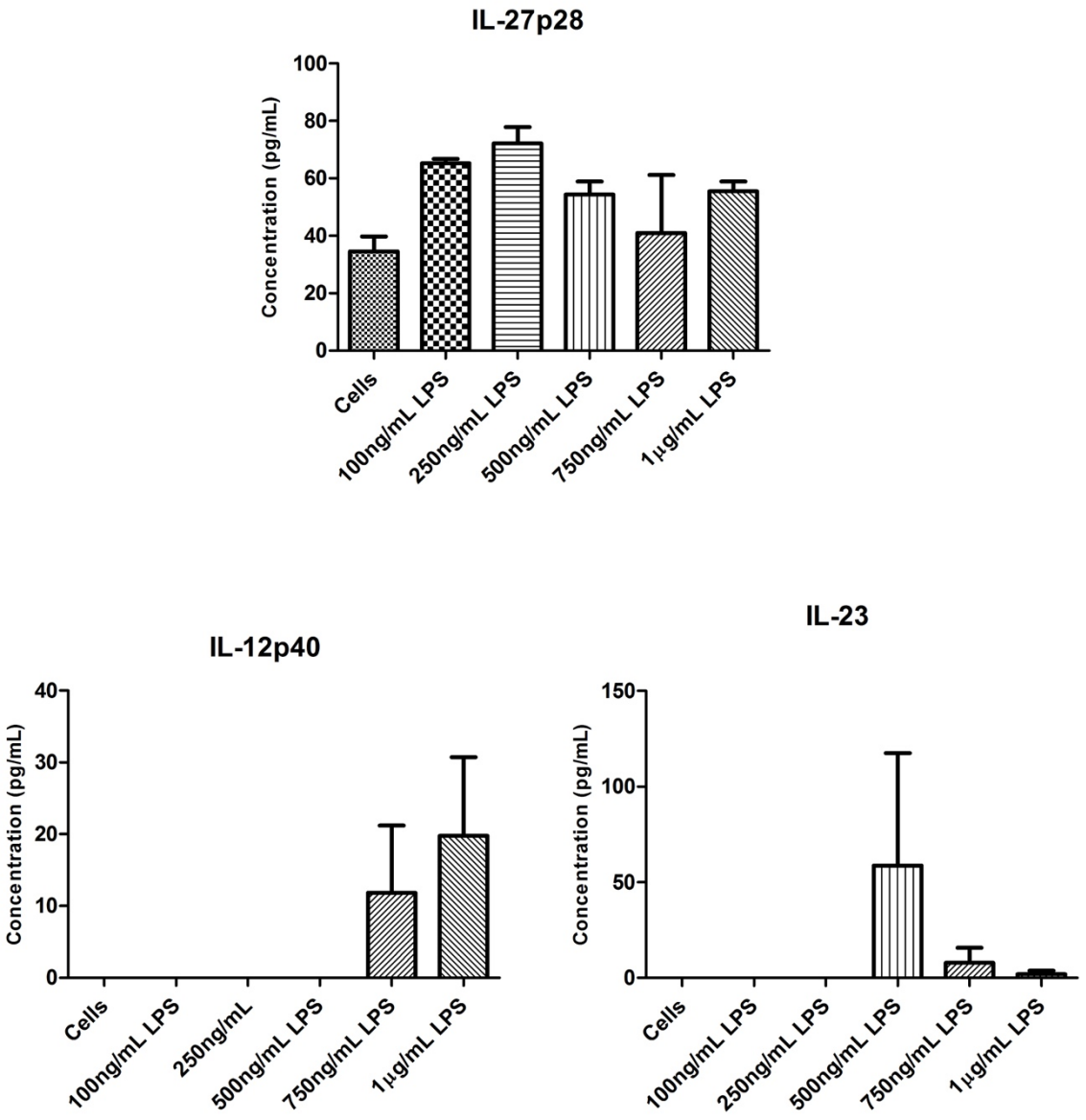


Figure 3.13 J774A.1 macrophage do not secrete key inflammatory cytokines, IL-12p40 and IL-23 J774A.1 Macrophage were stimulated with increasing doses of LPS, ranging from 100ng/mL to 1μg/mL. IL-12p40, IL-23 and IL-27p38 concentrations were determined using specific ELISA kits as previously described. IL-27p28 expression was affected in a dose dependant manner. IL-12p40 and IL-23 secretion was only detectable in small quantities at high doses of LPS. Data is presented as mean ± SEM of three replicates.

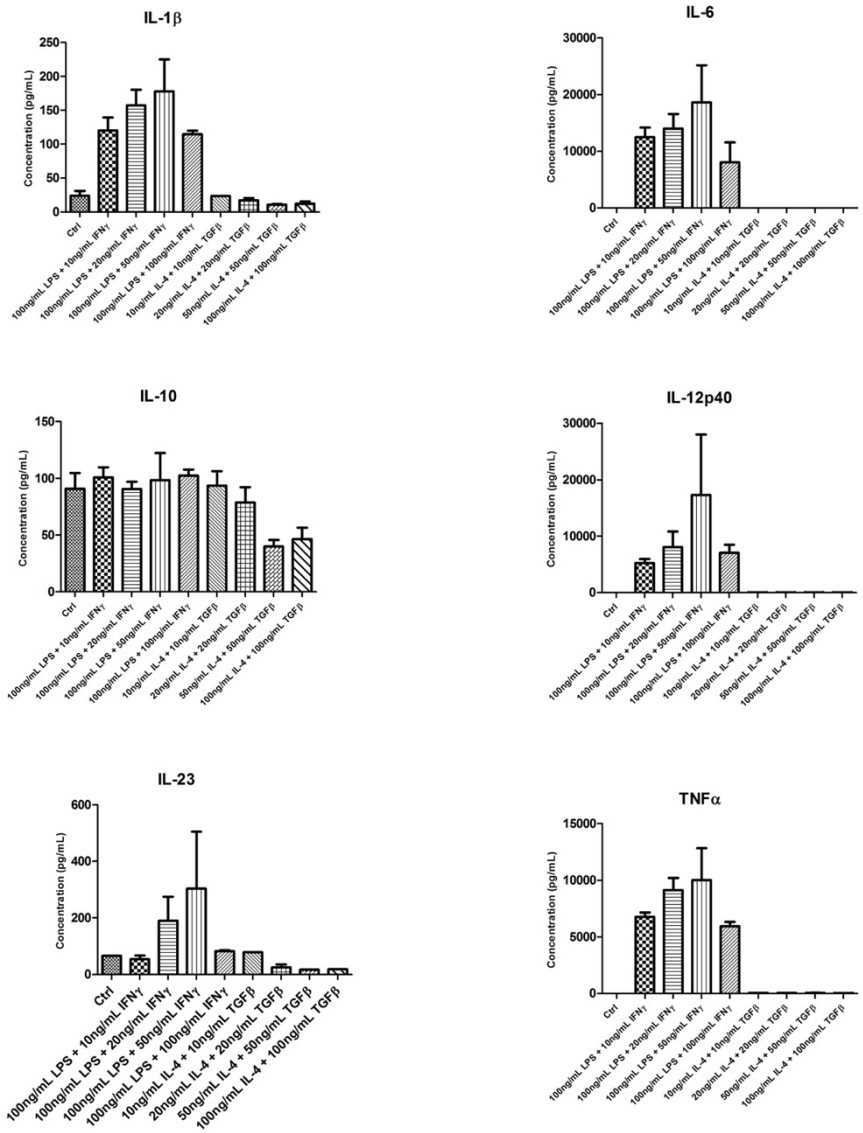


Figure 3.14 - IFNγ, IL-4 and TGFβ affect cytokine secretion in BMDMs BMDM Macrophage were stimulated with 100ng/mL LPS and a dose range of 10ng/mL to 100ng/mL IFNγ for M1 polarisation and IL-4 and TGFβ for M2 polarisation. Specific cytokine concentrations were assessed using ELISA kits as previously described in section 2.2.5. Data is presented as mean ± SEM of three replicates. ***p<0.001, **p<0.01, *p<0.05 LPS treated cells vs. cytokine stimulated cells. Significance was determined using one-way ANOVA with a Newman-Keuls post-test.

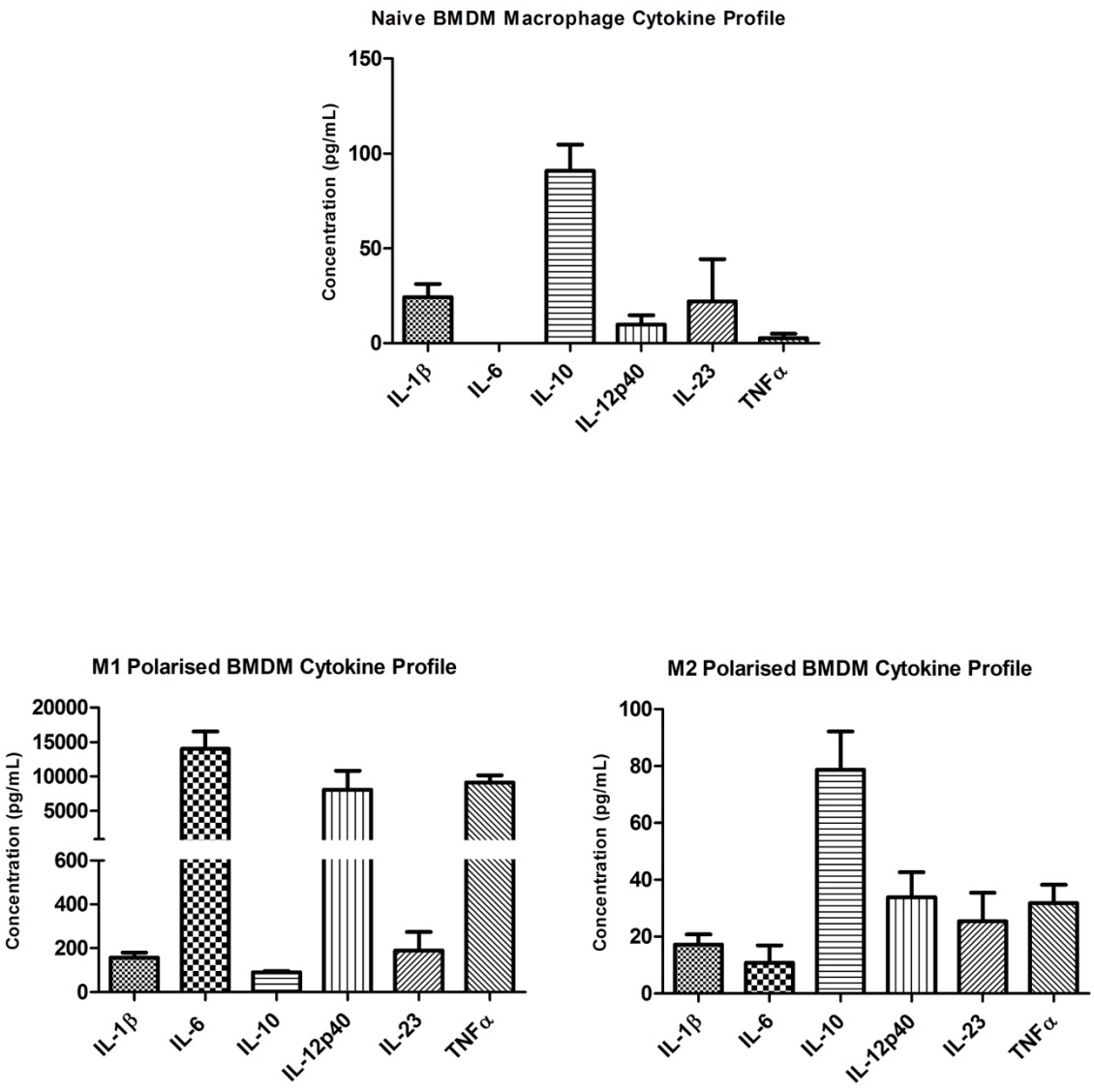


Figure 3.15 - BMDMs exhibit differential cytokine profiles consistent with M1 and M2 macrophage phenotypes BMDMs were stimulated with M1 polarising factors 20ng/mL IFNγ and 100ng/mL LPS, and M2 polarising factors 20ng/mL IL-4 and 20ng/mL TGFβ for 24hr at 37°C in 5% CO_2. Polarisation of BMDM macrophage to M1 and M2 subtypes elicits differing cytokine profiles, illustrated above, in naïve M1 and M2 polarised macrophage. Data is presented as mean ± SEM of three replicates.

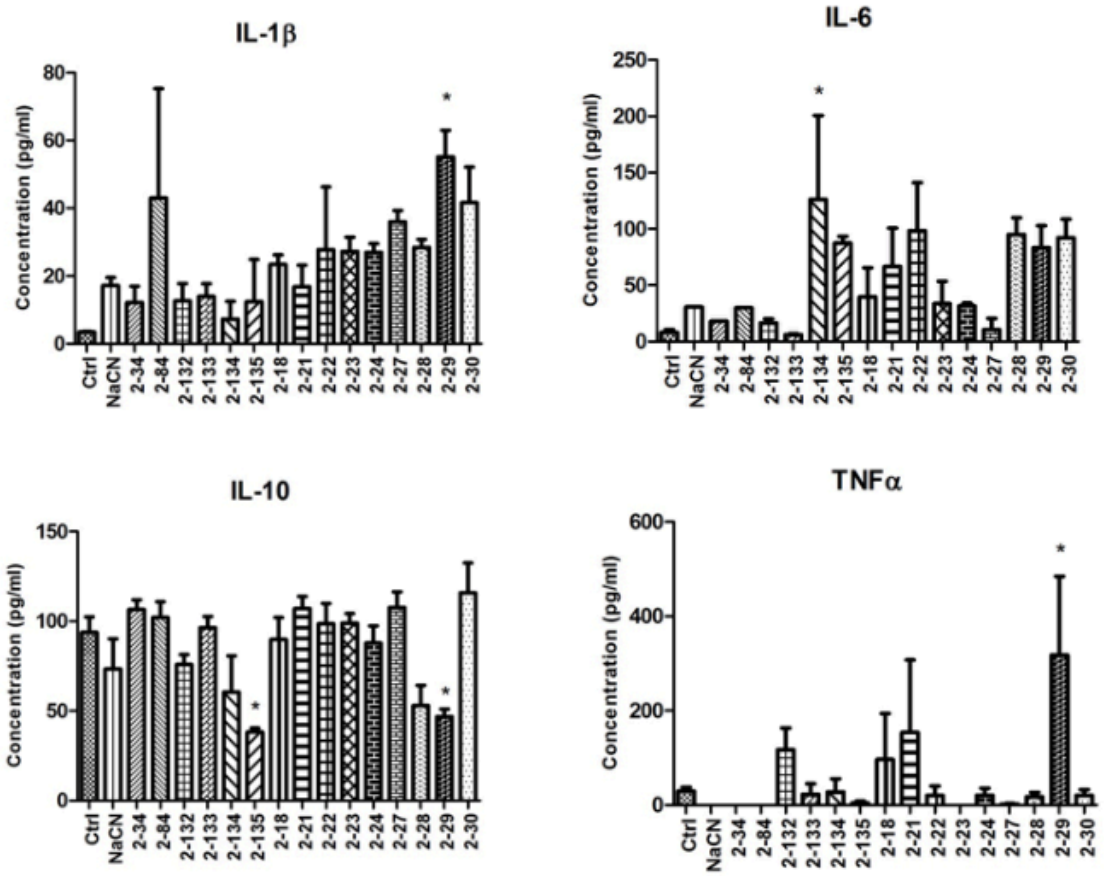


Figure 3.16 - Casein derived hydrolysates show the ability to modulate the cytokine secretion in naïve J774A.1 macrophage J774A.1 murine macrophage were stimulated with M1 polarising factors 20ng/mL IFNγ and 100ng/mL LPS and M2 polarising factors 20ng/mL IL-4 and 20ng/mL IL-13 in the presence and absence of 1mg/mL casein derived hydrolysate and whole protein contorl NaCN. Specific cytokine concentration in each sample was assessed using unique ELISA kits as previously described in section 2.2.5. Data is presented as mean $\pm$ SEM of three. ***p<0.001, **p<0.01, *p<0.05 comparing unstimulated cells vs. hydrolysate stimulated cells. Significance was determined using one-way ANOVA with a Newman-Keuls post-test.

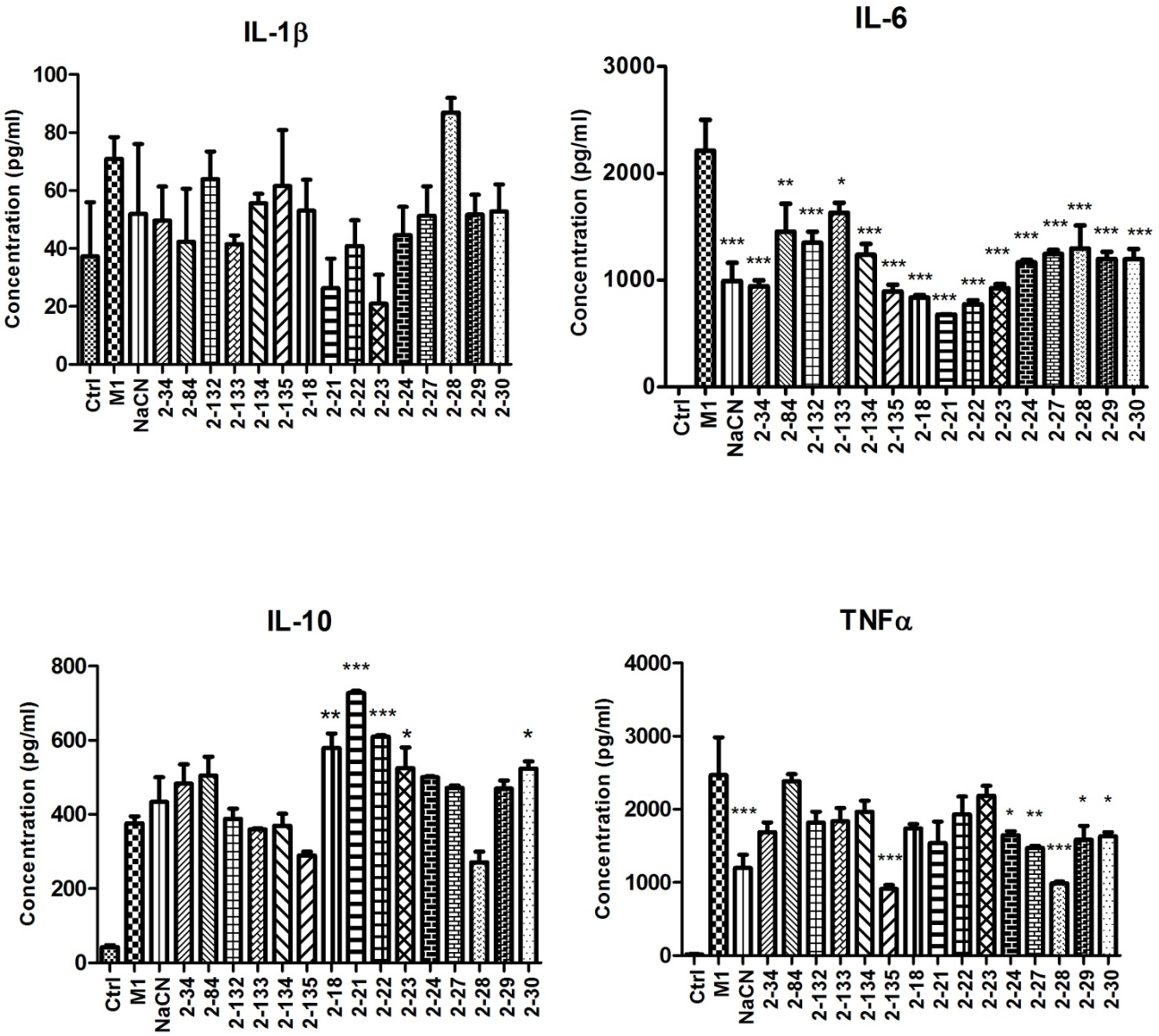


Figure 3.17 - Casein derived hydrolysates show the ability to modulate the cytokine secretion in M1 polarised J774A.1 macrophage J774A.1 murine macrophage were stimulated with M1 polarising factors 20ng/mL IFNγ in the presence and absence of 1mg/mL casein derived hydrolysate and whole protein contorl NaCN. Specific cytokine concentration in each sample was assessed using unique ELISA kits as previously described in section 2.2.5. Data is presented as mean ± SEM of three replicates. ***p<0.001, **p<0.01, *p<0.05 comparing M1 polarised cells vs. hydrolysate stimulated cells. Significance was determined using one-way

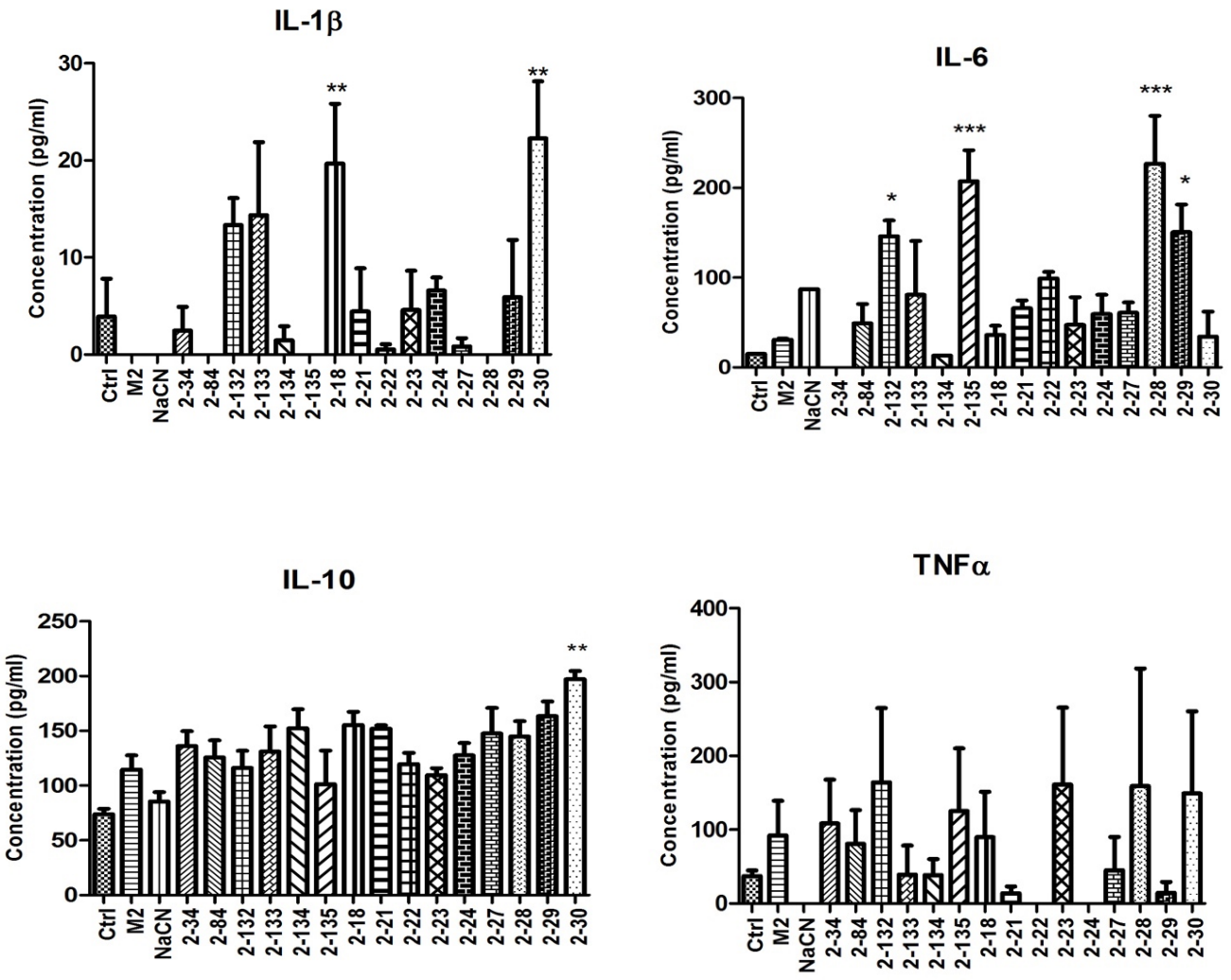


Figure 3.18 - Casein derived hydrolysates show the ability to modulate the M2 driven phenotype in J774A.1 macrophage. J774A.1 murine macrophage were stimulated with M2 polarising factors 20ng/mL IL-4 and 20ng/mL IL-13 in the presence and absence of 1mg/mL casein derived hydrolysate and whole protein contorl NaCN. Specific cytokine concentration in each sample was assessed using unique ELISA kits as previously described in section 2.2.5. Data is presented as mean ± SEM of three. ***p<0.001, **p<0.01, *p<0.05 comparing M2 polarised macrophage vs. hydrolysate stimulated cells. Significance was determined using one- way ANOVA with a Newman-Keuls post-test.

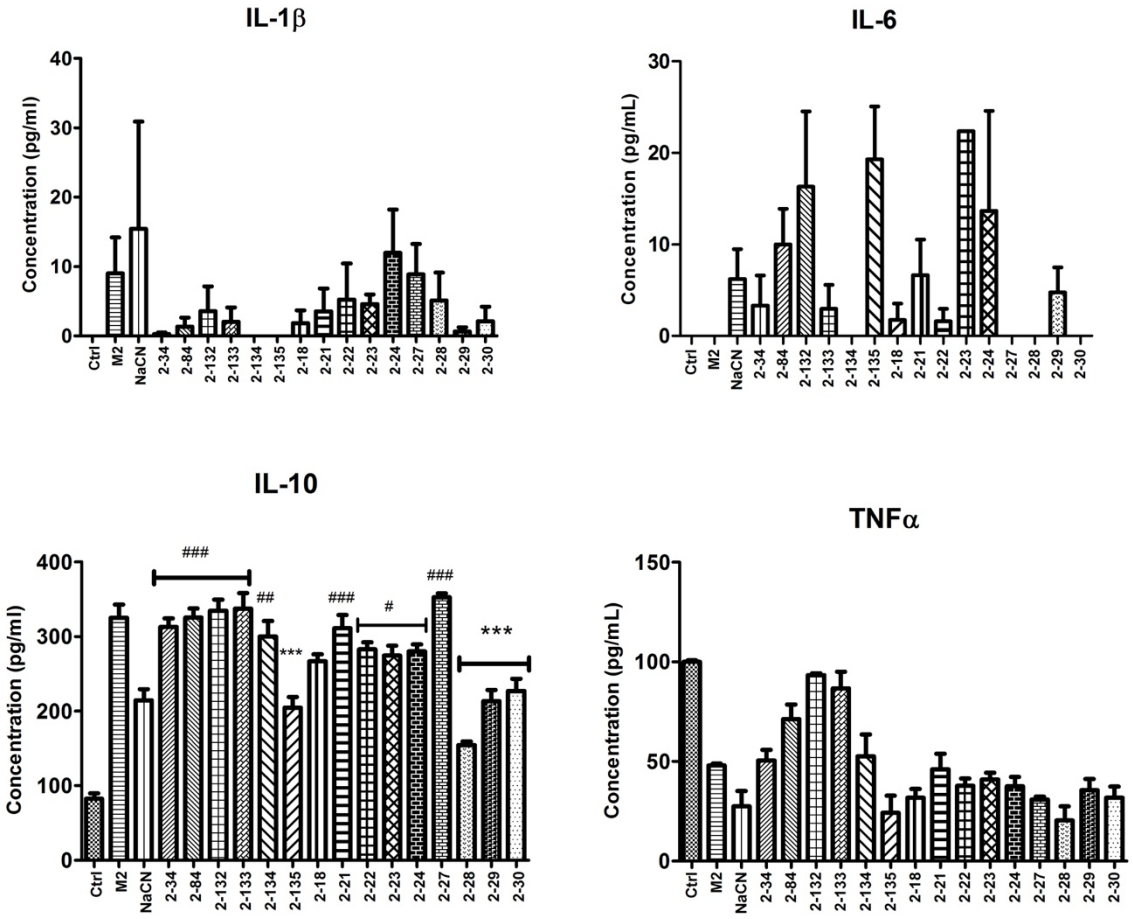


Figure 3.19 - Casein derived hydrolysates show the ability to modulate the M2 driven phenotype in J774A.1 macrophage. J774A.1 murine macrophage were stimulated with M2 polarising 20ng/mL IL-4 and TGFβ in the presence and absence of 1mg/mL casein derived hydrolysate and whole protein control (NaCN). Specific cytokine concentration in each sample was assessed using unique ELISA kits as previously described. Data is presented as mean ± SEM of three replicates. ***/### p<0.001, **/## p<0.01, *p/#<0.05 . Statistics denoted by: ***/**/* comparing M2 polarised macrophage vs. hydrolysate stimulated cells and, statistics denoted by: ###/##/# comparing NaCN/M2 polarised macrophage vs. hydrolysate stimulated cells. Significance was determined using one- way ANOVA with a Newman-Keuls post-test.

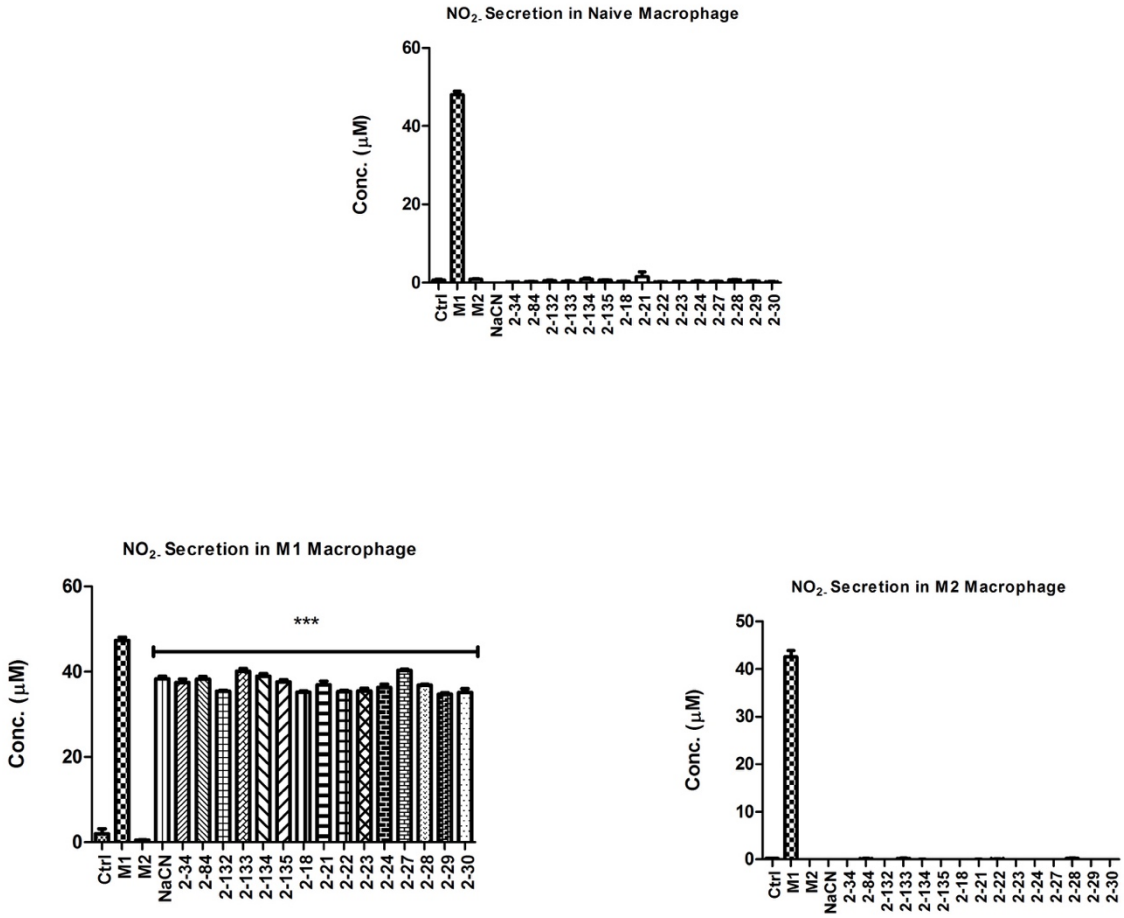


Figure 3.20 - Casein derived hydrolysates show the ability to modulate Nitrite production polarised in J774A.1 macrophage. J774A.1 murine macrophage were stimulated with M1 polarising factors 20ng/mL IFNγ and 100ng/mL LPS and M2 polarising factors 20ng/mL IL-4 and 20ng/mL TGFβ in the presence and absence of 1mg/mL casein derived hydrolysate and whole protein contorl NaCN. Nitrite production was measured as previously described using the Greiss reagent assay system. Data is presented as mean ± SEM of three replicates. ***p<0.001, **p<0.01, *p<0.05 comparing M1/M2 polarised macrophage vs. M1/M1/hydrolysate stimulated cells. Significance was determined using one- way ANOVA with a Newman-Keuls post-test.

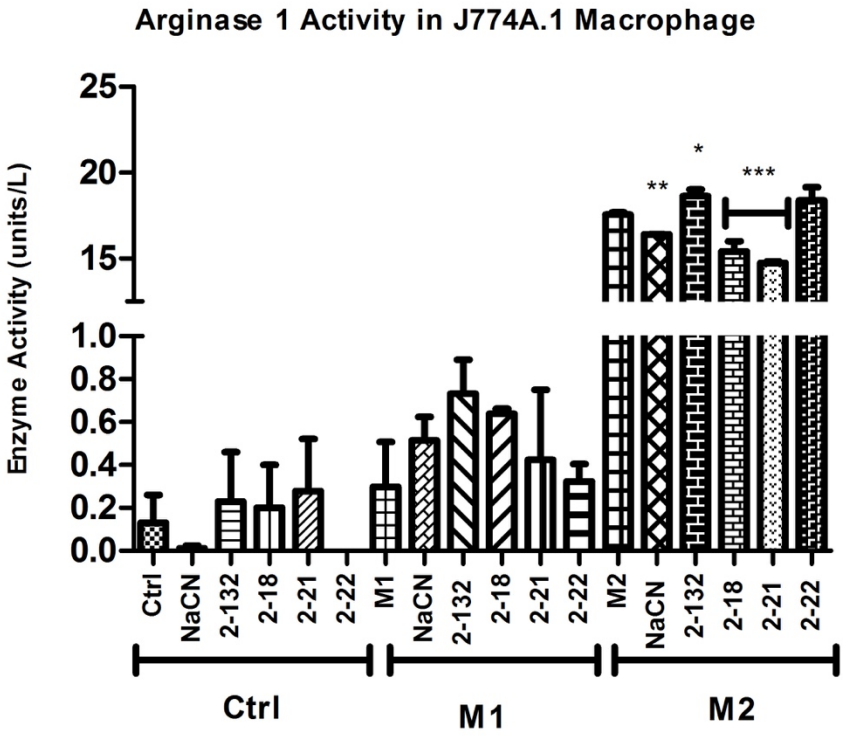


Figure 3.21 - Candidate casein derived hydrolysates show the ability to modulate the activity of key M2 macrophage marker Arginase 1. Arginase 1 activity was assessed in Naïve, M1 and M2 polarised macrophage treated with candidate sample s UL-2-132. UL-2-18, UL-2-21 and UL-2-22 that displayed specific anti-inflammatory immunomodulatory properties in polarised J774A.1 murine macrophage. Data is presented as mean ± SEM of three replicates. ***p<0.001, **p<0.01, *p<0.05 comparing M1 polarised macrophage vs. M1/hydrolysate stimulated cells. Significance was determined using one- way ANOVA with a Newman-Keuls post-test.

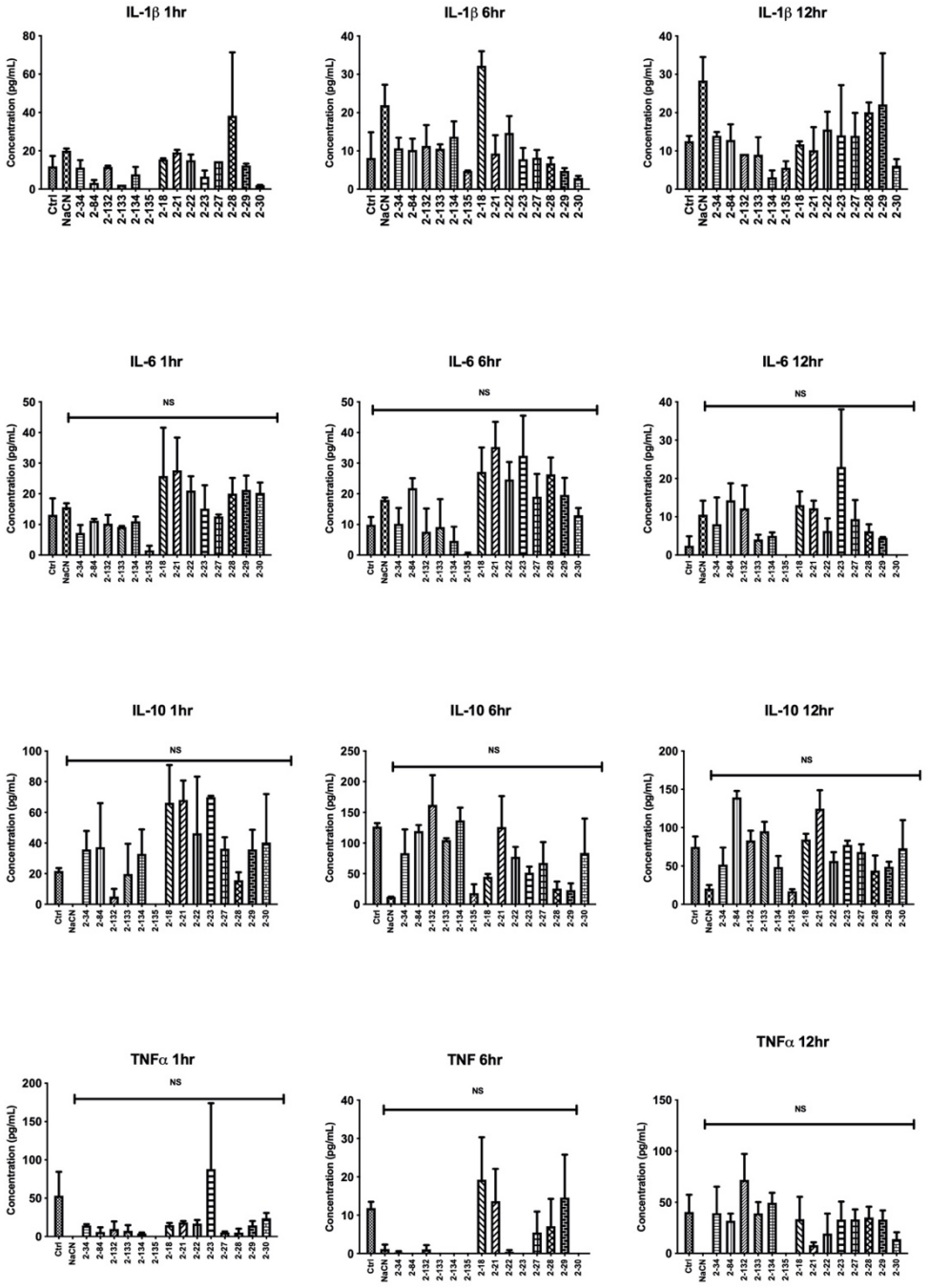


Figure 3.22 - Casein Derived Protein Hydrolysates Modulate Expression of Cytokines in Naïve J774A.1 Macrophage in a Time Dependant Manner. J774A.1 murine macrophage were stimulated with 1mg/mL casein derived hydrolysate and whole protein contorl NaCN for 1hr, 6hr and 12hr. Specific cytokine concentration in each sample was assessed using unique ELISA kits as previously described in section 2.2.5. Data is presented as mean ± SEM of three. ***p<0.001, **p<0.01, *p<0.05 comparing unstimulated cells vs. hydrolysate stimulated cells. Significance was determined using one-way ANOVA with a Newman-Keuls post-test.

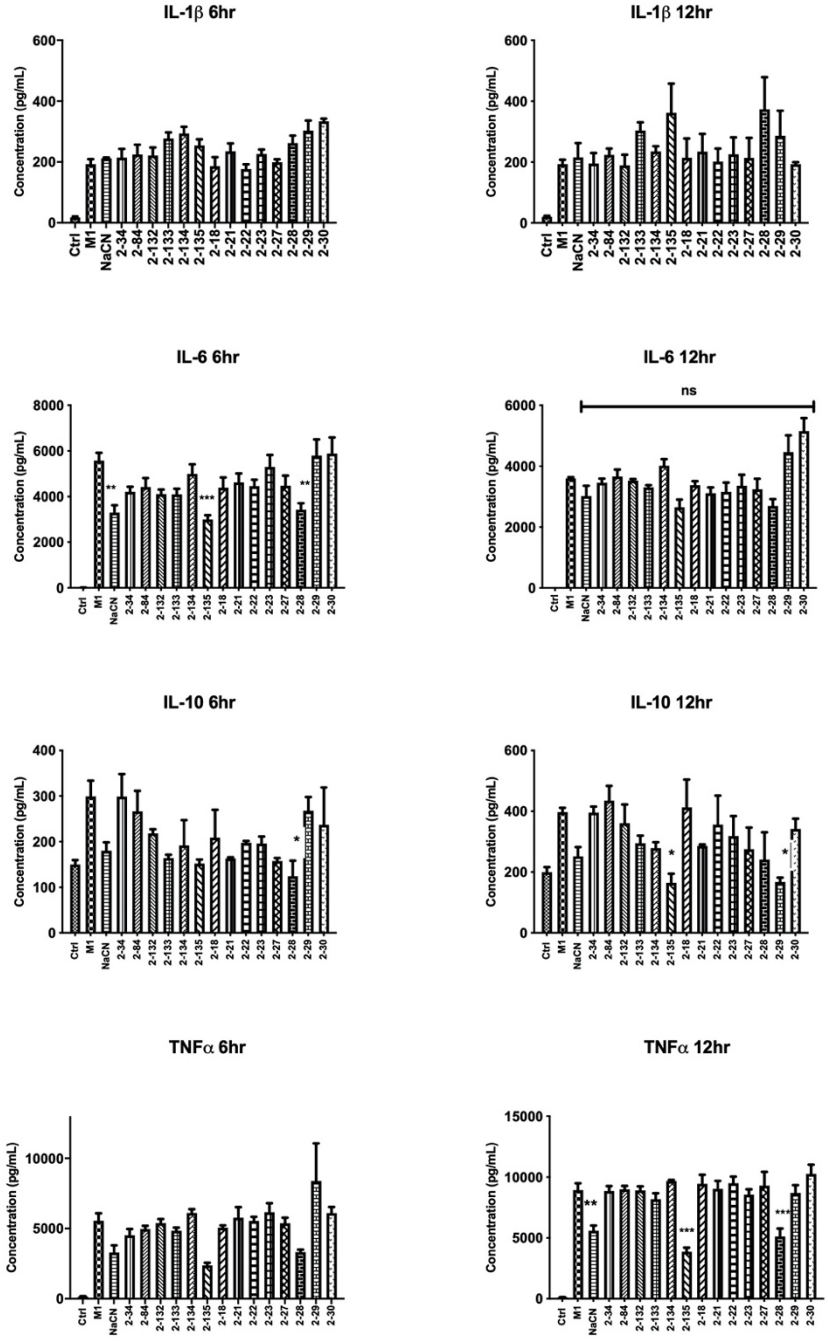


Figure 3.23 - Casein Derived Hydrolysates Demonstrate loss of TNFα and IL-6 Suppressive Bioactivity as Length of Pre-Incubation Increases. J774A.1 murine macrophage were stimulated with M1 polarising factors 20ng/mL IFNγ in the presence and absence of 1mg/mL casein derived hydrolysate and whole protein contorl NaCN for 6hr and 12hr. Specific cytokine concentration in each sample was assessed using unique ELISA kits as previously described in section 2.2.5. Data is presented as mean ± SEM of three replicates. ***p<0.001, **p<0.01, *p<0.05 comparing M1 polarised cells vs. M1/hydrolysate stimulated cells. Significance was determined using one-way ANOVA with a Newman-Keuls post-test.

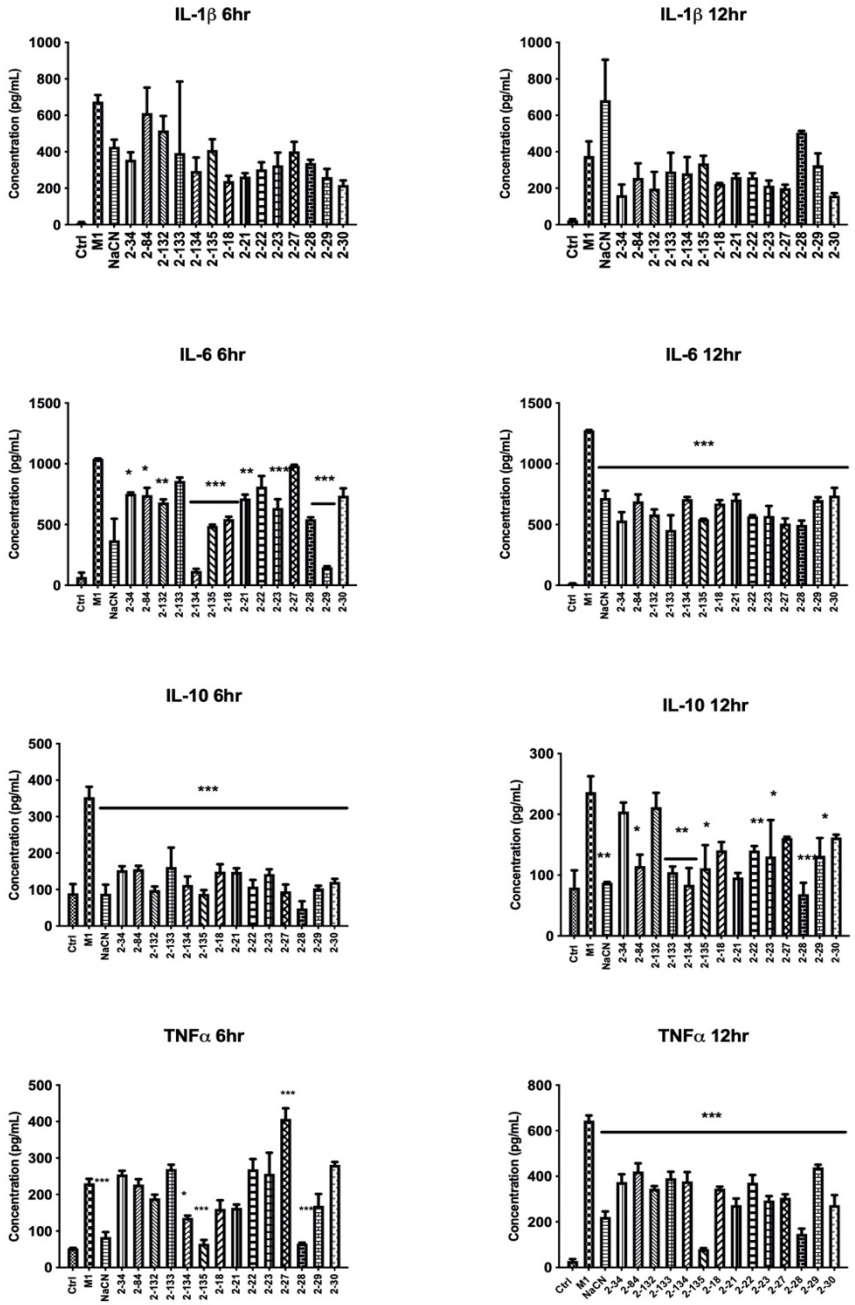


Figure 3.24 - Re-Stimulation of J774A.1 Macrophage with Casein Derived Hydrolysates Recovers Anti-Inflammatory Bioactivity in M1 Polarised J774A.1 Macrophage. J774A.1 murine macrophage were stimulated with M1 polarising factors 20ng/mL IFNγ in the presence and absence of 1mg/mL casein derived hydrolysate and whole protein contorl NaCN for 6hr and 12hr. Specific cytokine concentration in each sample was assessed using unique ELISA kits as previously described in section 2.2.5. Data is presented as mean ± SEM of three replicates. ***p<0.001, **p<0.01, *p<0.05 comparing M1 polarised cells vs. M1/hydrolysate stimulated cells. Significance was determined using one-way ANOVA with a Newman-Keuls post-test.

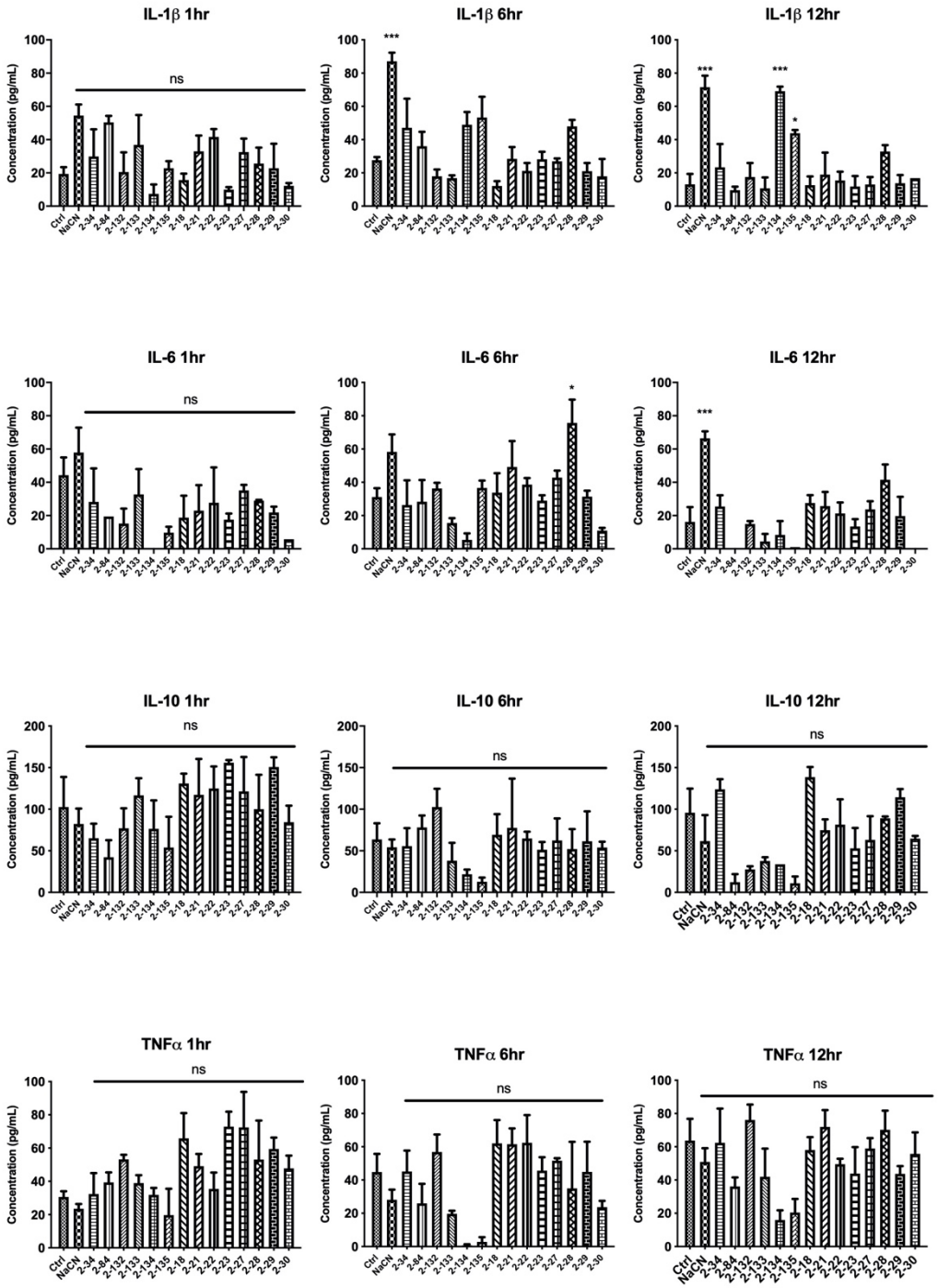


Figure 3.25 - Casein Derived Protein Hydrolysates Modulate Expression of Cytokines in Naïve J774A.1 Macrophage in a Time Dependant Manner at a Dose of 2mg/mL. J774A.1 murine macrophage were stimulated with 2mg/mL casein derived hydrolysate and whole protein contorl NaCN for 1hr, 6hr and 12hr. Specific cytokine concentration in each sample was assessed using unique ELISA kits as previously described in section 2.2.5. Data is presented as mean ± SEM of three. ***p<0.001, **p<0.01, *p<0.05 comparing unstimulated cells vs. hydrolysate stimulated cells. Significance was determined using one-way ANOVA with a Newman-Keuls post-test.

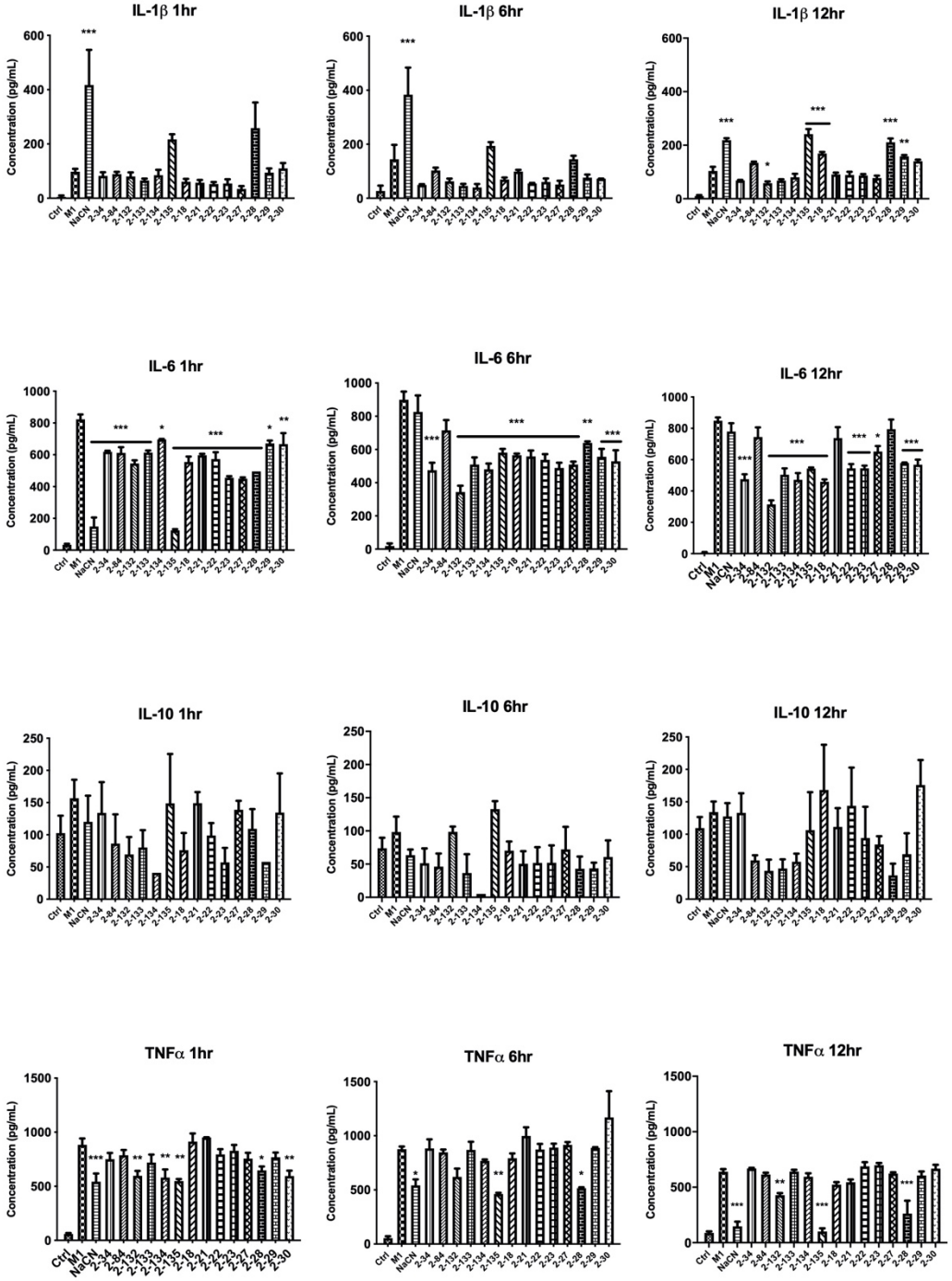


Figure 3.26 - Casein Derived Protein Hydrolysates Modulate Expression of Cytokines in M1 Stimulated J774A.1 Macrophage in a Time Dependant Manner at a Dose of 2mg/mL. J774A.1 murine macrophage were stimulated with 2mg/mL casein derived hydrolysate and whole protein contorl NaCN for 1hr, 6hr and 12hr. Specific cytokine concentration in each sample was assessed using unique ELISA kits as previously described in section 2.2.5. Data is presented as mean ± SEM of three. ***p<0.001, **p<0.01, *p<0.05 comparing M1 cells vs. hydrolysate stimulated cells. Significance was determined using one-way ANOVA with a Newman-Keuls post-test.

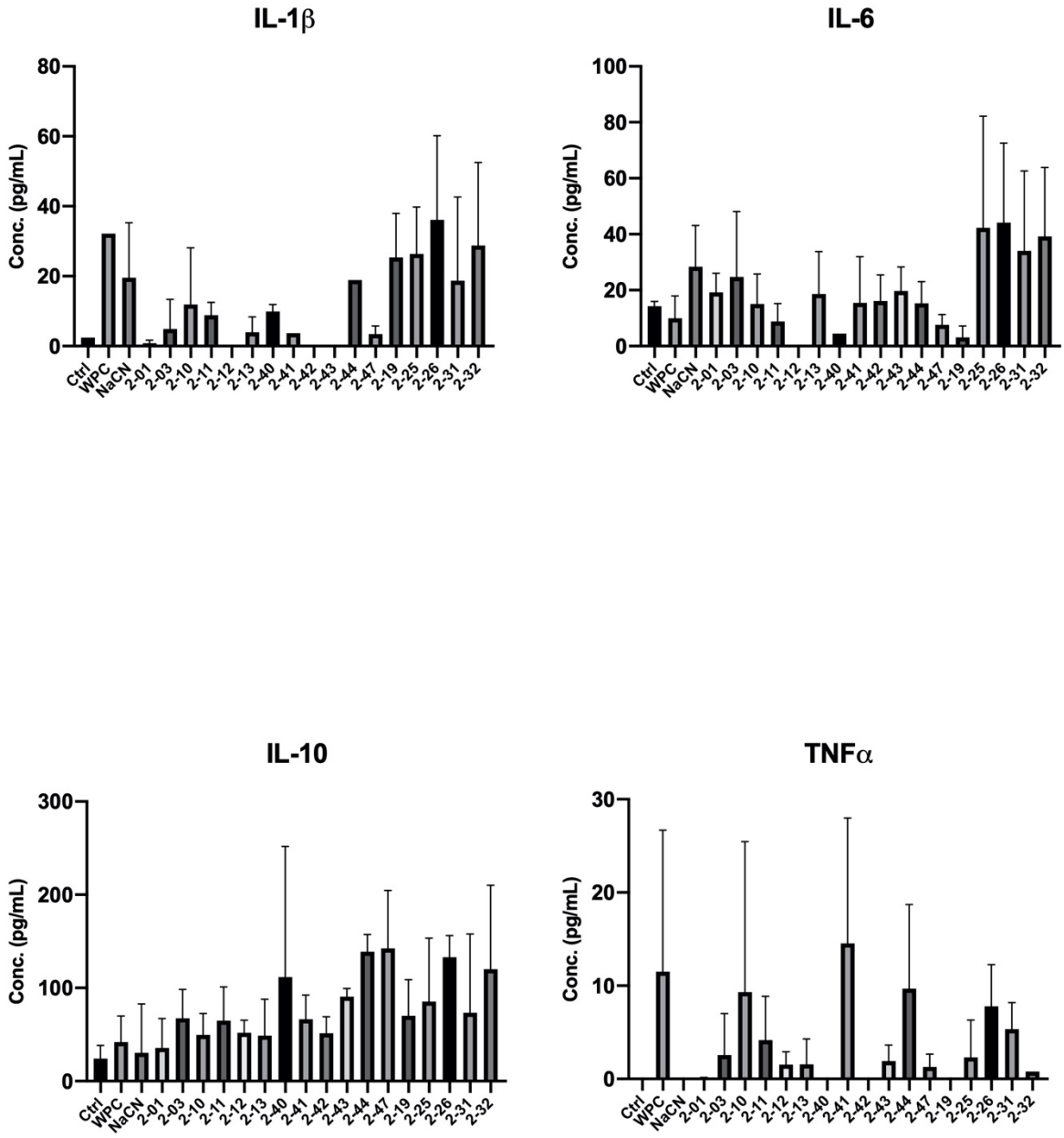


Figure 3.27 – Casein (NaCN) and Whey Protein (WPC) derived hydrolysates show the ability to modulate the cytokine secretion in naïve J774A.1 macrophage J774A.1 murine macrophage were stimulated with 1mg/mL casein and whey protein derived. Specific cytokine concentration in each sample was assessed using unique ELISA kits as previously described in section 2.2.5. Data is presented as mean ± SEM of three. ***p<0.001, **p<0.01, *p<0.05 comparing unstimulated cells vs. hydrolysate stimulated cells. Significance was determined using one-way ANOVA with a Newman-Keuls post-test.

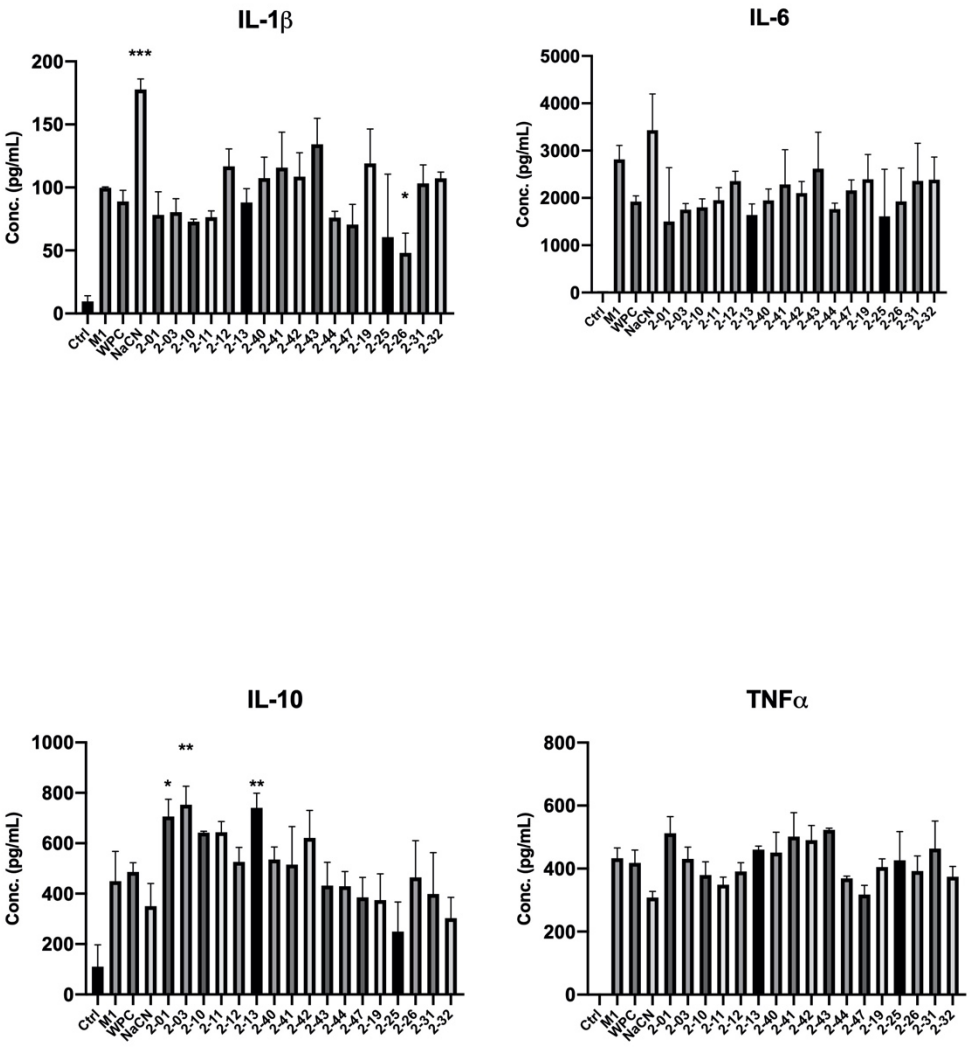


Figure 3.28– Casein and Whey protein derived hydrolysates show the ability to modulate the cytokine secretion in M1 polarised J774A.1 macrophage J774A.1 murine macrophage were stimulated with M1 polarising factors 20ng/mL IFNγ in the presence and absence of 1mg/mL casein/whey derived hydrolysate and whole protein contorl NaCN/WPC. Specific cytokine concentration in each sample was assessed using unique ELISA kits as previously described. Data is presented as mean ± SEM of three replicates. ***p<0.001, **p<0.01, *p<0.05 comparing M1 polarised cells vs. M1/hydrolysate stimulated cells. Significance was determined using one-way ANOVA with a Newman-Keuls post-test.

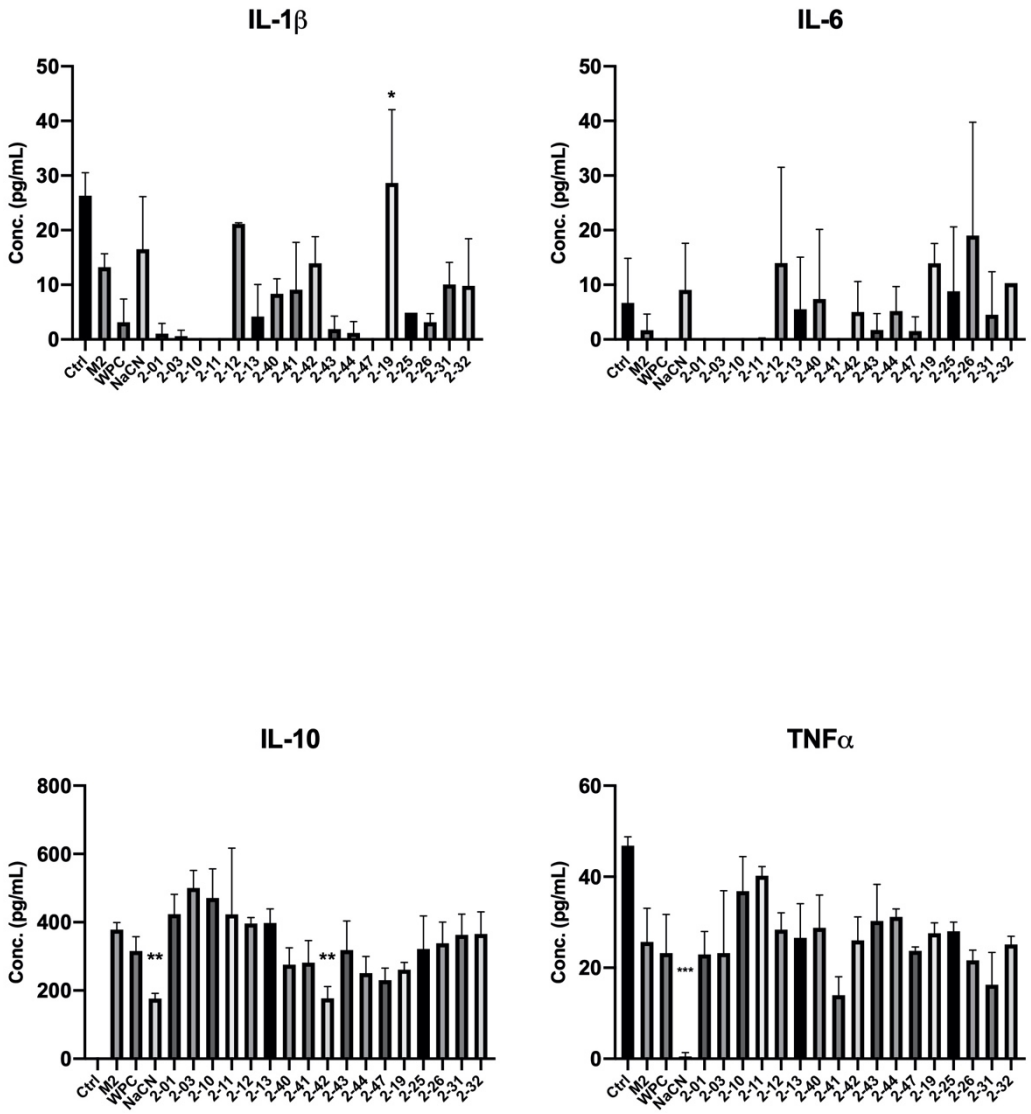


Figure 3.29 - Casein and Whey protein derived hydrolysates show the ability to modulate the M2 driven phenotype in J774A.1 macrophage. J774A.1 murine macrophage were stimulated with M2 polarising 20ng/mL IL-4 and TGFβ in the presence and absence of 1mg/mL casein/whey derived hydrolysate and whole protein control NaCN/WPC. Specific cytokine concentration in each sample was assessed using unique ELISA kits as previously described in section 2.2.5. Data is presented as mean ± SEM of three replicates. *** p<0.001, ** p<0.01, *p<0.05. Statistics denoted by: * comparing M2 polarised macrophage vs. M2/hydrolysate stimulated cell. Significance was determined using one- way ANOVA with a Newman-Keuls post-test.

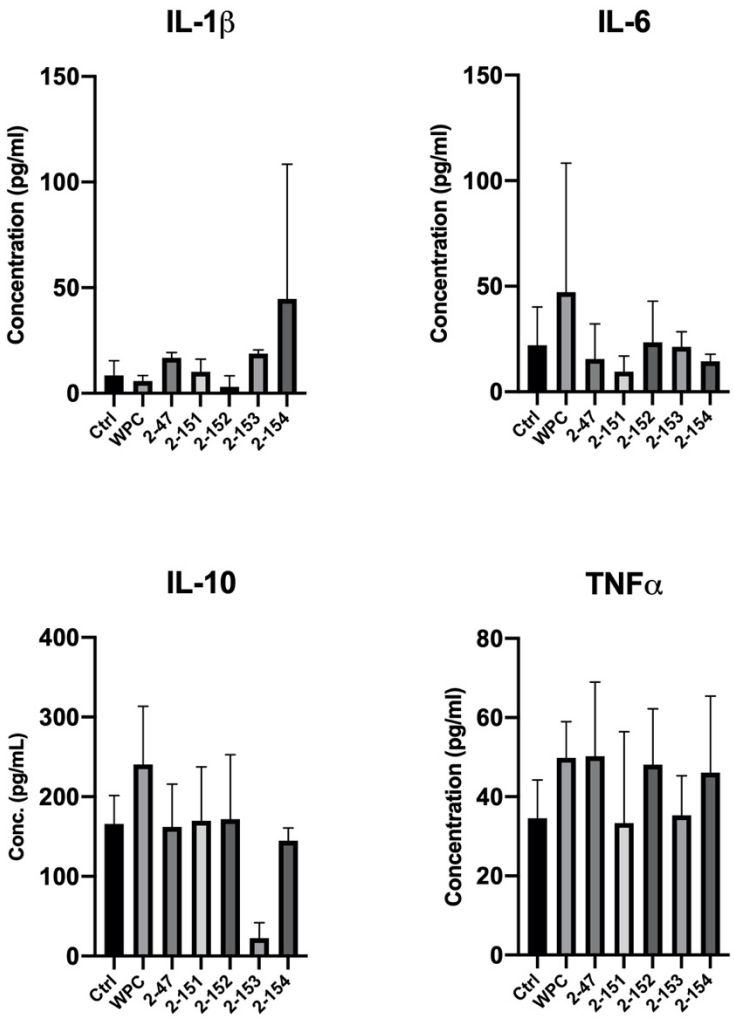


Figure 3.30 - Whey Protein (WPC) derived hydrolysates 2-47 and its regenerates show the ability to modulate the cytokine secretion in naïve J774A.1 macrophage J774A.1 murine macrophage were stimulated with 1mg/mLof Whey Protein (WPC) derived hydrolysates 2-47 and its regenerates. Specific cytokine concentration in each sample was assessed using unique ELISA kits as previously described in section 2.2.5. Data is presented as mean ± SEM of three. ***p<0.001, **p<0.01, *p<0.05 comparing unstimulated cells vs. hydrolysate stimulated cells. Significance was determined using one-way ANOVA with a Newman-Keuls post-test.

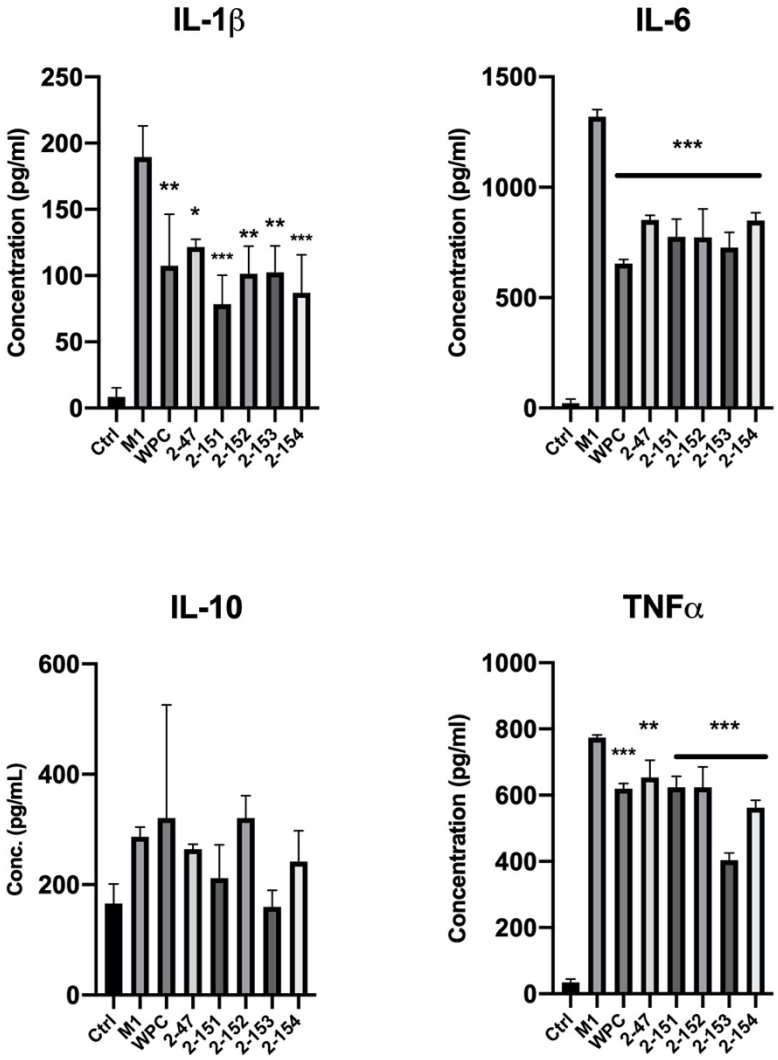


Figure 3.31 - Whey Protein (WPC) derived hydrolysates 2-47 and its regenerates show the ability to modulate the cytokine secretion in M1 Polarised J774A.1 macrophage J774A.1 murine macrophage were stimulated with M1 polarising factors 20ng/mL IFNγ and 100ng/mL LPS in the presence and absence of 1mg/mL of Whey Protein (WPC) derived hydrolysates 2-47 and its regenerates. Specific cytokine concentration in each sample was assessed using unique ELISA kits as previously described in section 2.2.5. Data is presented as mean ± SEM of three. ***p<0.001, **p<0.01, *p<0.05 comparing unstimulated cells vs. hydrolysate stimulated cells. Significance was determined using one-way ANOVA with a Newman-Keuls post-test.

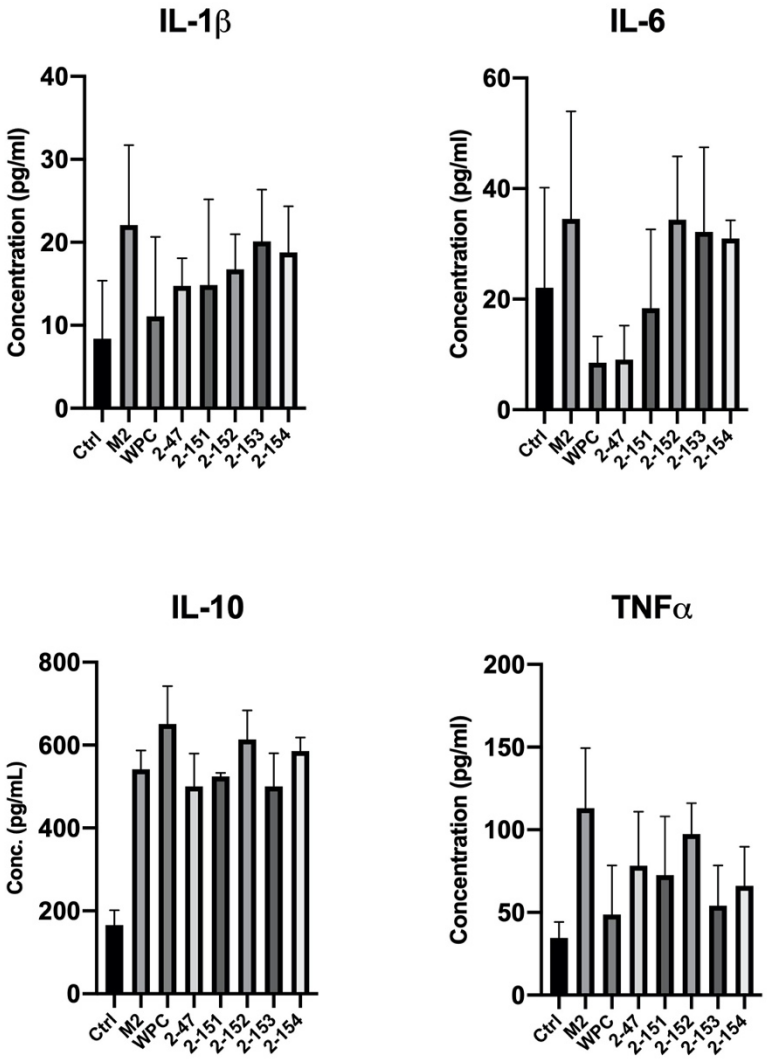


Figure 3.32 - Whey Protein (WPC) derived hydrolysates 2-47 and its regenerates show the ability to modulate the cytokine secretion in M2 Polarised J774A.1 macrophage J774A.1 murine macrophage were stimulated with M2 polarising factors M2 polarising 20ng/mL IL-4 and TGFβ in the presence and absence of 1mg/mL of Whey Protein (WPC) derived hydrolysates 2-47 and its regenerates. Specific cytokine concentration in each sample was assessed using unique ELISA kits as previously described in section 2.2.5. Data is presented as mean ± SEM of three. ***p<0.001, **p<0.01, *p<0.05 comparing unstimulated cells vs. hydrolysate stimulated cells. Significance was determined using one-way ANOVA with a Newman-Keuls post-test.

3.4 Discussion

Macrophage display a wide degree of plasticity regarding their phenotype. Macrophage polarization refers to the ability of macrophage to exhibit a distinct phenotype as determined by the nature of the stimulus encountered (Murray, 2017; Shapouri-Moghaddam et al., 2018). For example, exposure to bacterial antigens such as lipopolysaccharide are known to induce an inflammatory phenotype in several immune cell types. However, with regard to true M1 macrophage polarization, it has been documented that LPS alone is not sufficient to drive a genotype and phenotype consistent with M1 macrophage (Martinez and Gordon, 2014). Inflammatory cytokines such as IFNγ or TNFα are required in combination with LPS (Martinez and Gordon, 2014; Paulina Achita, 2015). M1 activation is transduced through the downstream effectors of the IFNγ receptor STAT1/JAK1/JAK2, in combination with the TLR4 signaling pathway which induces NF-κB activity (Martinez and Gordon, 2014). Traditionally, M1 polarised macrophage are defined as secreting high levels of nitric oxide through the activity of the iNOS enzyme, with prominent phagocytosis activity. The M1 cytokine secretome is also heavily skewed towards a Th1, pro-inflammatory phenotype, characterized by high levels of secretion of IL-1β, IL-6, IL-12p40, IFNγ and TNFα and comparatively low levels of secretion of the anti-inflammatory cytokine IL-10 (Iqbal and Kumar, 2016; Martinez and Gordon, 2014).

J774A.1 macrophage, are a commonly used immortalized cell line in immunological based studies. Although a robust cell line for studying inflammation, findings in this study uncovered an inability of M1 polarised J774A.1s to secrete key members of the IL-12 family, specifically IL-12p40 and IL-23. M1 macrophage are consistently cited and documented to secreted high levels of IL-12p40 and IL-23 (Martinez and Gordon, 2014; Murray, 2017; Wang et al., 2014). It has been demonstrated that IL-12 stimulation can revert an M2 macrophage back to an M1 phenotype, suggesting it plays a critical role in sustaining M1 functionality (Yu et al., 2016). As a result, detecting and measuring changes IL-12 and IL-23 secretion may be a critical point in uncovering how potential immunomodulators can impact on M1 macrophage functionality.

IL-12p40 and IL-23 secretion was inducible in our primary bone marrow derived macrophage. Due to the genetic augmentation required to immortalize cell lines, like J774A.1 macrophage, the representative *in vivo* functionality of a cell is compromised (Pastor et al., 2010). BMDMs are commonly isolated and differentiated from bone marrow using conditioned media from L929 cells, which secrete M-CSF, among other growth factors the drive BMDM differentiation and proliferation (Weischenfeldt and Porse, 2008). However, it has been demonstrated that using recombinant murine M-CSF it is possible to differentiate and drive BMDMs expressing CD11b and F4/80. These BMDMs also display the ability to polarize towards M1 and M2 phenotypes with cytokine secretome consistent with each phenotype. While we confirmed that these cells could secrete IL-12 and IL-23 we decided that BMDMs were not appropriate for this study. Due to the high-volume screening of casein and whey derived hydrolysates to be screened in M1 and M2 polarised BMDMs, resources and time constraints surrounding the use of animals , we deemed it not appropriate. Despite the loss of IL-12 family cytokine data, physiologically meaningful data can be gleaned from using M1 and M2 polarised J774s. The primary inflammatory cytokines secreted by M1 J774A.1 macrophage; IL-1β, IL-6 and TNFα have all been documented to have key functions in the progression of chronic inflammatory disease. In the context of muscle health, high levels of circulating IL-1β,IL-6 and TNFα are implicated with muscle atrophy and metabolic disruption (Haddad et al., 2005; Li et al., 2009; Reid and Li, 2001). Therefore, gathering data surrounding the impact of hydrolysate modulation on IL-1β, IL-6 and TNFα from M1 polarised macrophage, will allow us to extrapolate and predict potential effects hydrolysates may have on immune function *in vivo*.

Following optimization of the M1 and M2 polarization model we next wanted to assess whether the milk derived hydrolysates could alter this polarization and therefore the cytokines being secreted by these cells. This is due to the fact that novel anti-inflammatory bioactive food ingredients may provide a natural avenue to treating chronic inflammation and improving poor healing in wounds, particularly in the context of muscle recovery (Marcone, Simone et al., 2017; S Lopez-Varela, 2002). Initially, a panel of Sodium Caseinate (NaCN) derived hydrolysates were chosen due to their ability to promote Th2, anti-inflammatory phenotypes naïve T cells and T cell subsets in another study undertaken in our laboratory as part of the Food for Health Programme. This is a partnership between

multinational enterprise and public research organisations with the singular goal of researching, developing, manufacturing, and marketing novel, bioactive food ingredients isolated from bovine milk that have a proven health benefit.

Our preliminary data generated using this method in the established M1 and M2 macrophage models, demonstrated that candidate NaCN derived hydrolysates exhibit potent anti-inflammatory bioactivity. Of note, is that in modulated M1 macrophage, although reduced, pro-inflammatory factors were not knocked out completely. For example, sample 2-21 down regulates IL-1β, IL-6 and TNFα, while driving IL-10 in M1 polarised J774A.1s. Sample 2-21 also drove IL-10 secretion in M2 polarised J774A.1s. While it is important that inflammation is not completely abrogated so as to induce immunosuppression (Lillehoj, 1987), it is also a critical point of interest in the context of muscle and wound recovery.

Inflammation is beneficial for muscle recovery in the early stages of regeneration as it drives proliferation and early differentiation of progenitor cells to support healing (Chazaud, 2016; James G. Tidball, 2017). This is exemplified in a study conducted by Jetten *et. al*, where exogenous M2 polarised macrophage were administered to subcutaneous wounds during the inflammatory phase of recovery, and delayed the recovery of the wounds (Jetten et al., 2014). Moreover, early delivery of ibuprofen to tendon injuries significantly impaired wound healing (Connizzo et al., 2014). IL-1β concentrations are known to increase in skeletal muscle following exercise. Though, to promote initial regenerative inflammation, there is evidence to support that IL-1β modulates secretion of myokine IL-6, which promotes metabolic health and adaptation to modified muscle use (Chiba et al., 2015). Although several studies note that abrogation of IL-6 can benefit muscle recovery (Wada et al., 2017), the acute downregulation may lead to an impaired inflammatory response due to the potentiating role of IL-6, and may negatively impact the proliferation and activation of skeletal muscle progenitor cells and adaptation to exercise (Paniri and Akhavan-Niaki, 2020; Rogeri et al., 2020). The same can be said for TNFα, where down regulation of TNFα in acute wounds can delay wound healing in muscle via promotion of catabolic pathways and inhibiting myogenesis (Demirkapi et al., 2017). The suppression we see in inflammatory cytokines fromm M1 macrophage, and the subsequent benefit for

wound healing and metabolic heath for skeletal muscle becomes positive in the context of chronic muscle injury where the injury micro-environment is kept in state of perpetual low-grade inflammation perpetuating a degenerative cycle of damage and unresolved healing (Raziyeva et al., 2021). For example, administration of *Infliximab*, a monoclonal TNFα inhibitor has been shown to improve whole body insulin sensitivity (Sun et al., 2017). Raimondo et al. further demonstrated that M2 polarisation *in vivo*, using IL-4 tagged nano particles, improved muscle function in mice following ischemic injury (Raimondo and Mooney, 2018). Therefore, the consequences of acute down regulation of key M1 cytokines may have a negative influence on outputs of skeletal muscle function. The effect of this on glucose metabolism, muscle protein synthesis and *in vitro* wound healing will be examined in detail in subsequent thesis chapters.

Promoting IL-10 in the context of skewing an M1 phenotype and promoting an M2 phenotype in the context of chronic muscle injury is a therapeutic strategy being followed worldwide. Due to the importance that IL-10 has as a quencher of inflammation, and the detrimental effects chronic inflammation has on muscle health, reducing pro-inflammatory cytokines and/or driving IL-10 secretion to promote an anti-inflammatory healer immune cell type is desired (Saclier et al., 2013; T Koh and L DiPietro, 2013). Villata et. al demonstrated that abolition of IL-10 *in vivo* promoted mdx induced muscle damage. Administration of exogenous IL-10 led to improved muscle function related to a deactivation of M1 macrophage in mdx injured muscle (Villalta et al., 2011). Therefore, we were particularly interested in our study to see whether the milk derived hydrolysates influenced this cytokine as it would indicate it may have beneficial effects on muscle. Indeed Krzyszcyk et al. showed that modulating the functions of macrophages during the wound healing process can have beneficial outcomes (Krzyszczyk et al., 2018). Goren et. al documented that administration of anti-TNFα and anti-F4/80 antibodies to inhibit inflammatory macrophage, one week post injury resulted in enhanced healing (Goren et al., 2007). Anti-inflammatory glucans have been shown to have beneficial effects on wound healing (T Koh and L DiPietro, 2013). The use of growth factor therapies has also been shown to drive healing, particularly with the approved therapeutic Regranex. Regranex, has been shown to increase macrophage accumulation in non-healing ulcers and drive them towards and M2-like phenotype, improving healing (Krzyszczyk et al., 2018). A PGE2

hydrogel has also been shown to promote wounding healing through enhancing M2 macrophage polarisation (Zhang et al., 2018). Our preliminary findings of increased IL-10 following exposure to the milk-derived hydrolysates indicates their beneficial potential in muscle health.

During the initial screening experiments, variability was noticed in the levels of IL-10 being secreted from the polarized J774.1 cells. It is often believed that M2 macrophage should secrete more IL-10 than their inflammatory M1 counterparts (Martinez and Gordon, 2014; Shapouri-Moghaddam et al., 2018). However, the data presented in this thesis demonstrates that wide variability was observed in the IL-10 secretion in response to IL-4 and IL-13 stimulation in M2 polarised J774A.1s when directly compared to M1 polarised cells. In J774A.1s however, regardless of the M2 IL-10 secretion levels, IL-4 and IL-13 stimulation ensured that there was more IL-10 present than the inflammatory cytokines measured, with concomitant Arg1 upregulation and nitric oxide downregulation. Therefore, before proceeding further, we examined several options for the optimization of the IL-10 secretion from the M2 cells. These including changing the polarization factors and using primary derived cells.

In the context of *in vitro* M2 macrophage polarization, studies that use M2 macrophage are often polarizing towards an M2a phenotype with polarization achieved using IL-4 and IL-13 alone or in combination (Hallowell et al., 2017; Iqbal and Kumar, 2016; Paulina Achita, 2015; Saclier et al., 2013). We attempted to boost IL-10 secretion in M2 polarised macrophage, using the alternate polarization strategies to included TGFβ. This is a potent anti-inflammatory, Th2 cytokine that plays critical roles in immunoregulation. It has been documented that TGFβ stimulation is cable of inducing an M2-like phenotype in macrophage (Blobe et al., 2002; Zhang et al., 2016). In combination with IL-4 we demonstrated that TGFβ was able to enhance IL-10 secretion relative to IL-4 and IL-13 stimulated macrophage in J774A.1 macrophage.

Another polarization strategy we attempted involved the use of a molecule called Prostaglandin E2 (PGE2). PGE2 is a fatty acid attached to the eicosanoid family (Park et al., 2006). PGE2 is generated by the metabolizing of arachidonic acid by the enzymes COX-1 and COX-2 (Park et al., 2006). PGE2 is a multifunctional regulator of the inflammatory response. Knockout studies in mice suggest that abolition of COX-1 leads to a decreased inflammatory response, suggesting an key role in promoting inflammation (Park et al., 2006). Furthermore, PGE2 was found to be integral in the skewing of macrophage towards and M1 phenotype during a *Salmonella Typhimurium* infection (Sheppe et al., 2018). However, the immunomodulatory role of PGE2 is multifaceted, as with many immune mediators, and appears to be context dependent. Several studies have linked PGE2 to the polarization of M2 like phenotypes in macrophages (Liu et al., 2012; Montero et al., 2016). PGE2 also appears to play a critical role in the resolution of inflammation. Loynes et. al, demonstrated in an *in vivo* wounding model in Zebrafish, that macrophage derived PGE2 is essential deactivation inflammatory neutrophil and promoting their migration away from the site of injury. This resolution of neutrophilic inflammation was associated with improved healing of the wounds (Loynes et al., 2018). Furthermore, *in vitro* studies have demonstrated that PGE2 augments cellular responses to LPS. In bovine epithelial cells it has been demonstrated that PGE2 and LPS stimulation suppresses the expression of TLR4 and IL-8 (Shen et al., 2018). In macrophage, PGE2 and LPS stimulation was indicated to suppress the expression of IFNβ and TNFα, while maintaining or enhancing IL-10 secretion (Tang et al., 2017; Treffkorn et al., 2004; Xu et al., 2008).

In our experiments this combination of LPS and PGE2 suppressed the LPS mediated secretion of IL-1β, IL-6 and TNFα while promoting IL-10 secretion. This generated a cytokine secretome profile comparable to the IL-4 and TGFβ polarised cells, suggesting skewing towards an M2-like phenotype. However, LPS/PGE2 cells failed to induce expression of Arginase 1, a key phenotypic marker of M2 macrophage. Significant upregulation of nitric oxide secretion was also observed. It is likely that this is related to the lack of Arginase 1 activity due to both Arginase 1 and iNOS relying on the availability of the same substrate, Arginine (Rath et al., 2014).

Therefore, moving forward it was decided that a cocktail of IL-4 and TGFβ would be employed for *in vitro* M2 polarization in J774A.1 macrophage based on the M2-like secretome profile and functional Arginase 1 expression in treated cells. However, IL-10 levels were still consistently lower or the same as M1 stimulated cells. Consequently, it was necessary to observe M1 and M2 macrophage independently of each other, in the context of this study.

Given that several groups in FHI were examining the immunomodulatory potential of milk protein hydrolysates, it was critical for the sake of cross institutional comparisons of experimental outcomes, that the variability of hydrolysate preparation was accounted for. In 2015, an SOP for cross institutional hydrolysate preparation and stimulation was agreed upon. This describes cells being exposed to 1mg/mL of protein hydrolysate for 1hr prior to activation with inflammatory or anti-inflammatory mediators. Therefore, we assessed whether the 1 hr time exposure and indeed the 1mg/ml concentration were optimal for our model, before proceeding further. Furthermore, the fate of an immunomodulatory hydrolysate identified by FHI, is to be included in a functional food, applicable to specific area to promote health benefits. Consequently, it is important to examine what happens when macrophage are exposed to the hydrolysates for a longer period of time prior to polarisation. Considerable effects on M1 polarised macrophage cytokine and NO_2^- secretion were observed after 1 hour. However, at the same concentration, the anti-inflammatory potential of the same panel of hydrolysates was diminished after 6hr and 12hr, with associated reduction in IL-10 secretion. Interestingly, after 1 hour, TNFα levels in unpolarised J774A.1 macrophage was suppressed, while IL-10 secretion was enhanced. However, after 6hr and 12hr TNFα and IL-10 levels returned to basal concentrations. It is possible that the anti-inflammatory potential of these hydrolysates is mediated by the driving of M2 associated IL-10 and the suppression of TNFα, given it has integral role in driving an M1 phenotype (Lin et al., 2018). Upon re-exposure to the same dose at the time of polarisation, the return of pro-inflammatory cytokine suppression was observed, however significant reductions in IL-10 were also observed. This observation raised the question, is the anti-inflammatory effect of the re-exposure due to A) more total hydrolysate present or B) fresh unmetabolized hydrolysate present?

To answer this, J774A.1 macrophage were exposed to 2mg/mL of hydrolysate for 1hr, 6hr and 12hr prior to polarisation to an M1 phenotype. At this dose, anti-inflammatory activity in several samples was maintained across the time points, however IL-10 concentrations were trending downwards compared to M1 stimulated cells, as seen when cells were re-exposed to the hydrolysate previously. This raises the possibility that increased doses and incubation times before polarisation *in vitro* may have immunosuppressive effects, rather that specific anti-inflammatory effects. Some evidence exists to show that specific fractions of hydrolysed NaCN do indeed suppress inflammatory cytokine secretion and suppress IL-10 (Mukhopadhya et al., 2014). This will have implications in future studies looking at the *in vivo* effects of specific samples. Therefore, we maintained our protocol of 1mg/ml for 1 hour.

With both the M1, M2 polarisation model optimisation and the time and concentration of exposure finalised, we next continued with screening of an expanded set of milk derived hydrolysates. Cow's milk is comprised two major protein families, Whey and Casein. In the context of sports nutrition and supporting recovery from intense exercise, whey protein is the go-to due to its solubility and rate of absorption when compared to casein (Phillips, 2011). Whey protein hydrolysates have been examined extensively for their health boosting effects. For example, whey protein hydrolysates have been associated with improved muscle recovery in runners (Bibby et al., 2015). Several whey protein hydrolysates have also been found to be immunomodulatory (Dullius et al., 2018; Marcone, Simone et al., 2017; Reyes-Diaz et al., 2018).

As whey protein is digested and absorbed rapidly, a hydrolysate derived from whey may have major benefits as a functional food for muscle recovery post exercise. A panel of Whole Whey protein (WPC) and their hydrolysates were found to have several immunomodulatory effects in M1 and M2 polarised J774A.1 macrophage. Observations noted that several samples such as 2-10 and 2-11 displayed anti-TNFα and anti-IL-6 properties, while boosting IL-10 secretion in M1 macrophage. Similarly, in M2 macrophage IL-10 secretion was enhanced by samples 2-10 and 2-11. Samples 2-47 and regenerates derived from further hydrolysis of 2-47 (2-151 to 2-152) also exhibited anti-inflammatory

properties, significantly downregulating IL-1β, IL-6 and TNFα secretion, furthermore these hydrolysates also maintained IL-10 secretion in M2 polarised macrophage. It has been noted that inhibition of TNFα can improve wound healing (Goren et al., 2007) and inhibition of IL-6 can increase the regenerative capacity of skeletal muscle in chronic muscle injury (Narsale and Carson, 2015). Enhancement of IL-10 secretion may also drive phenotypic shifts from M1 to M2 phenotypes, potentially aiding in the resolution of inflammation in skeletal muscle (Jiang et al., 2016; Makita et al., 2015). These findings again demonstrate the potential of the milk-derived hydrolysates to modulate M1 and M2 phenotypes which could have subsequent effects on muscle health.

To summarise the findings of this chapter:

1. A model of M1 and M2 macrophage polarisation was developed in J774A.1 macrophage. Each of the polarised phenotypes express cytokine secretome profiles and phenotypic markers consistent with current knowledge of macrophage biology.

2. It has been demonstrated that the effects of milk derived hydrolysates are transient and that doses of specific hydrolysates can illicit varying cytokine responses in M1 polarised macrophage. This allowed for further optimisation the method of hydrolysate stimulation, to be of use in later models in this thesis.

3. It was shown, using this model of macrophage polarisation, that both whey and casein derived milk hydrolysates can influence M1 and M2 macrophage phenotypes in terms of cytokine secretion, with many exhibiting potent anti-inflammatory bioactivities.

This chapter has provided the basis for which selection of specific candidate samples for crosstalk studies with skeletal muscle cells will be made to study the effects of anti-inflammatory modulated immune function on measures of skeletal muscle health. The next chapter will now screen these identified immunomodulatory hydrolysates for additional bioactivities directly on skeletal muscle cell models.

Chapter 4

Establishment of *in vitro* Screening Platforms to Study the Effect of Cows Milk Protein Hydrolysates on Glucose Metabolism, Protein Anabolism and Wound Healing in Skeletal Muscle

4.1 Introduction

Skeletal muscle is one of the most abundant tissues in the body. Beyond its prime function of locomotion, skeletal muscle is a primary metabolic site in the body (Frontera and Ochala, 2015). The metabolic functions of skeletal muscle have roles in the utilization of ingested nutrients for energy production and tissue maintenance (Egan and Zierath, 2013a) Three critical functions that muscle requires to maintain homeostasis is the ability to intake and utilize glucose, regulate protein synthesis and be able to heal itself post injury.

The rate of glucose uptake and utilization increases during exercise and during nutrient intake (Egan and Zierath, 2013b). The primary glucose transporter, GLUT4, is responsible for facilitating glucose transport across the cell membrane in skeletal muscle. GLUT4 is constantly being translocated to the cell membrane and recycled internally to allow for a consistent and steady uptake of glucose (Bryant et al., 2002; Richter and Hargreaves, 2013). GLUT4 translocation and subsequent activity, is facilitated by the contraction of muscle fibers during movement and exercise (Messina et al., 2015). However, GLUT4 activity is primarily promoted by the activity of insulin. Insulin is secreted from the pancreas in response to nutrient intake, and its primary function is to induce nutrient uptake and metabolic processes to support bodily activity (Bryant et al., 2002). Insulin binds to the insulin receptors, such as IRS-1, located on the cell surface which initiates a signaling cascade which, in the context of GLUT4, drives receptor gene expression, processing and translocation to the cell membrane (Jiao et al., 2015; Wang et al., 1998) Due to the importance of clearing glucose from the blood stream, efficient GLUT4 function is paramount (Bryant et al., 2002).

Dysfunction in GLUT4 activity, directly coincides with the pathogenesis of insulin resistance and subsequently T2DM (Jiao et al., 2015). Nutritional and exercise interventions appear to offer therapeutic potential to restore GLUT4 function and attenuate insulin resistance. For example, a rodent model of insulin resistance demonstrated that intake of dietary cod protein sources has the potential to re-sensitise the host to the effects of insulin (Frederic Tremblay, Charles Lavigne, Helene Jacques, 2003). Several human studies, concerning the

elderly, have demonstrated that physical exercise can attenuate insulin resistance (Cartee et al., 2016; Richter and Hargreaves, 2013).

The catabolic pathways in muscle enable appropriate energy production, to support physical activity and homeostatic bodily function (McCarthy and Esser, 2010)**.** Metabolic efficiency is a critical process in skeletal muscle for appropriate utilization of nutrients and significantly, in order to self-regulate its mass If this efficiency is compromised, the balance of catabolic to anabolic processes is tipped towards catabolism and this can deleteriously impact muscle function, namely in the process of muscle protein synthesis (MPS), a critical pathway for the regulation of muscle mass (Kalyani et al., 2014). A decrease in protein synthesis can result in a loss of muscle mass over time and due to the decreased muscle mass, a decrease in the metabolic potential of skeletal muscle (Haran et al., 2012; Yoon, 2017). The primary regulator of the muscle protein synthesis pathway is the mammalian target or rapamycin (mTOR) multi-protein complex. The mTOR signaling cascade is responsible for regulating muscle protein synthesis and maintaining muscle mass (Torre-Villalvazo et al., 2019)**.** Downstream of the primary mTOR complex, there are several signaling proteins, whose activity is directly proportional to the activity of mTOR, and can thus be correlated to the rate of muscle protein synthesis (Egan and Zierath, 2013b). One of these markers is 4-eukaryotic binding protein 1 (4-EBP1). 4-EBP1s phosphorylation (activation) allows for an indirect measurement of MPS rates (Haran et al., 2012). mTOR is activated in response to anabolic signals such as nutrients and hormones. One of the primary activators is the hormone Insulin which drives mTOR activation via IRS-1 (Shen et al., 2005). Insulin mediated activation of the mTORC1 complex initiates phosphorylation 4-EBP1 and drives translation initiation and protein production. Age and inflammation have both been identified to play significant roles in the inhibition of mTOR signaling and as a result, protein synthesis in muscle tissue (Breen and Phillips, 2011; Haran et al., 2012). Furthermore, failure to adequately in take enough dietary protein is known to contribute to this process. It has been documented previously that driving mTOR activity via protein supplementation, in combination with resistance training can have beneficial impacts on muscle mass and function (Deldicque et al., 2005; Yoon, 2017).

Skeletal muscle, along with the liver, is one of the few organs in the body that is capable of regenerating itself from injury and damage (George K. Michalopoulos, 2007; Tidball and Villalta, 2010). As mentioned previously, the initial proliferative response of resident stem cells and myoblasts within the muscle structure is critical in order to provide enough new tissue initiate wound closure. During the process of myogenesis there is temporal activation and deactivation of specific genes that promote the proliferation and differentiation of myoblasts to myotubes (Krook et al., 2014). Although an acute inflammatory response is critical for initiating wound healing, chronic inflammation has been demonstrated *in vitro* and *in vivo* to diminish the capacity of myoblasts to form myotubes via co-culture and conditioned medium experiments using human monocytes (Saclier et al., 2013). The process of myogenesis can be negatively impacted through chronic inflammation and protein malnutrition, leading to muscle atrophy and loss of mechanical and metabolic functions overtime, detrimentally impacting the persons quality of life (Londhe and Guttridge, 2015; Pourhassan et al., 2020). In contrast, opioid like peptides found in chicken feed have been shown to inhibit myoblast migration in chickens, negatively affecting muscle mass and overall yield of meat from these animals, demonstrating the importance that nutrition, adequate or otherwise, has on the ability of damaged muscle to heal properly and maintain its mass (Nihashi et al., 2019).

Given the anti-inflammatory activity of many of the hydrolysates derived from whey and casein sources found in bovine milk demonstrated in the previous chapter, the aims of this chapter are to screen the immunomodulatory hydrolysates, for additional bioactivities that may directly provide health benefits in skeletal muscle based on the critical aspects of muscle functions discussed above, glucose metabolism, muscle protein synthesis and regeneration. The specific objectives are:

1. To establish a GLUT4 *in vitro* screening platform in a skeletal muscle cell line. This *in vitro* model will be used to assess the impact of immune mediators and bovine milk derived hydrolysates on GLUT4 translocation in skeletal muscle. For this, the L6-GLUT4myc myotubes will be employed. This cell model has long been employed in investigations concerning glucose metabolism and GLUT4 activity (Huang et al., 2002; Ishikura et al., 2010b).

2. To establish an *in vitro* screening platform to detect and quantify the levels of phosphorylated 4-EBP1$^{(Thr37/46)}$ via western blot and image analysis in parental L6 myotubes. This platform will then be employed to examine the effects of whey and casein derived protein hydrolysates on the levels of 4-EBP1 activation.

3. To optimize an *in vitro* wound healing assay using a scratch assay method of injury induction. Using this method, it will be possible to visualize, quantify and measure the effect that treatment with whey and casein derived protein hydrolysates has on wound closure, alluding to potential pro-myogenic functions *in vivo*.

4.2 Results

4.2.1 Growth and Culture of L6 GLUT4myc Rat Derived Skeletal Muscle Cells

The L6 skeletal muscle cell line (Kerafast), originally isolated from the quadricep muscle of rats, is a myoblast cell line that can readily fuse and differentiate into mature skeletal myotubes. Myogenic differentiation can be observed microscopically (figure 4.1), as seen by the distinct differences in cellular structure between the myoblast and myotube stages of the L6 myoblast cell life cycle. Initially, L6 GLUT4myc skeletal muscle cells were seeded in 6 well plates at $4x10^4$ cells/mL in L6 growth medium. Images of cell growth and differentiation were taken on days one through eight. Over the course of four days, the myoblasts expanded and proliferated and covered the surface of the cell culture plate in a single monolayer. Once confluent, L6 myoblasts begin to orientate together and line up end to end (Figure 4.1). At this point, cell monolayers were maintained in L6 differentiation medium for a further four days. Over the period of day four to eight, orientated myoblasts subsequently underwent cellular fusion, forming the large multinucleated myotubes. The L6 GLUT4myc myoblast cell lines carries a plasmid that allows for over expression of the primary insulin stimulated transporter GLUT4. The recombinant GLUT4 contains a myc tag, located on the extracellular portion of the transporter. This myc tag allows for GLUT4myc immuno-detection and quantification and is a valuable tool in researching glucose metabolism in several contexts.

4.2.2 100nM Insulin Induces GLUT4myc Translocation to the cell surface of both myoblasts and myotubes

It has been established that a super-physiological concentration of insulin is able to induce a roughly 1.5 to 2.0 fold change in cell surface GLUT4 in L6 GLUT4myc myoblasts and myotubes (Ishikura et al., 2010b). 100nM insulin is routinely used to induce this fold change in cell surface GLUT4. In order to confirm that the originally described method of inducing GLUT4 translocation *in vitro* is a viable method to detect changes in cell surface GLUT4 in our experiments, GLUT4myc translocation in response to 100nM insulin was assessed. L6 GLUT4myc myoblasts were seeded at $8x10^4$ cells/mL and grown to confluence at 37°C in 5% CO_2. For myotube differentiation, cells were seeded at $4x10^4$ cells/mL and grown to

confluence at 37°C in 5% CO_2. After four days, confluent L6 monolayers were subsequently cultured in low serum, differentiation medium as previously described. Cells were serum starved for three hours at 37°C in 5% CO_2. Once the serum starve incubation was complete, L6 GLUT4myc myoblasts or myotubes were incubated with 100nM insulin for 20 min at 37°C in 5% CO_2. Cell surface GLUT4myc was detected and quantified as previously described in section 2.2.9. As detailed in figure 4.2, 100nM insulin is capable of driving a significant increase in cell surface GLUT4myc is both the myoblast ($p<0.001$) and myotube ($p<0.001$) stage of this muscle cell line compared to the untreated controls (UTC).

4.2.3 Treatment of L6 GLUT4myc Myoblasts with 100ng/mL of Th1 and Th2 cytokines, impacts basal and insulin stimulated GLUT4myc

In order to assess if changes in GLUT4myc translocation can be detected using the baseline assay previously described, it was decided to assess the impact of recombinant Th1 and Th2 cytokines on GLIT4 translocation to the membrane in L6 GLUT4myc myoblasts. Due to the cross talk between the immune system and skeletal muscle *in vivo*, and the link between inflammation and insulin related metabolic syndromes such as diabetes the effect of chronic stimulation with respective inflammatory Th1 and anti-inflammatory Th2 cytokines was assessed, as illustrated in figure 4.3. L6 GLUT4myc myoblasts were seeded at $8x10^4$ cells/mL and grown to confluence at 37°C in 5% CO_2. Cells were incubated with 100ng/mL of the Th2 cytokines IL-2, IL-4 and TGFβ and the Th1 cytokines IL-6, IFNγ, and TNFα (Th1) for 24 hours at 37°C in 5% CO_2. Cells were subsequently serum starved for three hours. Once the serum starve incubation was complete, L6 GLUT4myc myoblasts were incubated with 100nM insulin for 20 min. In the case of IL-2, IL-4 ($P<0.05$), IFNγ, TGFβ ($p<0.001$) and TNFα ($p<0.001$), basal levels of GLUT4myc was increased compared to the untreated control, suggesting a positive insulinotrophic effect. IL-2 ($p<0.01$), TGFβ ($p<0.001$) and IL-4 (ns), in the presence of 100nM insulin increased cell surface GLUT4 compared to the insulin stimulated control, suggesting a potential synergy between the Th2 cytokines and insulin. In contrast, there was no synergy observed between IL-6 and insulin as treatment did not appear to impact GLUT4myc translocation negatively or positively in the basal and insulin treated conditions.

4.2.4 Assessment of a 96 well GLUT4myc Assay Format

Previous data presented was obtained using the classic 24 well cell culture plate approach. Although appropriate for detecting changes in cell surface GLUT4myc, there are limitations in the variety of conditions that can be measured on a given plate. Development of a 96 well assay format for the measurement of cell surface GLUT4myc is desirable, as it will allow for the comparison of more samples.

4.2.4.1 100nM Insulin stimulation leads to varied response in cell surface GLUT4myc

L6 GLUT4myc myoblasts were seeded at $8x10^4$ cells/mL and grown to confluence at 37°C in 5% CO_2. Cells were subsequently serum starved for three hours at 37°C in 5% CO_2. Once the serum starve incubation was complete, L6 GLUT4myc myoblasts were incubated with 100nM insulin for 20 min. Cell surface GLUT4myc was detected and quantified as previously described. Fold changes are considerably lower relative to the 24 well assay fold change presented previously. Illustrated in supplementary figure SF1.12, through four independent experiments, changes in insulin stimulated GLUT4 translocation varies from a 1.2 to a 1.6 fold change. This variability and unpredictability in cell insulin response is problematic, as it will make interpretation of our sample hydrolysate's effects on GLUT4 translocation difficult. Of note, L6 GLUT4myc myotubes were unable to proliferate sufficiently and differentiate in a 96 well cell culture plate, for this assay. Perhaps due to due to the lack of sufficient space and cell numbers to support successful differentiation into mature myotubes.

4.2.4.2 Insulin Induces GLUT4 Translocation to the Cell Membrane of L6 GLUT4myc Myoblasts in a dose dependant manner however, fails to induce and adequate fold change in cell surface GLUT4

In attempt to ameliorate variability and lower fold changes in response to 100nM insulin via a 96 well format, a dose response with insulin was performed to try and drive GLUT4myc translocation in myoblasts (figure 4.5). L6 GLUT4myc myoblasts were seeded at $8x10^4$ cells/mL and grown to confluence at 37°C in 5% CO_2. Cells were subsequently serum starved for three hours at 37°C in 5% CO_2. Once the serum starve incubation was complete, L6 GLUT4myc myoblasts were incubated with the following doses of Bovine Insulin; 10nM, 50nM, 100nM and 1μM; for 20 min at 37°C in 5% CO_2. Cell surface GLUT4myc was detected and quantified as previously described in in section 2.2.9. Although GLUT4my changes were altered in a dose dependant manner, the fold changes relative to the unstimulated control are not sufficient, outlined in supplementary figure SF1.13. This perhaps due to the high relative signal of the UTC. However, given the knowledge than insulin stimulation leads to a significant increase in cell surface GLUT4myc, these fold changes in a 96 well plate are not acceptable.

4.2.4.3 Variability and inconsistencies in detectable fold changes between the unstimulated control and insulin stimulated control lead to an inability to interpret the effects of casein and casein derived hydrolysates on basal and insulin stimulated GLUT4myc translocation

L6 GLUT4myc myoblasts were seeded in 96 well plates at $8x10^4$ cells/mL and grown to confluence at 37°C in 5% CO_2. Cells were subsequently serum starved for three hours at 37°C in 5% CO_2. Once the serum starve incubation was complete, L6 GLUT4myc myoblasts were incubated with either 1mg/mL candidate hydrolysate in the presence or absence 100nM bovine insulin for 20 min. As illustrated in figure 4.4 only a 1.2 fold change between the unstimulated and insulin stimulated controls was detected. With this in mind, the hydrolysate data suggests that a selection of hydrolysates are having the same effect as 100nM insulin, in the absence of 100nM insulin. In the presence of 100nM insulin (figure 4.7), a decreased response was observed in several samples, which contradicts the basal data. Thus, due to the lack of fold change between the unstimulated and insulin stimulated controls it is not possible to derive if these changes are in fact meaningful. As a result, the

96 well GLUT4 assay option does not appear to be a viable option for bioactivity screening of milk derived hydrolysates.

4.2.5 Optimisation of an in vitro screening platform for the detection of cell surface GLUT4 in L6 GLUT4myc myoblasts and myotubes.

It has been demonstrated previously that the original GLUT4 translocation assay that uses 100nM insulin as a driver is sufficient to allow us to detect changes in cell surface GLUT4. The 96 well assay format has also been shown to be a non-viable option for the screening of hydrolysate effects on GLUT4 translocation. Moving forward, the 24 well plate assay format will be used to measure GLUT4myc translocation and how samples or immune-environmental conditions impact this translocation. Consequently, further optimisations to ensure a clear, interpretable signal, relating to GLUT4 translocation is required.

4.2.5.1 Insulin Induces GLUT4 Translocation to the Cell Membrane of L6 GLUT4myc Myoblasts in a dose dependant manner

L6 GLUT4myc myoblasts were seeded at $8x10^4$ cells/mL and grown to confluence at 37°C in 5% CO_2. Cells were subsequently serum starved for three hours at 37°C in 5% CO_2. Once the serum starve incubation was complete, L6 GLUT4myc myoblasts were incubated with the following doses of Bovine Insulin; 10nM, 50nM, 100nM, 1μM and 2μM; for 20 min at 37°C in 5% CO_2. Cell surface GLUT4myc was detected and quantified as previously described. Illustrated in Figure 4.5, Across all dose ranges, levels of cell surface GLUT4myc were significantly upregulated ($p<0.001$). A 1μM insulin concentration, yielded the highest fold change of cell surface GLUT4myc compared to the unstimulated control. Of note, there is a significant change in cell surface GLUT4myc in the 100nM insulin ($p<0.05$) and 2μM insulin ($p<0.001$) compared to the 1μM insulin dose. Considering this, the 1μM insulin dose was brought forward to assess the effect of insulin incubation time on GLUT4myc translocation in L6 GLUT4myc myoblasts.

4.2.5.2 Time course analysis of GLUT4myc translocation in response to 1μM Insulin in L6 GLUT4myc myoblasts

L6 GLUT4myc myoblasts were seeded at $8x10^4$ cells/mL and grown to confluence at 37°C in 5% CO_2. Cells were subsequently serum starved for three hours at 37°C in 5% CO_2. Once the serum starve incubation was complete, L6 GLUT4myc myoblasts were incubated with 1μM insulin for 10min, 20min, 30min, 45min and 60min at 37°C in 5% CO_2. As can be observed in figure 4.6, there is a temporal effect on GLUT4 translocation stimulated with 1μM. Cell surface GLUT4myc peaked at both the 20 minute and 30-minute time points, there is no significant difference between these time points. Cell surface GLUT4myc then began to drop off at times exceeding 30 min. Although a 10minute incubation induced GLUT4myc translocation, cell surface levels were significantly lower ($p<0.001$) than the 20- and 30-minute incubation times. It was subsequently concluded that a 1μM insulin stimulation for 20 min at 37°C in 5% CO_2 will be used to assess the impact of casein derived hydrolysates of GLUT4 translocation.

4.2.5.3 Insulin induces GLUT4 translocation to the cell membrane of L6 GLUT4myc Myotubes in a dose dependant manner

L6 GLUT4myc myoblasts were seeded at $4x10^4$ cells/mL and grown to confluence at 37°C in 5% CO_2 where they were subsequently differentiated in myotubes as previously described. Cells were subsequently serum starved for three hours at 37°C in 5% CO_2. Once the serum starve incubation was complete, L6 GLUT4myc myoblasts were incubated with the following doses of Bovine Insulin; 10nM, 50nM, 100nM, 1μM and 2μM; for 20 min, as determined in the myoblast time course, at 37°C in 5% CO_2. Cell surface GLUT4myc was detected and quantified as previously described. As illustrated in figure 4.7, all doses of insulin significantly enhanced the levels of detectable GLUT4myc on the surface of the myotubes ($p<0.001$). There was statistically significant change between successive doses, however a peak at 1μM insulin after 20mins was observed.

4.2.5.4 Time course analysis of GLUT4myc translocation in response to 1μM Insulin in L6 GLUT4myc Myotubes

L6 GLUT4myc myoblasts were seeded at $4x10^4$ cells/mL and grown to confluence at 37°C in 5% CO_2 where they were subsequently differentiated in myotubes as previously described. Cells were subsequently serum starved for three hours at 37°C in 5% CO_2. Once the serum starve incubation was complete, L6 GLUT4myc myoblasts were incubated with 1μM insulin for 10min, 20min, 30min, 45min and 60min at 37°C in 5% CO_2. As illustrated in figure 4.8 incubation with 1μM insulin is differentially affected by time. At each time points, there was a significant increase in cell surface GLUT4myc translocation ($p<0.001$). GLUT4myc translocation peaked at 20mins and proceeded to drop off as time increased. There were significant difference between 10min vs. 20min ($p<0.001$), 20min vs 30min ($p<0.01$), 20min vs 45min ($p<0.001$) and 20min vs 60min ($p<0.001$). Moving forward, It was subsequently concluded that a 1μM insulin stimulation for 20 min at 37°C in 5% CO_2 will be used to assess the impact of milk derived hydrolysates of GLUT4 translocation.

4.2.6 Representative doses of recombinant Th1 and Th2 cytokines secreted from J774A.1 macrophage modulate GLUT4 translocation in L6 GLUT4myc myotubes

Soluble, secreted immune factors have been shown to have considerable effects on muscle metabolism both *in vitro* and in vivo. To assess the robustness of the optimised GLUT4 translocation assay, recombinant Th1 and Th2 cytokines with documented effects on GLUT4 function were used to assess whether varying stimuli can change GLUT4 translocation *in vitro* . L6 GLUT4myc myoblasts were seeded at $4x10^4$ cells/mL and grown to confluence at 37°C in 5% CO_2 where they were subsequently differentiated in myotubes as previously described. Cells were subsequently serum starved for three hours at 37°C in 5% CO_2. Cells were subsequently incubated with a dose range of 500pg/mL to 10ng/mL of recombinant IL-1β, IL-6, IL-10 and TNFα for 24hr. This dose range was chosen as it is representative of the range of secreted cytokines from the established M1 and M2 polarisation model in J774A.1 macrophage as presented in the previous chapter. As

illustrated in figure 4.9. Pro-inflammatory cytokines IL-1β, IL-6 and TNFα dose dependently increased both the basal and insulin stimulated levels of cell surface GLUT4myc. Anti-inflammatory (Th2) IL-10 however appeared to have the opposite effect with significantly decreased levels of insulin stimulated cell surface GLUT4. Basal GLUT4 in response to IL-10 trended downwards as dose increased resulting in a significant reduction of cell surface GLUT4myc at 10ng/mL.

4.2.7 Preliminary Analysis of the Effect of Casein Derived Protein Hydrolysates on GLUT4myc Translocation in L6 GLUT4myc Myoblasts

Having assessed the effect of altering cytokine concentrations on GLUT4 translocation, we have demonstrated that the assay is cable of detecting changes in cell surface GLUT4myc. Initial screening of a cohort of casein hydrolysates, in the presence and absence of 1μM insulin, was performed in myoblasts in order to assess whether previously identified immunomodulatory hydrolysates could modulate GLUT4 translocation in muscle cells.

4.2.7.1 Casein derived protein hydrolysates differentially effect the basal levels of GLUT4myc is L6 GLUT4myc Myoblasts

L6 GLUT4myc myoblasts were seeded at $8x10^4$ cells/mL and grown to confluence at 37°C in 5% CO_2. Cells were subsequently serum starved for three hours at 37°C in 5% CO_2. Once the serum starve incubation was complete, L6 GLUT4myc myoblasts were incubated with either 1mg/mL candidate hydrolysate or 1μM bovine insulin for 20 min at 37°C in 5% CO_2. Represented in Figure 4.10, cell surface GLUT4myc was detected and quantified as previously described. Whole intact casein (NaCN), 2-34, 2-134, 2-135 significantly ($p<0.001$) and deleteriously impacted on cell surface GLUT4myc in the basal state. Remaining samples do not appear to have negatively affected basal cell surface GLUT4myc with modest increases observed in samples 2-133, 2-18, 2-21, 2-22 and 2-29 ($p<0.05$).

4.2.7.2 Casein derived protein hydrolysates differentially effect the insulin stimulated levels of Cell Surface GLUT4myc is L6 GLUT4myc Myoblasts

L6 GLUT4myc myoblasts were seeded at $8x10^4$ cells/mL and grown to confluence at 37°C in 5% CO_2. Cells were subsequently serum starved for three hours at 37°C in 5% CO_2. Once the serum starve incubation was complete, L6 GLUT4myc myoblasts were co-incubated with 1mg/mL candidate hydrolysate and 1μM bovine insulin for 20 min at 37°C in 5% CO_2. Cell surface GLUT4myc was detected and quantified as previously described. Illustrated in figure 4.11, samples 2-18, 2-21, 2-22, 2-29, 2-30 ($p<0.001$) and 2-27 ($p<0.05$) exhibited strong synergistic effects with insulin, significantly boosting the abundance of cell surface GLUT4myc compared to the 1μM insulin control.

4.2.8 Casein and Whey derived protein hydrolysates differentially modulate GLUT4 translocation to the cell surface of L6 GLUT4myc Myotubes.

Initial data has demonstrated that milk derived hydrolysates can, in some cases beneficially modulate GLUT4 translocation in myoblasts. Myotubes are the primary contractile component in function skeletal muscle, and as a result adequate glucose uptake and utilisation is essential for their role in locomotion. Due to this fact, the full panel of whey and casein hydrolysates was screened for GLUT4 modulating bioactivity in L6 GLUT4myc myotubes. L6 GLUT4myc myoblasts were seeded at $4x10^4$ cells/mL and grown to confluence at 37°C in 5% CO_2 where they were subsequently differentiated in myotubes as previously described. Cells were subsequently serum starved for three hours at 37°C in 5% CO_2. Once the serum starve incubation was complete, L6 GLUT4myc myotubes were incubated with 1mg/mL of whole protein controls, WPC/NaCN or derived hydrolysate in the presence or absence of 1μM bovine insulin for 25 min at 37°C in 5% CO_2. Cell surface GLUT4myc was detected and quantified as previously described. Data is summarised in table 4.1 and table 4.2 and represented in figures 4.12 to 4.17 inclusive.

4.2.8.1 Effect of Whey Derived Hydrolysates on GLUT4 Translocation in L6 GLUT4myc Myotubes.

Whey family derived hydrolysates exhibited significant insulinotrophic effects on the basal level of cell surface GLUT4 in L6 GLUT4myc myotubes. In most cases, WPC hydrolysats significantly drove the basal levels of cell surface GLUT4 with the exception of samples 2-153 and 2-154 (figure 4.20) , where a modest decrease compared to the UTC was observed. Varying effects of were observed with the WPC substrate control. This may be due to the fact that this is a whole protein source and is metabolised to a varying degree each and every time, subtly effecting bioactivity. In the presence of 1uM insulin, samples 2-12, 2-13 ($p<0.001$) and 2-153 had deleterious consequences for insulin stimulated levels of GLUT4. In contrast, samples 2-40 ($p<0.05$), 2-47 ($p<0.001$), 2-152 ($p<0.05$) and 2-154 ($p<0.01$) (Figures 4.13 and 4.17 respectively) were able to considerably enhance the levels of cell surface GLUT4 in response to 1µM insulin.

4.2.8.2 Effect of Casein Derived Hydrolysates on GLUT4 Translocation in L6 GLUT4myc Myotubes

In contrast to the whey protein hydrolysates previously discussed, casein derived hydrolysates have been shown to induce more significant and beneficial changes in cell surface GLUT4 in the presence and absence of insulin. Several casein hydrolysates both significantly enhanced the basal levels of GLUT4 on the myotube cell surface, notably samples: 2-18 ($p<0.001$), 2-21 ($p<0.001$), 2-22 ($p<0.001$), 2-23 ($p<0.01$), 2-28 ($p<0.01$) and 2-132 ($p<0.05$) (figures 4.16, 4.18, and 4.19 respectively). Theses samples also exhibited potent synergistic effects with insulin driving significant increases in cell surface GLUT4; 2-18 ($p<0.001$), 2-21 ($p<0.01$), 2-22 ($p<0.001$), 2-23 ($p<0.001$), 2-28 ($p<0.001$) and 2-132 ($p<0.01$) (figures 4.13, 4.15, and 4.16 respectively). In contrast to the whey protein derived hydrolysates, none of the candidate casein derived hydrolysates exhibited detrimental effects on GLUT4 translocation. In every case, cell surface expression of GLUT4myc was enhanced or maintained. Like the whole whey protein substrate, variations in cell responses to the whole casein (NaCN) were observed, perhaps indicating that the whole protein source is metabolised to a varying degree each time, effecting its bioactivity.

4.2.8.3 Notable Hydrolysates Affect GLUT4myc Translocation in a dose dependant manner

Five hydrolysates were noted to have positive effects on GLUT4myc translocation in L6 GLUT4myc myotubes. 2-18, 2-21, 2-47, 2-132 and 2-152 all exhibited pro-GLUT4 bioactivity at 1mg/mL alone and in the presence of 1µM insulin. Therefore it was decided to investigate the effect of increasing dosages on GLUT4myc translocation. L6 GLUT4myc myoblasts were seeded at $4x10^4$ cells/mL and grown to confluence at 37°C in 5% CO_2 where they were subsequently differentiated into myotubes as previously described. Cells were subsequently serum starved for three hours at 37°C in 5% CO_2. Once the serum starve incubation was complete, L6 GLUT4myc myotubes were incubated with 0.5mg/mL, 1mg/mL, 2mg/mL and 5mg/mL for 20min in the presence or absence of 1µM insulin at 37°C in 5% CO_2. As outlined in Figure 4.18, In the absence of insulin, Samples 2-18 and 2-47 dose dependently increased the levels of GLUT4myc on the cell surface of myotubes. Samples 2-21 and 2-132, GLUT4 translocation peaked at 1mg/mL in the absence of insulin. In the presence of 1µM insulin, increasing doses of samples 2-18, 2-21 and 2-132 exhibited dose dependant decreases in cell surface GLUT4myc. Sample 2-47 in contrast exhibited no dose dependant effects in the presence of 1µM insulin.

Substrate	Sample	Basal	+ 1uM Insulin
WPC	2-01	↑ ***	---
	2-03	↑ **	---
	2-10	↑ *	---
	2-11	↑ ***	---
	2-12	↑ ***	↓
	2-13	-	↓***
	2-40	↑	↑ *
	2-41	-	---
	2-42	↑	---
	2-43	↑ ***	---
	2-44	↑ ***	---
	2-47	↑ ***	↑ ***
	2-151	↑	---
	2-152	↑	↑ *
	2-153	↓	↓
	2-154	↓	↑ **
NaCN	2-18	↑ ***	↑ ***
	2-19	↑	---
	2-21	↑ ***	↑ **
	2-22	↑ ***	↑ ***
	2-23	↑ **	↑ ***
	2-25	---	---
	2-26	↑	↑
	2-27	---	---
	2-28	↑ **	↑ ***
	2-29	↑ ***	---
	2-30	↑ ***	---
	2-31	↑ ***	---
	2-34	---	---
	2-84	---	↑ ***
	2-132	↑ *	↑ **
	2-133	↑ ***	---
	2-134	↑ ***	---
	2-135	---	---

Table 4.1: Summary of the effect of NacN and WPC derived protein hydrolysates at 1mg/mL, on the translocation of GLUT4 in L6 GLUT4myc myotubes. Data is presented as mean ± SEM of three replicates. ***p<0.001, **p<0.01, *p<0.05 comparing UTC/1µM Insulin to hydrolysate treated cells.

Substrate	Sample	Basal GLUT4				1µM Insulin			
		0.5mg/mL	1mg/mL	2mg/mL	5mg/mL	0.5mg/mL	1mg/mL	2mg/mL	5mg/mL
NaCN	2-18	↑**	↑**	↑**	↑***	↓*	↑***	↑***	-------
	2-21	----	↑*	----	-----	↑***	↑***	------	------
	2-132	------	↑**	-----	-----	↑***	↑*	------	↓*
WPC	2-47	↑***	↑***	↑***	↑***	------	↑*	------	------

Table 4.2: Summary of the dose response effect of NacN and WPC derived protein hydrolysates at on the translocation of GLUT4 in L6 GLUT4myc myotubes. Data is presented as mean ± SEM of three replicates. ***p<0.001, **p<0.01, *p<0.05 comparing UTC/1uM Insulin to hydrolysate treated cells.

4.2.9 Detection and Quantification of phospho-4EBP1 in L6 Myotubes

Muscle mass is directly linked to the ability of muscle to function both physically and metabolically. The mammalian target of rapamycin (mTOR) signalling pathway is the considered the master regulator of protein synthesis and caretaker of skeletal muscle mass (Yoon, 2017). There are two functional mTOR complexes within the cell, mTORC1 and mTORC2, the former of which is responsible for regulating proteins synthesis. 4EBP1 is a member of small proteins that are inhibitors of protein translation. When mTORC1 is activated 4EBP1 is phosphorylated and translation of mRNA is initiated. As a result, measuring 4EBP1 phosphorylation will allow for an indirect measure of muscle anabolism regarding protein synthesis.

4.2.9.1 100M Insulin Stimulates 4EBP1 phosphorylation in L6 Myotubes

L6 myoblasts were seeded at $4x10^4$cells/mL. Confluent myoblasts were differentiated into myotubes as previously described. Cells were serum starved for three hours and subsequently incubated with 100nM insulin for 20 min. Cells were lysed via mechanical syringe lysis and proteins separated and blotted as previously described. Following staining with specific secondary antibodies the nitrocellulose membrane was incubated with a TMB western blot substrate for 20 min. Blot images were captured using a digital camera. As presented in supplementary figure SF1.14, 100nM insulin is able to drive 4EBP1 phosphorylation, as indicated by the presence of two separate bands at/below the 20kDa marker. Although it can be qualitatively observed that there is an increase in phosphorylation. this method of visualization does not allow for accurate quantification of phosphorylation levels due to the reflection of light back from the membrane and the lack of band definition.

4.2.9.2 Detection of phospho-4EBP1 in L6 Myotubes using a chemi-luminescent substrate

L6 myoblasts were seeded at $4x10^4$cells/mL. Confluent myoblasts were differentiated into myotubes as previously described. Cells were serum starved for three hours and subsequently incubated with 100nM insulin for 25 min. Cells were lysed via mechanical syringe lysis and proteins separated and blotted as previously described. Following staining with specific secondary antibodies, the nitrocellulose membrane was incubated with a chemi-luminescent ECL western blot substrate for 2 min. Blot images were captured using a G-Box. Blots were exposed for 5 min. 100nM insulin clearly and defiantly induces 4EPB1 phosphorylation, illustrated in supplementary figure SF1.15. The extent of this phosphorylation is more defined qualitatively, than the TMB incubated blots previously.

4.2.9.3 Exposure times dictate relative intensity of signal observable in Western Blots

L6 myoblasts were seeded at $4x10^4$cells/mL. Confluent myoblasts were differentiated into myotubes as previously described. Cells were incubated with 1mg/mL of whole casein (NaCN) and whey (WPC) protein for 24hr. Cells were serum starved for three hours and subsequently incubated with 100nM insulin for 25 min. Cells were lysed via mechanical syringe lysis and proteins separated and blotted as previously described. Following staining with specific secondary antibodies, the nitrocellulose membrane was incubated with a chemi-luminescent ECL western blot substrate for 2 min. Blot images were captured using a G-Box. Images were exposed for 1 minute (supplementary figure SF1.16) and 5 min (supplementary figure SF1.17). 1-minute exposure time allowed for visualization of loading control, β-actin and phospho-4EBP1$^{(Thr37/46)}$ bands. Subtle changes in wells in the presence and absence of 100nM insulin can be observed with regard to phospho-4EBP1$^{(Thr37/46)}$. However, this band instensity is too low to allow for accurate qualitative and quantitative difference to be observed in NaCN and WPC stimulated wells. An exposure time of 5 min however allowed for clear differences to be made between wells containing insulin and those not. Higher intensities of phospho-4EBP1$^{(Thr37/46)}$ activity can be observed both in the presence and absence of 100nM insulin in both NaCN and WPC stimulated cells compared to the unstimulated control and 100nM insulin control

4.2.9.4 Whole Casein and Whey protein drive 4-EBP1 phosphorylation in L6 myotubes in the presence and absence of 100nM insulin

L6 myoblasts were seeded at $4x10^4$cells/mL. Confluent myoblasts were differentiated into myotubes as previously described. Cells were serum starved for three hours and subsequently incubated with 1mg/mL of whole casein (NaCN) and whey (WPC) protein in the presence and absence of 100nM insulin for 25 min. Cells were lysed via mechanical syringe lysis and proteins separated and blotted as previously described. Following staining with specific secondary antibodies, the nitrocellulose membrane was incubated with a chemi-luminescent ECL western blot substrate for 2 min. Blot images were captured using a G-Box. Blots were exposed for 5 min. The intensity of each band was quantified using ImageJ, image analysis software. Pixel values were normalized to the untreated control cells and expressed as arbitrary units (AU). Illustrated in figure 4.19, 100nM insulin drove 4EBP1 phosphorylation significantly, compared to the untreated cells ($p<0.001$). NaCN and WPC increased basal levels of phospho-4EBP1$^{(Thr37/46)}$. Insulin and both NaCN and WPC80 exhibited synergistic effects with one another, both driving phospho-4EBP1$^{(Thr37/46)}$. Interestingly however, there is a significant difference in phospho-4EBP1$^{(Thr37/46)}$ levels in favour of NaCN compared to WPC80 ($p<0.01$). The intention from this point forward will be to see if casein derived hydrolysates can further boost phospho-4EBP1$^{(Thr37/46)}$ activity and benefit muscle protein anabolism.

4.2.9.5 Dose Response Optimisation of 4-EBP1 phosphorylation in L6 myotubes

L6 myoblasts were seeded at $4x10^4$cells/mL. Confluent myoblasts were differentiated into myotubes as previously described. Cells were serum starved for three hours and subsequently incubated with the following dose range of bovine insulin; 10nM, 50nM, 100nM, 1µM and 2µM for 20 min at 37°C in 5% CO2. Cells were lysed via mechanical syringe lysis and proteins separated and blotted as previously described. Following staining with specific secondary antibodies, the nitrocellulose membrane was incubated with a chemi-luminescent ECL western blot substrate for 2 min. Blot images were captured using a G-Box. Blots were exposed for 5 min. Illustrated in figure 4.20, phospho-4EBP1$^{(Thr37/46)}$ was activated in response to insulin stimulation. No significant trend was observed, other than 4EBP1 was phosphorylated to a similar degree irrespective of insulin dose applied.

4.2.9.6 Time Course Optimisation of 4-EBP1 phosphorylation in L6 myotubes

L6 myoblasts were seeded at $4x10^4$cells/mL. Confluent myoblasts were differentiated into myotubes as previously described. Cells were serum starved for three hours and subsequently incubated with 1µM bovine insulin for 10min, 20min, 30min, 45min and 60min at 37^oC in 5% CO2. Cells were lysed via mechanical syringe lysis and proteins separated and blotted as previously described. Following staining with specific secondary antibodies, the nitrocellulose membrane was incubated with a chemi-luminescent ECL western blot substrate for 2 min. Blot images were captured using a G-Box. Blots were exposed for 5 min. As illustrated in figure 4.21, measurements of 4EBP1 activation were determined through analysis of the gamma and alpha chain phosphorylation levels. A time dependent effect of insulin stimulation on gamma chain phosphorylation was observed. Phosphorylation of the gamma chain peaked following 20min of incubation with 1µM insulin, after which, a decrease in this phosphorylation activity was observed. A similar trend was also documented with alpha chain phosphorylation. Phosphorylation levels peaked between 10min and 20min incubation times, where a time dependant drop off in activity was observed. These findings fall in line with previous optimisation experiments regarding GLUT4 translocation, that 1µM bovine insulin for 20mins at 37^oC in 5% CO2, drive maximal levels of both GLUT4 translocation and phospho-4EBP1$^{(Thr37/46)}$.

4.2.9.7 Casein and Whey Protein Derived Hydrolysates differentially modulate basal 4-EBP1 phosphorylation in L6 myotubes

L6 myoblasts were seeded at $4x10^4$cells/mL. Confluent myoblasts were differentiated into myotubes as previously described. Cells were serum starved for three hours and subsequently incubated with 1mg/mL of specific whey and casein derived hydrolysates for 20mins at 37^oC in 5% CO2. Cells were lysed via mechanical syringe lysis and proteins separated and blotted as previously described. Following staining with specific secondary antibodies, the nitrocellulose membrane was incubated with a chemi-luminescent ECL western blot substrate for 2 min. Blot images were captured using a G-Box. Blots were exposed for 5 min. Western blots were quantified using ImageJ analysis software. Quantitative analysis of the western blot date, outlined in figure 4.22, revealed that both casein and whey proteins can modulate phospho-4EBP1$^{(Thr37/46)}$ activity. Casein derived hydrolysates 2-18 ($p<0.05$), 2-22 ($p<0.001$) and 2-133 ($p<0.01$) enhanced basal phospho-4EBP1$^{(Thr37/46)}$ activity. In contrast sample 2-134 ($p<0.01$) downregulated this activity suggesting negative outcomes for MPS in skeletal muscle. Whey derived hydrolysates 2-03, 2-10, 2-12 ($p<0.001$) and 2-47 ($p<0.01$) similarly enhanced activity levels of phospho-4EBP1$^{(Thr37/46)}$**.** Whey hydrolysate Sample 2-41 down regulated ($p<0.01$).

4.2.9.8 Casein and Whey Protein Derived Hydrolysate Modulate Insulin Stimulated 4-EBP1 phosphorylation in L6 myotubes

L6 myoblasts were seeded at $4x10^4$cells/mL. Confluent myoblasts were differentiated into myotubes as previously described. Cells were serum starved for three hours and subsequently incubated with 1mg/mL of specific whey and casein derived hydrolysates and 1µM insulin for 20mins at 37°C in 5% CO2. Cells were lysed via mechanical syringe lysis and proteins separated and blotted as previously described. Following staining with specific secondary antibodies, the nitrocellulose membrane was incubated with a chemi-luminescent ECL western blot substrate for 2 min. Blot images were captured using a G-Box. Blots were exposed for 5 min. Western blots were quantified using ImageJ analysis software. Divergent from observations at the basal level of 4-EBP1 activation, significant down regulation was noted, presented in figure 4.23. Sample 2-133 was previously observed to boost the basal phosphorylation of 4-EBP1 ($p<0.01$), however in the presence of 1µM insulin, 2-133 significantly down regulated 4-EBP1 activation ($p<0.01$). In contrast to this, two samples were able to promote 4-EBP1 activation. Sample 2-22 ($p<0.001$) and 2-18 (ns) increased gamma chain phosphorylation. A similar pattern of activity was observed with the whey protein hydrolysates. Samples 2-10 ($p<0.05$), 2-12 ($p<0.05$) and 2-13 ($p<0.001$) enhanced 4-EBP1 activation relative to insulin alone. Significant down regulation was observed with sample 2-41 ($p<0.05$), 2-43, 2-47 and 2-152 ($p<0.01$).

4.2.10 Development of an in vitro model of wound healing in L6 Myoblasts

The ability of skeletal muscle to regenerate is an important characteristic of muscle function. Adequate regeneration allows for muscle health and function to be maintained overtime culminating longevity and healthy ageing, Analysing muscle wound healing can be a cost ineffective, however there is an established, cost effective method that allows for the monitoring of myoblast migration *in vitro* called the scratch assay. This method involves scratching a line of cell monolayer and tracking migration at specific time points. This method can allow us to elucidate potential muscle healing properties of bioactive whey and casein derived hydrolysates.

4.2.10.1 Recombinant Th1 and Th2 cytokines modulate wound healing in an in vitro model of wound healing in L6 myoblasts.

Immune function is a key regulator of muscle regeneration. In order to assess whether changes in the rate of wound healing can be measured, the effect of recombinant Th1 and Th2 cytokines were analysed. L6 GLUT4myc myoblasts were seeded at $8x10^4$ cells/mL and grown to confluence at 37°C in 5% CO_2 in 24 well plates. The confluent monolayer of L6 myoblasts was subsequently injured by scraping a sterile P1000 micropipette tip, down the centre of the well of cells. The injured monolayer was then washed twice via aspiration with prewarmed, sterile 1X DPBS. Cells were then refed with L6 GM and incubated with 10ng/mL of recombinant IL-1β, IL-6, IL-10 and TNFα. Images were then taken at a specific, predetermined area within the well using the iDu Optics LabCam iPhone adaptor mount for an Olympus CKX31 microscope under 10x magnification. Images were taken at 0hr, 24hr and 48hr post injury. The area of wound closure was measured using ImageJ analysis software as previously described. Stimulation with recombinant Th1 and Th2 cytokines appeared to have contrasting effects of the rate of wound closure in L6 myoblasts. As outline in Fig. 4.24 IL-1β increased the rate of wound closure at T24 (ns) and T48 (ns). Stimulation with IL-6 in contrast had no enhancing or detrimental effect on the rate of wound closure in L6 myoblasts. Similarly, recombinant IL-10 and TNFα (figure 4.32) both boost the rate of wound closure at T24 (ns, ns) and T48 (ns, ns).

4.2.10.2 Increased rates of in vitro wound closure is associated with an increased secretion of chemokine MCP-1/CCL2 from L6 myoblasts.

CCL2/MCP-1 is a key chemokine involved in recruiting circulating monocytes and promoting satellite cell migration to the site of wound injury and has been shown to be integral to the wound healing process. As a result, CCL2/MCP-1 was measured from Th1 and Th2 cytokine stimulated myoblasts to detect if changes in CCl2/MCP-1 secretion were associated with increased rates of *in vitro* wound healing. L6 GLUT4myc myoblasts were seeded at $8x10^4$ cells/mL and grown to confluence at 37°C in 5% CO_2 in 24 well plates. The confluent monolayer of L6 myoblasts was subsequently injured by scraping a sterile P1000, down the centre of the well of cells. The injured monolayer was then washed twice via aspiration with prewarmed, sterile 1X DPBS. Cells were then refed with L6 GM and incubated with 10ng/mL of recombinant IL-1β, IL-6, IL-10 and TNFα for 48hr. Following analysis of wound closure using an in vitro model of wound healing, supernatants were analysed for the concentration of secreted MCP-1/CCL2 using chemokine specific ELISA. As outlined in fig. 4.25 IL-1β ($p<0.001$), IL-10 (ns) and TNFα ($p<0.001$) all boosted secretion of MCP-1/CCL2 from injured L6 myoblasts. Recombinant IL-6 did not induce secretion of MCP-1/CCL2 from L6 myotubes. This increase in MCP-1/CCL2 secretion was positively associated with increased rates of wound closure in an in vitro model of wound healing.

4.2.10.3 Whey and Casein derived hydrolysates modulate secretion of MCP-1/CCL2 from TNFα activated L6 myoblasts.

Due to the role that TNFα has during the early phases of muscle healing in vivo, and the effect on healing and MCP-1/CCL2 secretion previously shown. It was decided to investigate whether the whey and casein derived hydrolysates could bolster the secretion of CCL2/MCP-1 secretion from TNFα activated L6 myoblasts. L6 GLUT4myc myoblasts were seeded at $8x10^4$ cells/mL and grown to confluence at 37°C in 5% CO_2 in 24 well plates. Cells were incubated with 1mg/mL of specific casein or whey protein derived hydrolysates for 1 hour at 37°C in 5% CO_2. Cells were subsequently stimulated with 10ng/mL rTNF for 24hr at 37°C in 5% CO_2. Resulting supernatants were analysed for MCP-1/CCL2 secretion using Chemokine specific ELISA. Results are outlined in figure 4.26. Whole casein (NaCN) modestly increased secretion of MCP-1/CCL2 while secretion was maintained by whole whey protein (WPC). NaCN derived hydrolysates exhibited potent pro-MCP-1/CCL2 bioactivities. Samples 2-29 ($p<0.05$), 2-19, 2-34, 2-84, 2-134 ($p<0.01$), 2-22, 2-23, 2-25, 2-26, 2-27, 2-28, 2-132, 2-1332-18 ($p<0.001$) all significantly boosted MCP-1/CCL2 secretion relative to the 10ng/mL TNFα control suggesting potential benefits for increased rates of wound healing. In contrast to the NaCN derived hydrolysates, although secretion of MCP-1/CCL2 was maintained throughout only 2-47 ($p<0.05$), 2-152 ($p<0.01$) and 2-154 ($p<0.001$) significantly enhanced secretion of MCP-1/CCL2 relative to the 10ng/mL TNFα control.

4.2.10.4 Casein and Whey derived hydrolysates differentially modulate the rate of wound healing in an in vitro model of muscle injury in L6 myoblasts.

We have shown that Th1 and Th2 cytokines can positively influence myoblast migration and wound healing in vitro . Moreover we have shown that hydrolysate stimulation can bolster secretion of CCL2/MCP-1 in myoblasts, a key component of the regeneration process. The next step was to analyse the effect of hydrolysate stimulation of wound healing unactivated myoblasts and TNFα activated myoblasts, to represent the early phases of skeletal muscle regeneration. L6 GLUT4myc myoblasts were seeded at $8x10^4$ cells/mL and grown to confluence at 37°C in 5% CO_2 in 24 well plates. The confluent monolayer of L6 myoblasts was subsequently injured by scraping a sterile P1000, down the centre of the well of cells. The injured monolayer was then washed twice via aspiration with prewarmed, sterile 1X DPBS. Cells were then refed with L6 GM and incubated with 1mg/mL of specific NaCN or WPC derived hydrolysate in the presence or absence of 10ng/mL TNFα. Images were then taken at a specific, predetermined area within the well using the iDu Optics LabCam iPhone adaptor mount for an Olympus CKX31 microscope under 10x magnification. Images were taken at 0hr, 24hr and 48hr post injury. The area of wound closure was measured using ImageJ analysis software as previously described. Several WPC and NaCN derived hydrolysates promoted increased rates of wound closure. As outlined in figure 4.29, sample 2-01 and 2-11 significantly boosted the rates of wound closure at T24 ($p<0.05$, $p<0.05$) and T48 ($p<0.01$, $p<0.05$) relative to the UTC. Furthermore, samples WPC, 2-03 and trended to increase the rate of wound closure. Sample 2-12 did not augment the rate of wound healing. Similar trends were observed with 2-13, 2-42 and 2-43 whilst wound closure was unchanged relative to the UTC with samples 2-40 and 2-41 (figure 4.30).). Samples 2-47, 2-151, 2-154 and 2-133 (figure 4.31, 4.37 respectively) and 2-154 all appeared to boost or maintain the rate of recovery with 2-151 at T48 showing a significant benefit for wound healing as illustrated in Fig. 4.31 ($p<0.05$). In contrast sample 2-153 observably blocked the rate of wound healing relative to the UTC (4.31).

As detailed in the figures 4.32, 4.33 and 4.34 whey protein derived hydrolysates in the presence of 10ng/mL TNFα did not inhibit or promote the rate of wound closure in injured L6 myoblasts. With the single exception of sample 2-154, where significant reductions in the rate of wound closure were observed at T24 ($p<0.01$) and T48 ($p<0.01$) suggesting interference with the wound healing process (Figure 4.34). Regarding the effect of NaCN derived hydrolysates on TNFα activated myoblasts, several samples exhibited significant interference with the wound healing process. Sample 2-21 and 2-22 blocked healing at T24 ($p<0.05$) and T48 ($p<0.05$) as shown in figure 4.38. Sample 2-135 (figure 4.40) significantly interfered with the ability of myoblasts to recovery appearing to halt migration at T24 leading to significant difference between TNFα alone and TNFα in the presence of 2mg/mL 2-135.

4.3 Figures

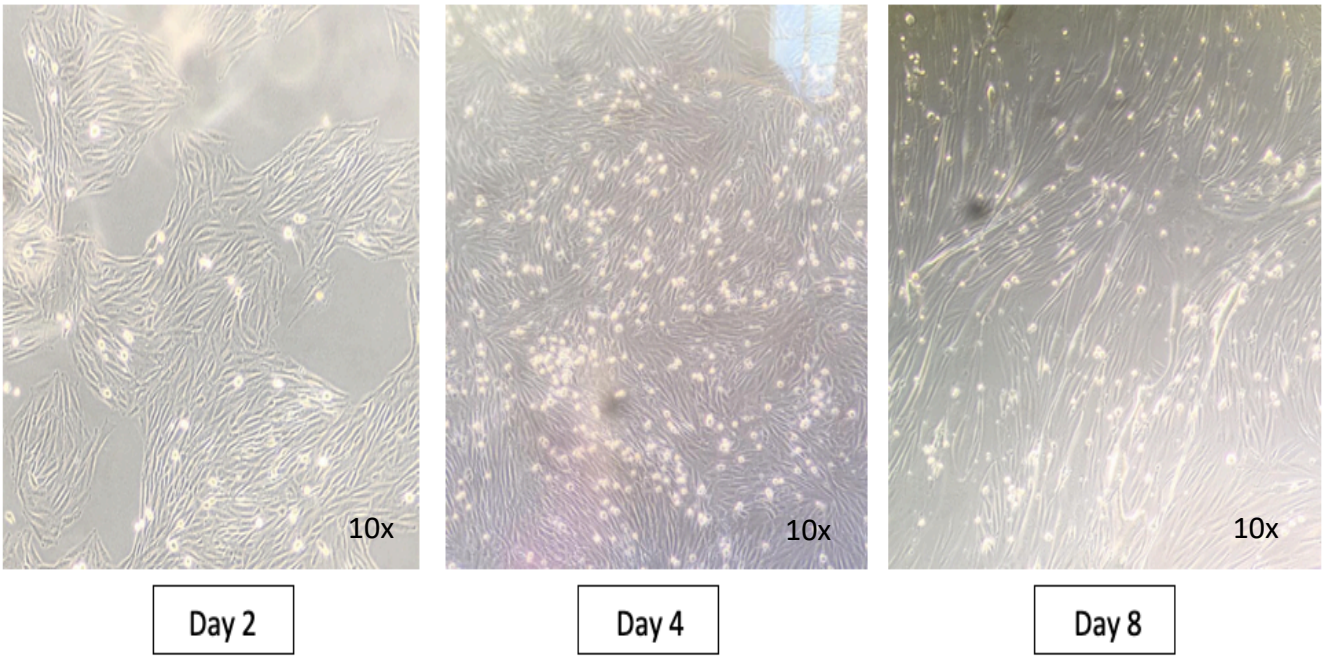


Figure 4.1 Myogenic differentiation of L6 and L6 GLUT4myc myoblasts. L6 GLUT4myc Myoblasts were seeded at $4x10^4$cells/mL in 24 well Nunc treated tissue culture plates. Cells were cultured at 37°C in 5% CO_2. Cell monolayers were cultured in fully supplemented growth medium and fed every 48hr. On day four, the cell culture medium was switched to low serum (2%) differentiation medium to induce differentiation of confluent myoblasts to myotubes. Cells were cultured for a further four days and fed every 48hr. Representative images of L6 myoblast and L6 GLUT4myc myoblasts during the myogenic differentiation process into mature, multinucleated myotubes were taken using a smart phone placed on a lens compatible bracket for an Olympus Microscope.

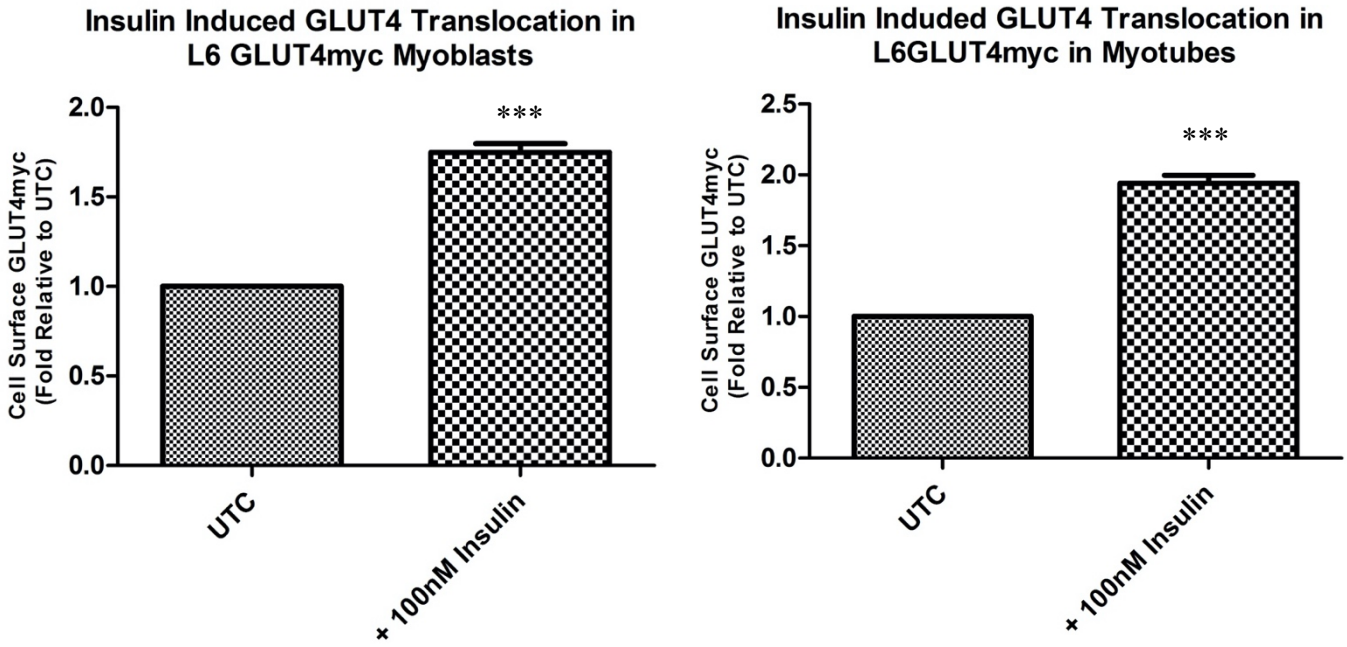


Figure 4.2 Insulin from bovine pancreas at super physiological concentrations induces GLUT4 translocation to the cell membrane in L6 GLUT4myc Myoblasts and Myotubes L6 GLUT4myc myoblasts were seeded at $4x10^4$cells/mL and differentiated into myotubes as previously described or seeded at $8x10^4$cells/mL and cultured to confluence for myoblasts. Cells were incubated with 100nM insulin for 20 min at 37°C in 5% CO_2. Cell surface GLUT4myc was quantified as previously described in section 2.2.9. Changes in cell surface GLUT4myc are expressed as a fold change relative to the untreated, basal (UTC) control. Data is presented as mean ± SEM of three replicates. ***p<0.001, **p<0.01, *p<0.05 comparing UTC to insulin stimulated cells. Significance was determined using one- way ANOVA with a Newman-Keuls post-test.

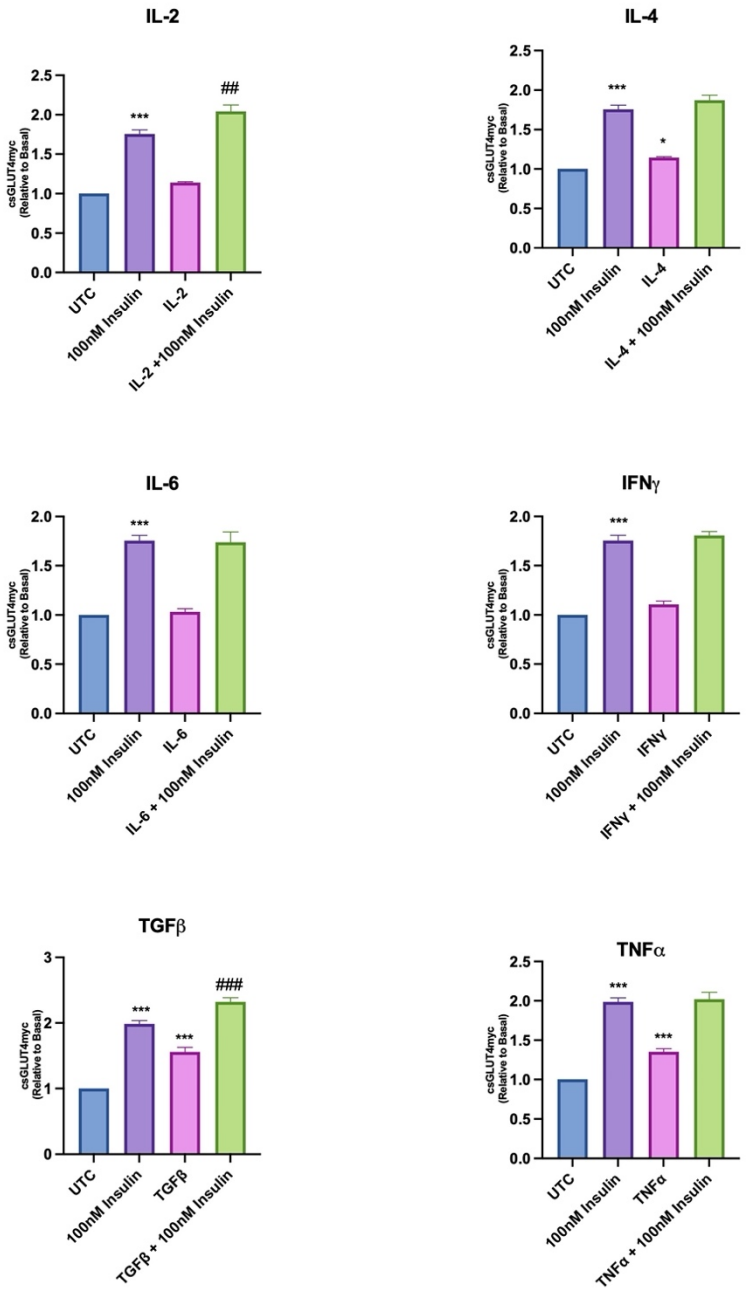


Figure 4.3 Recombinant Murine Th1 and Th2 cytokines modulate GLUT4 translocation in L6 GLUT4myc Myoblasts in the presence and absence of 100nM Insulin. L6 GLUT4myc myoblasts were seeded at $8x10^4$cells/mL and cultured to confluence. Cells were stimulated with 100ng/mL of each cytokine (IL-2, IL-4, IL-6, IFN$\boldsymbol{\gamma}$, TGFβ and TNFα) for 24hr and subsequently incubated with 100nM insulin for 20 min. Cell surface GLUT4myc was quantified as previously described. Changes in cell surface GLUT4myc are expressed as a fold change relative to the untreated, basal (UTC) control. Data is presented as mean ± SEM of three replicates. ***p<0.001, **p<0.01, *p<0.05 comparing UTC to treated conditions, $^{###}$p<0.001, $^{##}$p<0.01, $^{#}$p<0.05 comparing 100nM insulin treated cells to other treated conditions. Significance was determined using one- way ANOVA with a Newman-Keuls post-test.

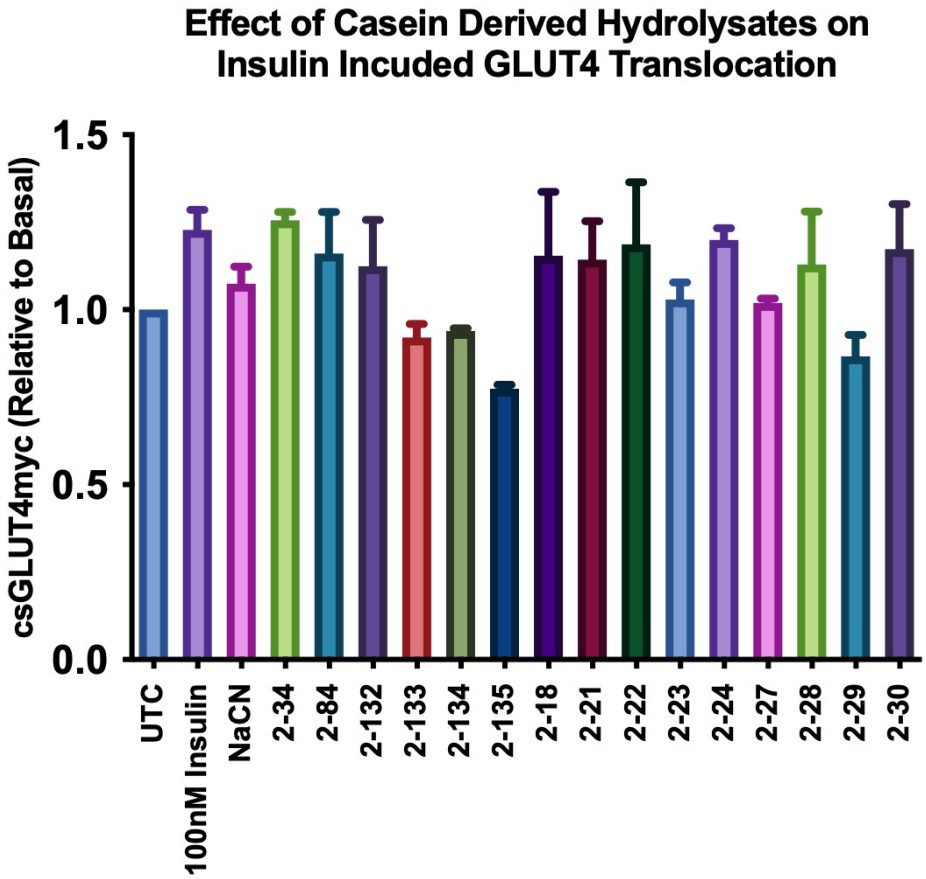


Figure 4.4 Variability and inconsistencies in detectable fold changes between the unstimulated control and insulin-stimulated control lead to an inability to interpret the effects of casein and casein derived hydrolysates on basal GLUT4myc translocation L6 GLUT4myc myoblasts were seeded at $8x10^4$ cells/mL and grown to confluence at 37°C in 5% CO_2. Cells were subsequently serum starved for three hours at 37°C in 5% CO_2. Once the serum starve incubation was complete, L6 GLUT4myc myoblasts were incubated with either 1mg/mL candidate hydrolysate or 1μM bovine insulin for 20 min. Changes in cell surface GLUT4myc are expressed as a fold change relative to the untreated, basal (UTC) control. Data is presented as mean ± SEM of three replicates. Data is presented as mean ± SEM of three replicates. ***p<0.001, **p<0.01, *p<0.05 comparing UTC to treated conditions. Significance was determined using one- way ANOVA with a Newman-Keuls post-test.

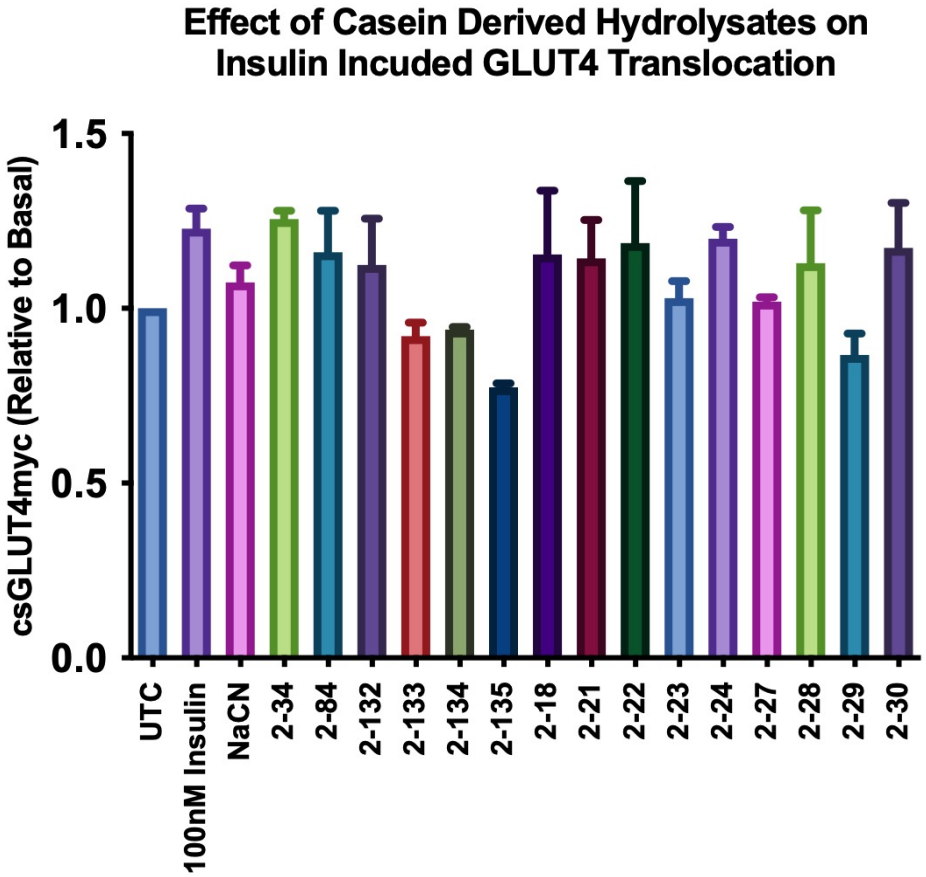


Figure 4.5 Variability and inconsistencies in detectable fold changes between the unstimulated control and insulin-stimulated control lead to an inability to interpret the effects of casein derived hydrolysates on insulin stimulated GLUT4myc translocation L6 GLUT4myc myoblasts were seeded at $8x10^4$ cells/mL and grown to confluence at 37°C in 5% CO_2. Cells were subsequently serum starved for three hours at 37°C in 5% CO_2. Once the serum starve incubation was complete, L6 GLUT4myc myoblasts were incubated with either 1mg/mL candidate hydrolysate or 1μM bovine insulin for 20 min. Changes in cell surface GLUT4myc are expressed as a fold change relative to the untreated, basal (UTC) control. Data is presented as mean ± SEM of three replicates. ***p<0.001, **p<0.01, *p<0.05 comparing UTC to treated conditions. Significance was determined using one- way ANOVA with a Newman-Keuls post-test.

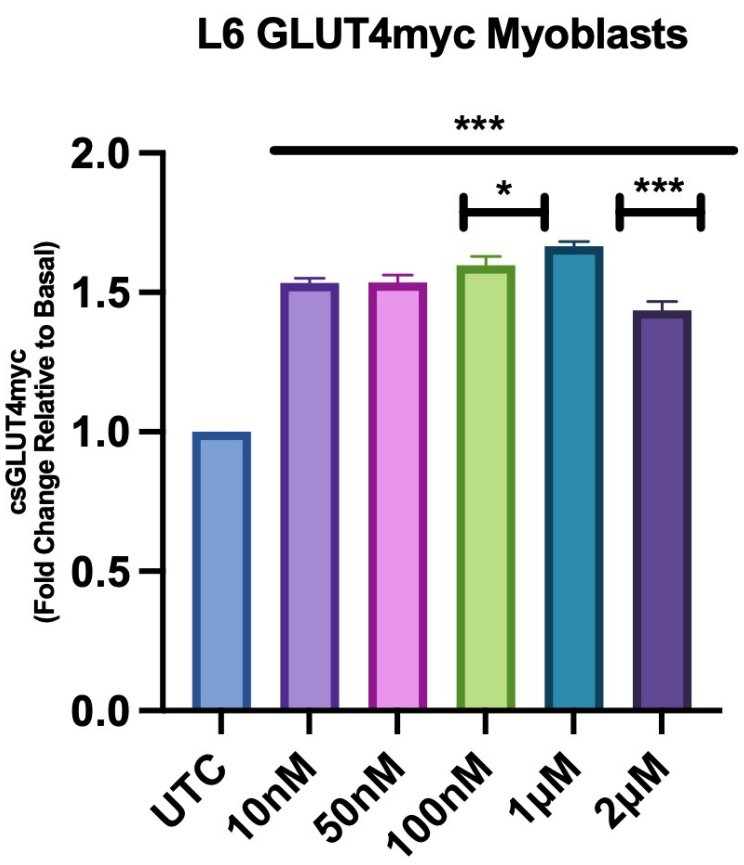


Figure 4.6 Insulin drives GLUT4 Translocation in L6 GLUT4myc Myoblasts in a dose dependant manner L6 GLUT4myc myoblasts were seeded in 24 well plates at $8x10^4$cells/mL and grown to confluence. Cells were subsequently starved in serum free αMEM cell culture medium for 3 hours at 37°C in 5% CO_2. Cells were then stimulated with 10nM, 50nM, 100nM and 1μM Bovine Insulin for 20 min at 37°C in 5% CO_2. Cell surface GLUT4myc was then assessed as previously described. Changes in cell surface GLUT4myc are expressed as a fold change relative to the untreated, basal (UTC) control. Data is presented as mean ± SEM of three replicates. ***p<0.001, **p<0.01, *p<0.05 comparing UTC to treated conditions. Significance was determined using one- way ANOVA with a Newman-Keuls post-test.

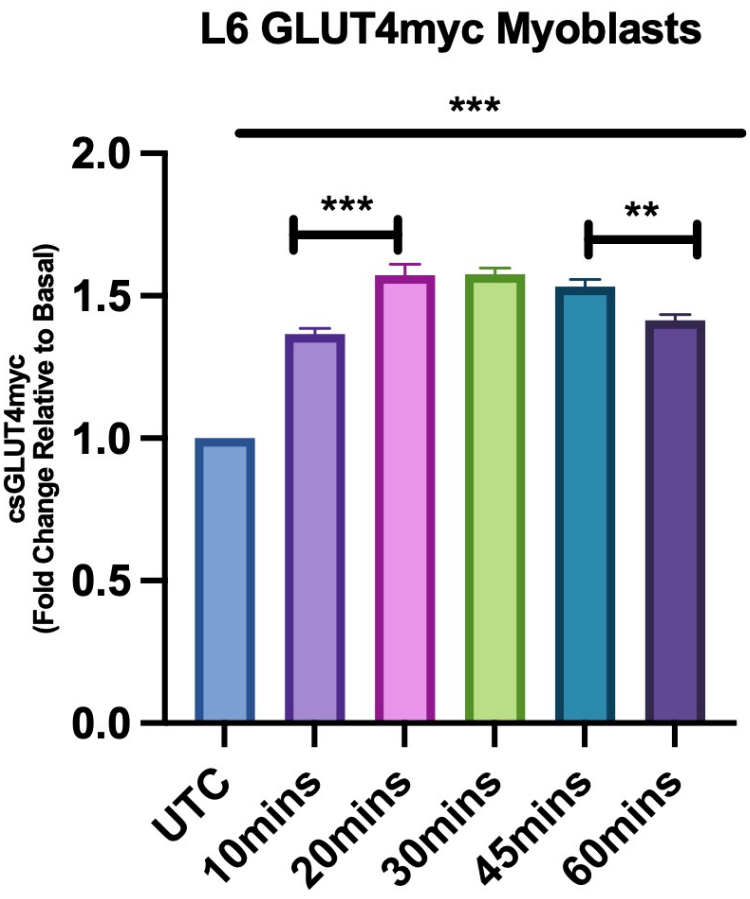


Figure 4.7 Time course Insulin drives GLUT4 Translocation in L6 GLUT4myc Myoblasts L6 GLUT4myc myoblasts were seeded in 24 well plates at $4x10^4$cells/mL and grown to confluence. Cells were differentiated into mature myotubes as previously described. Cells were subsequently starved in serum free αMEM cell culture medium for 3 hours at 37°C in 5% CO_2. Cells were then stimulated with 10nM, 50nM, 100nM and 1μM Bovine Insulin for 20 min at 37°C in 5% CO_2. Cell surface GLUT4myc was then assessed as previously described. Changes in cell surface GLUT4myc are expressed as a fold change relative to the untreated, basal (UTC) control. Data is presented as mean ± SEM of three replicates. ***p<0.001, **p<0.01, *p<0.05 comparing UTC to treated conditions. Significance was determined using one- way ANOVA with a Newman-Keuls post-test

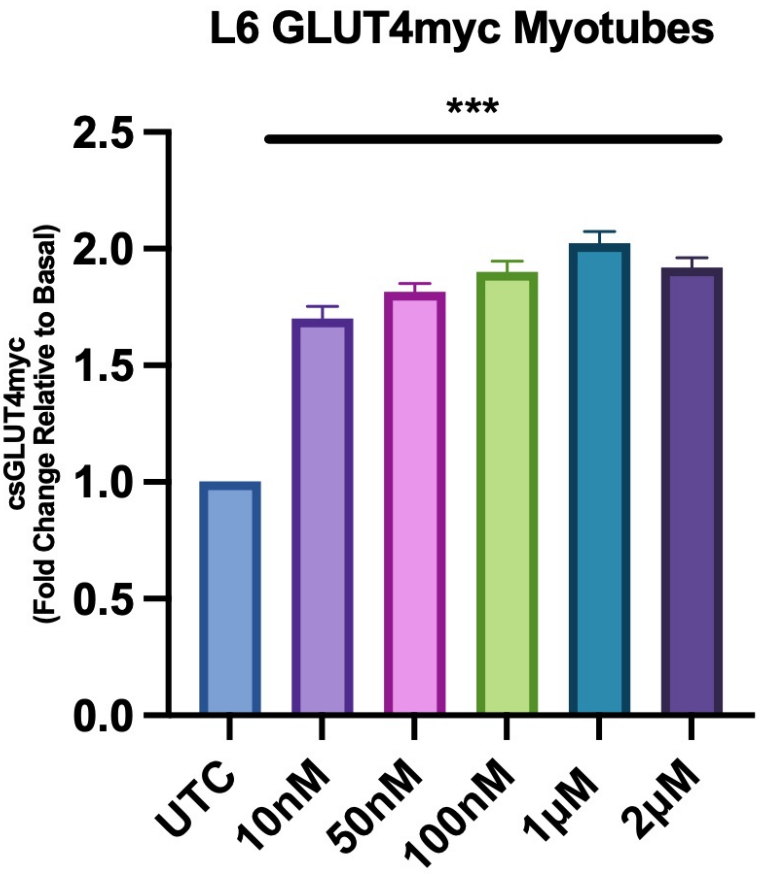


Figure 4.8 Dose response of GLUT4myc translocation to the cell membrane of L6 GLUT4myc myoblasts in response to stimulation with 1μM Bovine Insulin. L6 GLUT4myc myoblasts were seeded in 24 well plates at 8x10^{4}cells/mL and grown to confluence. Cells were subsequently starved in serum free αMEM cell culture medium for 3 hours at 37°C in 5% CO_2. Cells were then stimulated 1μM and incubated for 60, 45, 30, 20 and 10 min at 37°C in 5% CO_2. Cell surface GLUT4myc was then assessed as previously described. Changes in cell surface GLUT4myc are expressed as a fold change relative to the untreated, basal (UTC) control. Data is presented as mean ± SEM of three replicates Data is presented as mean ± SEM of three replicates. ***p<0.001, **p<0.01, *p<0.05 comparing UTC to treated conditions. Significance

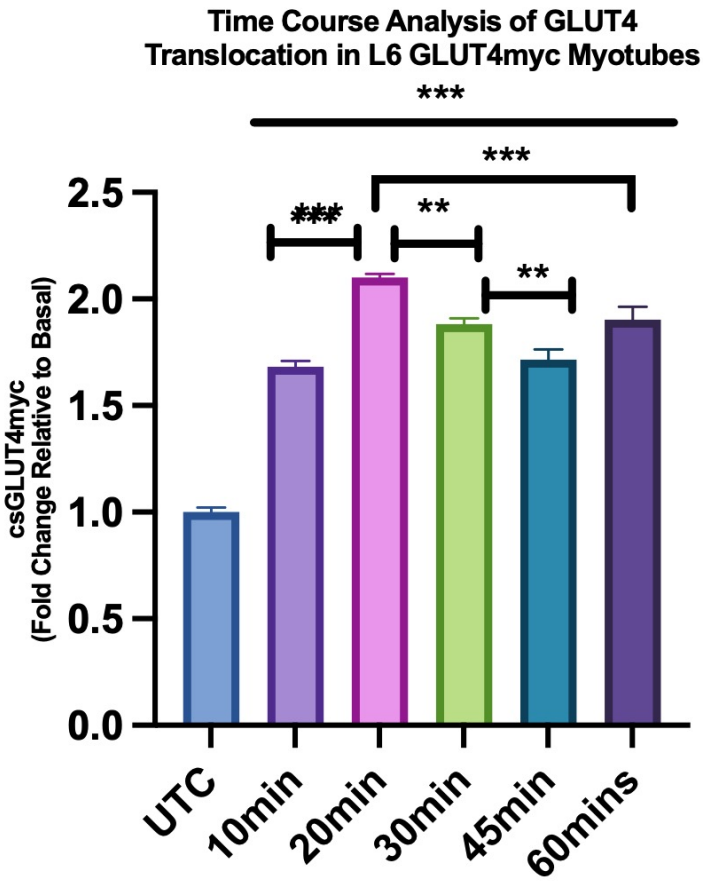


Figure 4.9 Time course Insulin drives GLUT4 Translocation in L6 GLUT4myc Myoblasts i L6 GLUT4myc myoblasts were seeded in 24 well plates at $4x10^4$cells/mL and grown to confluence. Cells were differentiated into mature myotubes as previously described. Cells were subsequently starved in serum free αMEM cell culture medium for 3 hours at 37°C in 5% CO_2. Cells were then stimulated with 10nM, 50nM, 100nM and 1μM Bovine Insulin for 20 min at 37°C in 5% CO_2. Cell surface GLUT4myc was then assessed as previously described. Changes in cell surface GLUT4myc are expressed as a fold change relative to the untreated, basal (UTC) control. Data is presented as mean ± SEM of three replicates. ***p<0.001, **p<0.01, *p<0.05 comparing UTC to treated conditions. Significance was determined using one- way ANOVA with a Newman-Keuls post-test

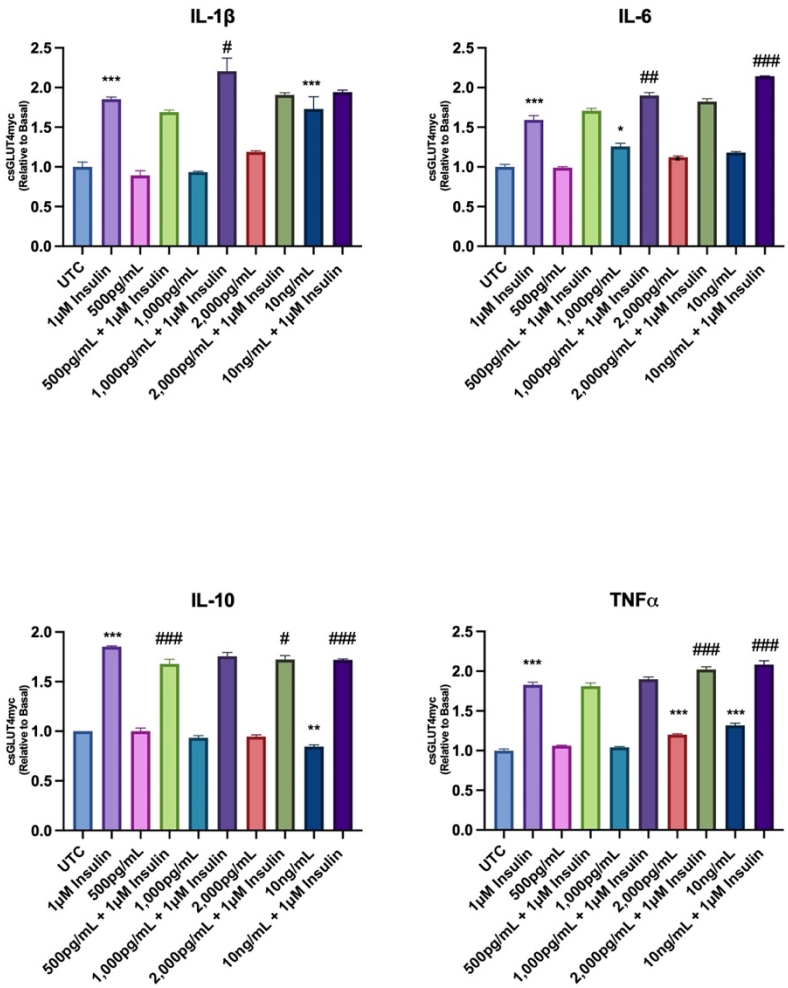


Figure 4.10 Recombinant Murine Th1 and Th2 Macrophage specific cytokines modulate GLUT4 translocation in L6 GLUT4myc Myotubes in a dose dependant manner in the presence and absence of 1μM Insulin. L6 GLUT4myc myoblasts were seeded in 24 well plates at 4x10^4cells/mL and grown to confluence. Cells were differentiated into mature myotubes as previously described. Cells were subsequently starved in serum free αMEM cell culture medium for 3 hours at 37°C in 5% CO_2. Differentiated myotubes were then incubated with increasing doses of specific recombinant Th1 and Th2 cytokines for 24hr at 37°C in 5% CO_2. Cells were then stimulated with 1μM insulin for 20mins at 37°C in 5% CO_2. Cell surface GLUT4myc was then assessed as previously described. Changes in cell surface GLUT4myc are expressed as a fold change relative to the untreated, basal (UTC) control. Data is presented as mean ± SEM of three replicates. ***p<0.001, **p<0.01, *p<0.05 comparing UTC to treated conditions, $^{###}$p<0.001, $^{##}$p<0.01, $^{#}$p<0.05 comparing 1μM insulin treated cells to other treated conditions. Significance was determined using one- way ANOVA with a Newman-Keuls post-test.

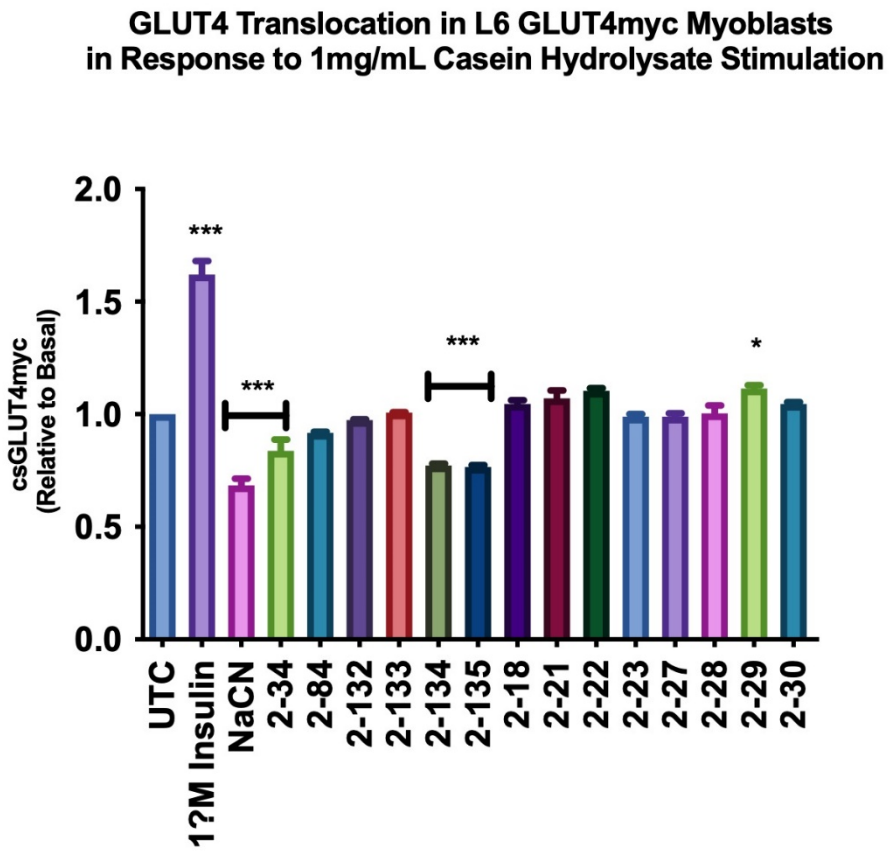


Figure 4.11 Analysis of the effects of casein derived hydrolysates on the basal expression of cell surface GLUT4myc in L6 GLUT4myc Myoblasts. L6 GLUT4myc myoblasts were seeded in 24 well plates at 8x10^4cells/mL and grown to confluence. Cells were subsequently starved in serum free αMEM cell culture medium for 3 hours at 37°C in 5% CO_2. Cells were then stimulated with 1mg/mL candidate hydrolysate or whole protein control for 25 min at 37°C in 5% CO_2. Cell surface GLUT4myc was then assessed as previously described. Changes in cell surface GLUT4myc are expressed as a fold change relative to the untreated, basal (UTC) control. Data is presented as mean ± SEM of three replicates and is representative of two biological replicates. ***p<0.001, **p<0.01, *p<0.05 comparing UTC to insulin/hydrolysate stimulated cells. Significance was determined using one- way ANOVA with a Newman-Keuls post-test

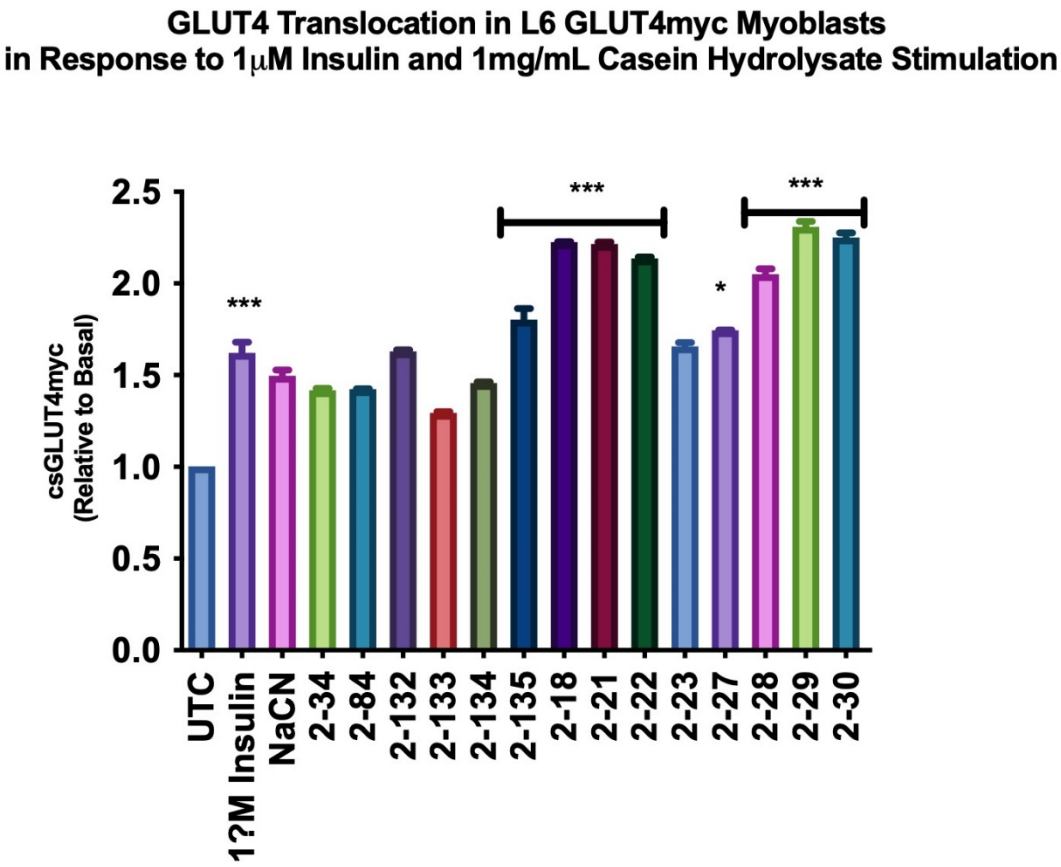


Figure 4.12 Analysis of the effects of casein derived hydrolysates on the basal expression of cell surface GLUT4myc in L6 GLUT4myc Myoblasts. L6 GLUT4myc myoblasts were seeded in 24 well plates at 8x10^4cells/mL and grown to confluence. Cells were subsequently starved in serum free αMEM cell culture medium for 3 hours at 37°C in 5% CO_2. Cells were then stimulated with 1mg/mL and 1μM Bovine Insulin candidate hydrolysate or whole protein control for 25 min at 37°C in 5% CO_2. Cell surface GLUT4myc was then assessed as previously described. Changes in cell surface GLUT4myc are expressed as a fold change relative to the untreated, basal (UTC) control. Data is presented as mean ± SEM of three replicates and is representative of two biological replicates. ***p<0.001, **p<0.01, *p<0.05 comparing UTC to insulin/hydrolysate stimulated cells. Significance was determined using one- way ANOVA with a Newman-Keuls post-test

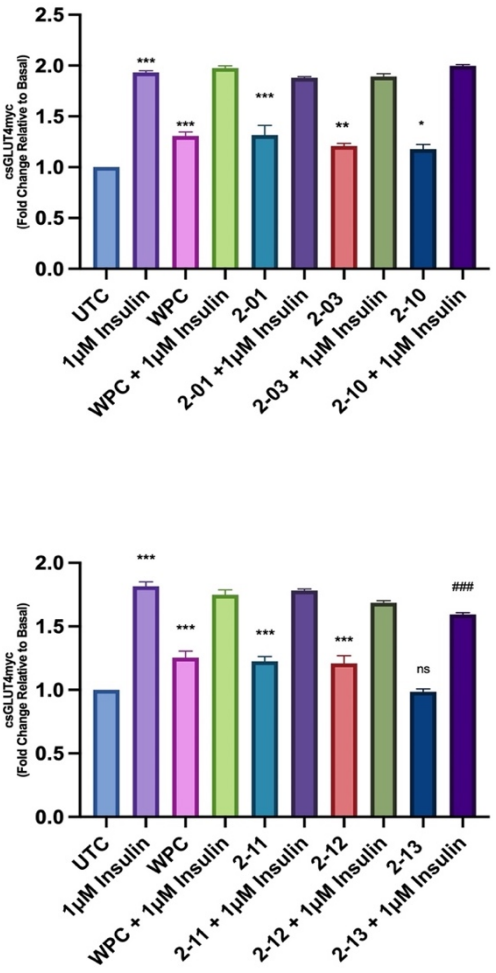


Figure 4.13 Whey protein derived protein hydrolysates modulate the translocation of GLUT4 to the cell surface of L6 GLUT4myc Myotubes. L6 GLUT4myc myoblasts were seeded in 24 well plates at $4x10^4$cells/mL and grown to confluence. Cells were differentiated into mature myotubes as previously described. Cells were subsequently starved in serum free αMEM cell culture medium for 3 hours at 37°C in 5% CO_2. Cells were then stimulated with 1mg/mL of whole protein of derived hydrolysate in the presence and absence of 1µM bovine insulin for 20 min at 37°C in 5% CO_2. Cell surface GLUT4myc was then assessed as previously described. Changes in cell surface GLUT4myc are expressed as a fold change relative to the untreated, basal (UTC) control. Data is presented as mean ± SEM of three replicates. . ***p<0.001, **p<0.01, *p<0.05 comparing UTC to hydrolsyates minus 1µM insulin, $^{###}$p<0.001, $^{##}$p<0.01, $^{#}$p<0.05 comparing 1µM insulin to hydrolysates plus 1µM insulin. Significance was determined using one- way ANOVA with a Newman-Keuls post-test

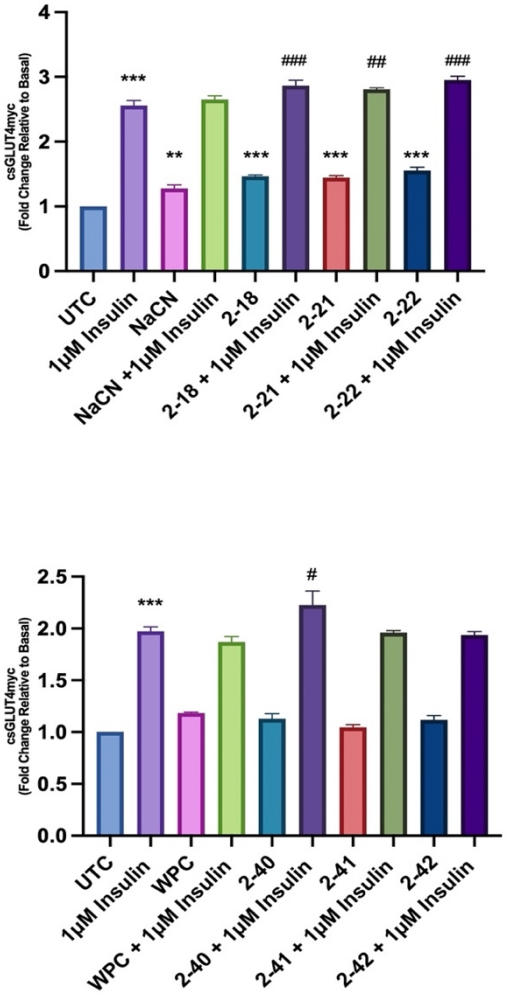


Figure 4.14 Whey and casein protein derived protein hydrolysates modulate the translocation of GLUT4 to the cell surface of L6 GLUT4myc Myotubes. L6 GLUT4myc myoblasts were seeded in 24 well plates at $4x10^4$cells/mL and grown to confluence. Cells were differentiated into mature myotubes as previously described. Cells were subsequently starved in serum free αMEM cell culture medium for 3 hours at 37°C in 5% CO_2. Cells were then stimulated with 1mg/mL of whole protein of derived hydrolysate in the presence and absence of 1μM bovine insulin for 20 min at 37°C in 5% CO_2. Cell surface GLUT4myc was then assessed as previously described. Changes in cell surface GLUT4myc are expressed as a fold change relative to the untreated, basal (UTC) control. Data is presented as mean ± SEM of three replicates. ***p<0.001, **p<0.01, *p<0.05 comparing UTC to hydrolsyates minus 1μM insulin, $^{###}$p<0.001, $^{##}$p<0.01, $^{#}$p<0.05 comparing 1μM insulin to hydrolysates plus 1μM insulin. Significance was determined using one- way ANOVA with a Newman-Keuls post-test

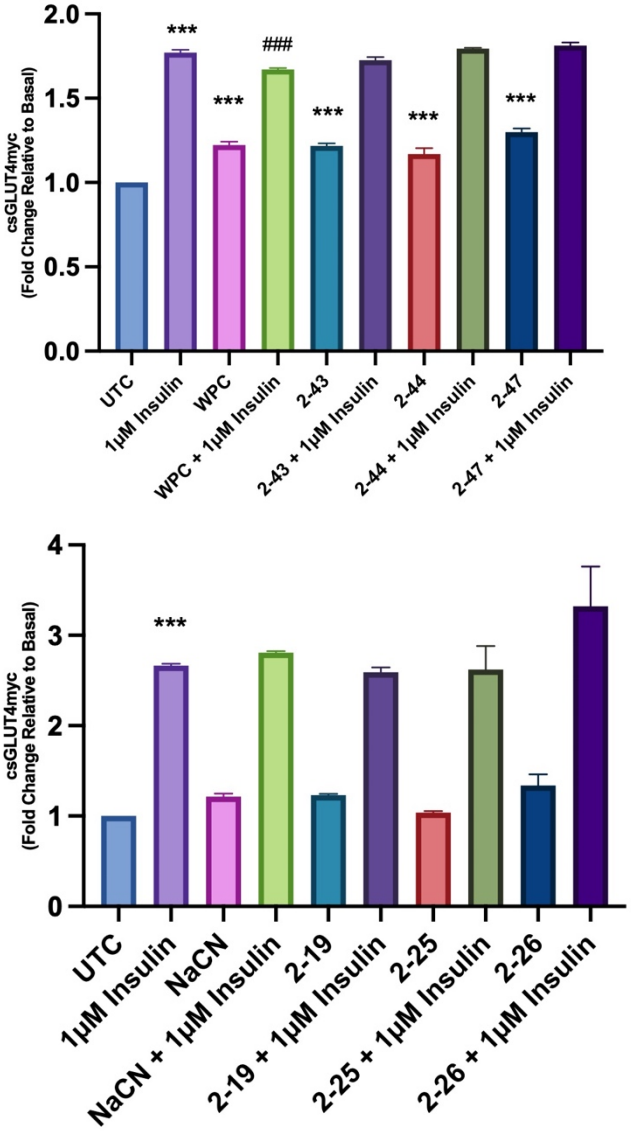
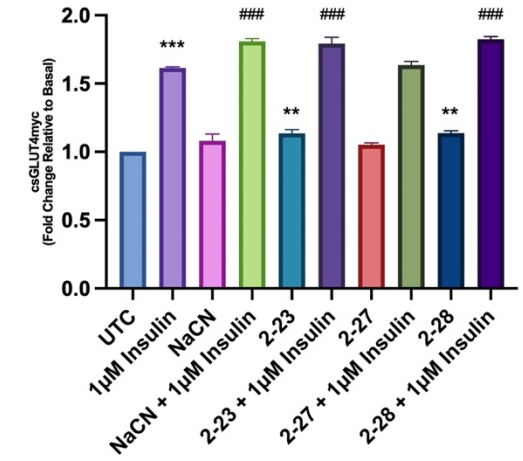


Figure 4.15 Whey and casein protein derived protein hydrolysates modulate the translocation of GLUT4 to the cell surface of L6 GLUT4myc Myotubes. L6 GLUT4myc myoblasts were seeded in 24 well plates at $4x10^4$cells/mL and grown to confluence. Cells were differentiated into mature myotubes as previously described. Cells were subsequently starved in serum free αMEM cell culture medium for 3 hours at 37°C in 5% CO_2. Cells were then stimulated with 1mg/mL of whole protein of derived hydrolysate in the presence and absence of 1μM bovine insulin for 20 min at 37°C in 5% CO_2. Cell surface GLUT4myc was then assessed as previously described. Changes in cell surface GLUT4myc are expressed as a fold change relative to the untreated, basal (UTC) control. Data is presented as mean ± SEM of three replicates. . ***p<0.001, **p<0.01, *p<0.05 comparing UTC to hydrolsyates minus 1μM insulin, $^{###}$p<0.001, $^{##}$p<0.01, $^{#}$p<0.05 comparing 1μM insulin to hydrolysates plus 1μM insulin. Significance was determined using one- way ANOVA with a Newman-Keuls post-test



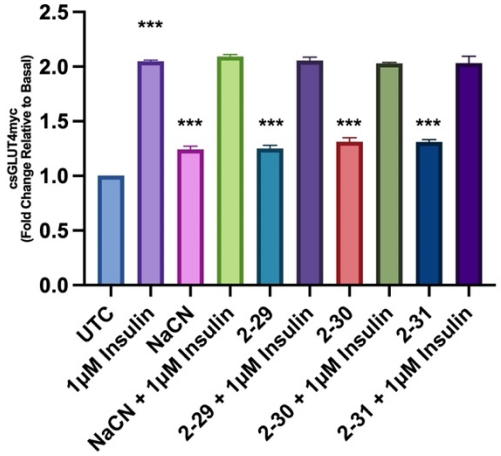


Figure 4.16 Casein protein derived protein hydrolysates modulate the translocation of GLUT4 to the cell surface of L6 GLUT4myc Myotubes. L6 GLUT4myc myoblasts were seeded in 24 well plates at $4x10^4$cells/mL and grown to confluence. Cells were differentiated into mature myotubes as previously described. Cells were subsequently starved in serum free αMEM cell culture medium for 3 hours at 37°C in 5% CO_2. Cells were then stimulated with 1mg/mL of whole protein of derived hydrolysate in the presence and absence of 1µM bovine insulin for 20 min at 37°C in 5% CO_2. Cell surface GLUT4myc was then assessed as previously described. Changes in cell surface GLUT4myc are expressed as a fold change relative to the untreated, basal (UTC) control. Data is presented as mean ± SEM of three replicates. . ***p<0.001, **p<0.01, *p<0.05 comparing UTC to hydrolsyates minus 1µM insulin, $^{###}$p<0.001, $^{##}$p<0.01, $^{#}$p<0.05 comparing 1µM insulin to hydrolysates plus 1µM insulin. Significance was determined using one- way ANOVA with a Newman-Keuls post-test

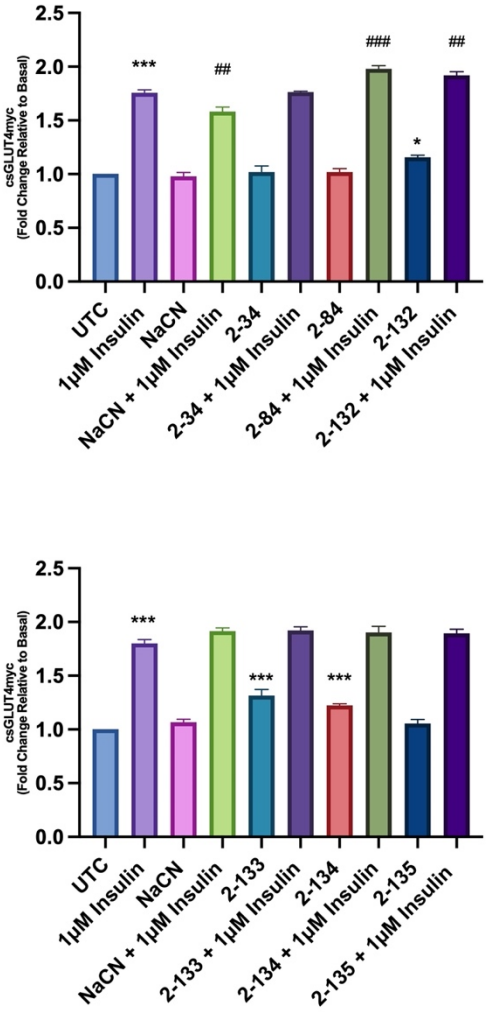


Figure 4.17 Casein protein derived protein hydrolysates modulate the translocation of GLUT4 to the cell surface of L6 GLUT4myc Myotubes. L6 GLUT4myc myoblasts were seeded in 24 well plates at $4x10^4$cells/mL and grown to confluence. Cells were differentiated into mature myotubes as previously described. Cells were subsequently starved in serum free αMEM cell culture medium for 3 hours at 37°C in 5% CO_2. Cells were then stimulated with 1mg/mL of whole protein of derived hydrolysate in the presence and absence of 1μM bovine insulin for 20 min at 37°C in 5% CO_2. Cell surface GLUT4myc was then assessed as previously described. Changes in cell surface GLUT4myc are expressed as a fold change relative to the untreated, basal (UTC) control. Data is presented as mean ± SEM of three replicates. . ***p<0.001, **p<0.01, *p<0.05 comparing UTC to hydrolsyates minus 1μM insulin, $^{###}$p<0.001, $^{##}$p<0.01, $^{#}$p<0.05 comparing 1μM insulin to hydrolysates plus 1μM insulin. Significance was determined using one- way ANOVA with a Newman-Keuls post-test

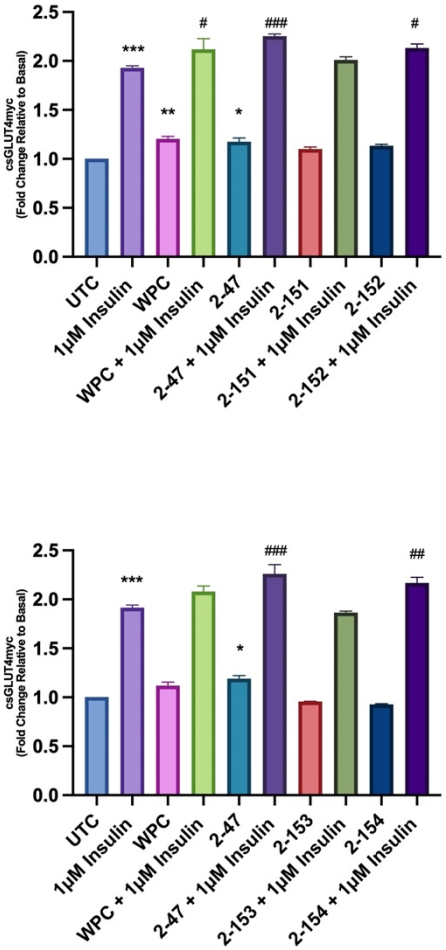


Figure 4.18 Whey protein derived protein hydrolysates modulate the translocation of GLUT4 to the cell surface of L6 GLUT4myc Myotubes. L6 GLUT4myc myoblasts were seeded in 24 well plates at $4x10^4$cells/mL and grown to confluence. Cells were differentiated into mature myotubes as previously described. Cells were subsequently starved in serum free αMEM cell culture medium for 3 hours at 37°C in 5% CO_2. Cells were then stimulated with 1mg/mL of whole protein of derived hydrolysate in the presence and absence of 1μM bovine insulin for 20 min at 37°C in 5% CO_2. Cell surface GLUT4myc was then assessed as previously described. Changes in cell surface GLUT4myc are expressed as a fold change relative to the untreated, basal (UTC) control. Data is presented as mean ± SEM of three replicates. ***p<0.001, **p<0.01, *p<0.05 comparing UTC to hydrolsyates minus 1μM insulin, $^{###}$p<0.001, $^{##}$p<0.01, $^{#}$p<0.05 comparing 1μM insulin to hydrolysates plus 1μM insulin. Significance was determined using one- way ANOVA with a Newman-Keuls post-test

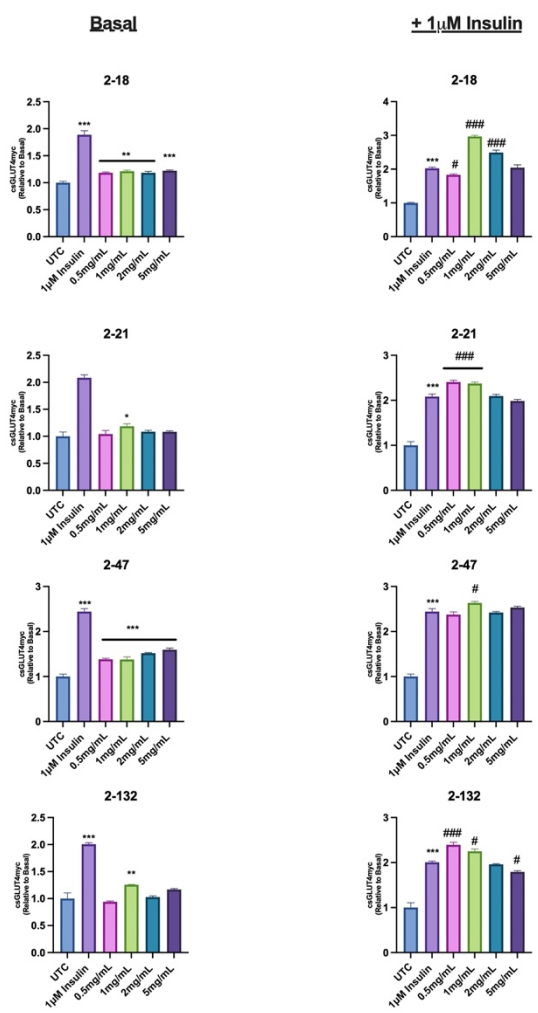


Figure 4.19 Whey and Casein Derived Hydrolysates dose dependently affect basal and insulin stimulated GLUT4 translocation in L6 GLUT4myc Myotubes. L6 GLUT4myc myoblasts were seeded in 24 well plates at $4x10^4$cells/mL and grown to confluence. Cells were differentiated into mature myotubes as previously described. Cells were subsequently starved in serum free αMEM cell culture medium for 3 hours at 37°C in 5% CO_2. Cells were then stimulated with increasing doses of specific whey and casein derived hydrolysates for 20mins at 37°C in 5% CO_2. Cell surface GLUT4myc was then assessed as previously described. Changes in cell surface GLUT4myc are expressed as a fold change relative to the untreated, basal (UTC) control. Data is presented as mean ± SEM of three replicates. . ***p<0.001, **p<0.01, *p<0.05 comparing UTC to hydrolsyates minus 1μM insulin, $^{###}$p<0.001, $^{##}$p<0.01, $^{#}$p<0.05 comparing 1μM insulin to hydrolysates plus 1μM insulin. Significance was determined using one- way ANOVA with a Newman-Keuls post-test

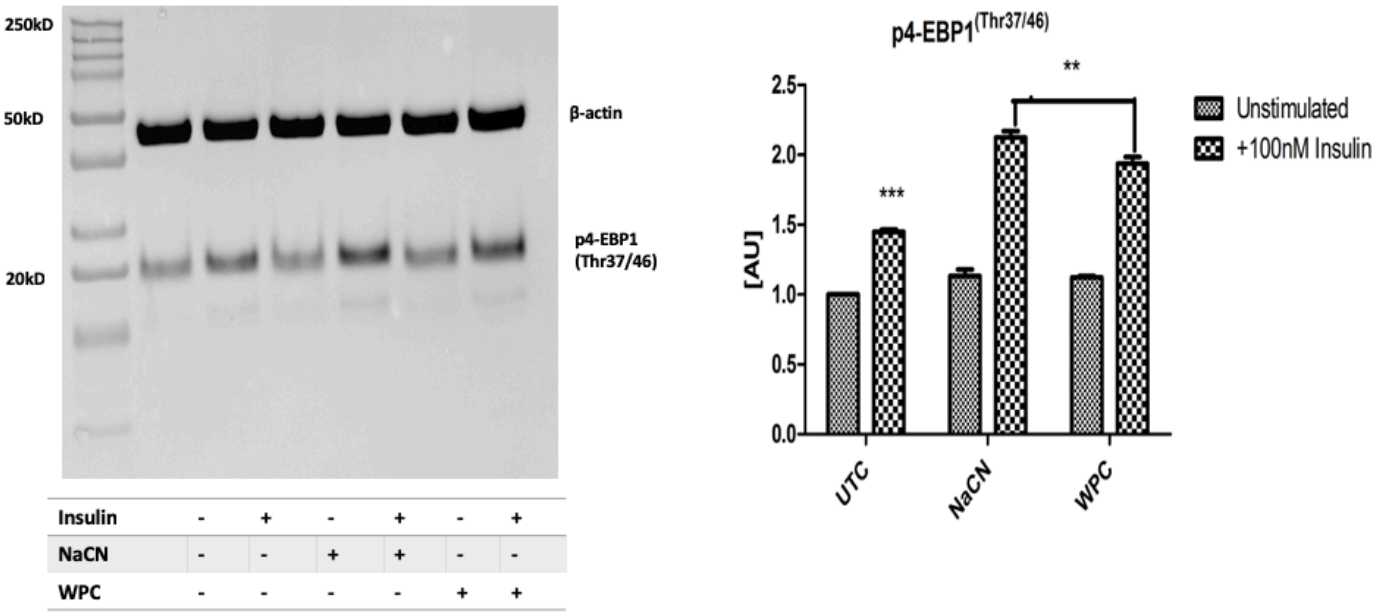


Figure 4.20 Representative western blot image of phospho-4EBP1$^{(Thr37/46)}$ activation and associated densitometric data derived using Image J image analysis software. L6 myotubes were stimulated with 1mg/mL of either whole, intact casein (NaCN) or whey (WPC) protein isolates in the presence or absence of 100nM insulin. NaCN and WPC can beneficially affect 4EBP1 activity in isolation and in combination with 100nM insulin. Data presented as ± SEM of two independent experiments. ***p<0.001, **p<0.01, *p<0.05 comparing untreated control (UTC) vs. 100nM insulin stimulated cells and NaCN/WPC + 100nM insulin vs. 100nM insulin. Significance was determined using one- way ANOVA with a Newman-Keuls post-test.

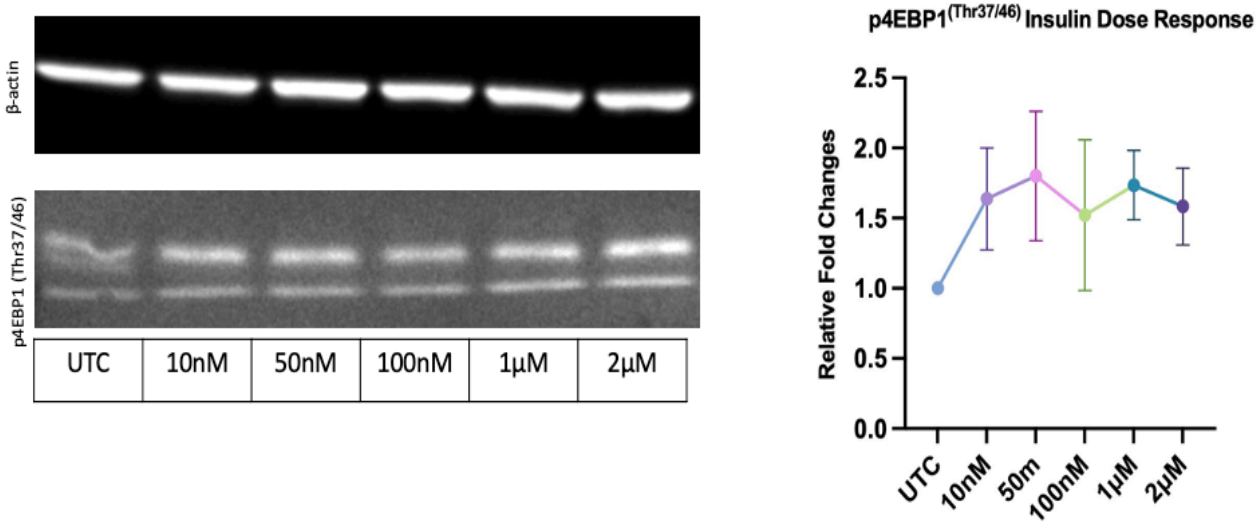


Figure 4.21: The effect of insulin on the levels of p4-EPB1$^{Thr(37/46)}$ in L6 myotubes. L6 myoblasts were seeded at 4x10^{4}cells/mL. Confluent myoblasts were differentiated into myotubes as previously described. Myotubes were subsequently stimulated with a dose range of insulin from bovine pancreas (10nM, 50nM, 100nM, 1µM and 2µM) for 20mins at 37^{0}C in 5% CO_2. Total protein was isolated and quantified as previously described. . Following immunoblotting with specific antibodies against β-actin (loading control) and p-4EBP1$^{(Thr37/46)}$ nitrocellulose membrane was incubated with a chemi-luminescent ECL western blot substrate for 2 min. Blot images were captured using a G-Box. Blots were quantified using the Image J analysis software as previously described. Data presented as ± SEM of three independent replicates . ***p<0.001, **p<0.01, *p<0.05 comparing to the untreated contro (UTC)l. Significance was determined using a two-way ANOVA with a Holm-Sidak post-test.

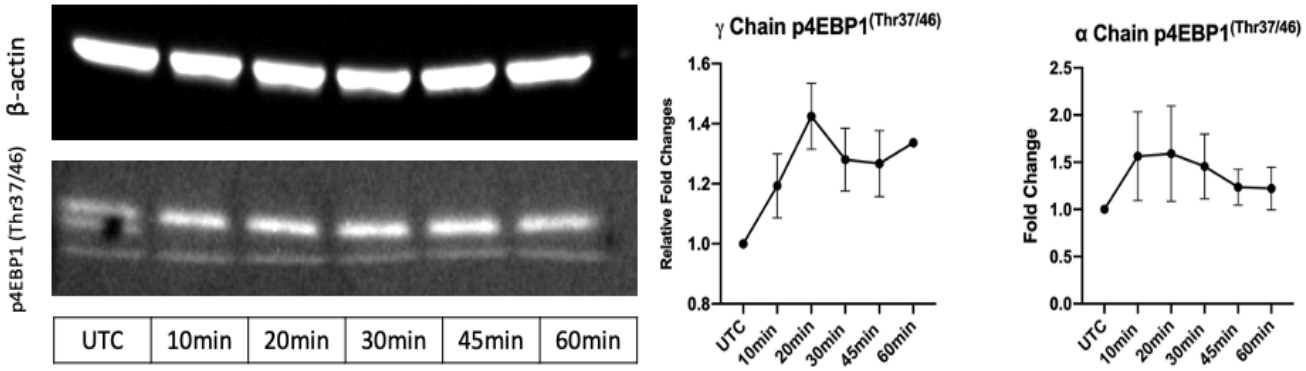
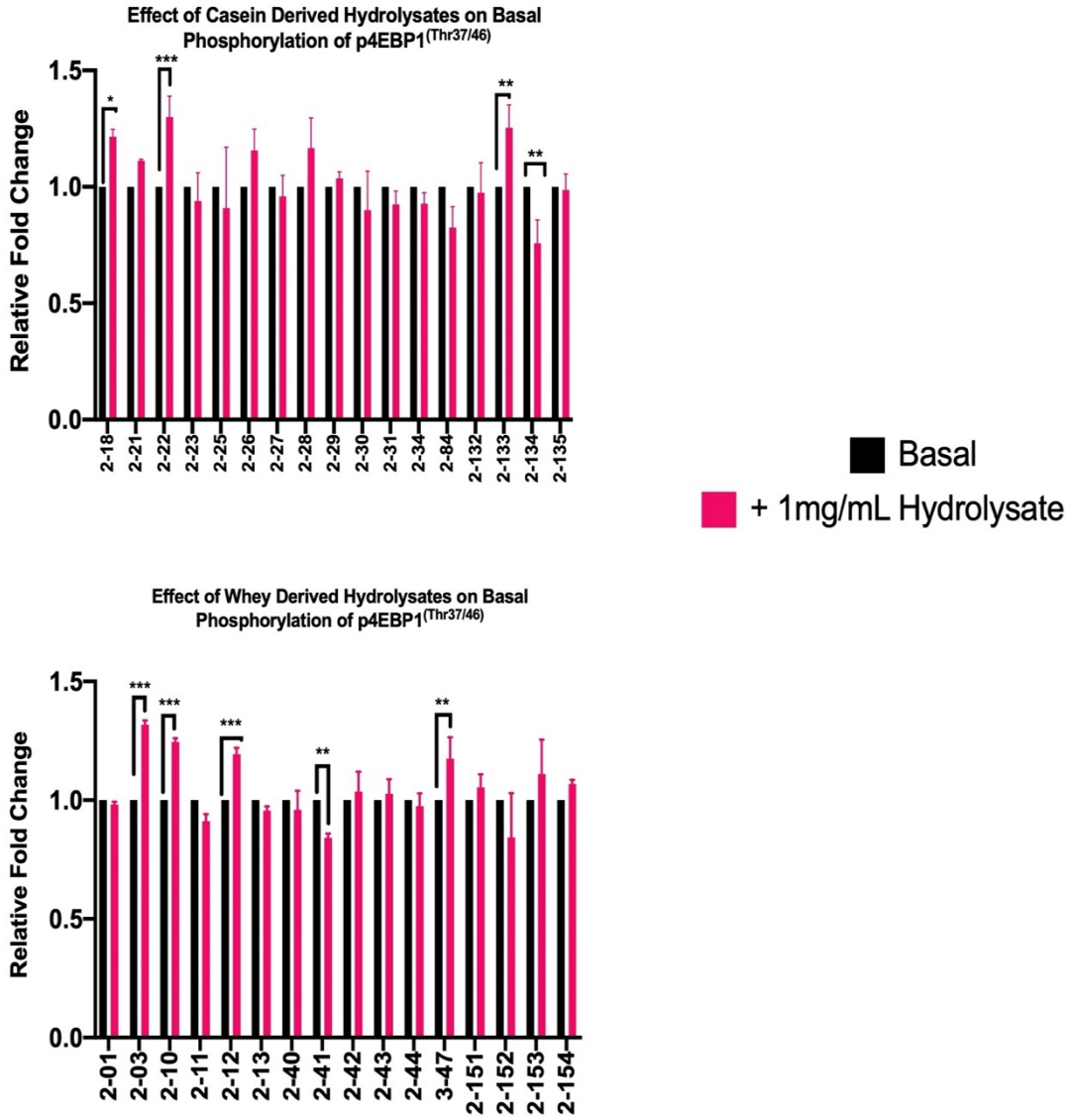


Figure 4.22: The effect of insulin incubation time on the levels of p4-EPB1$^{Thr(37/46)}$ in L6 myotubes. L6 myoblasts were seeded at 4x10^{4}cells/mL. Confluent myoblasts were differentiated into myotubes as previously described. Myotubes were subsequently stimulated with 1μM insulin from bovine pancreas at 37^{0}C in 5% CO_2 at specific time points (10min, 20min, 30min, 45min and 60min). Total protein was isolated and quantified as previously described. . Following immunoblotting with specific antibodies against β-actin (loading control) and p-4EBP1$^{(Thr37/46)}$ nitrocellulose membrane was incubated with a chemi-luminescent ECL western blot substrate for 2 min. Blot images were captured using a G-Box. Blots were quantified using the Image J analysis software as previously described. Data presented as ± SEM of three independent replicates . ***p<0.001, **p<0.01, *p<0.05 comparing untreated control. Significance was determined using a two-way ANOVA with a Holm-Sidak post-test.



F**igure 4.23: The effect of whey (WPC) and casein derived hydrolysates on the on the levels of basal p4-EPB1$^{Thr(37/46)}$ in L6 myotubes.** L6 myoblasts were seeded at 4x10^{4}cells/mL. Confluent myoblasts were differentiated into myotubes as previously described. Myotubes were subsequently stimulated with 1mg/mL hydrolysate in the presence or absence of 1µM insulin. Total protein was isolated and quantified as previously described. . Following immunoblotting with specific antibodies against β-actin (loading control) and p-4EBP1$^{(Thr37/46)}$ nitrocellulose membrane was incubated with a chemi-luminescent ECL western blot substrate for 2 min. Blot images were captured using a G-Box. Blots were quantified using the Image J analysis software as previously described. Data presented as ± SEM of three independent replicates . ***p<0.001, **p<0.01, *p<0.05 comparing untreated control to hydrolysate treated cells. Significance was determined using a two-way ANOVA with a Holm-Sidak post-test.

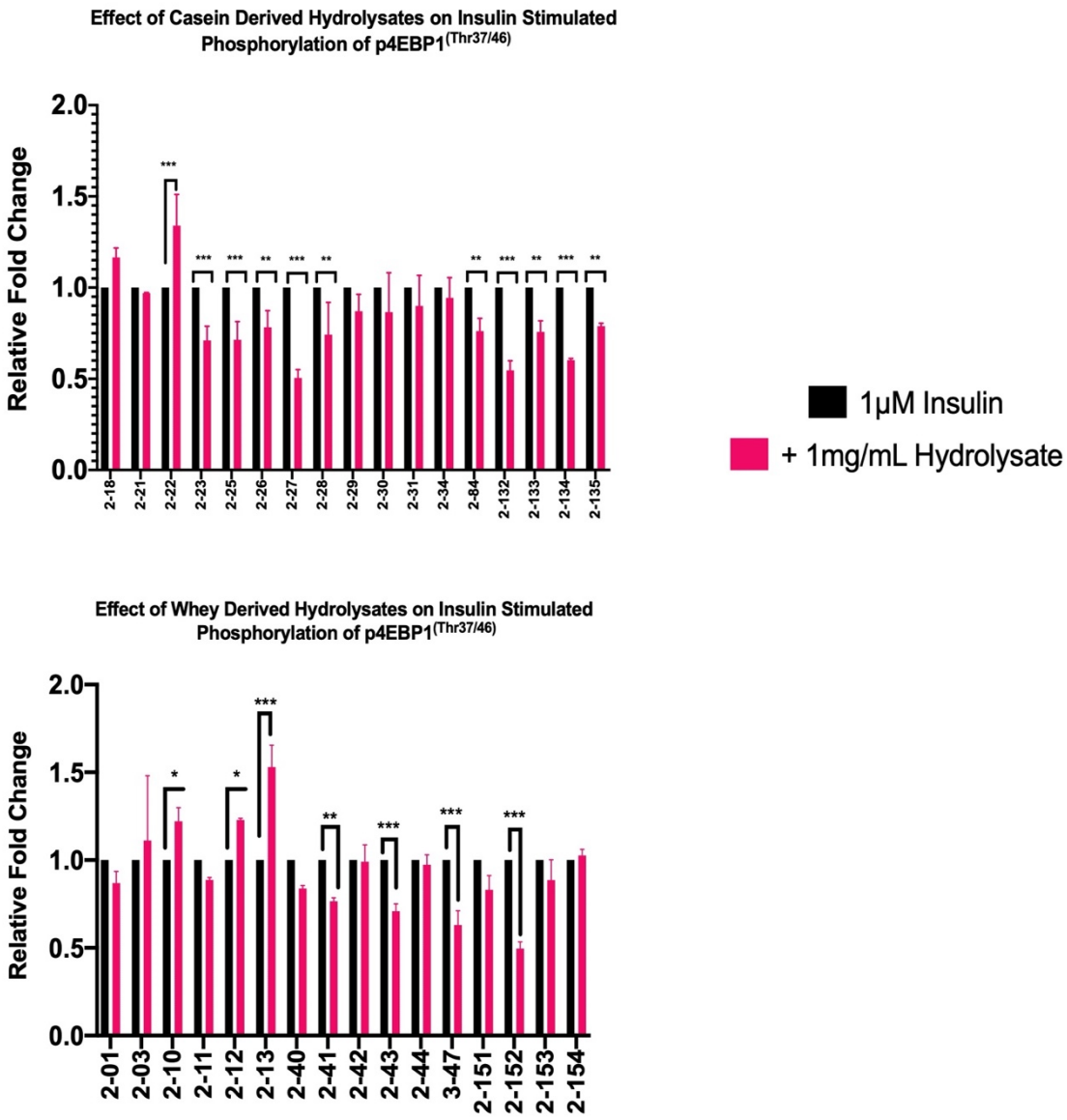


Figure 4.24: The effect of whey (WPC) and casein derived hydrolysates on the on the levels of insulin stimulated p4-EPB1$^{Thr(37/46)}$ in L6 myotubes.. L6 myoblasts were seeded at 4x10^{4}cells/mL. Confluent myoblasts were differentiated into myotubes as previously described. Myotubes were subsequently stimulated with 1mg/mL hydrolysate in the presence or absence of 1µM insulin. Total protein was isolated and quantified as previously described. . Following immunoblotting with specific antibodies against β-actin (loading control) and p-4EBP1$^{(Thr37/46)}$ nitrocellulose membrane was incubated with a chemi-luminescent ECL western blot substrate for 2 min. Blot images were captured using a G-Box. Blots were quantified using the Image J analysis software as previously described. Data presented as ± SEM of three independent replicates. ***p<0.001, **p<0.01, *p<0.05 comparing untreated control cells to hydrolysate treated cells. Significance was determined using a two-way ANOVA with a Holm-Sidak post-test.

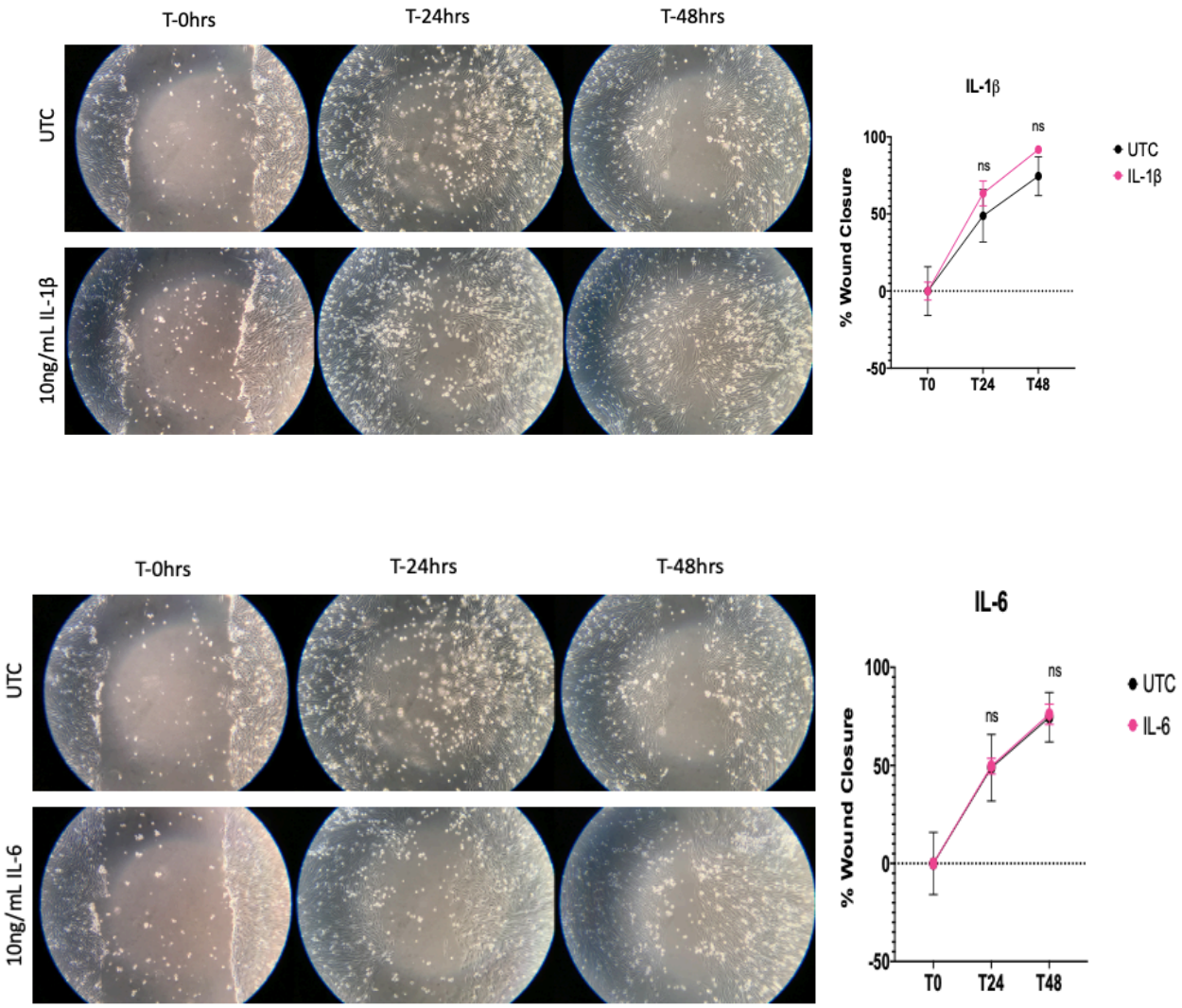


Figure 4.25: Recombinant Th1 and Th2 cytokines modulate wound healing in an in vitro assay of wound healing. L6 myoblasts were seeded at $8x10^6$ cells/mL at cultured to confluence as previously described. Cells were seeded in triplicate for each condition. Once confluent, the monolayer was wounded using a sterile P1000 micropipette tip to create a uniform scratch down the centre of the monolayer. Cells were then washed to remove injury debris and images were taken at a specific point within the well. Cells were subsequently incubated with 10ng/mL recombinant IL-1β, IL-6, IL-10 and TNFα. Images were taken at this point at 0hr (T0), 24hr (T24) and 48hr (T48). Wound closure is expressed as percentage closure of the original wound relating to each condition. Data is presented as mean ± SEM of three replicates. ***p<0.001, **p<0.01, *p<0.05 comparing the percentage wound closure at each time point. Significance was determined using two- way ANOVA with a Holm-Sidak post-test

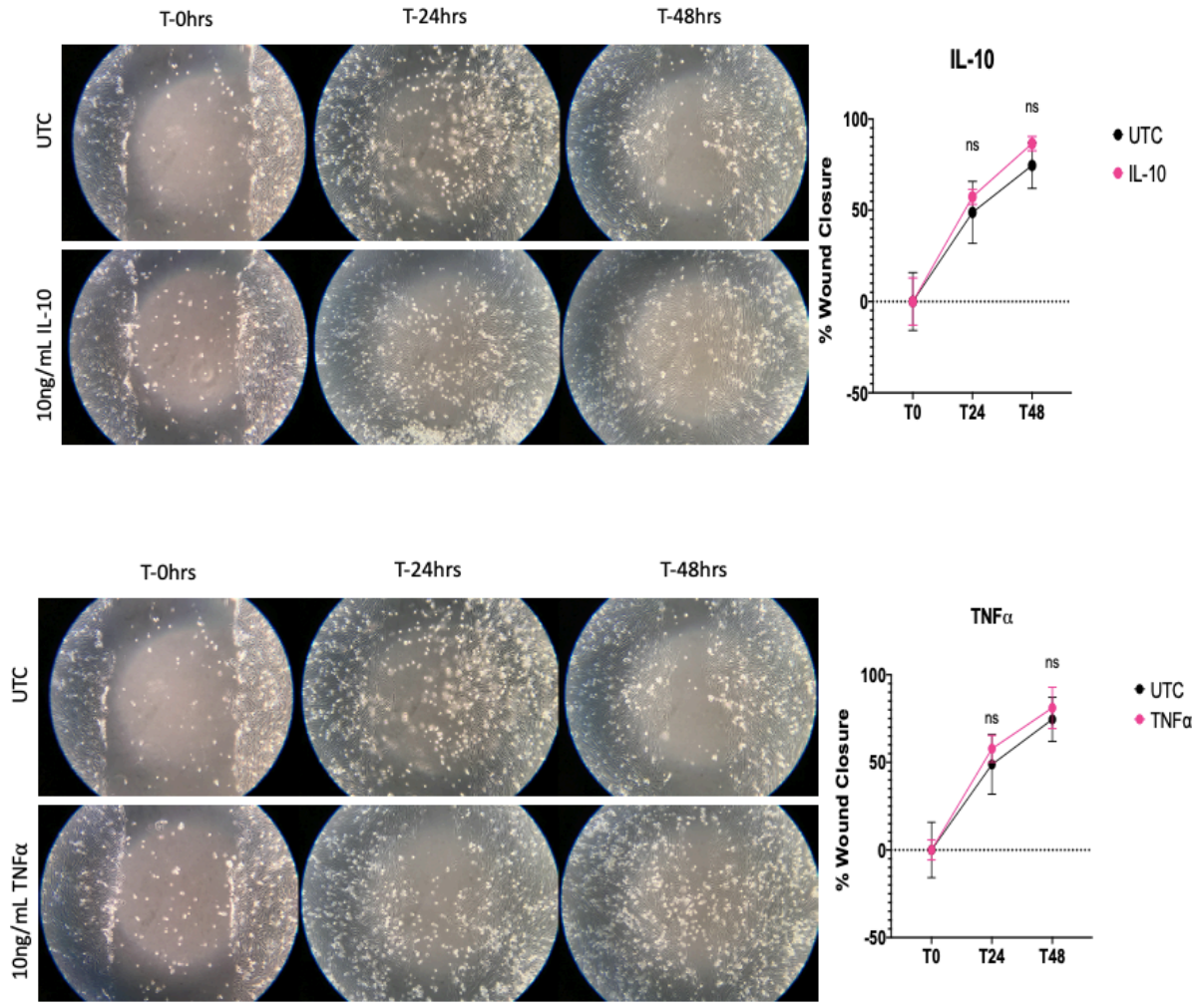


Figure 4.26: Recombinant Th1 and Th2 cytokines modulate wound healing in an in vitro assay of wound healing. L6 myoblasts were seeded at 8x10^6 cells/mL at cultured to confluence as previously described. Cells were seeded in triplicate for each condition. Once confluent, the monolayer was wounded using a sterile P1000 micropipette tip to create a uniform scratch down the centre of the monolayer. Cells were then washed to remove injury debris and images were taken at a specific point within the well. Cells were subsequently incubated with 10ng/mL recombinant IL-1β, IL-6, IL-10 and TNFα. Images were taken at this point at 0hr (T0), 24hr (T24) and 48hr (T48). Wound closure is expressed as percentage closure of the original wound relating to each condition. Data is presented as mean ± SEM of three replicates. ***p<0.001, **p<0.01, *p<0.05 comparing the percentage wound closure at each time point. Significance was determined using two- way ANOVA with a Holm-Sidak post-test

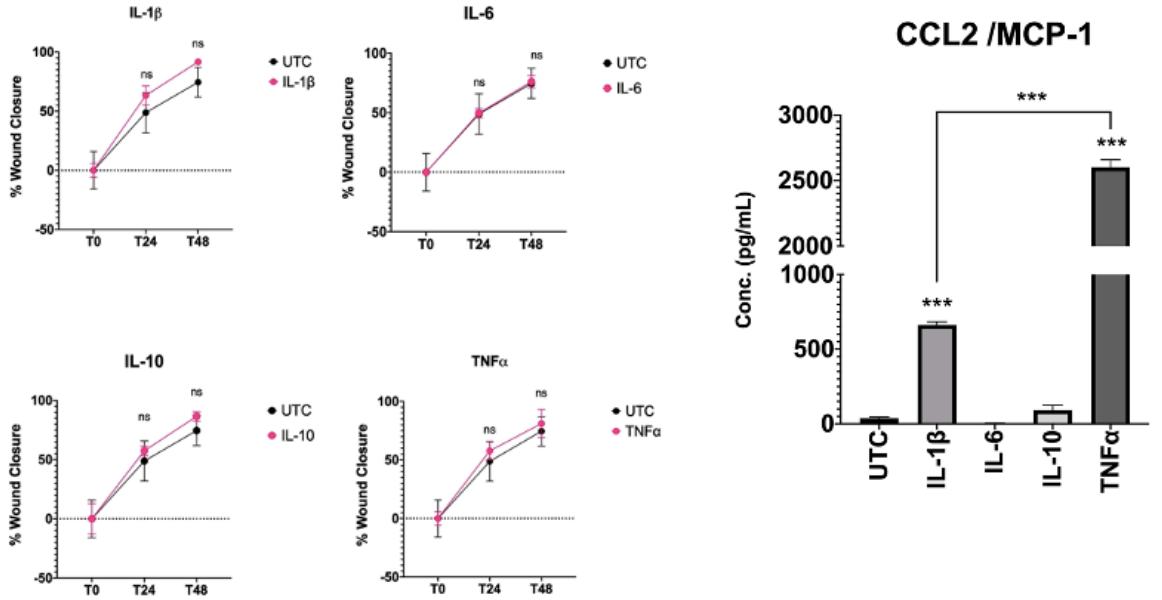


Figure 4.27: Recombinant Th1 and Th2 cytokines induce CCL2/MCP-1 chemokine secretion in L6 myoblasts associated with increased rates of in vitro wound closure. L6 myoblasts were seeded at $8x10^6$ cells/mL at cultured to confluence as previously described. Cells were subsequently stimulated with 10ng/mL Cells were recombinant IL-1β, IL-6, IL-10 and TNFα for 24hr. CCL2/MCP-1 chemokine secretion was measured using ELISA as previously described. Data is presented as mean ± SEM of three replicates. ***p<0.001, **p<0.01, *p<0.05 as determined via one-way ANOVA using a Newman-Keuls post-test.

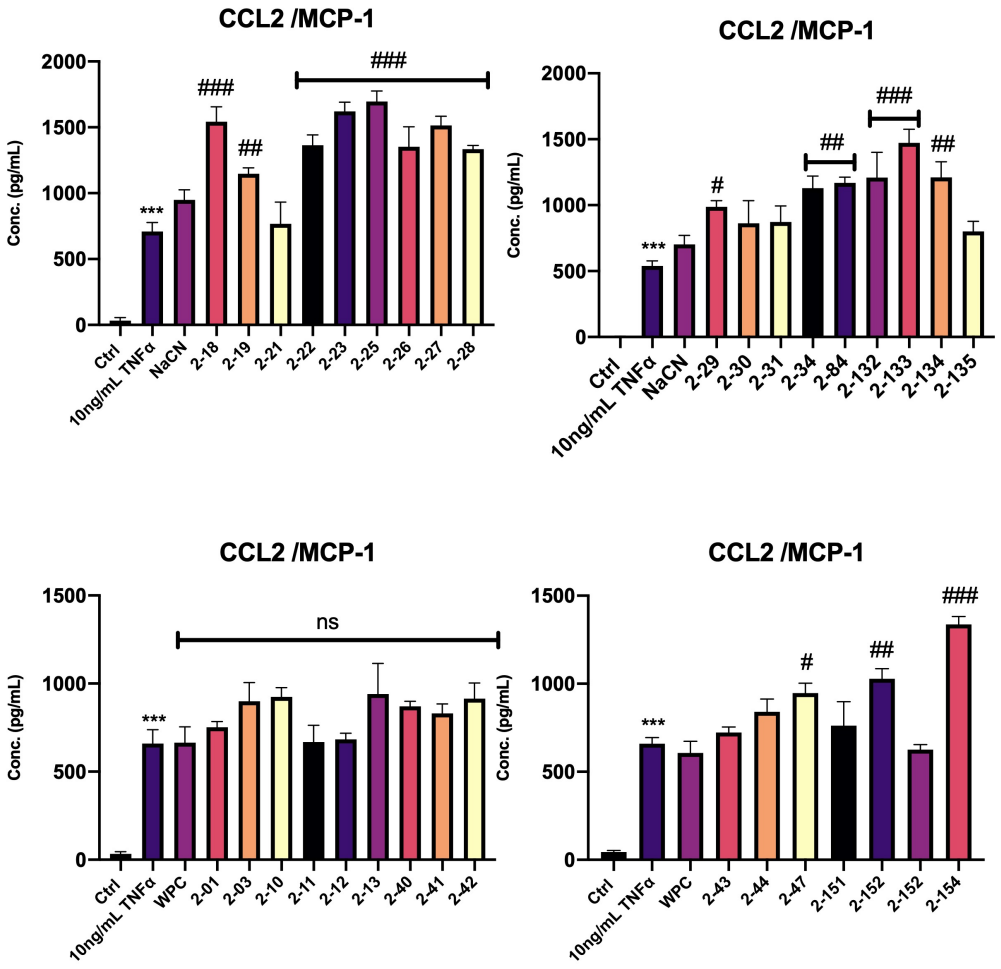


Figure 4.28: Whey and Casein derived hydrolysates drive CCL2/MCP-1 secretion in TNFα activated L6 myoblasts. L6 myoblasts were seeded at $8x10^6$ cells/mL at cultured to confluence as previously described. Cells were pre-incubated with 1mg/mL of hydrolysate sample for 1hr at 37°C in 5% CO_2. Cells were subsequently stimulated with 10ng/mL Cells were recombinant TNFα for 24hr. CCL2/MCP-1 chemokine secretion was measured using ELISA as previously described. Data is presented as mean ± SEM of three replicates. ***p<0.001, **p<0.01, *p<0.05 comparing UTC to 10ng/mL TNFα treated cells, $^{###}$p<0.001, $^{##}$p<0.01, $^{#}$p<0.05 comparing 10ng/mL TNFα treated cells to hydrolysate treated cells. Significance was determined using one- way ANOVA with a Newman-Keuls post-test.

.

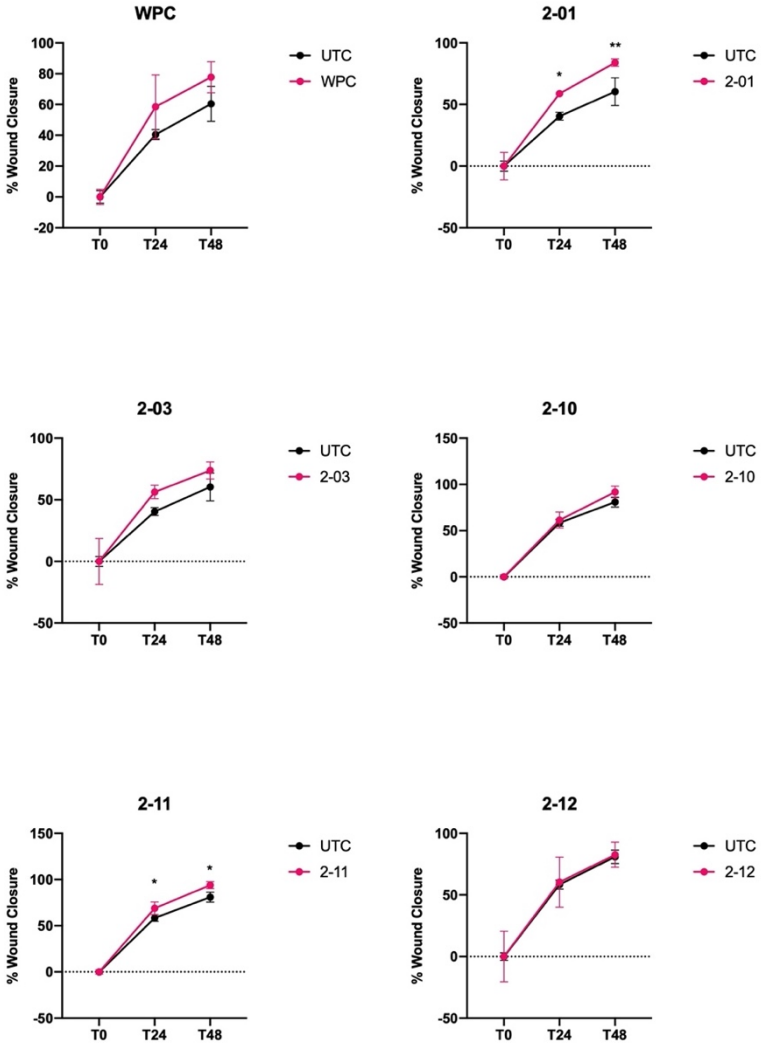


Figure 4.29: Whey (WPC) derived hydrolysates modulate the recovery of an in vitro wound in L6 myoblasts. L6 myoblasts were seeded at $8x10^6$ cells/mL at cultured to confluence as previously described. Cells were seeded in triplicate for each condition. Once confluent, the monolayer was wounded using a sterile P1000 micropipette tip to create a uniform scratch down the centre of the monolayer. Cells were then washed to remove injury debris and images were taken at a specific point. Cells were then incubated with 1mg/mL of specific hydrolysate. Images were taken at this point at 0hr (T0), 24hr (T24) and 48hr (T48). Wound closure is expressed as percentage closure of the original wound relating to each condition. Data is presented as mean ± SEM of three replicates. ***p<0.001, **p<0.01, *p<0.05 comparing the percentage wound closure at each time point. Significance was determined using two- way ANOVA with a Holm-Sidak post-test

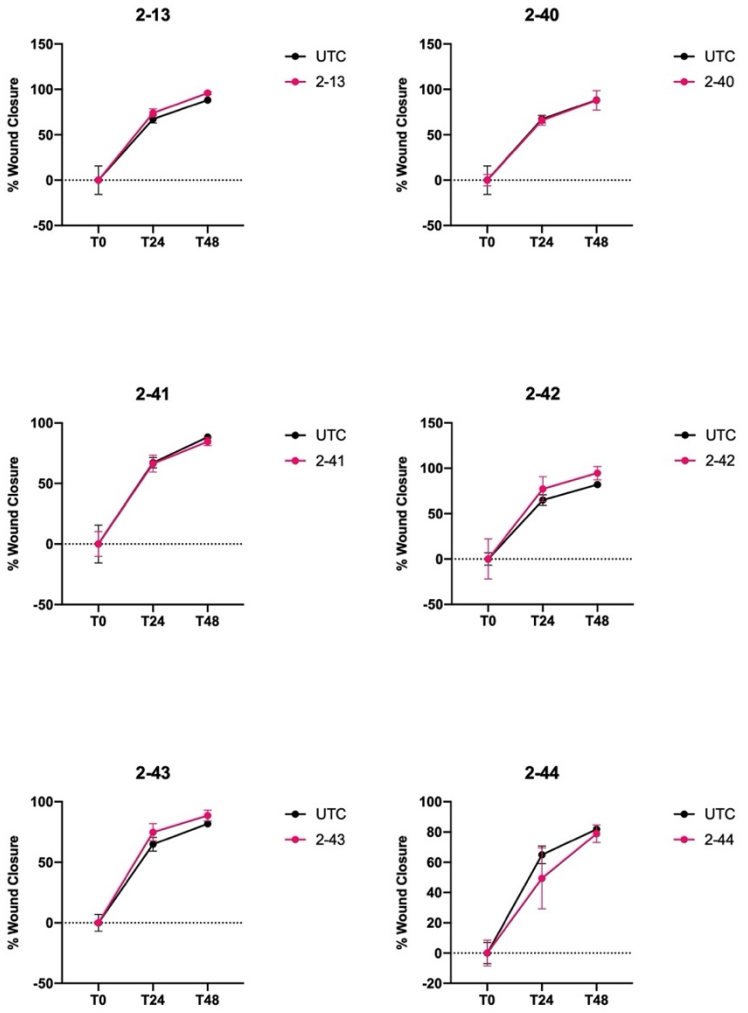


Figure 4.30: Whey (WPC) derived hydrolysates modulate the recovery of an in vitro wound in L6 myoblasts. L6 myoblasts were seeded at $8x10^6$ cells/mL at cultured to confluence as previously described. Cells were seeded in triplicate for each condition. Once confluent, the monolayer was wounded using a sterile P1000 micropipette tip to create a uniform scratch down the centre of the monolayer. Cells were then washed to remove injury debris and images were taken at a specific point. Cells were then incubated with 1mg/mL of specific hydrolysate Images were taken at this point at 0hr (T0), 24hr (T24) and 48hr (T48). Wound closure is expressed as percentage closure of the original wound relating to each condition. Data is presented as mean ± SEM of three replicates. ***p<0.001, **p<0.01, *p<0.05 comparing the percentage wound closure at each time point. Significance was determined using two- way ANOVA with a Holm-Sidak post-test

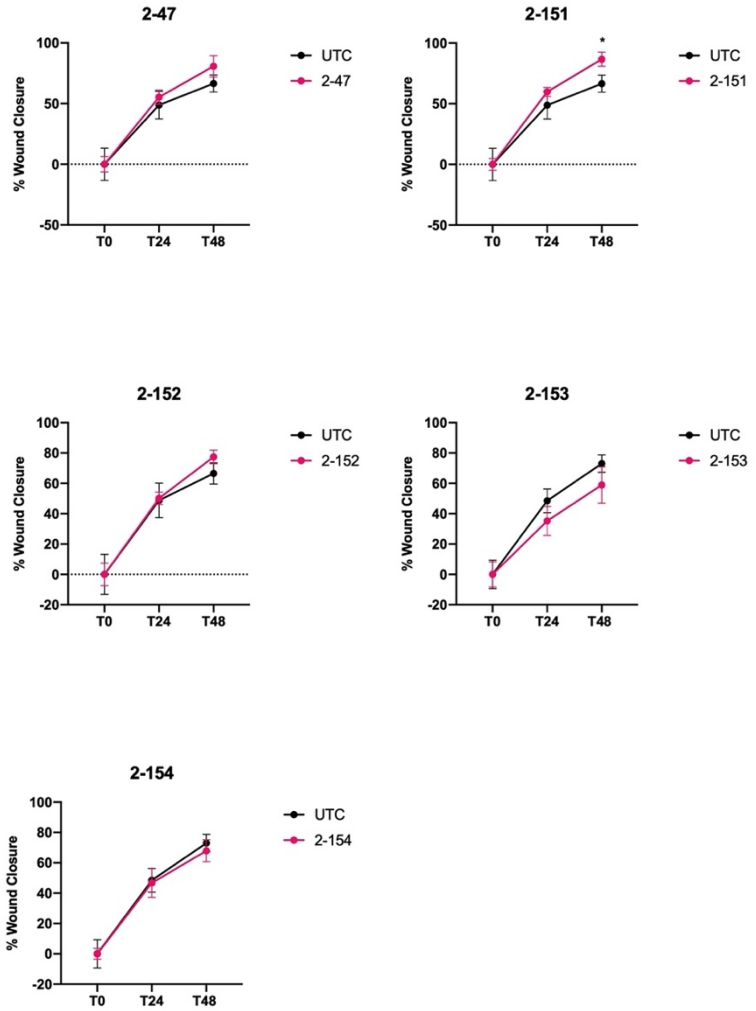


Figure 4.31: Whey (WPC) derived hydrolysates modulate the recovery of an in vitro wound in L6 myoblasts. L6 myoblasts were seeded at $8x10^6$ cells/mL at cultured to confluence as previously described. Cells were seeded in triplicate for each condition. Once confluent, the monolayer was wounded using a sterile P1000 micropipette tip to create a uniform scratch down the centre of the monolayer. Cells were then washed to remove injury debris and images were taken at a specific point. Cells were then incubated with 1mg/mL of specific hydrolysate Images were taken at this point at 0hr (T0), 24hr (T24) and 48hr (T48). Wound closure is expressed as percentage closure of the original wound relating to each condition. Data is presented as mean ± SEM of three replicates. ***p<0.001, **p<0.01, *p<0.05 comparing the percentage wound closure at each time point. Significance was determined using two- way ANOVA with a Holm-Sidak post-test

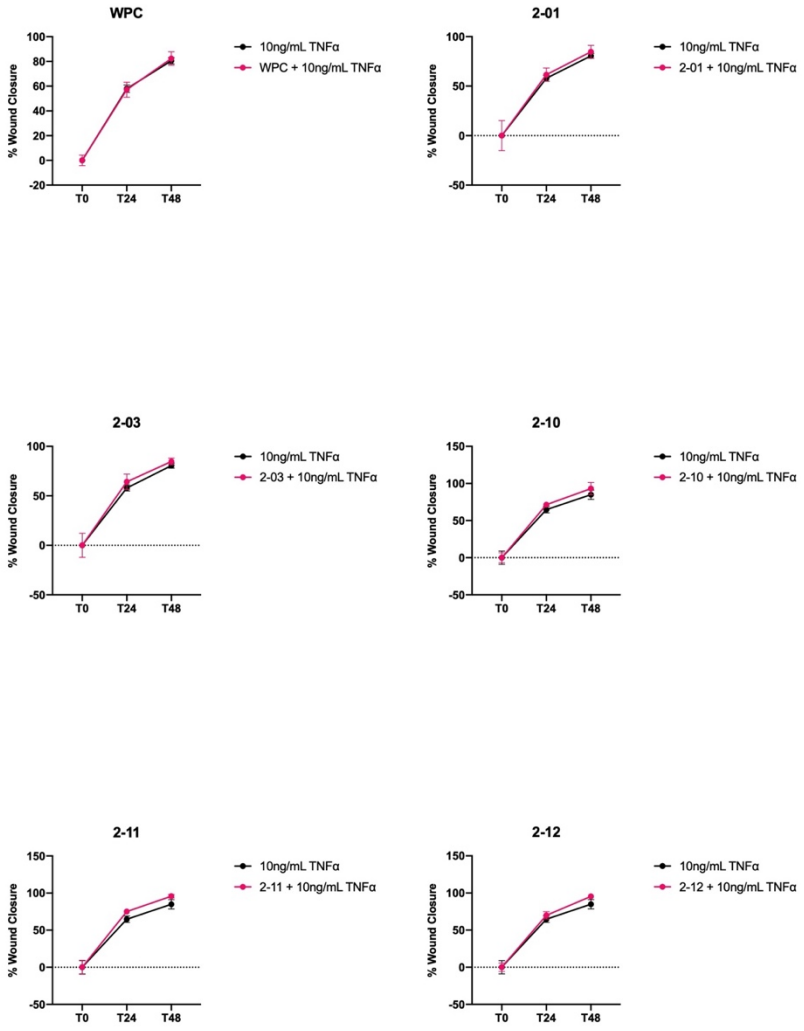


Figure 4.32: Whey (WPC) derived hydrolysates modulate the recovery of an in vitro wound in TNFα activated L6 myoblasts. L6 myoblasts were seeded at $8x10^6$ cells/mL at cultured to confluence as previously described. Cells were seeded in triplicate for each condition. Once confluent, the monolayer was wounded using a sterile P1000 micropipette tip to create a uniform scratch down the centre of the monolayer. Cells were then washed to remove injury debris and images were taken at a specific point. Cells were then incubated with 1mg/mL of specific hydrolysate in the presence of 10ng/mL recombinant TNFα. Images were taken at this point at 0hr (T0), 24hr (T24) and 48hr (T48). Wound closure is expressed as percentage closure of the original wound relating to each condition. Data is presented as mean ± SEM of three replicates. ***p<0.001, **p<0.01, *p<0.05 comparing the percentage wound closure at each time point. Significance was determined using two-way ANOVA with a Holm-Sidak post-test

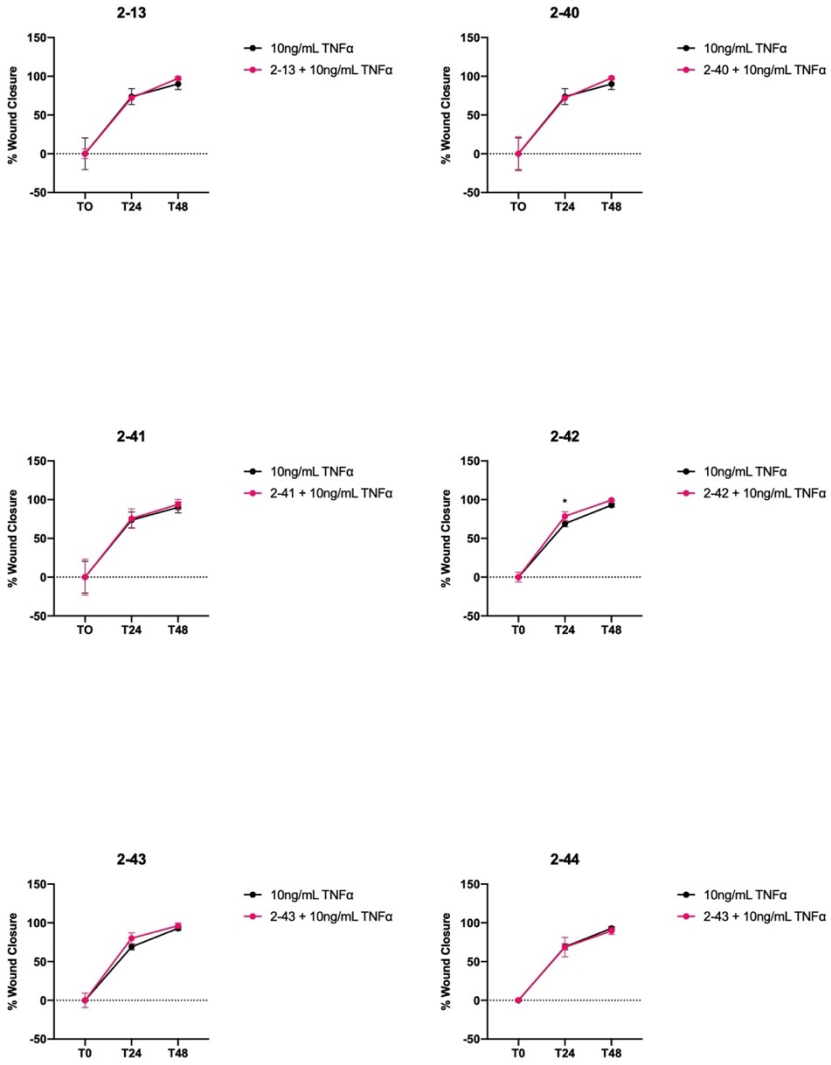


Figure 4.33: Whey (WPC) derived hydrolysates modulate the recovery of an in vitro wound in TNFα activated L6 myoblasts. L6 myoblasts were seeded at $8x10^6$ cells/mL at cultured to confluence as previously described. Cells were seeded in triplicate for each condition. Once confluent, the monolayer was wounded using a sterile P1000 micropipette tip to create a uniform scratch down the centre of the monolayer. Cells were then washed to remove injury debris and images were taken at a specific point. Cells were then incubated with 1mg/mL of specific hydrolysate in the presence of 10ng/mL recombinant TNFα. Images were taken at this point at 0hr (T0), 24hr (T24) and 48hr (T48). Wound closure is expressed as percentage closure of the original wound relating to each condition. Data is presented as mean ± SEM of three replicates. ***p<0.001, **p<0.01, *p<0.05 comparing the percentage wound closure at each time point. Significance was determined using two-way ANOVA with a Holm-Sidak post-test

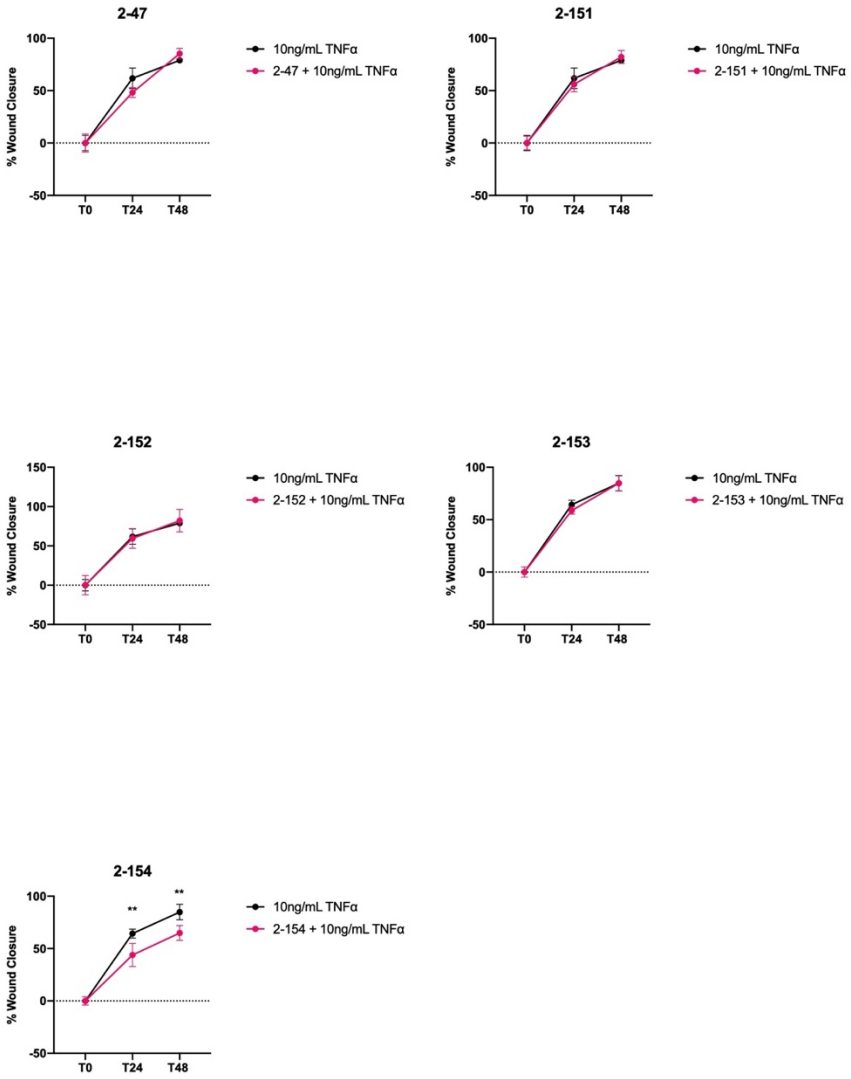


Figure 4.34: Whey (WPC) derived hydrolysates modulate the recovery of an in vitro wound in TNFα activated L6 myoblasts. L6 myoblasts were seeded at $8x10^6$ cells/mL at cultured to confluence as previously described. Cells were seeded in triplicate for each condition. Once confluent, the monolayer was wounded using a sterile P1000 micropipette tip to create a uniform scratch down the centre of the monolayer. Cells were then washed to remove injury debris and images were taken at a specific point. Cells were then incubated with 1mg/mL of specific hydrolysate in the presence of 10ng/mL recombinant TNFα. Images were taken at this point at 0hr (T0), 24hr (T24) and 48hr (T48). Wound closure is expressed as percentage closure of the original wound relating to each condition. Data is presented as mean ± SEM of three replicates. ***p<0.001, **p<0.01, *p<0.05 comparing the percentage wound closure at each time point. Significance was determined using two-way ANOVA with a Holm-Sidak post-test

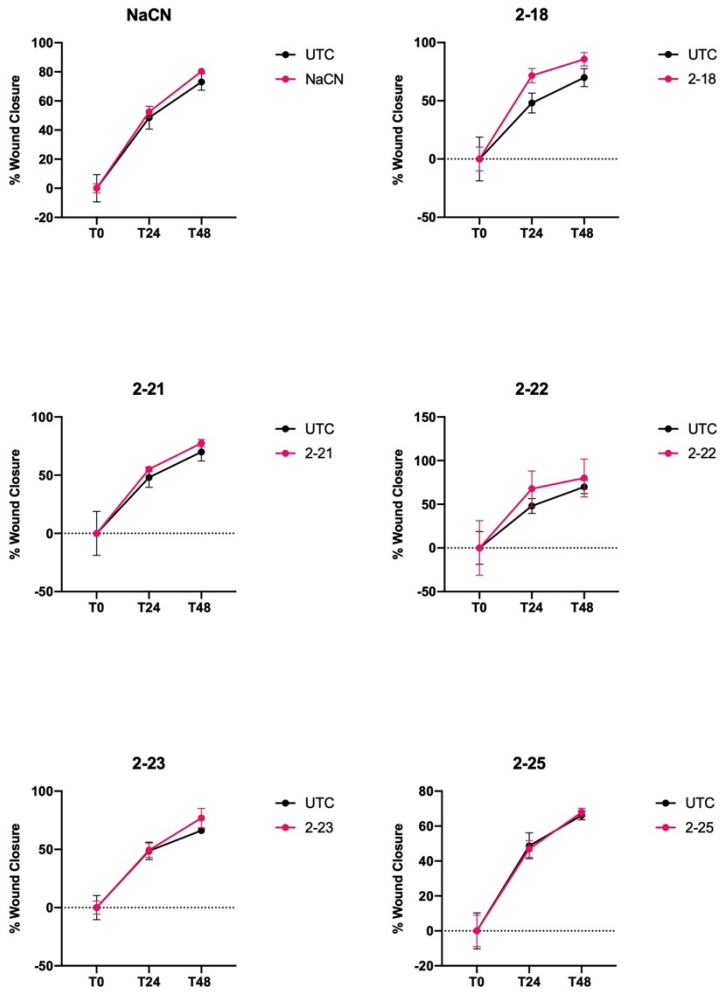


Figure 4.35: Casein (NaCN) derived hydrolysates modulate the recovery of an in vitro wound in L6 myoblasts. L6 myoblasts were seeded at $8x10^6$ cells/mL at cultured to confluence as previously described. Cells were seeded in triplicate for each condition. Once confluent, the monolayer was wounded using a sterile P1000 micropipette tip to create a uniform scratch down the centre of the monolayer. Cells were then washed to remove injury debris and images were taken at a specific point. Cells were then incubated with 1mg/mL of specific hydrolysate. Images were taken at this point at 0hr (T0), 24hr (T24) and 48hr (T48). Wound closure is expressed as percentage closure of the original wound relating to each condition. Data is presented as mean ± SEM of three replicates. ***p<0.001, **p<0.01, *p<0.05 comparing the percentage wound closure at each time point. Significance was determined using two- way ANOVA with a Holm-Sidak post-test

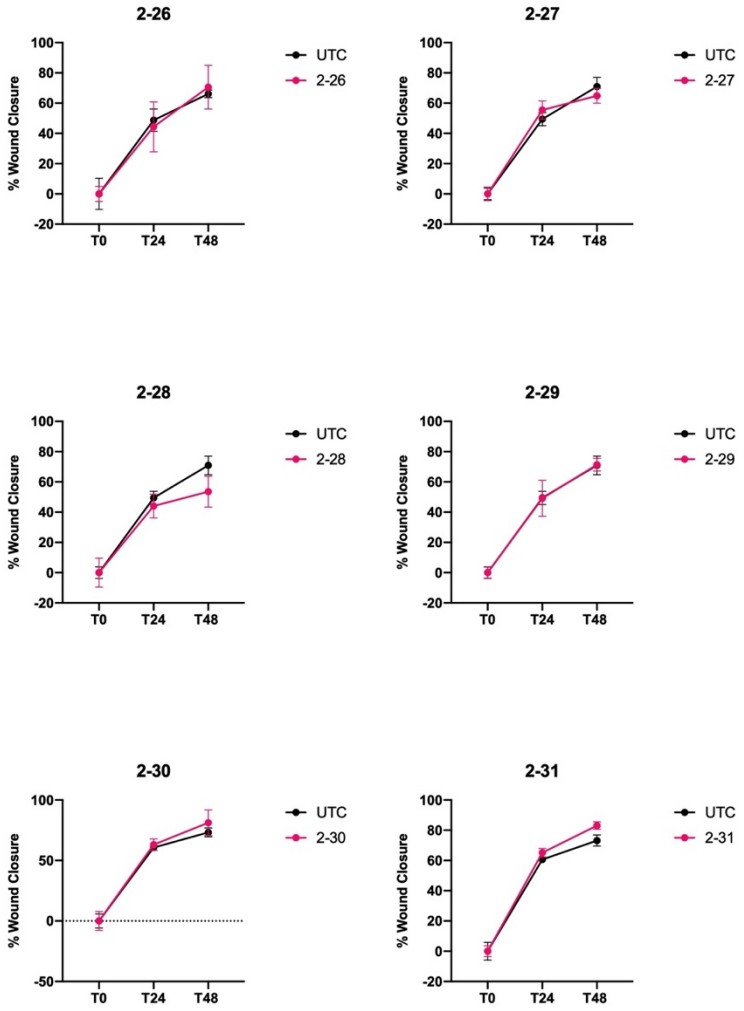


Figure 4.36: Casein (NaCN) derived hydrolysates modulate the recovery of an in vitro wound in L6 myoblasts. L6 myoblasts were seeded at $8x10^6$ cells/mL at cultured to confluence as previously described. Cells were seeded in triplicate for each condition. Once confluent, the monolayer was wounded using a sterile P1000 micropipette tip to create a uniform scratch down the centre of the monolayer. Cells were then washed to remove injury debris and images were taken at a specific point. Cells were then incubated with 1mg/mL of specific hydrolysate. Images were taken at this point at 0hr (T0), 24hr (T24) and 48hr (T48). Wound closure is expressed as percentage closure of the original wound relating to each condition. Data is presented as mean ± SEM of three replicates. ***p<0.001, **p<0.01, *p<0.05 comparing the percentage wound closure at each time point. Significance was determined using two- way ANOVA with a Holm-Sidak post-test

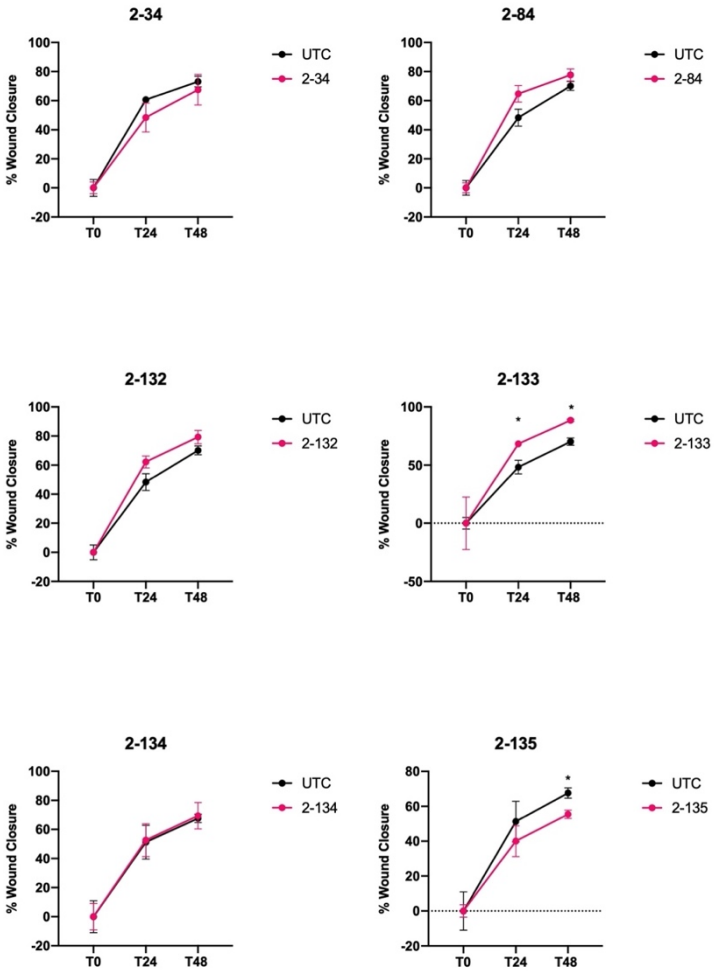


Figure 4.37: Casein (NaCN) derived hydrolysates modulate the recovery of an in vitro wound in L6 myoblasts. L6 myoblasts were seeded at $8x10^6$ cells/mL at cultured to confluence as previously described. Cells were seeded in triplicate for each condition. Once confluent, the monolayer was wounded using a sterile P1000 micropipette tip to create a uniform scratch down the centre of the monolayer. Cells were then washed to remove injury debris and images were taken at a specific point. Cells were then incubated with 1mg/mL of specific hydrolysate. Images were taken at this point at 0hr (T0), 24hr (T24) and 48hr (T48). Wound closure is expressed as percentage closure of the original wound relating to each condition. Data is presented as mean ± SEM of three replicates. ***p<0.001, **p<0.01, *p<0.05 comparing the percentage wound closure at each time point. Significance was determined using two- way ANOVA with a Holm-Sidak post-test

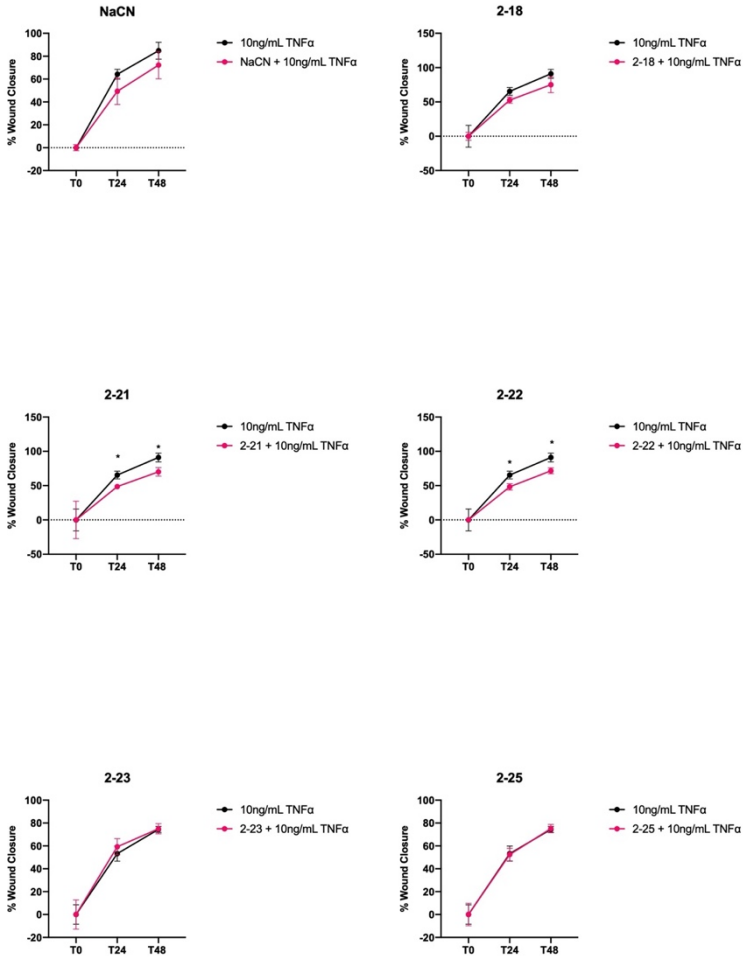


Figure 4.38: Casein (NaCN) derived hydrolysates modulate the recovery of an in vitro wound in TNFα activated L6 myoblasts. L6 myoblasts were seeded at $8x10^6$ cells/mL at cultured to confluence as previously described. Cells were seeded in triplicate for each condition. Once confluent, the monolayer was wounded using a sterile P1000 micropipette tip to create a uniform scratch down the centre of the monolayer. Cells were then washed to remove injury debris and images were taken at a specific point. Cells were then incubated with 1mg/mL of specific hydrolysate in the presence of 10ng/mL recombinant TNFα. Images were taken at this point at 0hr (T0), 24hr (T24) and 48hr (T48). Wound closure is expressed as percentage closure of the original wound relating to each condition. Data is presented as mean ± SEM of three replicates. ***p<0.001, **p<0.01, *p<0.05 comparing the percentage wound closure at each time point. Significance was determined using two-way ANOVA with a Holm-Sidak post-test

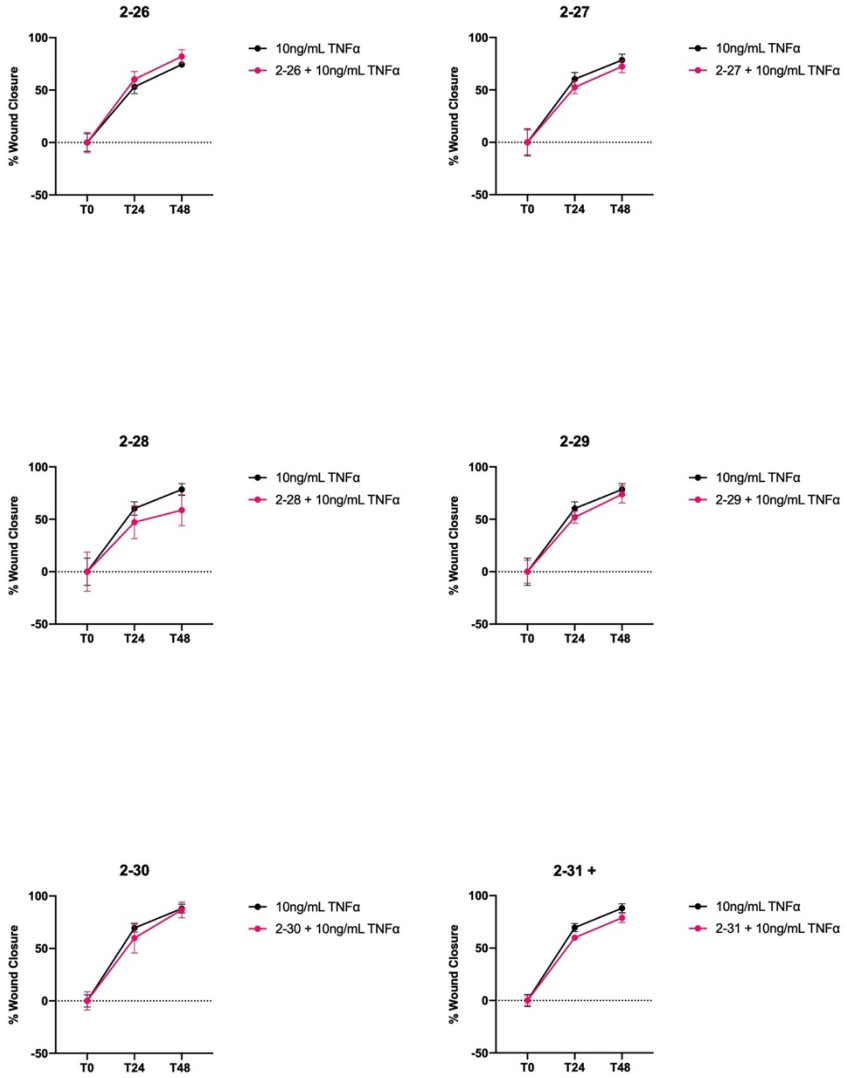


Figure 4.39: Casein (NaCN) derived hydrolysates modulate the recovery of an in vitro wound in TNFα activated L6 myoblasts. L6 myoblasts were seeded at $8x10^6$ cells/mL at cultured to confluence as previously described. Cells were seeded in triplicate for each condition. Once confluent, the monolayer was wounded using a sterile P1000 micropipette tip to create a uniform scratch down the centre of the monolayer. Cells were then washed to remove injury debris and images were taken at a specific point. Cells were then incubated with 1mg/mL of specific hydrolysate in the presence of 10ng/mL recombinant TNFα. Images were taken at this point at 0hr (T0), 24hr (T24) and 48hr (T48). Wound closure is expressed as percentage closure of the original wound relating to each condition. Data is presented as mean ± SEM of three replicates. ***p<0.001, **p<0.01, *p<0.05 comparing the percentage wound closure at each time point. Significance was determined using two-way ANOVA with a Holm-Sidak post-test

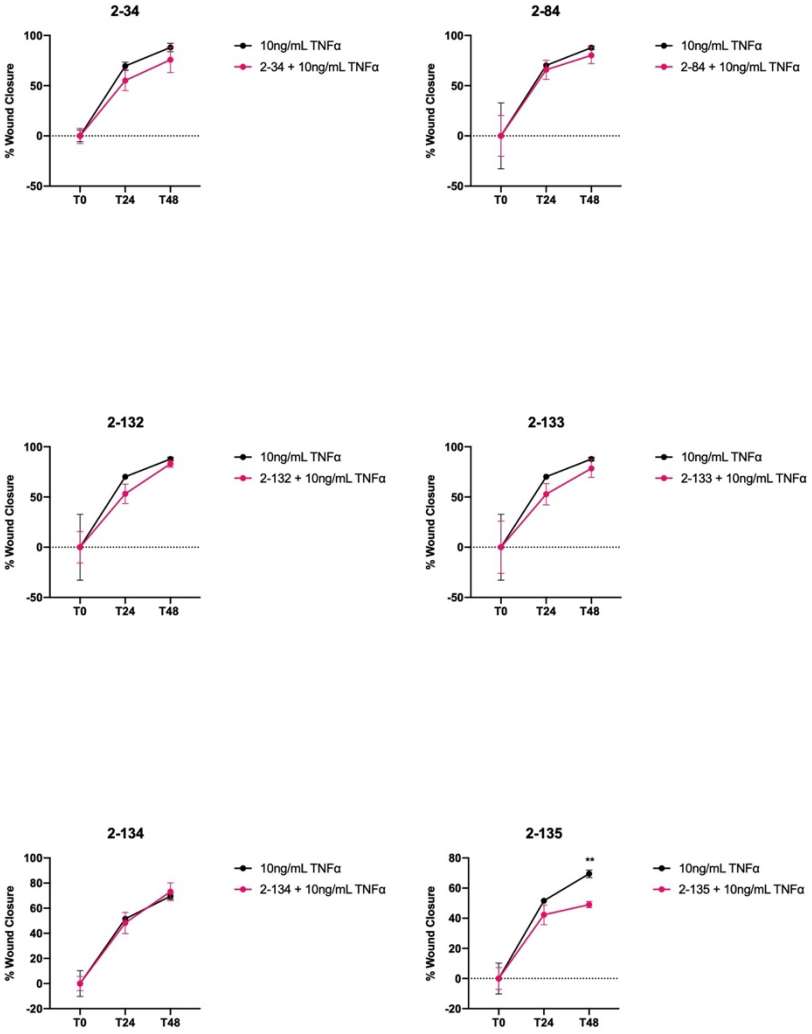


Figure 4.40: Casein (NaCN) derived hydrolysates modulate the recovery of an in vitro wound in TNFα activated L6 myoblasts. L6 myoblasts were seeded at $8x10^6$ cells/mL at cultured to confluence as previously described. Cells were seeded in triplicate for each condition. Once confluent, the monolayer was wounded using a sterile P1000 micropipette tip to create a uniform scratch down the centre of the monolayer. Cells were then washed to remove injury debris and images were taken at a specific point. Cells were then incubated with 1mg/mL of specific hydrolysate in the presence of 10ng/mL recombinant TNFα. Images were taken at this point at 0hr (T0), 24hr (T24) and 48hr (T48). Wound closure is expressed as percentage closure of the original wound relating to each condition. Data is presented as mean ± SEM of three replicates. ***p<0.001, **p<0.01, *p<0.05 comparing the percentage wound closure at each time point. Significance was determined using two-way ANOVA with a Holm-Sidak post-test.

4.4 Discussion

The aims of this chapter was to screen whey and casein hydrolysates for bioactivity that could indicate a health benefit in skeletal muscle. The main focus was on their potential effects on glucose metabolism, muscle protein synthesis and regeneration. The first step was therefore to establish an optimized cellular model for the screening. The L6-GLUT4myc myoblast cell line has long been employed in investigations concerning glucose metabolism and GLUT4 activity (Huang et al., 2002; Ishikura et al., 2010b). The cell line, originally isolated from the rat quadriceps, has been altered to stably express a myc tagged GLUT4 receptor, which like the endogenous receptor, is translocated to the membrane of these cells in response to insulin, a detailed description of the plasmid structure can be found at the following source (Wang et al., 1998). The cell line was developed, as the sensitivity of unaltered L6 myoblasts to insulin is relatively low compared to the differentiated L6 myotubes. However, upon being stably transfected with the GLUT4myc plasmid it has become possible to study glucose metabolism in the L6 myoblasts (Atsunori Ueyama, Karan L. Yaworsky, Qinghua Wang, Yousuke Ebina, 1999). These cells can also be driven to differentiate into multinucleated myotubes. GLUT4 is all but absent from the cell surface (Bryant et al., 2002). Owing to the myc epitope on the recombinant GLUT4 in the L6 GLUT4myc cell line being located on the extracellular portion of the transporter, it is possible to detect GLUT4myc on the cell surface using an already established immunofluorescence assay as described by *Wang et. al 1998*. Stimulation of L6 GLUT4-myc with 100nM insulin has been documented to induce a 1.5 to 2.0 fold increase in detectable cell surface GLUT4myc (Huang et al., 2002; Wang et al., 1998). Furthermore, this myc tag does not appear to negatively impact the wildtype functionality of GLUT4 with regards to translocation and ability to uptake circulating glucose *in vitro* . In accordance with previous studies, it has been shown in the results presented that using the method employed by Wang et. al is robust enough to detect this fold change in both L6 GLUT4myc myoblasts and myotubes (Wang et al., 1998) .

Due to the increased range of wells on a 96 well plate versus a 24 well plate, optimisation an employment of a 96 well format of this assay would allow for comprehensive high throughput platform for screening of the effects of specific analytes on GLUT4 trafficking.

The primary GLUT4 translocation assay is performed in 24 well plates. There are very few published instances of analysing GLUT4 translocation via a 96 well method (Fazakerley et al., 2010). The findings of the investigations of this thesis demonstrate a large variability in the response of L6 GLUT4myc myoblasts to 100nM insulin in 96 well plates. Although an insulin dose effect can be observed, the signal from the unstimulated control is too high to discern any meaningful information, particularly when observing the effects of hydrolysate stimulation. The lack of fold change seen in 96 well versus 24 well plate formats could be due to several reasons. One possibility is that 96 well culture plate displays a high affinity for the primary and secondary antibodies, making removal difficult during washing. This may result in the blanket signal in unstimulated and stimulated wells being observed. Likewise, the small, compressed channels of an individual well of a 96 well plate may make washing excess antibody from the cells within more difficult. However, these assumptions are unsubstantiated and will need to be investigated further. Given our findings we continued with the 24 well format for our screening and next optimised this format with a focus on insulin concentration and time exposure.

A dose of 100nM insulin for 20 min is considered to be a super physiological dose and is commonly used to drive GLUT4 translocation *in vitro* (Huang et al., 2002; Wang et al., 1998). To examine whether it is possible to optimise the dose and time of incubation, to drive maximal GLUT4, an insulin dose response and time course analysis was performed. As also demonstrated by *Cogan, 2018*, 1μM insulin was able to drive significant levels of GLUT4 translocation (Cogan, 2018). Further investigations revealed that an incubation of 20 min with 1μM insulin yielded maximal GLUT4 translocation in L6 GLUT4myc myoblasts and myotubes. Despite primary investigations being performed with the original 100nM insulin, which still represents relevant physiologically meaningful data, 1μM insulin was employed for later experiments into the effect of various stimuli on GLUT4 translocation in L6 GLUT4myc myotubes.

There is a key point which must be addressed when interpreting results using the GLUT4 translocation method. As mentioned previously, 100nM insulin induces a 1.5-to-2.0-fold change in cell surface GLUT4myc. The primary question is do whether to analyse the ΔGLUT4myc or treat conditions in the presence and absence of insulin as separate

conditions in order to extrapolate potential benefits *in vivo*. Under normal conditions, the afore mentioned fold change in cell surface GLUT4myc is representative of a healthy insulin response. Thus, a decrease in the ΔGLUT4myc may indicated negative consequences. For example, in humans, excessive levels of circulating TNFα has been shown to inhibit nominal glucose uptake via impaired activation of Akt Substrate 160, a key regulator involved in GLUT4 trafficking, providing a molecular link between chronic inflammation and metabolic dysfunction in skeletal muscle (Bouzakri et al., 2005). However in vitro , the data appears to be conflicting the in vivo data. Roher et al demonstrated that dose dependently, recombinant TNF increased the basal and insulin stimulated levels of cell surface GLUT4 in L6 GLUT4myc myoblasts and myotubes. Crucially however, is that the ΔGLUT4myc was strikingly decreased as a result. Despite this, in both myoblasts and myotubes, enhanced levels of cell surface GLUT4myc increased basal and insulin stimulated 2-DG glucose uptake (Roher et al., 2008a). In addition, Huang et al demonstrated that reduction in total cell surface GLUT4myc as a result of chronic glucose stimulation impaired the insulin stimulated levels of 2-DG glucose uptake. They did however note that there was an increased level of basal 2-DG glucose uptake despite reductions in basal GLUT4. This affected was attributed to the compensatory effects of a second glucose transporter GLUT1, whose total abundance was increased in response to chronic pre-treatment with high levels of glucose (Huang et al., 2002).

Taken together it appears that the fold change differences in the presence and absence of insulin are not the determining factor as to whether there is an impaired response to a certain stimulus. Furthermore, the study conducted by Bouzakri et al. used an infusion of TNFα in human subjects, which is likely to have induced the expression and secretion of pro-inflammatory mediators which may have exacerbated host inflammatory responses leading to a multifactorial effect on glucose metabolism suggesting that a single cytokine or factor alone is insufficient to drive deleterious effects on skeletal muscle metabolism. Ultimately, the effects of specific treatments on GLUT4 translocation should be interpreted by analysing the changes in the presence and absence of insulin separately and not the ΔGLUT4myc between treatments.

Following optimisation of the cellular model, we next wanted to provide proof of principle that GLUT4 translocation could be influenced by external factors and indeed that the L6-GLUT4myc model was robust enough to detect changes in basal and insulin stimulated levels of cell surface GLUT4 following exposure to such external factors. It has been well documented , that cytokines, both pro- and anti-inflammatory can interact with and influence muscle cells, both to the detriment and benefit of muscle health (Chazaud, 2016; Li, 2003; James G. Tidball, 2017). Therefore, we incubated several recombinant Th1 and Th2 cytokines with the muscle cells in order to confirm that we could detect any changes in basal and insulin stimulated GLUT4. . Th2 cytokines IL-2, IL-4 and TGFβ had a positive influence and promoted cell surface GLUT4myc, consistent with previous reports (Budi et al., 2015; Chang et al., 2012). The Th2 cytokine IL-10 in contrast, dose dependently reduced both insulin and insulin stimulated levels of cell surface GLUT4. This directly contradicts reports that improved serum IL-10 levels correlates with improved measures of diabetes and insulin resistance (Leon-Cabrera et al., 2015). Modulation of GLUT4 translocation was also detected following exposure to Th1 cytokines IL-6, TNFα and IFN$\boldsymbol{\gamma}$. Each cytokine increased basal cell surface GLUT4, while IL-6 and TNF dose dependently increased both basal and insulin stimulated levels of cell surface GLUT4. These observations are consistent with studies that investigated the effect of these inflammatory cytokines in skeletal muscle (BÉDARD et al., 1997; Carey et al., 2006; Roher et al., 2008b).

Our data confirmed our model was indeed robust enough to detect changes in GLUT4 following exposure to external factors, therefore we next exposed these cells to our whey and casein hydrolysates. Our data clearly indicates thatwhey protein and whey protein hydrolysates have the ability to upregulate basal GLUT4myc on the surface of L6 GLUT4myc myotubes, independent of insulin in some cases, indicating sub maximal insulinotrophic bioactivity. Whey protein hydrolysates had no negative effect on insulin stimulated controls relative to insulin alone. In the presence of insulin, in many cases GLUT4 translocation was unaffected relative to insulin alone. Regarding sample 2-47, this hydrolysate could induce significant increases in GLUT4 translocation at the basal and insulin stimulated levels. Similar patterns of pro-GLUT4 activity were observed with the casein hydrolysate group.

There are two sets of data relating to the casein hydrolysate cohort of samples. Initial experiments were conducted in myoblasts since they were ready to use quicker than the eight days required to culture mature myotubes and that they expressed a similar upregulation of GLUT4 translocation in response to insulin. In myoblasts, significant down regulation of basal GLUT4 was observed with several hydrolysates, while insulin stimulated cells in the presence of hydrolysate showed significant increases. The observations of the effects of these hydrolysates in myotubes, 2-18 for example , do not translate fully. This could be in part due to varying metabolic signalling pathways between myoblasts and myotubes being active or inactive, as myoblasts grow and become confluent gene expression profiles change to promote myotube formation (Krook et al., 2014). Moreover, myotubes are the structural and functional subunits of skeletal muscle fibre structure, data relating to GLUT4 translocation in myotubes is therefore physiologically relevant (Chanon et al., 2017; Yang and Hu, 2018). In myotubes, casein hydrolysates enhanced basal GLUT4 translocation and insulin stimulated GLUT4 translocation, exhibiting both insulinotrophic and insulin-synergy bioactivity respectively. Several key hydrolysates in this regard were identified, 2-18, 2-21, 2-132 and 2-47, and were examined further to determine whether there was a dose effect on GLUT4 translocation. As presented, at the basal level all samples dose dependently promoted GLUT4 translocation, further enforcing the theory of insulinotrophic bioactivity. However, in the presence of 1µM insulin, a dose dependant decrease in pro-GLUT4 activity was observed with samples 2-18, 2-21 and 2-132 while sample 2-47 stabilised at an increase of cell surface GLUT4 across all doses ranging from 0.5mg/mL to 5mg/mL. This dose dependant decrease may indicate that the cells are becoming stressed at higher doses of hydrolysate and as a result decrease their GLUT4 abundance on the cell surface. The consequence of this observation *in vivo* is unclear; however, it may indicate potential negative side effects for glucose uptake and utilisation if excess amounts of one of these bioactive components were consumed. This, however, will need to be investigated further with an increased dose range while also taking the timing of incubation into consideration.

Cow's milk is a complex matrix of proteins, branch chained amino acids (BCAA), BAPS, sugars and fats, and globally considered one of the most nutrient dense substances available for human consumption. Consequently, in depth studies of what dairy components illicit the positive health benefits for animal and human health are required (Marcone, Simone et al., 2017). Of the total native proteins found in cows milk, casein proteins account for approximately 80% and whey proteins making up the remaining 20% of the total protein (Marcone, Simone et al., 2017). Whey protein has been studied extensively with regard to its biological effects (Sousa et al., 2012). Whey protein is often discarded as a biproduct of the dairy industry. As a result, due to the excess whey produced as waste, and move towards more sustainable practices, researchers are attempting to uncover potential applications to reduce total waste from the dairy industry. Due to its readily and consistent availability, and the fact that it is acid soluble, whey protein is often used as a source of rapidly bioavailable protein and amino acids to support recovery in athletes and overall homeostasis (West et al., 2017).

Whey protein has been studied extensively in its ability to beneficially regulate glucose metabolism in skeletal muscle. Morato et.al demonstrated *in vivo*, that diets consisting of whole whey protein or a whey protein hydrolysate was able to enhance glucose uptake in Wistar Rats over a diet supplemented with whole caseins as a protein source. This improved metabolic response coincided with an increase in cell surface GLUT4 to the plasma membrane in hind limb skeletal muscle, in which the hydrolysed whey significantly outperformed the whole whey protein. Moreover, this increased GLUT4 activity and glucose utilization occurred independent of changes in serum insulin concentrations, suggesting two potential mechanisms; the whey protein enhances muscles sensitivity to circulating insulin or that the whey protein and hydrolysate exhibit an insulinotrophic bioactivity (Morato et al., 2013). Using an ex vivo serum screening platform in L6 GLUT4myc myotubes, Cogan et. al demonstrated that serum from human subjects who consumed a whey protein hydrolysate enhanced GLUT4 translocation in vitro in L6 GLUT4myc myotubes 60 min following consumption compared to baseline. Importantly, the whole whey protein control and a cocktail of non-essential amino acids failed to drive GLUT4 to the same extent (Cogan et al., 2019).

Casein protein comprises approximately 80% of the total protein fraction of dairy milk. Ingestion of dairy foods has long been associated with several health benefits, including immunomodulatory properties and benefits for glucose metabolism Whey protein comprises 20% of the total protein in milk and in terms of glucose metabolism, whey protein and its hydrolysates have been the most extensively studied in their ability to regulate glucose metabolism (Comerford and Pasin, 2016). Although not as extensively studied, there is promising data that Casein protein can positively impact glucose metabolism in skeletal muscle. For example, a Casein derived peptide has been shown to inhibit high glucose induced insulin resistance *in vitro* (Song et al., 2017). An *in vivo* mouse model of exercise also demonstrated that pre-exercise casein supplementation can improve glucose tolerance by enhancing GLUT4 in skeletal muscle. Reductions in serum TNFα were also observed in this study and it is postulated that this reduction may contribute to glucose tolerance (Matsunaga et al., 2017). Yuan et. al further demonstrated that a casein glycomacropeptide hydrolysate improved insulin signalling in diabetic mice, enhancing GLUT4 abundance on the surface of subject muscle (Song et al., 2017). Our data in myotubes, concerning GLUT4 translocation, suggests that at 1mg/mL both casein and whey derived hydrolysates can promote GLUT4 translocation and may help in promoting glucose uptake and utilisation in both healthy and diabetic individuals aiding muscle function and improving quality of life.

Given that the hydrolysates modulated glucose metabolism, we next examined their potential effects on muscle protein synthesis. In skeletal muscle**,** the mammalian target of rapamycin (mTOR) signalling pathway is the overarching regulator of skeletal muscle protein synthesis (Yoon, 2017). Downstream of the primary mTORC1 complex in the cell, there is a protein complex 4EBP1, which in its inactive, unphosphorylated stated is bound to a translation initiation factor eIF4E. Once phosphorylated, 4EBP1 releases eIF4E which allows for translation initiation and protein synthesis (Qin et al., 2016). Contextually, 4EBP1 activity is often observed and study in terms of cancer, where its chronic state of activation drives uncontrolled protein synthesis and cellular growth (Musa et al., 2016). However in the context of muscle health, upregulation of 4EBP1 activity and phosphorylation is associated with an increase of muscle protein synthesis rates in response to muscle injury and nutrient uptake (Kumar et al., 2009). Stimulation with insulin promoted p4E-BP1

phosphorylation of three isoforms of p4E-BP1 in L6 myotubes. Each of these three primary isoforms are designated, alpha (α), beta (β) and gamma ($\boldsymbol{\gamma}$) with the $\boldsymbol{\gamma}$ chain being the largest isoform. Insulin induced hyper phosphorylation of the $\boldsymbol{\gamma}$ isoform which is consistent with a study which investigated the phosphorylated states of each isoform in rat liver and skeletal muscle (Yoshizawa et al., 1998). Furthermore this insulin phosphorylation is correlated with increased MPS in skeletal muscle (Nakashima et al., 2020; Shen et al., 2005; Vary et al., 2001). Time course analysis revealed that, like GLUT4 translocation, an incubation time of 20mins at a dose of 1μM induced maximal $\boldsymbol{\gamma}$ isoform phosphorylation. As a result, measurement of $\boldsymbol{\gamma}$ isoform p4E-BP1 was used to measure the degree of activation of this anabolic pathway.

Given that whole casein and whey consists of intact protein, and that both enhanced p4E-BP1 signalling, it is predicted that due to the nature of the casein and whey derived hydrolysates and the potential higher bioavailability of "ready to use" priming amino acids, that hydrolysates can enhance 4E-BP1 phosphorylation, driving muscle protein synthesis (Morgan and Breen, 2021). Our data demonstrated that hydrolysates 2-18, 2-22, 2-133, 2-03, 2-10, 2-12 and 2-47 significantly increased the 4-EBP1 phosphorylation relative to the controls in the absence of insulin. This increase in gamma chain phosphorylation is positively associated with increased rates of protein synthesis in skeletal muscle (Shen et al., 2005). Conversely, in the presence of insulin, except for hydrolysates 2-18, 2-22, 2-03 and 2-12, hydrolysate treatment appeared to induce dephosphorylation of gamma chain p4-4BP1, which would indicate that these hydrolysates alone, are antagonistic to the functions and effects of insulin on mTOR and subsequent p4E-BP1 activation.

Many studies analysing the effect of proteins or nutritional supplementation on muscle hypertrophy have been performed in human or animal exercise intervention trials. Kakigi et. al demonstrated that ingestion of a whole whey protein following resistance training enhanced markers of muscle hypertrophy signalling (Kakigi et al., 2014). Moreover, Nakayama et. al further demonstrated that a whey protein hydrolysate was capable of inducing enhanced mTOR, 4EBP1 and S6K1 activity in an animal model of exercise (Nakayama et al., 2019). Cogan et. al, demonstrated that ingestion of a casein derived hydrolysate in conjunction with a carbohydrate source can drive anabolic signalling via

4EBP1, which may benefit the maintenance of muscle mass (Cogan et al., 2018). The confounding effects of exercise, circulating hormones and even the effects of immune function, may limit the ability of an *in vitro* assay to fully elucidate the bioactivity of candidate nutritional interventions. Our data however, does indicate that several casein and whey derived hydrolysates can beneficially promote 4E-BP1 phosphorylation, therefore MPS, eluding to potential benefits in vivo for maintenance of skeletal muscle mass. A hydrolysate with activity such as this, would be applicable in areas such as promoting recovery from exercise and maintaining muscle mass in the elderly.

The final part of this chapter was to assess the effects of the hydrolysates on muscle regeneration. Our skeletal muscle structure is kept in a constant state of injury and recovery. As with each movement, from steps to typing on a keyboard, muscle fibers are broken and require time to regenerate for our bodies to continue to function optimally. As discussed previously, myogenesis is the process in which our muscle tissue is renewed and restored. Orchestrated in large part by the immune system, a key step in this process is the ability of muscle progenitors and myoblasts to migrate to the site of injury to facilitate the wound healing process (James G Tidball, 2017). Assessing the effect of a specific treatment on wound healing capacity, can be done in several ways. *In vivo,* inducing a tissue wound using established procedures and measuring the rate of wound closure combined with other biomarkers of wound healing is one strategy (Jetten et al., 2014) . However, methods such as these are often expensive, time consuming and require ethical approval for deployment.

Despite muscle regeneration being a multifaceted, multilayered process, it is possible to gain insight on potential wound healing benefits *in vitro* . One cost effective method for studying wound healing *in vitro* is the use of the scratch assay method. This assay involves scraping a uniform scratch through a confluent layer of cells and measuring either the relative rate of wound closure or the comparative area of wound closure from one treatment to the next. This method of in vitro wound healing analysis has been employed extensively in several tissue models of wound healing (Goetsch and Niesler, 2011).

The immune system as previously discussed is a key regulator of skeletal muscle healing (Bosurgi et al., 2011). An initial proinflammatory response is critical for the induction wound the wound healing process (Brunelli and Rovere-Querini, 2008). To assess whether differences in rates of wound healing could be measured, we first employed the scratch assay and exposed then to recombinant pro- and anti-inflammatory cytokines typical of M1 and M2 macrophage, IL-1β, IL-6, IL-10 and TNFα. IL-1β, IL-10 and TNFα increased the rate of wound repair relative to the untreated control. This data is consistent with observations made within the literature regarding skeletal muscle injury (Li, 2013; Nitahara-Kasahara et al., 2021; Otis et al., 2014). IL-6 had no measurable effect on wound healing *in vitro* , despite IL-6 being documented extensively as being a major component of promoting muscle wound healing (Serrano et al., 2008).

We next exposed the cells in the scratch assay to our whey and casein derived hydrolysates. Our data clearly demonstrates that they exhibited the ability to support muscle recovery *in vitro* in the presence and absence of recombinant TNFα, used to replicate the injury micro-environment *in vivo*. Several hydrolysates exhibited enhanced proliferative bioactivities in injured skeletal muscle cells. In the absence of TNFα, hydrolysates 2-01, 2-11, 2-133 and 2-151 significantly increased proliferation and wound closure whereas no detrimental or positive impact was observed in the presence of TNFα. Some hydrolysates appeared to negatively impact wound healing in the presence and absence of TNF indicating potential negative consequences for acute wound healing *in vivo.* These hydrolysates included 2-28, 2-153, 2-153, 2-21 and 2-22.

The pro-regenerative effects of bioactive food components have been previously documented. The human intestinal tract is one tissue that, like muscle, is in a constant state of injury and recovery due to peristaltic contractions moving expired food matter through the gut. Nielsen et. al demonstrated in the Rat IEC-6 intestinal cell line that whole bovine casein, differentially digested with the proteolytic enzyme's pepsin and pancreatin, were able to induce cell proliferation and wound healing in a scratch assay *in vitro* model of wound healing by over 40%. Moreover, 15 peptides isolated from digest fractions of interest from this study were previously identified to have several additional bioactivities (Nielsen et al., 2019). Brown et. al set out to study the effect of replicative ageing on wound

healing in skeletal muscle C2C12 and the effect that Leucine and β-Hydroxy β-methyl butyric (HMB) acid supplementation had on the rates of wound closure in aged and young C2C12 myoblasts. Researchers cultured C2C12 myoblasts to a high passage number to replicate the ageing process *in vitro* . "Aged" cells were seeded and scratched alongside "young" low passage control myoblasts and the rate at which the wound closed was measured. Cells were subsequently incubated with leucine or HMB for 48 hours and the rate of wound closure was assessed. Leucine or HMB supplementation enhanced the rate of wound closure in both aged and young C2C12 myoblasts, supporting their use as exercise recovery supplements (Brown et al., 2017).

Previous studies show that increased rate of wound closure induced by cytokines is associated with increased secretion of the chemokine CCL2/MCP-1 from muscle cells. CCL2/MCP-1 is a key chemoattractant molecule, that in the context of skeletal muscle, is key for attracting infiltrating macrophage and other immune cells to aid in the direction of skeletal muscle generation (Lu et al., 2011; Yahiaoui et al., 2008). Given the significance of CCL2/MCP-1, we decided to assess the effect that hydrolysates would have on the secretion of CCL2/MCP-1 from TNFα activated L6 myoblasts, to represent the initial inflammatory response to acute muscle injury. The data presented in this thesis indicates that, with the exceptions of samples WPC, 2-21 and 2-152, both whey and casein derived hydrolysates were able to enhance CCL2/MCP-1 secretion from activated L6 myoblasts. This indicates the potential for these hydrolysates to be able increase the rate of skeletal muscle regeneration through the rapid attraction of circulating monocytes and macrophage to support regeneration *in vivo*. Moreover, considering the previously identified anti-inflammatory activity of these hydrolysates, combined with increased CCL2/MCP-1 secretion, that ingestion of these hydrolysates may improve healing of chronic muscle damage associated ageing. Support for CCL2/MCP-1 mediated therapies was demonstrated by Ishida et. al who showed that topical administration of a CCL2/MCP-1 enhanced recovery of diabetic wounds in a mouse model of diabetes (Ishida et al., 2019). In support of this, Wood et. al demonstrated in a CCL2 knockout mouse model of diabetes, that wound healing was significantly impaired and that a single 60ng dose of exogenous CCL2 applied to the wound area was able to improve the recovery of the wound compared to control diabetic mice (Wood et al., 2014).

In summary, this thesis chapter has identified the following:

1. Casein and whey protein hydrolysates can beneficially modulate basal, and insulin stimulated GLUT4 translocation in L6 GLUT4myc myotubes, which may have health boosting properties relating to glucose uptake and utilization in several human cohorts.
2. Casein and whey protein hydrolysates differentially affect protein synthesis pathways in L6 myotubes. Although several hydrolysates show promising pro-anabolic activity, this will need to be confirmed in a cell line or ex vivo myocyte culture, such as C2C12s which express genes associated with muscle anabolism.
3. Casein and whey protein hydrolysates enhance secretion of CCL2/MCP-1 from TNFα activated myoblasts which is associated with improved wound healing in skeletal muscle.
4. Casein and whey protein hydrolysates can beneficially modulate the healing of an in vitro wound in L6 myoblasts, suggesting a role in promoting muscle healing following injury or damage.

Chapter 5

Establishment of *in vitro* Conditioned Medium and Co-Culture Models to Assess the Impact of Candidate Cow's Milk Protein Hydrolysate Modulated Immune Profiles on Outputs of Skeletal Muscle Function

5.1 Introduction:

Skeletal muscle can be considered, among other things, one of the largest organs in the human body. Essential for locomotion and survival, in recent times the importance of muscle homeostasis for metabolic outputs and whole-body homeostasis as a result has become apparent (Brouns et al., 2002). It has been estimated that the rate of nuclei turnover in denervated muscle tissue is approximately 1% to 2% per week (Schmalbruch and Lewis, 2000). However, upon each muscle contraction from walking, typing or running, muscle fibers are damaged during this process, and consequently, damaged muscle tissue requires healing (Proske and Morgan, 2001).

As discussed in detail in Chapter One the immune system is the primary conductor and regulator of skeletal acute muscle wound healing (Yang and Hu, 2018). To recap, the process of healing is a stepwise and time dependent process. Initially, tissue resident monocytes and macrophage are activated and begin to recruit circulating monocytes and neutrophils to the site of injury. These cells begin to secrete pro-inflammatory stimulators such as CCL2, IFNγ and TNFα which skew occupying immune populations towards a Th1 phenotype. These Th1 skewed populations begin to secrete more inflammatory stimulators. IFNγ and TNFα function directly on muscle resident stem cells to initiate proliferation and differentiation into myoblasts. Concomitantly, inflammatory M1 macrophage necrotise and phagocytose damaged muscle tissue to clear the site of injury. As the healing timeline progresses, the immune microenvironment at the site of injury begins to phenotypically shift towards an anti-inflammatory Th2 environment, characterised by the abundance of M2 macrophage and muscle specific Treg populations. Together, the activity of these Th2 cell populations promote the resolution of residual inflammatory activity, promote myoblast bonding to myotube formation and induce ECM deposition from infiltrating fibroblasts (Burzyn et al., 2013; James G Tidball, 2017; Tidball and Villalta, 2010; Wood et al., 2014).

However, due to dystrophic disease, lifestyle factors and age the pro-wound healing interaction between muscle and immunity can be detrimentally affected to induce a stage of chronic muscle injury promoting fibrosis in the muscle and reduced functional capacity of skeletal muscle tissue (Sass et al., 2018; James G Tidball, 2017). This sustained inflammation has been linked with the induction of Sarcopenia, the age related metabolic disease which is characterised by a loss of muscle mass and function overtime (Haran et al., 2012; Kalinkovich and Livshits, 2017). Moreover, chronic inflammation is also linked with the onset of insulin resistance, a key disease hallmark of T2DM

As presented in Chapters Three and Four of this thesis, several cow's milk derived hydrolysates have shown muscle health boosting and anti-inflammatory bioactivities in the models employed for this work. However, due to the extensively characterised direct and indirect interactions between the immune system and skeletal, the question of how hydrolysate modulated immunity impacts key measurements of skeletal muscle function remain unanswered. Several nutraceutical/ bioactive food ingredients have been found to have pro-wound healing effects through modulating both the wound area and immune function (Ibrahim et al., 2018). In a model of intramuscular dexamethasone injury, Mani et. al demonstrated that topical treatment of the wound area with a 0.1% curcumin-based ointment enhanced wound healing. This was associated with an increase in expression of the immunoregulatory cytokine TGFβ-1 in the wound area. Moreover, TGFβ-1 mRNA levels were significantly elevated in macrophages occupying the wound area, suggesting that Curcumin modulated immunity plays a role in improved wound healing (Mani et al., 2002). In 3T3L1 adipocytes, vitamin D supplementation was shown to enhance GLUT4 translocation and glucose uptake, associated with a decrease in inflammatory CCL2 secretion (Manna and Jain, 2012).

The next step in this research is to assess the impact of hydrolysate modulated immune function on the following metrics of muscle function *in vitro* : GLUT4 translocation, 4EBP1 Phosphorylation levels (MPS indicator) and wound healing using the *in vitro* scratch wound assay. The goals of this chapter are as follows:

1. To optimise the generation of M1 and M2 polarised macrophage conditioned medium.
2. To investigate the effects of M1 and M2 polarised macrophage conditioned medium on the measurements of muscle function.
3. To investigate the effects of hydrolysate-modulated M1 and M2 polarised macrophage conditioned medium on the measurements of muscle function.
4. To investigate the effect of M1 and M2 polarised macrophage co-culture on the measurements of muscle function.
5. To investigate the effect of hydrolysate-modulated M1 and M2 polarised macrophage co-culture on the measurements of muscle function.

5.2 Results:

5.2.1 Generation of Differentially Activated Macrophage Conditioned Medium

The L6 GLUT4myc and L6 muscle cell lines used throughout this study are cultured primarily in three formulations of αMEM; growth medium (10% FBS) differentiation medium (2% FBS) and starvation medium (0% FBS), all of which contain a low glucose content of 1g/L. J774A.1 macrophage in contrast require a high glucose DMEM formulation of 5g/L which is critical to supporting immune polarisation. The muscle cell lines have documented sensitivity to high glucose exposure (Huang et al., 2002). As a result, to generate conditioned medium for use in studying crosstalk between immunity and skeletal muscle, strategies around αMEM:DMEM ratio formulations were attempted. We examined effect on cell viability and cytokine production.

5.2.1.1 Increasing concentrations of αMEM Growth Medium Negatively affects J774A.1 Macrophage Cell Viability

J774A.1 macrophage were seeded at $1x10^6$cells/mL in the following ratios of αMEM:DMEM; neat DMEM, 1:5, 2:5, 3:5, 4:5, neat αMEM and incubated for three hours at 37°C in 5% CO_2. Following this incubation, cells were stimulated with 100ng/mL LPS for 24hr at 37°C in 5% CO_2. Cell viability was deterimined using the CellTiter AQueous One MTS assay as previously described in section 2.2.8. As outlined in figure 5.1, baseline DMEM has no negative consequences for cell viability. Macrophage viability appears to peak significantly ($p<0.001$) at an αMEM:DMEM ratio of 2:5 and 3:5. Increasing αMEM ratios subsequently lead to a drop off in cell viability with neat αMEM significantly downregulating LPS activated cell viability ($p<0.001$).

5.2.1.2 Increasing concentrations of αMEM Growth Medium Negatively affects IL-6 and TNFα secretion in LPS activated J774A.1 Macrophage.

J774A.1 macrophage were seeded at $1x10^6$cells/mL in the following ratios of αMEM:DMEM; neat DMEM, 1:5, 2:5, 3:5, 4:5, neat αMEM and incubated for three hours at 37°C in 5% CO_2. Following this incubation, cells were stimulated with 100ng/mL LPS for 24hr at 37°C in 5% CO_2. Secreted cytokine concentrations were determined using specific cytokine ELISA as previously described in section 2.2.5. Increasing αMEM to DMEM ratios had significant negative consequences for IL-1β, IL-6 and TNFα secretion from LPS activated J774A.1 macrophage. As outlined in figure 5.2, significant decreases in both IL-6 and TNFα secretion were observed dose dependently as the αMEM:DMEM ratio increased ($p<0.001$). Similar effects were observed with IL-1β secretion. However, when activated in neat αMEM a significant increase relative to the LPS activated DMEM control was observed ($p<0.001$). With regards to IL-10 secretion, the only significant change was observed at the LPS activated 4:5 dose where a significant increase relative to the LPS DMEM control was observed ($p<0.05$). Despite this, no clear pattern of the effect of medium ratios on IL-10 secretion can be observed.

5.2.1.3 αMEM Negatively affects cell viability in M1 and M2 polarised J774A.1 macrophage phenotypes.

J774A.1 macrophage were seeded at $1x10^6$cells/mL and cultured in either αMEM or DMEM cell culture medium and incubated for three hours at 37°C in 5% CO_2. Following this, cells were polarised to the M1 and M2 phenotypes are previously described. Cell viability was deterimined using the CellTiter AQueous One MTS assay as previously described in section 2.2.8. Detailed in figure 5.3, baseline DMEM has no effect on polarised J774A.1 cell viability. However, when cultured in αMEM, significant negative consequences for cell viability were observed for M1 polarised ($p<0.001$) and M2 polarised ($p<0.05$) macrophage.

5.2.1.4 αMEM Negatively affects cytokine secretion profiles in M1 and M2 polarised J774A.1 macrophage phenotypes.

J774A.1 macrophage were seeded at 1x10^{6}cells/mL and cultured in either αMEM or DMEM cell culture medium and incubated for three hours at 37°C in 5% CO_2. Following this, cells were polarised to the M1 and M2 phenotypes are previously described. Secreted cytokine concentrations were determined using specific cytokine ELISA as previously described in section 2.2.5. As outlined figure 5.4, polarisation of J774A.1 macrophage has a significant impact on stereotypical cytokine profiles. In naïve macrophage a significant increase in IL-10 ($p<0.05$) was observed. As seen previously in LPS activated J774A.1 macrophage, M1 polarisation profiles are significantly impacted. IL-6 ($p<0.001$) and TNFα ($p<0.05$) were significantly down regulated in αMEM M1 polarised macrophage. Similar affects were observed in M2 polarised macrophage with downregulation of both IL-10 ($p<0.05$) and TNFα ($p<0.05$) being noted. Based on the data presented thus far, conditioned medium for crosstalk experiments will be generated in DMEM to ensure adequate immune functionality.

5.2.1.5 Varying cell densities affects secreted cytokine concentrations in M1 and M2 polarised J774A.1 macrophage.

In order to maximise the concentrations of cytokines in the conditioned media for future experiments we next assessed the effect of changing the cell density. J774A.1 macrophage were seeded at the following densities: M1/2 Ctrl, 1x10^{6}cells/mL in 2mL, M1/2A 1x10^{6}cells/mL in 1mL, M1/2B 2x10^{6}cells/mL in 1mL and M1/2C 2x10^{6}cells/mL in 2mL and incubated for three hours at 37°C in 5% CO_2. Following this, cells were polarised to the M1 and M2 phenotypes are previously described in section 2.2.5. Secreted cytokine concentrations were determined using specific cytokine ELISA as previously described. M1/2 Ctrl represents the macrophage cell density that has been used throughout this thesis as a control. In M1 polarised macrophage, altering cell densities increases the levels of detectable IL-6, IL-10, and TNFα. M1B resulted in an increase in IL-6 ($p<0.001$), IL-10 ($p<0.001$) and TNFα ($p<0.001$) whilst IL-1β secretion was maintained (figure 5.5). Outlined in figure 5.6, in M2 polarised Macrophage, M2B cell densities increased IL-6 (ns) IL-10 ($p<0.05$) and TNFα ($p<0.05$). M2C cell density significantly boosted IL-6 secretion ($p<0.01$).

Based on this data, generation of conditioned medium for optimisation experiments will be generated using M1 and M2 polarised macrophage at the following densities: $1x10^6$cells/mL in 2mL as a control and $2x10^6$cells/mL in 1mL as concentrated medium.

5.2.1.6 Generation of hydrolysate modulated M1 and M2 macrophage conditioned growth medium.

Following optimisation of the parameters for generation of conditioned media we next exposed the macrophage to hydrolysates prior to differentiation to M1 and M2 phenotype. J774A.1 macrophage were seeded at $1x10^6$cells/mL and cultured DMEM and incubated for three hours at 37°C in 5% CO_2. Cells were subsequently stimulated with 1mg/mL of whole protein control (NaCN/WPC), casein derived hydrolysate (2-18, 2-132) or whey derived hydrolysate (2-47, 2-152) for one hour at 37°C in 5% CO_2. Following this, cells were polarised to M1 and M2 phenotypes as previously described. Secreted cytokine concentrations were determined using specific cytokine ELISA as previously described in section 2.2.5. In M1 macrophage (figure 5.7) Casein derived hydrolysate 2-18 exhibited ant-IL-1β ($p<0.05$), anti-IL-6 (ns) and pro-IL-10 (ns) bioactivity while TNFα was unaffected. Casein hydrolysate 2-132 exhibited anti-IL-1β (ns) anti-IL-6 ($p<0.001$), anti-TNFα ($p<0.001$) and pro-IL-10 bioactivity. Whole casein (NaCN) had exhibited differential effects on IL-6 secretion but consistently exhibited anti-IL-10 ($p<0.05$) and anti-TNFα ($p<0.01$, $p<0.001$) bioactivity consistent with previous observations. 2-18 and 2-132 suppressed IL-6 ($p<0.001$, $p<0.001$) compared to NaCN. Furthermore, both 2-18 and 2-132 increased IL-10 secretion ($p<0.01$, $p<0.05$) compared to NaCN. 2-132 also reduced TNFα secretion to a greater degree than NaCN ($p<0.001$). Whey derived 2-47 and 2-152 exhibited anti-IL-6 ($p<0.001$, $p<0.05$) and anti-TNFα ($p<0.001$, $p<0.001$) bioactivity. Whole whey protein, WPC, exhibited comparable bioactivity with the hydrolysates down regulating IL-6 ($p<0.001$) and TNFα ($p<0.001$) secretion. In M2 polarised macrophage, figure 5.8, samples 2-18 and 2-132 exhibited comparable effects: pro-IL-10 ($p<0.001$) and pro-TNFα ($p<0.001$) activity. Whole NaCN knocked down IL-10 secretion ($p<0.01$, $p<0.05$). NaCN derived hydrolysates were able to restore and boost IL-10 secretion ($p<0.001$). WPC promoted IL-10 secretion ($p<0.001$) while hydrolysate 2-152 boosted (ns) and 2-47 ($p<0.05$) downregulated IL-10 secretion. WPC significantly improved IL-10 secretion over hydrolysate 2-47 ($p<0.001$).

Hydrolysate modulated conditioned medium stocks were generated and stored at -20°C until required for crosstalk experiments.

5.2.2 The Effect of M1 and M2 Macrophage Conditioned medium on GLUT4 Translocation in L6 GLUT4myc Myotubes.

5.2.2.1 Changes in secreted cytokines from M1 and M2 macrophage augments GLUT4 translocation in L6 GLUT4myc myotubes.

L6 GLUT4myc myoblasts were seeded at 4x10^{4}cells/mL and differentiated into myotubes as previously described. Mature myotubes were subsequently exposed to standard (1x10^{6}cells/mL in 2mL) or concentrated (2x10^{6}cells/mL in 1mL) M1 and M2 J774A.1 macrophage conditioned medium for 24hr at 37°C in 5%. Cell surface GLUT4myc was quantified as previously described in section 2.2.9. Results presented in figure 5.9. Standard M1 conditioned medium increased the basal ($p<0.001$) and insulin ($p<0.001$) stimulated levels of cell surface GLUT4myc. When compared to the standard M1 conditioned medium in the presence of insulin, the concentrated M1 conditioned medium enhanced GLUT4 translocation ($p<0.001$). Basal levels of GLUT4myc between standard and concentrated were unchanged. Similar findings were observed with the M2 standard and concentrated growth medium. M2 conditioned medium increased the basal ($p<0.001$) and insulin ($p<0.001$) stimulated levels of cell surface GLUT4myc. Moreover, basal and insulin levels of cell surface GLUT4myc were significantly upregulated in the M2 concentrated cells compared to the standard M2 conditioned medium ($p<0.01$).This data highlights that changes in relative cytokine concentrations can have a significant effect on the ability of GLUT4 to translocate to the cell surface of L6 GLUT4myc myotubes.

5.2.2.2 Hydrolysate Modulated M1 J774A.1 Macrophage Conditioned modulates GLUT4 translocation in L6 GLUT4myc Myotyubes.

L6 GLUT4myc myoblasts were seeded at $4x10^4$cells/mL and differentiated into myotubes as previously described. Mature myotubes were subsequently exposed to hydrolysate modulated M1 conditioned medium for medium for 24hr at 37^oC in 5%. Cell surface GLUT4myc was quantified as previously described in section 2.2.9. NaCN ($p<0.05$) and 2-132 ($p<0.001$) M1 modulated medium significantly increased cell surface GLUT4myc compared to unmodulated M1 growth medium. NaCN (ns) and 2-132 ($p<0.05$) also enhanced insulin stimulated cell surface GLUT4myc. 2-18 modulated M1 medium did not affect cell surface GLUT4myc at either the basal or insulin stimulated levels (Figure 5.10). WPC modulated medium maintained basal GLUT4myc levels and promoted insulin stimulated levels ($p<0.001$). A similar effect was seen with hydrolysate 2-152, in which basal levels were maintained and insulin stimulated GLUT4 was increased ($p<0.001$). Hydrolysate 2-47 maintained insulin stimulated levels of cell surface GLUT4 and increased basal levels of cell surface GLUT4 ($p<0.05$). Data available in figure 5.12. This data, combined with the modulated cytokine profiles available in figure 5.7, appear to indicate that skewing the immune microenvironment towards a Th2 environment can beneficially promote basal and insulin stimulated GLUT4 translocation in myotubes.

5.2.2.3 2 Hydrolysate Modulated M2 J774A.1 Macrophage Conditioned modulates GLUT4 translocation in L6 GLUT4myc Myotyubes.

L6 GLUT4myc myoblasts were seeded at $4x10^4$cells/mL and differentiated into myotubes as previously described. Mature myotubes were subsequently exposed to hydrolysate modulated M1 conditioned medium for medium for 24hr at 37^oC in 5%. Cell surface GLUT4myc was quantified as previously described in section 2.2.9. Outlined in figure 5.11, at both the basal and insulin stimulated levels, 2-18 ($p<0.05$, $p<0.05$) and 2-132 ($p<0.001$, $p<0.001$) promoted GLUT4 translocation compared to unmodulated M2 conditioned medium. NaCN modulated medium maintained basal GLUT4 levels and promoted insulin stimulated levels ($p<0.05$). WPC promoted basal levels of GLUT4 ($p<0.001$) and maintained insulin stimulated levels relative to unmodulated M2 medium. 2-47 boosted basal (ns) and insulin stimulated ($p<0.05$) GLUT4. Hydrolysate 2-152 maintained basal GLUT4, however significantly decreased insulin stimulated levels ($p<0.001$). Data available in figure 5.13. Considering the results in section 5.2.2.2 and the M2 modulated cytokine profiles available in figure 5.8, promoting an Th2 anti-inflammatory immune environment appears to be beneficial for basal and insulin stimulated levels of GLUT4 in myotubes.

5.2.3 The Effect of M1 and M2 Macrophage Conditioned medium on p4E-BP1$^{Thr37/46}$ activation in L6 Myotubes.

5.2.3.1 Changes in secreted cytokines from M1 and M2 macrophage augments p4E-BP1$^{(Thr37/46)}$ activation in L6 Myotubes

After establishing the effects of M1 and M2 conditioned media on GLUT4, we next examined a potential effect on p4E-BP1$^{Thr37/46}$ activation. L6 myoblasts were seeded at 4x10^{4}cells/mL and differentiated into myotubes as previously described. Mature myotubes were subsequently exposed to standard (1x10^{6}cells/mL in 2mL) or concentrated (2x10^{6}cells/mL in 1mL) M1 and M2 J774A.1 macrophage conditioned medium for 24hr at 37°C in 5%. Immunoblotting, detection, and quantification was performed as previously described in section 2.2.10. Results are Illustrated in figure 5.14. Stimulation with standard M1 ($p<0.01$) and M2 ($p<0.01$) enhanced basal gamma chain p4E-BP1$^{(Thr37/46)}$ compared to the untreated control. Similar effects were observed, to a greater degree with the concentrated M1 and M2 conditioned medium. M1 ($p<0.001$) and M2 ($p<0.001$) conditioned medium significantly promoted basal gamma chain p4E-BP1$^{(Thr37/46)}$. Moreover, at the concentrated level, M2 conditioned medium promoted significant gamma chain p4E-BP1$^{(Thr37/46)}$ compared to the concentrated M1 conditioned medium ($p<0.05$). In the presence of 1µM insulin (figure 5.15), gamma chain p4E-BP1$^{(Thr37/46)}$ was unaffected by the standard conditioned medium. In the presence the concentrated conditioned medium gamma chain p4E-BP1$^{(Thr37/46)}$ trended upwards without significance.

5.2.3.2 Hydrolysate Modulated M1 J774A.1 Macrophage Conditioned modulates p4E-BP1$^{(Thr37/46)}$ activation in L6 Myotubes.

After establishing the effect of M1 and M2 conditioned media on p4E-BP1$^{Thr37/46}$ activation, we next examined the hydrolysate-modulated M1 and M2 conditioned media on signalling. L6 myoblasts were seeded at 4x10^{4}cells/mL and differentiated into myotubes as previously described. Mature myotubes were subsequently exposed to hydrolysate modulated M1 conditioned medium for medium for 24hr at 37°C in 5% CO2. Immunoblotting, detection, and quantification was performed as previously described in section 2.2.10. NaCN ($p<0.05$), 2-18 ($p<0.01$) and 2-132 ($p<0.05$) modulated M1 conditioned promoted basal gamma chain

p4E-BP1$^{(Thr37/46)}$ relative to the untreated control. There was no significant change between unmodulated and modulated growth medium. Results are Illustrated in figure 5.16. In the presence of 1µM insulin, hydrolysate modulate conditioned medium trended to increase gamma chain p4E-BP1$^{(Thr37/46)}$, however these results were not statistically significant (figure 5.18). WPC ($p<0.001$), 2-47 ($p<0.01$) and 2-152 (ns) all enhanced basal gamma chain p4E-BP1$^{(Thr37/46)}$ relative to the unmodulated M1 conditioned medium (figure 5.20). In the presence of 1µM insulin, hydrolysate modulate conditioned medium trended to increase gamma chain p4E-BP1$^{(Thr37/46)}$, however these results were not statistically significant, similar to what was observed with the casein derived hydrolysates (figure 5.22).

5.2.3.2 Hydrolysate Modulated M2 J774A.1 Macrophage Conditioned modulates p4E-BP1$^{(Thr37/46)}$ activation in L6 Myotubes.

L6 myoblasts were seeded at $4x10^4$cells/mL and differentiated into myotubes as previously described. Mature myotubes were subsequently exposed to hydrolysate modulated M2 conditioned medium for medium for 24hr at 37°C in 5% CO2. Immunoblotting, detection, and quantification was performed as previously described. As illustrated in figure 5.17, NaCN ($p<0.05$), 2-18 ($p<0.001$) and 2-132 ($p<0.05$) modulated M2 conditioned promoted basal gamma chain p4E-BP1$^{(Thr37/46)}$ relative to the untreated control. There was no significant change between unmodulated and modulated growth medium. In the presence of 1µM insulin, hydrolysate modulate conditioned medium trended to increase gamma chain p4E-BP1$^{(Thr37/46)}$, NaCN ($p<0.05$), 2-18 ($p<0.05$) however there was no statistical significance between unmodulated and modulated M2 conditioned medium (figure 5.19). WPC ($p<0.001$), 2-47 ($p<0.01$) and 2-152 (ns) all enhanced basal gamma chain p4E-BP1$^{(Thr37/46)}$ relative to the unmodulated M2 conditioned medium (figure 5.21). In the presence of 1µM insulin, WPC (0.05), 2-47 ($p<0.01$) and 2-152 ($p<0.05$) promoted gamma chain p4E-BP1$^{(Thr37/46)}$, relative to the unmodulated M2 conditioned growth medium (Figure 5.23).

Taken together this data appears to support the hypothesis that promotion of a Th2 immune microenvironment can positively impact of mTOR signalling and protein synthesis pathways by promoting phosphorylation of p4E-BP1$^{(Thr37/46)}$.

5.2.4 The Effect of M1 and M2 Macrophage Conditioned medium on Wound Healing In vitro

The final parameter we assessed was the potential impact of hydrolysate-modulated M1 and M2 macrophages on muscle repair using the scratch assay. We first examined the effects of M1 and M2 media alone in this assay.

5.2.4.1 Naïve, M1 and M2 Conditioned growth medium promotes wound healing in vitro

L6 Myoblasts were seeded at $8x10^4$cells/mL and grown to confluence. Once confluent, the monolayer was wounded using a sterile P1000 micropipette tip to create a uniform scratch down the centre of the monolayer. Cells were then washed to remove injury debris and images were taken at a specific point within the well. Cells were subsequently incubated with naïve, M1 and M2 conditioned medium at 37°C in 5% CO_2. Images were taken at T0, T24 and T48. Images were analysed using ImageJ analysis software. Wound closure is expressed as percentage closure of the original wound relating to each condition. Naïve macrophage conditioned medium promoted wound healing compared to the untreated control at T0 ($p<0.001$) and T48 ($p<0.05$). Similar observations were made for M1 conditioned medium at T24 ($p<0.01$) and T48 ($p<0.01$). M2 conditioned medium also promoted recovery relative the UTC, although these changes were not significant (figure 5.24).

5.2.4.2 NacN, 2-18 and 2-132 Modulated M1 Conditioned Medium Beneficially modulates wound healing in vitro

L6 Myoblasts were seeded at $8x10^4$cells/mL and grown to confluence. Once confluent, the monolayer was wounded using a sterile P1000 micropipette tip to create a uniform scratch down the centre of the monolayer. Cells were then washed to remove injury debris and images were taken at a specific point within the well. Cells were subsequently incubated with M1 conditioned and hydrolysate-modulated, M1 conditioned medium at 37^oC in 5% CO_2. Images were taken at T0, T24 andT48. Images were analysed using ImageJ analysis software Wound closure is expressed as percentage closure of the original wound relating to each condition. NaCN modulated M1 conditioned medium promoted recovery at all time points relative to both the untreated control and to the unmodulated conditioned medium. Similar effects were observed with samples 2-18 and 2-132. A tabular representation of statistical analysis is presented as follows, ***p<0.001, **p<0.01, *p<0.05. Based on this data, hydrolysate modulated immunity exhibits the ability enhance wound healing relative to unmodulated inflammatory M1 conditioned medium. Data is illustrated in figure 5.25.

Sample	Time Point	UTC vs M1	UTC vs Hy CM	M1 CM vs. Hy CM
NaCN	T0	ns	ns	ns
	T24	↑**	↑***	↑*
	T48	ns	↑***	↑***
2-18	T0	ns	ns	ns
	T24	↑**	↑***	↑**
	T48	ns	↑**	↑**
2-132	T0	ns	ns	ns
	T24	↑**	↑*	↑*
	T48	ns	↑*	ns

Table 5.1 *Tabular representation of statistical analysis of M1 NaCN Hydrolysate Modulated wound healing in vitro . CM, conditioned medium, Hy CM, hydrolysate modulated medium***p<0.001, **p<0.01, *p<0.05*

5.2.4.3 NacN, 2-18 and 2-132 -Modulated M2 Conditioned Medium modulates wound healing in vitro

L6 Myoblasts were seeded at $8x10^4$cells/mL and grown to confluence. Once confluent, the monolayer was wounded using a sterile P1000 micropipette tip to create a uniform scratch down the centre of the monolayer. Cells were then washed to remove injury debris and images were taken at a specific point within the well. Cells were subsequently incubated with M2 conditioned and M2 hydrolysate modulated conditioned medium at 37°C in 5% CO_2. Images were taken at T0, T24 andT48. Images were analysed using ImageJ analysis software Wound closure is expressed as percentage closure of the original wound relating to each condition. NaCN and 2-132 had no significant effect on wound healing *in vitro* . Sample 2-18 however, increased wound healing at T24 ($p<0.05$) and T48 ($p<0.05$) relative to the untreated control. A tabular representation of statistical analysis is presented as follows, ***p<0.001, **p<0.01, *p<0.05. Based on this data, hydrolysate modulated Th2 immunity can support wound healing *in vitro* . Data is illustrated in figure 5.26.

Sample	Time Point	UTC vs M2	UTC vs Hy CM	M2 CM vs. Hy CM
NaCN	T0	ns	ns	ns
	T24	ns	ns	ns
	T48	ns	ns	ns
2-18	T0	ns	ns	ns
	T24	ns	↑*	ns
	T48	ns	↑*	ns
2-132	T0	ns	ns	ns
	T24	ns	ns	ns
	T48	ns	ns	ns

Table 5.2 *Tabular representation of statistical analysis of M2 NaCN Hydrolysate Modulated wound healing in vitro . CM, conditioned medium, Hy CM, hydrolysate modulated medium***p<0.001, **p<0.01, *p<0.05*

5.2.4.4 WPC, 2-47 and 2-152 - Modulated M1 Conditioned Medium Beneficially modulates wound healing in vitro

L6 Myoblasts were seeded at $8x10^4$cells/mL and grown to confluence. Once confluent, the monolayer was wounded using a sterile P1000 micropipette tip to create a uniform scratch down the centre of the monolayer. Cells were then washed to remove injury debris and images were taken at a specific point within the well. Cells were subsequently incubated with M1 conditioned and M1 hydrolysate-modulated conditioned medium at 37°C in 5% CO_2. Images were taken at T0, T24 andT48. Images were analysed using ImageJ analysis software Wound closure is expressed as percentage closure of the original wound relating to each condition. Hydrolysate treatment had no significant affect at boosting wound healing relative to unmodulated conditioned medium. WPC, 2-47 and 2-152 treatment significantly increased wound healing relative to the untreated control. A tabular representation of statistical analysis is presented as follows ***p<0.001, **p<0.01, *p<0.05. Based on this data, hydrolysate modulated immunity exhibits the ability enhance wound healing relative to unmodulated inflammatory M1 conditioned medium. Data is illustrated in figure 5.27.

Sample	Time Point	UTC vs M1	UTC vs Hy CM	M1 CM vs. Hy CM
WPC	T0	ns	ns	ns
	T24	↑**	↑***	ns
	T48	ns	↑**	ns
2-47	T0	ns	ns	ns
	T24	↑**	↑***	ns
	T48	ns	↑***	ns
2-152	T0	ns	ns	ns
	T24	↑**	↑***	ns
	T48	ns	↑*	ns

Table 5.3 *Tabular representation of statistical analysis of M1 WPC Hydrolysate Modulated in vitro . CM, conditioned medium, Hy CM, hydrolysate modulated medium***p<0.001, **p<0.01, *p<0.05*

5.2.4.4 WPC, 2-47 and 2-152 -Modulated M2 Conditioned Medium Beneficially modulates wound healing in vitro

L6 Myoblasts were seeded at $8x10^4$cells/mL and grown to confluence. Once confluent, the monolayer was wounded using a sterile P1000 micropipette tip to create a uniform scratch down the centre of the monolayer. Cells were then washed to remove injury debris and images were taken at a specific point within the well. Cells were subsequently incubated with M2 conditioned and M2 hydrolysate modulated conditioned medium at 37°C in 5% CO_2. Images were taken at T0, T24 andT48. Images were analysed using ImageJ analysis software Wound closure is expressed as percentage closure of the original wound relating to each condition. WPC, 2-47 and 2-152 treatment significantly increased wound healing relative to the untreated control. The wound healing was increased relative to the unmodulated M2 conditioned medium however, this change was not significant. A tabular representation of statistical analysis is presented as follows ***p<0.001, **p<0.01, *p<0.05. Based on this data, hydrolysate modulated immunity exhibits the ability enhance wound healing relative to unmodulated inflammatory M1 conditioned medium. Data is illustrated in figure 5.28.

Sample	Time Point	UTC vs M2	UTC vs Hy CM	M2 CM vs. Hy CM
WPC	T0	ns	ns	ns
	T24	↑**	↑***	ns
	T48	ns	↑**	ns
2-47	T0	ns	ns	ns
	T24	↑**	↑**	ns
	T48	ns	↑*	ns
2-152	T0	ns	ns	ns
	T24	↑**	↑***	ns
	T48	ns	↑*	ns

Table 5.4 *Tabular representation of statistical analysis of M1 WPC Hydrolysate Modulated wound healing in vitro . CM, conditioned medium, Hy CM, hydrolysate modulated medium***p<0.001, **p<0.01, *p<0.05*

5.2.5 The Effect of Co-Culture with modulated and non-modulated J774A.1 Macrophage on Critical Outputs of Skeletal Muscle Function.

Thus far we have demonstrated that soluble secreted factors from hydrolysate-modulated and non-modulated M1 and M2 J774A.1 macrophage have considerable effects on glucose metabolism, muscle protein synthesis pathways and wound healing *in vitro* . However, since both resident and infiltrating macrophage directly contact skeletal muscle *in vivo* (Bird, 2016), the effect of direct co-culture with modulated and non-modulated J774A.1 Macrophage needs to be investigated.

5.2.5.1 Increasing densities of M1 and M2 polarised macrophage promote GLUT4 translocation in L6 GLUT4myc Myotubes.

L6 GLUT4myc myoblasts were seeded at $4x10^4$cells/mL and differentiated into myotubes as previously described. J774A.1 macrophage were polarised to M1 and M2 phenotypes for three hours as previously described. Once incubation was complete, polarised J774A.1 macrophage were harvested and added directly to the L6 GLUT4myc myotube culture, in numbers ranging from 5,000 cells to 100,000 cells, for 24hr at 37°C in 5% CO_2. Cells were subsequently stimulated with or without 1µM insulin for 20mins at 37°C in 5% CO_2. Cell surface GLUT4myc was quantified as previously described. As outlined in figure 5.29, Increasing populations of both M1 and M2 polarised J774A.1 macrophage promote both basal and insulin stimulated cell surface GLUT4. Regarding the M1 phenotype, cell surface GLUT4 peaked at 100,000 cells per well both at basal ($p<0.01$) and insulin stimulated ($p<0.001$) levels. A similar observation can be seen regarding the M2 population at 100,000 cells with basal ($p<0.001$) and insulin stimulated ($p<0.001$) levels peaking. Considering this, activating and subsequent modulation of M1 and M2 phenotypes for four hours, and at a concentration of 100,000 cells per well will be used for future co-culture experiments.

5.2.5.2 Co-Culture with Hydrolysate- Modulated M1 Polarised Macrophage Modulates GLUT4 Translocation in L6 GLUT4myc Myotubes.

L6 GLUT4myc myoblasts were seeded at $4x10^4$cells/mL and differentiated into myotubes as previously described. J774A.1 macrophage were incubated with 1mg/mL of whole protein or hydrolysate for one hour prior to being polarised to an M1 phenotype for three hours as previously described. Once incubation was complete, polarised J774A.1 macrophage were harvested, and 100,000 cells added directly to the L6 GLUT4myc myotube culture for 24hr at 37°C in 5% CO_2. Cells were subsequently stimulated with or without 1µM insulin for 20mins at 37°C in 5% CO_2. Cell surface GLUT4myc was quantified as previously described. As outlined in figure 5.30, NaCN ($p<0.05$), 2-18 ($p<0.001$) and 2-132 ($p<0.001$) M1 modulated macrophage upregulated basal GLUT4 translocation significantly relative to unmodulated M1 macrophage. In the presence of 1µM insulin NaCN modulated cells did not affect GLUT4 translocation, where 2-18 ($p<0.001$) and 2-132 ($p<0.001$) increased GLUT4 translocation relative to the insulin stimulated, unmodulated M1 macrophage. Regarding whey protein hydrolysate modulated cells (figure 5.32), it appeared to induce down regulation of GLUT4 translocation. WPC ($p<0.05$) down regulated basal GLUT4 relative to unmodulated M1 cells. WPC ($p<0.001$) and 2-47 ($p<0.05$) down regulated insulin stimulated GLUT4 translocation relative to the unmodulated M1 cells. Importantly, the insulin stimulated GLUT4 translocation stimulated by WPC ($p<0.01$) and 2-47 ($p<0.001$) upregulated GLUT4 translocation relative insulin alone.

5.2.5.3 Co-Culture with Hydrolysate-Modulated M2 Polarised Macrophage Modulates GLUT4 Translocation in L6 GLUT4myc Myotubes.

L6 GLUT4myc myoblasts were seeded at $4x10^4$cells/mL and differentiated into myotubes as previously described. J774A.1 macrophage were incubated with 1mg/mL of whole protein or hydrolysate for one hour prior to being polarised to an M2 phenotype for three hours as previously described. Once incubation was complete, polarised J774A.1 macrophage were harvested, and 100,000 cells added directly to the L6 GLUT4myc myotube culture for 24hr at 37°C in 5% CO_2. Cells were subsequently stimulated with or without 1µM insulin for 20mins at 37°C in 5% CO_2. Cell surface GLUT4myc was quantified as previously described. Basal GLUT4 was significantly increased by co-culture with M2 polarised cells modulated with NaCN ($p<0.01$), 2-18 ($p<0.001$) and 2-132 ($p<0.001$). This positive regulation of GLUT4 translated to the insulin stimulated state where NaCN ($p<0.01$), 2-18 ($p<0.001$) and 2-132 ($p<0.05$) upregulated GLUT4 translocation relative to unmodulated M2 cells (figure 5.31). In contrast to their effects in the M1 phenotype, whey derived peptides exhibited a positive effect on GLUT4 translocation in modulated M2 macrophage. Basal GLUT4 was significantly increased by WPC ($p<0.05$), 2-47 ($p<0.001$) and 2-152 ($p<0.001$). In the presence of insulin, whole whey protein (WPC) and the derived hydrolysates significantly increased cell surface GLUT4 as detailed in figure 5.33 ($p<0.001$).

5.2.5.4 Co-Culture with Hydrolysate Modulated M1 Polarised Macrophage Modulates modulates p4E-BP1$^{(Thr37/46)}$ activation in L6 Myotubes.

L6 myoblasts were seeded at $4x10^4$cells/mL and differentiated into myotubes as previously described. J774A.1 macrophage were incubated with 1mg/mL of whole protein or hydrolysate for one hour prior to being polarised to an M1 phenotype for three hours as previously described. Once incubation was complete, polarised J774A.1 macrophage were harvested, and 100,000 cells added directly to the L6 myotube culture for 24hr at 37°C in 5% CO_2. Immunoblotting was performed as previously described. NaCN, 2-18 and 2-132 significantly boosted p4E-BP1$^{(Thr37/46)}$ activation relative to the unstimulated control ($p<0.01$). Although not significant, levels were boosted compared the unmodulated M1 polarised cells, there was a trend to increase p4E-BP1$^{(Thr37/46)}$ activation (figure 5.34). In the

presence of 1µM insulin NaCN ($p<0.01$), 2-18 ($p<0.01$) and 2-132 ($p<0.001$) increased p4E-BP1$^{(Thr37/46)}$ activation relative to the untreated control. Moreover, NaCN ($p<0.05$), 2-18 ($p<0.05$) and 2-132 ($p<0.01$) increased p4E-BP1$^{(Thr37/46)}$ activation relative to unmodulated M1 cells (figure 5.36). WPC modulated cells increased basal p4E-BP1$^{(Thr37/46)}$ activation ($p<0.05$) relative to unmodulated M1 cells, while 2-47 and 2-152 also boosted basal p4E-BP1$^{(Thr37/46)}$ activation (ns) as illustrated in figure 5.38 In the presence of insulin (figure 5.40), there was no effect on p4E-BP1$^{(Thr37/46)}$ activation.

5.2.5.5 Co-Culture with Hydrolysate Modulated M2 Polarised Macrophage Modulates p4E-BP1(Thr37/46) activation in L6 Myotubes.

L6 myoblasts were seeded at $4x10^4$cells/mL and differentiated into myotubes as previously described. J774A.1 macrophage were incubated with 1mg/mL of whole protein or hydrolysate for one hour prior to being polarised to an M2 phenotype for three hours as previously described. Once incubation was complete, polarised J774A.1 macrophage were harvested, and 100,000 cells added directly to the L6 myotube culture for 24hr at 37^oC in 5% CO_2. Immunoblotting was performed as previously described. NaCN ($p<0.01$), 2-18 ($p<0.01$) and 2-132 ($p<0.05$) increased basal p4E-BP1$^{(Thr37/46)}$ activation relative to untreated cells. These samples also enhanced p4E-BP1$^{(Thr37/46)}$ activation relative to unmodulated cells (figure 5.35) . In the presence of p4E-BP1$^{(Thr37/46)}$ activation, NaCN and 2-18 maintained p4E-BP1$^{(Thr37/46)}$ levels, while 2-132 significantly increased p4E-BP1$^{(Thr37/46)}$ relative to untreated cells (figure 5.37). Basal p4E-BP1$^{(Thr37/46)}$ activation was unaffected by WPC, 2-47 and 2-152 modulated M2 cells (figure 5.39). In the presence of p4E-BP1$^{(Thr37/46)}$ activation was significantly down regulated relative to untreated cells by sample WPC ($p<0.05$) and 2-152 ($p<0.05$). Moreover, p4E-BP1$^{(Thr37/46)}$ activation was significantly down regulated by WPC ($p<0.01$), 2-47 ($p<0.05$) and 2-152 ($p<0.05$) when compared to unmodulated M2 cells (figure 5.41).

5.2.5.6 Co-Culture with NaCN Hydrolysate-Modulated M1 Polarised Macrophage Maintains pro wound healing properties of the M1 phenotype in vitro

L6 Myoblasts were seeded at $8x10^4$cells/mL and grown to confluence. Once confluent, the monolayer was wounded using a sterile P1000 micropipette tip to create a uniform scratch down the centre of the monolayer. Cells were then washed to remove injury debris and images were taken at a specific point within the well. J774A.1 macrophage were incubated with 1mg/mL of whole protein or hydrolysate for one hour prior to being polarised to an M1 phenotype for three hours as previously described. Once incubation was complete, polarised J774A.1 macrophage were harvested, and 100,000 cells added directly to the L6 myotube culture for 24hr at 37°C in 5% CO_2. Images were taken at T0, T24 andT48. Images were analysed using ImageJ analysis software Wound closure is expressed as percentage closure of the original wound relating to each condition. Hydrolysate modulated cells and unmodulated cells tracked similarly over time during wound healing with no significant changes at any time point. Data presented in figure 5.42 illustrates the supportive properties of modulated immunity regarding wound healing *in vitro* . A tabular representation of statistical analysis is presented as follows ***p<0.001, **p<0.01, *p<0.05.

Sample	Time Point	UTC vs M1 CC	UTC vs Hy CC	M1 CC vs. Hy CC
NaCN	T0	ns	ns	ns
	T24	↑**	ns	ns
	T48	↑**	↑**	ns
2-18	T0	ns	ns	ns
	T24	↑**	ns	ns
	T48	↑**	↑*	ns
2-132	T0	ns	ns	ns
	T24	↑**	↑*	ns
	T48	↑**	↑*	ns

Table 5.5 *Tabular representation of statistical analysis of NaCN Hydrolysate M1 Modulated Cells on wound healing in vitro . CC, conditioned cells, Hy CM, hydrolysate modulated cells ***p<0.001, **p<0.01, *p<0.05*

5.2.5.7 Co-Culture with NaCN Hydrolysate Modulated M2 Polarised Macrophage Maintains pro wound healing properties of the M2 phenotype in vitro

L6 Myoblasts were seeded at $8x10^4$cells/mL and grown to confluence. Once confluent, the monolayer was wounded using a sterile P1000 micropipette tip to create a uniform scratch down the centre of the monolayer. Cells were then washed to remove injury debris and images were taken at a specific point within the well. J774A.1 macrophage were incubated with 1mg/mL of whole protein or hydrolysate for one hour prior to being polarised to an M2 phenotype for three hours as previously described. Once incubation was complete, polarised J774A.1 macrophage were harvested, and 100,000 cells added directly to the L6 myotube culture for 24hr at 37°C in 5% CO_2. Images were taken at T0, T24 and T48. Images were analysed using ImageJ analysis software. Wound closure is expressed as percentage closure of the original wound relating to each condition. Hydrolysate-modulated cells and unmodulated cells tracked similarly over time during wound healing with no significant changes at any time point. Data presented in figure 5.43 illustrates the supportive properties of modulated immunity regarding wound healing *in vitro* . A tabular representation of statistical analysis is presented as follows ***p<0.001, **p<0.01, *p<0.05.

Sample	Time Point	UTC vs M2 CC	UTC vs Hy CC	M2 CC vs. Hy CC
NaCN	T0	ns	ns	ns
	T24	↑*	↑**	ns
	T48	↑*	↑*	ns
2-18	T0	ns	ns	ns
	T24	↑*	↑*	ns
	T48	↑*	↑*	ns
2-132	T0	ns	ns	ns
	T24	↑*	↑*	ns
	T48	↑*	↑*	ns

Table 5.6 *Tabular representation of statistical analysis of NaCN Hydrolysate M2 Modulated Cells wound healing in vitro . CC, conditioned cells, Hy CM, hydrolysate modulated cells ***p<0.001, **p<0.01, *p<0.05*

5.2.5.8 Co-Culture with WPC Hydrolysate Modulated M1 Polarised Macrophage Maintains pro wound healing properties of the M1 phenotype in vitro

L6 Myoblasts were seeded at $8x10^4$cells/mL and grown to confluence. Once confluent, the monolayer was wounded using a sterile P1000 micropipette tip to create a uniform scratch down the centre of the monolayer. Cells were then washed to remove injury debris and images were taken at a specific point within the well. J774A.1 macrophage were incubated with 1mg/mL of whole protein or hydrolysate for one hour prior to being polarised to an M1 phenotype for three hours as previously described. Once incubation was complete, polarised J774A.1 macrophage were harvested, and 100,000 cells added directly to the L6 myotube culture for 24hr at 37^oC in 5% CO_2. Images were taken at T0, T24 and T48. Images were analysed using ImageJ analysis software Wound closure is expressed as percentage closure of the original wound relating to each condition. Hydrolysate modulated cells and unmodulated cells tracked similarly over time during wound healing with no significant changes at any time point. Data presented in figure 5.44 illustrates the supportive properties of modulated immunity regarding wound healing in vitro A tabular representation of statistical analysis is presented as follows ***p<0.001, **p<0.01, *p<0.05.

Sample	Time Point	UTC vs M1 CC	UTC vs Hy CC	M1 CC vs. Hy CC
WPC	T0	ns	ns	ns
	T24	↑**	↑*	ns
	T48	↑***	↑**	ns
2-47	T0	ns	ns	ns
	T24	↑**	↑**	ns
	T48	↑***	↑***	ns
2-152	T0	ns	ns	ns
	T24	↑**	↑**	ns
	T48	↑***	↑***	ns

Table 5.7 *Tabular representation of statistical analysis of WPC Hydrolysate M1 Modulated Cells wound healing in vitro . CC, conditioned cells, Hy CM, hydrolysate modulated cells ***p<0.001, **p<0.01, *p<0.05*

5.2.5.9 Co-Culture with WPC Hydrolysate Modulated M2 Polarised Macrophage Maintains pro wound healing properties of the M2 phenotype in vitro

L6 Myoblasts were seeded at $8x10^4$cells/mL and grown to confluence. Once confluent, the monolayer was wounded using a sterile P1000 micropipette tip to create a uniform scratch down the centre of the monolayer. Cells were then washed to remove injury debris and images were taken at a specific point within the well. J774A.1 macrophage were incubated with 1mg/mL of whole protein or hydrolysate for one hour prior to being polarised to an M2 phenotype for three hours as previously described. Once incubation was complete, polarised J774A.1 macrophage were harvested, and 100,000 cells added directly to the L6 myotube culture for 24hr at 37°C in 5% CO_2. Images were taken at T0, T24 and T48. Images were analysed using ImageJ analysis software Wound closure is expressed as percentage closure of the original wound relating to each condition. Hydrolysate modulated cells and unmodulated cells tracked similarly over time during wound healing with no significant changes at any time point. Data presented in figure 5.45 illustrates the supportive properties of modulated immunity regarding wound healing in vitro A tabular representation of statistical analysis is presented as follows ***p<0.001, **p<0.01, *p<0.05.

Sample	Time Point	UTC vs M2 CC	UTC vs Hy CC	M2 CC vs. Hy CC
WPC	T0	ns	ns	ns
	T24	ns	↑**	ns
	T48	↑**	↑***	ns
2-47	T0	ns	ns	ns
	T24	ns	ns	ns
	T48	↑**	↑**	ns
2-152	T0	ns	ns	ns
	T24	ns	ns	ns
	T48	↑**	↑**	ns

Table 5.8 *Tabular representation of statistical analysis of WPC Hydrolysate M2 Modulated Cells wound healing in vitro . CC, conditioned cells, Hy CM, hydrolysate modulated cells ***p<0.001, **p<0.01, *p<0.05*

5.3 Figures:

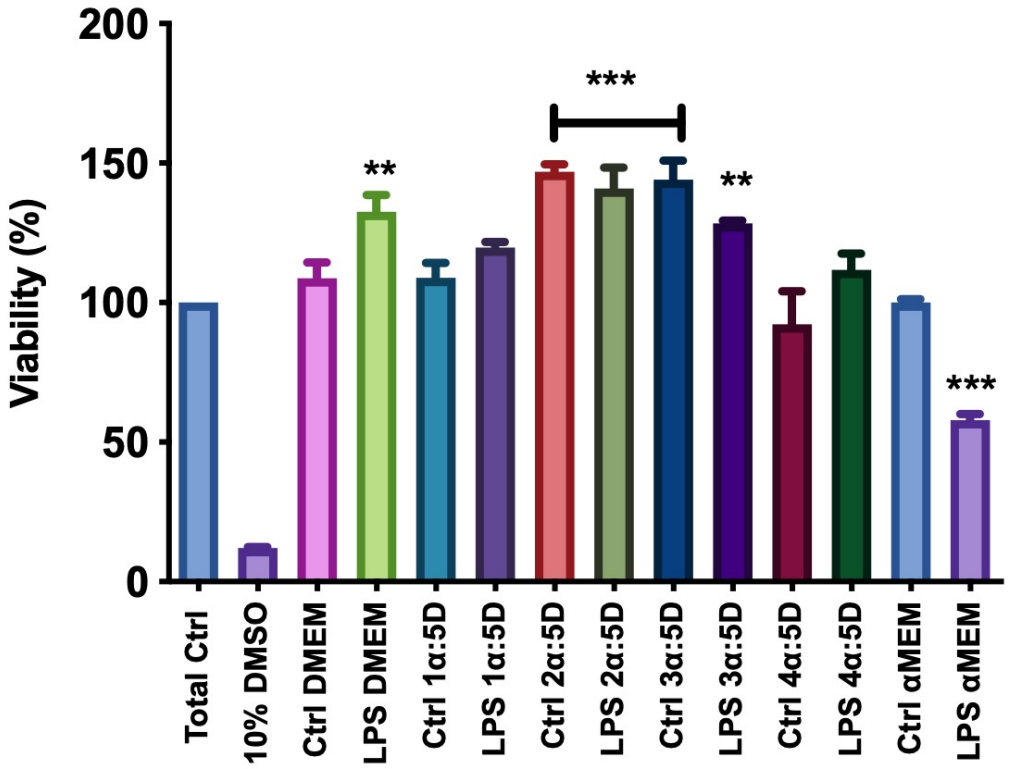


Figure 5.1 Increasing ratios of αMEM to DMEM growth medium negatively impacts on J774A.1 macrophage cell viability. J774A.1 macrophage were seeded at 1x10^6cells/mL in varying ration of αMEM to DMEM cell culture growth medium and incubated for three hours at 37°C in 5% CO_2. Cells were subsequently incubated with 100ng/mL LPS or 10% DMSO for 24hr 37°C in 5% CO_2. Cell viability was determined using the MTS Cell Titre AQueous One assay as previously described. Data presented as ±SEM of three replicates. ***p<0.001, **p<0.01, *p<0.05 comparing treated conditions to total control cells. Significance was determined using one- way ANOVA with a Newman-Keuls post-test.

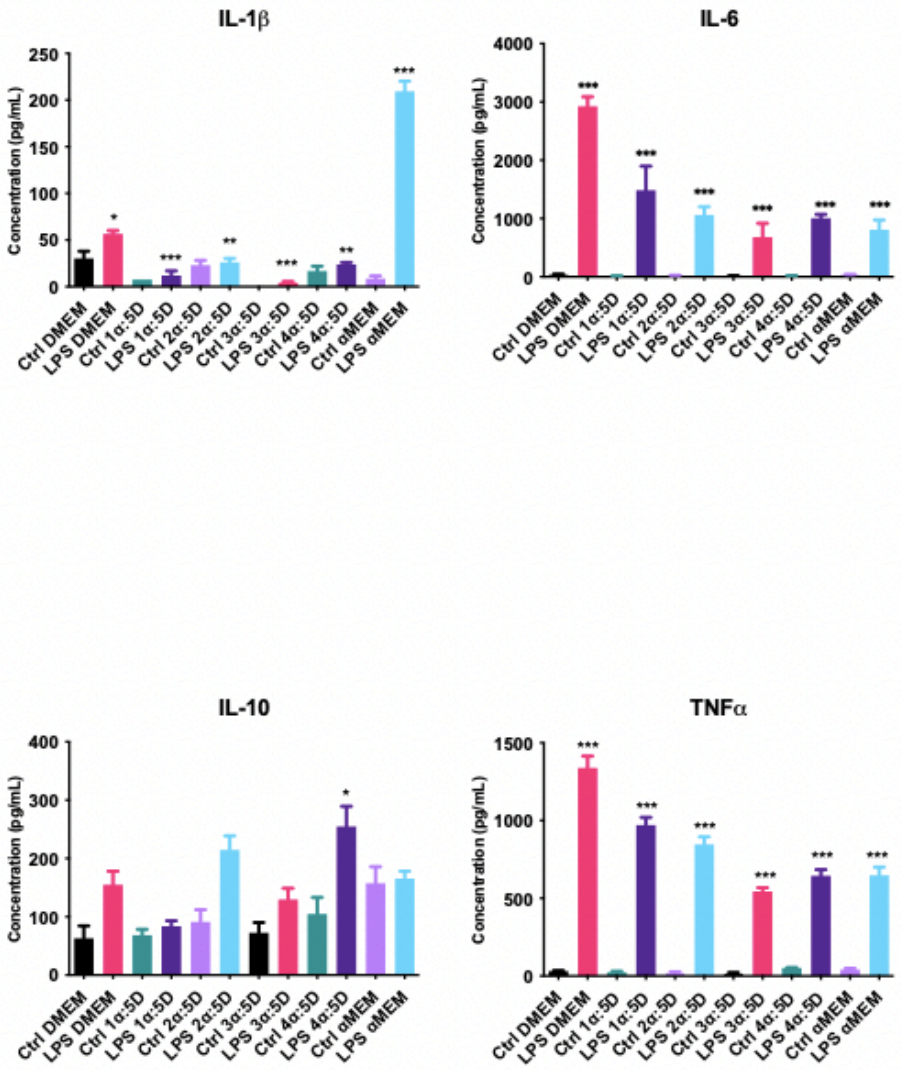


Figure 5.2 Increasing ratios of αMEM to DMEM growth medium modulates cytokine secretion in LPS activated J774A.1 macrophage. J774A.1 macrophage were seeded at 1x10^{6}cells/mL in varying ration of αMEM to DMEM cell culture growth medium and incubated for three hours at 37°C in 5% CO_2. Cells were subsequently stimulated with 100ng/mL LPS for 24hr at 37°C in 5% CO_2. Secreted cytokine concentrations were determined using a cytokine specific ELISA as previously described. Data presented as ±SEM of three replicates. ***p<0.001, **p<0.01, *p<0.05 comparing treated conditions to total control cells. Significance was determined using one- way ANOVA with a Newman-Keuls post-test.

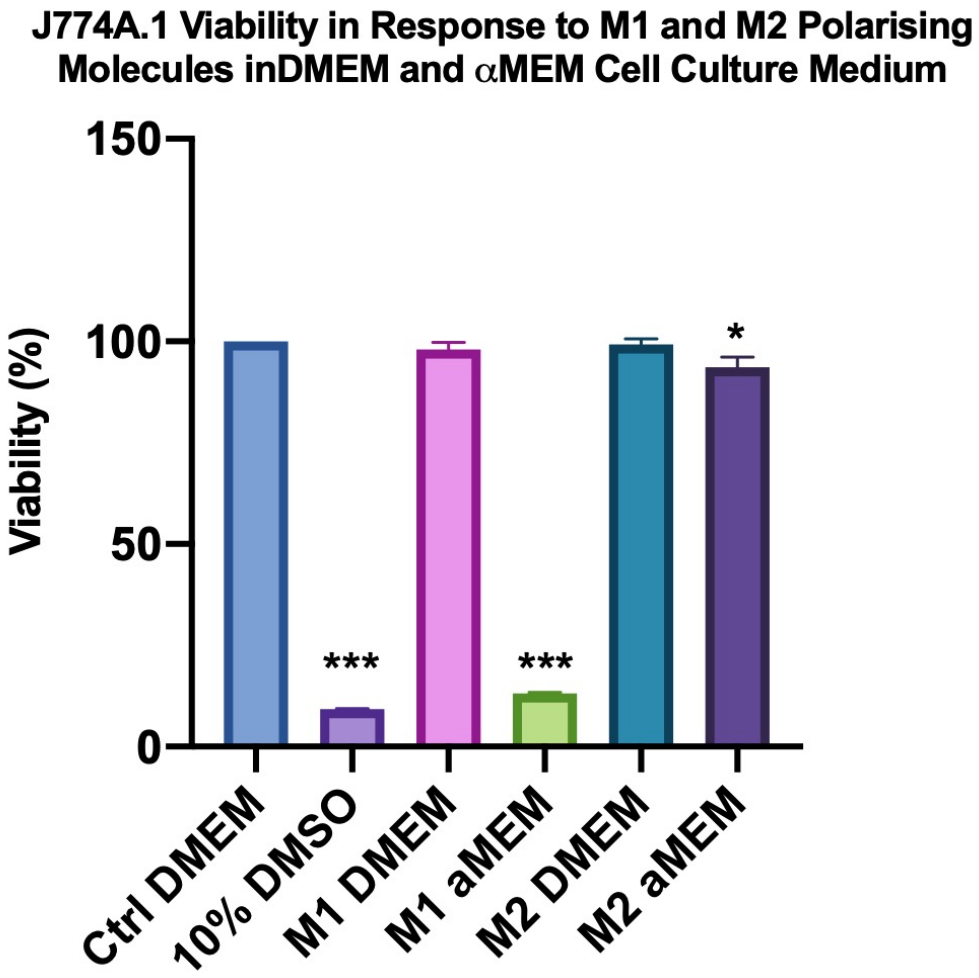


Figure 5.3 The effect of different medium supplementation on M1 and M2 polarised J774A.1 macrophage. J774A.1 macrophage were seeded at 1x10^{6}cells/mL in either αMEM or DMEM cell culture growth medium and incubated for three hours at 37°C in 5% CO_2. Cells were subsequently polarised to either M1 or M2 macrophage phenotypes as previously described. viability was determined using the MTS Cell Titre AQueous One assay as previously described. Data presented as ±SEM of three replicates. ***p<0.001, **p<0.01, *p<0.05 comparing treated conditions to total control cells. Significance was determined using one- way ANOVA with a Newman-Keuls post-test.

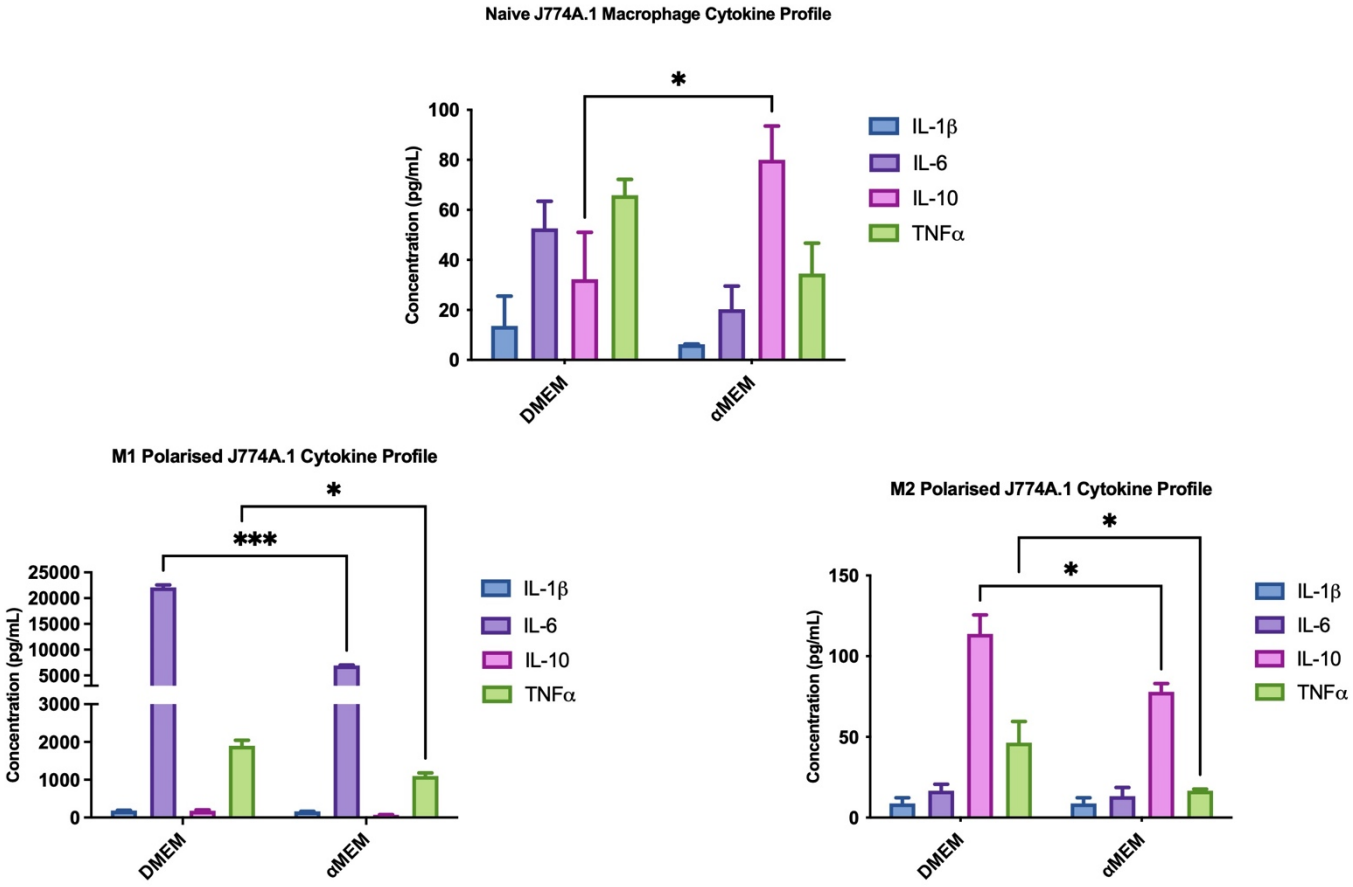


Figure 5.4 The effect of different medium supplementation on M1 and M2 polarised J774A.1 macrophage cytokine secretion profiles. J774A.1 macrophage were seeded at 1x10^{6}cells/mL in either αMEM or DMEM cell culture growth medium and incubated for three hours at 37°C in 5% CO_2. Cells were subsequently polarised to either M1 or M2 macrophage phenotypes as previously described. Secreted cytokine concentrations were determined using a cytokine specific ELISA as previously described. ***p<0.001, **p<0.01, *p<0.05 comparing treated conditions to total control cells. Significance was determined using one- way ANOVA with a Newman-Keuls post-test.

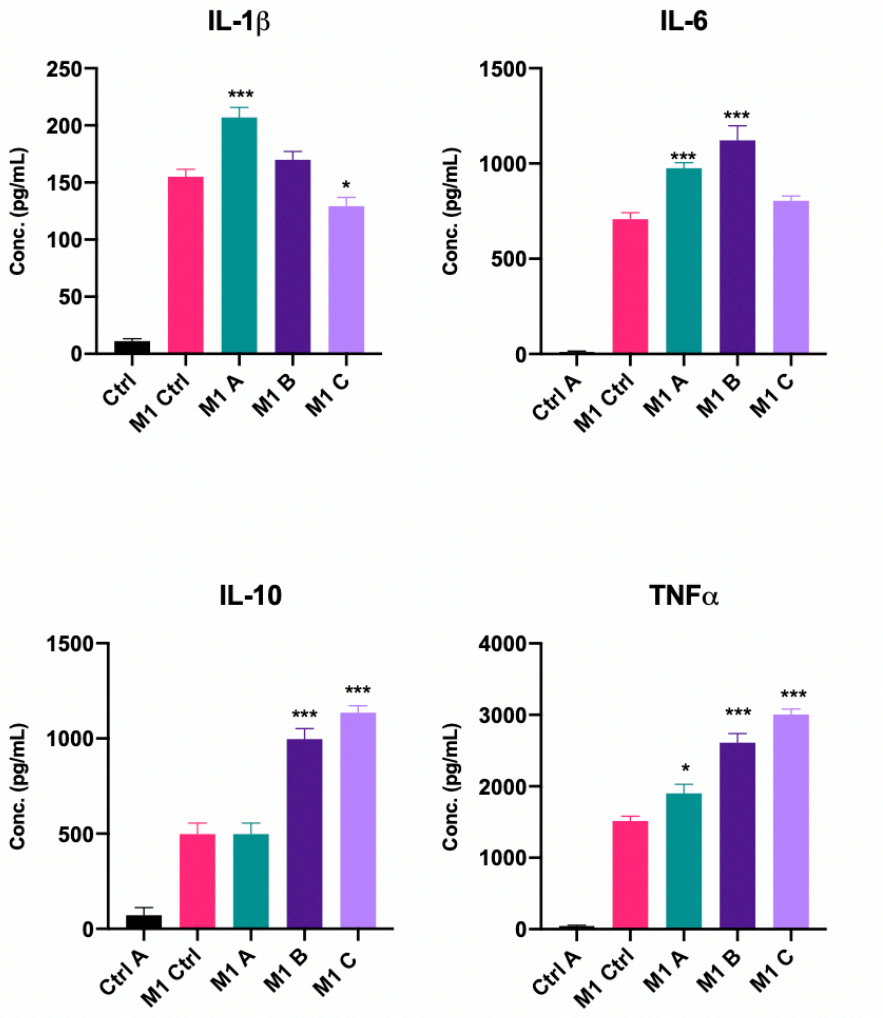


Figure 5.5 Varying seeding density of cells concentrates detectable levels of secreted cytokines in M1 Polarised J774A.1 Macrophage. J774A.1 macrophage were seeded at M1 Ctrl, 1x10^{6}cells/mL in 2mL, M1A 1x10^{6}cells/mL in 1mL, M1B 2x10^{6}cells/mL in 1mL and M1C 2x10^{6}cells/mL and were subsequently polarised to the M1 macrophage phenotype as previously described. Secreted cytokine concentrations were determined using a cytokine specific ELISA as previously described. Data presented as ±SEM of three replicates. ***p<0.001, **p<0.01, *p<0.05 comparing treated conditions to total control cells. Significance was determined using one- way ANOVA with a Newman-Keuls post-test.

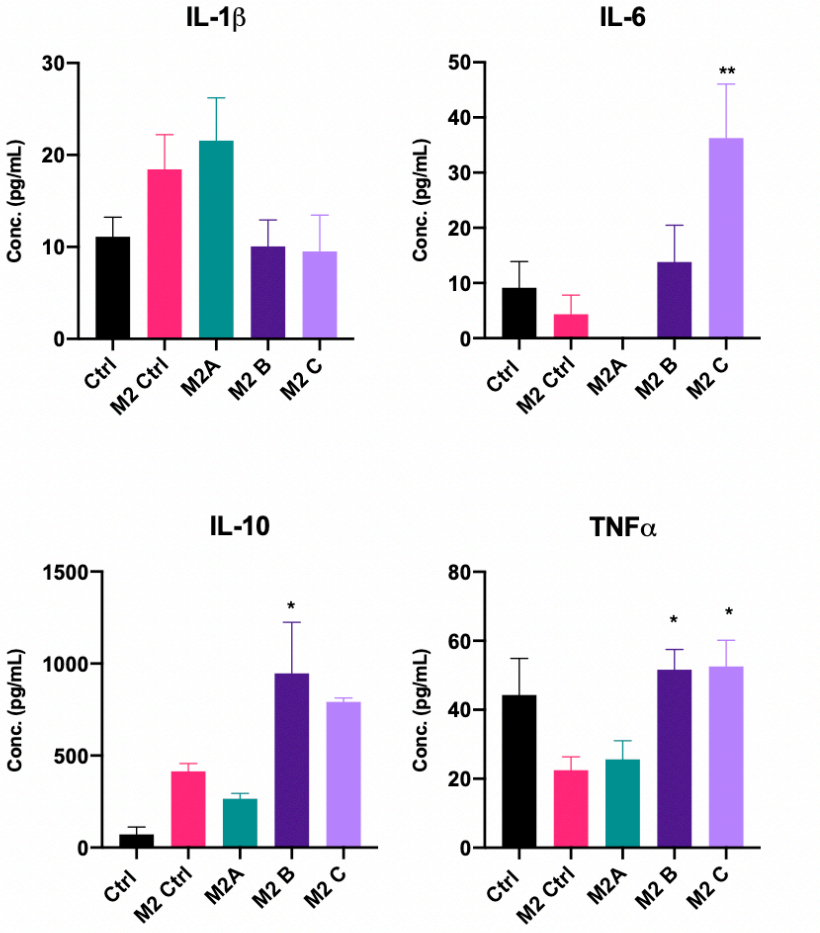


Figure 5.6 Varying seeding density of cells concentrates detectable levels of secreted cytokines in M2 Polarised J774A.1 Macrophage. . J774A.1 macrophage were seeded at M2 Ctrl, 1x10^{6}cells/mL in 2mL, M2A 1x10^{6}cells/mL in 1mL, M2B 2x10^{6}cells/mL in 1mL and M2C 2x10^{6}cells/mL and were subsequently polarised to the M1 macrophage phenotype as previously described. Secreted cytokine concentrations were determined using a cytokine specific ELISA as previously described. Data presented as ±SEM of three replicates. ***p<0.001, **p<0.01, *p<0.05 comparing treated conditions to total control cells. Significance was determined using one- way ANOVA with a Newman-Keuls post-test

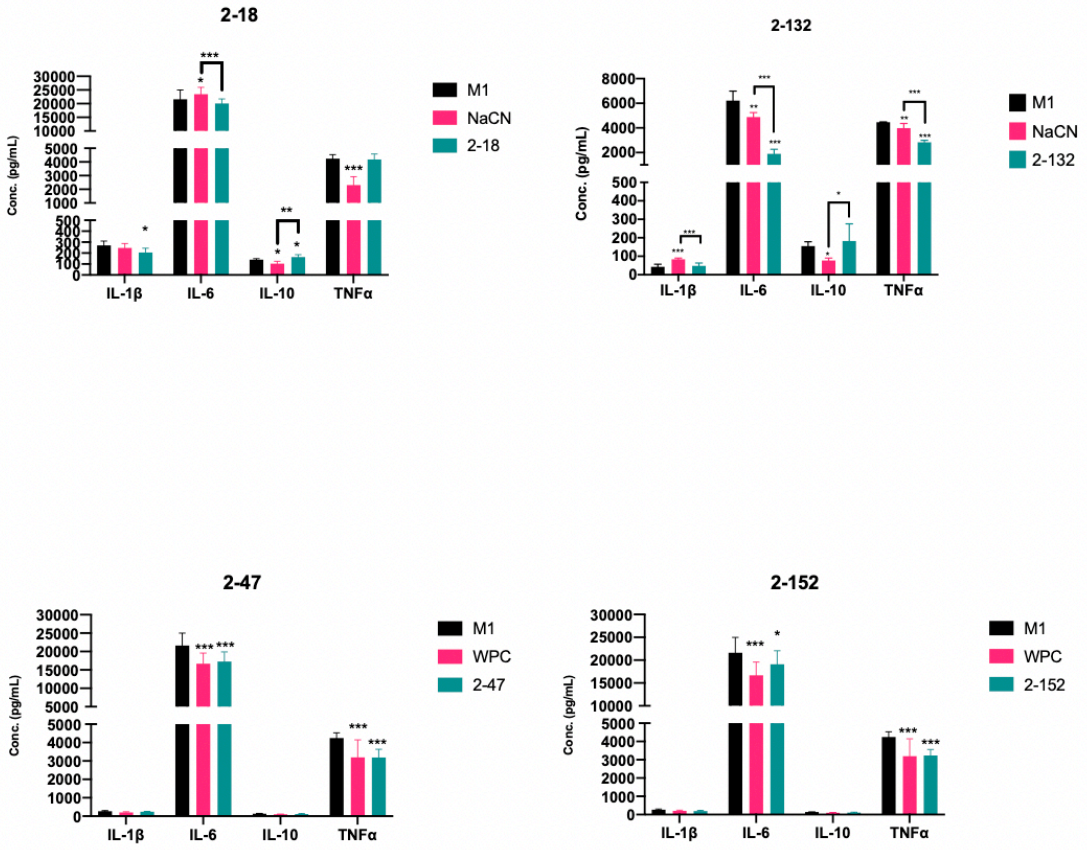


Figure 5.7 Candidate Casein and Whey Derived Hydrolysates Exhibit Anti-Inflammatory Bioactivity in M1 Polarised J774A.1 Macrophage. J774A.1 macrophage were seeded at 1x10^{6}cells/mL and incubated for three hours at 37°C in 5% CO_2. Cells were pre-incubated with 1mg/mL of candidate hydrolysate for 1 hour at 37°C in 5% CO_2. Cells were subsequently polarised to the M1 phenotype as previously described 37°C in 5% CO_2. Secreted cytokine concentrations were determined using a cytokine specific ELISA as previously described. ***p<0.001, **p<0.01, *p<0.05 comparing treated conditions to total control cells. Significance was determined using one- way ANOVA with a Newman-Keuls post-test.

cates. Significance

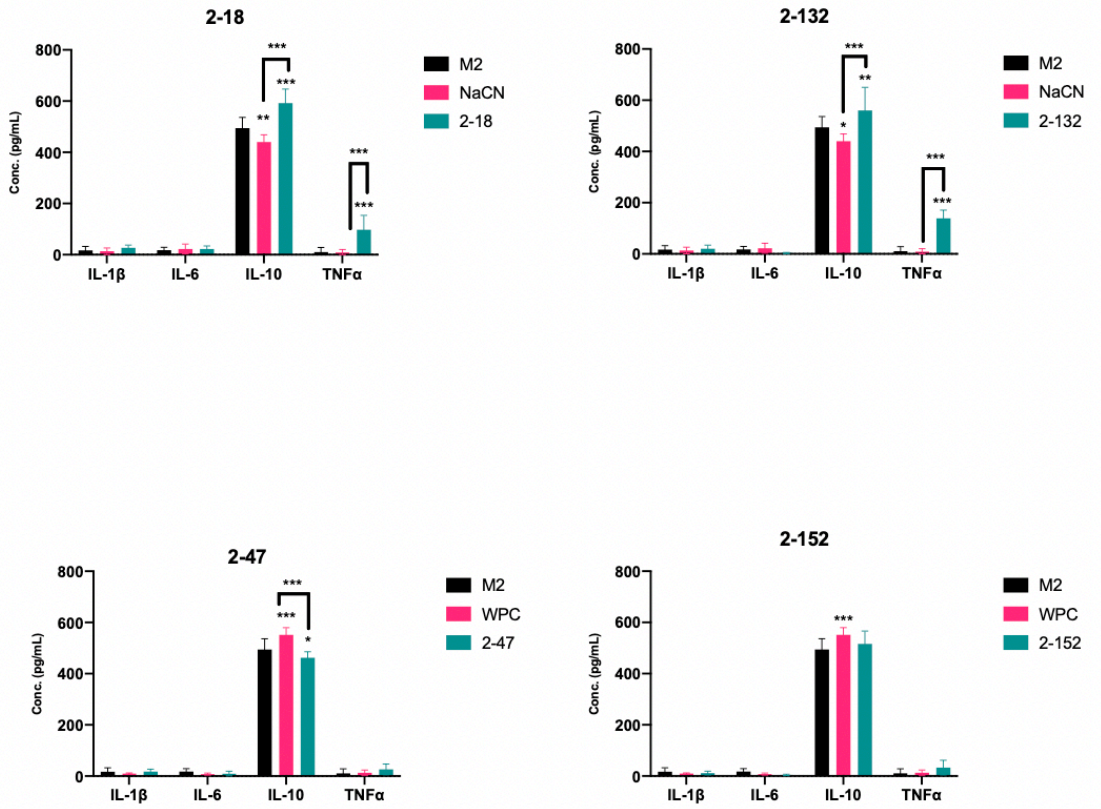


Figure 5.8 Candidate Casein and Whey Derived Hydrolysates Exhibit Anti-Inflammatory Bioactivity in M2 Polarised J774A.1 Macrophage. J774A.1 macrophage were seeded at 1x10^{6}cells/mL and incubated for three hours at 37°C in 5% CO_2. Cells were pre-incubated with 1mg/mL of candidate hydrolysate for 1 hour at 37°C in 5% CO_2. Cells were subsequently polarised to the M2 phenotype as previously described 37°C in 5% CO_2. Secreted cytokine concentrations were determined using a cytokine specific ELISA as previously described. ***p<0.001, **p<0.01, *p<0.05 comparing treated conditions to total control cells. Significance was determined using one- way ANOVA with a Newman-Keuls post

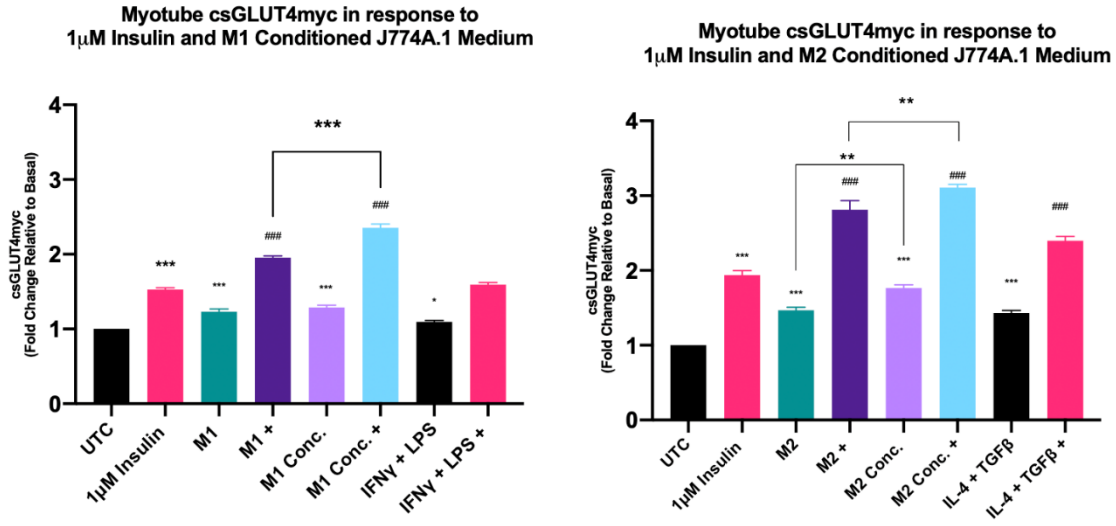


Figure 5.9 Concentrating the levels of secreted M1 and M2 specific cytokines modulates translocation of GLUT4 in L6 GLUT4myc myotubes. L6 GLUT4myc myoblasts were seeded at 4x10^{4}cells/mL and differentiated into myotubes as previously described. Mature myotubes were subsequently exposed to standard or concentrated M1 and M2 J774A.1 macrophage conditioned medium for 24hr at 37°C in 5% CO_2. Cells were subsequently stimulated with or without 1μM bovine insulin for 20mins at 37°C in 5% CO_2. Cell surface GLUT4myc was quantified as previously described. Data presented as ±SEM of three replicates. ***p<0.001, **p<0.01, *p<0.05 comparing UTC to conditioned medium minus 1μM insulin, $^{###}$p<0.001, $^{##}$p<0.01, $^{#}$p<0.05 comparing 1μM insulin to conditioned medium plus 1μM insulin, unless otherwise indicated through use of bracket indicators.. Significance determined using a one way ANOVA with a Dunnett's post-test. ***/$^{###}$/p<0.001, **/$^{##}$p<0.01, */$^{#}$p<0.05.

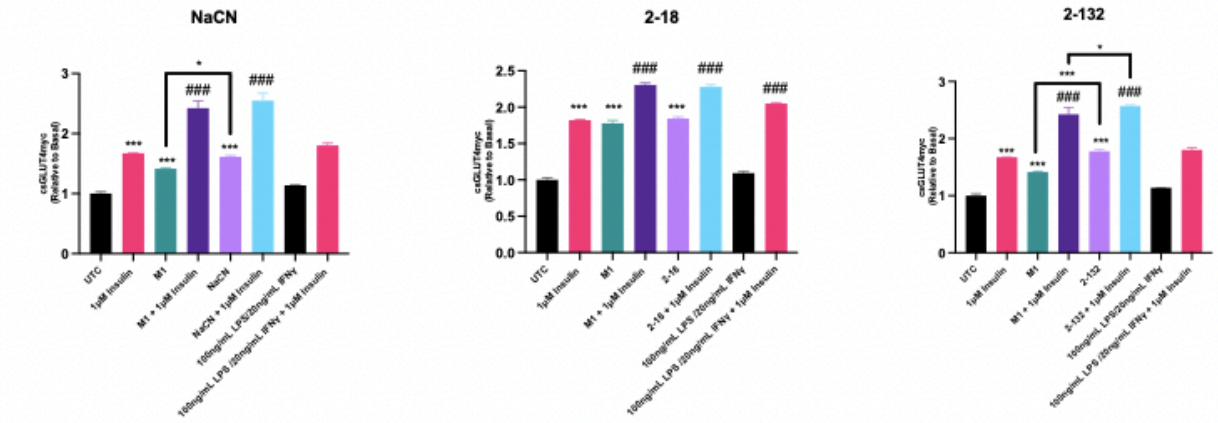


Figure 5.10 NacN, 2-18 and 2-132 Hydrolysate Modulated M1 J774A.1 Macrophage Conditioned medium promotes GLUT4 translocation in L6 GLUT4myc Myotyubes. L6 GLUT4myc myoblasts were seeded at 4x10^{4}cells/mL and differentiated into myotubes as previously described. Mature myotubes were subsequently exposed to baseline or whole protein/hydrolysate modulated M1 J774A.1 macrophage conditioned medium for 24hr at 37°C in 5% CO_2. Cells were subsequently stimulated with or without 1µM bovine insulin for 20mins at 37°C in 5% CO_2. Cell surface GLUT4myc was quantified as previously described. Data presented as ±SEM of three replicates.***p<0.001, **p<0.01, *p<0.05 comparing UTC to conditioned medium minus 1µM insulin, $^{###}$p<0.001, $^{##}$p<0.01, $^{#}$p<0.05 comparing 1µM insulin to conditioned medium plus 1µM insulin, unless otherwise indicated through use of bracket indicators.. Significance determined using a one way ANOVA with a Dunnett's post-test. ***/$^{###}$/p<0.001, **/$^{##}$p<0.01, */$^{#}$p<0.05.

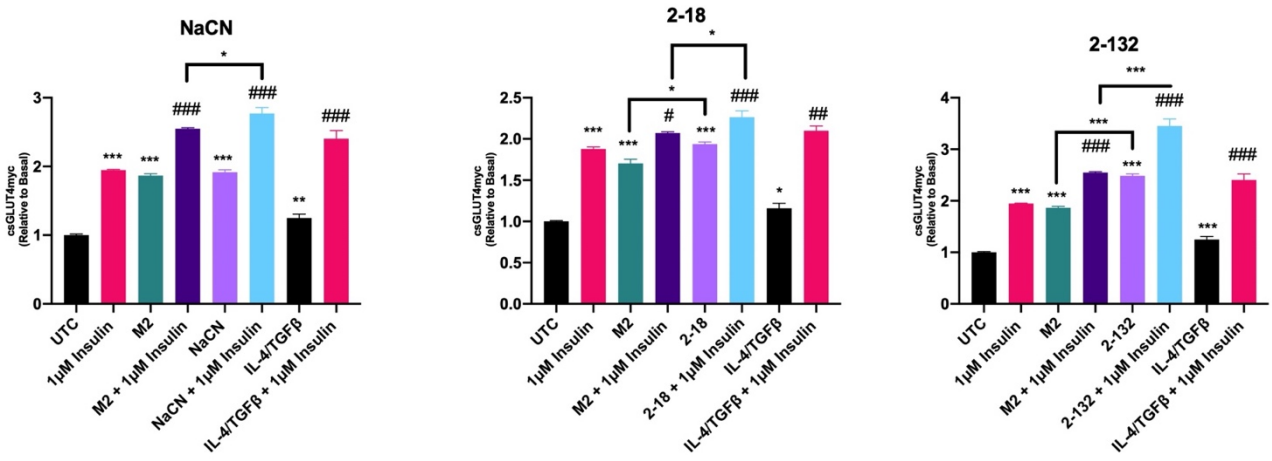


Figure 5.11 NacN, 2-18 and 2-132 Hydrolysate Modulated M2 J774A.1 Macrophage Conditioned medium promotes GLUT4 translocation in L6 GLUT4myc Myotyubes. L6 GLUT4myc myoblasts were seeded at $4x10^4$cells/mL and differentiated into myotubes as previously described. Mature myotubes were subsequently exposed to baseline or whole protein/hydrolysate modulated M2 J774A.1 macrophage conditioned medium for 24hr at 37°C in 5% CO_2. Cells were subsequently stimulated with or without 1μM bovine insulin for 20mins at 37°C in 5% CO_2. Cell surface GLUT4myc was quantified as previously described. Data presented as ±SEM of three replicates. ***p<0.001, **p<0.01, *p<0.05 comparing UTC to conditioned medium minus 1μM insulin, $^{###}$p<0.001, $^{##}$p<0.01, $^{#}$p<0.05 comparing 1μM insulin to conditioned medium plus 1μM insulin, unless otherwise indicated through use of bracket indicators. Significance determined using a one way ANOVA with a Dunnett's post-test. ***/$^{###}$/p<0.001, **/$^{##}$p<0.01, */$^{#}$p<0.05.

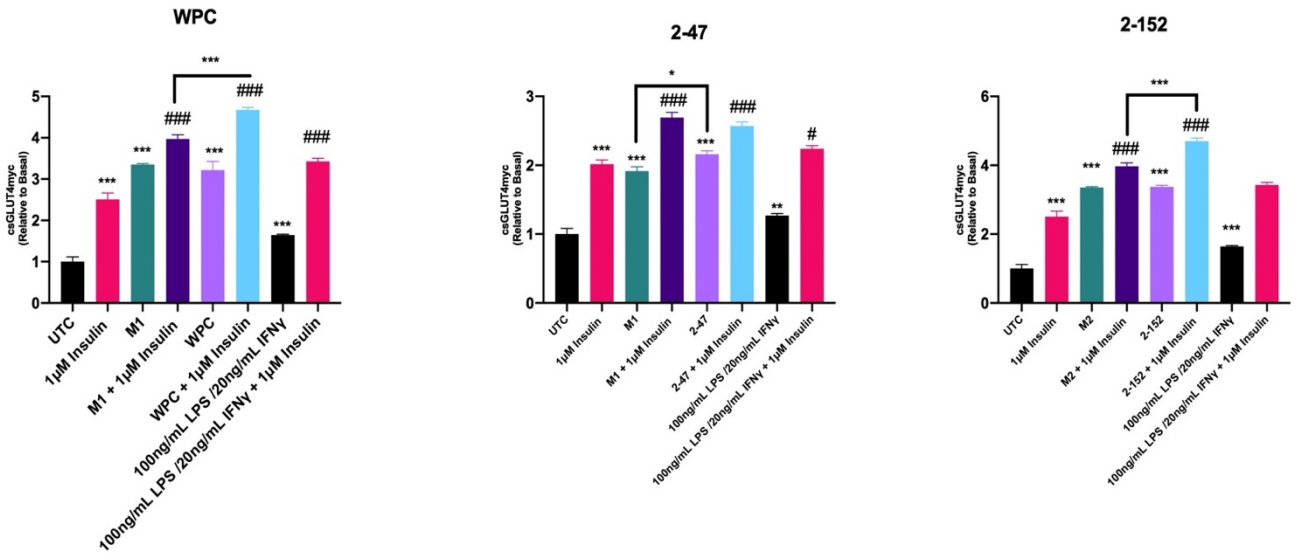


Figure 5.12 WPC, 2-47 and 2-152 Hydrolysate Modulated M1 J774A.1 Macrophage Conditioned medium promotes GLUT4 translocation in L6 GLUT4myc Myotyubes. L6 GLUT4myc myoblasts were seeded at 4x10^{4}cells/mL and differentiated into myotubes as previously described. Mature myotubes were subsequently exposed to baseline or whole protein/hydrolysate modulated M1 J774A.1 macrophage conditioned medium for 24hr at 37°C in 5% CO_2. Cells were subsequently stimulated with or without 1µM bovine insulin for 20mins at 37°C in 5% CO_2. Cell surface GLUT4myc was quantified as previously described. Data presented as ±SEM of three replicates.***p<0.001, **p<0.01, *p<0.05 comparing UTC to conditioned medium minus 1µM insulin, $^{###}$p<0.001, $^{##}$p<0.01, $^{#}$p<0.05 comparing 1µM insulin to conditioned medium plus 1µM insulin, unless otherwise indicated through use of bracket indicators. Significance determined using a one way ANOVA with a Dunnett's post-test. ***/$^{###}$/p<0.001, **/$^{##}$p<0.01, */$^{#}$p<0.05.

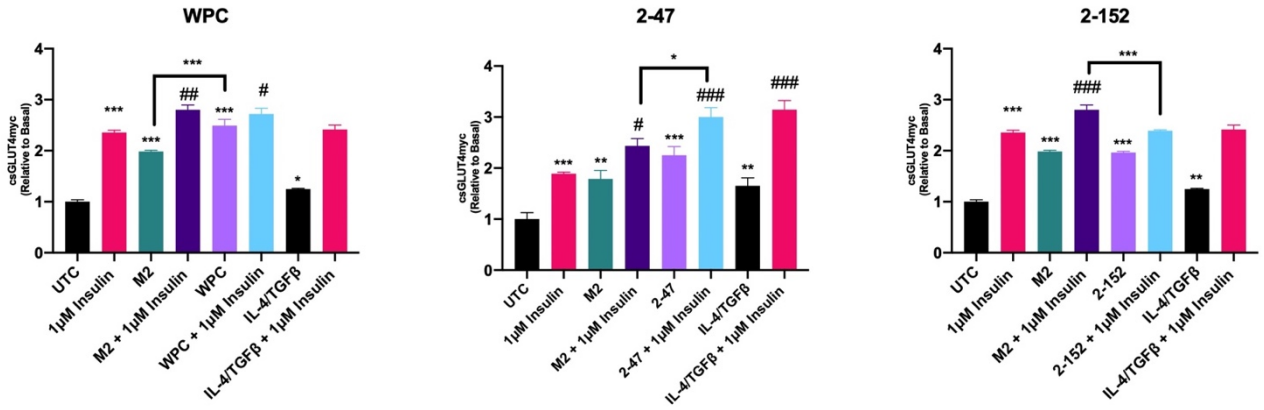


Figure 5.13 WPC, 2-47 and 2-152 Hydrolysate Modulated M2 J774A.1 Macrophage Conditioned medium promotes GLUT4 translocation in L6 GLUT4myc Myotyubes. L6 GLUT4myc myoblasts were seeded at $4x10^4$cells/mL and differentiated into myotubes as previously described. Mature myotubes were subsequently exposed to baseline or whole protein/hydrolysate modulated M2 J774A.1 macrophage conditioned medium for 24hr at 37°C in 5% CO_2. Cells were subsequently stimulated with or without 1μM bovine insulin for 20mins at 37°C in 5% CO_2. Cell surface GLUT4myc was quantified as previously described. Data presented as ±SEM of three replicates.***p<0.001, **p<0.01, *p<0.05 comparing UTC to conditioned medium minus 1μM insulin, $^{###}$p<0.001, $^{##}$p<0.01, $^{#}$p<0.05 comparing 1μM insulin to conditioned medium plus 1μM insulin, unless otherwise indicated through use of bracket indicators. Significance determined using a one way ANOVA with a Dunnett's post-test. ***/$^{###}$/p<0.001, **/$^{##}$p<0.01, */$^{#}$p<0.05.

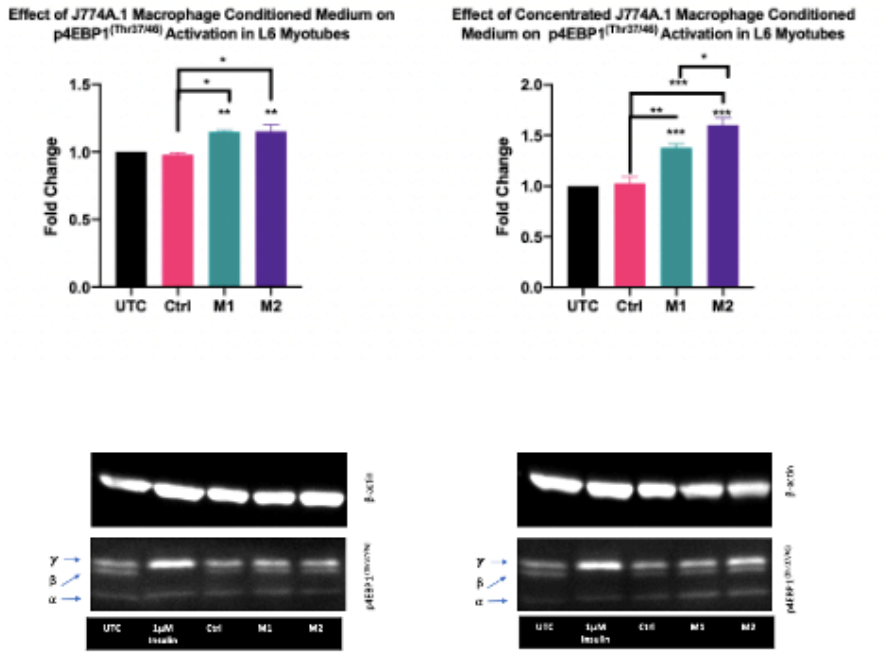


Figure 5.14 Concentrated M1 and M2 J774A.1 macrophage conditioned medium differentially modulates basal p4E-BP1$^{(Thr37/46)}$ in L6 Myotubes. L6 myoblasts were seeded at 4x10^{4}cells/mL and differentiated into myotubes as previously described. Mature myotubes were subsequently exposed to standard or concentrated M1 and M2 J774A.1 macrophage conditioned medium for 24hr at 37°C in 5% CO_2. Immunoblotting was performed as previously described. Data presented as ±SEM of three replicates. Significance determined using a one way ANOVA with a Newmans-Kuels post-test. ***p<0.001, **p<0.01, *p<0.05.

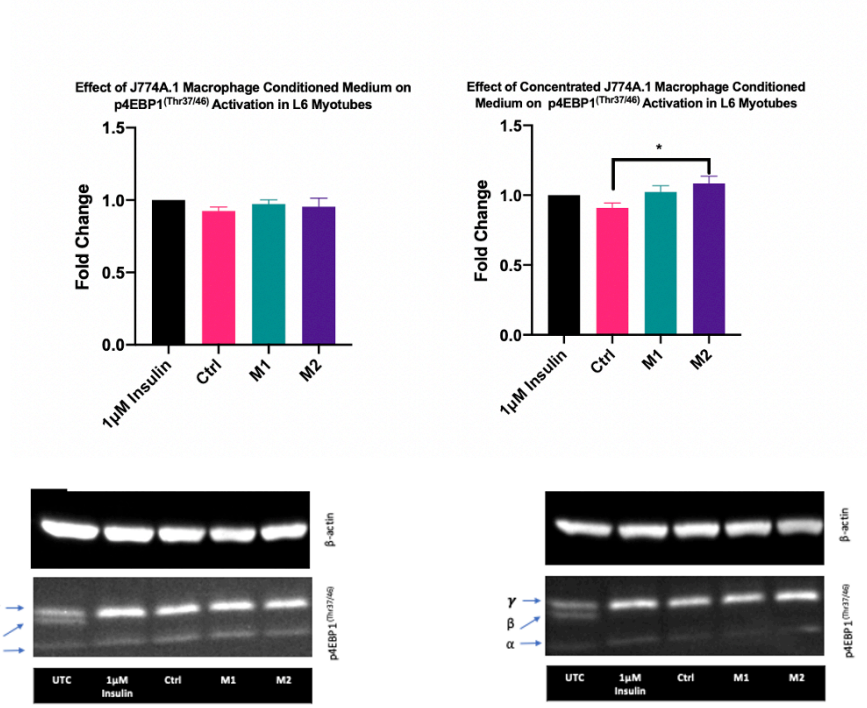


Figure 5.15 Concentrated M1 and M2 J774A.1 macrophage conditioned medium differentially modulate insulin stimulated p4E-BP1$^{(Thr37/46)}$ in L6 Myotubes. L6 myoblasts were seeded at 4x10^{4}cells/mL and differentiated into myotubes as previously described. Mature myotubes were subsequently exposed to standard or concentrated M1 and M2 J774A.1 macrophage conditioned medium for 24hr at 37°C in 5% CO_2. Immunoblotting was performed as previously described. Data presented as ±SEM of three replicates. Significance determined using a one way ANOVA with a Newmans-Kuels post-test. ***p<0.001, **p<0.01, *p<0.05.

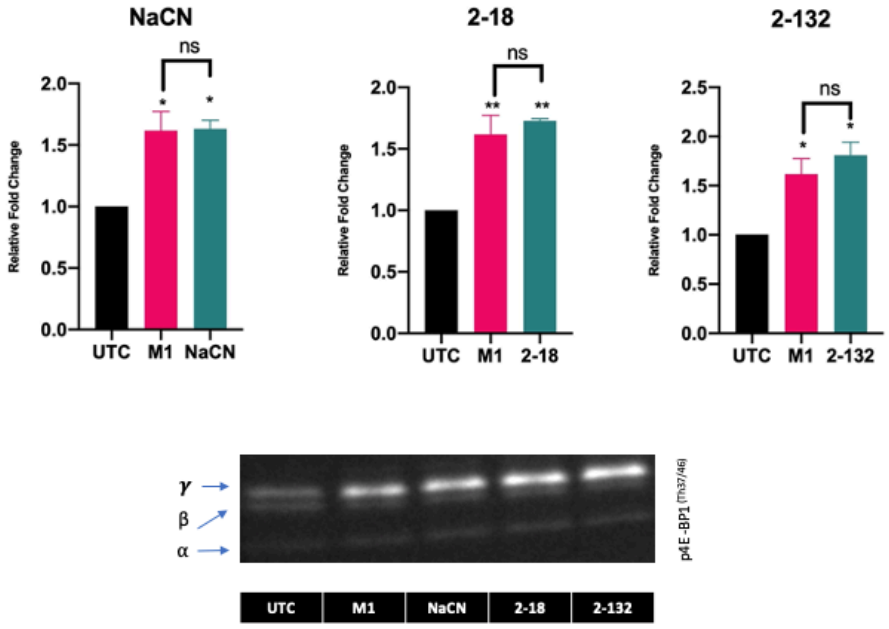


Figure 5.16 NacN, 2-18 and 2-132 Hydrolysate Modulated M1 J774A.1 Macrophage Conditioned medium beneficially modulates basal p4E-BP1$^{(Thr37/46)}$ in L6 Myotubes. L6 myoblasts were seeded at 4x10^{4}cells/mL and differentiated into myotubes as previously described. Mature myotubes were subsequently exposed to baseline or whole protein/hydrolysate modulated M1 J774A.1 macrophage conditioned medium for 24hr at 37°C in 5% CO_2. Cells were subsequently stimulated with or without 1µM bovine insulin for 20mins at 37°C in 5% CO_2. Immunoblotting was performed as previously described. Data presented as ±SEM of three replicates. Significance determined using a one way ANOVA with a Newmans-Kuels post-test. ***p<0.001, **p<0.01, *p<0.05.

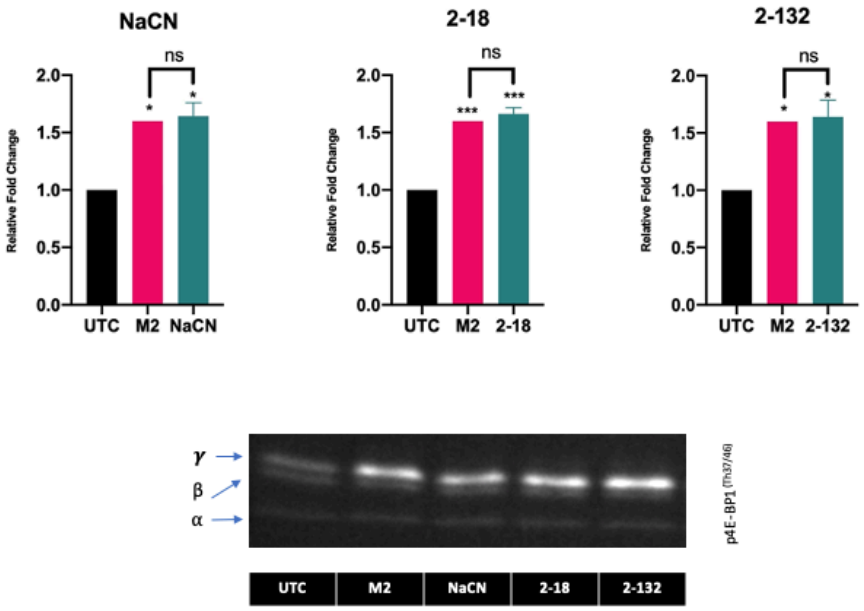


Figure 5.17 NacN, 2-18 and 2-132 Hydrolysate Modulated M2 J774A.1 Macrophage Conditioned medium beneficially modulates basal p4E-BP1$^{(Thr37/46)}$ in L6 Myotubes. L6 myoblasts were seeded at 4x10^{4}cells/mL and differentiated into myotubes as previously described. Mature myotubes were subsequently exposed to baseline or whole protein/hydrolysate modulated M2 J774A.1 macrophage conditioned medium for 24hr at 37°C in 5% CO_2. Cells were subsequently stimulated with or without 1µM bovine insulin for 20mins at 37°C in 5% CO_2. Immunoblotting was performed as previously described. Data presented as ±SEM of three replicates. Significance determined using a one way ANOVA with a Newmans-Kuels post-test. ***p<0.001, **p<0.01, *p<0.05.

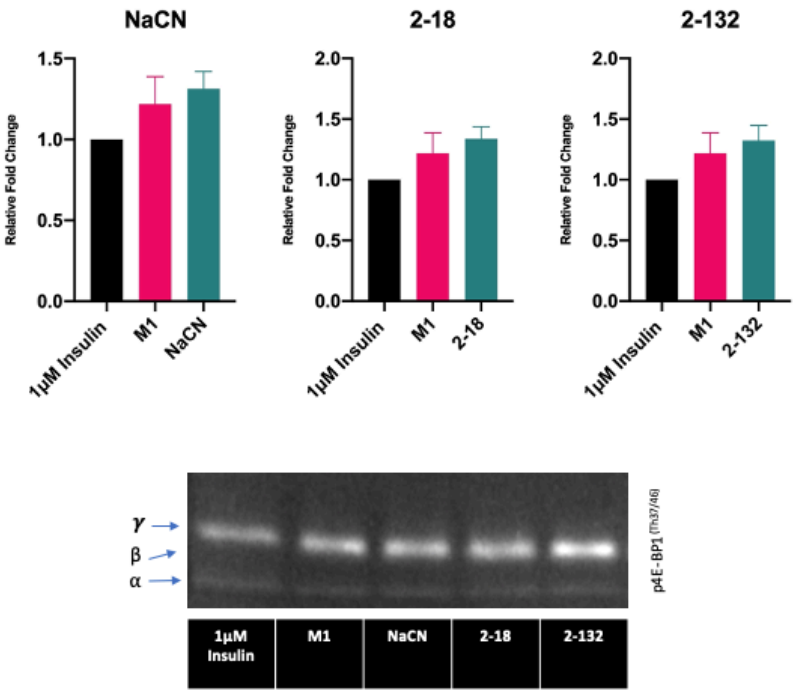


Figure 5.18 NacN, 2-18 and 2-132 Hydrolysate Modulated M1 J774A.1 Macrophage Conditioned medium beneficially modulates insulin stimulated p4E-BP1$^{(Thr37/46)}$ in L6 Myotubes. L6 myoblasts were seeded at 4x10^{4}cells/mL and differentiated into myotubes as previously described. Mature myotubes were subsequently exposed to baseline or whole protein/hydrolysate modulated M1 J774A.1 macrophage conditioned medium for 24hr at 37°C in 5% CO_2. Cells were subsequently stimulated with or without 1µM bovine insulin for 20mins at 37°C in 5% CO_2. Immunoblotting was performed as previously described. Data presented as ±SEM of three replicates. Significance determined using a one way ANOVA with a Newmans-Kuels post-test. ***p<0.001, **p<0.01, *p<0.05.

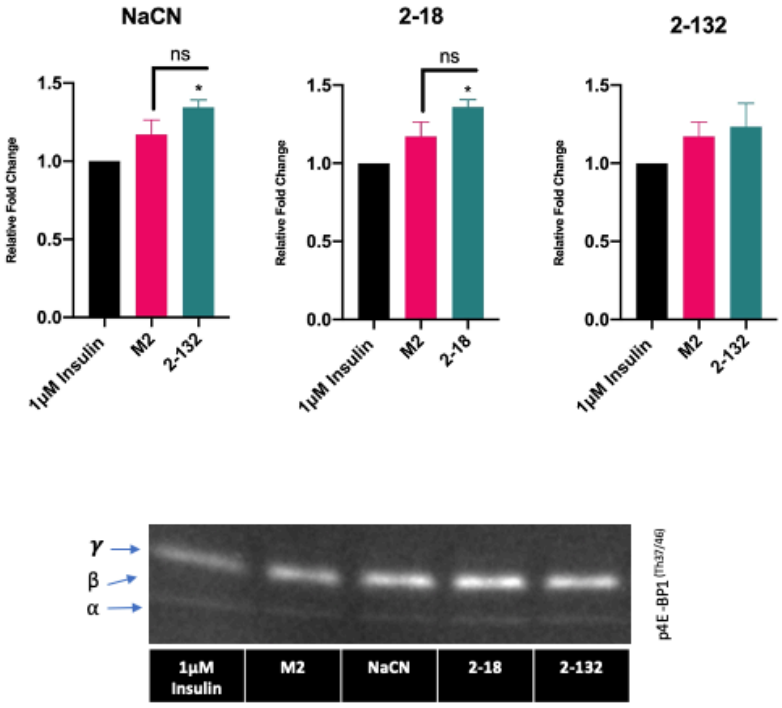


Figure 5.19 NacN, 2-18 and 2-132 Hydrolysate Modulated M2 J774A.1 Macrophage Conditioned medium beneficially modulates insulin stimulated p4E-BP1$^{(Thr37/46)}$ in L6 Myotubes. L6 myoblasts were seeded at 4x10^{4}cells/mL and differentiated into myotubes as previously described. Mature myotubes were subsequently exposed to baseline or whole protein/hydrolysate modulated M2 J774A.1 macrophage conditioned medium for 24hr at 37°C in 5% CO_2. Cells were subsequently stimulated with or without 1μM bovine insulin for 20mins at 37°C in 5% CO_2. Immunoblotting was performed as previously described. Data presented as ±SEM of three replicates. Significance determined using a one way ANOVA with a Newmans-Kuels post-test. ***p<0.001, **p<0.01, *p<0.05.

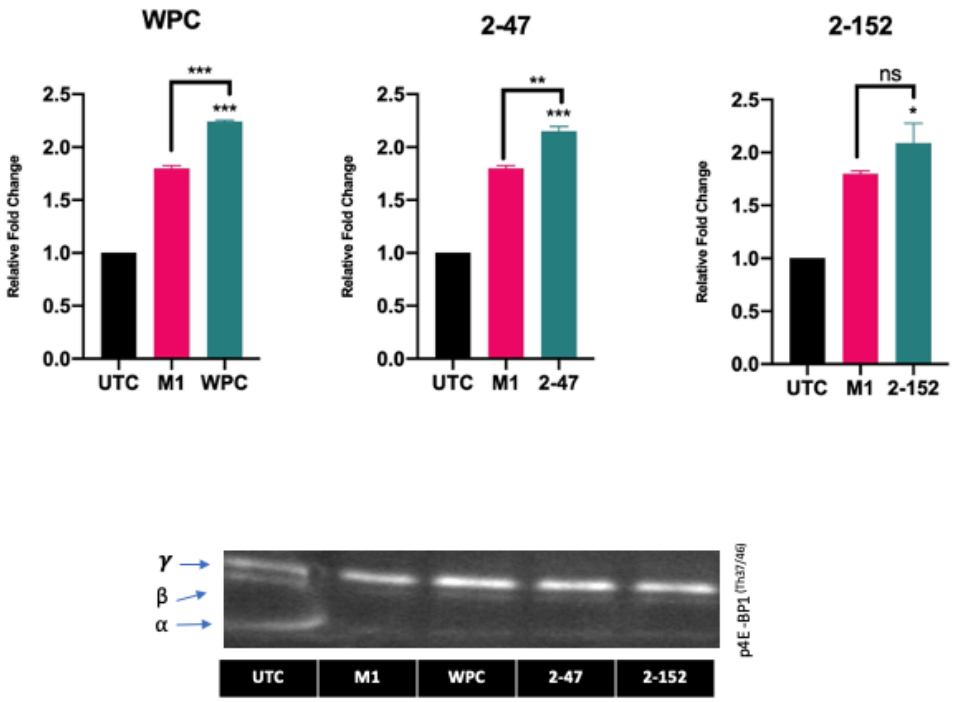


Figure 5.20 WPC, 2-47, 2-152 Hydrolysate Modulated M1 J774A.1 Macrophage Conditioned medium beneficially modulates basal p4E-BP1$^{(Thr37/46)}$ in L6 Myotubes. L6 myoblasts were seeded at 4x10^{4}cells/mL and differentiated into myotubes as previously described. Mature myotubes were subsequently exposed to baseline or whole protein/hydrolysate modulated M1 J774A.1 macrophage conditioned medium for 24hr at 37°C in 5% CO_2. Cells were subsequently stimulated with or without 1µM bovine insulin for 20mins at 37°C in 5% CO_2. Immunoblotting was performed as previously described. Data presented as ±SEM of three replicates. Significance determined using a one way ANOVA with a Newmans-Kuels post-test. ***p<0.001, **p<0.01, *p<0.05.

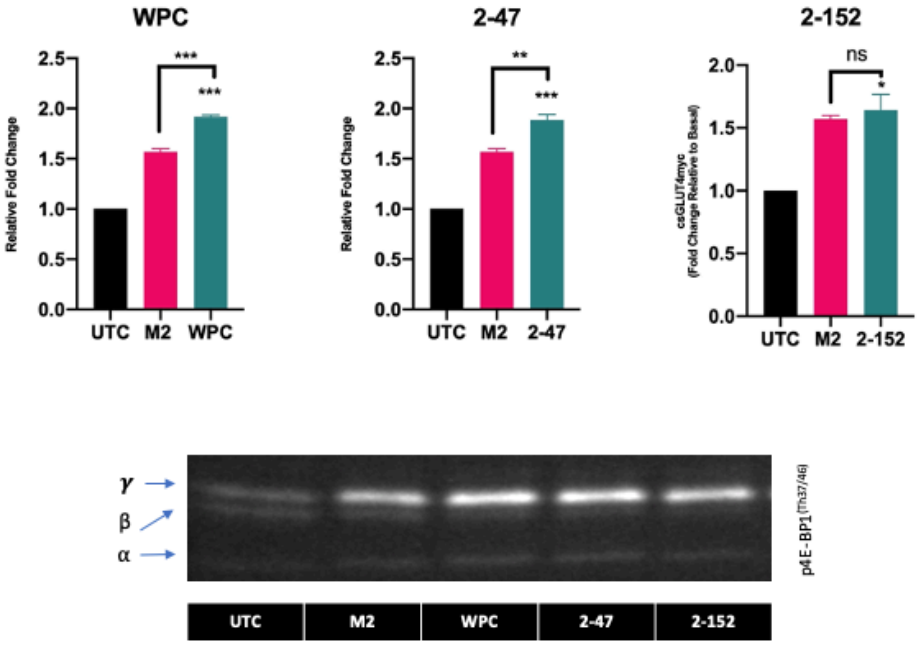


Figure 5.21 WPC, 2-47, 2-152 Hydrolysate Modulated M2 J774A.1 Macrophage Conditioned medium beneficially modulates basal p4E-BP1$^{(Thr37/46)}$ in L6 Myotubes. L6 myoblasts were seeded at 4x10^{4}cells/mL and differentiated into myotubes as previously described. Mature myotubes were subsequently exposed to baseline or whole protein/hydrolysate modulated M2 J774A.1 macrophage conditioned medium for 24hr at 37°C in 5% CO_2. Cells were subsequently stimulated with or without 1µM bovine insulin for 20mins at 37°C in 5% CO_2. Immunoblotting was performed as previously described. Data presented as ±SEM of three replicates. Significance determined using a one way ANOVA with a Newmans-Kuels post-test. ***p<0.001, **p<0.01, *p<0.05.

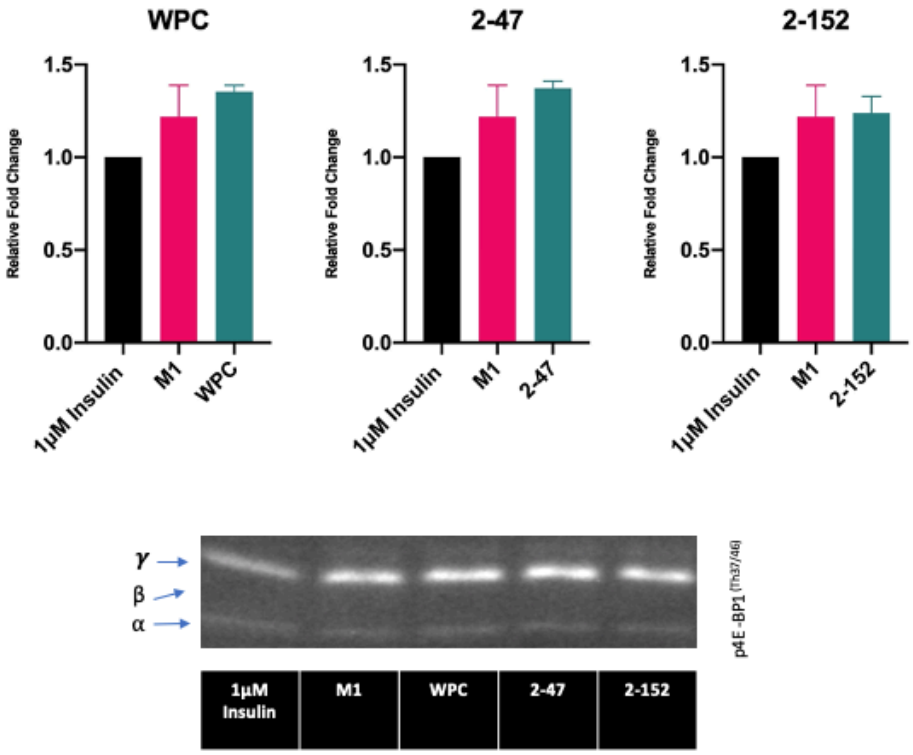


Figure 5.22 WPC, 2-47, 2-152 Hydrolysate Modulated M1 J774A.1 Macrophage Conditioned medium beneficially modulates insulin stimulated p4E-BP1$^{(Thr37/46)}$ in L6 Myotubes. L6 myoblasts were seeded at 4x10^{4}cells/mL and differentiated into myotubes as previously described. Mature myotubes were subsequently exposed to baseline or whole protein/hydrolysate modulated M1 J774A.1 macrophage conditioned medium for 24hr at 37°C in 5% CO_2. Cells were subsequently stimulated with or without 1µM bovine insulin for 20mins at 37°C in 5% CO_2 Immunoblotting was performed as previously described. Data presented as ±SEM of three replicates. Significance determined using a one way ANOVA with a Newmans-Kuels post-test. ***p<0.001, **p<0.01, *p<0.05.

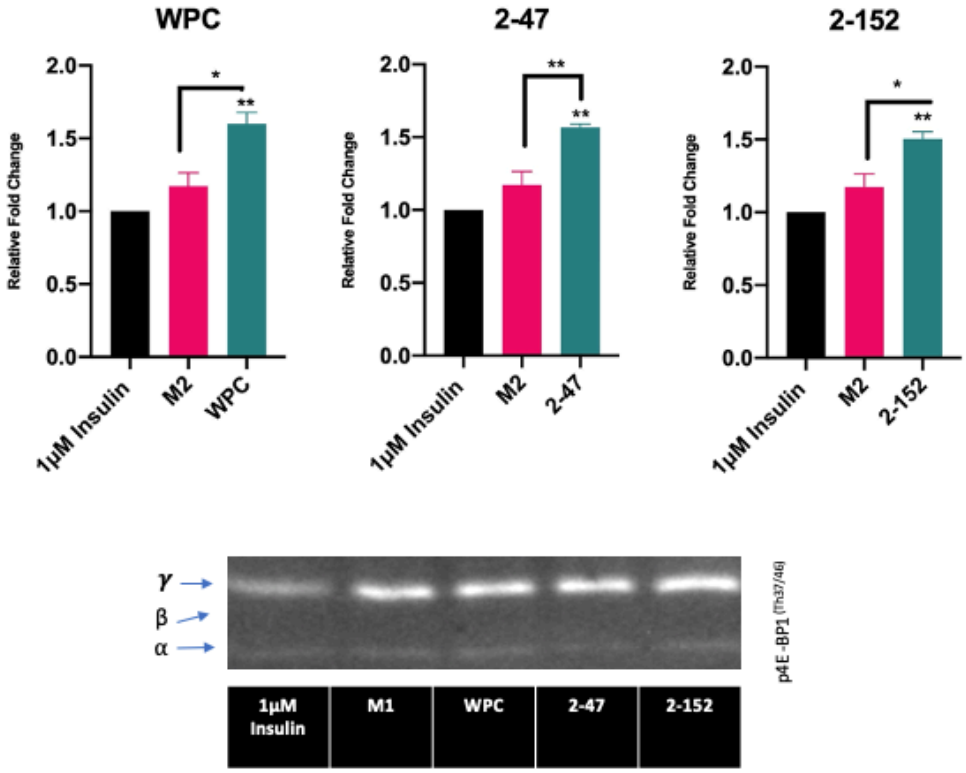


Figure 5.23 WPC, 2-47, 2-152 Hydrolysate Modulated M2 J774A.1 Macrophage Conditioned medium beneficially modulates insulin stimulated p4E-BP1$^{(Thr37/46)}$ in L6 Myotubes. L6 myoblasts were seeded at 4x10^{4}cells/mL and differentiated into myotubes as previously described. Mature myotubes were subsequently exposed to baseline or whole protein/hydrolysate modulated M2 J774A.1 macrophage conditioned medium for 24hr at 37°C in 5% CO_2. Cells were subsequently stimulated with or without 1μM bovine insulin for 20mins at 37°C in 5% CO_2. Immunoblotting was performed as previously described. Data presented as ±SEM of three replicates. Significance determined using a one way ANOVA with a Newmans-Kuels post-test. ***p<0.001, **p<0.01, *p<0.05.

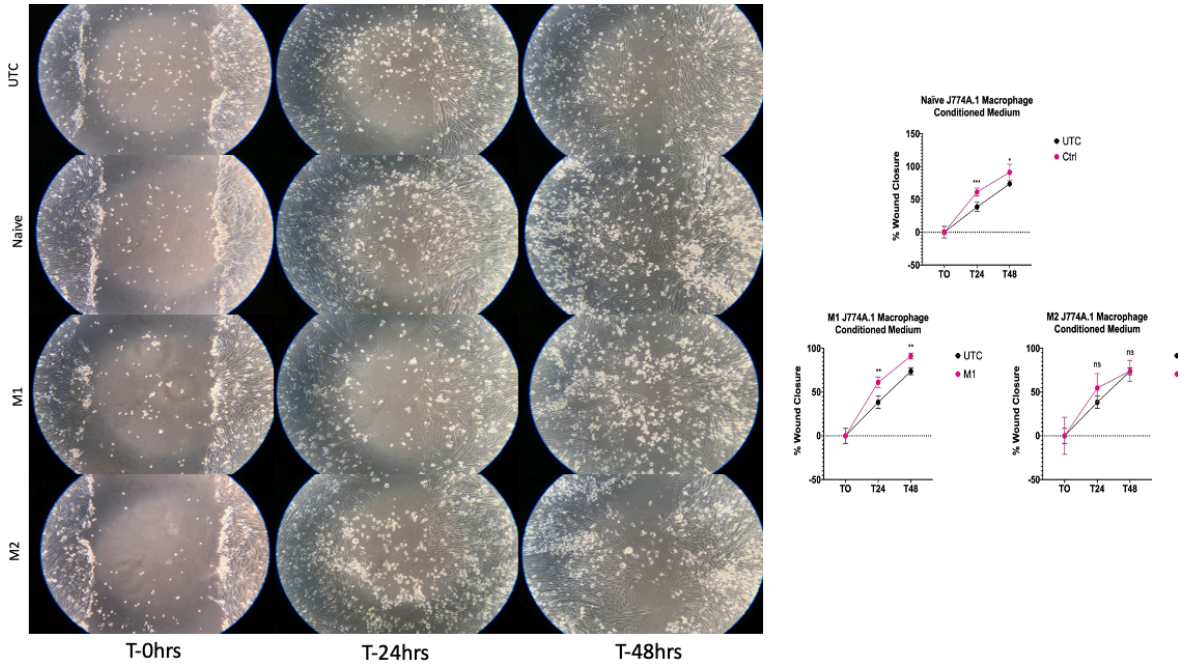
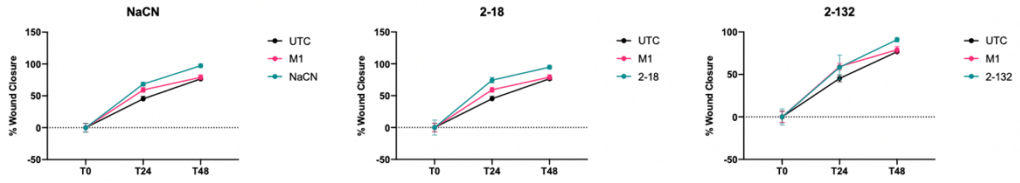
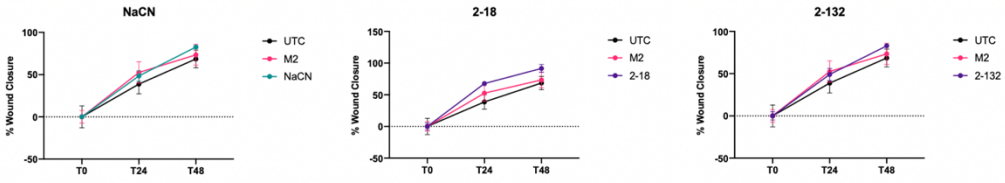


Figure 5.24 Naïve, M1 and M2 Modulated Macrophage Conditioned Medium Beneficially modulated wound healing in vitro . L6 Myoblasts were seeded at 8x10^{4}cells/mL and grown to confluence. Once confluent, the monolayer was wounded using a sterile P1000 micropipette tip to create a uniform scratch down the centre of the monolayer. Cells were then washed to remove injury debris and images were taken at a specific point within the well. Cells were subsequently incubated with naïve, M1 and M2 conditioned medium at 37°C in 5% CO_2. Images were taken at T0, T24 andT48. Wound closure is expressed as percentage closure of the original wound relating to each condition. Data is presented as mean ± SEM of three replicates. ***p<0.001, **p<0.01, *p<0.05 comparing the percentage wound closure at each time point. Significance was determined using two- way ANOVA with a Holm-Sidak post-test



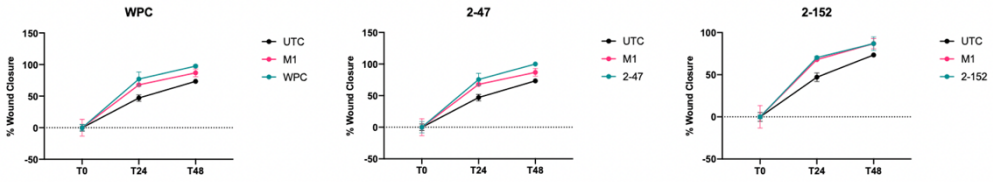
Sample	Time Point	UTC vs M1	UTC vs Hy CM	M1 CM vs. Hy CM
NaCN	T0	ns	ns	ns
	T24	↑**	↑***	↑*
	T48	ns	↑***	↑***
2-18	T0	ns	ns	ns
	T24	↑**	↑***	↑**
	T48	ns	↑**	↑**
2-132	T0	ns	ns	ns
	T24	↑**	↑*	↑*
	T48	ns	↑*	ns

Figure 5.25 NacN, 2-18 and 2-132 Hydrolysate Modulated Conditioned Medium Beneficially modulates wound healing in vitro . L6 Myoblasts were seeded at $8x10^4$cells/mL and grown to confluence. Once confluent, the monolayer was wounded using a sterile P1000 micropipette tip to create a uniform scratch down the centre of the monolayer. Cells were then washed to remove injury debris and images were taken at a specific point within the well. Cells were subsequently exposed to baseline or whole protein/hydrolysate modulated M1 J774A.1 macrophage conditioned medium at 37°C in 5% CO_2. Images were taken at T0, T24 andT48. Wound closure is expressed as percentage closure of the original wound relating to each condition. Data is presented as mean ± SEM of three replicates. ***p<0.001, **p<0.01, *p<0.05 comparing the percentage wound closure at each time point. Significance was determined using two- way ANOVA with a Holm-Sidak post-test



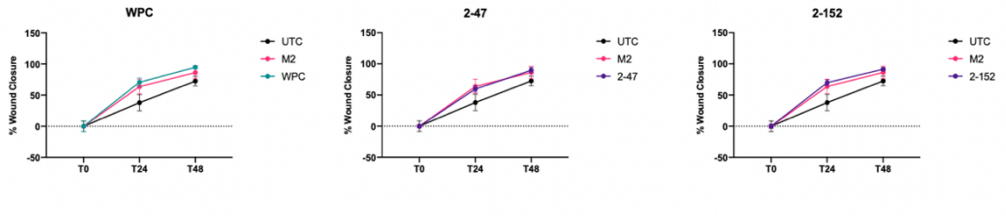
Sample	Time Point	UTC vs M2	UTC vs Hy CM	M2 CM vs. Hy CM
NaCN	T0	ns	ns	ns
	T24	ns	ns	ns
	T48	ns	ns	ns
2-18	T0	ns	ns	ns
	T24	ns	↑*	ns
	T48	ns	↑*	ns
2-132	T0	ns	ns	ns
	T24	ns	ns	ns
	T48	ns	ns	ns

Figure 5.26 NacN, 2-18 and 2-132 Hydrolysate Modulated Conditioned Medium Beneficially modulates wound healing in vitro . L6 Myoblasts were seeded at $8x10^4$cells/mL and grown to confluence. Once confluent, the monolayer was wounded using a sterile P1000 micropipette tip to create a uniform scratch down the centre of the monolayer. Cells were then washed to remove injury debris and images were taken at a specific point within the well. Cells were subsequently exposed to baseline or whole protein/hydrolysate modulated M2 J774A.1 macrophage conditioned medium at 37°C in 5% CO_2. Images were taken at T0, T24 andT48. Wound closure is expressed as percentage closure of the original wound relating to each condition. Data is presented as mean ± SEM of three replicates. ***p<0.001, **p<0.01, *p<0.05 comparing the percentage wound closure at each time point. Significance was determined using two- way ANOVA with a Holm-Sidak post-test.



Sample	Time Point	UTC vs M1	UTC vs Hy CM	M1 CM vs. Hy CM
WPC	T0	ns	ns	ns
	T24	↑**	↑***	ns
	T48	ns	↑**	ns
2-47	T0	ns	ns	ns
	T24	↑**	↑***	ns
	T48	ns	↑***	ns
2-152	T0	ns	ns	ns
	T24	↑**	↑***	ns
	T48	ns	↑*	ns

Figure 5.27 WPC, 2-47 and 2-152 Hydrolysate Modulated Conditioned Medium Beneficially modulates wound healing in vitro . L6 Myoblasts were seeded at $8x10^4$cells/mL and grown to confluence. Once confluent, the monolayer was wounded using a sterile P1000 micropipette tip to create a uniform scratch down the centre of the monolayer. Cells were then washed to remove injury debris and images were taken at a specific point within the well. Cells were subsequently exposed to baseline or whole protein/hydrolysate modulated M1 J774A.1 macrophage conditioned medium at 37°C in 5% CO_2. Images were taken at T0, T24 andT48. Wound closure is expressed as percentage closure of the original wound relating to each condition. Data is presented as mean ± SEM of three replicates. ***p<0.001, **p<0.01, *p<0.05 comparing the percentage wound closure at each time point. Significance was determined using two- way ANOVA with a Holm-Sidak post-test



Sample	Time Point	UTC vs M2	UTC vs Hy CM	M2 CM vs. Hy CM
WPC	T0	ns	ns	ns
	T24	↑**	↑***	ns
	T48	ns	↑**	ns
2-47	T0	ns	ns	ns
	T24	↑**	↑**	ns
	T48	ns	↑*	ns
2-152	T0	ns	ns	ns
	T24	↑**	↑***	ns
	T48	ns	↑*	ns

Figure 5.28 WPC, 2-47 and 2-152 Hydrolysate Modulated Conditioned Medium Beneficially modulates wound healing in vitro . L6 Myoblasts were seeded at $8x10^4$cells/mL and grown to confluence. Once confluent, the monolayer was wounded using a sterile P1000 micropipette tip to create a uniform scratch down the centre of the monolayer. Cells were then washed to remove injury debris and images were taken at a specific point within the well. Cells were subsequently exposed to baseline or whole protein/hydrolysate modulated M2 J774A.1 macrophage conditioned medium at 37°C in 5% CO_2. Images were taken at T0, T24 andT48. Wound closure is expressed as percentage closure of the original wound relating to each condition. Data is presented as mean ± SEM of three replicates. ***p<0.001, **p<0.01, *p<0.05 comparing the percentage wound closure at each time point. Significance was determined using two- way ANOVA with a Holm-Sidak post-test

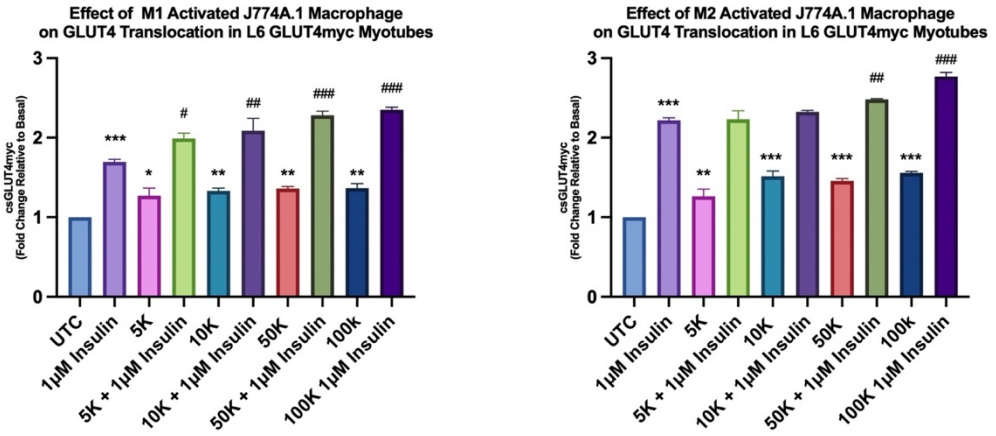


Figure 5.29 Co-Culture of M1 and M2 Activated J774A.1 Macrophage drives GLUT4 translocation in L6 GLUT4myc Myotubes. L6 GLUT4myc myoblasts were seeded at $4x10^4$cells/mL and differentiated into myotubes as previously described. J774A.1 macrophage were polarised to M1 and M2 phenotypes for three hours as previously described. Once incubation was complete, polarised J774A.1 macrophage were harvested and added directly to the L6 GLUT4myc myotube culture for 24hr at 37°C in 5% CO_2. Cells were subsequently stimulated with or with out 1µM insulin for 20mins at 37°C in 5% CO_2. Cell surface GLUT4myc was quantified as previously described. Data presented as ±SEM of three replicates.***p<0.001, **p<0.01, *p<0.05 comparing UTC to M1/M2 cells minus 1µM insulin, $^{###}$p<0.001, $^{##}$p<0.01, $^{#}$p<0.05 comparing 1µM insulin to M1/M2 plus 1µM insulin, unless otherwise indicated through use of bracket indicators.Significance determined using a one way ANOVA with a Dunnett's post-test. ***/$^{###}$/p<0.001, **/$^{##}$p<0.01, */$^{#}$p<0.05.

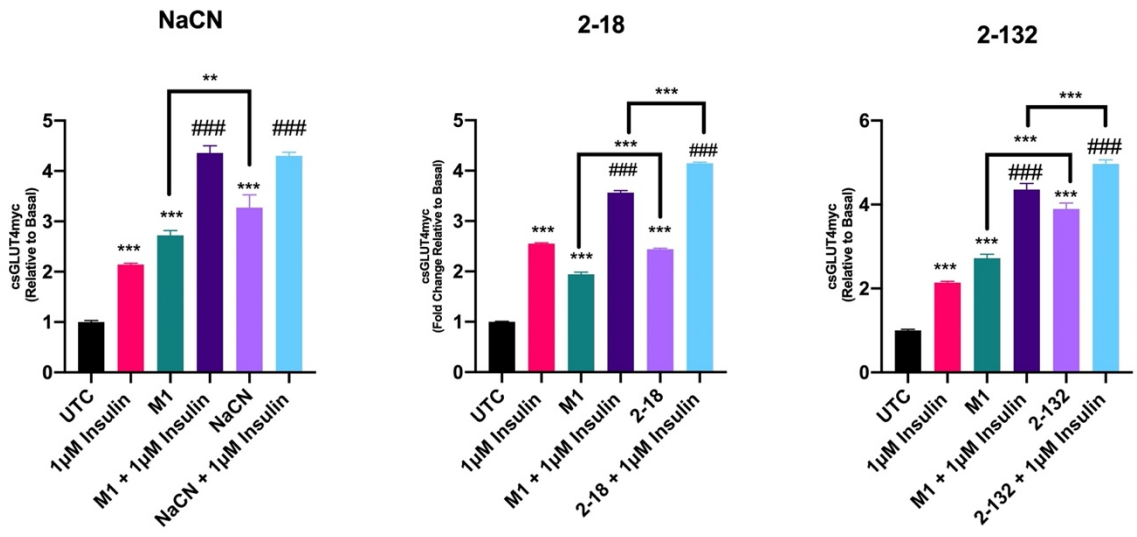


Figure 5.30 Co-Culture with NaCN, 2-18 and 2-132 modulated M1 J77A.1 macrophage promotes GLUT4 translocation in L6 GLUT4myc Myotubes. L6 GLUT4myc myoblasts were seeded at 4x10^{4}cells/mL and differentiated into myotubes as previously described. J774A.1 macrophage were incubated with 1mg/mL of whole protein or hydrolysate for one hour prior to being polarised to an M1 phenotype for three hours as previously described. Once incubation was complete, polarised J774A.1 macrophage were harvested and 100,000 cells added directly to the L6 GLUT4myc myotube culture for 24hr at 37°C in 5% CO_2. Cells were subsequently stimulated with or with out 1µM insulin for 20mins at 37°C in 5% CO_2. Cell surface GLUT4myc was quantified as previously described. Data presented as ±SEM of three replicates. .***p<0.001, **p<0.01, *p<0.05 comparing UTC to M1 cells minus 1µM insulin, $^{###}$p<0.001, $^{##}$p<0.01, $^{#}$p<0.05 comparing 1µM insulin to M1 cells plus 1µM insulin, unless otherwise indicated through use of bracket indicators.Significance determined using a one way ANOVA with a Dunnett's post-test. ***/$^{###}$/p<0.001, **/$^{##}$p<0.01, */$^{#}$p<0.05.

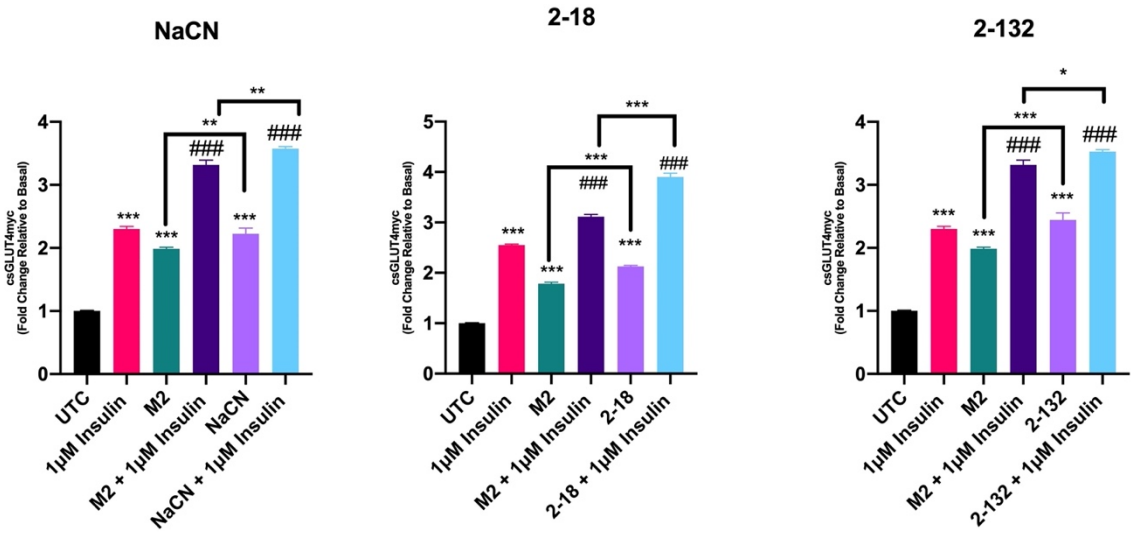


Figure 5.31 Co-Culture with NaCN, 2-18 and 2-132 modulated M2 J77A.1 macrophage promotes GLUT4 translocation in L6 GLUT4myc Myotubes. L6 GLUT4myc myoblasts were seeded at $4x10^4$cells/mL and differentiated into myotubes as previously described. J774A.1 macrophage were incubated with 1mg/mL of whole protein or hydrolysate for one hour prior to being polarised to an M2 phenotype for three hours as previously described. Once incubation was complete, polarised J774A.1 macrophage were harvested and 100,000 cells added directly to the L6 GLUT4myc myotube culture for 24hr at 37°C in 5% CO_2. Cells were subsequently stimulated with or with out 1µM insulin for 20mins at 37°C in 5% CO_2. Cell surface GLUT4myc was quantified as previously described. Data presented as ±SEM of three replicates. ***p<0.001, **p<0.01, *p<0.05 comparing UTC to M2 cells minus 1µM insulin, $^{###}$p<0.001, $^{##}$p<0.01, $^{#}$p<0.05 comparing 1µM insulin to M2 cells plus 1µM insulin, unless otherwise indicated through use of bracket indicators.Significance determined using a one way ANOVA with a Dunnett's post-test. ***/$^{###}$/p<0.001, **/$^{##}$p<0.01, */$^{#}$p<0.05.

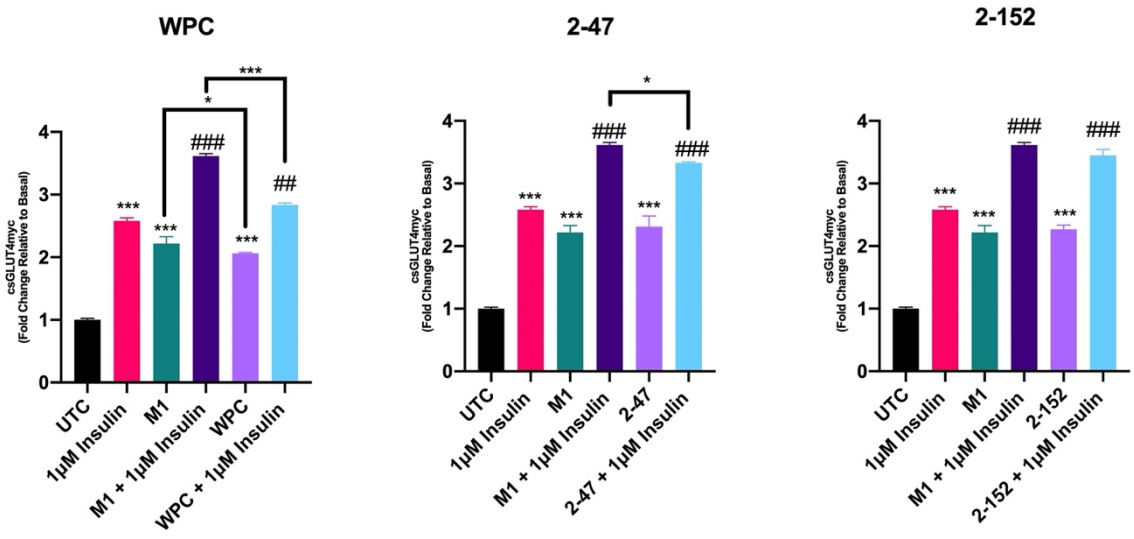


Figure 5.32 Co-Culture with WPC, 2-47 and 2-152 modulated M1 J77A.1 macrophage promotes GLUT4 translocation in L6 GLUT4myc Myotubes. L6 GLUT4myc myoblasts were seeded at $4x10^4$cells/mL and differentiated into myotubes as previously described. J774A.1 macrophage were incubated with 1mg/mL of whole protein or hydrolysate for one hour prior to being polarised to an M1 phenotype for three hours as previously described. Once incubation was complete, polarised J774A.1 macrophage were harvested and 100,000 cells added directly to the L6 GLUT4myc myotube culture for 24hr at 37°C in 5% CO_2. Cells were subsequently stimulated with or with out 1µM insulin for 20mins at 37°C in 5% CO_2. Cell surface GLUT4myc was quantified as previously described. Data presented as ±SEM of three replicates.***p<0.001, **p<0.01, *p<0.05 comparing UTC to M2 cells minus 1µM insulin, $^{###}$p<0.001, $^{##}$p<0.01, $^{#}$p<0.05 comparing 1µM insulin to M1 cells plus 1µM insulin, unless otherwise indicated through use of bracket indicators.Significance determined using a one way ANOVA with a Dunnett's post-test. ***/$^{###}$/p<0.001, **/$^{##}$p<0.01, */$^{#}$p<0.05.

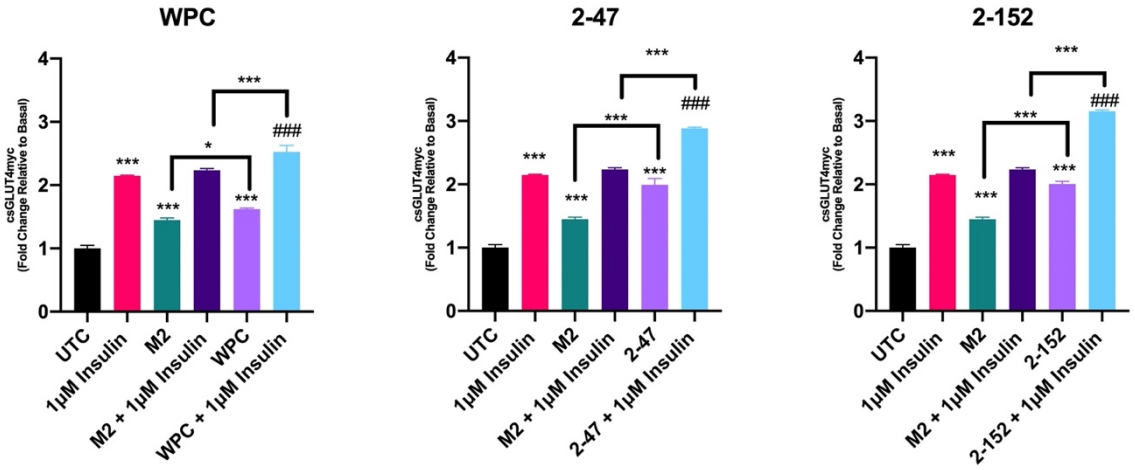


Figure 5.33 Co-Culture with WPC, 2-47 and 2-152 modulated M2 J77A.1 macrophage promotes GLUT4 translocation in L6 GLUT4myc Myotubes. L6 GLUT4myc myoblasts were seeded at $4x10^4$cells/mL and differentiated into myotubes as previously described. J774A.1 macrophage were incubated with 1mg/mL of whole protein or hydrolysate for one hour prior to being polarised to an M2 phenotype for three hours as previously described. Once incubation was complete, polarised J774A.1 macrophage were harvested and 100,000 cells added directly to the L6 GLUT4myc myotube culture for 24hr at 37°C in 5% CO_2. Cells were subsequently stimulated with or with out 1μM insulin for 20mins at 37°C in 5% CO_2. Cell surface GLUT4myc was quantified as previously described. Data presented as ±SEM of three replicates. .***p<0.001, **p<0.01, *p<0.05 comparing UTC to M2 cells minus 1μM insulin, $^{###}$p<0.001, $^{##}$p<0.01, $^{#}$p<0.05 comparing 1μM insulin to M2 cells plus 1μM insulin, unless otherwise indicated through use of bracket indicators. Significance determined using a one way ANOVA with a Dunnett's post-test. ***/$^{###}$/p<0.001, **/$^{##}$p<0.01, */$^{#}$p<0.05

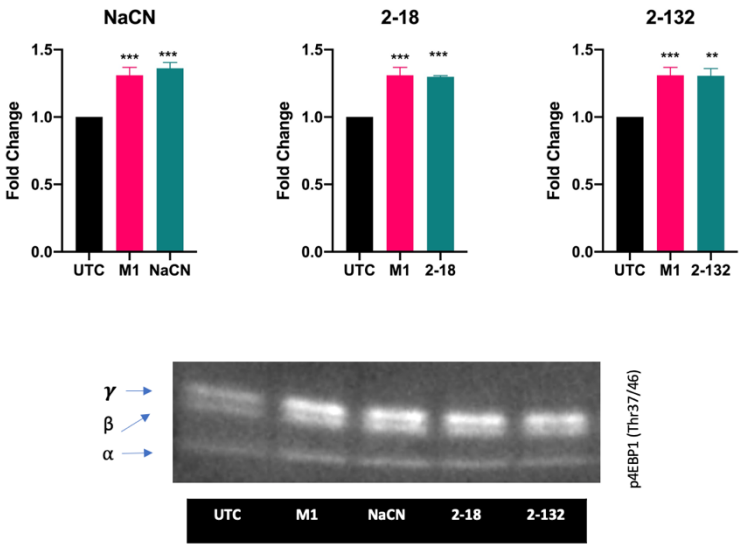


Figure 5.34 Co-Culture with NacN, 2-18 and 2-132 Hydrolysate Modulated M1 J774A.1 Macrophage beneficially modulates basal p4E-BP1$^{(Thr37/46)}$ in L6 Myotubes. L6 myoblasts were seeded at 4x10^{4}cells/mL and differentiated into myotubes as previously described. J774A.1 macrophage were incubated with 1mg/mL of whole protein or hydrolysate for one hour prior to being polarised to an M1 phenotype for three hours as previously described. Once incubation was complete, polarised J774A.1 macrophage were harvested, and 100,000 cells added directly to the L6 myotube culture for 24hr at 37°C in 5% CO_2. Immunoblotting was performed as previously described. Data presented as ±SEM of three replicates. Significance determined using a one way ANOVA with a Newmans-Kuels post-test. ***p<0.001, **p<0.01, *p<0.05.

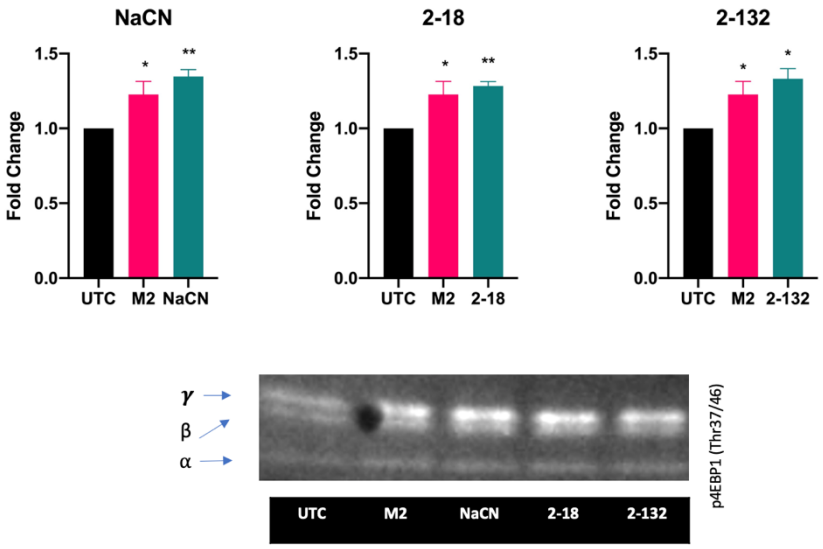


Figure 5.35 Co-Culture with NacN, 2-18 and 2-132 Hydrolysate Modulated M2 J774A.1 Macrophage beneficially modulates basal p4E-BP1$^{(Thr37/46)}$ in L6 Myotubes. L6 myoblasts were seeded at 4x10^{4}cells/mL and differentiated into myotubes as previously described. J774A.1 macrophage were incubated with 1mg/mL of whole protein or hydrolysate for one hour prior to being polarised to an M2 phenotype for three hours as previously described. Once incubation was complete, polarised J774A.1 macrophage were harvested, and 100,000 cells added directly to the L6 myotube culture for 24hr at 37°C in 5% CO_2. Immunoblotting was performed as previously described. Data presented as ±SEM of three replicates. Significance determined using a one way ANOVA with a Newmans-Kuels post-test. ***p<0.001, **p<0.01, *p<0.05.

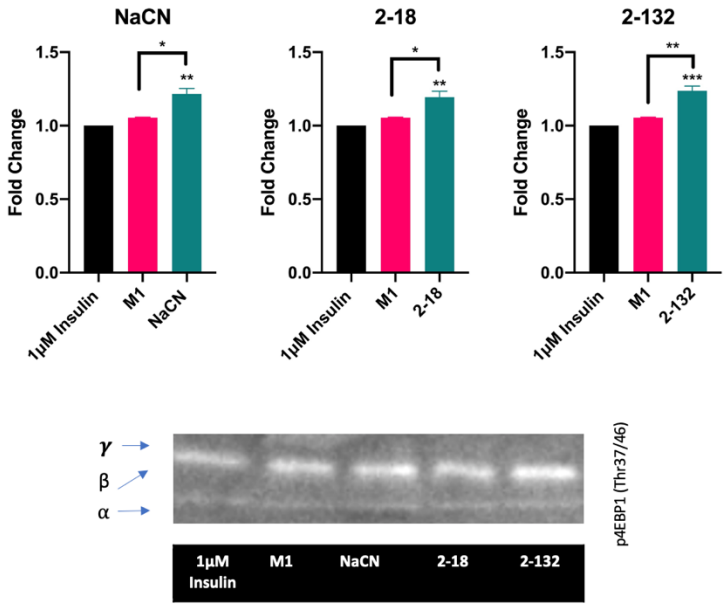


Figure 5.36 Co-Culture with NacN, 2-18 and 2-132 Hydrolysate Modulated M1 J774A.1 Macrophage beneficially modulates insulin stimulated p4E-BP1$^{(Thr37/46)}$ in L6 Myotubes. L6 myoblasts were seeded at 4x10^{4}cells/mL and differentiated into myotubes as previously described. J774A.1 macrophage were incubated with 1mg/mL of whole protein or hydrolysate for one hour prior to being polarised to an M1 phenotype for three hours as previously described. Once incubation was complete, polarised J774A.1 macrophage were harvested, and 100,000 cells added directly to the L6 myotube culture for 24hr at 37°C in 5% CO_2. Immunoblotting was performed as previously described. Data presented as ±SEM of three replicates. Significance determined using a one way ANOVA with a Newmans-Kuels post-test. ***p<0.001, **p<0.01, *p<0.05.

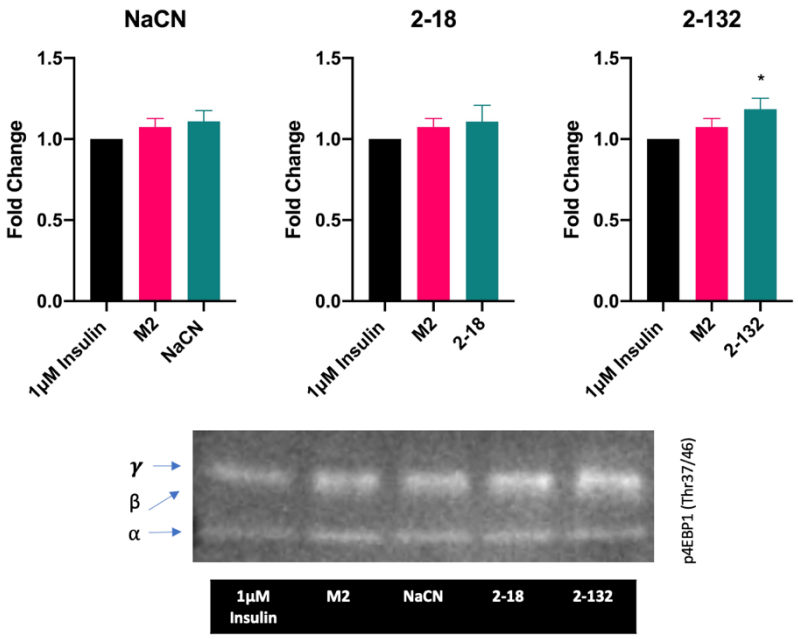


Figure 5.37 Co-Culture with NacN, 2-18 and 2-132 Hydrolysate Modulated M2 J774A.1 Macrophage beneficially modulates insulin stimulated p4E-BP1$^{(Thr37/46)}$ in L6 Myotubes. L6 myoblasts were seeded at 4x10^{4}cells/mL and differentiated into myotubes as previously described. J774A.1 macrophage were incubated with 1mg/mL of whole protein or hydrolysate for one hour prior to being polarised to an M1 phenotype for three hours as previously described. Once incubation was complete, polarised J774A.1 macrophage were harvested, and 100,000 cells added directly to the L6 GLUT4myc myotube culture for 24hr at 37°C in 5% CO_2. Immunoblotting was performed as previously described. Data presented as ±SEM of three replicates. Significance determined using a one way ANOVA with a Newmans-Kuels post-test. ***p<0.001, **p<0.01, *p<0.05.

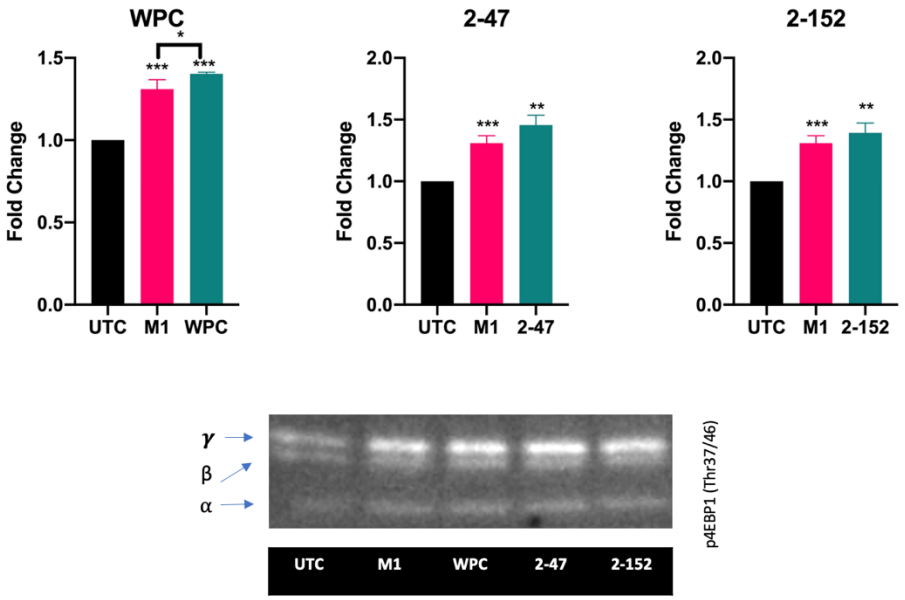


Figure 5.38 Co-Culture with WPC, 2-47 and 2-152 Hydrolysate Modulated M1 J774A.1 Macrophage beneficially modulates basal p4E-BP1$^{(Thr37/46)}$ in L6 Myotubes. L6 myoblasts were seeded at 4x10^{4}cells/mL and differentiated into myotubes as previously described. J774A.1 macrophage were incubated with 1mg/mL of whole protein or hydrolysate for one hour prior to being polarised to an M1 phenotype for three hours as previously described. Once incubation was complete, polarised J774A.1 macrophage were harvested, and 100,000 cells added directly to the L6 myotube culture for 24hr at 37°C in 5% CO_2. Immunoblotting was performed as previously described. Data presented as ±SEM of three replicates. Significance determined using a one way ANOVA with a Newmans-Kuels post-test. ***p<0.001, **p<0.01, *p<0.05.

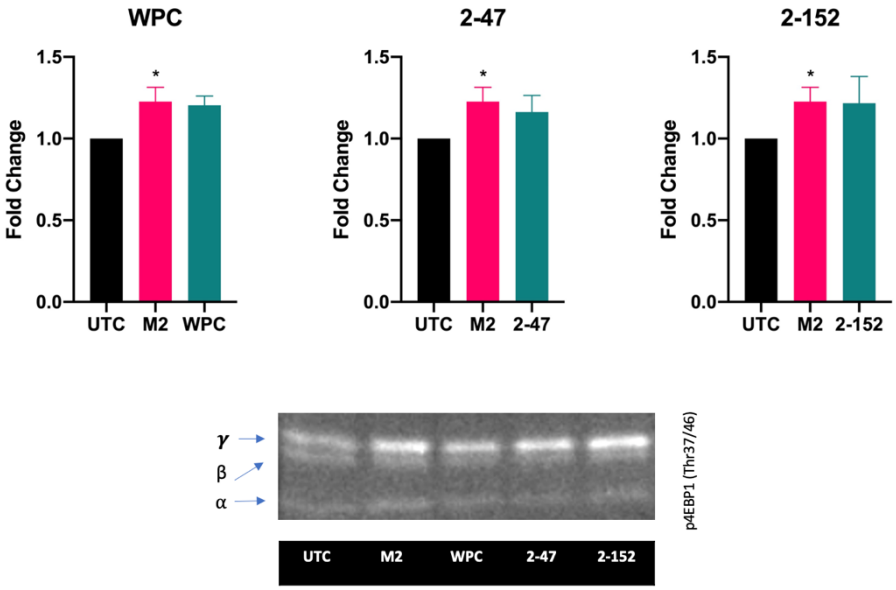


Figure 5.39 Co-Culture with WPC, 2-47 and 2-152 Hydrolysate Modulated M2 J774A.1 Macrophage modulates basal p4E-BP1$^{(Thr37/46)}$ in L6 Myotubes. L6 myoblasts were seeded at 4x10^{4}cells/mL and differentiated into myotubes as previously described. J774A.1 macrophage were incubated with 1mg/mL of whole protein or hydrolysate for one hour prior to being polarised to an M2 phenotype for three hours as previously described. Once incubation was complete, polarised J774A.1 macrophage were harvested, and 100,000 cells added directly to the L6 myotube culture for 24hr at 37°C in 5% CO_2. Immunoblotting was performed as previously described. Data presented as ±SEM of three replicates. Significance determined using a one way ANOVA with a Newmans-Kuels post-test. ***p<0.001, **p<0.01, *p<0.05.

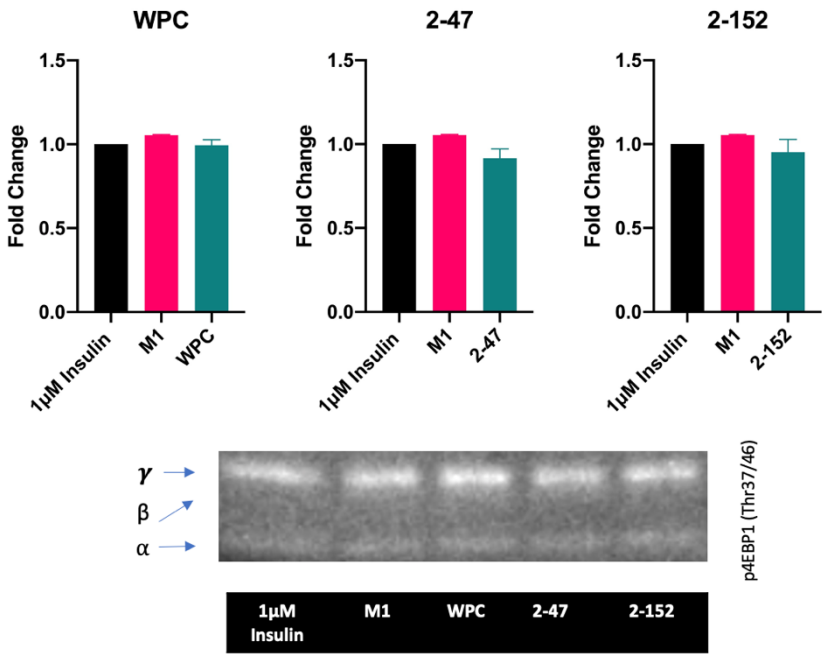


Figure 5.40 Co-Culture with WPC, 2-47 and 2-152 Hydrolysate Modulated M1 J774A.1 Macrophage modulates insulin stimulated p4E-BP1$^{(Thr37/46)}$ in L6 Myotubes. L6 myoblasts were seeded at 4x10^{4}cells/mL and differentiated into myotubes as previously described. J774A.1 macrophage were incubated with 1mg/mL of whole protein or hydrolysate for one hour prior to being polarised to an M1 phenotype for three hours as previously described. Once incubation was complete, polarised J774A.1 macrophage were harvested, and 100,000 cells added directly to the L6 myotube culture for 24hr at 37°C in 5% CO_2. Immunoblotting was performed as previously described. Data presented as ±SEM of three replicates. Significance determined using a one way ANOVA with a Newmans-Kuels post-test. ***p<0.001, **p<0.01, *p<0.05.

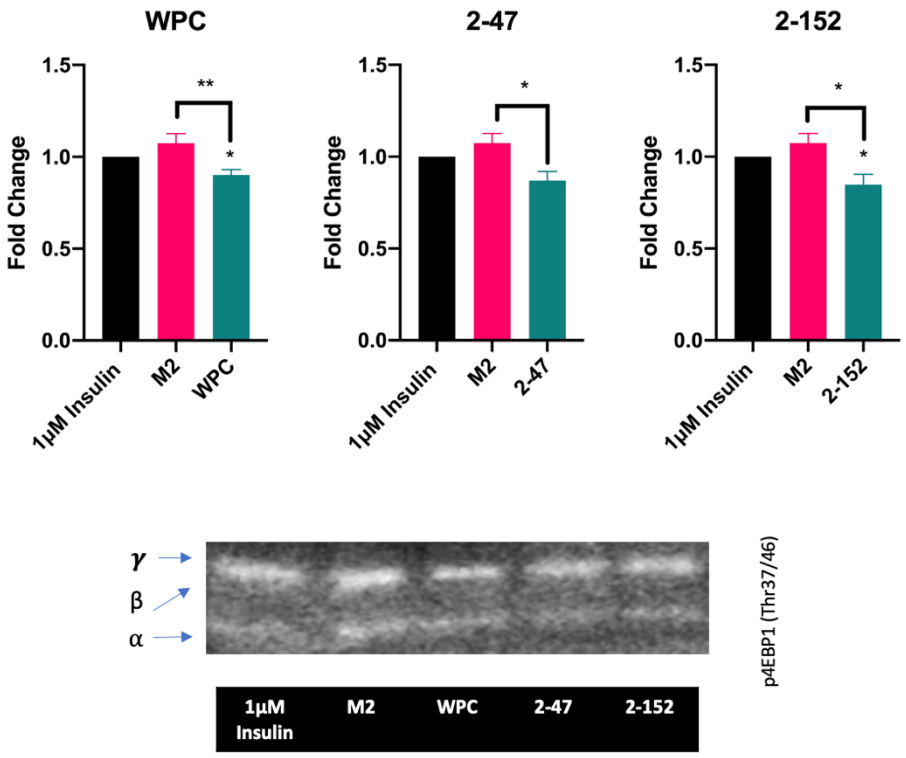
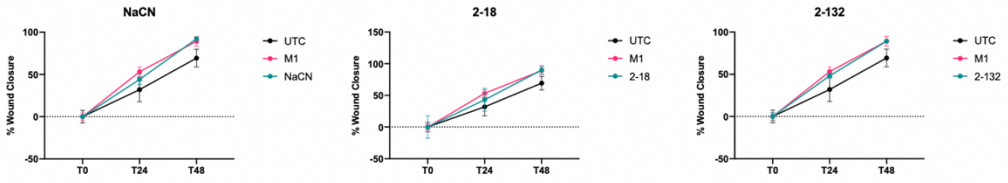
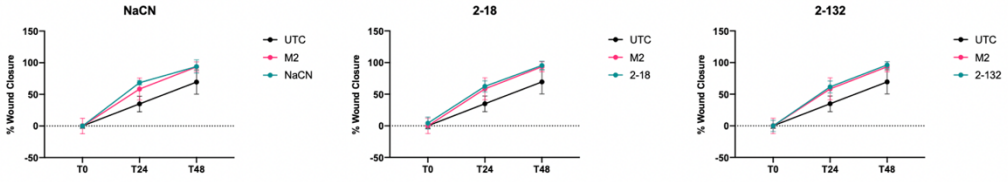


Figure 5.41 Co-Culture with WPC, 2-47 and 2-152 Hydrolysate Modulated M2 J774A.1 Macrophage modulates insulin stimulated p4E-BP1$^{(Thr37/46)}$ in L6 Myotubes. L6 myoblasts were seeded at 4x10^{4}cells/mL and differentiated into myotubes as previously described. J774A.1 macrophage were incubated with 1mg/mL of whole protein or hydrolysate for one hour prior to being polarised to an M2 phenotype for three hours as previously described. Once incubation was complete, polarised J774A.1 macrophage were harvested, and 100,000 cells added directly to the L6 myotube culture for 24hr at 37°C in 5% CO_2. Immunoblotting was performed as previously described. Data presented as ±SEM of three replicates. Significance determined using a one way ANOVA with a Newmans-Kuels post-test. ***p<0.001, **p<0.01, *p<0.05.



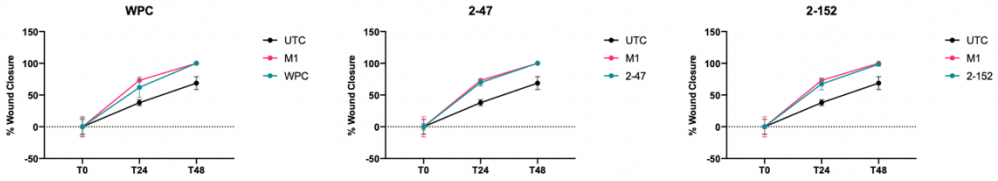
Sample	Time Point	UTC vs M1 CC	UTC vs Hy CC	M1 CC vs. Hy CC
NaCN	T0	ns	ns	ns
	T24	↑**	ns	ns
	T48	↑**	↑**	ns
2-18	T0	ns	ns	ns
	T24	↑**	ns	ns
	T48	↑**	↑*	ns
2-132	T0	ns	ns	ns
	T24	↑**	↑*	ns
	T48	↑**	↑*	ns

Figure 5.42 Co-Culture with NaCN, 2-18 and 2-132 Hydrolysate Modulated M1 J774A.1 Macrophage beneficially modulate wound healing in vitro . L6 myoblasts were seeded at 8x10^{4}cells/mL grown to confluence. Once confluent, the monolayer was wounded using a sterile P1000 micropipette tip to create a uniform scratch down the centre of the monolayer. Cells were then washed to remove cell debris. J774A.1 macrophage were incubated with 1mg/mL of whole protein or hydrolysate for one hour prior to being polarised to an M1 phenotype for three hours as previously described. Once incubation was complete, polarised J774A.1 macrophage were harvested, and 100,000 cells added directly to the L6 myoblast culture. Images were taken at T0, T24 andT48. Wound closure is expressed as percentage closure of the original wound relating to each condition. Data is presented as mean ± SEM of three replicates. ***p<0.001, **p<0.01, *p<0.05 comparing the percentage wound closure at each time point. Significance was determined using two-way ANOVA with a Holm-Sidak post-test



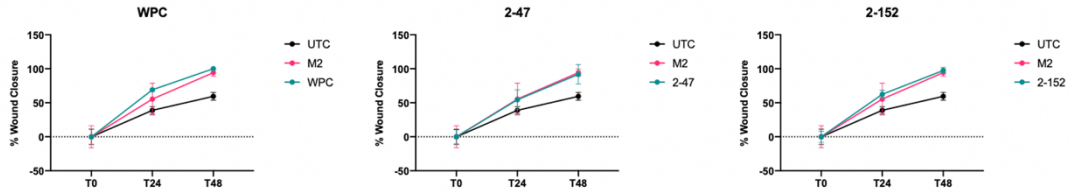
Sample	Time Point	UTC vs M2 CC	UTC vs Hy CC	M2 CC vs. Hy CC
NaCN	T0	ns	ns	ns
	T24	↑*	↑**	ns
	T48	↑*	↑*	ns
2-18	T0	ns	ns	ns
	T24	↑*	↑*	ns
	T48	↑*	↑*	ns
2-132	T0	ns	ns	ns
	T24	↑*	↑*	ns
	T48	↑*	↑*	ns

Figure 5.43 Co-Culture with NaCN, 2-18 and 2-132 Hydrolysate Modulated M2 J774A.1 Macrophage beneficially modulate wound healing in vitro . L6 myoblasts were seeded at 8x10^{4}cells/mL grown to confluence. Once confluent, the monolayer was wounded using a sterile P1000 micropipette tip to create a uniform scratch down the centre of the monolayer. Cells were then washed to remove cell debris. J774A.1 macrophage were incubated with 1mg/mL of whole protein or hydrolysate for one hour prior to being polarised to an M1 phenotype for three hours as previously described. Once incubation was complete, polarised J774A.1 macrophage were harvested, and 100,000 cells added directly to the L6 myoblast culture. Images were taken at T0, T24 andT48. Wound closure is expressed as percentage closure of the original wound relating to each condition. Data is presented as mean ± SEM of three replicates. ***p<0.001, **p<0.01, *p<0.05 comparing the percentage wound closure at each time point. Significance was determined using two-way ANOVA with a Holm-Sidak post-test



Sample	Time Point	UTC vs M1 CC	UTC vs Hy CC	M1 CC vs. Hy CC
WPC	T0	ns	ns	ns
	T24	↑**	↑*	ns
	T48	↑***	↑**	ns
2-47	T0	ns	ns	ns
	T24	↑**	↑**	ns
	T48	↑***	↑***	ns
2-152	T0	ns	ns	ns
	T24	↑**	↑**	ns
	T48	↑***	↑***	ns

Figure 5.44 Co-Culture with WPC, 2-47 and 2-152 Hydrolysate Modulated M1 J774A.1 Macrophage beneficially modulate wound healing in vitro . L6 myoblasts were seeded at $8x10^4$cells/mL grown to confluence. Once confluent, the monolayer was wounded using a sterile P1000 micropipette tip to create a uniform scratch down the centre of the monolayer. Cells were then washed to remove cell debris. J774A.1 macrophage were incubated with 1mg/mL of whole protein or hydrolysate for one hour prior to being polarised to an M1 phenotype for three hours as previously described. Once incubation was complete, polarised J774A.1 macrophage were harvested, and 100,000 cells added directly to the L6 myoblast culture. Images were taken at T0, T24 andT48. Wound closure is expressed as percentage closure of the original wound relating to each condition. Data is presented as mean ± SEM of three replicates. ***p<0.001, **p<0.01, *p<0.05 comparing the percentage wound closure at each time point. Significance was determined using two-way ANOVA with a Holm-Sidak post-test



Sample	Time Point	UTC vs M2 CC	UTC vs Hy CC	M2 CC vs. Hy CC
WPC	T0	ns	ns	ns
	T24	ns	↑**	ns
	T48	↑**	↑***	ns
2-47	T0	ns	ns	ns
	T24	ns	ns	ns
	T48	↑**	↑**	ns
2-152	T0	ns	ns	ns
	T24	ns	ns	ns
	T48	↑**	↑**	ns

Figure 5.45 Co-Culture with WPC, 2-47 and 2-152 Hydrolysate Modulated M2 J774A.1 Macrophage beneficially modulate wound healing in vitro . L6 myoblasts were seeded at 8x10^{4}cells/mL grown to confluence. Once confluent, the monolayer was wounded using a sterile P1000 micropipette tip to create a uniform scratch down the centre of the monolayer. Cells were then washed to remove cell debris. J774A.1 macrophage were incubated with 1mg/mL of whole protein or hydrolysate for one hour prior to being polarised to an M2 phenotype for three hours as previously described. Once incubation was complete, polarised J774A.1 macrophage were harvested, and 100,000 cells added directly to the L6 myoblast culture. Images were taken at T0, T24 andT48. Wound closure is expressed as percentage closure of the original wound relating to each condition. Data is presented as mean ± SEM of three replicates. ***p<0.001, **p<0.01, *p<0.05 comparing the percentage wound closure at each time point. Significance was determined using two-way ANOVA with a Holm-Sidak post-test

5.4 Discussion:

To achieve the objectives of this chapter, we first had to optimise a method by which we could generate macrophage conditioned growth medium to analyse the effects of secreted, soluble factors from both hydrolysate-modulated and non-modulated M1 and M2 polarised J774A.1 macrophage, on outputs of skeletal muscle function. Initially, it was attempted to sensitize macrophage to the growth medium of the L6 and L6 GLUT4myc muscle cells. Normally, J774A.1 macrophage are cultured in DMEM medium containing 5g/L D-Glucose. In contrast, the αMEM used to culture the muscle cells contains 1g/L D-Glucose. This was attempted due to the documented effect of high glucose exposure in skeletal muscle, down regulating GLUT4 activity (Huang et al., 2002).

Initially we examined the effect of increasing ratios of αMEM: DMEM on macrophage viability and typical cytokine secretion. In LPS activated macrophage increasing rations of αMEM: DMEM resulted in a decrease in cell viability and a dose dependant decrease in IL-6 and TNFα secretion. Polarisation to M1 and M2 phenotypes, in αMEM, similarly resulted in down regulation of cell viability and more significantly, had a detrimental impact on typical cytokine profiles of M1 and M2 macrophage. This observation can primarily be attributed to the abundance and availability of nutrients, mainly glucose in the cell culture medium. Aerobic glycolysis is a key metabolic pathway in TLR4 activated immune cells (Kelly and O'Neill, 2015). Tan et. al demonstrated that promotion of PDK1 signalling, a key mediator of glycolysis was associated with M1 phenotype polarisation, where inhibition, and subsequent promotion of M2 polarisation (Tan et al., 2015). M2 polarised macrophage in contrast rely more on oxidative metabolism and fatty acid oxidation for their energy requirements (Viola et al., 2019). This data supports the fact that glucose is essential to support M1 and M2 macrophage polarisation due to the significant cellular demand for ATP, and that inhibition or interference with glycolytic and oxidative pathways can significantly impact on immune function (Silvia and O'Neill, 2014). As a result, we used DMEM conditioned medium for conditioned medium experiments, as maintaining healthy M1 and M2 macrophage phenotypes was critical for understanding effects of secreted soluble factors on skeletal muscle health.

Using the standard DMEM cell culture growth medium, two sets of conditioned mediums were generated. The first was an attempt to increase cytokine concentrations in M1 and M2 polarised macrophage. The rationale for this was that in the initial set up of the conditioned medium experiments to be conducted for this chapter, it was desirable to show that altering cytokine concentrations in growth medium can impact on outputs of skeletal muscle function. To do this, cells were seeded at the following densities: $1x10^6$cells/mL (Ctrl), $1x10^6$cells/mL in 1mL (A), $2x10^6$cells/mL in 1mL (B) and $2x10^6$cells/mL in 2mL (C). The attempts to concentrate secreted cytokines from both M1 and M2 polarised macrophage were successful. Conditioned medium for optimisation experiments was generated using a cell density of $2x10^6$cells/mL in 1mL, as this density in M1 macrophage, significantly promoted IL-6, IL-10, and TNF secretion. In M2 macrophage, this cell density also led to significantly higher levels of M2 specific IL-10 being secreted over the standard (Ctrl) density used throughout this thesis.

The second set of conditioned medium generated was the hydrolysate modulated conditioned growth medium. Conditioned medium was generated using NaCN and derived hydrolysates 2-18 and 2-132, and WPC and derived hydrolysates 2-47 and 2-152. These hydrolysates were chosen on the basis that they all exhibited anti-inflammatory properties in M1 and M2 polarised macrophage. Moreover, they also elicited positive effects directly on skeletal muscle cells; promoting GLUT4 translocation, protein anabolic signalling and they also supported aspects of skeletal muscle regeneration. These results were presented in the previous two results chapters. Conditioned medium was generated using the standard cell density of $1x10^6$cells/mL. In M1 macrophage, NaCN hydrolysates had a significantly more potent anti-inflammatory profile than the whole protein. 2-18 reduced IL-1β and IL-6 secretion and promoted IL-10 secretion. 2-132 also exhibited these properties with the added reduction of TNFα secretion. WPC hydrolysates 2-47 and 2-152 had comparable down regulation of both IL-6 and TNFα secretion and no effect on IL-10 was observed. In M2 macrophage, 2-18 and 2-132 enhanced IL-10 and TNFα secretion, whilst NaCN exhibited anti-IL-10 bioactivity. WPC enhanced IL-10 secretion in M2 macrophage whilst 2-47 modestly reduced IL-10 whilst 2-152 maintained IL-10 secretion.

Initial experiments concerning the effect of conditioned medium of GLUT4 were performed in myotubes. Normal M1 conditioned medium from both M1 and M2 macrophage enhanced the translocation of GLUT4 to the membrane in myotubes. Concentrating the secreted cytokines had a considerable effect of GLUT4 translocation, driving increased levels of both basal and insulin stimulated GLUT4. Interestingly, M2 conditioned medium, could drive a higher magnitude of cell surface GLUT4 compared to the M1 conditioned medium. These changes between the normal and concentrated growth medium coincided with increases in IL-6, IL-10, and TNFα in both M1 and M2 conditioned medium.

Having demonstrated that altering cytokine concentrations could impact GLUT4 translocation, the next step was to study the effect of hydrolysate-modulated conditioned medium on GLUT4 translocation. Regarding the NaCN cohort of hydrolysates, samples NaCN modulated M1 conditioned medium boosted basal levels of GLUT4. In contrast hydrolysate 2-18 did not alter GLUT4 levels relative to unmodulated M1 conditioned medium. M1 2-132-modulated medium altered GLUT4 levels to a considerable extent, promoting translocation at both the insulin stimulated and basal levels. In the modulated M2 conditioned media 2-18 and 2-132 hydrolysates promoted both basal and insulin stimulated levels of cell surface GLUT4, whereas only the insulin stimulated levels were affected with NaCN. WPC and 2-152 modulated M1 media enhanced insulin stimulated GLUT4 translocation while a benefit for basal GLUT4 translocation was seen with hydrolysate 2-47. In contrast to the NaCN M2 modulated cohort, a variable effect was seen with the WPC cohort. 2-47 promoted insulin stimulated and basal GLUT4m whilst, 2-152 blocked GLUT4 translocation relative to unmodulated cells. No effect on insulin stimulated GLUT4 was observed with M2 WPC conditioned medium, while basal GLUT4 was enhanced.

These observations, although variable appear to follow a trend. With M1 modulated conditioned medium, down regulation of TNFα and/or promotion of IL-10 secretion increased basal, and insulin stimulated GLUT4. NaCN and 2-132 down regulate TNFα, while 2-132 also promotes IL-10 secretion leading to enhanced GLUT4 translocation at both basal and insulin stimulated states. In contrast, although pro-IL-10 activity was observed with sample 2-18, a failure to down regulate TNFα led to no change in GLUT4 translocation compared to unmodulated M1 conditioned medium. WPC hydrolysates down regulated TNFα secretion, which were associated with benefits for GLUT4 translocation, however these benefits did not appear as potent as the casein hydrolysate 2-132, where both IL-10 and TNFα was altered. In the M2 modulated conditioned medium cohort, 2-18 and 2-132 enhanced IL-10 and TNFα secretion, which was associated with a considerable upregulation of cell surface GLUT4 at both basal and insulin-stimulated states, compared to NaCN where both IL-10 and TNFα were downregulated. Interestingly, although IL-10 was down regulated, NaCN modulated M2 macrophage promoted insulin stimulated GLUT4, which was an effect also observed with the whey hydrolysate 2-47. We have previously shown, in Chapter Four, that increasing doses of IL-10 can be detrimental for GLUT4 translocation. Although the basal state was unaffected, 2-152 M2 modulated media detrimentally affected insulin stimulated GLUT4, whilst basal levels were unaffected. This was associated with a driving of IL-10 secretion. Although WPC was also associated with increased IL-10 secretion, basal GLUT4 was promoted.

This data appears to indicate a balance between the relative abundances of inflammatory TNFα and anti-inflammatory IL-10 is required to promote GLUT4 translocation and as a result glucose uptake and utilisation. Inflammation is strongly associated with insulin resistance, with studies showing correlation between high levels of circulating inflammatory cytokines and T2DM (Kalinkovich and Livshits, 2017). Bouzakri et. al demonstrated that infusion of TNF in humans induced skeletal muscle insulin resistance in healthy human subjects (Bouzakri et al., 2005). However, TNFα has also been shown to promote Glucose uptake. Roher et. al demonstrated that TNFα dose dependently increases both cell surface GLUT4 abundance and 2-DG glucose uptake in myoblasts and myotubes (Roher et al., 2008a). These findings were substantiated further by Vraskou et al. *in vitro* . Using primary trout derived myocytes, this study demonstrated that recombinant TNFα

induced glucose uptake which coincided with increased GLUT4 abundance in the trout tissue. Moreover, this effect was replicated using conditioned medium from LPS stimulated trout derived macrophage, supporting the findings of this results chapter (Vraskou et al., 2011). IL-10 status also plays a significant role with in supporting glucose metabolism. Reduced serum IL-10 concentrations are negatively associated insulin sensitivity (Kim et al., 2004; Leon-Cabrera et al., 2015). In a mouse model of diabetes, transgenic mice over expressing IL-10, exhibited enhanced levels of insulin sensitivity and glucose uptake in skeletal muscle in mice fed a high fat diet (Hong et al., 2009). This study exemplified the protective effects of IL-10 *in vivo*.

Regarding IL-6 modulation, it is a pleotropic cytokine, believed to exert both pro- and anti-inflammatory effects which are both tissue specific and time dependent (Muñoz-Cánoves et al., 2013). We have demonstrated that reduction of IL-6 secretion in M1 modulated macrophage conditioned medium translates to positive outcomes for GLUT4 translocation. There are several sources of IL-6, including immune cells, the liver, adipose tissue and skeletal muscle (Hoene and Weigert, 2008). IL-6 production in the liver is thought to induce insulin resistance in these tissues (Hoene and Weigert, 2008; Rotter et al., 2003). Kim et. al demonstrated *in vivo*, that IL-6 infusions in mice, decreased insulin stimulated glucose disposal. Interestingly this effect was ameliorated by co-infusion of IL-6 and IL-10, further suggesting the protective roles of IL-10 as an anti-inflammatory and metabolic regulator (Kim et al., 2004). However, we have previously demonstrated that recombinant IL-6 promotes GLUT4 translocation, and by association glucose uptake and utilisation. In humans, Krogh-Madsen demonstrated that infusion of recombinant TNF and not IL-6, negatively impacted insulin metabolism despite increases in serum plasma concentrations of each cytokine (Krogh-Madsen et al., 2006). Moreover, Caery et. al demonstrated that acute IL-6 stimulation in L6 myotubes promoted insulin stimulated GLUT4 translocation (Carey et al., 2006). Indeed, our findings and those discussed suggest a dual role for IL-6 in glucose metabolism. Acute IL-6 stimulation appears to have positive effects for glucose metabolism, however the association of high levels of circulating inflammatory IL-6 cannot be ignored. Therefore, we propose that the modulation of IL-6 presented, although down regulated in many cases, is not enough to prevent the acute benefits of IL-6 on skeletal muscle health, and may play a protective role in attenuating chronic inflammatory activity

in skeletal muscle due to the progressive effects of IL-6 on inflammation (Villar-Fincheira et al., 2021). Considering the balance of TNFα and IL-10 abundance, and the dual role of IL-6, it does appear from the *in vitro* data that skewing immune function towards an M2 phenotype in M1 macrophage and promoting M2 activity is beneficial for glucose metabolism.

Our second measurement of skeletal muscle function was analysing the effect on muscle protein synthesis, through measuring the downstream mTOR effector 4E-BP1. Using the concentrated and normal M1 and M2 conditioned growth medium, we observed that promotion of the M2 phenotype significantly enhanced basal and insulin stimulated 4E-BP1 activation compared to the M1 phenotype. Modulation of M1 and M2 phenotypes with NaCN, 2-18 and 2-132 modestly increased basal and insulin stimulated 4E-PB1 activation relative to unmodulated M1 and M2 phenotypes. In contrast, modulation of M1 and M2 phenotypes with WPC and 2-47 considerably enhanced basal 4E-BP1 activation. In the presence of insulin, WPC, 2-47 and 2-152 M2 modulated conditioned significantly 4E-BP1 signalling in myotubes. A noticeable difference between the casein- and whey-modulated M2 phenotypes is the absence of TNFα promotion in the whey cohort, which may be attributable to the enhanced 4E-BP1 activation versus the casein-modulated cohort.

TNFα has been long implicated in the inhibition of protein synthesis in skeletal muscle (Lang et al., 2002). *In vitro* , Williamson et. al demonstrated in C2C12 skeletal myotubes, that acute TNF stimulation decreased insulin stimulated muscle protein synthesis. Interestingly, acute TNF stimulation promoted basal 4E-BP1 $\boldsymbol{\gamma}$ form phosphorylation but inhibited the insulin stimulated levels (Williamson et al., 2005). Lang et. al demonstrated in vivo, that TNF inhibited 4E-BP1 activation in both heart and skeletal muscle tissue samples, resulting in increased 4E-BP1:EIF4E association, culminating in a reduction of protein synthesis in the respective tissues (Lang et al., 2002). 2-18 and 2-132 M2 modulated conditioned medium exhibited enhanced TNFα secretion, whilst WPC, 2-47 and 2-152 TNF levels were unaltered. The absence, or lack of TNFα promotion in M2 phenotype, may explain why increased 4E-BP1 activation is being seen, over and above the casein modulated M2 conditioned medium Considering the roll that TNFα plays in mTOR regulation, the

reduction in TNFα secretion in modulated M1 phenotypes by NaCN and 2-132 may not be a sufficient lowering of TNFα abundance to induce a significant increase in 4E-BP1 activation compared to the whey protein and hydrolysate modulated conditioned medium. Nevertheless, data presented suggests that skewing the secretome of immune environment towards that of ananti-inflammatory Th2 can beneficially promote muscle protein synthesis in skeletal muscle.

The immune system is an overarching arbiter of skeletal muscle regeneration. Dysfunction to the temporal and spacial regulation of immunity during healing induces detrimental effects for the regenerative and metabolic functions of skeletal muscle overtime (Tidball and Villalta, 2010). Therefore, modulation of M1 and M2 macrophage function, could potentially have considerable consequences for skeletal muscle healing *in vitro* . Initial analysis showed that both M1 and M2 conditioned growth medium promoted muscle wound injury healing in the scratch assay model of injury. This observation is consistent lines of observation concerning macrophage function and their role in wound healing. The role of M1 macrophage in the initial stages of muscle injury, promoting satellite cell and myoblast proliferation has been extensively documented (Dort et al., 2019). M2 macrophage were shown to be instrumental in promoting myoblast migration through upregulation of key chemokine pathways in skeletal muscle (Sakaguchi et al., 2014). Moreover, M2 macrophage are instrumental in promoting myoblast to myotube differentiation, a critical step in the generation of new muscle fibres (Saclier et al., 2013). Observations concerning NaCN, 2-18 and 2-132 M1 modulated growth medium, suggest that skewing of M1 phenotypes towards an M2 phenotype promoted increased wound healing compared to unmodulated M1 conditioned medium. Ko et. al demonstrated that although inflammatory activated conditioned medium promoted myoblast and myotube migration, naïve macrophage medium, with reduced levels of inflammatory cytokines, promoted more complete closure of the *in vitro* wound (Ko et al., 2016). Supporting this, reductions in IL-1, IL-6 and TNFα appear to function separately or in unison to support skeletal muscle healing in the M1 phenotype. Similarly with WPC, 2-47 and 2-152, although not as significantly boosted, reduction in an M1 phenotype did not negatively influence myoblast migration. Similar observations were also made with the modulated M2 phenotype conditioned medium. Together this information indicates that hydrolysate

modulated immunity, directly and positively influences the migration of injured myoblasts, suggesting that modulate immunity may be supportive during muscle injury regeneration.

Thus far, we have provided evidence, that altering secreted factors from both M1 and M2 polarised macrophage can induce beneficial metabolic changes that promote aspects essential to maintaining muscle health and function. During muscle injury, and even in a quiescence skeletal muscle, both healthy and diseased contains macrophage that are in direct cell to cell contact with the muscle structure (Brigitte et al., 2010; Pillon et al., 2013; Tidball and Villalta, 2010). As a result, deciphering the effect of modulated immune function in a scenario of direct cell to cell contact is essential to alluding to potential clinical benefits *in vivo*. Co-culture was performed using modulated and non-modulated M1 and M2 polarised J774A.1 macrophage that were activated for four hours prior to being harvested and incubated with either mature myotubes or myoblasts. This time point was chosen as previous research in the lab has previously demonstrated that in LPS activated dendritic cells, IL-6 and TNFα secretion was significantly upregulated (Collins, 2014). Moreover, Liu et. al demonstrated that key markers of M2 activation are elevated after three hours (Liu et al., 2020).

In the context of GLUT4 trafficking, we demonstrated that co-culture with M1 and M2 modulated NaCN, 2-18 and 2-132 macrophage beneficially increase GLUT4 translocation in both the insulin and stimulated states. This increase in cell surface GLUT4 over the unmodulated M1 and M2 modulated cells appears to be more potent that the effects seen with the conditioned medium, suggesting that direct cell contact is integral to promoting GLUT4 translocation. In contrast, modulation of the M1 phenotype, with WPC and 2-47 suppressed GLUT4 translocation relative to unmodulated M1 macrophage, meanwhile 2-152-modulated cells had no effect relative to the M1 control cells. In M2 modulated macrophage we observed significant benefits for GLUT4 translocation with WPC, 2-47 and 2-152-modulated M2 macrophage significantly boosting cell surface GLUT4. The difference concerning conditioned medium and co-culture and the whey protein hydrolysate immunity suggest an involvement of direct cell contact and sufficient secreted cytokines and growth factors are required to promote and support GLUT4 trafficking *in vitro* .

This data further adds credence to the hypothesis that modulating aspects of inflammation can be beneficial for glucose metabolism in skeletal muscle. Infiltration and sustained activation of inflammatory cells is closely linked with the onset of insulin resistance and the dysregulation of glucose metabolism (Kanter et al., 2012; Wu and Ballantyne, 2017; Zhang et al., 2015). Song et. al demonstrated that primary macrophage derived from GRP94$^{(-/-)}$ knockout mice, exhibited traits more akin to the anti-inflammatory M2 phenotype and reduced infiltration in liver and adipose tissue, improving whole body insulin sensitivity (Song et al., 2020). Further evidence that increasing M2 polarised macrophage phenotypes can have benefits for insulin metabolism was presented by Ikeda et. al that showed that increasing M2 populations in skeletal muscle post exercise, was positively correlated with improved glucose disposal in muscle tissue. Although researchers noted that these changes were made independent of change in GLUT4, total GLUT4, and not translocated (cell surface) was measured (Ikeda et al., 2013). Moreover, Resveratrol treatment attenuated M1 polarisation in mouse skeletal muscle, enhanced M2 populations and promoted infiltration of T regulatory lymphocytes, boosting signalling of pro-metabolic pathways in skeletal muscle. This study offered insight into to the potential health benefits of promoting a Th2 environment in skeletal muscle (Shabani et al., 2020).

M1 and M2 modulated co-culture induced similar changes in 4E-BP1 activation compared to unmodulated cells. In the presence of insulin, NaCN, 2-18 and 2-132 cells considerably enhanced 4E-BP1 activation. This trend was also observed with the M2 modulated phenotypes. WPC, 2-47 and 2-152 M1 and M2 modulated co-culture enhanced basal 4E-BP1 levels. However, in the presence of insulin, 4E-BP1 was down regulated because of direct cell contact. This is counter to observations concerning conditioned medium experiments suggesting two possibilities; secreted factors play an integral role in 4E-BP1 signalling and that potential changes in cell surface molecule adhesion could be at play in the regulation of 4E-BP1 signalling. Walton et. al demonstrated that increased populations of M2 macrophage in skeletal muscle post resistance exercise training was positively associated with upregulation of hypertrophic pathways in skeletal muscle (Walton et al., 2019).

One potential mechanism of interference of 4E-BP1 activation is the potential regulation of key adhesion molecules in either skeletal muscle or macrophage. Sonnett et. al demonstrated that cellular adhesion between human macrophage and both myoblasts and myotubes resulted in rescuing of muscle viability through anti-apoptotic signals. In this study, they identified that adhesion between macrophage and muscle cells was mediated through the following cell adhesions: VCAM-1–VLA-4, ICAM-1–LFA-1, PECAM1–PECAM-1 and CX3CL1-CX3CR1. These adhesion molecules deliver anti-apoptotic signals through increased Akt phosphorylation and increased BCL-2 expression (Sonnet et al., 2006). Increases in Akt phosphorylation and BCL-2 expression are positively associated with skeletal muscle hypertrophy and glucose metabolism (Bodine et al., 2001; He et al., 2012). It is possible that immunomodulation may have augmented the abundance of the adhesion receptor and ligands or the activity of Akt and BLC-2 mediate cell proliferation, culminating in the differential effects observed. The degree at which these markers were modulated is unknown, however altering adhesion molecules such as VCAM-1 has a documented effect. Choo et. al demonstrated that knock down of VCAM-1 delayed muscle fibre hypertrophy in a non-inflammatory state, but in the presence of inflammation it was shown to be essential for promoting expansion and differentiation of muscle satellite cells (Choo et al., 2017).

Interestingly, unlike what we observed with the conditioned medium experiments, modulated direct cell: cell contact did not alter the rate of wound healing relative to the unmodulated M1 and M2 phenotypes. This information, indicates only one possibility, which is that modulation of soluble factors secreted by both M1 and M2 phenotypes plays a more prominent role in the promotion of wound healing. This knowledge lends to the hypothesis that down regulating inflammatory pathway, critical in the early stages of muscle regeneration, using immunomodulatory hydrolysates, may not impact on the ability of muscle to regenerate. Evidence concerning the use of Ibuprofen for muscle and tendon injury, indicates that knocking out initial inflammation can have detrimental impacts for healing these tissues (Connizzo et al., 2014; Liao et al., 2019).

In conclusion we have demonstrated the following:

1. That conditioned medium from M1 and M2 function differentially impacts on outputs of muscle health GLUT4 translocation, 4E-BP1 signalling and drives skeletal muscle wound healing.

2. That modulating macrophage soluble function towards a M2/Th2 phenotype promotes GLUT4 translocation, 4E-BP1 signalling and drives skeletal muscle wound healing.

3. That co-culture with M1 and M2 macrophage have differential effects on outputs of muscle function over the secreted factors in conditioned medium

4. That co-culture with Th2 skewed/modulated M1 and M2 polarised macrophage can promote GLUT4 translocation and 4E-BP1 signalling in skeletal muscle

5. Down regulating inflammation with casein and whey derived hydrolysates do not negatively impact the early phases of myoblast migration during in vitro wound healing.

This thesis chapter further adds to the hypothesis that surprising chronic inflammatory activity can have positive influences on skeletal, to promote muscle health and function (Nicklas and Brinkley, 2009).

Chapter 6:

General Discussion

Scientific research is continually reinforcing and substantiating the effects that nutrition has on our overall health, from the benefits of superfoods such as blue berries, to the detriments of excess dietary fat on our cardiovascular health (Lenihan-Geels et al., 2013; PROESTOS, 2018). The term “functional foods” describes a set of foods that possess the ability to beneficially enhance the health and wellbeing of the consumer (PROESTOS, 2018). Functional foods are foods that contain added specific bioactive ingredients, that when consumed beneficially impact the consumer in several ways, beyond the effects of basic “wild type” nutrition (Hasler, 2002). Protein is a potent source of functional ingredients. Functional bioactive peptides and hydrolysates can be decrypted from their parent protein sequences through natural digestive process, however due to the variability in native digestion, which is based on numerous factors, consistent and concentrated release of functional peptides may be difficult (Udenigwe and Aluko, 2012). Therefore, identifying, isolating, and fortifying whole foods with specific bioactive peptides or hydrolysates allows for the creation of a functional food designed specifically to support aspects of both human and animal health. Protein-derived functional foods have been shown to beneficially improve several systems of human health including immune function, cardiovascular health, metabolic function and even antimicrobial properties (Peighambardoust et al., 2021).

Cow’s milk is a complex matrix consisting of a plethora of health promoting nutrients. Protein in cow’s milk exists in two forms, 20% of which is casein and the remaining 80% is casein. In their whole form, both casein and whey have been shown to have health promoting properties including anticarcinogenic, immunomodulatory, anti-microbial and antiviral (Davoodi et al., 2016). However, hydrolysed bioactive peptides and hydrolysates can induce a range of health promoting benefits beyond that of the whole parent proteins (Marcone, Simone et al., 2017) Lalor et. al demonstrated that the k-casein subunit is potently anti-inflammatory driving M2 like macrophage phenotypes (Lalor and O’Neill, 2019b). Silva et. al demonstrated that a whey derived hydrolysate can inhibit ACE mediated conversion of angiotensin I to angiotensin II, promoting cardiovascular health (Silva et al., 2014).

Due to whey and casein being produced as excess waste products from several dairy processes, they present an opportunity to mine and commercialise cows milk protein derived health boosting functional foods. Furthermore, the EU and EFSA have passed legislation that requires that any health boosting food or supplement that goes to market requires scientifically accredited health claims (EC1924/2006). At FHI, the goal is to research, develop, manufacture, and commercialise milk derived functional foods with proven, scientifically supported health claims.

Muscle tissue is a primary metabolic site in the human body and has key functions in locomotion. Chronic inflammation has been shown to detrimentally affect both the regenerative and metabolic functions of skeletal muscle tissue. In the elderly, chronic inflammation leads to an increase lipid accumulation in skeletal muscle which further exacerbates the inflammatory response, which damages muscle tissue further resulting in a deleterious, degenerative loss of muscle mass and function overtime (Dalle et al., 2017). This is a metabolic syndrome called Sarcopenia. The functional loss of skeletal muscle is also linked to disruption in key metabolic pathways of skeletal muscle: glucose uptake and utilisation and anabolic signalling pathways; culminating in T2DM and a loss of independence (Hunter et al., 2019). NSAIDs have been shown to be effective in restoring muscle mass and function in sarcopenic individuals (Dalle et al., 2017; Landi et al., 2013). We hypothesised that identification of an anti-inflammatory myomodulatory cows' milk derived hydrolysate could reduce chronic inflammation associated with sarcopenia, and further improve the metabolic efficiency in affected muscle. Moreover, due to the implications of inflammation negatively regulating skeletal muscle metabolism, suppressing excess inflammation during recovery from exercise to promote muscle growth, energy efficiency and reduce delayed onset muscle soreness (DOMs), an anti-inflammatory milk hydrolysate could find application as a functional food to promote recovery from intense exercise and therefore supporting athletic performance.

Throughout this PhD project the goal to identify novel immunomodulatory milk derived hydrolysates, which could potentially benefit the metabolic and regenerative health of skeletal muscle tissue. Chapter Three allowed us to optimize and screen a panel of whey and casein derived hydrolysates for bioactivities relating to immunomodulation of M1 and M2 macrophage phenotypes involved in muscle repair and homeostasis. In Chapter Four, we further analyzed the identified immunomodulators on key outputs of skeletal muscle function. Combining the observations from these two chapters, we identified four candidate hydrolysates that may be beneficial in modulating skeletal muscle health *in vivo*, in the context of acute and chronic inflammation. Two casein derived hydrolysates, 2-18 and 2-132, and two whey derived hydrolysates, 2-47 and 2-152, were selected to study the effects of modulated immunity both directly and indirectly. We examined this in Chapter Five using a co-culture system which could assess both the effects of soluble and cell-to-cell contact factors.

2-132, is a casein derived hydrolysate, that has been studied in multiple contexts through the FHI research consortium. Unpublished work from our research group demonstrated that 2-132 can down regulate Th1 and DC responses and promote gut membrane integrity in a DSS model of colitis in mice (Hunt et al, unpublished). Based on this data uncovering novel applications in the context of other critical bodily functions needed to be investigated. We have demonstrated that in the context of M1 polarised macrophage, modulation with 1mg/mL 2-132 down regulated IL-1, IL-6, and TNFα secretion. IL-10 secretion was also enhanced by 2-132, suggesting that it may have a role in promoting an M1 to M2 phenotypic shift in macrophage populations. Furthermore, this hydrolysate showed the capacity to promote and enhance an M2 anti-inflammatory phenotype in the macrophage polarization model. This was indicted by significant promotion of the regulatory cytokine IL-10. In our models of skeletal muscle measurement, 2-132 showed previously unidentified bioactivity beyond its immunomodulatory potential. 2-132 was able to boost basal levels of cell surface GLUT4 in myotubes. Moreover, it was demonstrated that 2-132 can synergize with insulin, to further promote GLUT4 translocation over insulin alone. 2-132 also showed the ability to maintain the activation status of basal levels of phosphorylated 4E-BP1, indicating a role in the maintenance of skeletal muscle mass. In the context of skeletal muscle healing, 2-132 showed the ability to

enhance CCL2/MCP-1 secretion from myoblasts, whilst also promoting muscle wound healing *in vitro* . Based on this data, the effect of 2-132 immuno- and myomodulatory was examined in models of crosstalk, looking at the impacts of soluble mediators via conditioned medium and via direct cell to cell contact in a 2D model of cell culture. We demonstrated that 2-132 modulated M1 and M2 conditioned medium, induced greater GLUT4 translocation to cell surface, in both basal and insulin stimulated states compared to unmodulated M1 and M2 growth medium. The same effect was also observed in a model of direct cell contact in both M1 and M2 phenotypes. Positive effects were also observed with the activation of the mTOR signaling cascade via 4E-BP1 activation. Modulation of 2-132 M1 and M2 soluble factors-maintained activation of 4E-BP1. In the co-culture model similar observations were shown, however insulin stimulation in the co-culture model led to significantly higher levels of 4E-BP1 activation and inferred muscle protein synthesis. Wound healing was also beneficially modulated by soluble factor modulation. 2-132 modulated M1 conditioned medium led to a significant improvement in wound healing, over unmodulated M1 conditioned medium while there was no change in the M2 conditioned medium. M1 and 2-132 modulated macrophage did not promote wound healing to the same degree as seen with the conditioned medium data. A similar observation with 2-132 M2 modulated cells was also observed. This indicates that modulation of soluble factors, and not cell contact points, is fundamental to the increased regenerative capacity observed.

This profile of activity may suggest that immuno- and myomodulation with 2-132 may have benefits in the treatment of chronic inflammatory disease in skeletal muscle, due to the pro-M2 anti-inflammatory and pro-metabolic effects observed. As mentioned sarcopenia is an inflammatory disease of muscle characterized by metabolic disfunction and a loss of skeletal muscle mass overtime (Bunchorntavakul and Reddy, 2020). Often associated with ageing and increased morbidity, patients presenting with sarcopenia exhibit an elevated inflammatory profile, insulin resistance and/or T2DM and blunted protein synthesis (Haran et al., 2012). Indeed, several studies implicate excess levels of IL-1, IL-6 and TNFα and reductions in circulating IL-10 as key indicators of sarcopenia (Fan et al., 2016; Rong et al., 2018)

The use of anti-inflammatory strategies to promote tissue function has been investigated extensively. A comprehensive literature survey indicates that anti-inflammatory strategies can promote restoration of skeletal muscle function in the elderly (Alturki et al., 2018). In the elderly use of NSAIDs such as ibuprofen have been shown to positively influence muscle inflammation and muscle health (Dalle et al., 2017). The use of a food derived immunomodulator may offer a natural, safer method to promote muscle health and modulate inflammation in sarcopenic individuals. Sumi et. al demonstrated in a mouse model of chronic inflammation, that the use of anti-inflammatory food components EPA, DHA and α-lactalbumin following resistance exercise, resulted in a decrease in inflammatory cytokines IL-1β, IL-6 and TNFα that was directly correlated with benefits for muscle health and mass (Sumi et al., 2020). Directly targeting muscle macrophage *in vivo* with IL-4 tagged nanoparticles promoted muscle mass and function *in vivo,* induced an M1 to M2 phenotypic shift in muscle resident macrophage (Raimondo and Mooney, 2018). Dietary protein has also been a proven source of immuno- and myomodulators that can promote aspects of muscle health, relating to sarcopenia. Son et. al demonstrated that egg white protein derived hydrolysates can overcome TNFα mediated suppression of glucose uptake, a hallmark of sarcopenia, through promotion of GLUT4 translocation to the cell surface of L6 myotubes (Son and Wu, 2019). Furthermore, the pro-GLUT4 bioactivity observed with sample 2-132 suggests that in combination with its anti-inflammatory capacity, it can promote increased basal and insulin glucose uptake. Indeed, these observations of M2-skewing in the literature appear to align with observations around the potential impact of 2-132 bioactivity on M1 and M2 macrophage function and subsequent impact on muscle tissue. This data has provided a basis for further research and the potential commercialization of hydrolysate 2-132 as a functional food to support healthy ageing by supporting muscle health.

The second casein derived hydrolysate we investigated was 2-18. 2-18 exhibited many similarities with the bioactivity of 2-132. In M2 macrophage, 2-18 significantly promoted IL-10 secretion, whereas in M1 macrophage, although IL-10 was upregulated TNFα secretion was unaffected. Unlike 2-132, which appears to promote M1 to M2 phenotype skewing, 2-18's immunomodulatory capacity appears to be in promoting and sustaining an M2 anti-inflammatory phenotype. Regarding the effects directly on muscle, 2-18

significantly enhanced basal and insulin stimulated GLUT4 translocation. Moreover, 4E-BP1 activation was enhanced in both basal and insulin stimulated states. Wound healing in the context of the scratch assay was boosted and this was associated with increased CCL2/MCP-1 secretion. Modulated M1 conditioned medium from 2-18 maintained GLUT4 translocation, enhanced basal and insulin stimulated 4E-BP1 activation and promoted increased wound healing in the scratch assay model. M2 conditioned medium, in contrast, promoted a significant increase in GLUT4 translocation, upregulation of 4E-BP1 activity and maintenance of wound healing. In contrast to the conditioned medium, co-culture with 2-18 modulated M1 macrophage, we observed significant improvements in GLUT4 translocation, which contrasts with conditioned medium experiments, suggesting that modulation of the cell surface phenotype may be influencing the GLUT4 translocation pathway. Promotion of GLUT4 was also observed in M2 modulated cells. 2-18 M1 and M2 modulated cells, promoted activation of 4E-B1 and similarly did not negatively impact on muscle regeneration. We have demonstrated that 2-18 shares similar functional properties of 2-132. in terms of immunomodulation, myomodulation and influencing crosstalk between macrophage and skeletal muscle. However, the inability to significantly suppress the M1 phenotype, suggests that 2-18 may have commercial potential in the sports nutrition market.

The initial inflammatory response to muscle injury is a critical step in the regeneration pathway. Upregulation of inflammatory markers such as IL-6 and TNFα are essential for conditioning the site of injury with inflammatory signals to drive monocyte and leukocyte infiltration, and subsequent proliferation of skeletal muscle progenitor cells (Tidball and Villalta, 2010). NSAIDs are known to inhibit M1 macrophage function, skewing towards an anti-inflammatory phenotype (Liu et al., 2017). Connizzo et. al demonstrated that the timing and delivery of an anti-inflammatory to treat tendon injury was critical. Researchers showed that early administration of ibuprofen delayed tendon injury healing; macrophage are also a key regulator of tendon injury like muscle (Connizzo et al., 2014; Sunwoo et al., 2020). Moreover ibuprofen has also been shown to directly inhibit muscle satellite cell proliferation (Liao et al., 2019). This blunting is likely contributable to a deactivation of the initial inflammatory response to tissue injury likely mediated through down regulation of the COX-2 signaling pathway in neutrophils and macrophage (Shen et al., 2006).

Furthermore, a successful transition from M1 to M2 anti-inflammatory microenvironments are absolutely required for the resolution of residual inflammatory activity as well as extracellular matrix deposition and finalization of wound healing (James G Tidball, 2017). 2-18 as mentioned appears to be pro-M2 and not necessarily anti-M1, evident from the maintenance of TNFα secretion. It's unlikely, therefore to interfere with M1 macrophage during the initial inflammatory phase, and likely to promote the later M1 to M2 environment transition, 2-18 may therefore be applicable in the resolution of acute muscle injury, often seen in the young sporting population (Barroso and Thiele, 2011). Furthermore, we have also shown that 2-18 modulated soluble factors can directly benefit metabolic and regenerative outputs of skeletal muscle. Further evidence to support the use of 2-18 as a functional food to support athletes is the direct effects observed in skeletal muscle health is evident from its positive effects on GLUT4 and 4EBP1 activation. 2-18 promoted basal and insulin stimulated GLUT4 translocation. GLUT4 translocation is directly correlated with glucose uptake and utilization (RYDER et al., 1999). Due to the energy demands of skeletal muscle during exercise and the importance of glucose uptake during recovery for glycogen resynthesis, it is imperative that GLUT4 functions optimally (KUO et al., 1999). Oosthuyse et. al provides evidence that a casein hydrolysate-CHO mix can better influence time trial performance in cyclists compared to whey hydrolysate-CHO mix by altering metabolic parameters such as plasma glucose, insulin and lactate concentrations (Oosthuyse et al., 2015) . Moreover, promotion of basal 4E-BP1 activation suggests a role in promoting molecular and structural adaption to exercise. Cogan et. al demonstrated that ingestion of a casein derived hydrolysate was able to boost mTOR and 4E-BP1 activity, pathways critical to muscle growth and repair following exercise (Cogan et al., 2018). Identification of a casein derived hydrolysate that has a benefit in for applications in areas such as supporting athletic performance presents a possible commercial opportunity. Normally in the context of protein-based supplements and functional foods that support sporting performance, whey protein is the standard source. This is partly due to the ease of access to excess whey from other processes in the dairy industry, but also since whey protein is acid soluble and absorbed rapidly once ingested, it makes it a desirable choice in the sports nutrition space (West et al., 2017). Thus, identification of a casein derived hydrolysate that can promote similar, if not more potent, benefits than a whey hydrolysate

opens up the possibility of mining casein as a source of novel bioactives for a range of applications.

Thus far, we have discussed the findings of this research in relation to casein derived hydrolysates. In Chapter Three we identified a range of immunomodulatory whey hydrolysates, including 2-47 and 2-152. In the M1 and M2 macrophage model, both hydrolysates exhibited potent anti-inflammatory anti-M1 bioactivities evident through down regulation of both myeloid TNFα and IL-6. Furthermore, they showed the ability to maintain the M2 phenotype through sustained IL-10 secretion. In terms of the direct effects on skeletal muscle; 2-47 dose dependently boosted basal GLUT4 translocation, and increased the insulin stimulated levels. Furthermore, 2-47 significantly increased basal 4E-BP1 activity. 2-47 boosted CCL2/MCP-1 secretion in muscle cells which was positively correlated with increased wound healing after 48hr. 2-152 also boosted basal and insulin stimulated GLUT4 translocation, maintained 4E-BP1 activation, boosted CCL2/MCP-1 and promoted skeletal muscle healing. In our models of immune-muscle crosstalk, 2-47-modulated M1 conditioned medium boosted basal GLUT4 translocation, while 2-152 boosted insulin stimulated GLUT4 translocation. 2-47-M2 modulated conditioned medium showed potent benefits for GLUT4 translocation. In contrast, 2-152 M2 modulation significantly impaired insulin stimulated GLUT4 translocation, relative to the unmodulated M2 conditioned medium, but critically, not less than the insulin controls. Modulation of secreted factors from both M1 and M2 macrophage conditioned with 2-47 and 2-152 had positive effects in boosting 4E-BP1 activation. Moreover, modulation of secreted cytokines, did not impair wound healing. Interestingly some contrasting observations were noted in the direct model of co-culture. M1 activated macrophage modulated with 2-47 negatively affected insulin stimulated GLUT4 translocation, while 2-152 modulations did not impact GLUT4 translocation. Significant improvements in GLUT4 translocation were noted regarding modulation of 2-47 and 2-152 M2 macrophage, with both basal and insulin stimulated GLUT4 being enhanced. 2-47- and 2-152- modulated M1 and M2 macrophage both maintained 4E-BP1 activity in muscle cells. However, in the presence of insulin 2-47- and 2-152-modulated M1 and M2 macrophage, had considerable negative consequences, down regulating 4E-BP1 activity. Co-culture with 2-47/152-M1 and M2 modulated cells did not impact on wound healing *in vitro* .

Whey protein has been a constant source of bioactive hydrolysates and peptides for many years. Hydrolysate 2-47 and 2-152, in a similar manner to 2-132, showed potent anti-inflammatory effects, down regulating IL-6 and TNFα. Unlike the casein hydrolysates, 2-47 and 2-152 did not augment IL-10 secretion. Despite this, the application of an IL-6 and TNFα inhibitor in a chronic inflammatory muscle disease cannot be understated. In a cohort of over 60s females, supplementation with hydrolyzed whey protein enhanced chest, bicep, and knee extensor strength. This effect was correlated with decreased levels of IL-6, TNFα and CRP (Nabuco et al., 2019). Moreover, we have demonstrated that 2-47 and 2-152 beneficially modulated GLUT4 translocation and 4E-BP1 in skeletal muscle. Whey protein ingestion is positively associated with improvements in metabolic health (Sousa et al., 2012). Whole whey consumption is positively associated with increases in muscle anabolic signaling (West et al., 2017). McKinley et. al demonstrated that in adolescent swimmers, whey ingestion improved metrics of muscle recovery (McKinlay et al., 2020). Borack et. al further demonstrated that ingestion of a whey isolate enhanced muscle protein synthesis pathways via mTOR activation (Borack et al., 2016). Whey consumption is also positively associated with whole body insulin sensitivity, due to the extensive evidence supporting the insulinotrophic properties of whey (Adams and Broughton, 2016). Regarding the effects of whey hydrolysates on GLUT4 in skeletal muscle Morato et. al demonstrated *in vivo* that ingestion of a whey hydrolysate enhanced GLUT4 translocation in rats, to a noticeably greater extent than unhydrolyzed whey (Morato et al., 2013). We observed contrasting consequences on outputs of muscle function concerning the effect of either modulated soluble factor secretion or direct cell contact with our candidate whey hydrolysates. It is possible that these effects are as a result of unquantified components of modulated medium such as chemokines, but also due to potential changes in cell adhesion markers that are known to induce proliferative signaling in skeletal muscle via Akt and BLC2 signaling pathways (Sonnet et al., 2006). Despite the blurred clarity around the direct consequence of 2-47 and 2-152 immunomodulation modulation on muscle function, based on the evidence surrounding 2-47 and 2-152, they may have application in suppressing chronic inflammatory diseases of skeletal muscle. Moreover, the pro-metabolic effects and

pro-healing bioactivates directly observed on skeletal muscle by 2-47 and 2-152 make these hydrolysates a candidate for also supporting post-exercise recovery.

This thesis has provided evidence that cow's milk whey and casein derived protein hydrolysates can modulate immune function, muscle function and in some cases can positively impact the interaction that occurs between these two systems. The data presented provides evidence that these hydrolysates can improve measures of inflammatory disease in skeletal muscle, through down regulation of key M1 and upregulation of M2 cytokines. Direct effects of hydrolysates on skeletal muscle also indicate a role in beneficially modulating glucose and protein metabolism in muscle cells. We do however acknowledge that there are several limitations to this *in vitro* study.

Throughout this study we have consistently demonstrated that M1 polarised macrophage and their secreted mediators, can benefit our measures of skeletal muscle function, despite conflicting reports that categorically link inflammation to metabolic disruption in skeletal muscle (Lee and Olefsky, 2021). A potential factor contributing to these divergent observations *in vitro* is the contextualization of inflammatory macrophage activation. Chronic inflammation in skeletal muscle, not only reduces muscle mass over time, it also promotes the infiltration and accumulation of ectopic lipids within the muscle structure (Mei et al., 2011). As a result, the presence of increased lipids and fatty acids can influence macrophage activity. A principal fatty acid in skeletal muscle is palmitic acid (PA), which is a 16-carbon chain saturated fatty acid. PA has been shown to induce skeletal muscle insulin resistance and reduce glucose uptake directly in L6 myotubes, through promotion of NF-κB activation, although insulin resistance to PA can occur independently of NF-κB status (Hommelberg et al., 2011). In macrophage, PA can influence TLR4-mediated activation. Riera-Borrull et. al demonstrated that macrophage activated with PA and LPS induced cytokine secretion of IL-1β, IL-6 and TNFα over and above that of LPS activated macrophage alone. Moreover, it was demonstrated that IL-10 secretion was significantly down regulated (Riera-Borrull et al., 2017). Conditioned medium from PA-activated macrophage was shown to induce insulin resistance in L6 GLUT4myc myotubes through down regulation of IRS-1, ultimately reducing GLUT4 translocation. This GLUT4 down regulation reduced 2D-glucose uptake also (Kewalramani et al., 2011). Importantly, however, is that Samokhvalov

et. al demonstrated differential consequences on GLUT4 and insulin sensitivity in L6 GLUT4myc myoblasts depending on the mode of macrophage activation. According to this study, PA activated macrophage blocked 2D-glucose uptake and significantly down regulated GLUT4 translocation. In contrast, LPS activated macrophage, improved 2D-Glucose uptake and promoted GLUT4 translocation, which aligns with the observations of this thesis (Samokhvalov et al., 2009). Indeed, the plasticity and heterogeneity of macrophage phenotypes extends beyond the many subsets of M2 macrophage, to the M1 phenotype whose environment dictates subtle nuances between M1 macrophage in other tissues in the body. Due to the role that fatty acids play in the progression of chronic muscle inflammatory disease, optimization of an M1 polarized macrophage model, potentially using a combination of IFN$\boldsymbol{\gamma}$, TNFα, PA and LPS may induce an M1-like macrophage phenotype, from which high definition, contextual and physiologically relevant data can be gathered from *in vitro* .

The metabolic health and function of skeletal muscle is dependent on an array of factors. Notably is the influence adipokines, a class of cytokines released from adipose tissue. Like skeletal muscle, inflammation in adipose tissue is a potential mechanism by which whole body metabolic homeostasis can be disrupted, with expression of inflammatory adipokines being linked in numerous *in vivo* studies (Kwon and Pessin, 2013). Anatomically, skeletal muscle and adipose tissue are in close proximity to one another, thus dysregulation in adipokine activity can have potent effects on skeletal muscle. Several adipokines such as Leptin, Resistin and Visfatin have been shown to positively regulate insulin metabolic pathways in skeletal muscle, conversely overexpression of adipokine Pref-1 has been shown *in vivo* to negatively regulate insulin metabolic pathways (Nicholson et al., 2018). Chronic inflammation in adipose tissue is mediated through the effects of a specialized subgroup of macrophage called adipose tissue macrophage (ATM), whose persistent activation can lead to the expansion of adipose tissue and a cycle of chronic low-grade inflammation which is linked to impairment of metabolic processes medium in both adipose tissue and skeletal muscle (Russo and Lumeng, 2018). Jakkawanpitak et al. demonstrated that conditioned medium from TLR2 activated macrophage elicits NF-KB activation and inflammatory cytokine secretion in 3T3-L1 adipocytes (Jakkawanpitak et al., 2020). Furthermore, hypoxia-induced inflammatory conditioned, characterised by IL-6 and

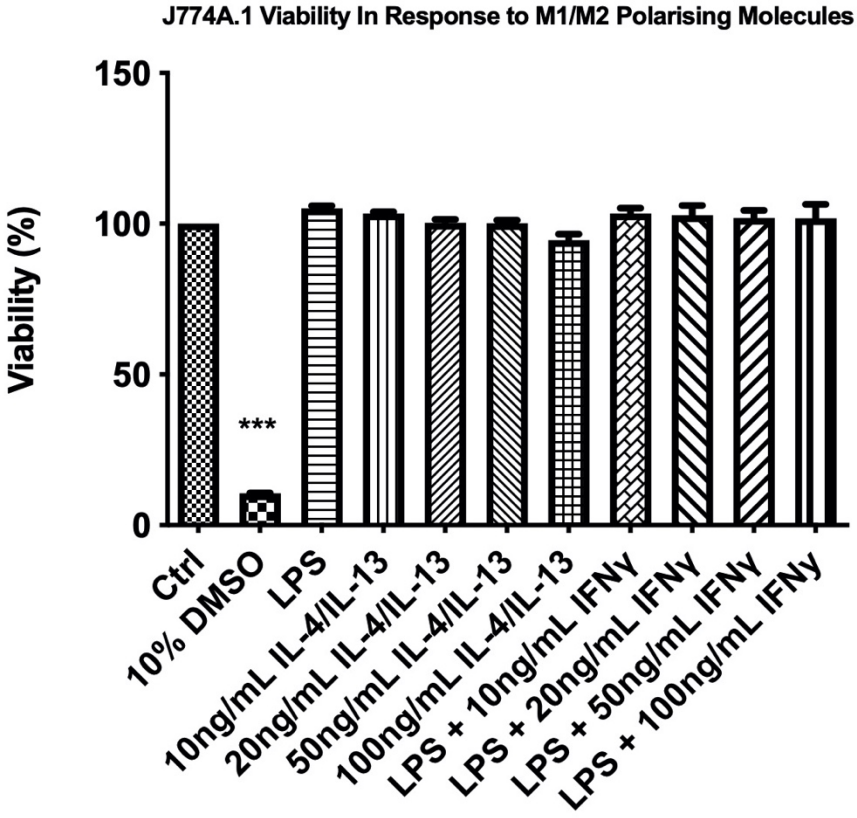
TNFα upregulation, from 3T3-L1 adipocytes was found to impair GLUT4 trafficking in C2C12-GLUT4myc myotubes (Yu et al., 2011). Indeed this does provide evidence that chronic inflammation in adipose tissue can influence crosstalk with skeletal muscle and detrimentally effect metabolic signalling. Therefore, establishment of a more complex, physiologically relevant crosstalk *in vitro* model would be required. In terms of conditioned medium, analysing the effects of hydrolysate-modulated adipocyte conditioned medium would allow us to expand our view, on how cow's milk derived hydrolysates can indirectly influence skeletal muscle metabolism. Furthermore, development of a triple co-culture method, would allow us to replicate the *in vivo* microenvironment which coordinates metabolic status in skeletal muscle, and allow us to study the influence of immunomodulatory hydrolysates in a physiologically relevant context. Triple co-culture models can be achieved with a combination of both direct co-culture and the use of trans well inserts (Noonan et al., 2019).

Rat derived L6 and L6 GLUT4myc myocytes are the principal cell line employed for studying glucose metabolic pathways in muscle cells *in vitro* (Barnes et al., 2018; Cheong et al., 2014). Conversely, the C2C12 myocyte cell line is often used in metabolic studies relating to anabolic and catabolic pathways in skeletal muscle (Marín de Mas et al., 2017). A recent publication conducted direct comparisons between the metabolic profiles of L6 and C2C12 myocytes. Abdelmoez et. al identified that genes involved in ATP processing, such as glycolysis, and glucose oxidation were significantly upregulated compared to C2C12s. In tandem, genes related to muscle tissue hypertrophy were upregulated in C2C12s and down regulated in L6s (Abdelmoez et al., 2020). Amino acid and protein supplementation is known to have a pro-anabolic effect in muscle tissue, promoting mTOR activation (Farnfield et al., 2009). However, we have observed in this thesis that hydrolysate stimulation in many cases, can detrimentally inhibit mTOR signaling via dephosphorylation of 4E-BP1. Given the implications of divergent metabolic gene expression profiles it may be necessary to conduct hydrolysate screening, and its potential effects, in the C2C12 cell model. Re-confirming observations of immune cross talk in the C2C12 model will also be required.

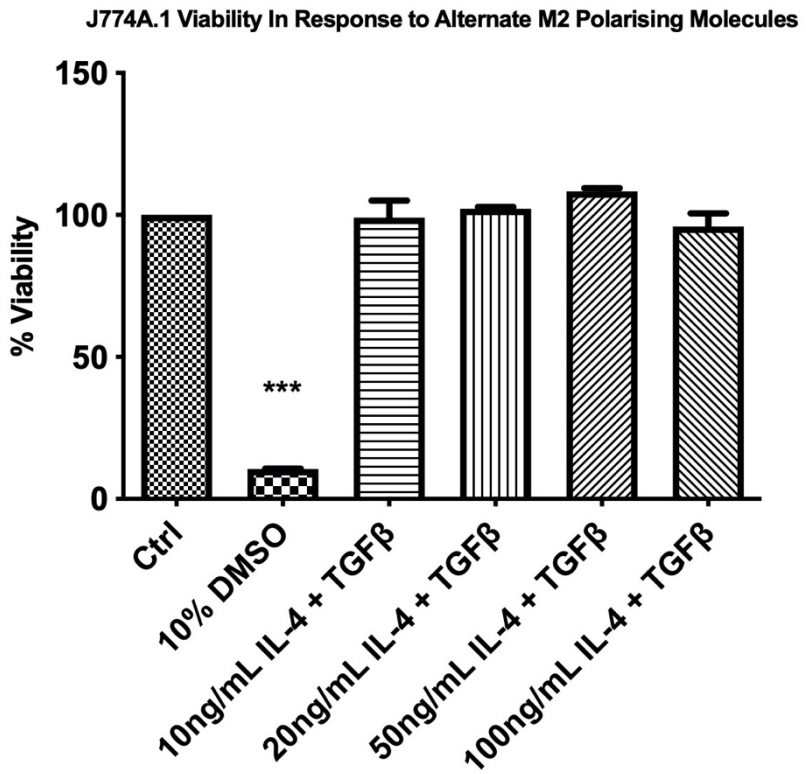
Throughout this thesis, we have identified candidate ant-inflammatory hydrolysates, that can influence skeletal muscle health *in vitro* . However, due to the desired application of these hydrolysates in reducing inflammation and promoting an M1 to M2 phenotypic shift, we have not considered the potential application of an immune boosting hydrolysate on skeletal muscle health. It has been documented that in small doses that TNFα can accelerate the healing of bone fractures (Chan et al., 2015; Glass et al., 2011). Moreover, TNFα has also been shown to drive GLUT4 translocation and wound healing in skeletal muscle (Li, 2013; Vraskou et al., 2011). Several whey derived hydrolysates, such as 2-01 for example enhanced TNFα secretion in M1 macrophage, promoted basal GLUT4 translocation, promoted 4E-BP1 signaling and promoted wound healing. This profile suggests that an immune boosting hydrolysate may have a role in accelerating muscle healing following exercise. Furthermore, the next phase of FHI funded research is examining the effect of fermented casein and whey on immune function both in the anti-inflammatory and immune boosting context. Expanding the pool of samples to those with immune boosting activity and fermented milk protein fractions, for screening in our models, we can further identify samples that can beneficially promote aspects of skeletal muscle health.

Chapter 7:

Supplementary Figures

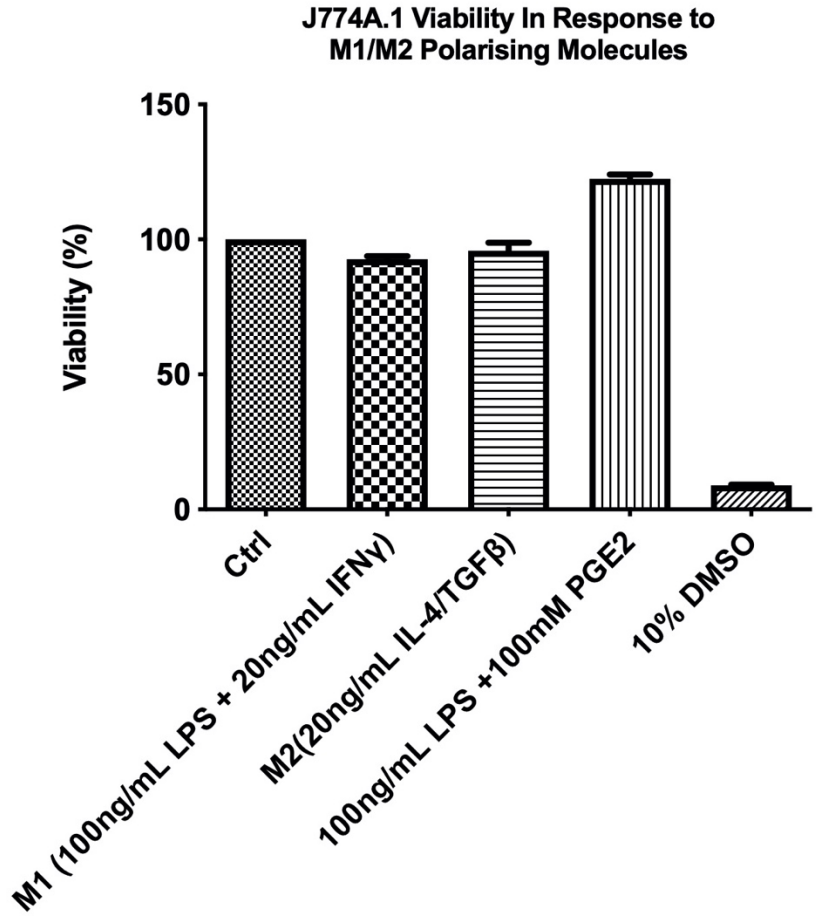


SF1.1 - M1 and M2 polarising factors do not impact J774A.1 Cell Viability: J774A.1 were stimulated with M1 polarising factors using various doses of IFNγ, IL-4 and IL-13. As a negative control DMSO was added to certain cells to induce cell death. Cells weres subsequently incubated with MTS cell titre aquos one solution for 3 hours at 37^0C Viability is represented as a percentage compared to viable, untreated cells. Data is presented as mean ± SEM of three replicates. ***p<0.001, **p<0.01, *p<0.05 comparing control, unstimulated cells vs. stimulated cells. Significance was determined using one- way ANOVA with a Newman-Keuls post-test.

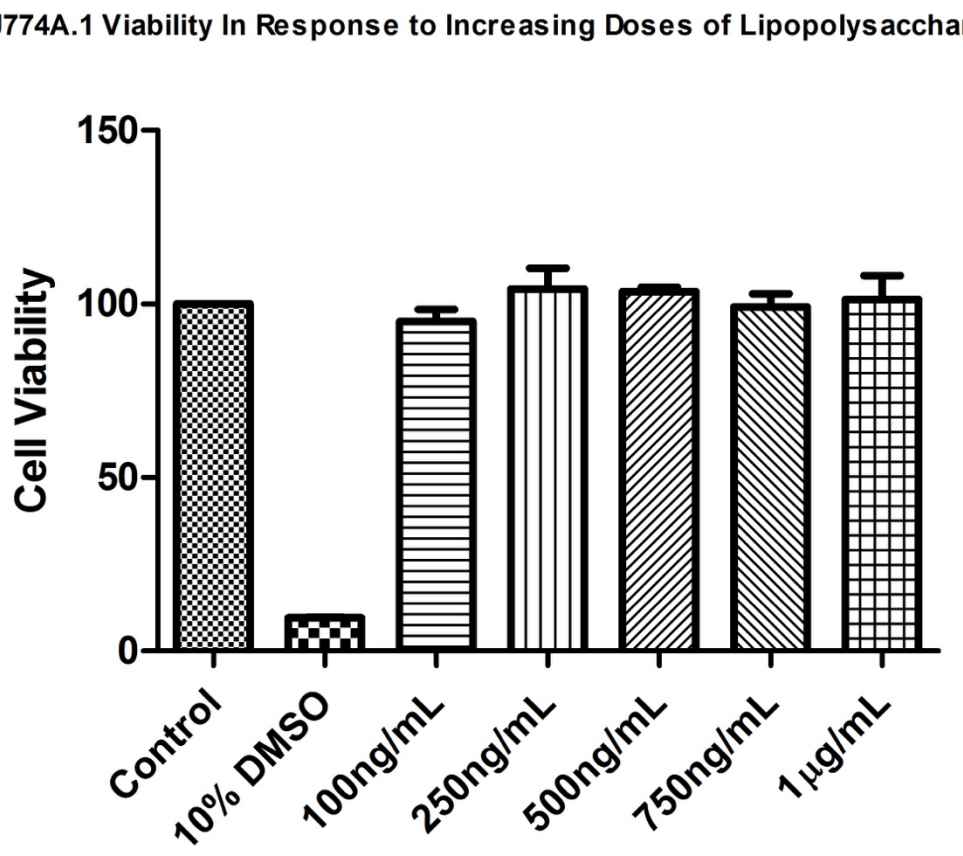


SF1.2 - IL-4 and TGFβ does not negetitvely impact on J774A.1 Macrophage cell viability

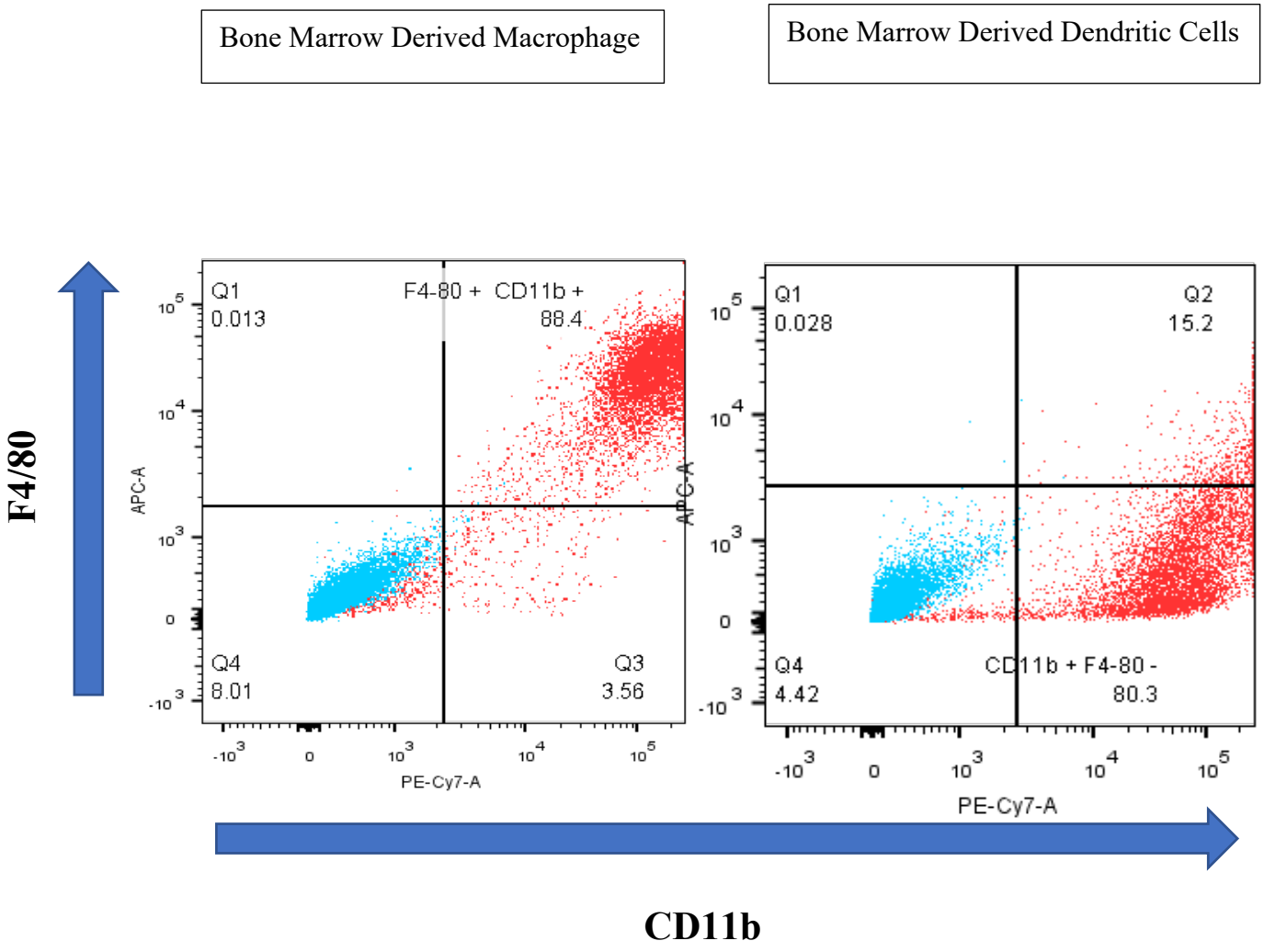
J774A.1 Macrophage were stimulated with increasing doses of IL-4 and TGFβ, ranging from 10ng/mL to 100ng/mL. J774A.1 viability was not negetively affected by treatment with increasing doses of IL-4 and TGFβ. Viability is represented as a percentage compared to viable, untreated cells. Data is presented as mean ± SEM of three replicates. ***p<0.001, **p<0.01, *p<0.05 comparing control, unstimulated cells vs. stimulated cells. Significance was determined using one- way ANOVA with a Newman-Keuls post-test.



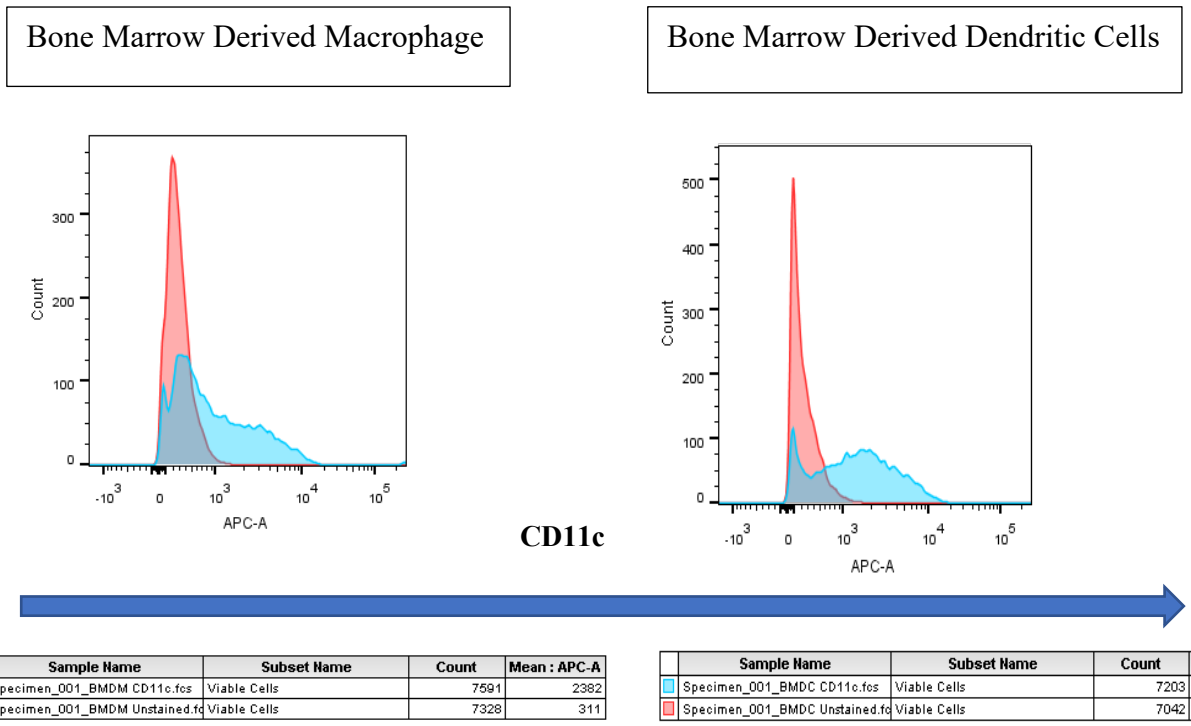
SF1.3 - Co-Stimulation with 100mM PGE2 and 100ng/mL LPS does not Negatively Impact J774A.1 Cell Viability. J774A.1 Macrophage were seeded at 1x10^6cells/mL and stimulated with M1 polarising factors 20ng/mL IFNγ and 100ng/mL LPS, M2 polarising factors 20ng/mL IL-4 and 20ng/mL TGFβ , and 100mM PGE2 and 100ng/mL LPS for 24hrs at 37°C in 5% CO_2. As a negative control, DMSO was added to specific cells to induce cell death. Cells weres subsequently incubated with MTS cell titre aquos one solution for 3 hours at 37^{0}C . Viability is represented as a percentage compared to viable, untreated cells. Data is presented as mean ± SEM of three replicates.



SF1.4- Increasing doses of LPS do not negetively on J774A.1 Macrophage Viability J774A.1 Macrophage were stimulated with increasing doses of LPS, ranging from 100ng/mL to 1μg/mL. J774A.1 viability was not negetively affected by treatment with increasing doses of LPS. Viability is represented as a percentage compared to viable, untreated cells. Data is presented as mean ± SEM of three replicates.



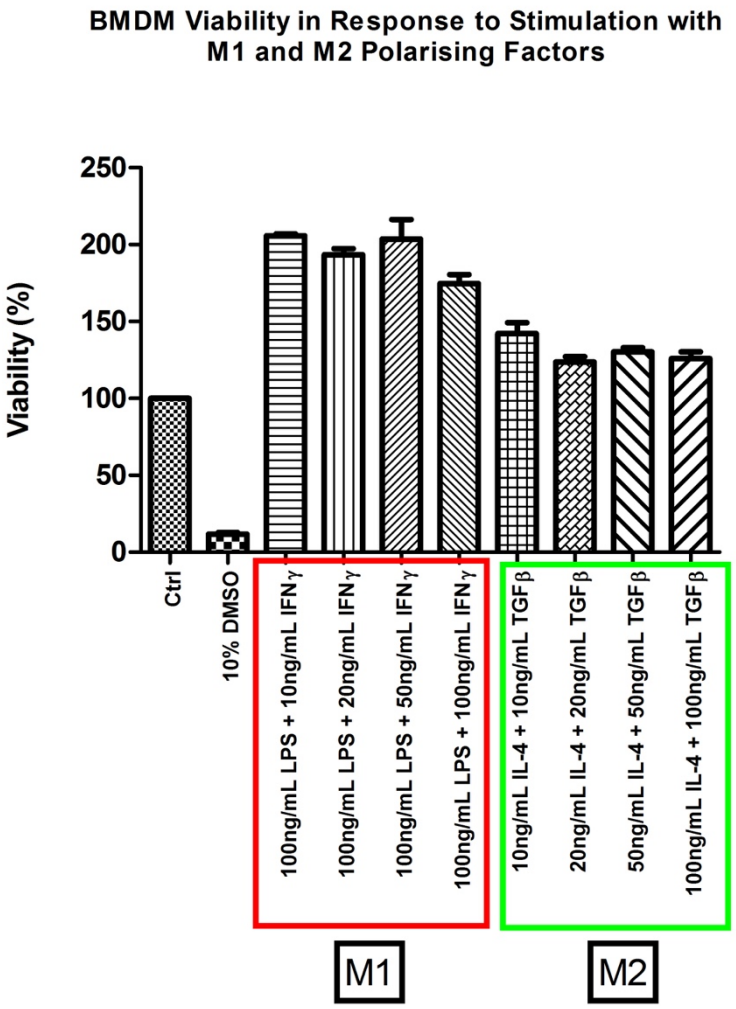
SF1.5 - Isolated Bone Marrow Derived Macrophage Express Key Surface Markers of the Macrophage Lineage F4/80 and CD11b Bone marrow was isolate from 6-8 week-old Balb/C female mice as previously described. Macrophage were cultured in the presence of 25ng/mL M-CSF and Dendritic cells were cultured in the presence of 50ng/mL GM-CSF. Cultured BMDMs were fluorescently labelled for flowcytometry as previously described. Both BMDMs and BMDCs express comparable CD11b. F4/80, a key macrophage marker is only present on the cells cultured in 25ng/mL M-CSF, a key growth factor required for macrophage proliferation and differentiation. Red cells correspond to those stained with specific antibodies, and blue corresponds to those that are unstained.



	Sample Name	Subset Name	Count	Mean : APC-A
	Specimen_001_BMDM CD11c.fcs	Viable Cells	7591	2382
	Specimen_001_BMDM Unstained.fc	Viable Cells	7328	311

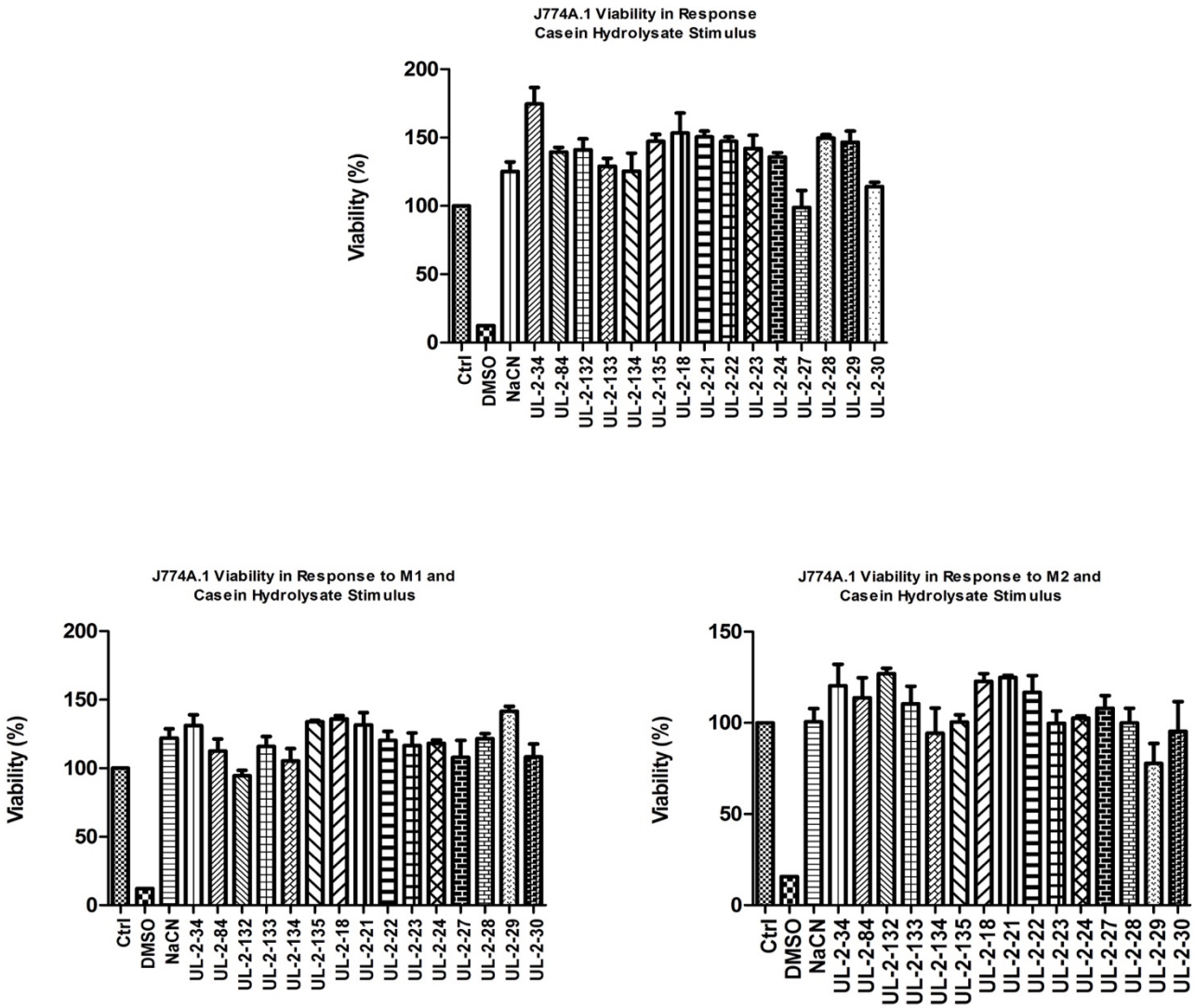
	Sample Name	Subset Name	Count	Mean : APC-A
	Specimen_001_BMDC CD11c.fcs	Viable Cells	7203	2663
	Specimen_001_BMDC Unstained.fc	Viable Cells	7042	262

SF1.6 - Isolated Bone Marrow Derived Macrophage Express differential levels of key Dendritic cell marker CD11c Bone marrow was isolate from 6-8 week-old Balb/C female mice as previously described. Macrophage were cultured in the presence of 25ng/mL M-CSF and Dendritic cells were cultured in the presence of 50ng/mL GM-CSF. Cultured BMDMs were fluorescently labelled for flowcytometry as previously described. Both BMDMs and BMDCs express CD11c. However there a greater proportion of the Dendritic cells population expressing CD11c compared to the macrophage population. Blue cells correspond to those stained with specific antibodies, and red corresponds to those that are unstained.

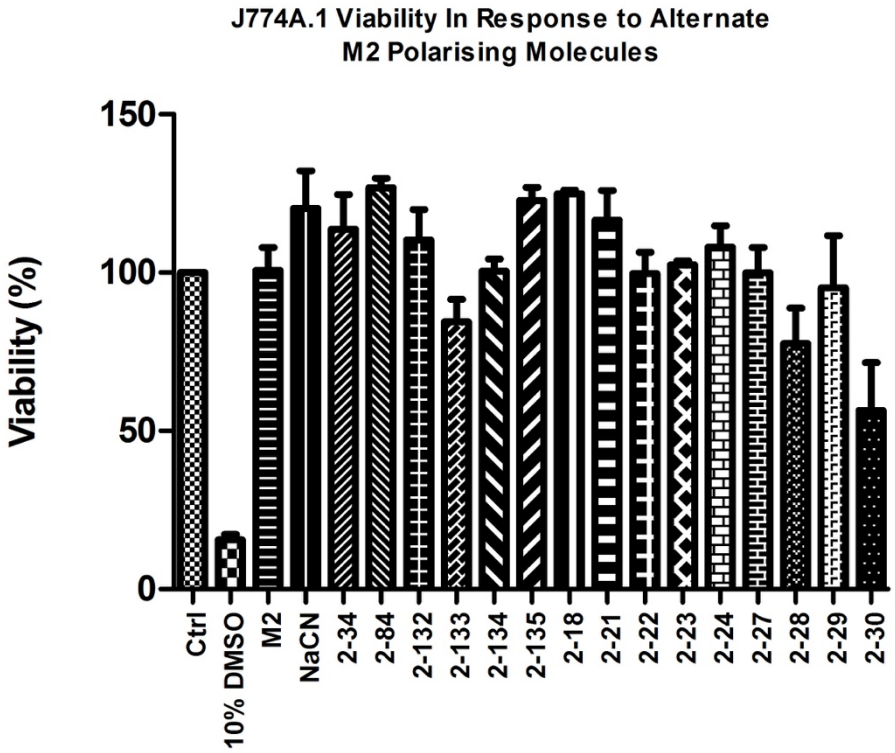


SF1.7 - Varying doses of IFNγ, IL-4 and TGFβ do not negatively impact of BMDM viability

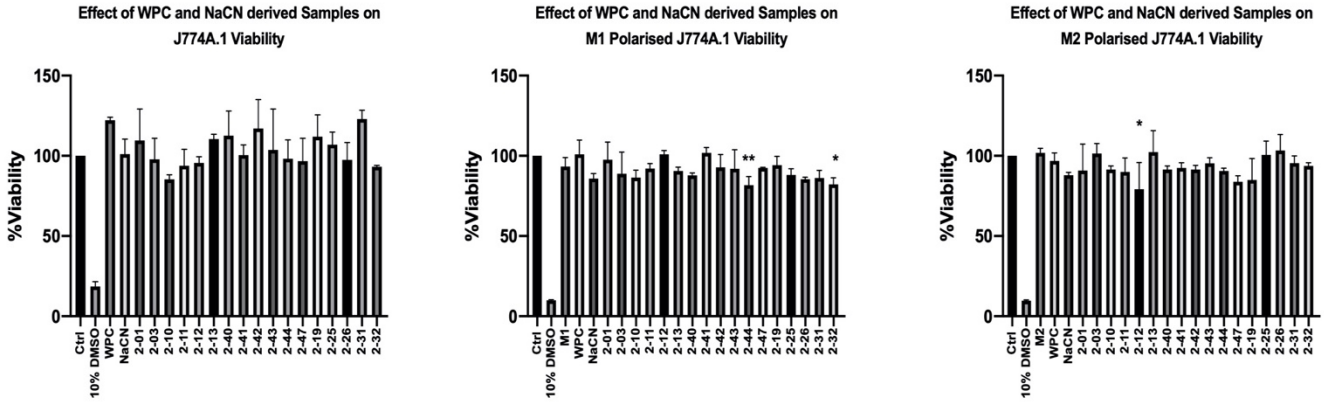
BMDMs were stimulated with M1 and M2 polarising factors at various doses of IFNγ, L IL-4 and TGFβ, ranging from 10ng/mL to 100ng/mL. BMDM viability was not negetively affected by treatment with polarising molecules. Viability is represented as a percentage compared to viable, untreated cells. Data is presented as mean ± SEM of three replicates.



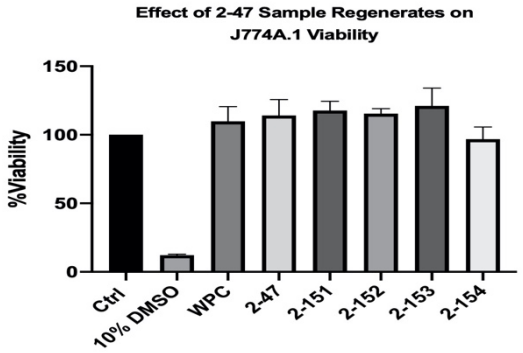
SF1.8 J774A.1 Murine Macrophage viability is not negatively impacted by hydrolysate stimulation in the presence and absence of M1 and M2 polarising factors. J774A.1 murine macrophage were stimulated with M1 polarising factors 20ng/mL IFNγ and 100ng/mL LPS and M2 polarising factors 20ng/mL IL-4 and 20ng/mL IL-13 in the presence and absence of 1mg/mL casein derived hydrolysate and whole protein contorl NaCN. As a negative control DMSO was added to certain cells to induce cell death. Cells weres subsequently incubated with MTS cell titre aquos one solution for 3 hours at 37^0C , in order to assess whether samples possessed cytotoxic properties. Viability is represented as a percentage compared to viable, untreated cells. Data is presented as mean $\pm$ SEM of three replicates.

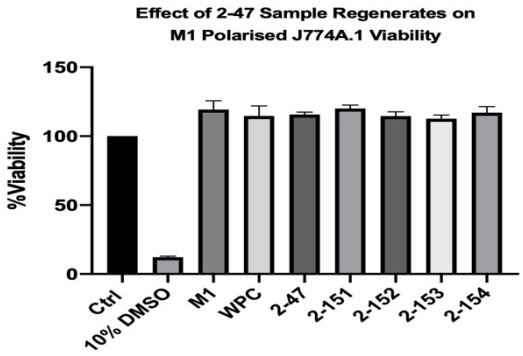


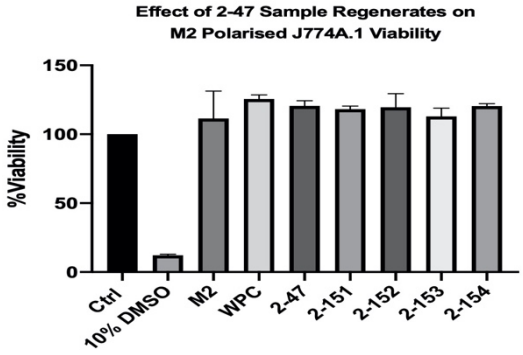
SF1.9 - J774A.1 Murine Macrophage viability is not negatively impacted my hydrolysate stimulation in the presence and absence M2 polarising factors. J774A.1 murine macrophage were stimulated with M2 polarising factors 20ng/mL IL-4 and TGFβ in the presence and absence of 1mg/mL casein derived hydrolysate and whole protein control (NaCN). As a negative control, 10% DMSO was used to induce cell death. Viability is represented as a percentage compared to viable, untreated cells. Data is presented as mean ± SEM of three replicates.



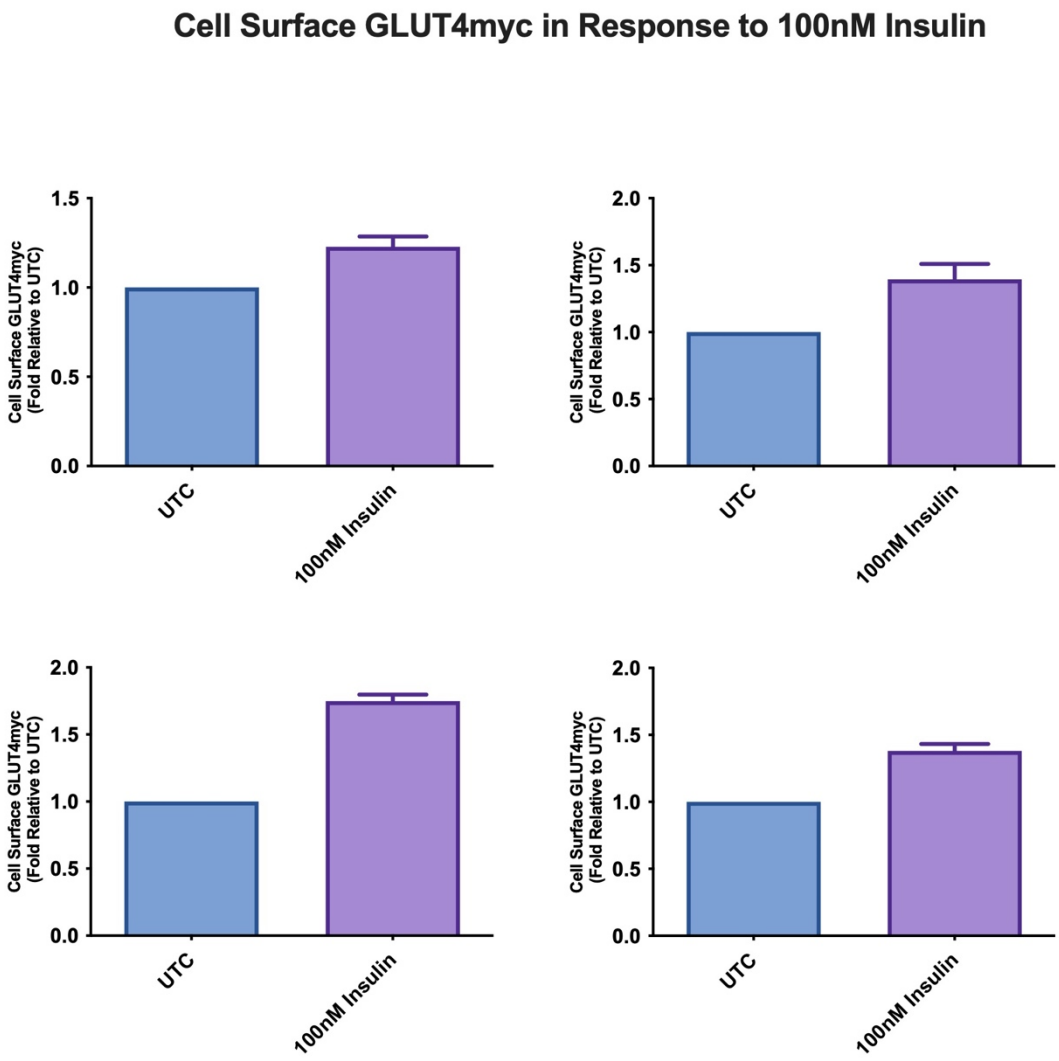
SF1.10 - J774A.1 Murine Macrophage viability is not negatively impacted by casein and whey protein hydrolysate stimulation in the presence and absence of M1 and M2 polarising factors. J774A.1 murine macrophage were stimulated with M1 polarising factors 20ng/mL IFNγ and 100ng/mL LPS and M2 polarising factors 20ng/mL IL-4 and 20ng/mL IL-13 in the presence and absence of 1mg/mL casein derived hydrolysate and whole protein contorl NaCN. As a negative control DMSO was added to certain cells to induce cell death. Cells weres subsequently incubated with MTS cell titre aquos one solution for 3 hours at 37^0C , in order to assess whether samples possessed cytotoxic properties. Viability is represented as a percentage compared to viable, untreated cells. Data is presented as mean $\pm$ SEM of three replicates. ***p<0.001, **p<0.01, *p<0.05 comparing unstimulated cells vs. hydrolysate stimulated cells. Significance was determined using one-way ANOVA with a Newman-Keuls post-test.



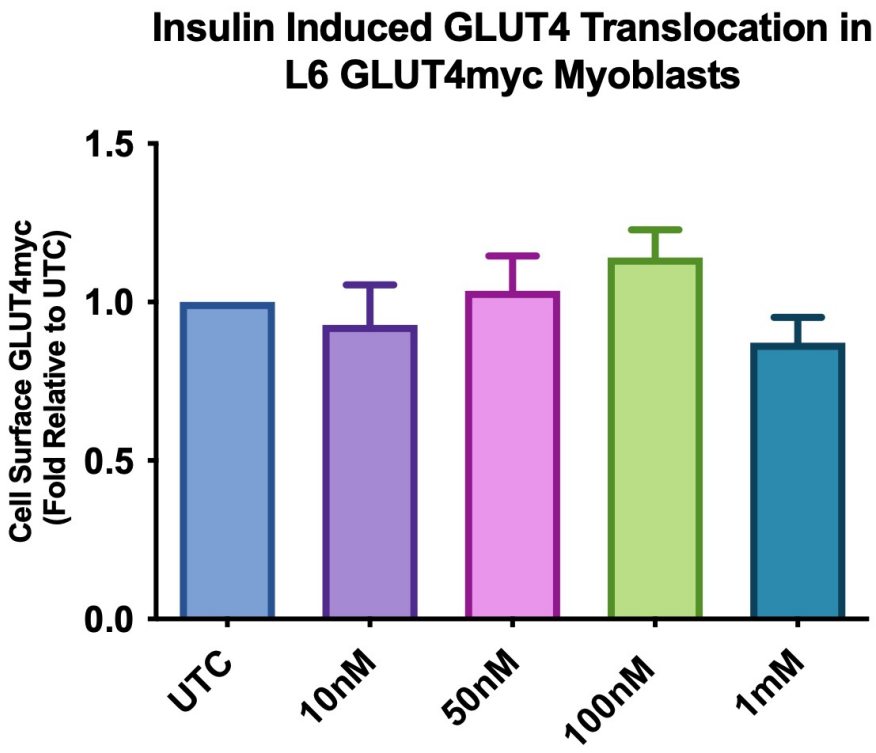




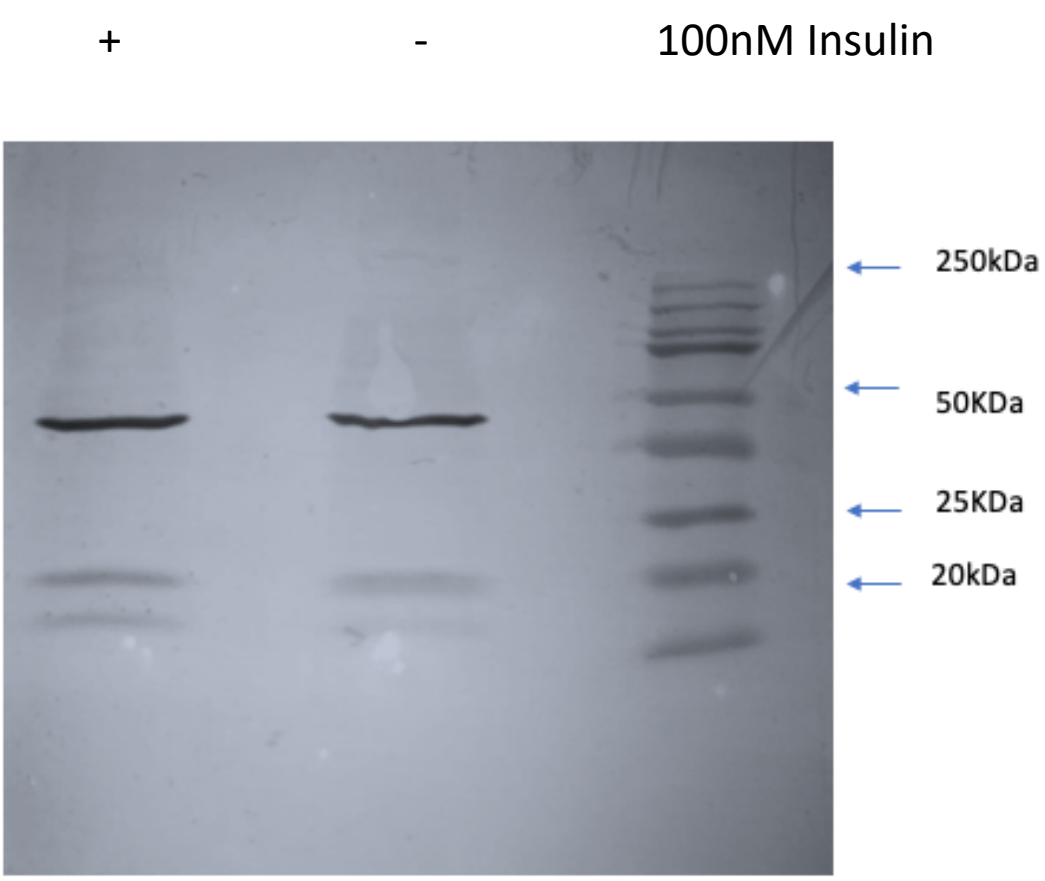
SF1.11 - Whey Protein (WPC) derived hydrolysates 2-47 and its regenerates do not negatively affect polarised J774A.1 Viability J774A.1 murine macrophage were stimulated with M1 polarising factors 20ng/mL IFNγ and 100ng/mL LPS and M2 polarising factors 20ng/mL IL-4 and 20ng/mL TGFβin the presence and absence of 1mg/mL Whey Protein (WPC) derived hydrolysates 2-47 and its regenerates. As a negative control DMSO was added to certain cells to induce cell death. Cells weres subsequently incubated with MTS cell titre aquos one solution for 3 hours at 37^0C , in order to assess whether samples possessed cytotoxic properties. Viability is represented as a percentage compared to viable, untreated cells. Data is presented as mean ± SEM of three replicates. ***p<0.001, **p<0.01, *p<0.05 comparing unstimulated cells vs. hydrolysate stimulated cells. Significance was determined using one-way ANOVA with a Newman-Keuls post-test.



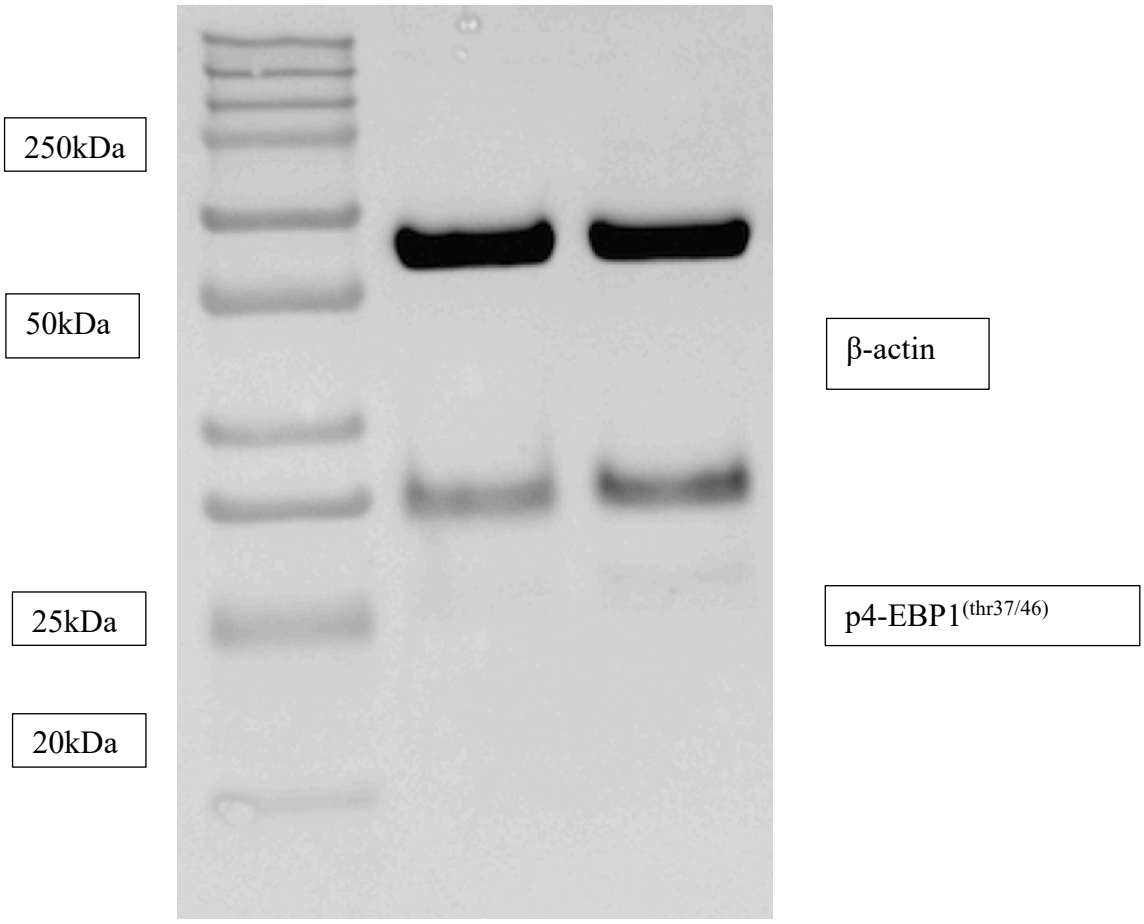
SF1.12 - 100nM Insulin stimulation leads to varied response in cell surface GLUT4myc in a 96 well plate format of the GLUT4 translocation assay. L6 GLUT4myc myoblasts were seeded at $8x10^4$cells/mL and cultured to confluence. Cells were incubated with 100nM insulin for 20 minutes. Cell surface GLUT4myc was quantified as previously described. Changes in cell surface GLUT4myc are expressed as a fold change relative to the untreated, basal (UTC) control. Data is presented as mean ± SEM of three replicates. ***p<0.001, **p<0.01, *p<0.05 comparing UTC to treated conditions. Significance was determined using one- way ANOVA with a Newman-Keuls post-test.



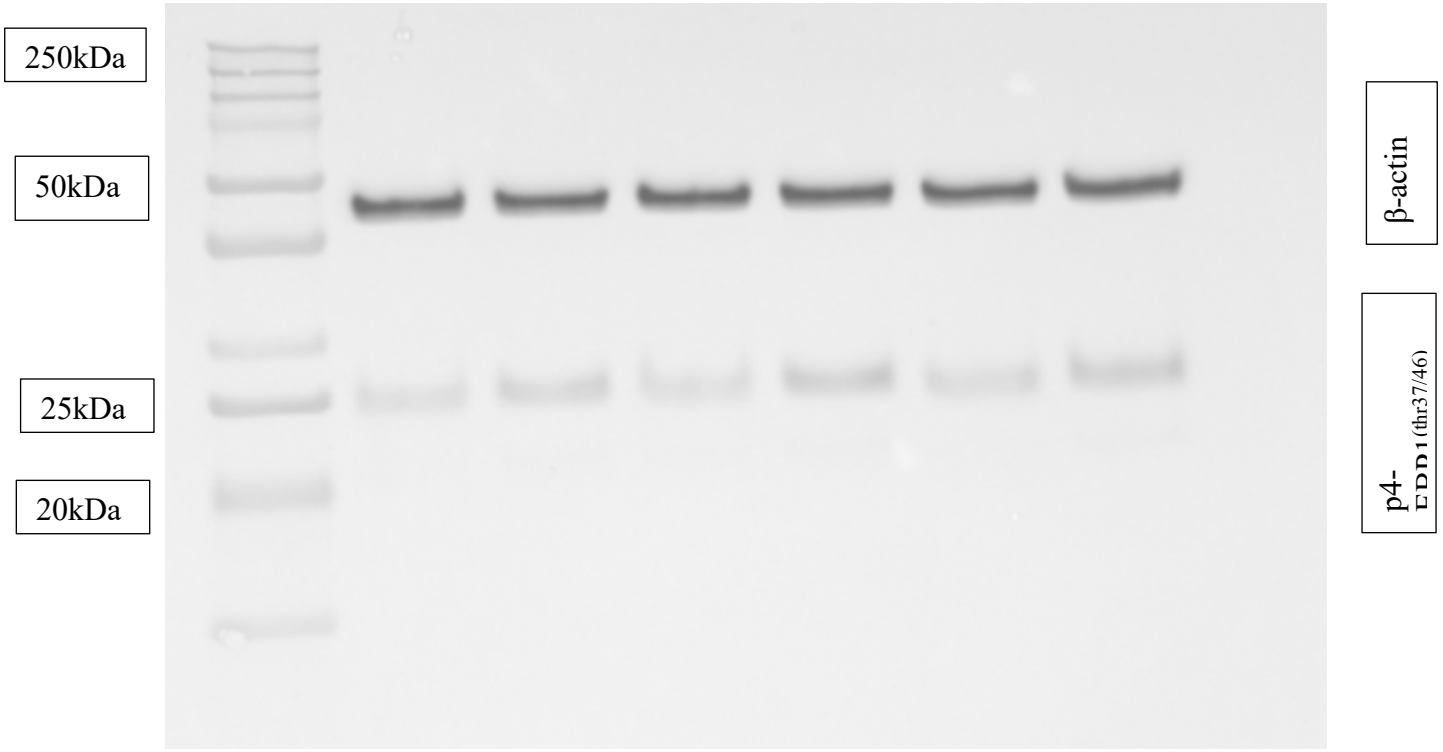
SF1.13 Insulin fails to induce a significant change in cell surface GLUT4 in L6 GLUT4myc Myoblasts in a dose dependant manner L6 GLUT4myc myoblasts were seeded in 24 well plates at $8x10^4$cells/mL and grown to confluence. Cells were subsequently starved in serum free αMEM cell culture medium for 3 hours at 37°C in 5% CO_2. Cells were then stimulated with 10nM, 50nM, 100nM, 1μM and 2μM Bovine Insulin for 20 minutes at 37°C in 5% CO_2. Cell surface GLUT4myc was then assessed as previously described. Data is presented as mean ± SEM of three replicates. Data is presented as mean ± SEM of three replicates. ***p<0.001, **p<0.01, *p<0.05 comparing UTC to treated conditions. Significance was determined using one- way ANOVA with a Newman-Keuls post-test



SF1.14 100nM Insulin Stimulates 4EBP1 phosphorylation in L6 Myotubes L6 myoblasts were seeded at $4x10^4$cells/mL and cultured at 37°C in 5% CO_2. Confluent myoblasts were differentiated into myotubes as previously described. Following immunoblotting with specific antibodies against β-actin (loading control) and p-4EBP1$^{(Thr37/46)}$**.** Following staining with specific secondary antibodies, the nitrocellulose membrane was incubated with a TMB western blot substrate for 2 minutes. Images were captured using a digital camera on a lighted background.

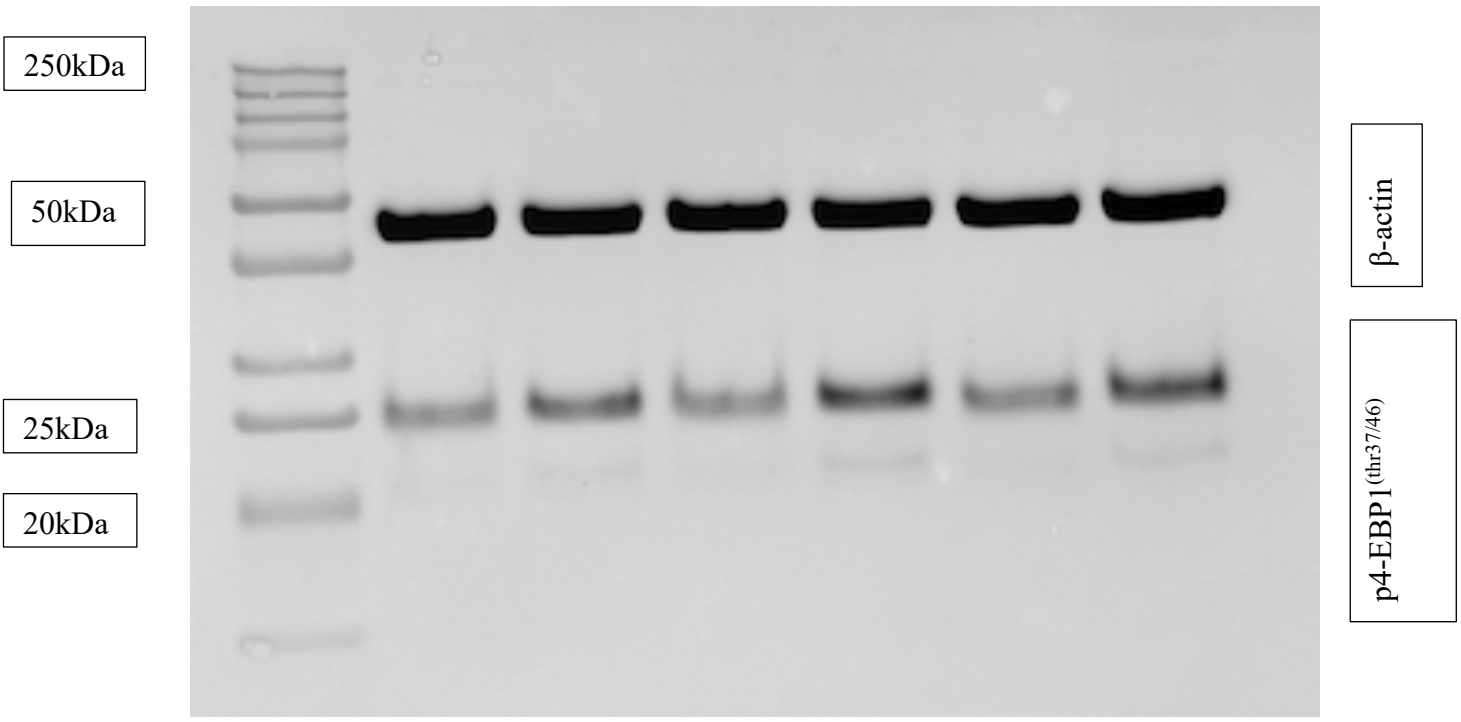


SF1.14 - Detection of phospho-4EBP1 in L6 Myotubes using a chemi-luminescent substrate L6 myoblasts were seeded at $4x10^4$cells/mL and cultured at 37°C in 5% CO_2. Confluent myoblasts were differentiated into myotubes as previously described. Following staining with specific secondary antibodies, the nitrocellulose membrane was incubated with a chemi-luminescent ECL western blot substrate for 2 minutes. Blot images were captured using a G-Box with a 5 minute exposure time.



Insulin	-	+	-	+	-	+
NaCN	-	-	+	+	-	-
WPC	-	-	-	-	+	+

SF1.16 Exposure times dictate relative intensity of signal observable in Western Blot, 1-minute exposure time L6 myoblasts were seeded at 4x10^{4}cells/mL. Confluent myoblasts were differentiated into myotubes as previously described. Cells were incubated with 1mg/mL of whole casein (NaCN) and whey (WPC) protein. Following immunoblotting with specific antibodies against β-actin (loading control) and p-4EBP1$^{(Thr37/46)}$**.** Following staining with specific secondary antibodies, the nitrocellulose membrane was incubated with a chemi-luminescent ECL western blot substrate for 2 minutes. Blot images were captured using a G-Box.



Insulin	-	+	-	+	-	+
NaCN	-	-	+	+	-	-
WPC	-	-	-	-	+	+

SF1.17 Exposure times dictate relative intensity of signal observable in Western Blot - 5 minute exposure time L6 myoblasts were seeded at 4x10^{4}cells/mL. Confluent myoblasts were differentiated into myotubes as previously described. Cells were incubated with 1mg/mL of whole casein (NaCN) and whey (WPC) protein. Following immunoblotting with specific antibodies against β-actin (loading control) and p-4EBP1$^{(Thr37/46)}$**.** Following staining with specific secondary antibodies, the nitrocellulose membrane was incubated with a chemi-luminescent ECL western blot substrate for 2 minutes. Blot images were captured using a G-Box.

Chapter 8:

Bibliography

Abdelmoez, A.M., Puig, L.S., Smith, J.A.B., Gabriel, B.M., Savikj, M., Dollet, L., Chibalin, A. V., Krook, A., Zierath, J.R., Pillon, N.J., 2020. Comparative profiling of skeletal muscle models reveals heterogeneity of transcriptome and metabolism. Am. J. Physiol. - Cell Physiol. 318, C615–C626. https://doi.org/10.1152/ajpcell.00540.2019

Adams, R.L., Broughton, K.S., 2016. Insulinotropic Effects of Whey: Mechanisms of Action, Recent Clinical Trials, and Clinical Applications. Ann. Nutr. Metab. 69, 56–63. https://doi.org/10.1159/000448665

Altan-Bonnet, G., Mukherjee, R., 2019. Cytokine-mediated communication: a quantitative appraisal of immune complexity. Nat. Rev. Immunol. 19, 205–217. https://doi.org/10.1038/s41577-019-0131-x

Alturki, M., Beyer, I., Mets, T., Bautmans, I., 2018. Impact of drugs with anti-inflammatory effects on skeletal muscle and inflammation: A systematic literature review. Exp. Gerontol. 114, 33–49. https://doi.org/10.1016/j.exger.2018.10.011

Álvarez-Rodríguez, L., López-Hoyos, M., Muñoz-Cacho, P., Martínez-Taboada, V.M., 2012. Aging is associated with circulating cytokine dysregulation. Cell. Immunol. 273, 124–132. https://doi.org/10.1016/j.cellimm.2012.01.001

Arango Duque, G., Descoteaux, A., 2014. Macrophage Cytokines: Involvement in Immunity and Infectious Diseases. Front. Immunol. 5, 1–12. https://doi.org/10.3389/fimmu.2014.00491

Arnold, L., Henry, A., Poron, F., Baba-Amer, Y., van Rooijen, N., Plonquet, A., Gherardi, R.K., Chazaud, B., 2007. Inflammatory monocytes recruited after skeletal muscle injury switch into antiinflammatory macrophages to support myogenesis. J. Exp. Med. 204, 1057–1069. https://doi.org/10.1084/jem.20070075

Atherton, P.J., Kumar, V., Selby, A.L., Rankin, D., Hildebrandt, W., Phillips, B.E., Williams, J.P., Hiscock, N., Smith, K., 2017. Enriching a protein drink with leucine augments muscle protein synthesis after resistance exercise in young and older men. Clin. Nutr. 36, 888–895. https://doi.org/10.1016/j.clnu.2016.04.025

Atsunori Ueyama, Karan L. Yaworsky, Qinghua Wang, Yousuke Ebina, A.K., 1999. GLUT4-myc ectopic expression in L6 myoblasts generates a GLUT-4-specific pool conferring insulin sensitivity. Am. J. Physiol. Endocrinol. Metab. 40, E572–E578. https://doi.org/10.1016/0009-8981(71)90060-X

Barnes, T., Di Sebastiano, K.M., Vlavcheski, F., Quadrilatero, J., Tsiani, E.L., Mourtzakis, M., 2018. Glutamate increases glucose uptake in L6 myotubes in a concentration- and time-dependent manner that is mediated by AMPK. Appl. Physiol. Nutr. Metab. 43, 1307–1313. https://doi.org/10.1139/apnm-2018-0174

Barroso, G.C., Thiele, E.S., 2011. MUSCLE INJURIES IN ATHLETES. Rev. Bras. Ortop. (English Ed. 46, 354–358. https://doi.org/10.1016/S2255-4971(15)30245-7

BÉDARD, S., MARCOTTE, B., MARETTE, A., 1997. Cytokines modulate glucose transport in skeletal muscle by inducing the expression of inducible nitric oxide synthase. Biochem. J. 325, 487–493. https://doi.org/10.1042/bj3250487

Bibby, B.M., Jensen, J., Madsen, K., Hansen, M., Bangsbo, J., 2015. Effect of Whey Protein Hydrolysate on Performance and Recovery of Top-Class Orienteering Runners. Int. J. Sport Nutr. Exerc. Metab. 25, 97–109.

Bird, L., 2016. Macrophages: Macrophage muscle man. Nat. Rev. Immunol. 16, 720–721. https://doi.org/10.1038/nri.2016.133

Blandizzi, C., Gionchetti, P., Armuzzi, A., Caporali, R., Chimenti, S., Cimaz, R., Cimino, L., Lapadula, G., Lionetti, P., Marchesoni, A., Marcellusi, A., Mennini, F.S., Salvarani, C., Girolomoni, G., 2014. The Role of Tumour Necrosis Factor in the Pathogenesis of Immune-Mediated Diseases. Int. J. Immunopathol. Pharmacol. 27, 1–10. https://doi.org/10.1177/03946320140270S101

Blobe, G.C., Schiemann, W.P., Lodish, H.F., 2002. Role of Transforming Growth Factor β in Human Disease. N. Engl. J. Med. 342, 1350–1358. https://doi.org/10.1056/nejm200005043421807

Bodine, S.C., Stitt, T.N., Gonzalez, M., Kline, W.O., Stover, G.L., Bauerlein, R., Zlotchenko, E., Scrimgeour, A., Lawrence, J.C., Glass, D.J., Yancopoulos, G.D., 2001. Akt/mTOR pathway is a crucial regulator of skeletal muscle hypertrophy and can prevent muscle atrophy in vivo. Nat. Cell Biol. 3, 1014–1019. https://doi.org/10.1038/ncb1101-1014

Borack, M.S., Reidy, P.T., Husaini, S.H., Markofski, M.M., Deer, R.R., Richison, A.B., Lambert, B.S., Cope, M.B., Mukherjea, R., Jennings, K., Volpi, E., Rasmussen, B.B., 2016. Soy-Dairy Protein Blend or Whey Protein Isolate Ingestion Induces Similar Postexercise Muscle Mechanistic Target of Rapamycin Complex 1 Signaling and Protein Synthesis Responses in Older Men. J. Nutr. 146, 2468–2475. https://doi.org/10.3945/jn.116.231159

Bosurgi, L., Manfredi, A.A., Rovere-Querini, P., 2011. Macrophages in injured skeletal muscle: A perpetuum mobile causing and limiting fibrosis, prompting or restricting resolution and regeneration. Front. Immunol. 2, 1–10. https://doi.org/10.3389/fimmu.2011.00062

Bouzakri, K., Plomgaard, P., Krogh-Madsen, R., Pedersen, B.K., Zierath, J., 2005. TNF-alpha induces skeletal muscle insulin resistance in healthy human subjects via inhibition of AS160 phosphorylation. Ann. Endocrinol. (Paris). 66, 415. https://doi.org/10.1016/S0003-4266(05)81866-9

Breen, L., Phillips, S.M., 2011. Skeletal muscle protein metabolism in the elderly : Interventions to counteract the ‘ anabolic resistance ’ of ageing. Nutr. Metab. 6, 1–11.

Brigitte, M., Schilte, C., Plonquet, A., Baba-Amer, Y., Henri, A., Charlier, C., Tajbakhsh, S., Albert, M., Gherardi, R.K., Chrétien, F., 2010. Muscle resident macrophages control the immune cell reaction in a mouse model of notexin-induced myoinjury. Arthritis Rheum. 62, 268–279. https://doi.org/10.1002/art.27183

Brouns, F., van Nieuwenhoven, M., Jeukendrup, A., van Marken Lichtenbelt, W., 2002. Functional foods and food supplements for athletes: from myths to benefit claims substantiation through the study of selected biomarkers. Br. J. Nutr. 88, S177–S186. https://doi.org/10.1079/bjn2002683

Brown, A.D., Close, G.L., Sharples, A.P., Stewart, C.E., 2017. Murine myoblast migration: influence of replicative ageing and nutrition. Biogerontology 18, 947–964. https://doi.org/10.1007/s10522-017-9735-3

Brunelli, S., Rovere-Querini, P., 2008. The immune system and the repair of skeletal muscle. Pharmacol. Res. 58, 117–121. https://doi.org/10.1016/j.phr.2008.06.008

Bryant, N.J., Govers, R., James, D.E., 2002. Regulated transport of the glucose transporter GLUT4. Nat. Rev. Mol. Cell Biol. 3, 267–277. https://doi.org/10.1038/nrm782

Budi, E.H., Muthusamy, B.-P., Derynck, R., 2015. The insulin response integrates increased TGF-β signaling through Akt-induced enhancement of cell surface delivery of TGF-β receptors. Sci. Signal. 8, ra96–ra96. https://doi.org/10.1126/scisignal.aaa9432

Bunchorntavakul, C., Reddy, K.R., 2020. Review article: malnutrition/sarcopenia and frailty in patients with cirrhosis. Aliment. Pharmacol. Ther. 51, 64–77. https://doi.org/10.1111/apt.15571

Burzyn, D., Kuswanto, W., Kolodin, D., Shadrach, J.L., Cerletti, M., Jang, Y., Sefik, E., Tan, T.G., Wagers, A.J., Benoist, C., Mathis, D., 2013. A Special Population of regulatory T Cells Potentiates muscle repair. Cell 155, 1282–1295. https://doi.org/10.1016/j.cell.2013.10.054

Calder, P.C., Kew, S., 2018. The immune system : a target for functional foods ? https://doi.org/10.1079/BJN2002682

Carey, A.L., Steinberg, G.R., Macaulay, S.L., Thomas, W.G., Holmes, A.G., Ramm, G., Prelovsek, O., Hohnen-Behrens, C., Watt, M.J., James, D.E., Kemp, B.E., Pedersen, B.K., Febbraio, M.A., 2006. Interleukin-6 increases insulin-stimulated glucose disposal in humans and glucose uptake and fatty acid oxidation in vitro via AMP-activated protein kinase. Diabetes 55, 2688–2697. https://doi.org/10.2337/db05-1404

Cartee, G.D., Hepple, R.T., Bamman, M.M., Zierath, J.R., 2016. Exercise Promotes Healthy Aging of Skeletal Muscle. Cell Metab. 23, 1034–1047. https://doi.org/10.1016/j.cmet.2016.05.007

Chan, J.K., Glass, G.E., Ersek, A., Freidin, A., Williams, G.A., Gowers, K., Espirito Santo, A.I., Jeffery, R., Otto, W.R., Poulsom, R., Feldmann, M., Rankin, S.M., Horwood, N.J., Nanchahal, J., 2015. Low-dose TNF augments fracture healing in normal and osteoporotic bone by up-regulating the innate immune response. EMBO Mol. Med. 7, 547–561. https://doi.org/10.15252/emmm.201404487

Chang, Y.H., Ho, K.T., Lu, S.H., Huang, C.N., Shiau, M.Y., 2012. Regulation of glucose/lipid metabolism and insulin sensitivity by interleukin-4. Int. J. Obes. 36, 993–998. https://doi.org/10.1038/ijo.2011.168

Chanon, S., Durand, C., Vieille-Marchiset, A., Robert, M., Dibner, C., Simon, C., Lefai, E., 2017. Glucose Uptake Measurement and Response to Insulin Stimulation in In vitro Cultured Human Primary Myotubes. J. Vis. Exp. 2017, 1–7. https://doi.org/10.3791/55743

Chaplin, D.D., 2010. Overview of the Immune Response. J. Allergy Clin. Immunol. 125, 826–828. https://doi.org/10.1016/j.jaci.2009.12.980.Overview

Chazaud, B., 2016. Inflammation during skeletal muscle regeneration and tissue remodeling-application to exercise-induced muscle damage management. Immunol. Cell Biol. 94, 140–145. https://doi.org/10.1038/icb.2015.97

Chen, L., Tredget, E.E., Wu, P.Y.G., Wu, Y., Wu, Y., 2008. Paracrine factors of mesenchymal stem cells recruit macrophages and endothelial lineage cells and enhance wound healing. PLoS One 3. https://doi.org/10.1371/journal.pone.0001886

Cheong, S.H., Furuhashi, K., Ito, K., Nagaoka, M., Yonezawa, T., Miura, Y., Yagasaki, K., 2014. Daidzein promotes glucose uptake through glucose transporter 4 translocation to plasma membrane in L6 myocytes and improves glucose homeostasis in Type 2 diabetic model mice. J. Nutr. Biochem. 25, 136–143. https://doi.org/10.1016/j.jnutbio.2013.09.012

Chiba, K., Tsuchiya, M., Koide, M., Hagiwara, Y., Sasaki, K., Hattori, Y., Watanabe, M., Sugawara, S., Kanzaki, M., Endo, Y., 2015. Involvement of IL-1 in the Maintenance of Masseter Muscle Activity and Glucose Homeostasis. PLoS One 10, e0143635. https://doi.org/10.1371/journal.pone.0143635

Choo, H.-J., Canner, J.P., Vest, K.E., Thompson, Z., Pavlath, G.K., 2017. A tale of two niches: differential functions for VCAM-1 in satellite cells under basal and injured conditions. Am. J. Physiol. Physiol. 313, C392–C404. https://doi.org/10.1152/ajpcell.00119.2017

Cogan, K.E., 2018. Identification of bioactive milk-derived protein hydrolysates and investigation of effects on postprandial glycemia and recovery from exercise in humans. Doctoral Dissertation, University College Dublin.

Cogan, K.E., Carson, B.P., Patel, B., Amigo-Benavent, M., Jakeman, P.M., Egan, B., 2019. Regulation of GLUT4 translocation in an in vitro cell model using postprandial human serum ex vivo. Exp. Physiol. 104, 800–807. https://doi.org/10.1113/EP087356

Cogan, K.E., Evans, M., Iuliano, E., Melvin, A., Susta, D., Neff, K., De Vito, G., Egan, B., 2018. Co-ingestion of protein or a protein hydrolysate with carbohydrate enhances anabolic signaling, but not glycogen resynthesis, following recovery from prolonged aerobic exercise in trained cyclists. Eur. J. Appl. Physiol. 118, 349–359. https://doi.org/10.1007/s00421-017-3775-x

Collins, L.E., 2014. Defining a Role for SNARE Proteins in Dendritic Cell Secretion. Dublin City University.

Comerford, K.B., Pasin, G., 2016. Emerging evidence for the importance of dietary protein source on glucoregulatory markers and type 2 diabetes: Different effects of dairy, meat, fish, egg, and plant protein foods. Nutrients 8. https://doi.org/10.3390/nu8080446

Connizzo, B.K., Yannascoli, S.M., Tucker, J.J., Caro, A.C., Riggin, C.N., Mauck, R.L., Soslowsky, L.J., Steinberg, D.R., Bernstein, J., 2014. The Detrimental Effects of Systemic Ibuprofen Delivery on Tendon Healing Are Time-Dependent. Clin. Orthop. Relat. Res. 472, 2433–2439. https://doi.org/10.1007/s11999-013-3258-2

Costamagna, D., Costelli, P., Sampaolesi, M., Penna, F., 2015. Role of Inflammation in Muscle Homeostasis and Myogenesis. Mediators Inflamm. 2015, 1–14. https://doi.org/10.1155/2015/805172

D'Souza, K., Mercer, A., Mawhinney, H., Pulinilkunnil, T., Udenigwe, C.C., Kienesberger, P.C., 2020. Whey Peptides Stimulate Differentiation and Lipid Metabolism in Adipocytes and Ameliorate Lipotoxicity-Induced Insulin Resistance in Muscle Cells. Nutrients 12, 425. https://doi.org/10.3390/nu12020425

Dai, Q., Zhou, D., Xu, L., Song, X., 2018. Curcumin alleviates rheumatoid arthritis-induced inflammation and synovial hyperplasia by targeting mTOR pathway in rats. Drug Des. Devel. Ther. 12, 4095–4105. https://doi.org/10.2147/DDDT.S175763

Daig, R., 2000. Human intestinal epithelial cells secrete interleukin-1 receptor antagonist and interleukin-8 but not interleukin-1 or interleukin-6. Gut 46, 350–358. https://doi.org/10.1136/gut.46.3.350

Dalle, S., Rossmeislova, L., Koppo, K., 2017. The Role of Inflammation in Age-Related Sarcopenia. Front. Physiol. 8. https://doi.org/10.3389/fphys.2017.01045

Dardevet, D., Rémond, D., Peyron, M.A., Papet, I., Savary-Auzeloux, I., Mosoni, L., 2012. Muscle wasting and resistance of muscle anabolism: The "anabolic threshold concept"

for adapted nutritional strategies during sarcopenia. Sci. World J. 2012. https://doi.org/10.1100/2012/269531

Davoodi, S.H., Shahbazi, R., Esmaeili, S., Sohrabvandi, S., Mortazavian, A., Jazayeri, S., Taslimi, A., 2016. Health-Related Aspects of Milk Proteins. Iran. J. Pharm. Res. IJPR 15, 573–591. https://doi.org/10.22037/ijpr.2016.1897

Defronzo, R.A., 2009. From the triumvirate to the ominous octet: A new paradigm for the treatment of type 2 diabetes mellitus. Diabetes 58, 773–795. https://doi.org/10.2337/db09-9028

Deldicque, L., Theisen, D., Francaux, M., 2005. Regulation of mTOR by amino acids and resistance exercise in skeletal muscle. Eur. J. Appl. Physiol. 94, 1–10. https://doi.org/10.1007/s00421-004-1255-6

Demirkapi, M., Yildizgören, M.T., Güler, H., Turhanoğlu, A.D., 2017. The effect of anti-tumor necrosis factor-alpha treatment on muscle performance and endurance in patients with ankylosing spondylitis: A prospective follow-up study. Arch. Rheumatol. 32, 309–314. https://doi.org/10.5606/ArchRheumatol.2017.6335

Dinarello, C. a, 2007. Historical insights into cytokines. Eur. J. Immunol. 37 Suppl 1, S34-45. https://doi.org/10.1002/eji.200737772

Dort, J., Fabre, P., Molina, T., Dumont, N.A., 2019. Macrophages Are Key Regulators of Stem Cells during Skeletal Muscle Regeneration and Diseases. Stem Cells Int. 2019, 1–20. https://doi.org/10.1155/2019/4761427

Dullius, A., Inês, M., Fernanda, C., Souza, V. De, 2018. Whey protein hydrolysates as a source of bioactive peptides for functional foods – Biotechnological facilitation of industrial scale-up. J. Funct. Foods 42, 58–74. https://doi.org/10.1016/j.jff.2017.12.063

Egan, B., Zierath, J.R., 2013a. Exercise metabolism and the molecular regulation of skeletal muscle adaptation. Cell Metab. 17, 162–184. https://doi.org/10.1016/j.cmet.2012.12.012

Egan, B., Zierath, J.R., 2013b. Exercise metabolism and the molecular regulation of skeletal muscle adaptation. Cell Metab. 17, 162–184. https://doi.org/10.1016/j.cmet.2012.12.012

El Sohaimy, S., 2012. Functional foods and nutraceuticals-modern approach to food science. World Appl. Sci. J. 20, 691–708. https://doi.org/10.5829/idosi.wasj.2012.20.05.66119

Fan, J., Kou, X., Yang, Y., Chen, N., 2016. MicroRNA-regulated proinflammatory cytokines in sarcopenia. Mediators Inflamm. 2016. https://doi.org/10.1155/2016/1438686

Farnfield, M., Carey, K., Gran, P., Trenerry, M., Cameron-Smith, D., 2009. Whey Protein Ingestion Activates mTOR-dependent Signalling after Resistance Exercise in Young Men: A Double-Blinded Randomized Controlled Trial. Nutrients 1, 263–275. https://doi.org/10.3390/nu1020263

Farrugia, M., Baron, B., 2016. The role of TNF-α in rheumatoid arthritis: a focus on regulatory T cells. J. Clin. Transl. Res. 2, 84–90.

Fazakerley, D.J., Holman, G.D., Marley, A., James, D.E., Stöckli, J., Coster, A.C.F., 2010. Kinetic evidence for unique regulation of GLUT4 trafficking by insulin and AMP-activated protein kinase activators in L6 myotubes. J. Biol. Chem. 285, 1653–1660. https://doi.org/10.1074/jbc.M109.051185

Ferrucci, L., Fabbri, E., 2018. Inflammageing: chronic inflammation in ageing, cardiovascular disease, and frailty. Physiol. Behav. 176, 139–148. https://doi.org/10.1016/j.physbeh.2017.03.040

Frederic Tremblay, Charles Lavigne, Helene Jacques, A.M., 2003. Dietary Cod Protein Restores Insulin-Induced Activation of Phosphatidylinositol 3-Kinase/Akt and GLUT4 Translocation to the T-Tubules in Skeletal Muscle of High-Fat–Fed Obese Rats. Diabetes 52, 29–37.

Frontera, W.R., Ochala, J., 2015. Skeletal Muscle: A Brief Review of Structure and Function. Calcif. Tissue Int. 96, 183–195. https://doi.org/10.1007/s00223-014-9915-y

George K. Michalopoulos, 2007. Liver Regeneration. J. Cell. Physiol. 2, 286–300. https://doi.org/10.1002/jcp.21172.Liver

Glass, G.E., Chan, J.K., Freidin, A., Feldmann, M., Horwood, N.J., Nanchahal, J., 2011. TNF-promotes fracture repair by augmenting the recruitment and differentiation of muscle-derived stromal cells. Proc. Natl. Acad. Sci. 108, 1585–1590. https://doi.org/10.1073/pnas.1018501108

Goetsch, K.P., Niesler, C.U., 2011. Optimization of the scratch assay for in vitro skeletal muscle wound healing analysis. Anal. Biochem. 411, 158–160. https://doi.org/10.1016/j.ab.2010.12.012

Gong, T., Liu, L., Jiang, W., Zhou, R., 2020. DAMP-sensing receptors in sterile inflammation and inflammatory diseases. Nat. Rev. Immunol. 20, 95–112. https://doi.org/10.1038/s41577-019-0215-7

Gordon, S., Taylor, P.R., 2005. Monocyte and macrophage heterogeneity. Nat. Rev. Immunol. 5, 953–964. https://doi.org/10.1038/nri1733

Goren, I., Mu, E., Schiefelbein, D., Christen, U., Pfeilschifter, J., Mu, H., Frank, S., 2007. Systemic Anti-TNF a Treatment Restores Diabetes-Impaired Skin Repair in ob / ob Mice by Inactivation of Macrophages 2259–2267. https://doi.org/10.1038/sj.jid.5700842

Guo, Q., Wang, Y., Xu, D., Nossent, J., Pavlos, N.J., Xu, J., 2018. Rheumatoid arthritis: pathological mechanisms and modern pharmacologic therapies. Bone Res. 6, 15. https://doi.org/10.1038/s41413-018-0016-9

Gylling, H., Plat, J., Turley, S., Ginsberg, H.N., Ellegård, L., Jessup, W., Jones, P.J., Lütjohann, D., Maerz, W., Masana, L., Silbernagel, G., Staels, B., Borén, J., Catapano, A.L., De Backer, G., Deanfield, J., Descamps, O.S., Kovanen, P.T., Riccardi, G., Tokgözoglu, L., Chapman, M.J., 2014. Plant sterols and plant stanols in the management of dyslipidaemia and prevention of cardiovascular disease. Atherosclerosis 232, 346–360. https://doi.org/10.1016/j.atherosclerosis.2013.11.043

Haddad, F., Zaldivar, F., Cooper, D.M., Adams, G.R., 2005. IL-6-induced skeletal muscle atrophy. J. Appl. Physiol. 98, 911–917. https://doi.org/10.1152/japplphysiol.01026.2004

Hallowell, R.W., Collins, S.L., Craig, J.M., Zhang, Y., Oh, M., Illei, P.B., Chan-Li, Y., Vigeland, C.L., Mitzner, W., Scott, A.L., Powell, J.D., Horton, M.R., 2017. MTORC2 signalling regulates M2 macrophage differentiation in response to helminth infection and adaptive thermogenesis. Nat. Commun. 8. https://doi.org/10.1038/ncomms14208

Haran, P.H., Rivas, D.A., Fielding, R.A., 2012. Role and potential mechanisms of anabolic resistance in sarcopenia. J. Cachexia. Sarcopenia Muscle 3, 157–162. https://doi.org/10.1007/s13539-012-0068-4

Hartmann, R., Meisel, H., 2007. Food-derived peptides with biological activity : from research to food applications 163–169. https://doi.org/10.1016/j.copbio.2007.01.013

Hasler, C.M., 2002. Issues and Opinions Functional Foods : Benefits , Concerns and Challenges — A Position Paper from the American Council on Science and Health 1 3772–3781.

He, C., Bassik, M.C., Moresi, V., Sun, K., Wei, Y., Zou, Z., An, Z., Loh, J., Fisher, J., Sun, Q., Korsmeyer, S., Packer, M., May, H.I., Hill, J.A., Virgin, H.W., Gilpin, C., Xiao, G., Bassel-Duby, R., Scherer, P.E., Levine, B., 2012. Exercise-induced BCL2-regulated autophagy is required for muscle glucose homeostasis. Nature 481, 511–515. https://doi.org/10.1038/nature10758

Hirano, T., 2021. IL-6 in inflammation, autoimmunity and cancer. Int. Immunol. 33, 127–148. https://doi.org/10.1093/intimm/dxaa078

Hoene, M., Weigert, C., 2008. The role of interleukin-6 in insulin resistance, body fat

distribution and energy balance. Obes. Rev. 9, 20–29. https://doi.org/10.1111/j.1467-789X.2007.00410.x

Hommelberg, P.P.H., Plat, J., Sparks, L.M., Schols, A.M.W.J., van Essen, A.L.M., Kelders, M.C.J.M., van Beurden, D., Mensink, R.P., Langen, R.C.J., 2011. Palmitate-induced skeletal muscle insulin resistance does not require NF-κB activation. Cell. Mol. Life Sci. 68, 1215–1225. https://doi.org/10.1007/s00018-010-0515-3

Hong, E.-G., Ko, H.J., Cho, Y.-R., Kim, H.-J., Ma, Z., Yu, T.Y., Friedline, R.H., Kurt-Jones, E., Finberg, R., Fischer, M.A., Granger, E.L., Norbury, C.C., Hauschka, S.D., Philbrick, W.M., Lee, C.-G., Elias, J.A., Kim, J.K., 2009. Interleukin-10 Prevents Diet-Induced Insulin Resistance by Attenuating Macrophage and Cytokine Response in Skeletal Muscle. Diabetes 58, 2525–2535. https://doi.org/10.2337/db08-1261

Huang, C., Somwar, R., Patel, N., Niu, W., Török, D., Klip, A., 2002. Sustained exposure of L6 myotubes to high glucose and insulin decreases insulin-stimulated GLUT4 translocation but upregulates GLUT4 activity. Diabetes 51, 2090–2098. https://doi.org/10.2337/diabetes.51.7.2090

Huang, S., Czech, M.P., 2007. The GLUT4 Glucose Transporter. Cell Metab. 5, 237–252. https://doi.org/10.1016/j.cmet.2007.03.006

Hunter, G.R., Singh, H., Carter, S.J., Bryan, D.R., Fisher, G., 2019. Sarcopenia and Its Implications for Metabolic Health. J. Obes. 2019. https://doi.org/10.1155/2019/8031705

Ibrahim, N., Wong, S., Mohamed, I., Mohamed, N., Chin, K.-Y., Ima-Nirwana, S., Shuid, A., 2018. Wound Healing Properties of Selected Natural Products. Int. J. Environ. Res. Public Health 15, 2360. https://doi.org/10.3390/ijerph15112360

Ikeda, S., Tamura, Y., Kakehi, S., Takeno, K., Kawaguchi, M., Watanabe, T., Sato, F., Ogihara, T., Kanazawa, A., Fujitani, Y., Kawamori, R., Watada, H., 2013. Exercise-induced enhancement of insulin sensitivity is associated with accumulation of M2-polarized macrophages in mouse skeletal muscle. Biochem. Biophys. Res. Commun. 441, 36–41. https://doi.org/10.1016/j.bbrc.2013.10.005

Iqbal, S., Kumar, A., 2016. Characterization of In vitro Generated Human Polarized Macrophages. J. Clin. Cell. Immunol. 06. https://doi.org/10.4172/2155-9899.1000380

Ishida, Y., Kuninaka, Y., Nosaka, M., Furuta, M., Kimura, A., Taruya, A., Yamamoto, H., Shimada, E., Akiyama, M., Mukaida, N., Kondo, T., 2019. CCL2-Mediated Reversal of Impaired Skin Wound Healing in Diabetic Mice by Normalization of Neovascularization and Collagen Accumulation. J. Invest. Dermatol. 139, 2517-2527.e5. https://doi.org/10.1016/j.jid.2019.05.022

Ishikura, S., Antonescu, C.N., Klip, A., 2010a. Documenting GLUT4 exocytosis and endocytosis in muscle cell monolayers. Curr. Protoc. Cell Biol. 15151–151519. https://doi.org/10.1002/0471143030.cb1515s46

Ishikura, S., Antonescu, C.N., Klip, A., 2010b. Documenting GLUT4 exocytosis and endocytosis in muscle cell monolayers. Curr. Protoc. Cell Biol. 15151–151519. https://doi.org/10.1002/0471143030.cb1515s46

Iyer, S.S., Cheng, G., 2012. Role of Interleukin 10 Transcriptional Regulation in Inflammation and Autoimmune Disease. Crit. Rev. Immunol. 32, 23–63. https://doi.org/10.1615/CritRevImmunol.v32.i1.30

Jakkawanpitak, C., Hutadilok-Towatana, N., Sermwittayawong, D., 2020. Fungal-like particles and macrophage-conditioned medium are inflammatory elicitors for 3T3-L1 adipocytes. Sci. Rep. 10, 9437. https://doi.org/10.1038/s41598-020-66283-4

Jetten, N., Roumans, N., Gijbels, M.J., Romano, A., Post, M.J., De Winther, M.P.J., Van Der Hulst, R.R.W.J., Xanthoulea, S., 2014. Wound administration of M2-polarized macrophages does not improve murine cutaneous healing responses. PLoS One 9, 1–9. https://doi.org/10.1371/journal.pone.0102994

Jiang, J., Jia, T., Gong, W., Ning, B., Wooley, P.H., Yang, S.Y., 2016. Macrophage Polarization in IL-10 Treatment of Particle-Induced Inflammation and Osteolysis. Am. J. Pathol. 186, 57–66. https://doi.org/10.1016/j.ajpath.2015.09.006

Jiao, B., Yu, Z.-B., Xu, P.-T., Zhang, W.-C., Song, Z., 2015. Impaired Translocation of GLUT4 Results in Insulin Resistance of Atrophic Soleus Muscle. Biomed Res. Int. 2015, 1–11. https://doi.org/10.1155/2015/291987

Kaiko, G.E., Horvat, J.C., Beagley, K.W., Hansbro, P.M., 2008. Immunological decision-making: How does the immune system decide to mount a helper T-cell response? Immunology 123, 326–338. https://doi.org/10.1111/j.1365-2567.2007.02719.x

Kakigi, R., Yoshihara, T., Ozaki, H., Ogura, Y., Ichinoseki-Sekine, N., Kobayashi, H., Naito, H., 2014. Whey protein intake after resistance exercise activates mTOR signaling in a dose-dependent manner in human skeletal muscle. Eur. J. Appl. Physiol. 114, 735–742. https://doi.org/10.1007/s00421-013-2812-7

Kalinkovich, A., Livshits, G., 2017. Sarcopenic obesity or obese sarcopenia: A cross talk between age-associated adipose tissue and skeletal muscle inflammation as a main mechanism of the pathogenesis. Ageing Res. Rev. 35, 200–221. https://doi.org/10.1016/j.arr.2016.09.008

Kalyani, R.R., Corriere, M., Ferrucci, L., 2014. Age-related and disease-related muscle loss: The effect of diabetes, obesity, and other diseases. Lancet Diabetes Endocrinol. 2, 819–829. https://doi.org/10.1016/S2213-8587(14)70034-8

Kanter, J.E., Kramer, F., Barnhart, S., Averill, M.M., Vivekanandan-Giri, A., Vickery, T., Li, L.O., Becker, L., Yuan, W., Chait, A., Braun, K.R., Potter-Perigo, S., Sanda, S., Wight, T.N., Pennathur, S., Serhan, C.N., Heinecke, J.W., Coleman, R.A., Bornfeldt, K.E., 2012. Diabetes promotes an inflammatory macrophage phenotype and atherosclerosis through acyl-CoA synthetase 1. Proc. Natl. Acad. Sci. U. S. A. 109. https://doi.org/10.1073/pnas.1111600109

Kelly, B., O'Neill, L.A.J., 2015. Metabolic reprogramming in macrophages and dendritic cells in innate immunity. Cell Res. 25, 771–784. https://doi.org/10.1038/cr.2015.68

Kewalramani, G., Fink, L.N., Asadi, F., Klip, A., 2011. Palmitate-Activated Macrophages Confer Insulin Resistance to Muscle Cells by a Mechanism Involving Protein Kinase C θ and ε. PLoS One 6, e26947. https://doi.org/10.1371/journal.pone.0026947

Kiewiet, Mensiena; Faas, Maria; de Vos, P., 2018. University of Groningen Immunomodulatory Protein Hydrolysates and Their Application Kiewiet, Mensiena; Faas, Maria; de Vos, Paulus. https://doi.org/10.3390/nu10070904

Kim, H.-J., Higashimori, T., Park, S.-Y., Choi, H., Dong, J., Kim, Y.-J., Noh, H.-L., Cho, Y.-R., Cline, G., Kim, Y.-B., Kim, J.K., 2004. Differential Effects of Interleukin-6 and -10 on Skeletal Muscle and Liver Insulin Action In vivo. Diabetes 53, 1060–1067. https://doi.org/10.2337/diabetes.53.4.1060

Ko, M.H., Li, C.Y., Lee, C.F., Chang, C.K., Fang, S.H., 2016. Scratch wound closure of myoblasts and myotubes is reduced by inflammatory mediators. Int. Wound J. 13, 680–685. https://doi.org/10.1111/iwj.12346

Koca, I., Tasci, B., 2016. Garlic as a functional food. Acta Hortic. 1143, 139–146. https://doi.org/10.17660/ActaHortic.2016.1143.20

Krogh-Madsen, R., Plomgaard, P., Møller, K., Mittendorfer, B., Pedersen, B.K., 2006. Influence of TNF-α and IL-6 infusions on insulin sensitivity and expression of IL-18 in humans. Am. J. Physiol. Metab. 291, E108–E114. https://doi.org/10.1152/ajpendo.00471.2005

Krook, A., Sjögren, R.J.O., Zierath, J.R., Katayama, M., Egan, B., 2014. Temporal analysis of reciprocal miRNA-mRNA expression patterns predicts regulatory networks during differentiation in human skeletal muscle cells. Physiol. Genomics 47, 45–57. https://doi.org/10.1152/physiolgenomics.00037.2014

Krzyszczyk, P., Schloss, R., Palmer, A., Berthiaume, F., 2018. The Role of Macrophages in Acute and Chronic Wound Healing and Interventions to Promote Pro-wound Healing Phenotypes 9, 1–22. https://doi.org/10.3389/fphys.2018.00419

Kumar, V., Selby, A., Rankin, D., Patel, R., Atherton, P., Hildebrandt, W., Williams, J., Smith, K., Seynnes, O., Hiscock, N., Rennie, M.J., 2009. Age-related differences in the dose-response relationship of muscle protein synthesis to resistance exercise in young and old men. J. Physiol. 587, 211–217. https://doi.org/10.1113/jphysiol.2008.164483

KUO, BROWNING, IVY, 1999. Regulation of GLUT4 protein expression and glycogen storage after prolonged exercise. Acta Physiol. Scand. 165, 193–201. https://doi.org/10.1046/j.1365-201x.1999.00489.x

Kwon, H., Pessin, J.E., 2013. Adipokines Mediate Inflammation and Insulin Resistance. Front. Endocrinol. (Lausanne). 4, 1–13. https://doi.org/10.3389/fendo.2013.00071

Lai, Y., Dong, C., 2016. Therapeutic antibodies that target inflammatory cytokines in autoimmune diseases. Int. Immunol. 28, 181–188. https://doi.org/10.1093/intimm/dxv063

Lalor, R., O'Neill, S., 2019a. Bovine κ-casein fragment induces hypo-responsive m2-like macrophage phenotype. Nutrients 11. https://doi.org/10.3390/nu11071688

Lalor, R., O'Neill, S., 2019b. Bovine κ-Casein Fragment Induces Hypo-Responsive M2-Like Macrophage Phenotype. Nutrients 11, 1688. https://doi.org/10.3390/nu11071688

Landi, F., Marzetti, E., Liperoti, R., Pahor, M., Russo, A., Martone, A.M., Colloca, G., Capoluongo, E., Bernabei, R., 2013. Nonsteroidal Anti-Inflammatory Drug (NSAID) Use and Sarcopenia in Older People: Results From the ilSIRENTE Study. J. Am. Med. Dir. Assoc. 14, 626.e9-626.e13. https://doi.org/10.1016/j.jamda.2013.04.012

Lang, C.H., Frost, R.A., Nairn, A.C., MacLean, D.A., Vary, T.C., 2002. TNF-α impairs heart and skeletal muscle protein synthesis by altering translation initiation. Am. J. Physiol. Metab. 282, E336–E347. https://doi.org/10.1152/ajpendo.00366.2001

Lee, Y.S., Olefsky, J., 2021. Chronic tissue inflammation and metabolic disease. Genes Dev. 35, 307–328. https://doi.org/10.1101/gad.346312.120

Lenihan-Geels, G., Bishop, K., Ferguson, L., 2013. Alternative Sources of Omega-3 Fats: Can We Find a Sustainable Substitute for Fish? Nutrients 5, 1301–1315. https://doi.org/10.3390/nu5041301

Leon-Cabrera, S., Arana-Lechuga, Y., Esqueda-León, E., Terán-Pérez, G., Gonzalez-Chavez, A., Escobedo, G., Velázquez Moctezuma, J., 2015. Reduced Systemic Levels of IL-10 Are Associated with the Severity of Obstructive Sleep Apnea and Insulin Resistance in Morbidly Obese Humans. Mediators Inflamm. 2015, 1–9. https://doi.org/10.1155/2015/493409

Lester, S.N., Li, K., 2014. Toll-Like Receptors in Antiviral Innate Immunity. J. Mol. Biol. 426,

1246–1264. https://doi.org/10.1016/j.jmb.2013.11.024

Li-chan, E.C.Y., 2015. Bioactive peptides and protein hydrolysates : research trends and challenges for application as nutraceuticals and functional food ingredients. Curr. Opin. Food Sci. 1, 28–37. https://doi.org/10.1016/j.cofs.2014.09.005

Li, W., Moylan, J.S., Chambers, M.A., Smith, J., Reid, M.B., 2009. Interleukin-1 stimulates catabolism in C2C12 myotubes. Am. J. Physiol. Physiol. 297, C706–C714. https://doi.org/10.1152/ajpcell.00626.2008

Li, Y.-P., 2013. TNF-α is a mitogen in skeletal muscle. Am. J. Physiol. Physiol. 285, C370–C376. https://doi.org/10.1152/ajpcell.00453.2002

Liao, C.H., Lin, L.P., Yu, T.Y., Hsu, C.C., Pang, J.H.S., Tsai, W.C., 2019. Ibuprofen inhibited migration of skeletal muscle cells in association with downregulation of p130cas and CrkII expressions. Skelet. Muscle 9, 1–11. https://doi.org/10.1186/s13395-019-0208-z

Lillehoj, H.S., 1987. Effects of immunosuppression on avian coccidiosis: Cyclosporin A but not hormonal bursectomy abrogates host protective immunity. Infect. Immun. 55, 1616–1621.

Lin, S.H., Chuang, H.Y., Ho, J.C., Lee, C.H., Hsiao, C.C., 2018. Treatment with TNF-α inhibitor rectifies M1 macrophage polarization from blood CD14+ monocytes in patients with psoriasis independent of STAT1 and IRF-1 activation. J. Dermatol. Sci. 91, 276–284. https://doi.org/10.1016/j.jdermsci.2018.05.009

Liu, L., Ge, D., Ma, L., Mei, J., Liu, S., Zhang, Q., Ren, F., Liao, H., Pu, Q., Wang, T., You, Z., 2012. Interleukin-17 and prostaglandin E2 are involved in formation of an M2 macrophage-dominant microenvironment in lung cancer. J. Thorac. Oncol. 7, 1091–1100. https://doi.org/10.1097/JTO.0b013e3182542752

Liu, S.X., Gustafson, H.H., Jackson, D.L., Pun, S.H., Trapnell, C., 2020. Trajectory analysis quantifies transcriptional plasticity during macrophage polarization. Sci. Rep. 10, 12273. https://doi.org/10.1038/s41598-020-68766-w

Liu, Yitong, Fang, S., Li, X., Feng, J., Du, J., Guo, L., Su, Y., Zhou, J., Ding, G., Bai, Y., Wang, S., Wang, H., Liu, Yi, 2017. Aspirin inhibits LPS-induced macrophage activation via the NF-κB pathway. Sci. Rep. 7, 1–11. https://doi.org/10.1038/s41598-017-10720-4

Londhe, P., Guttridge, D.C., 2015. Inflammation induced loss of skeletal muscle. Bone 80, 131–142. https://doi.org/10.1016/j.bone.2015.03.015

Loynes, C.A., Lee, J.A., Robertson, A.L., Steel, M.J.G., Ellett, F., Feng, Y., Levy, B.D., Whyte, M.K.B., Renshaw, S.A., 2018. PGE2 production at sites of tissue injury promotes an

anti-inflammatory neutrophil phenotype and determines the outcome of inflammation resolution in vivo. Sci. Adv. 4. https://doi.org/10.1126/sciadv.aar8320

Lu, H., Huang, D., Ransohoff, R.M., Zhou, L., 2011. Acute skeletal muscle injury: CCL2 expression by both monocytes and injured muscle is required for repair. FASEB J. 25, 3344–3355. https://doi.org/10.1096/fj.10-178939

Makita, N., Hizukuri, Y., Yamashiro, K., Murakawa, M., Hayashi, Y., 2015. IL-10 enhances the phenotype of M2 macrophages induced by IL-4 and confers the ability to increase eosinophil migration. Int. Immunol. 27, 131–141. https://doi.org/10.1093/intimm/dxu090

Mani, H., Sidhu, G.S., Kumari, R., Gaddipati, J.P., Seth, P., Maheshwari, R.K., 2002. Curcumin differentially regulates TGF-β1, its receptors and nitric oxide synthase during impaired wound healing. BioFactors 16, 29–43. https://doi.org/10.1002/biof.5520160104

Manna, P., Jain, S.K., 2012. Vitamin D Up-regulates Glucose Transporter 4 (GLUT4) Translocation and Glucose Utilization Mediated by Cystathionine-γ-lyase (CSE) Activation and H2S Formation in 3T3L1 Adipocytes. J. Biol. Chem. 287, 42324–42332. https://doi.org/10.1074/jbc.M112.407833

Marcone, Simone, Belton, O., J. Fitzgerald, D., 2017. Milk-derived bioactive peptides and their health promoting effects : a potential role in atherosclerosis. Br. J. Clin. Pharmacol. 83, 152–152. https://doi.org/10.1111/bcp.13002

Marín de Mas, I., Marín, S., Pachón, G., Rodríguez-Prados, J.C., Vizán, P., Centelles, J.J., Tauler, R., Azqueta, A., Selivanov, V., López de Ceraín, A., Cascante, M., 2017. Unveiling the Metabolic Changes on Muscle Cell Metabolism Underlying p-Phenylenediamine Toxicity. Front. Mol. Biosci. 4, 1–12. https://doi.org/10.3389/fmolb.2017.00008

Marko, D.M., Foran, G., Vlavcheski, F., Baron, D.C., Hayward, G.C., Baranowski, B.J., Necakov, A., Tsiani, E., MacPherson, R.E.K., 2020. Interleukin-6 Treatment Results in GLUT4 Translocation and AMPK Phosphorylation in Neuronal SH-SY5Y Cells. Cells 9, 1114. https://doi.org/10.3390/cells9051114

Martinez, F.O., Gordon, S., 2014. The M1 and M2 paradigm of macrophage activation: time for reassessment. F1000Prime Rep. 6, 1–13. https://doi.org/10.12703/p6-13

Matsunaga, Y., Tamura, Y., Sakata, Y., Nonaka, Y., Saito, N., Nakamura, H., Shimizu, T., Takeda, Y., Terada, S., Hatta, H., 2017. Comparison between pre-exercise casein peptide and intact casein supplementation on glucose tolerance in mice fed a high-fat diet. Appl. Physiol. Nutr. Metab. 43, 355–362. https://doi.org/10.1139/apnm-2017-0485

McCarthy, J.J., Esser, K.A., 2010. Anabolic and catabolic pathways regulating skeletal muscle mass. Curr. Opin. Clin. Nutr. Metab. Care 13, 230–235. https://doi.org/10.1097/MCO.0b013e32833781b5

McKinlay, B.J., Theocharidis, A., Adebero, T., Kurgan, N., Fajardo, V.A., Roy, B.D., Josse, A.R., M. Logan-Sprenger, H., Falk, B., Klentrou, P., 2020. Effects of Post-Exercise Whey Protein Consumption on Recovery Indices in Adolescent Swimmers. Int. J. Environ. Res. Public Health 17, 7761. https://doi.org/10.3390/ijerph17217761

Mei, M., Zhao, L., Li, Qing, Chen, Y., Huang, A., Varghese, Z., Moorhead, J.F., Zhang, S., Powis, S.H., Li, Qifu, Ruan, X.Z., 2011. Inflammatory stress exacerbates ectopic lipid deposition in C57BL/6J mice. Lipids Health Dis. 10, 110. https://doi.org/10.1186/1476-511X-10-110

Messina, G., Palmieri, F., Monda, V., Messina, A., Dalia, C., Viggiano, A., Tafuri, D., Messina, A., Moscatelli, F., Valenzano, A., Cibelli, G., Chieffi, S., Monda, M., 2015. Exercise causes muscle GLUT4 translocation in an insulin-independent manner. Biol. Med. 7, 2–5. https://doi.org/10.4172/0974-8369.1000S3007

Mills, C.D., Kincaid, K., Alt, J.M., Heilman, M.J., Hill, A.M., 2000. M-1/M-2 Macrophages and the Th1/Th2 Paradigm. J. Immunol. 164, 6166–6173. https://doi.org/10.4049/jimmunol.164.12.6166

Montero, J., Gómez-Abellán, V., Arizcun, M., Mulero, V., Sepulcre, M.P., 2016. Prostaglandin E2 promotes M2 polarization of macrophages via a cAMP/CREB signaling pathway and deactivates granulocytes in teleost fish. Fish Shellfish Immunol. 55, 632–641. https://doi.org/10.1016/j.fsi.2016.06.044

Morato, P.N., Lollo, P.C.B., Moura, C.S., Batista, T.M., Camargo, R.L., Carneiro, E.M., Amaya-Farfan, J., 2013. Whey Protein Hydrolysate Increases Translocation of GLUT-4 to the Plasma Membrane Independent of Insulin in Wistar Rats. PLoS One 8. https://doi.org/10.1371/journal.pone.0071134

Morgan, P.T., Breen, L., 2021. The role of protein hydrolysates for exercise-induced skeletal muscle recovery and adaptation: a current perspective. Nutr. Metab. (Lond). 18, 44. https://doi.org/10.1186/s12986-021-00574-z

Mosmann, T.R., Cherwinski, H., Bond, M.W., Giedlin, M.A., Coffman, R.L., 1986. Two types of murine helper T cell clone. I. Definition according to profiles of lymphokine activities and secreted proteins. J. Immunol. 136, 2348–57.

Mukhopadhya, A., Noronha, N., Bahar, B., Ryan, M.T., Murray, B.A., Kelly, P.M., Loughlin, I.B.O., Doherty, J.V.O., Sweeney, T., 2014. Anti-inflammatory effects of a casein hydrolysate and its peptide-enriched fractions on TNF a - challenged Caco-2 cells and LPS-challenged porcine colonic explants. Food Sci. Nutr. 2, 712–723. https://doi.org/10.1002/fsn3.153

Muñoz-Cánoves, P., Scheele, C., Pedersen, B.K., Serrano, A.L., 2013. Interleukin-6 myokine signaling in skeletal muscle: A double-edged sword? FEBS J. 280, 4131–4148.

https://doi.org/10.1111/febs.12338

Murray, P.J., 2017. Macrophage Polarization. Annu. Rev. Physiol. 79, 541–566. https://doi.org/10.1146/annurev-physiol-022516-034339

Murray, P.J., Allen, J.E., Biswas, S.K., Fisher, E.A., Gilroy, D.W., Goerdt, S., Gordon, S., Hamilton, J.A., Ivashkiv, L.B., Lawrence, T., Locati, M., Mantovani, A., Martinez, F.O., Mege, J.L., Mosser, D.M., Natoli, G., Saeij, J.P., Schultze, J.L., Shirey, K.A., Sica, A., Suttles, J., Udalova, I., vanGinderachter, J.A., Vogel, S.N., Wynn, T.A., 2014. Macrophage Activation and Polarization: Nomenclature and Experimental Guidelines. Immunity 41, 14–20. https://doi.org/10.1016/j.immuni.2014.06.008

Musa, J., Orth, M.F., Dallmayer, M., Baldauf, M., Pardo, C., Rotblat, B., Kirchner, T., Leprivier, G., Grünewald, T.G.P., 2016. Eukaryotic initiation factor 4E-binding protein 1 (4E-BP1): A master regulator of mRNA translation involved in tumorigenesis. Oncogene 35, 4675–4688. https://doi.org/10.1038/onc.2015.515

Nabuco, H.C.G., Tomeleri, C.M., Fernandes, R.R., Sugihara Junior, P., Cavalcante, E.F., Cunha, P.M., Antunes, M., Nunes, J.P., Venturini, D., Barbosa, D.S., Burini, R.C., Silva, A.M., Sardinha, L.B., Cyrino, E.S., 2019. Effect of whey protein supplementation combined with resistance training on body composition, muscular strength, functional capacity, and plasma-metabolism biomarkers in older women with sarcopenic obesity: A randomized, double-blind, placebo-controlled t. Clin. Nutr. ESPEN 32, 88–95. https://doi.org/10.1016/j.clnesp.2019.04.007

Nakashima, K., Ishida, A., Shimamoto, S., Ijiri, D., Ohtsuka, A., 2020. Insulin Stimulation of Protein Synthesis and mTOR Signaling in Chick Myotube Cultures. J. Poult. Sci. 57, 205–209. https://doi.org/10.2141/jpsa.0190082

Nakayama, K., Tagawa, R., Saito, Y., Sanbongi, C., 2019. Effects of whey protein hydrolysate ingestion on post-exercise muscle protein synthesis compared with intact whey protein in rats. Nutr. Metab. (Lond). 16, 90. https://doi.org/10.1186/s12986-019-0417-9

Narsale, A., Carson, J., 2015. Role of IL-6 In Cachexia – Therapeutic Implications. Curr Opin Support Palliat Care 8, 321–327. https://doi.org/10.1097/SPC.0000000000000091.Role

Navarro, J.F., Mora, C., 2006. Diabetes, Inflammation, Proinflammatory Cytokines, and Diabetic Nephropathy. Sci. World J. 6, 908–917. https://doi.org/10.1100/tsw.2006.179

Németh, K., Leelahavanichkul, A., Yuen, P.S.T., Mayer, B., Parmelee, A., Doi, K., Robey, P.G., Leelahavanichkul, K., Koller, B.H., Brown, J.M., Hu, X., Jelinek, I., Star, R.A., Mezey, É., 2009. Bone marrow stromal cells attenuate sepsis via prostaglandin E 2-dependent reprogramming of host macrophages to increase their interleukin-10 production. Nat. Med. 15, 42–49. https://doi.org/10.1038/nm.1905

Nicholson, T., Church, C., Baker, D.J., Jones, S.W., 2018. The role of adipokines in skeletal muscle inflammation and insulin sensitivity. J. Inflamm. 15, 9. https://doi.org/10.1186/s12950-018-0185-8

Nicklas, B.J., Brinkley, T.E., 2009. Exercise training as a treatment for chronic inflammation in the elderly. Exerc. Sport Sci. Rev. 37, 165–170. https://doi.org/10.1097/JES.0b013e3181b7b3d9

Nielsen, S.D., Purup, S., Larsen, L.B., 2019. Effect of casein hydrolysates on intestinal cell migration and their peptide profiles by LC-ESI/MS/MS. Foods 8. https://doi.org/10.3390/foods8030091

Nihashi, Y., Umezawa, K., Shinji, S., Hamaguchi, Y., Kobayashi, H., Kono, T., Ono, T., Kagami, H., Takaya, T., 2019. Distinct cell proliferation, myogenic differentiation, and gene expression in skeletal muscle myoblasts of layer and broiler chickens. Sci. Rep. 9, 1–15. https://doi.org/10.1038/s41598-019-52946-4

Nitahara-Kasahara, Y., Kuraoka, M., Oda, Y., Hayashita-Kinoh, H., Takeda, S., Okada, T., 2021. Enhanced cell survival and therapeutic benefits of IL-10-expressing multipotent mesenchymal stromal cells for muscular dystrophy. Stem Cell Res. Ther. 12, 105. https://doi.org/10.1186/s13287-021-02168-1

Noonan, J., Grassia, G., MacRitchie, N., Garside, P., Guzik, T.J., Bradshaw, A.C., Maffia, P., 2019. A novel triple-cell two-dimensional model to study immune vascular interplay in atherosclerosis. Front. Immunol. 10, 1–9. https://doi.org/10.3389/fimmu.2019.00849

Oosthuyse, T., Carstens, M., Millen, A.M.E., 2015. Whey or Casein Hydrolysate with Carbohydrate for Metabolism and Performance in Cycling. Int. J. Sports Med. 36, 636–646. https://doi.org/10.1055/s-0034-1398647

Orecchioni, M., Ghosheh, Y., Pramod, A.B., Ley, K., 2019. Macrophage Polarization: Different Gene Signatures in M1(LPS+) vs. Classically and M2(LPS–) vs. Alternatively Activated Macrophages. Front. Immunol. 10, 1–14. https://doi.org/10.3389/fimmu.2019.01084

Otis, J.S., Niccoli, S., Hawdon, N., Sarvas, J.L., Frye, M.A., Chicco, A.J., Lees, S.J., 2014. Pro-Inflammatory Mediation of Myoblast Proliferation. PLoS One 9, e92363. https://doi.org/10.1371/journal.pone.0092363

Paniri, A., Akhavan-Niaki, H., 2020. Emerging role of IL-6 and NLRP3 inflammasome as potential therapeutic targets to combat COVID-19: Role of lncRNAs in cytokine storm modulation. Life Sci. 257, 118114. https://doi.org/10.1016/j.lfs.2020.118114

Papamichael, K., Lin, S., Moore, M., Papaioannou, G., Sattler, L., Cheifetz, A.S., 2019. Infliximab in inflammatory bowel disease. Ther. Adv. Chronic Dis. 10, 204062231983844. https://doi.org/10.1177/2040622319838443

Park, J.Y., Pillinger, M.H., Abramson, S.B., 2006. Prostaglandin E2 synthesis and secretion: The role of PGE2 synthases. Clin. Immunol. 119, 229–240. https://doi.org/10.1016/j.clim.2006.01.016

Pastor, D.M., Poritz, L.S., Olson, T.L., Kline, C.L., Iii, L.R.H., Koltun, A., Chinchilli, V.M., Irby, R.B., 2010. Primary cell lines: false representation or model system? a comparison of four human colorectal tumors and their coordinately established cell lines 3, 1–15.

Paulina Achita, A.B., 2015. Immortalized Murine Macrophage Cell Line as a Model for Macrophage Polarization into Classically Activated M(IFNγ+LPS) or Alternatively Activated M(IL-4) Macrophages. J. Clin. Cell. Immunol. 06, 1–7. https://doi.org/10.4172/2155-9899.1000318

Peighambardoust, S.H., Karami, Z., Pateiro, M., Lorenzo, J.M., 2021. A Review on Health-Promoting, Biological, and Functional Aspects of Bioactive Peptides in Food Applications. Biomolecules 11, 631. https://doi.org/10.3390/biom11050631

Phillips, S.M., 2011. A comparison of whey to caseinate. Am. J. Physiol. Metab. 300, E610–E610. https://doi.org/10.1152/ajpendo.00647.2010

Pi-Sunyer, X., 2010. The Medical Risks of Obeisity. PMC 121, 21–33. https://doi.org/10.3810/pgm.2009.11.2074.The

Pillon, N.J., Arane, K., Bilan, P.J., Chiu, T.T., Klip, A., 2012. Muscle cells challenged with saturated fatty acids mount an autonomous inflammatory response that activates macrophages. Cell Commun. Signal. 10, 1–12. https://doi.org/10.1186/1478-811X-10-30

Pillon, N.J., Bilan, P.J., Fink, L.N., Klip, A., 2013. Cross-talk between skeletal muscle and immune cells: muscle-derived mediators and metabolic implications. AJP Endocrinol. Metab. 304, E453–E465. https://doi.org/10.1152/ajpendo.00553.2012

Pourhassan, M., Rommersbach, N., Lueg, G., Klimek, C., Schnatmann, M., Liermann, D., Janssen, G., Wirth, R., 2020. The impact of malnutrition on acute muscle wasting in frail older hospitalized patients. Nutrients 12, 1–12. https://doi.org/10.3390/nu12051387

PROESTOS, C., 2018. Superfoods: Recent Data on their Role in the Prevention of Diseases. Curr. Res. Nutr. Food Sci. J. 6, 576–593. https://doi.org/10.12944/CRNFSJ.6.3.02

Proske, U., Morgan, D.L., 2001. Muscle damage from eccentric exercise: mechanism,

mechanical signs, adaptation and clinical applications. J. Physiol. 537, 333–345. https://doi.org/10.1111/j.1469-7793.2001.00333.x

Qin, X., Jiang, B., Zhang, Y., 2016. 4E-BP1, a multifactor regulated multifunctional protein. Cell Cycle 15, 781–786. https://doi.org/10.1080/15384101.2016.1151581

Raimondo, T.M., Mooney, D.J., 2018. Functional muscle recovery with nanoparticle-directed M2 macrophage polarization in mice. Proc. Natl. Acad. Sci. 115, 10648–10653. https://doi.org/10.1073/pnas.1806908115

Rasmussen, B.B., Tipton, K.D., Miller, S.L., Wolf, S.E., Wolfe, R.R., Blake, B., Tipton, K.D., Sharon, L., Wolf, S.E., Wolfe, R.R., 2018. An oral essential amino acid-carbohydrate supplement enhances muscle protein anabolism after resistance exercise 386–392.

Rath, M., Müller, I., Kropf, P., Closs, E.I., Munder, M., 2014. Metabolism via arginase or nitric oxide synthase: Two competing arginine pathways in macrophages. Front. Immunol. 5, 1–10. https://doi.org/10.3389/fimmu.2014.00532

Raziyeva, K., Kim, Y., Zharkinbekov, Z., Kassymbek, K., Jimi, S., Saparov, A., 2021. Immunology of Acute and Chronic Wound Healing. Biomolecules 11, 700. https://doi.org/10.3390/biom11050700

Reid, M.B., Li, Y.P., 2001. Tumor necrosis factor-alpha and muscle wasting: a cellular perspective. Respir. Res. 2, 269–72. https://doi.org/10.1186/rr67

Reyes-Diaz, A., F Gonzalez-Cordova, A., Hernandez-Mendoza, A., Reyes-Diaz, R., Vallejo-Cordoba, B., 2018. Immunomodulation by hydrolysates and peptides derived from milk proteins. Int. J. Dairy Technol. 71, 1–9. https://doi.org/10.1111/1471-0307.12421

Richter, E.A., Hargreaves, M., 2013. Exercise, GLUT4, and Skeletal Muscle Glucose Uptake. Physiol. Rev. 93, 993–1017. https://doi.org/10.1152/physrev.00038.2012

Riera-Borrull, M., Cuevas, V.D., Alonso, B., Vega, M.A., Joven, J., Izquierdo, E., Corbí, Á.L., 2017. Palmitate Conditions Macrophages for Enhanced Responses toward Inflammatory Stimuli via JNK Activation. J. Immunol. 199, 3858–3869. https://doi.org/10.4049/jimmunol.1700845

Rigamonti, E., Zordan, P., Sciorati, C., Rovere-Querini, P., Brunelli, S., 2014. Macrophage plasticity in skeletal muscle repair. Biomed Res. Int. 2014. https://doi.org/10.1155/2014/560629

Rogeri, P.S., Gasparini, S.O., Martins, G.L., Costa, L.K.F., Araujo, C.C., Lugaresi, R., Kopfler, M., Lancha, A.H., 2020. Crosstalk Between Skeletal Muscle and Immune System: Which Roles Do IL-6 and Glutamine Play? Front. Physiol. 11, 1–11. https://doi.org/10.3389/fphys.2020.582258

Roh, J.S., Sohn, D.H., 2018. Damage-Associated Molecular Patterns in Inflammatory Diseases. Immune Netw. 18, 1–14. https://doi.org/10.4110/in.2018.18.e27

Roher, N., Samokhvalov, V., Díaz, M., MacKenzie, S., Klip, A., Planas, J. V., 2008a. The proinflammatory cytokine tumor necrosis factor-α increases the amount of glucose transporter-4 at the surface of muscle cells independently of changes in interleukin-6. Endocrinology 149, 1880–1889. https://doi.org/10.1210/en.2007-1045

Rong, Y.-D., Bian, A.-L., Hu, H.-Y., Ma, Y., Zhou, X.-Z., 2018. Study on relationship between elderly sarcopenia and inflammatory cytokine IL-6, anti-inflammatory cytokine IL-10. BMC Geriatr. 18, 308. https://doi.org/10.1186/s12877-018-1007-9

Rotter, V., Nagaev, I., Smith, U., 2003. Interleukin-6 (IL-6) Induces Insulin Resistance in 3T3-L1 Adipocytes and Is, Like IL-8 and Tumor Necrosis Factor-α, Overexpressed in Human Fat Cells from Insulin-resistant Subjects. J. Biol. Chem. 278, 45777–45784. https://doi.org/10.1074/jbc.M301977200

Russo, L., Lumeng, C.N., 2018. Properties and functions of adipose tissue macrophages in obesity. Immunology 155, 407–417. https://doi.org/10.1111/imm.13002

RYDER, J.W., KAWANO, Y., GALUSKA, D., FAHLMAN, R., WALLBERG-HENRIKSSON, H., CHARRON, M.J., ZIERATH, J.R., 1999. Postexercise glucose uptake and glycogen synthesis in skeletal muscle from GLUT4-deficient mice. FASEB J. 13, 2246–2256. https://doi.org/10.1096/fasebj.13.15.2246

S Lopez-Varela, M.G.-G. and A.M., 2002. Functional foods and the immune system : a review. Eur. J. Clin. Nutr. 56, 29–33.

Sabaka, P., Koščálová, A., Straka, I., Hodosy, J., Lipták, R., Kmotorková, B., Kachlíková, M., Kušnírová, A., 2021. Role of interleukin 6 as a predictive factor for a severe course of Covid-19: retrospective data analysis of patients from a long-term care facility during Covid-19 outbreak. BMC Infect. Dis. 21, 308. https://doi.org/10.1186/s12879-021-05945-8

Saclier, M., Yacoub-Youssef, H., Mackey, A.L., Arnold, L., Ardjoune, H., Magnan, M., Sailhan, F., Chelly, J., Pavlath, G.K., Mounier, R., Kjaer, M., Chazaud, B., 2013. Differentially activated macrophages orchestrate myogenic precursor cell fate during human skeletal muscle regeneration. Stem Cells 31, 384–396. https://doi.org/10.1002/stem.1288

Saini, J., McPhee, J.S., Al-Dabbagh, S., Stewart, C.E., Al-Shanti, N., 2016. Regenerative function of immune system: Modulation of muscle stem cells. Ageing Res. Rev. 27, 67–76. https://doi.org/10.1016/j.arr.2016.03.006

Sakaguchi, S., Shono, J., Suzuki, T., Sawano, S., Anderson, J.E., Do, M.-K.Q., Ohtsubo, H., Mizunoya, W., Sato, Y., Nakamura, M., Furuse, M., Yamada, K., Ikeuchi, Y., Tatsumi, R., 2014. Implication of anti-inflammatory macrophages in regenerative moto-neuritogenesis: Promotion of myoblast migration and neural chemorepellent semaphorin 3A expression in injured muscle. Int. J. Biochem. Cell Biol. 54, 272–285. https://doi.org/10.1016/j.biocel.2014.05.032

Samokhvalov, V., Bilan, P.J., Schertzer, J.D., Antonescu, C.N., Klip, A., 2009. Palmitate- and lipopolysaccharide-activated macrophages evoke contrasting insulin responses in muscle cells. Am. J. Physiol. Endocrinol. Metab. 296, E37-46. https://doi.org/10.1152/ajpendo.90667.2008

Samuel, V.T., Shulman, G.I., 2012. Mechanisms for insulin resistance: Common threads and missing links. Cell 148, 852–871. https://doi.org/10.1016/j.cell.2012.02.017

Sass, F., Fuchs, M., Pumberger, M., Geissler, S., Duda, G., Perka, C., Schmidt-Bleek, K., 2018. Immunology Guides Skeletal Muscle Regeneration. Int. J. Mol. Sci. 19, 835. https://doi.org/10.3390/ijms19030835

Scheller, J., Chalaris, A., Schmidt-Arras, D., Rose-John, S., 2011. The pro- and anti-inflammatory properties of the cytokine interleukin-6. Biochim. Biophys. Acta - Mol. Cell Res. 1813, 878–888. https://doi.org/10.1016/j.bbamcr.2011.01.034

Schilling, A.F., Lehman, W., Böker, K.O., Liu, J., Ernst, J., Saul, D., 2018. Current Methods for Skeletal Muscle Tissue Repair and Regeneration. Biomed Res. Int. 2018, 1–11. https://doi.org/10.1155/2018/1984879

Schmalbruch, H., Lewis, D.M., 2000. Dynamics of nuclei of muscle fibers and connective tissue cells in normal and denervated rat muscles. Muscle Nerve 23, 617–626. https://doi.org/10.1002/(SICI)1097-4598(200004)23:4<617::AID-MUS22>3.0.CO;2-Y

Serrano, A.L., Baeza-Raja, B., Perdiguero, E., Jardí, M., Muñoz-Cánoves, P., 2008. Interleukin-6 Is an Essential Regulator of Satellite Cell-Mediated Skeletal Muscle Hypertrophy. Cell Metab. 7, 33–44. https://doi.org/10.1016/j.cmet.2007.11.011

Shabani, M., Sadeghi, A., Hosseini, H., Teimouri, M., Babaei Khorzoughi, R., Pasalar, P., Meshkani, R., 2020. Resveratrol alleviates obesity-induced skeletal muscle inflammation via decreasing M1 macrophage polarization and increasing the regulatory T cell population. Sci. Rep. 10, 3791. https://doi.org/10.1038/s41598-020-60185-1

Shapouri-Moghaddam, A., Mohammadian, S., Vazini, H., Taghadosi, M., Esmaeili, S.A., Mardani, F., Seifi, B., Mohammadi, A., Afshari, J.T., Sahebkar, A., 2018. Macrophage plasticity, polarization, and function in health and disease. J. Cell. Physiol. 233, 6425–6440. https://doi.org/10.1002/jcp.26429

Shen, W.-H., Boyle, D.W., Wisniowski, P., Bade, A., Liechty, E.A., 2005. Insulin and IGF-I stimulate the formation of the eukaryotic initiation factor 4F complex and protein synthesis in C2C12 myotubes independent of availability of external amino acids. J. Endocrinol. 185, 275–289. https://doi.org/10.1677/joe.1.06080

Shen, W., Prisk, V., Li, Y., Foster, W., Huard, J., 2006. Inhibited skeletal muscle healing in cyclooxygenase-2 gene-deficient mice: the role of PGE 2 and PGF 2α. J. Appl. Physiol. 101, 1215–1221. https://doi.org/10.1152/japplphysiol.01331.2005

Shen, Y., Liu, B., Mao, W., Gao, R., Feng, S., Qian, Y., Wu, J., Zhang, S., Gao, L., Fu, C., Li, Q., Deng, Y., Cao, J., 2018. PGE2 downregulates LPS-induced inflammatory responses via the TLR4-NF-κB signaling pathway in bovine endometrial epithelial cells. Prostaglandins Leukot. Essent. Fat. Acids 129, 25–31. https://doi.org/10.1016/j.plefa.2018.01.004

Sheppe, A.E.F., Kummari, E., Walker, A., Richards, A., Hui, W.W., Lee, J.H., Mangum, L., Borazjani, A., Ross, M.K., Edelmann, M.J., 2018. PGE2 Augments Inflammasome Activation and M1 Polarization in Macrophages Infected With Salmonella Typhimurium and Yersinia enterocolitica. Front. Microbiol. 9, 1–16. https://doi.org/10.3389/fmicb.2018.02447

Shoelson, S.E., Lee, J., Goldfine, A.B., 2006. Inflammation and insulin resistance. J. Clin. Invest. 116, 1793–1801. https://doi.org/10.1172/JCI29069.and

Showkat, M., Beigh, M.A., Andrabi, K.I., 2014. mTOR Signaling in Protein Translation Regulation: Implications in Cancer Genesis and Therapeutic Interventions. Mol. Biol. Int. 2014, 1–14. https://doi.org/10.1155/2014/686984

Sidiropoulos, P.I., Boumpas, D.., 2006. Differential drug resistance to anti-tumour necrosis factor agents in rheumatoid arthritis. Ann. Rheum. Dis. 65, 701–703. https://doi.org/10.1136/ard.2005.049890

Silva, M.R., Silvestre, M.P.C., Silva, V.D.M., Souza, M.W.S., Lopes Junior, C.O., Afonso, W.O., Lana, F.C., Rodrigues, D.F., 2014. Production of ace-inhibitory whey protein concentrate hydrolysates: Use of pancreatin and papain. Int. J. Food Prop. 17, 1002–1012. https://doi.org/10.1080/10942912.2012.685821

Silvia, G.-P., O'Neill, L.A.J., 2014. Metabolic Reprograming in Macrophage Polarization. Front. Immunol. 5, 1–6. https://doi.org/10.3389/fimmu.2014.00420

Son, M., Wu, J., 2019. Egg white hydrolysate and peptide reverse insulin resistance associated with tumor necrosis factor-α (TNF-α) stimulated mitogen-activated protein kinase (MAPK) pathway in skeletal muscle cells. Eur. J. Nutr. 58, 1961–1969. https://doi.org/10.1007/s00394-018-1753-7

Song, J.J., Wang, Q., Du, M., Li, T.G., Chen, B., Mao, X.Y., 2017. Casein glycomacropeptide-derived peptide IPPKKNQDKTE ameliorates high glucose-induced insulin resistance in HepG2 cells via activation of AMPK signaling. Mol. Nutr. Food Res. 61, 1–12. https://doi.org/10.1002/mnfr.201600301

Song, L., Kim, D., Gou, W., Wang, J., Wang, P., Wei, Z., Liu, B., Li, Z., Gou, K., Wang, H., 2020. GRP94 regulates M1 macrophage polarization and insulin resistance. Am. J. Physiol. Metab. 318, E1004–E1013. https://doi.org/10.1152/ajpendo.00542.2019

Sonnet, C., Lafuste, P., Arnold, L., Brigitte, M., Poron, F., Authier, F.J., Chrétien, F., Gherardi, R.K., Chazaud, B., 2006. Human macrophages rescue myoblasts and myotubes from apoptosis through a set of adhesion molecular systems. J. Cell Sci. 119, 2497–2507. https://doi.org/10.1242/jcs.02988

Sousa, G.T., Lira, F.S., Rosa, J.C., de Oliveira, E.P., Oyama, L.M., Santos, R. V, Pimentel, G.D., 2012. Dietary whey protein lessens several risk factors for metabolic diseases: a review. Lipids Health Dis. 11, 67. https://doi.org/10.1186/1476-511X-11-67

Stevinson, C., 2000. Garlic for Treating Hypercholesterolemia. Ann. Intern. Med. 133, 420. https://doi.org/10.7326/0003-4819-133-6-200009190-00009

Sumi, K., Ashida, K., Nakazato, K., 2020. Resistance exercise with anti-inflammatory foods attenuates skeletal muscle atrophy induced by chronic inflammation. J. Appl. Physiol. 128, 197–211. https://doi.org/10.1152/japplphysiol.00585.2019

Sun, Q., Li, J., Gao, F., 2017. New insights into insulin: The anti-inflammatory effect and its clinical relevance. World J. Diabetes 5, 89. https://doi.org/10.4239/wjd.v5.i2.89

Sunwoo, J.Y., Eliasberg, C.D., Carballo, C.B., Rodeo, S.A., 2020. The role of the macrophage in tendinopathy and tendon healing. J. Orthop. Res. 38, 1666–1675. https://doi.org/10.1002/jor.24667

Swanson, D., Block, R., Mousa, S.A., 2012. Omega-3 Fatty Acids EPA and DHA : Health. J. Adv. Nutr. 3, 1–7. https://doi.org/10.3945/an.111.000893.Omega-3

T Koh and L DiPietro, 2013. Inflammation and wound healing: The role of the macrophage.Expert Rev Mol Med. Mol. Med. 16, 2011 Jul 11; 13: e23. https://doi.org/10.1017/S1462399411001943.Inflammation

Tan, Z., Xie, N., Cui, H., Moellering, D.R., Abraham, E., Thannickal, V.J., Liu, G., 2015. Pyruvate Dehydrogenase Kinase 1 Participates in Macrophage Polarization via Regulating Glucose Metabolism. J. Immunol. 194, 6082–6089. https://doi.org/10.4049/jimmunol.1402469

Tang, T., Scambler, T.E., Smallie, T., Cunliffe, H.E., Ross, E.A., Rosner, D.R., O'Neil, J.D., Clark, A.R., 2017. Macrophage responses to lipopolysaccharide are modulated by a feedback loop involving prostaglandin E2, dual specificity phosphatase 1 and tristetraprolin. Sci. Rep. 7, 1–13. https://doi.org/10.1038/s41598-017-04100-1

Tidball, James G., 2017. Regulation of muscle growth and regeneration by the immune system. Nat. Rev. Immunol. 17, 165–178. https://doi.org/10.1038/nri.2016.150

Tidball, J.G., Dorshkind, K., Wehling-henricks, M., 2015. Shared signaling systems in myeloid cell-mediated muscle regeneration. https://doi.org/10.1242/dev.098285

Tidball, J.G., Villalta, S.A., 2010. Regulatory interactions between muscle and the immune system during muscle regeneration. Am J Physiol Regul Integr Comp Physiol 298, R1173-87. https://doi.org/10.1152/ajpregu.00735.2009

Torre-Villalvazo, I., Alemán-Escondrillas, G., Valle-Ríos, R., Noriega, L.G., 2019. Protein intake and amino acid supplementation regulate exercise recovery and performance through the modulation of mTOR, AMPK, FGF21, and immunity. Nutr. Res. 72, 1–17. https://doi.org/10.1016/j.nutres.2019.06.006

Toth, M.J., 2004. Age-related differences in skeletal muscle protein synthesis: relation to markers of immune activation. AJP Endocrinol. Metab. 288, E883–E891. https://doi.org/10.1152/ajpendo.00353.2004

Treffkorn, L., Scheibe, R., Maruyama, T., Dieter, P., 2004. PGE 2 exerts its effect on the LPS-induced release of TNF-α, ET-1, IL-lα, IL-6 and IL-10 via the EP2 and EP4 receptor in rat liver macrophages. Prostaglandins Other Lipid Mediat. 74, 113–123. https://doi.org/10.1016/j.prostaglandins.2004.07.005

Udenigwe, C.C., Aluko, R.E., 2012. Food Protein-Derived Bioactive Peptides : Production , Processing , and Potential Health Benefits. https://doi.org/10.1111/j.1750-3841.2011.02455.x

Vary, T.C., Jefferson, L.S., Kimball, S.R., 2001. Insulin fails to stimulate muscle protein synthesis in sepsis despite unimpaired signaling to 4E-BP1 and S6K1. Am. J. Physiol. Metab. 281, E1045–E1053. https://doi.org/10.1152/ajpendo.2001.281.5.E1045

Vijayaraj, S.L., Feltham, R., Rashidi, M., Frank, D., Liu, Z., Simpson, D.S., Ebert, G., Vince, A., Herold, M.J., Kueh, A., Pearson, J.S., Dagley, L.F., Murphy, J.M., Webb, A.I., Lawlor, K.E., Vince, J.E., 2021. The ubiquitylation of IL-1β limits its cleavage by caspase-1 and targets it for proteasomal degradation. Nat. Commun. 12, 1–16. https://doi.org/10.1038/s41467-021-22979-3

Villalta, S.A., Rinaldi, C., Deng, B., Liu, G., Fedor, B., Tidball, J.G., 2011. Interleukin-10 reduces the pathology of mdx muscular dystrophy by deactivating M1 macrophages and modulating macrophage phenotype. Hum. Mol. Genet. 20, 790–805. https://doi.org/10.1093/hmg/ddq523

Villar-Fincheira, P., Sanhueza-Olivares, F., Norambuena-Soto, I., Cancino-Arenas, N., Hernandez-Vargas, F., Troncoso, R., Gabrielli, L., Chiong, M., 2021. Role of Interleukin-6 in Vascular Health and Disease. Front. Mol. Biosci. 8, 1–11. https://doi.org/10.3389/fmolb.2021.641734

Viola, A., Munari, F., Sánchez-Rodríguez, R., Scolaro, T., Castegna, A., 2019. The Metabolic Signature of Macrophage Responses. Front. Immunol. 10, 1–16. https://doi.org/10.3389/fimmu.2019.01462

Vraskou, Y., Roher, N., Díaz, M., Antonescu, C.N., MacKenzie, S.A., Planas, J. V., 2011. Direct involvement of tumor necrosis factor-α in the regulation of glucose uptake in rainbow trout muscle cells. Am. J. Physiol. Integr. Comp. Physiol. 300, R716–R723. https://doi.org/10.1152/ajpregu.00514.2010

Wada, E., Tanihata, J., Iwamura, A., Takeda, S., Hayashi, Y.K., Matsuda, R., 2017. Treatment with the anti-IL-6 receptor antibody attenuates muscular dystrophy via promoting skeletal muscle regeneration in dystrophin-/utrophin-deficient mice. Skelet. Muscle 7, 23. https://doi.org/10.1186/s13395-017-0140-z

Wajant, H., Siegmund, D., 2019. TNFR1 and TNFR2 in the Control of the Life and Death Balance of Macrophages. Front. Cell Dev. Biol. 7, 1–14. https://doi.org/10.3389/fcell.2019.00091

Walton, R.G., Kosmac, K., Mula, J., Fry, C.S., Peck, B.D., Groshong, J.S., Finlin, B.S., Zhu, B., Kern, P.A., Peterson, C.A., 2019. Human skeletal muscle macrophages increase following cycle training and are associated with adaptations that may facilitate growth. Sci. Rep. 9, 969. https://doi.org/10.1038/s41598-018-37187-1

Wang, L., Zhang, S., Wu, H., Rong, X., Guo, J., 2019. M2b macrophage polarization and its roles in diseases. J. Leukoc. Biol. 106, 345–358. https://doi.org/10.1002/JLB.3RU1018-378RR

Wang, N., Liang, H., Zen, K., 2014. Molecular mechanisms that influence the macrophage M1-M2 polarization balance. Front. Immunol. 5, 1–9. https://doi.org/10.3389/fimmu.2014.00614

Wang, Q., Khayat, Z., Kishi, K., Ebina, Y., Klip, A., 1998. GLUT4 translocation by insulin in intact muscle cells: Detection by a fast and quantitative assay. FEBS Lett. 427, 193–197. https://doi.org/10.1016/S0014-5793(98)00423-2

Wang, X., Ye, A., Lin, Q., Han, J., Singh, H., 2018. Gastric digestion of milk protein ingredients: Study using an in vitro dynamic model. J. Dairy Sci. 101, 6842–6852. https://doi.org/10.3168/jds.2017-14284

Weischenfeldt, J., Porse, B., 2008. Bone marrow-derived macrophages (BMM): Isolation and applications. Cold Spring Harb. Protoc. 3, 1–7. https://doi.org/10.1101/pdb.prot5080

West, D., Abou Sawan, S., Mazzulla, M., Williamson, E., Moore, D., 2017. Whey Protein Supplementation Enhances Whole Body Protein Metabolism and Performance Recovery after Resistance Exercise: A Double-Blind Crossover Study. Nutrients 9, 735. https://doi.org/10.3390/nu9070735

Williamson, D.L., Kimball, S.R., Jefferson, L.S., 2005. Acute treatment with TNF-α attenuates insulin-stimulated protein synthesis in cultures of C 2 C 12 myotubes through a MEK1-sensitive mechanism. Am. J. Physiol. Metab. 289, E95–E104. https://doi.org/10.1152/ajpendo.00397.2004

Wirsdörfer, F., Bangen, J.M., Pastille, E., Schmitz, D., Flohé, S., Schumak, B., Flohé, S.B., 2016. Dendritic cell-like cells accumulate in regenerating murine skeletal muscle after injury and boost adaptive immune responses only upon a microbial challenge. PLoS One 11, 1–19. https://doi.org/10.1371/journal.pone.0155870

Witkamp, R.F., van Norren, K., 2018a. Let thy food be thy medicine….when possible. Eur. J. Pharmacol. 836, 102–114. https://doi.org/10.1016/j.ejphar.2018.06.026

Witkamp, R.F., van Norren, K., 2018b. Let thy food be thy medicine….when possible. Eur. J. Pharmacol. 836, 102–114. https://doi.org/10.1016/j.ejphar.2018.06.026

Wood, S., Jayaraman, V., Huelsmann, E.J., Bonish, B., Burgad, D., Sivaramakrishnan, G., Qin, S., DiPietro, L.A., Zloza, A., Zhang, C., Shafikhani, S.H., 2014. Pro-inflammatory chemokine CCL2 (MCP-1) promotes healing in diabetic wounds by restoring the macrophage response. PLoS One 9, 1–8. https://doi.org/10.1371/journal.pone.0091574

Woods, C.B., Powell, C., Saunders, J.A., O'Brien, W., Murphy, M.H., Duff, C., Farmer, O., Johnston, A., Connolly, S., Belton, S., 2018. The children's sport participation and physical activity study 2018 (CSPPA 2018) 1–108.

Wu, H., Ballantyne, C.M., 2017. Skeletal muscle inflammation and insulin resistance in obesity. J. Clin. Invest. 127, 43–54. https://doi.org/10.1172/JCI88880

Wynn, T.A., Vannella, K.M., 2016. Macrophages in Tissue Repair, Regeneration, and Fibrosis. Immunity. https://doi.org/10.1016/j.immuni.2016.02.015

Xu, X.J., Reichner, J.S., Mastrofrancesco, B., Henry, W.L., Albina, J.E., 2008. Prostaglandin E 2 Suppresses Lipopolysaccharide-Stimulated IFN-β Production . J. Immunol. 180, 2125–2131. https://doi.org/10.4049/jimmunol.180.4.2125

Yahiaoui, L., Gvozdic, D., Danialou, G., Mack, M., Petrof, B.J., 2008. CC family chemokines directly regulate myoblast responses to skeletal muscle injury. J. Physiol. 586, 3991–4004. https://doi.org/10.1113/jphysiol.2008.152090

Yang, W., Hu, P., 2018. Skeletal muscle regeneration is modulated by inflammation. J. Orthop. Transl. 13, 25–32. https://doi.org/10.1016/j.jot.2018.01.002

Yin, H., Price, F., Rudnicki, M.A., 2013. Satellite Cells and the Muscle Stem Cell Niche. Am. Physiol. Soc. 93, 23–67. https://doi.org/10.1152/physrev.00043.2011

Yoon, M.S., 2017. mTOR as a key regulator in maintaining skeletal muscle mass. Front. Physiol. 8, 1–9. https://doi.org/10.3389/fphys.2017.00788

Yoshizawa, F., Kimball, S.R., Vary, T.C., Jefferson, L.S., 1998. Effect of dietary protein on translation initiation in rat skeletal muscle and liver. Am. J. Physiol. Metab. 275, E814–E820. https://doi.org/10.1152/ajpendo.1998.275.5.E814

Yu, J., Shi, L., Wang, H., Bilan, P.J., Yao, Z., Samaan, M.C., He, Q., Klip, A., Niu, W., 2011. Conditioned medium from hypoxia-treated adipocytes renders muscle cells insulin resistant. Eur. J. Cell Biol. 90, 1000–1015. https://doi.org/10.1016/j.ejcb.2011.06.004

Yu, X.L., Wu, B.T., Ma, T.T., Lin, Y., Cheng, F., Xiong, H.Y., Xie, C.L., Liu, C.Y., Wang, Q., Li, Z.W., Tu, Z.G., 2016. Overexpression of IL-12 reverses the phenotype and function of M2 macrophages to M1 macrophages. Int. J. Clin. Exp. Pathol. 9, 8963–8972.

Zhang, F., Wang, Hongsheng, Wang, X., Jiang, G., Liu, H., Zhang, G., Wang, Hao, Fang, R., Bu, X., Cai, S., Du, J., 2016. TGF-β induces M2-like macrophage polarization via SNAIL-mediated suppression of a pro-inflammatory phenotype. Oncotarget 7, 52294–52306. https://doi.org/10.18632/oncotarget.10561

Zhang, J., Fu, S., Sun, S., Li, Z., Guo, B., 2014. Inflammasome activation has an important role in the development of spontaneous colitis. Mucosal Immunol. 7, 1139–1150. https://doi.org/10.1038/mi.2014.1

Zhang, Q.-Z., Su, W.-R., Shi, S.-H., Wilder-Smith, P., Xiang, A.P., Wong, A., Nguyen, A.L., Kwon, C.W., Le, A.D., 2010. Human Gingiva-Derived Mesenchymal Stem Cells Elicit Polarization of M2 Macrophages and Enhance Cutaneous Wound Healing. Stem Cells 28, 1856–1868. https://doi.org/10.1002/stem.503

Zhang, S., Liu, Y., Zhang, X., Zhu, D., Qi, X., Cao, X., Fang, Y., Che, Y., Han, Z.C., He, Z.X., Han, Z., Li, Z., 2018. Prostaglandin E2 hydrogel improves cutaneous wound healing via M2 macrophages polarization. Theranostics 8, 5348–5361. https://doi.org/10.7150/thno.27385

Zhang, Y., Shi, L., Mei, H., Zhang, J., Zhu, Y., Han, X., Zhu, D., 2015. Inflamed macrophage microvesicles induce insulin resistance in human adipocytes. Nutr. Metab. (Lond). 12, 21. https://doi.org/10.1186/s12986-015-0016-3

Zhao, G., Dharmadhikari, G., Maedler, K., Meyer-Hermann, M., 2014. Possible Role of Interleukin-1β in Type 2 Diabetes Onset and Implications for Anti-inflammatory Therapy Strategies. PLoS Comput. Biol. 10, e1003798. https://doi.org/10.1371/journal.pcbi.1003798